SANDIA REPORT

SAND 2004-0001
Unlimited Release
Printed January 2004

Estimation Of Fatigue And Extreme Load Distributions From Limited Data With Application To Wind Energy Systems

LeRoy M. Fitzwater

Prepared by
Sandia National Laboratories
Albuquerque, New Mexico 87185 and Livermore, California 94550

Sandia is a multiprogram laboratory operated by Sandia Corporation,
a Lockheed Martin Company, for the United States Department of Energy's
National Nuclear Security Administration under Contract DE-AC04-94AL85000.

Issued by Sandia National Laboratories, operated for the United States Department of Energy by Sandia Corporation.

Available to DOE and DOE contractors from
U.S. Department of Energy
Office of Scientific and Technical Information
P.O. Box 62
Oak Ridge, TN 37831

Telephone: (865)576-8401
Facsimile: (865)576-5728
E-Mail: reports@adonis.osti.gov
Online ordering: http://www.doe.gov/bridge

Available to the public from
U.S. Department of Commerce
National Technical Information Service
5285 Port Royal Rd
Springfield, VA 22161

Telephone: (800)553-6847
Facsimile: (703)605-6900
E-Mail: orders@ntis.fedworld.gov
Online order: http://www.ntis.gov/help/ordermethods.asp?loc=7-4-0#online

SAND 2004-0001
Unlimited Release
Printed January 2004

ESTIMATION OF FATIGUE AND EXTREME LOAD DISTRIBUTIONS FROM LIMITED DATA WITH APPLICATION TO WIND ENERGY SYSTEMS

LeRoy M. Fitzwater
Department Of Civil And Environmental Engineering
Stanford University
Stanford,California

ABSTRACT

An estimate of the distribution of fatigue ranges or extreme loads for wind turbines may be obtained by separating the problem into two uncoupled parts, (1) a turbine specific portion, independent of the site and (2) a site-specific description of environmental variables. We consider contextually appropriate probability models to describe the turbine specific response for extreme loads or fatigue. The site-specific portion is described by a joint probability distribution of a vector of environmental variables, which characterize the wind process at the hub-height of the wind turbine. Several approaches are considered for combining the two portions to obtain an estimate of the extreme load, e.g., 50-year loads or fatigue damage. We assess the efficacy of these models to obtain accurate estimates, including various levels of epistemic uncertainty, of the turbine response.

This work was made under Contract BG-4054 with Sandia Corporation. The U.S. Government has a paid-up, non-exclusive, irrevokable worldwide license to reproduce, prepare derivative works, distribute copies to the public, and perform publicly and display publicly, by or on behalf of the Government.

Acknowledgments

I wish to express my gratitude to my principal advisor at Stanford University, professor Allin Cornell, for his advice and expert technical guidance, as well as Paul Veers from Sandia National Laboratories for his guidance, encouragement and especially his support throughout my entire course of study. A special word of thanks is given to the other members of my reading and defense committees, professors: Charles Menun, Greg Deierlein, and Holt Ashley, for their time and dedication. In addition I would like to acknowledge the support and encouragement I received for the members of the Wind Energy community at Sandia National Laboratories and the National Renewable Energy Laboratory: Marshall Buhl, Herb Sutherland, Bill Holley, Sandy Butterfield, Rick Santos, and Dale Berg. This work was supported by the United States Department of Energy.

Contents

Acknowledgments iii

List of Tables ix

List of Figures xv

1 Introduction 1

1.1 Motivation . . . 1
1.2 Background . . . 4
1.3 Wind Turbines . . . 10
1.3.1 Configuration and Operation . . . 10
1.3.2 Stationarity of the Wind Process . . . 14
1.4 Data Sets . . . 15
1.4.1 DOE/NREL/NWTC Unsteady Aerodynamics Experiment Phase III Turbine 15
1.4.2 Atlantic Orient Corporation, AOC 15/50 . . . 18
1.5 Moment-Based Models . . . 18
1.5.1 Expectation and Statistical Moments . . . 18
1.5.2 Estimating Statistical Moments . . . 24
1.5.3 Probability Models for Extreme Loads . . . 27
1.5.4 Global Extreme Model . . . 28
1.5.5 Random Peak Model . . . 29
1.5.6 Process Model . . . 30
1.6 Organization . . . 33

2 Short-term Extremes 35

2.1 Introduction . . . 35
2.2 Probability Models for Extreme Loads and Responses . . . 36

2.3 Data set . . . 37
2.4 Predicting Short-term Extreme Events . . . 38
2.4.1 Sample Time Histories . . . 38
2.4.2 Observed vs Predicted Distributions of Peaks . . . 43
2.4.3 Estimating 10-Minute Mean Maxima . . . 48
2.5 Conclusions . . . 59

3 Long-term Extremes **60**
3.1 Introduction . . . 60
3.2 Long-Term Loads—Short-Term Histories . . . 62
3.3 Data Set . . . 66
3.4 Long-Term Analysis Based on Modeling Global Extremes . . . 69
3.4.1 Short-Term Analysis . . . 69
3.4.2 Long-term Analysis . . . 77
3.4.3 Simplifying the Long-term Analysis . . . 80
3.4.4 Summary . . . 87
3.5 Long-Term Analysis Based on Modeling Local Peaks . . . 90
3.5.1 Short-Term Analysis . . . 90
3.5.2 Long-term Analysis . . . 109
3.5.3 Simplifying the Long-term Analysis . . . 111
3.5.4 Summary . . . 113
3.6 Comparison of Long-Term Estimates . . . 121
3.7 Conclusions . . . 123

4 Environmental Contours **124**
4.1 Introduction . . . 124
4.2 Estimating the Long-term Expected Response . . . 126
4.3 Overview of Examples . . . 128
4.4 Example 1 — IEC Model with Stall-Regulated Turbine . . . 129
4.4.1 Description of Environment . . . 129
4.4.2 Constructing the Environmental Contour . . . 131
4.4.3 Transform circle to contour . . . 132
4.4.4 Describing the Short-Term Response . . . 134
4.4.5 Environmental Contours vs. Full Integration Method . . . 137
4.5 Example 2 — Field Data Model with Stall-Regulated Turbine . . . 142
4.5.1 Description of Environment . . . 142

4.5.2 Constructing the Environmental Contour . . . 143
4.5.3 Description of Short-Term Response . . . 143
4.5.4 Environmental Contour vs. Full Integration Method . . . 144
4.6 Example 3 — Field Data Model with Pitch-Regulated Turbine . . . 146
4.6.1 Comparing Environmental Contour and Full Integration . . . 151
4.7 Including the Third Random Variable . . . 153
4.8 Conclusion . . . 155

5 Long-Term Fatigue Distributions **157**
5.1 Introduction . . . 157
5.2 Data Set . . . 159
5.3 Probability Models for Fatigue Loads . . . 159
5.3.1 The Standard Weibull Model . . . 160
5.3.2 The Quadratic Weibull Model . . . 161
5.3.3 The Damage-Based Weibull Model . . . 168
5.4 Long-Term Analysis Based on Quadratic Weibull Model . . . 169
5.4.1 Short-term Analysis . . . 169
5.4.2 Long-Term Analysis . . . 174
5.4.3 Summary . . . 185
5.5 Long-term Analysis with Damage-Based Weibull Model . . . 185
5.5.1 Short-Term Analysis . . . 185
5.5.2 Long-Term Analysis . . . 193
5.5.3 Summary . . . 195
5.6 Comparison of Long-term Estimates . . . 198
5.7 Conclusions . . . 201

6 Uncertainty Analysis **204**
6.1 Introduction . . . 205
6.1.1 Types of Uncertainty . . . 205
6.1.2 Motivation . . . 207
6.2 Data Set . . . 209
6.3 Uncertainty in Long-Term Environmental Distributions . . . 209
6.3.1 Estimating the Long-Term Distribution of Extreme Loads Considering Uncertain Parameters of the Distributions of Environmental Variables . . . 212
6.3.2 Summary . . . 222
6.4 Uncertainty in short-term load distribution . . . 222

6.4.1 Uncertain regression coefficients . . . 222
6.4.2 Using Bootstrap Method to Estimate Uncertainty in Regression Coefficients 224
6.4.3 Model Uncertainty . . . 233
6.5 Conclusions . . . 240

7 Summary and Conclusions **242**
7.1 Modeling Short-Term Extremes . . . 242
7.2 Estimating Long-Term Extreme Events . . . 243
7.2.1 Integration Method . . . 243
7.2.2 Environmental Contour Method . . . 244
7.3 Modeling Fatigue Ranges and Damage . . . 246
7.4 Quantifying Epistemic Uncertainty . . . 247

Bibliography **249**

A Filtering Pseudo-Parked Time Histories **256**

B Regression Analysis **260**
B.1 Introduction . . . 260
B.2 Multiple Linear Regression—Matrix Formulation . . . 261
B.3 Least Squares Estimation of β . . . 262
B.4 Expected Value and Variance of $\hat{\beta}$ . . . 263
B.5 Coefficient of Determination, R^2 . . . 264

C Long-Term Extremes—IEC Environment **265**
C.1 Introduction . . . 265
C.2 Data Set . . . 265
C.3 Long-Term Analysis Based on Modeling Global Extremes . . . 266
C.3.1 Short-Term Analysis . . . 266
C.3.2 Long-term Analysis . . . 271
C.3.3 Simplifying the Long-term Analysis . . . 274
C.3.4 Summary . . . 276
C.4 Long-Term Analysis Based on Modeling Local Peaks . . . 278
C.4.1 Short-Term Analysis . . . 278
C.4.2 Long-term Analysis . . . 279
C.4.3 Simplifying the Long-term Analysis . . . 287
C.4.4 Summary . . . 289

C.5 Comparison of Long-Term Estimates . . . 293

D First-Order Reliability Method **296**
D.1 Introduction . . . 296
D.2 Background . . . 296
D.3 First-Order Reliability Method (FORM) . . . 297
D.4 Affect of Multiple Design Points on FORM Estimate . . . 299

E Environmental Contours—IEC 61400-1 **305**
E.1 Introduction . . . 305
E.2 Definition of Environmental Random Variables . . . 305
E.2.1 Wind Speed . . . 305
E.2.2 Turbulence Intensity . . . 306
E.2.3 Joint Probability Density Function of Environmental Variables . . . 307
E.3 Transformation Equations . . . 308
E.3.1 Transformation of U_1 to basic space, wind speed, V . . . 308
E.3.2 Transformation of U_2, given V, to basic space, turbulence, I . . . 308
E.4 Plot of Environmental Contours for Wind Classes IA-IIIC . . . 309
E.5 Normalized Contours . . . 314

F Long-Term Fatigue Distributions—IEC Environment **316**
F.1 Introduction . . . 316
F.2 Data Set . . . 316
F.3 Long-Term Analysis Based on Quadratic Weibull Model . . . 317
F.3.1 Short-term Analysis . . . 317
F.3.2 Long-Term Analysis . . . 325
F.3.3 Summary . . . 331
F.4 Long-term Analysis with Damage-Based Weibull Model . . . 332
F.4.1 Short-Term Analysis . . . 332
F.4.2 Long-Term Analysis . . . 339
F.4.3 Summary . . . 341
F.5 Comparison of Long-term Estimates . . . 344

List of Tables

2.1 Correlation coefficient, ρ , between adjacent peaks y_i and y_{i+1} for various 10-minute mean wind speeds 43

3.1 Regression coefficients used in Equation 3.19 to fit statical moments of blade root flap bending loads as functions of the mean wind speed, V, and turbulence intensity, I. 76

3.2 Regression coefficients used in Equation 3.19 to fit statistical moments of blade root edge bending loads as functions of the mean wind speed, V, and turbulence intensity, I. 76

3.3 Regression coefficients used in Equation 3.27 to fit flap load moments as functions of the mean wind speed, V, and turbulence intensity, I. The wind turbine is operating for $V \leqq 24$m/s, otherwise the turbine is parked. 102

3.4 Regression coefficients used in Equation 3.27 to fit edge load moments as functions of the mean wind speed, V, and turbulence intensity, I. The wind turbine is operating for $V \leqq 24$m/s, otherwise the turbine is parked. 103

3.5 Estimates of one-year and 50-year blade root flap bending loads, considering deterministic fractiles of conditional short-term load, turbulence intensity, and wind speed. 116

3.6 Estimates of one-year and 50-year blade root edge bending loads, considering deterministic fractiles of conditional short-term load, turbulence intensity, and wind speed. 117

3.7 Comparison of long-term estimates of one-year and 50-year bending loads based on using Gumbel distribution fit to observed global maximum for the short-term load model versus fitting a quadratic Weibull distribution to the local peaks. 121

4.1 Regression coefficients used in Equation 4.17 to fit mean of the extreme 10-minute flap and edge bending loads as functions of the mean wind speed, V, and turbulence intensity, I. 136

4.2 Reference wind speed and turbulence values used in Equation 4.17 136
4.3 Regression coefficients used in Equation 4.17 to fit mean flap and edge bending loads as a functions of the mean wind speed, V, and turbulence intensity, I. 145
4.4 Reference wind speed and turbulence values used in Equation 4.17 145
4.5 Regression coefficients used in Equation 4.17 for flap load as a function of the mean wind speed, V, and turbulence intensity, T. 150
4.6 Comparison of one-year and 50-year blade root flap and edge bending loads, considering conditional short-term load alternatively either random, modeled by a Gumbel distribution, or deterministic. 155

5.1 Reference wind speed and turbulence values used in Equation 5.9 174
5.2 Regression coefficients used in Equation 5.9 to fit flap bending moment fatigue ranges as functions of the mean wind speed, V, and turbulence intensity, I. The turbine is operating for $V \leqq 24$m/s, otherwise the turbine is parked. 175
5.3 Regression coefficients used in Equation 5.9 to fit edge bending moment fatigue ranges as functions of the mean wind speed, V, and turbulence intensity, I. The turbine is operating for $V \leqq 24$m/s, otherwise the turbine is parked. 179
5.4 Regression coefficients used in Equation 5.9 to fit the expected number of fatigue ranges, $\mathsf{E}[N_0(v,i)]$, for blade root flap and edge bending, as functions of the mean wind speed, V, and turbulence intensity, I. 183
5.5 Estimate of damage measure, DM_{10}, for fatigue exponent values, $b_f = 1, \ldots, 10$, considering blade root flap and edge bending fatigue loads. 183
5.6 Regression coefficients used in Equation 5.9 to fit transformed ($z = 3$) flap bending moment fatigue ranges as functions of the mean wind speed and turbulence intensity. The turbine is operating for $V \leqq 24$m/s, otherwise the turbine is parked. . . . 188
5.7 Regression coefficients used in Equation 5.9 to fit transformed ($z = 3$) edge bending moment fatigue ranges as functions of the mean wind speed and turbulence intensity. The turbine is operating for $V \leqq 24$m/s, otherwise the turbine is parked. . 188
5.8 Regression coefficients used in Equation 5.9 to fit transformed ($z = 4$) flap bending moment fatigue ranges as functions of the mean wind speed and turbulence intensity. The turbine is operating for $V \leqq 24$m/s, otherwise the turbine is parked. . . . 189
5.9 Regression coefficients used in Equation 5.9 to fit transformed ($z = 4$) edge bending moment fatigue ranges as functions of the mean wind speed and turbulence intensity. The turbine is operating for $V \leqq 24$m/s, otherwise the turbine is parked. . 189

5.10 Regression coefficients used in Equation 5.9 to fit transformed ($z = 5$) flap bending moment fatigue ranges as functions of the mean wind speed and turbulence intensity. The turbine is operating for $V \leqq 24$m/s, otherwise the turbine is parked. . . . 190
5.11 Regression coefficients used in Equation 5.9 to fit transformed ($z = 5$) edge bending moment fatigue ranges as functions of the mean wind speed and turbulence intensity. The turbine is operating for $V \leqq 24$m/s, otherwise the turbine is parked. . 190
5.12 Regression coefficients used in Equation 5.9 to fit the expected number of fatigue ranges, for blade root flap and edge bending, as functions of the mean wind speed and turbulence intensity. The turbine is operating for $V \leqq 24$m/s, otherwise the turbine is parked. 195
5.13 Estimate of damage measure, DM_{10}, for fatigue exponent values, $b_f = 1, \ldots, 10$, considering blade root flap and edge bending loads. 198
5.14 Comparison of damage measure, DM_{10}, estimates for blade root flap bending fatigue loads between short-term quadratic Weibull(Q.W.) model and damage-based Weibull model for $z = 3, 4, 5$ ($z = b_f/2$). 199
5.15 Comparison of damage measure, DM_{10}, estimates for blade root edge bending fatigue loads between short-term quadratic Weibull(Q.W.) model and damage-based Weibull model for $z = 3, 4, 5$ ($z = b_f/2$). 201
5.16 Comparison of estimates of blade root flap bending fatigue damage measure, DM_{10}, for fatigue exponent values, $b_f = 1, \ldots, 10$, considering empirical, quadratic Weibull, and damage based models. 202
5.17 Comparison of estimates of blade root edge bending fatigue damage measure, DM_{10}, for fatigue exponent values, $b_f = 1, \ldots, 10$, considering empirical, quadratic Weibull, and damage based models. 202

6.1 Comparison of estimates of 50-year blade root flap bending moment, including uncertainty long-term environmental variable distribution parameters, with considering all parameters deterministic. 221
6.2 Comparison of estimates of 50-year blade root flap bending moment, considering uncertain regression coefficients. The bootstrap method was used to estimate uncertainty. Estimates of the 50-year blade root flap bending moment are compared with results obtained with regression coefficients considered deterministic. 226
6.3 Comparison of estimates of 50-year blade root flap bending moment, considering uncertain regression coefficients with known covariance. Estimates of the 50-year blade root flap bending moment are compared with results obtained with regression coefficients considered deterministic. 232

6.4 Numerical results of regression of the observed 10-minute maximum blade root flap bending moment on the predicted 10-minute maximum blade root flap bending moment from simulation. (Figure 6.10) 235

C.1 Regression coefficients used in Equation C.1 to fit statical moments of blade root flap bending loads as functions of the mean wind speed, V, and turbulence intensity, I. 268

C.2 Regression coefficients used in Equation C.1 to fit statistical moments of blade root edge bending loads as functions of the mean wind speed, V, and turbulence intensity, I. 268

C.3 Regression coefficients used in Equation C.1 to fit flap load moments as functions of the mean wind speed, V, and turbulence intensity, I. 280

C.4 Regression coefficients used in Equation C.1 to fit edge load moments as functions of the mean wind speed, V, and turbulence intensity, I. 281

C.5 Comparison of long-term estimates of one-year and 50-year bending loads based on using Gumbel distribution fit to observed extreme events for the short-term load model versus fitting a quadratic Weibull distribution to the local peaks for the short-term load model. 295

E.1 Mean value of annual distribution of 10-minute mean wind speed, for wind classes I-III. 306

E.2 Parameters I_{ref} and c for annual conditional distribution of turbulence, for Turbulence classes A-C. 307

F.1 Reference wind speed and turbulence values used in Equation F.1 319

F.2 Regression coefficients used in Equation 5.9 to fit flap bending moment fatigue ranges as functions of the mean wind speed, V, and turbulence intensity, I. The turbine is operating for $V \leqq 24$m/s, otherwise the turbine is parked. 320

F.3 Regression coefficients used in Equation 5.9 to fit edge bending moment fatigue ranges as functions of the mean wind speed, V, and turbulence intensity, I. The turbine is operating for $V \leqq 24$m/s, otherwise the turbine is parked. 321

F.4 Regression coefficients used in Equation 5.9 to fit the expected number of fatigue ranges, for blade root flap and edge bending, as functions of the mean wind speed, V, and turbulence intensity, I. 328

F.5 Estimate of damage measure, DM_{10}, for fatigue exponent values, $b_f = 1, \ldots, 10$, considering blade root flap and edge bending fatigue loads. 331

F.6 Regression coefficients used in Equation F.1 to fit transformed ($z = 3$) flap bending moment fatigue ranges as functions of the mean wind speed and turbulence intensity. The turbine is operating for $V \leqq$ 24m/s, otherwise the turbine is parked. . . . 334

F.7 Regression coefficients used in Equation F.1 to fit transformed ($z = 3$) edge bending moment fatigue ranges as functions of the mean wind speed and turbulence intensity. The turbine is operating for $V \leqq$ 24m/s, otherwise the turbine is parked. . 334

F.8 Regression coefficients used in Equation F.1 to fit transformed ($z = 4$) flap bending moment fatigue ranges as functions of the mean wind speed and turbulence intensity. The turbine is operating for $V \leqq$ 24m/s, otherwise the turbine is parked. . . . 335

F.9 Regression coefficients used in Equation F.1 to fit transformed ($z = 4$) edge bending moment fatigue ranges as functions of the mean wind speed and turbulence intensity. The turbine is operating for $V \leqq$ 24m/s, otherwise the turbine is parked. . 335

F.10 Regression coefficients used in Equation F.1 to fit transformed ($z = 5$) flap bending moment fatigue ranges as functions of the mean wind speed and turbulence intensity. The turbine is operating for $V \leqq$ 24m/s, otherwise the turbine is parked. . . . 336

F.11 Regression coefficients used in Equation F.1 to fit transformed ($z = 5$) edge bending moment fatigue ranges as functions of the mean wind speed and turbulence intensity. The turbine is operating for $V \leqq$ 24m/s, otherwise the turbine is parked. . 336

F.12 Regression coefficients used in Equation F.1 to fit the expected number of fatigue ranges, for blade root flap and edge bending, as functions of the mean wind speed and turbulence intensity. The turbine is operating for $V \leqq$ 24m/s, otherwise the turbine is parked. 341

F.13 Estimate of damage measure, DM_{10}, for fatigue exponent values, $b_f = 1, \ldots, 10$, considering blade root flap and edge bending loads. 341

F.14 Comparison of damage measure, DM_{10}, estimates for blade root flap bending fatigue loads between short-term quadratic Weibull(Q.W.) model and damage-based Weibull model for $z = 3, 4, 5$ ($z = b_f/2$). 346

F.15 Comparison of damage measure, DM_{10}, estimates for blade root edge bending fatigue loads between short-term quadratic Weibull(Q.W.) model and damage-based Weibull model for $z = 3, 4, 5$ ($z = b_f/2$). 346

F.16 Comparison of estimates of blade root flap bending fatigue damage measure, DM_{10}, for fatigue exponent values, $b_f = 1, \ldots, 10$, considering empirical, quadratic Weibull, and damage based models. 348

F.17 Comparison of estimates of blade root edge bending fatigue damage measure, DM_{10}, for fatigue exponent values, $b_f = 1, \ldots, 10$, considering empirical, quadratic Weibull, and damage based models. 348

List of Figures

1.1 Generic diagram of a two bladed horizontal axis turbine, showing the directions of out-of-plane, $M_{\text{out-of-plane}}$ and in-plane, $M_{\text{in-plane}}$, bending moments. 13

1.2 Cross-section through cord plane of generic wind turbine airfoil showing relation between out-of-plane and flap bending moments (also, in-plane and edge bending moments) through pitch angle α. 14

1.3 Department of Energy/National Renewable Energy Laboratory's Unsteady Aerodynamics Experiment Phase III turbine installed at the National Wind Technology Center. Photograph courtesy of the National Renewable Energy Laboratory, www.nrel.gov. 16

1.4 Close-up of DOE/NREL Unsteady Aerodynamics Experiment Phase III turbine installed at NWTC. Photograph courtesy of the National Renewable Energy Laboratory, www.nrel.gov. 17

1.5 Atlantic Orient Corporation's AOC 15/50 turbine installed in Burlington, Vermont. Photograph courtesy of the Atlantic Orient Corporation, www.aocwind.net. 19

1.6 Distributions with positive and negative skewness compared with the Gaussian distribution with zero skewness. Note, all distributions shown have the same mean and variance. 23

1.7 Distributions with higher and lower coefficients of kurtosis, $\kappa_X = 2$ and $\kappa_X = 6$ compared with the Gaussian distribution with κ_X=3. Note, all distributions shown have the same mean and variance. 23

1.8 Time scales versus amount of available data: Global maximum, Z; local random peaks, Y; random process, $X(t)$. 28

2.1 Simulated wind and blade responses; V=45m/s. 40

2.2 Simulated wind and blade responses; V=20m/s. 41

2.3 Simulated wind and blade responses; V=14m/s. 42

2.4 Histograms of the number of blade root edge bending peaks for V=20m/s and 14m/s. 43

2.5 Correlation between successive blade root bending peaks; V=45m/s. 44
2.6 Correlation between successive blade root bending peaks; V=20m/s. 45
2.7 Correlation between successive blade root peaks; V=14m/s. 46
2.8 Empirical and fitted quadratic Weibull probability distributions of response peaks; V=45m/s. 47
2.9 Empirical and fitted quadratic Weibull probability distributions of response peaks; V=20m/s. 49
2.10 Empirical and fitted quadratic Weibull probability distributions of *shifted* edge bending response peaks above 1.5; V=20m/s. 49
2.11 Empirical and fitted quadratic Weibull probability distributions of response peaks; V=14m/s. 50
2.12 Empirical and fitted quadratic Weibull probability distributions of *shifted* edge bending response peaks above 1.5; V=14m/s. 50
2.13 Bias and sigma reduction factors for three and four moment Hermite models and peak un-shifted quadratic Weibull model, V=45m/s. 52
2.14 Estimated expected maxima over various time intervals, V=45m/s 53
2.15 Bias and sigma reduction factors for three and four moment Hermite models, peak shifted, and un-shifted quadratic Weibull models, V=20m/s. 55
2.16 Bias and sigma reduction factors for three and four moment Hermite models, peak shifted, and un-shifted quadratic Weibull models, V=14m/s. 56
2.17 Estimated expected maxima over various time intervals, V=20m/s 57
2.18 Estimated expected maxima over various time intervals, V=14m/s 58

3.1 10-minute mean wind speed and turbulence intensity for 2400 10-minute Gaussian wind input processes. 67
3.2 Unfiltered and filtered time histories of blade root edge bending response for the parked turbine condition in a 24m/s turbulence class A wind environment. 68
3.3 Mean and standard deviation of 10-minute maximum blade root flap bending responses for given 10-minute mean wind speeds. The wind turbine is operating for $V \leqq 24$m/s, otherwise the turbine is parked. 71
3.4 Mean and standard deviation of 10-minute maximum blade root edge bending responses for given 10-minute mean wind speeds. The wind turbine is operating for $V \leqq 24$m/s, otherwise the turbine is parked. 72
3.5 Gumbel fit to observed blade root flap bending data for operating and parked wind speeds, turbulence class A. 73

3.6 Gumbel fit to observed blade root edge bending data for operating and parked wind speeds, turbulence class A. 74
3.7 Regression of the moments of 10-minute maximum on the 10-minute mean wind speed and turbulence intensity for blade root flap bending. 78
3.8 Regression of the moments of 10-minute maximum on the 10-minute mean wind speed and turbulence intensity for blade root edge bending. 79
3.9 Long-term distributions of 10-minute extreme blade root bending moment, $L_{10\,\mathrm{min}}$, considering three turbine conditions: 1) turbine operating over all wind speeds, 2) turbine parked over all wind speeds, 3) turbine operating below cutout wind speed and parked above cutout wind speed; for both: (a) flap and (b) edge bending. 81
3.10 Long-term distributions of 10-minute extreme blade root bending moment $L_{10\,\mathrm{min}}$, considering load, turbulence intensity, and wind speed deterministically for both: (a) flap and (b) edge bending. 83
3.11 Long-term distributions of 10-minute extreme blade root bending moment, $L_{10\,\mathrm{min}}$, considering the turbulence intensity at prescribed deterministic levels compared with the full distribution solution; for both: (a) flap and (b) edge bending. 85
3.12 Long-term distributions of 10-minute extreme blade root bending moment, $L_{10\,\mathrm{min}}$, considering the turbulence intensity at the 84% fractile and 10-minute mean wind speed at prescribed deterministic levels compared with the full distribution solution. 86
3.13 Long-term distributions of 10-minute extreme blade root bending moment, $L_{10\,\mathrm{min}}$, considering the short-term load at prescribed deterministic levels compared with the full distribution solution. 88
3.14 Long-term distributions of 10-minute extreme blade root bending moment, $L_{10\,\mathrm{min}}$, considering the short-term load at the 90% fractile and turbulence intensity at prescribed deterministic levels compared with the full distribution solution. 89
3.15 Process mean of 10-minute blade root flap and edge bending response, based on 100 pooled observations for each 10-minute mean wind speed and turbulence class. The wind turbine is operating for $V \leqq 24$m/s, otherwise the turbine is parked. . . . 92
3.16 Expected number of local peaks in 10-minute blade root flap and edge bending responses time histories, based on 100 pooled observations for each 10-minute mean wind speed and turbulence class. The wind turbine is operating for $V \leqq 24$m/s, otherwise the turbine is parked. 93
3.17 Pooled statistics of the mean of the local peaks in 10-minute blade root flap and edge bending responses time histories for given 10-minute mean wind speeds. The wind turbine is operating for $V \leqq 24$m/s, otherwise the turbine is parked. 95

3.18 Pooled statistics of the standard deviation of the local peaks in 10-minute blade root flap and edge bending responses time histories for given 10-minute mean wind speeds. The wind turbine is operating for $V \leqq 24$m/s, otherwise the turbine is parked. 96
3.19 Pooled statistics of the coefficient of skewness of the local peaks in 10-minute blade root flap and edge bending responses time histories for given 10-minute mean wind speeds. The wind turbine is operating for $V \leqq 24$m/s, otherwise the turbine is parked. 97
3.20 Quadratic Weibull model fit to observed blade root flap bending data for operating (18m/s) and parked (40m/s) wind speeds, turbulence class A. 98
3.21 Quadratic Weibull model fit to shifted and un-shifted observed blade root edge bending data for operating wind speed equal to 18m/s, turbulence class A. 100
3.22 Quadratic Weibull model fit to observed blade root edge bending data for parked wind speed equal to 40m/s, turbulence class A. 101
3.23 Regression of the process mean on the 10-minute mean wind speed and turbulence intensity for blade root flap and edge bending. 104
3.24 Regression of the expected number of local peaks on 10-minute mean wind speed and turbulence intensity for blade root flap and edge bending. 105
3.25 Regression of the mean of the local peaks on the 10-minute mean wind speed and turbulence intensity for blade root flap and edge bending. 106
3.26 Regression of the standard deviation of the local peaks on the 10-minute mean wind speed and turbulence intensity for blade root flap and edge bending. 107
3.27 Regression of the coefficient of skewness of the local peaks on the 10-minute mean wind speed and turbulence intensity for blade root flap and edge bending. 108
3.28 Long-term distributions of 10-minute extreme blade root bending moment, $L_{10\,\text{min}}$, considering three turbine conditions: 1) turbine operating over all wind speeds, 2) turbine parked over all wind speeds, 3) turbine operating below cutout wind speed and parked above cutout wind speed; for both (a) flap and (b) edge bending. 110
3.29 Long-term distributions of 10-minute extreme blade root bending moment, $L_{10\,\text{min}}$, considering load, turbulence intensity, and wind speed deterministically for both blade root (a) flap and (b) edge bending. 112
3.30 Long-term distributions of 10-minute extreme blade root bending moment, $L_{10\,\text{min}}$, considering the turbulence intensity at prescribed deterministic fractiles compared with the full distribution solution. 114
3.31 Long-term distributions of 10-minute extreme blade root bending moment, $L_{10\,\text{min}}$, considering the turbulence intensity at the 90% fractile and 10-minute mean wind speed at prescribed deterministic levels compared with the full distribution solution. 115

3.32 Long-term distributions of 10-minute extreme blade root bending moment, $L_{10\,\text{min}}$, considering the load term at prescribed deterministic levels compared with the full distribution solution. 118
3.33 Long-term distributions of 10-minute extreme blade root bending moment, $L_{10\,\text{min}}$, considering the short-term load at $\mu_Y + 7\sigma_Y$ level and turbulence intensity at prescribed deterministic fractiles compared with the full distribution solution. 119
3.34 Comparison of estimates of the long-term distribution of 10-minute extreme blade root bending moment, $L_{10\,\text{min}}$ based short-term Gumbel model for 10-minute extreme events or a short-term Weibull model for local peaks. 122

4.1 Joint probability density function based on wind class IA, μ_V=10m/s, I_{15}=0.18, a=2 130
4.2 Circle in 2-D standard normal space defined by $\beta^2 = u_1^2 + u_2^2$. 134
4.3 Environmental contour based on IEC IA wind class, one-year and 50-year return periods. 135
4.4 Environmental contour with blade root flap and edge bending iso-response curves. The ★'s represent the maximum response with the prescribed return period. 138
4.5 Extreme response as a function of angle, θ, in radians around circle in standard normal space for one-year and 50-year reliability levels. The ★'s represent the maximum extreme response. 139
4.6 Long-term distributions of 10-minute extreme blade root bending moment, $L_{10\,\text{min}}$, considering the short-term extreme load deterministic at mean level, for both: (a) flap and (b) edge bending. considered deterministic. 141
4.7 Joint probability density function for Lavrio, Greece site. 143
4.8 Environmental contour: Lavrio, Greece site. 144
4.9 Environmental contour with flap and edge bending iso-response curves. The ★'s represent the maximum response with the prescribed return period. 147
4.10 Extreme response as a function of angle, θ, in radians around circle in standard normal space for one-year and 50-year reliability levels. The ★'s represent the maximum extreme response. 148
4.11 Long-term distributions of 10-minute extreme blade root bending moment, $L_{10\,\text{min}}$, considering the short-term extreme load deterministic at mean level, for both: (a) flap and (b) edge bending. considered deterministic. 149
4.12 Constructed flap load response versus mean wind speed. 150
4.13 Environmental contour with flap bending iso-response curves. The ★'s represent the maximum response with the prescribed return period. 152

4.14 Extreme response as a function of angle, θ, in radians around circle in standard normal space for one-year and 50-year reliability levels. The ★'s represent the maximum extreme response. 152
4.15 Long-term distribution of 10-minute extreme blade root flap bending moment, $L_{10\text{ min}}$, considering the short-term extreme load deterministic at mean level. 153

5.1 Standard Weibull model fit to blade root flap and edge bending moment fatigue ranges for AOC 15/50 turbine operating in an environment with a 10-minute mean wind speed of 24m/s and turbulence class A. 162
5.2 Standard Weibull model fit to blade root flap and edge bending moment fatigue ranges for AOC 15/50 turbine parked in an environment with a 10-minute mean wind speed of 50m/s and turbulence class A. 163
5.3 Quadratic Weibull model fit to blade root flap and edge bending moment fatigue ranges for AOC 15/50 turbine operating in an environment with a 10-minute mean wind speed of 24m/s and turbulence class A. 165
5.4 Shifted quadratic Weibull model fit to blade root flap and edge bending moment fatigue ranges for AOC 15/50 turbine operating in an environment with a 10-minute mean wind speed of 24m/s and turbulence class A. 166
5.5 Quadratic Weibull model fit to blade root flap and edge bending moment fatigue ranges for AOC 15/50 turbine parked in an environment with a 10-minute mean wind speed of 50m/s and turbulence class A. 167
5.6 Damage-based Weibull model fit to blade root flap bending fatigue ranges for an AOC 15/50 turbine operating in an environment with a 10-minute mean wind speed of 24m/s and turbulence class A, for $z = 3, 4, 5$. 170
5.7 Damage-based Weibull model fit to blade root edge bending fatigue ranges for an AOC 15/50 turbine operating in an environment with a10-minute mean wind speed of 24m/s and turbulence class A, for $z = 3, 4, 5$. 171
5.8 Damage-based Weibull model fit to blade root flap bending fatigue ranges for an AOC 15/50 turbine parked in an environment with a 10-minute mean wind speed of 50m/s and turbulence class A, for $z = 3, 4, 5$. 172
5.9 Damage-based Weibull model fit to blade root edge bending fatigue ranges for an AOC 15/50 turbine parked in an environment with a 10-minute mean wind speed of 50m/s and turbulence class A, for $z = 3, 4, 5$. 173
5.10 Mean fatigue range of 10-minute blade root flap and edge bending response, based on 100 pooled observations for each 10-minute mean wind speed and turbulence class. The wind turbine is operating for $V \leqq 24$m/s, otherwise the turbine is parked. 176

5.11 Standard deviation of fatigue ranges for 10-minute blade root flap and edge bending response time histories, based on 100 pooled observations for each 10-minute mean wind speed and turbulence class. The wind turbine is operating for $V \leqq 24$m/s, otherwise the turbine is parked. 177

5.12 Coefficient of skewness of fatigue ranges for 10-minute blade root flap and edge bending response time histories, based on 100 pooled observations for each 10-minute mean wind speed and turbulence class. The wind turbine is operating for $V \leqq 24$m/s, otherwise the turbine is parked. 178

5.13 Long-term distributions of blade root fatigue bending moment ranges, R, considering three turbine conditions: 1) turbine operating over all wind speeds, 2) turbine parked over all wind speeds, 3) turbine operating below cutout wind speed and parked above cutout wind speed; for both: blade root (a) flap and (b) edge bending. 181

5.14 Expected number of fatigue ranges, $\mathsf{E}[N_0(v,i)]$, in 10-minute blade root flap and edge bending response time histories, based on 100 pooled observations for each 10-minute mean wind speed and turbulence class. The wind turbine is operating for $V \leqq 24$m/s, otherwise the turbine is parked. 184

5.15 Damage density for blade root flap and edge bending. 186

5.16 Mean of transformed ($z = 3$) fatigue ranges for 10-minute blade root flap and edge bending response, based on 100 pooled observations for each 10-minute wind speed and turbulence class. The wind turbine is operating for $V \leqq 24$m/s, otherwise the turbine is parked. 191

5.17 Standard deviation of transformed ($z = 3$) fatigue ranges for 10-minute blade root flap and edge bending response time histories, based on 100 pooled observations for each 10-minute mean wind speed and turbulence class. The wind turbine is operating for $V \leqq 24$m/s, otherwise the turbine is parked. 192

5.18 Long-term distributions of blade root fatigue bending moment ranges, R, considering three fatigue range transformations, $z = 3$, 4 and 5; for (a) flap and (b) edge bending. 194

5.19 Expected number of fatigue ranges in 10-minute blade root flap and edge bending response time histories, based on 100 pooled observations for each 10-minute mean wind speed and turbulence class. The wind turbine is operating for $V \leqq 24$m/s, otherwise the turbine is parked. 196

5.20 Damage density for blade root flap and edge bending. 197

5.21 Comparison of estimates of the long-term distribution of fatigue ranges based on quadratic or damage-based Weibull models for short-term distribution of fatigue ranges for (a) flap and (b) edge bending. 200

6.1 Median, mean, and 95% upper confidence level estimates of the long-term distribution of extreme blade root flap bending moment, considering the parameter of the Rayleigh distribution of 10-minute mean wind speed uncertain. Three conditions are presented, $\delta_{\mu_V} = 5\%, 10\%$ and 20%. Also shown, for comparison, is the long-term distribution with all parameter values considered deterministic, $\delta_{\mu_V} = 0$. 216

6.2 Median, mean, and 95% upper confidence level estimates of the long-term distributions of extreme blade root flap bending moment, considering the mean of the Gaussian distribution of conditional turbulence uncertain. Three conditions are presented, $\delta_{\mu_I|V} = 5\%, 10\%$ and 20%. Also shown, for comparison, is the long-term distribution with all parameter values considered deterministic. 218

6.3 Median, mean, and 95% upper confidence level estimates of the long-term distributions of extreme blade root flap bending moment, considering both the parameter of the Rayleigh distribution of 10-minute mean wind speed and the mean of the Gaussian distribution of conditional turbulence uncertain. Three conditions are presented, $\delta_{\mu_V} = \delta_{\mu_I|V} = 5\%, 10\%$ and 20%. Also shown, for comparison, is the long-term distribution with all parameter values considered deterministic. 220

6.4 Median and mean estimates of the long-term distribution of extreme blade root flap bending moment for an arbitrary 10-minutes, considering regression coefficients uncertain. The bootstrap method was used to estimate uncertainty in regression coefficients. 226

6.5 Median and mean estimates of the long-term distribution of extreme blade root flap bending moment, considering regression coefficients uncertain. The bootstrap method was used to estimate uncertainty in regression coefficients. 227

6.6 Median and mean estimates of the long-term distribution of extreme blade root flap bending moment for an arbitrary 10-minutes, considering regression coefficients uncertain with fixed covariance matrix. 230

6.7 Median and mean estimates of the annual long-term distributions of extreme blade root flap bending moment, considering regression coefficients uncertain. Regression coefficients considered uncertain with fixed covariance matrix. 231

6.8 Environmental conditions for 150 field recorded time histories. 234

6.9 Observed and predicted 10-minute maximum blade root flap bending moment versus 10-minute wind speed. 236

6.10 Observed versus predicted 10-minute maximum blade root flap bending moment. . 237
6.11 A measure of error: observed/predicted 10-minute maximum blade root flap bending moment versus 10-minute mean wind speed. 237
6.12 Mean long-term distribution of annual extreme blade root flap bending moment, including model uncertainty. 239

A.1 Unfiltered and filtered time histories of blade root edge bending response for the parked turbine condition in a 24m/s turbulence class A wind environment. 257
A.2 Unfiltered and filtered time histories of blade root edge bending response for the parked turbine condition in a 30m/s turbulence class A wind environment. 258
A.3 Unfiltered and filtered time histories of blade root edge bending response for the parked turbine condition in a 40m/s turbulence class A wind environment. 259

C.1 10-minute mean wind speed and turbulence intensity for 2400 10-minute Gaussian wind input processes. 266
C.2 Regression of the moments of 10-minute maximum on the 10-minute mean wind speed and turbulence intensity for blade root flap bending. 269
C.3 Regression of the moments of 10-minute maximum on the 10-minute mean wind speed and turbulence intensity for blade root edge bending. 270
C.4 Long-term distributions of 10-minute extreme blade root bending moment, $L_{10\,\mathrm{min}}$, considering three turbine conditions: 1) turbine operating over all wind speeds, 2) turbine parked over all wind speeds, 3) turbine operating below cutout wind speed and parked above cutout wind speed; for both: (a) flap and (b) edge bending. 273
C.5 Long-term distributions of 10-minute extreme blade root bending moment $L_{10\,\mathrm{min}}$, considering load, turbulence intensity, and wind speed deterministically for both: (a) flap and (b) edge bending. 275
C.6 Long-term distributions of 10-minute extreme blade root bending moment, $L_{10\,\mathrm{min}}$, considering the short-term load at prescribed deterministic levels compared with the full distribution solution. 277
C.7 Regression of the process mean on the 10-minute mean wind speed and turbulence intensity for blade root flap and edge bending. 282
C.8 Regression of the expected number of local peaks on 10-minute mean wind speed and turbulence intensity for blade root flap and edge bending. 283
C.9 Regression of the mean of the local peaks on the 10-minute mean wind speed and turbulence intensity for blade root flap and edge bending. 284

C.10 Regression of the standard deviation of the local peaks on the 10-minute mean wind speed and turbulence intensity for blade root flap and edge bending. 285
C.11 Regression of the coefficient of skewness of the local peaks on the 10-minute mean wind speed and turbulence intensity for blade root flap and edge bending. 286
C.12 Long-term distributions of 10-minute extreme blade root bending moment, $L_{10\,\mathrm{min}}$, considering three turbine conditions: 1) turbine operating over all wind speeds, 2) turbine parked over all wind speeds, 3) turbine operating below cutout wind speed and parked above cutout wind speed; for both blade root (a) flap and (b) edge bending. 288
C.13 Long-term distributions of 10-minute extreme blade root bending moment, $L_{10\,\mathrm{min}}$, considering load, turbulence intensity, and wind speed deterministically for both blade root (a) flap and (b) edge bending. 290
C.14 Long-term distributions of 10-minute extreme blade root bending moment, $L_{10\,\mathrm{min}}$, considering the 10-minute mean wind speed at prescribed deterministic fractiles compared with the full distribution solution. 291
C.15 Long-term distributions of 10-minute extreme blade root bending moment, $L_{10\,\mathrm{min}}$, considering the conditional short-term extreme load at prescribed deterministic levels compared with the full distribution solution. 292
C.16 Comparison of estimates of the long-term distribution of 10-minute extreme blade root bending moment, $L_{10\,\mathrm{min}}$ based short-term Gumbel model for 10-minute extreme events or a short-term Weibull model for local peaks. 294

D.1 Transformation of basic random variables to standard normal space. 298
D.2 Probability content behind first-order approximation of limit state function at design point, $\mathbf{u}^*$. 299
D.3 Plot of limit state functions in standard normal space for Example 1—IEC Model with Stall-Regulated Turbine, from Chapter 4, for (a) flap and (b) edge bending. . . 301
D.4 Plot of limit state functions in standard normal space for Example 2—Field Data Model with Stall-Regulated Turbine, from Chapter 4, for (a) flap and (b) edge bending. 303
D.5 Plot of limit state functions in standard normal space for Example 3—IEC Model with Pitch-Regulated Turbine, from Chapter 4, for blade root flap bending. 304

E.1 Joint probability density function for wind class IA, μ_V=10m/s, I_{ref}=0.16, c=3.8 . . 307
E.2 Environmental contour, wind class IA, 1-year and 50-year return periods. 309
E.3 Environmental contour, wind class IIA, 1-year and 50-year return periods. 310
E.4 Environmental contour, wind class IIIA, 1-year and 50-year return periods. 310
E.5 Environmental contour, wind class IB, 1-year and 50-year return periods. 311

E.6 Environmental contour, wind class IIB, 1-year and 50-year return periods. 311
E.7 Environmental contour, wind class IIIB, 1-year and 50-year return periods. 312
E.8 Environmental contour, wind class IC, 1-year and 50-year return periods. 312
E.9 Environmental contour, wind class IIC, 1-year and 50-year return periods. 313
E.10 Environmental contour, wind class IIIC, 1-year and 50-year return periods. 313
E.11 Environmental contour with normalized turbulence intensity, wind classes I-III, 1-year return period. 314
E.12 Environmental contour with normalized turbulence intensity, wind classes I-III,50-year return period. 315

F.1 10-minute mean wind speed and turbulence intensity for 2400 10-minute Gaussian wind input processes. 317
F.2 Mean fatigue range of 10-minute blade root flap and edge bending response, based on 100 pooled observations for each 10-minute mean wind speed and turbulence class. The wind turbine is operating for $V \leqq 24$m/s, otherwise the turbine is parked. 322
F.3 Standard deviation of fatigue ranges for 10-minute blade root flap and edge bending response time histories, based on 100 pooled observations for each 10-minute mean wind speed and turbulence class. The wind turbine is operating for $V \leqq 24$m/s, otherwise the turbine is parked. 323
F.4 Coefficient of skewness of fatigue ranges for 10-minute blade root and edge bending response time histories, based on 100 pooled observations for each 10-minute mean wind speed and turbulence class. The wind turbine is operating for $V \leqq 24$m/s, otherwise the turbine is parked. 324
F.5 Long-term distributions of blade root fatigue bending moment ranges, R, considering three turbine conditions: 1) turbine operating over all wind speeds, 2) turbine parked over all wind speeds, 3) turbine operating below cutout wind speed and parked above cutout wind speed; for both: blade root (a) flap and (b) edge bending. 327
F.6 Expected number of fatigue ranges in 10-minute blade root flap and edge bending response time histories, based on 100 pooled observations for each 10-minute mean wind speed and turbulence class. The wind turbine is operating for $V \leqq 24$m/s, otherwise the turbine is parked. 329
F.7 Damage density for blade root flap and edge bending. 330
F.8 Pooled statistics of the mean of transformed ($z = 3$) fatigue ranges in 10-minute blade root flap and edge bending response time histories for given 10-minute mean wind speeds. The wind turbine is operating for $V \leqq 24$m/s, otherwise the turbine is parked. 337

F.9 Pooled statistics of the standard deviation of transformed ($z = 3$) fatigue ranges in 10-minute blade root flap and edge bending response time histories for given 10-minute mean wind speeds. The wind turbine is operating for $V \leqq 24$m/s, otherwise the turbine is parked. 338
F.10 Long-term distributions of blade root fatigue bending moment ranges, R, considering three fatigue range transformations, $z = 3$, 4 and 5; for (a) flap and (b) edge bending. 340
F.11 Expected number of fatigue ranges in 10-minute blade root flap and edge bending response time histories, based on 100 pooled observations for each 10-minute mean wind speed and turbulence class. The wind turbine is operating for $V \leqq 24$m/s, otherwise the turbine is parked. 342
F.12 Damage density for blade root flap and edge bending. 343
F.13 Comparison of estimates of the long-term distribution of fatigue ranges based on quadratic or damage-based Weibull models for short-term distribution of fatigue ranges for (a) flap and (b) edge bending. 345

Chapter 1

Introduction

1.1 Motivation

Over 15,000 wind turbines, providing a clean and economical source of renewable energy, were installed in California during the 1980's, with a total combined power capacity of more than 1,500 Mega-Watts (MW) [1]. Today over 4,000 MW of wind power have been installed in the U.S. [2]. On average, one percent of electrical energy consumed throughout California is produced by these wind turbines. "Wind farms" provide an environmentally friendly alternative to fossil fuels. Since the 1970's energy crisis, research has been conducted to improve the efficiency and reliability of wind turbines in order to mitigate society's dependence on fossil fuels.

Electricity consumption is growing in most areas of the United States. Due to the continued low fuel costs and de-regulation, many U.S. utility companies are risk-averse, unwilling to make the investments that could reduce long-term energy costs and mitigate environmental risks. Worldwide installed capacity for wind-generated energy has grown from 5,000 Mega-Watts in 1995 to upwards of 24,000 MW today [1, 3]. Most of these new installations of wind power are in Europe and developing countries.

Many improvements in turbine design by manufacturers have made wind energy more attractive to electric utilities. Early installations of wind turbines were fairly unreliable. This has improved to where new installations have exceeded 95% availability. The levelized[1] cost of wind energy in the 1980's ranged from $.25 - $.30 per kilowatt-hour (kWh) [1, 5]. The American Wind Energy Association (AWEA) estimates that the current levelized cost of wind energy at state-of-the-art wind power plants with excellent site conditions is less than $0.05/kWh [6]. Typical levelized costs of other energy sources range between $0.039–$0.145/kWh (e.g., coal: $0.048–$0.055, natural gas:

[1] A levelized cost is the average cost over the lifetime of a facility with future costs discounted by the time value of money [4].

$0.039–$0.044, and nuclear: $0.111–$0.145) [4, 6]. Even with these improvements, the continued low cost of fossil fuels since the 1970's energy crisis has made the wind energy market more competitive among wind turbine manufacturers. This has led some manufacturers to operate with very narrow profit margins, and has pushed others into financial collapse.

The national and international structural design standards by which wind turbines are certified greatly impact the competitive edge of the companies participating in the wind energy industry. By developing methods to better predict both the extreme structural forces and the distribution of fatigue loads, we can reduce the cost of energy while improving safety and reliability. The need to reduce the cost of energy is self-evident; the means to achieve this through better understanding of structural forces acting on the wind turbines may not be as clear. Where current design practices and safety factors are too conservative, increased understanding in modeling the load process and associated uncertainties can permit reduced manufacturing and other start-up costs. Where they are non-conservative, improvement can extend component life and reduce maintenance and other service costs.

Engineering design performed in a purely deterministic way, i.e., where we assume that we know the forces applied to the structure and the strength of the material, can have surprising results when the component is put into service. Nature tells us that we cannot be certain about the demand (i.e., the forces applied) and the capacity (i.e., the strength of the material). The old adage of a chain being as strong as its weakest link is a very precious reality that is at times overlooked in design. Although failure can have a broad range of definitions, here we define it as the event where the forces on the structure exceed the ability of the material to withstand those forces. The reality is that it is not only a physical, but also an economic impossibility to eliminate the probability of failure. There is virtually always the possibility of a force being large enough to break the structure no matter how low the probability of that force occurring.

In order to negotiate this uncertainty we assign a safety factor when designing structural components. This factor is in general defined as the ratio of capacity to demand. If the capacity exactly matches the demand, by definition the safety factor is one. When the value falls below one, the part is inadequately designed. The question then arises how much added capacity is required to cover our seemingly unquantifiable uncertainty. Large safety factors are generally correlated with high levels of uncertainty, or extraordinary consequences of failure. As discussed previously these factors can impact both initial manufacturing and recurrent maintenance costs. The resulting economic impacts can be profound.

Let us look at the issue from the other direction, assigning an acceptable probability of failure. As stated earlier, it is impossible to remove the possibility of failure. Therefore resigning ourselves to this actuality, what level of probability of failure are we willing to accept? Engineering design

methods are generally calibrated to produce an acceptably low probability of failure (e.g., Madsen, et al. [7] or Melchers [8]), which in many cases may be established to be consistent with past acceptable experience. For instances when there is little experience, an acceptable probability of failure may be chosen based on economic cost/benefit analysis, or by analogy with risk levels inherent in other societal threats.

In the context of rotating machinery such as wind turbines, a technical challenge here is the development of a mathematical expression that covers the underlying uncertainty of both the material behavior and the fatigue loads. The complexities become intriguing when one realizes that in this type of analysis the analyst is presented with a suite of fatigue loads on the structure and not just one constant force. There is not just one material capacity; the capacities are now a function of the demand and the number of times that particular demand is seen by the structure. In addition, failure in this case is based on the accumulation of damage. With each cycle, microscopic cracks occur. It is the rate at which these cracks accumulate and propagate that cause damage to the structure and determines its useful life.

Current research efforts have focused on better prediction of the forces acting on the wind turbines. A number of statistical models have been proposed to predict both the once in a lifetime extreme structural forces and the day-to-day repeated operating forces. Systematic comparisons are underway between these various models and observed behavior, as estimated from either field data or computer model simulation. These statistical models hold the promise of providing robust force estimates for more reliable wind turbine design, while minimizing the cost of extensive simulation and/or field measurement projects.

Better estimation of extreme forces and the distribution of fatigue loads will enable us to find more realistic, and thereby more economic safety factors that meet an acceptable probability of failure. With well-founded safety factors, manufacturing processes and maintenance procedures can be optimized. All of this results in producing an economical, reliable, and clean energy resource.

In the remainder of this chapter we will discuss how we may proceed from prescribing a target probability of failure for a structural system to focusing on the long-term probability distribution of structural loads. This will be demonstrated through a formulation of the probability of failure as a relationship between the demand on the structure and the capacity of the structural system to withstand those demands. Based on this formulation we can develop a methodology for estimating the long-term distribution of loads on a structure by conditioning the loads by a set of environmental variables. Also, since this work is concerned with estimating these loads on horizontal axis wind turbines it seems appropriate to spend a little time describing the general configuration of these turbines, to facilitate the discussions that follow. In particular, some of the unique behavioral characteristics of wind turbines which we will have to deal with to make accurate estimates of the load

distributions will be discussed. We will briefly discuss the strict assumptions used to describe the behavior of the wind environment. Finally, we present a few moment-based probability models that will be used in the next several chapters to estimate the distributions of fatigue and extreme loads.

1.2 Background

The objective of reliability-based design methods is to provide a balance between sufficiently safe structures and reasonable costs while taking into account the randomness of design critical variables and the uncertainties associated with having only limited data. This is a formidable task. As a result, many methods ranging in complexity have been developed to address these issues. Structural reliability methods have been divided into four general levels characterized by the amount of data about the structural problem that is used or provided [7]. The most basic structural reliability methods are non-probabilistic in nature and employ only one "characteristic" value of each uncertain parameter and are called *Level I methods*. This is essentially the traditional safety factor and load factor formats. Partial safety factor approaches like AISC-LRFD[9] or AIC-318-89[10] are part of this category. *Level II methods* employ two values—usually the mean and standard deviation—to represent each random or uncertain variable. In addition, a measure of the correlation between each pair of random variables, typically the covariance, may be included. Reliability index methods–e.g., Cornell[11], Hasofer and Lind[12], and Ditlevsen[13]–are examples of this category. Methods which attempt to obtain the best estimate of the probability of failure based on probabilistic models and therefore require the knowledge of the joint distribution of all uncertain parameters are called *Level III methods*. Finally, *Level IV methods* use additional economic data to evaluate the system according to the principles of engineering economics under uncertainty. This classification of reliability methods is not exhaustive and it is not the intention here to provide a summary of the broad range of research, but moreover to provide a background to the development of the problems set forth in the coming sections and chapters.

In this section, our focus is on Level III reliability methods, which limit the probability of failure, p_f, of a structure—e.g., wind turbine—to a prescribed target value, $p_{f_{\text{target}}}$. The term "failure" can have a wide range of interpretations. Consider an office building structure which has sustained some damage from a recent earthquake. The tenant of the building may consider the system to have failed if he or his employees are not able to return to work immediately after the event. The work stoppage may be a result of "superficial" damage that requires the building to be unoccupied during the clean-up. Here the failure criteria is based on serviceability. The insurer may only consider the structure to have failed after a claim cost threshold has been exceeded. From this perspective the failure criterion is based on a repairability criteria. Further, the structural engineer may consider issues of

occurred or impending collapse of the structure in determining if the building has failed. Here, the failure criterion is based on issues of life-safety. Appropriate choice of $p_{f_{target}}$ depends on the type of failure considered. Higher target values are typically permitted where serviceability or economics are the dominant issues. On the other hand, much lower target values are generally required where personal injury or loss of life may occur. These target values of p_f are usually reported on an annual basis. In this way, it is easy to compare the reliability of different structures. In conditions where the probability of failure may increase over time, due to strength degradation (such as failures caused by fatigue or fatigue and over-load), $p_{f_{target}}$ may be specified for the lifetime of the structure.

Each of the failure conditions considered above qualitatively describes a different *limit state function*, $g(\mathbf{X})$, which divides the space of $\mathbf{X}$—the vector of basic variables which describe the state of the structure and the loads—between "failed" and "safe" regions.

$$\begin{aligned} g(\mathbf{X}) &> 0 \qquad \text{safe} \\ g(\mathbf{X}) &\leq 0 \qquad \text{failed} \end{aligned} \tag{1.1}$$

Variables typically included in, $\mathbf{X}$, are: *actions*, such as forces, temperature changes, and forced displacements; *material properties* such as yield strength and modulus of elasticity; *structural dimensions* and *model parameters*, such as blade pitch angle and drag coefficients. These variables may be stochastically dependent on one another, e.g., structural stiffness and displacement in a non-linear analysis. In addition the basic variables may also vary over time, i.e., be random processes, $\mathbf{X} = \mathbf{X}(t)$. We might describe the different failure mechanisms or types of failure as *failure modes*, each described by a different limit state function, $g_i(\mathbf{X})$. Then the probability of failing in mode, i, is the probability that there exists some time, t, less than the lifetime of the structure, T_L, such that the limit state function for that mode of failure is less than or equal to zero. This is expressed formally below:

$$p_{f_i} = P[\,\exists\, 0 \leq t \leq T_L \text{ s.t. } g_i(\mathbf{X}(t)) \leq 0] \tag{1.2}$$

where $P[\cdot]$ denotes the probability that the bracketed statement occurs. p_{f_i}, could also be calculated over some other time interval, e.g., one year, and in which case p_{f_i} is an annual probability of failure.

Given Equation 1.2, one way to calculate the probability of failure of a structural system would be to include all failure modes in the limit state function substituting $\mathbf{g}(\mathbf{X}(t))$ for $g_i(\mathbf{X}(t))$. Where, $\mathbf{g}$, is a vector in which each element is a limit state function associated with a different failure mode. Now the structural system is considered safe if and only if all the limit state functions in $\mathbf{g}(\mathbf{X}(t))$ are positive. This approach is the essence of expensive probabilistic risk analysis undertaken for nuclear reactors, for example [14]. In general, a structural system may contain several failure modes and $\mathbf{X}$

may contain hundreds of elements. The problem of solving Equation 1.2 in this form quickly becomes very complex. Alternatively, the probability of failure may by calculated separately for each structural element and failure mode. This type of analysis is referred to as component reliability analysis. The theory of system reliability then provides a set of methods as to how these "component" probabilities may be used, together with information about their associated dependencies, to find the probability of failure of the entire structural system. The reader is referred to Madsen, et al. [7] and Melchers [8] for further discussion on system reliability.

One approach for finding p_f from Equation 1.2 is to recognize the fact that $g(\mathbf{X}) < 0$ at some point over the time interval of interest if and only if the minimum value of the limit state function is less than zero over the prescribed time interval. In this case Equation 1.2 can be written as:

$$p_f = P[\min_{0 \le t \le T_L} g(\mathbf{X}(t)) < 0] \tag{1.3}$$

Formulating the problem in this way is sometimes referred to as the *time integrated* approach [8]. In addition, we may consider the case when some of the elements of $\mathbf{X}$, are assumed to be relatively independent of time when compared to the other constituents. Such that $g(\mathbf{X}(t))$ can be written as:

$$g(\mathbf{X}(t)) = g(\mathbf{X}_1) - g(\mathbf{X}_2(t)) \tag{1.4}$$

where $\mathbf{X}_1$ is the vector of time independent variables. Substituting Equation 1.4 into Equation 1.3 the probability of failure can be found from the expression below:

$$P_f = P[g_1(\mathbf{X}_1) \le \max_{0 \le t \le T_L} g_2(\mathbf{X}_2(t))] \tag{1.5}$$

The constituents of $\mathbf{X}_1$ are often basic variables that determine resistance or structural capacity, e.g., material properties and structure dimensions. Whereas the elements of $\mathbf{X}_2(t)$ are loads or actions applied to the structure. Of course there are exceptions: time-dependent material properties such as fatigue or creep may be included in $\mathbf{X}_2(t)$, and time independent loads or actions such as dead load or pre-tensioning may be included in $\mathbf{X}_1$. With this understanding in mind we may choose to let R represent the vector of time independent capacities, or in general resistance, and let $S(t)$ represent the vector of time dependent demands or "stresses" on the structure. With this new nomenclature Equation 1.5 may be written in terms of the scalar random variables R and S_{max}=$\max_{0 \le t \le T_L} S(t)$ as:

$$P_f = P[R \le S_{max}] \tag{1.6}$$

In the above equation the probability of failure is defined by the event $R \le S_{max}$ and can be found

from the joint distribution of R and S_{max}:

$$P_f = \int\int_{r \leq s} f_{R,S}(r,s)\ drds \tag{1.7}$$

where $f_{R,S}(r,s)$ denotes the joint probability density function (PDF) of R and S_{max}. If R and S_{max} are statistically independent where $f_{R,S}$=$f_R(r)f_S(s)$, then Equation 1.7 can be simplified as:

$$\begin{aligned} P_f &= \int\int_{r \leq s} f_R(r)f_S(s)\ drds \\ &= \int_{-\infty}^{\infty} F_R(s)f_S(s)ds \\ &= \int_{-\infty}^{\infty} f_R(r)G_S(s)ds \end{aligned} \tag{1.8}$$

where the notation $F_X(x)$ denotes the cumulative distribution function (CDF) of X defined as $F_X(x) = P[X \leq x]$, and $G_X(x) = P[X > x] = 1 - F_X(x)$.

Equation 1.8 reduces the problem of finding the probability of failure to that of finding the probability distributions of R and S_{max} independently. In this work we focus ourselves on finding the probability distribution of S_{max}, either for extremes or fatigue. This portion of the problem can often be more interesting, as not only are the demands on the structure usually time varying but they may usually dominate the problem as a result, e.g., of a larger coefficient of variation. This may imply that the demands on the structure may play a more dominant role in Equation 1.8 and need to be understood and modeled more carefully than the capacities. This is complicated by the fact that we may have only limited data with which to understand the nature of the demands, leading to greater "uncertainty" in the loads as compared to the capacities. We will come back to this notion of "uncertainty", as distinct from randomness, later in this discussion and again in regard to estimation of extreme loads in Chapter 6.

We have defined S_{max} as the maximum, over a specific duration of time, of the limit state function of $\mathbf{X}_2(t)$. Finding the distribution of S_{max} is not a trivial matter even if the marginal probability distributions of $\mathbf{X}_2$ are known. In general, the methods developed to resolve this problem require the marginal distribution of each load/demand and the dependencies between the loads and/or their rate of change with time. It may be a straight forward task to find the probability distribution of each load by measurements or simulations. These measurements or simulations must be carried out over the entire range of environmental conditions that may exist during the structure's intended operational lifetime, however. Therefore, very large sample sizes are required such that the long-term distribution of environmental events is represented and not biased toward a particular environmental condition.

Loads or demands on the structure may occur over very different time scales. The occurrence of load events may be sporadic in nature, e.g, the occurrence of earthquakes or storms, and the nature of the loading during an event may be slowly varying or fluctuate rapidly. Conversely, the loading may be constant, such as sustained live loads, or loads due to wind and wave action on the structure. Different load modeling techniques are used for these various loading conditions. In general, these loading conditions may be characterized by their relative time scales. One might consider loading events which have an inter-event time much longer than the duration of the event itself. If the load is constant during each event, such as extraordinary live loads, or varies slowly, such as snow loading, it is considered to have *macro-scale* time variability only. If, however, the loading fluctuates rapidly during the loading event, then it is considered to have both macro-scale and micro-scale time variability. In these latter cases, such as earthquakes, two separate models are used. The first models the probability of the occurrence of the event; the second models the probability distribution of the loads given the occurrence of an event. Similarly, loads due to wind and waves which fluctuate continuously while the gross characteristics change slowly over time are also considered to exhibit macro and micro time variability. When modeling the loads in these cases, it is convenient to consider these processes *stationary*[2] over short periods of time. These time periods are typically called environmental states. The duration for these environmental states is defined such that the assumption of stationarity is at least reasonably valid. Typical values are ten minutes for wind states and three - six hours for sea (wave) states.

In all the characterizations given above, each event or state is typically described by a set of *environmental variables*. For example, in the case of loads due to wave or wind action, the vector of environmental variables may be the wave period and significant wave height for wave loading or 10-minute mean wind speed and turbulence intensity for wind loading. With earthquakes, magnitude of the event, and source-to-site distance may be considered. In some cases the environmental variable may be a scalar quantity. In others, as cited above, it may be a vector of variables. In all cases, the probability distribution of the loads within the event is defined by these parameters.

The complication in finding the joint probability distribution of $\mathbf{X}_2$ directly is the requirement of having representative samples across all environmental conditions. This complication is often ameliorated by conditioning the joint probability distribution of $\mathbf{X}_2$ on the vector of environmental

[2] A stochastic process $X(t), t \geq 0$, is considered to be *strictly* stationary if for all n, s, $t_1, \ldots, t_n$ the random vectors $X(t_1), \ldots, X(t_n)$ and $X(t_1 + s), \ldots, X(t_n + s)$ have the same joint distribution. In other words, choosing any fixed point as the origin, the ensuing process has the same probability law. All the statistical moments are invariant with time. A stochastic process is considered to be *weakly* stationary if and only if the first two statistical moments are invariant with time, $\mathsf{E}[X(t)] = \mathsf{E}[X(t+s)]$ and the covariance, $\mathsf{Cov}[X(t_1), X(t+s)]$ does not depend on t. As the finite-dimensional distributions of a Gaussian process are uniquely determined by their means and covariances, it follows that a *weakly* stationary Gaussian process is also *strictly* stationary [15, 16].

parameters, $\mathbf{E}$:

$$f_{\mathbf{X}_2} = \int \cdots \int_{\text{all } \mathbf{E}} f_{\mathbf{X}_2|\mathbf{E}}(\mathbf{x}_2|\mathbf{e}) f_{\mathbf{E}}(\mathbf{e})\, d\mathbf{e} \tag{1.9}$$

where the notation $f_{X|Y}(x|y)$ denotes the conditional probability density function defined as:

$$f_{X|Y}(x|y) = \frac{f_{X,Y}(x,y)}{f_Y(y)} \tag{1.10}$$

Equation 1.9 is an application of the Law of Total Probability, where the probability distribution of the loads given a set of realizations of the environmental parameters are weighted by the probability of those realizations of the environmental parameters occurring. These results are then summed over the entire range of the environmental parameters. A caveat exists, however. That if the load distributions are affected by an environmental parameter, say E', that is not explicitly included in the vector of environmental variables $\mathbf{E}$, then the conditional probability distribution of the loads given the vector of environmental variables must be found from data which is sampled across a representative range of values of E'. If we know or can reasonably assume a distribution of E', then we could re-apply the Law of Total Probability and obtain:

$$f_{\mathbf{X}_2|\mathbf{E}}(\mathbf{x}_2|\mathbf{e}) = \int_{\text{all } E'} f_{\mathbf{X}_2|\mathbf{E},E'}(\mathbf{x}_2|\mathbf{e}, e') f_{E'|\mathbf{E}}(e'|\mathbf{e})\, de' \tag{1.11}$$

In other words while Equation 1.9 holds for any vector $\mathbf{E}$, if $\mathbf{E}$ does not include all the important, i.e., relevant environmental variables affecting $f_{\mathbf{X}_2}$, then this formulation may not hold much benefit. This is a condition of *sufficiency* [17] that is not easily verifiable. In practice, we may convince ourselves that a condition of sufficiency has been met by showing $f_{\mathbf{X}|\mathbf{E},E'} \cong f_{\mathbf{X}|\mathbf{E}}$, or (more easily but not completely—i.e., necessary but not sufficient) by assuming $\mathsf{E}[\mathbf{X}|\mathbf{E}, E'] = a + b\mathbf{E} + cE'$ and then show that the coefficient, c, is not statistically different from zero. If the data has been sampled over a broad range of environmental states and the variables chosen to be included in $\mathbf{E}$ are able to reasonably describe the load distribution, then there may be little increased benefit of including additional environmental variables.

One major benefit of the formulation given in Equation 1.9 is it separates the calculation of $f_{\mathbf{X}_2}$ into the need to provide two separate terms, a structure-dependent term $f_{\mathbf{X}_2|\mathbf{E}}(\mathbf{x}_2|\mathbf{e})$ and a decoupled site-dependent term, $f_{\mathbf{E}}(\mathbf{e})$. Therefore, if a robust probability distribution of the loads on the structure can be obtained for a broad range of realizations of the environmental variables, then one only needs the probability distribution of the environmental variables at a specific site in order to obtain the loads on the structure at that particular site. The "generic" structure-dependent model, $f_{\mathbf{X}_2|\mathbf{E}}(\mathbf{x}_2|\mathbf{e})$, can be used over and over at different sites where only, $f_{\mathbf{E}}(\mathbf{e})$, the probability distribution of the environmental variables changes from site to site. This only holds, however, if

either $\mathbf{E}$ contains all the important environmental variables, or if $f_{E'|\mathbf{E}}(e'|\mathbf{e})$ is identical at each site.

The joint probability distribution of $\mathbf{E}$ is often provided to the structural engineer by specialists in other fields such as meteorology for loading due to wind and waves, or seismology for earthquakes. Therefore, the structural engineer or analyst must consider both the importance of the environmental parameters as well as the availability of relevant data for determining their long-term distributions.

In this section a discussion has been presented where we proceed from prescribing a target probability of failure for a structural system to focusing on the long-term probability distribution of structural loads. This was demonstrated through a formulation of the probability of failure as a relationship between the demand on the structure and the capacity of the structural system to withstand those demands. Based on this formulation, the discussion focused on the development of a methodology for estimating the long-term distribution of loads on a structure by conditioning the loads on the structure by a set of environmental variables. The discussion presented here is based on the analysis of stochastic load models by Haghighi [18]. This sets the strategy that will be investigated throughout the rest of this work for the estimation of extreme loads and fatigue distributions on wind turbine structures.

1.3 Wind Turbines

This work is concerned with estimating fatigue and extreme load distributions on horizontal axis wind turbines. Therefore, it seems appropriate in this section to spend a little time describing the general configuration of these turbines to facilitate the discussions that follow. In particular, some of the unique behavior characteristics of wind turbines which we will have to deal with to make accurate estimates of the load distributions will be discussed. Also, since wind turbines do not operate in a vacuum, we will briefly discuss the strict assumptions used to describe the behavior of the wind environment. The general configuration of the turbine, and our assumptions of the behavior of the environment presented here, will be the basis from which we start our discussions on how we may estimate the fatigue and extreme loads encountered by these structural systems.

1.3.1 Configuration and Operation

A horizontal axis wind turbine generally consists of several standard components. The nacelle located at the top of the wind turbine tower, contains the key components of the wind turbine including the gearbox, which attaches the rotor hub to the electrical generator. The wind turbine blades convert kinetic energy of the wind into rotational mechanical energy of the low speed shaft. The blades of a wind turbine work much the same way as the wings of a fixed-wing aircraft or

the rotor-blades of a helicopter. The wind passes over both sides of the airfoil. As it passes over the longer upper surface of the airfoil, it creates an area of relative low pressure. The pressure differential between the upper and lower surfaces causes a lifting force to act on the blade. In an airplane or helicopter this lifting force supports the weight of the aircraft. For wind turbines, however, this lifting force causes the blades to turn, since they are constrained to move in a plane attached at the hub. A drag force, perpendicular to the lift, is also created as the wind passes over the airfoil. This drag force impedes the rotation of the rotor. Wind turbine blades are designed in such a way as to maximize the lift to drag ratio. The rotation, or pitch, of the blade about its long-axis may change along the longitudinal axis to control and optimize the turbines energy output, while limiting the structural loads on the turbine at varying wind speeds.

The low speed shaft connects the rotor hub to a gearbox, which determines the relative rotational speed of the low and high-speed shafts. The high-speed shaft connects the gearbox to the electrical generator. Generally, the rotor hub rotates too slowly for most generators to work efficiently. Low speed generators do exist and are efficient, but expensive. The gearbox makes the high-speed shaft turn faster and with lower torque. This then drives the electrical generator. The maximum power output of installed wind turbines ranges between 500 and 1,500kW. Wind turbines on the market today are 1,500kW machines, with up to 5MW machines in development. An electronic controller located in the turbine continuously monitors the condition of the wind turbine. It takes information from the anemometer and wind vane, which measure wind speed and direction, to turn the turbine on at *cut-in* wind speeds and turn the turbine off at *cut-out* wind speeds. The controller also regulates the yaw mechanism to turn the turbine into the direction of the wind. Usually the wind turbine only yaws a few degrees per minute, with changes in wind direction. Significant power loss results when the turbine is misaligned with the wind. Increasing the activity of the yaw controller can been associated with higher fatigue damage, however.

There are two general methods for regulating the power output of wind turbines. The power output is not allowed to greatly exceed the rated power, in order to avoid risk in damaging the gearbox or generator. Pitch control provides a mechanism for reducing the angle of attack along the entire length of the blade. The lower the angle of attack the less lift is generated. Stall-controlled turbines rely on the inherent aerodynamic tailoring of the airfoil to stall progressive sections of the blade during high wind speeds. As increasing sections of the blade stall, less of the blade is available to create lift. The controlling of the power output to protect the generator and gearbox also serves to mitigate the structural loads on the turbine. Other characteristics of wind turbines include: active versus free yaw machines, up-wind versus down-wind operation, teetered versus fixed machines, constant speed or variable speed operation, and of course the number of blades.

Figure 1.1 shows a generic two-bladed wind turbine. Of specific interest are the two loading

directions, on the wind turbine blade, that will be considered throughout the remaining chapters. In-plane bending, $M_{in-plane}$ results in deflections parallel to the swept surface of the rotating turbine blades. Out-of-plane bending $M_{out-of-plane}$ results in deflections perpendicular to the plane of rotation. Related to out-of-plane and in-plane bending are flap and edge bending. The flap direction is defined as the direction that is perpendicular to the swept surface of the undeformed rotor blade axis. Whereas the edge, or lead-lag, direction is defined as the direction which is parallel to the plane of the swept surface and perpendicular to the longitudinal axis of the undeformed rotor blade. Therefore the flap bending results in deformation of the blade perpendicular to the chord line. Edge bending results in deformation of the blade parallel to the chord line. For fixed pitch blades (stall-regulated turbines), where the angle between the angle of rotation and the leading edge of the airfoil does not change with changes in wind speed, only a simple constant coordinate transformation is required to relate flap and out-of plane bending moments (or edge and in-plane bending moments); see Figure 1.2. A more complicated time-dependent transformation is required to relate flap and out-of-plane bending moments (or edge and in-plane bending moments) for pitch-regulated turbines.

The loading on wind turbines can be considered to fall into one of two general conditions, parked and operating. When the turbine is parked it is much like other fixed structures and we might expect the statistics of the response of the turbine to the input wind process to be analogous to extreme winds on a building or other stationary structure. The other loading condition is when the turbine is operating. The out-of-plane loads in either condition are generally very similar. The details of this will be discussed in greater detail in subsequent chapters. The in-plane or edge loading on the other hand is very different in the operating condition than in the parked condition. With horizontal axis wind turbines, during the operating conditions as the blades turn in the wind field, they are also subjected to the effects of gravity which induces sinusoidal load cycles on the leading and trailing edges of the turbine blade. If we imagine a turbine blade starting at the top of the rotor, pointing straight up, the bending load on the leading edge and the trailing edge of the blade is zero, the gravity forces acts along the longitudinal axis of the blade. As the blade goes through one-quarter cycle, the leading edge of the blade is in compression and the trailing edge is in tension due to the gravity loading. When the blade is pointing straight down, the gravity force is acting along the longitudinal axis of the blade and there is no bending load. The blade continues through 3/4 of a revolution. Now, the leading edge is in tension and the trailing edge is in compression opposite to the loading it saw half a cycle ago. This periodic loading in the edge bending direction is a unique loading characteristic that will have to be carefully considered when we fit probabilistic models to these loads.

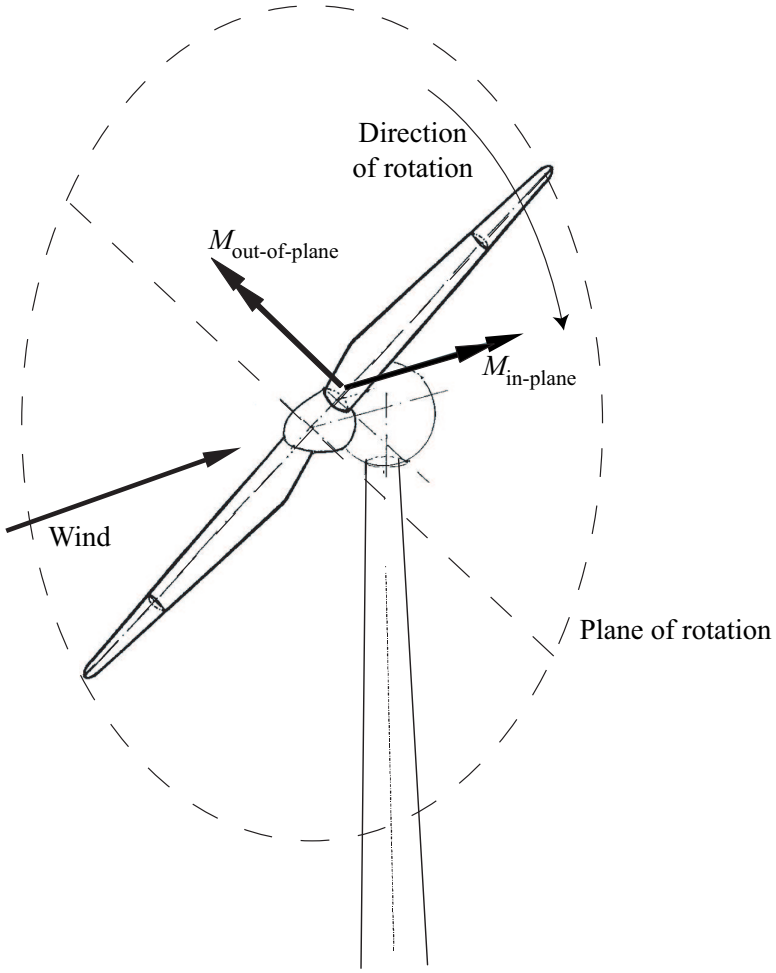

Figure 1.1: Generic diagram of a two bladed horizontal axis turbine, showing the directions of out-of-plane, $M_{\text{out-of-plane}}$ and in-plane, $M_{\text{in-plane}}$, bending moments.

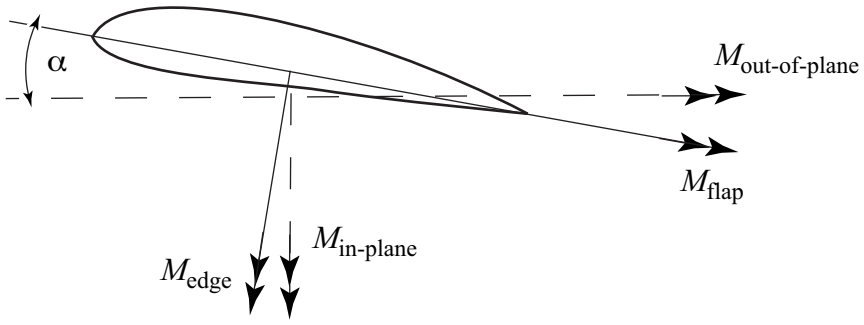

Figure 1.2: Cross-section through cord plane of generic wind turbine airfoil showing relation between out-of-plane and flap bending moments (also, in-plane and edge bending moments) through pitch angle α.

1.3.2 Stationarity of the Wind Process

In the discussion in Section 1.2 it was stated in Equation 1.9 that the probability distribution of the loads, $f_{\mathbf{X}_2}$ could be found by conditioning on a vector of variables, $\mathbf{E}$, which described the environmental process. For wind turbine design, typically the mean wind speed, V, and turbulence intensity, I, are the variables which are used to describe the wind process. Also wind loading is a process, like the loading due to waves, which has macro and micro time variability. The loads fluctuate continuously while the gross characteristics change slowly over time. In these cases it is convenient to consider these load processes stationary over a short reference period. For wind applications, seasonal, synoptic, and diurnal variations in the wind parameters make monthly, weekly, daily, or hourly values different from annual values. These conditions result in a selection of a reference time period during which the underlying environmental parameters can be considered to remain in a statistically steady-state condition. This reference time period is less than one hour and may commonly be taken as T=10 minutes. Therefore, V, is the 10-minute mean wind speed and I, is the 10-minute turbulence intensity. The turbulence intensity can be defined in two ways. Either the standard deviation of the 10-minute wind process, σ_V, or the coefficient of variation of the 10-minute wind process:

$$I = \frac{\sigma_V}{V} \tag{1.12}$$

Both definitions of turbulence intensity are used at different times in subsequent chapters. It will be clear when each definition is being applied.

1.4 Data Sets

Throughout this work several different sets of data are analyzed to illustrate the application of the theories developed. In this section we briefly describe each of these data sets. The data sets represent recorded or simulated data from three different horizontal-axis wind turbines.

1.4.1 DOE/NREL/NWTC Unsteady Aerodynamics Experiment Phase III Turbine

The Department of Energy/National Renewable Energy Laboratory/National Wind Technology Center Unsteady Aerodynamics Phase III horizontal axis test turbine is a modified Grumman Wind Stream 33. It is a three-bladed, fixed pitch, stall regulated turbine with a rotor diameter of 10 meters and a hub height of 25m. It operates in free yaw down wind of the tower with a cut-in wind speed of 6m/s and a nominal rotor speed of 72 RPM. The nominal rated power is 20kW [19]. The turbine is shown in Figure 1.3, and a close-up of the turbine hub is shown in Figure 1.4.

The data set described here was provided by the National Renewable Energy Laboratory and consisted of multiple 10-minute simulations performed for three target 10-minute mean wind speeds, V=14, 20, and 45m/s. The simulations were obtained using a general-purpose, commercially available structural analysis code, ADAMS, linked with the special purpose routines to estimate aerodynamic effects [20]. The details and assumptions in constructing the math-material model of the turbine are documented in the work by Madsen, et al. [21]. The three cases considered are described below:

1. V=14m/s, typical of nominal or "rated" wind conditions;
2. V=20m/s, the maximum or "cut-out" wind speed at which the turbine operates; and
3. V=45m/s, an extreme wind speed (e.g., 50-year level) during which the turbine is parked.

For each of the three cases, 100 simulation runs were performed. The duration of each simulation was 605 seconds with data recorded at 25Hz [21]. The first 5 seconds of each simulation were discarded to eliminate transients that may occur when the analysis is started. Seven data channels were "recorded" during each simulation. The three data channels that are important to this work are: wind speed, blade root out-of-plane (flap) bending moment, and blade root in-plane (edge) bending moment. Note, the terms flap and edge bending are used consistently throughout this work to refer to out-of-plane and in-plane bending, respectively. The remaining data channels correspond to loads on the yaw bearing of the turbine and are not used in the analysis presented in future chapters.

Figure 1.3: Department of Energy/National Renewable Energy Laboratory's Unsteady Aerodynamics Experiment Phase III turbine installed at the National Wind Technology Center. Photograph courtesy of the National Renewable Energy Laboratory, www.nrel.gov.

Figure 1.4: Close-up of DOE/NREL Unsteady Aerodynamics Experiment Phase III turbine installed at NWTC. Photograph courtesy of the National Renewable Energy Laboratory, www.nrel.gov.

1.4.2 Atlantic Orient Corporation, AOC 15/50

Atlantic Orient Corporation's AOC 15/50 horizontal axis turbine is a modified Enertech 44/60. It is a three-bladed, fixed pitch, stall-regulated turbine with a 15-meter rotor diameter and a hub height of 25 meters. It operates down wind of the tower with passive yaw control and a cut-in wind speed of 6m/s. The nominal rated power is 50kW in an 12m/s wind speed. The turbine has a fixed rotor speed of about 60 RPM [22] and is shown in Figure 1.5

The data set described here was provided by the National Renewable Energy Laboratory and consisted of multiple 10-minute simulations of Gaussian wind fields and corresponding in- and out-of-plane blade root bending moments. The wind input processes were recorded at the turbine hub height.

One hundred 10-minute simulations have been performed for various choices of wind speed and turbulence class with different random seed values. The simulations were carried out using YAWDYN, an aerodynamics and dynamics analysis code for wind turbines. Target 10-minute mean wind speeds, in the operating regime of the turbine were chosen from 10m/s to 24m/s in 2m/s increments. Simulations were run at each wind speed considering both class A and class B IEC turbulence classes[23]. Also, pseudo-parked conditions (turbine slowly idling) were run for both turbulence classes, with a target 10-min mean wind speeds of 24, 30, 40, and 50m/s. The original data set contained time histories corresponding to only the 50m/s environmental condition. The remaining pseudo-parked conditions were added later to the data set by the author.

1.5 Moment-Based Models

The purpose of this section is to present a brief review of probability concepts that will facilitate the discussion of future chapters. In particular, we are interested in how we might construct a small set of measures—statistical moments—which may adequately describe a random variable. Also, a topic of interest here, is given that we may have only limited observations of the random variable under consideration, how may we construct unbiased estimates of the statistical moments and what is the associated uncertainty in these estimates. A short discussion is presented here, and will be expanded in a later chapter. Finally, we present a few moment-based probability models that will be used in the next several chapters to estimate the distributions of fatigue and extreme loads.

1.5.1 Expectation and Statistical Moments

This section presents a summary of probability concepts used throughout this work. The reader may proceed to Section 1.5.2 if they are familiar with this material. Additional information on the

Figure 1.5: Atlantic Orient Corporation's AOC 15/50 turbine installed in Burlington, Vermont. Photograph courtesy of the Atlantic Orient Corporation, www.aocwind.net.

topics presented here can be found in Benjamin and Cornell [11], Grimmett and Stirzaker [16], and Rice [24].

A continuous random variable is completely defined by its probability density function. It is sometimes useful, however, to characterize a random variable by a set of measures which describe the overall features of its distribution. Commonly included in the set are measures of central tendency, breadth, and skewness of the distribution. Our interest here is in defining this set of measures as well as other useful measures. We will see later, (e.g., Chapter 2) that our problem will be that we only have estimates of these measures for a random variable and from these estimates infer an appropriate distribution of the random variable. In order to define this set of measures we first review the Expectation operator.

Expectation of Random Variables

The concept of the expectation of a random variable, X, is similar to the idea of a weighted average. The possible realizations of, X, are weighted by their associated probability of occurrence. It is sufficient for the discussion here to focus our attention on continuous random variables. Therefore, if X is a continuous random variable with probability density function, $f_X(x)$, then the expectation, denoted by $\mathsf{E}[\cdot]$, is given by

$$\mathsf{E}[X] = \int_{-\infty}^{\infty} x\, f_X(x)\, dx \tag{1.13}$$

More generally, the expectation operator may be applied to functions of random variables. Let $g(X)$ denote a function of the random variable, X. The expectation of $g(X)$ is then defined as:

$$\mathsf{E}[g(X)] = \int_{-\infty}^{\infty} g(x)\, f_X(x)\, dx \tag{1.14}$$

Expectation is a linear operation and its order can be interchanged with other linear operators as shown below, given $g_1(X)$ and $g_2(X)$.

$$\mathsf{E}[g_1(X) + g_2(X)] = \mathsf{E}[g_1(X)] + \mathsf{E}[g_2(X)] \tag{1.15}$$

The expectation of functions of joint random variables is given by

$$\mathsf{E}[g(X_1, X_2)] = \int_{-\infty}^{\infty} g(x_1, x_2)\, f_{X_1,X_2}(x_1, x_2)\, dx_1 dx_2 \tag{1.16}$$

Moments of Random Variables

The statistical moments of a random variable, X, are useful measures of the the probability distribution of X. Consider a function $g(X) = X^m$, where m is a deterministic constant. The m^{th} statistical moment of X is defined as:

$$\mathsf{E}[X^m] = \int_{-\infty}^{\infty} x^m \, f_X(x) \, dx \tag{1.17}$$

The first moment, $m = 1$, is called the *mean value*, denoted by μ_X, and is a common measure of central tendency of the probability mass.

Central Moments of Random Variables

Central moments of random variables are moments calculated about the mean. The m^{th} central moment of the random variable X is defined as:

$$\mathsf{E}[(X - \mu_X)^m] = \int_{-\infty}^{\infty} (x - \mu_X)^m \, f_X(x) \, dx \tag{1.18}$$

By applying Equation 1.15 we see that the value of the first central moment, $m = 1$, is always zero.

$$\mathsf{E}[(X - \mu_X)] = \mathsf{E}[X] - \mathsf{E}[\mu_X] = \mu_X - \mu_X = 0 \tag{1.19}$$

The variance of X is the second central moment ($m = 2$) and is denoted by $\mathsf{Var}[X]$ or σ_X^2, defined as

$$\mathsf{E}[(X - \mu_X)^2] = \int_{\infty}^{\infty} (x - \mu_X)^2 \, f_X(x) \, dx = \sigma_X^2 \tag{1.20}$$

and is a measure of the dispersion of the probability mass about $X = \mu_X$, the mean value, and is always ≥ 0. Alternatively, the variance may be found from the first two moments by applying Equation 1.15

$$\begin{aligned} \mathsf{E}[(X - \mu_X)^2] &= \mathsf{E}[X^2 - 2X\mu_X + \mu_X^2] && (1.21) \\ &= \mathsf{E}[X^2] - 2\mu_X \mathsf{E}[X] + \mathsf{E}[\mu_X^2] && (1.22) \\ &= \mathsf{E}[X^2] - \mu_X^2 && (1.23) \end{aligned}$$

Which can be written as

$$\mathsf{E}[(X - \mu_X)^2] = \mathsf{E}[X^2] - \mathsf{E}^2[X] \tag{1.24}$$

Two other measures of the dispersion of the probability mass are commonly used. These are the

standard deviation, σ_X, and the coefficient of variation, δ_X. The standard deviation of X, is defined as the positive square root of the variance,

$$\sigma_X = \sqrt{\mathsf{Var}[X]} \tag{1.25}$$

The coefficient of variation is defined as the ratio of the standard deviation to the mean, provided the mean is not equal to zero in which case the coefficient of variation is undefined. Note the coefficient of variation is a dimensionless quantity.

$$\delta_X = \frac{\sigma_X}{|\mu_X|} \tag{1.26}$$

The third central moment, $m = 3$, is a measure of skewness or asymmetry about the mean. The coefficient of skewness, γ_X, is defined as:

$$\gamma_X = \frac{\mathsf{E}[(X - \mu_X)^3]}{\sigma_X^3} \tag{1.27}$$

If the distribution of X is symmetric then $\gamma_X = 0$. When $\gamma_X > 0$, the distribution of X is said to be "*right-skewed*" and has a longer right-hand tail. Conversely, if $\gamma_X < 0$, then the distribution of X has a longer left-hand tail, and is "*left-skewed*". Examples of symmetric, right- and left-skewed distributions are shown in Figure 1.6

The fourth central moment, $m = 4$, is a measure of flatness. That is the weight of the tails compared with the weight of the body about the mean. The coefficient of kurtosis, κ_X, is defined as:

$$\kappa_X = \frac{\mathsf{E}[(X - \mu_X)^4]}{\sigma_X^4} \tag{1.28}$$

The normal or Gaussian distribution has a coefficient of kurtosis equal to 3.0. A value of the coefficient of kurtosis different than 3.0 is one measure of how much the distribution of a random variable deviates from the Gaussian distribution, as shown in Figure 1.7

Joint Central Moments

Two statistical moments that are commonly used to describe joint random variables (e.g. X_1 and X_2) are the covariance and the correlation coefficient. The first joint central moment is the covariance, Cov, and is defined as:

$$\mathsf{E}[(X_1 - \mu_{X_1})(X_2 - \mu_{X_2})] = \int_{-\infty}^{\infty} (X_1 - \mu_{X_1})(X_2 - \mu_{X_2})\, f_{X_1,X_2}(x_1, x_2)\, dx_1 dx_2 \tag{1.29}$$

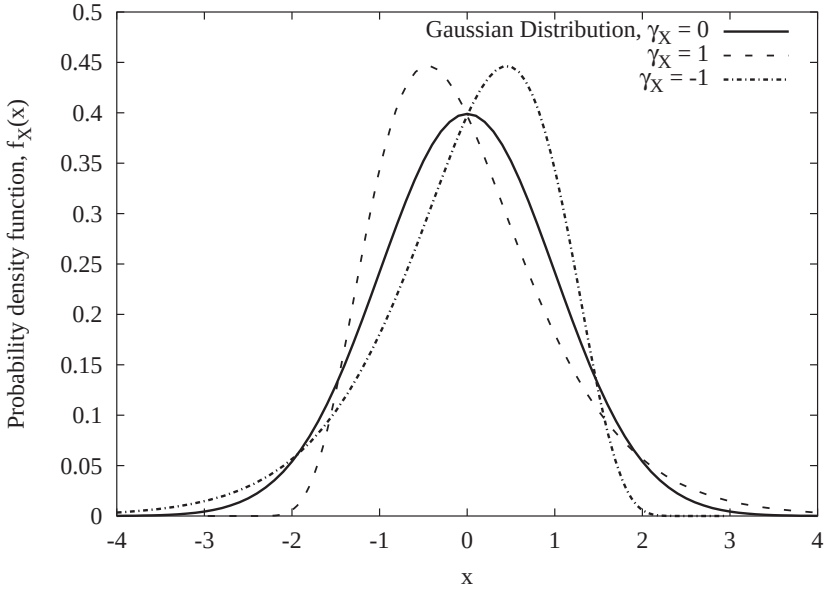

Figure 1.6: Distributions with positive and negative skewness compared with the Gaussian distribution with zero skewness. Note, all distributions shown have the same mean and variance.

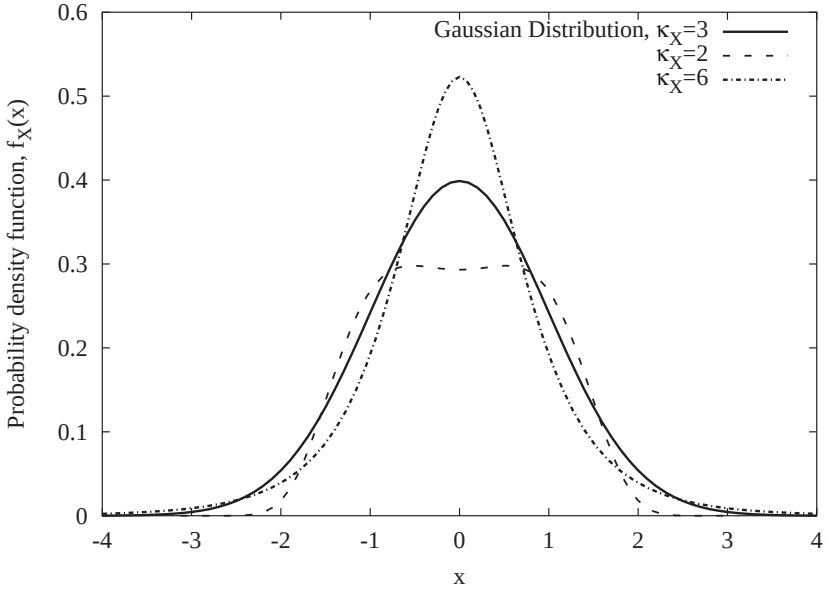

Figure 1.7: Distributions with higher and lower coefficients of kurtosis, $\kappa_X = 2$ and $\kappa_X = 6$ compared with the Gaussian distribution with κ_X=3. Note, all distributions shown have the same mean and variance.

and is a measure of the correlation between random variables X_1 and X_2. If X_1 and X_2 are independent then the $\mathsf{Cov}[X_1, X_2] = 0$. However, $\mathsf{Cov}[X_1, X_2] = 0$, does not imply that X_1 and X_2 are independent [25].

The correlation coefficient, ρ, is a dimensionless measure of linear dependence between two random variables and is defined as:

$$\rho_{1,2} = \frac{\mathsf{Cov}[X_1, X_2]}{\sigma_{X_1}\sigma_{X_2}} \qquad -1 \leq \rho \leq 1 \tag{1.30}$$

A value of $\rho_{1,2} = 1$, implies perfect positive linear dependence, i.e., a linear deterministic functional relationship exists between X_1 and X_2, e.g.,

$$X_2 = a + bX_1 \qquad (b > 0) \tag{1.31}$$

Whereas a value of $\rho_{1,2} = -1$, implies perfect negative linear dependence, e.g., $b < 0$ in Equation 1.31.

In this section we have reviewed a few probability concepts, in particular the expectation and statistical moments of random variables. The next section discusses how we may obtain estimates of these statistical moments from observed sample data and how good these sample statistics may be as estimators of the unknown moments of the random variables.

1.5.2 Estimating Statistical Moments

In this section we review how we may obtain estimates of statistical moments from sample data. Let us assume we have a set of, n, observations or realizations, $\{x_1, x_2, x_3, \ldots, x_n\}$, of the random variable X, from which we can calculate the sample mean

$$\bar{x} = \frac{1}{n}\sum_{i=1}^{n} x_i \tag{1.32}$$

and the sample variance is

$$s_X^2 = \frac{1}{n-1}\sum_{i=1}^{n} (x_i - \bar{x})^2 \tag{1.33}$$

We can interpret the observations of X, however, as realizations of n independent random variables, i.e., x_1 is a realization of X_1, x_2 is a realization of X_2, etc. We may further interpret X as the *population* from which the observations were randomly sampled. The distribution of X is a mathematical construction and therefore the moments, e.g., the population mean, μ_X, and the population variance, σ_X^2, are constants. Each random variable, X_i, shares the same distribution as X, and in

particular each variable has the same mean and variance as the population mean, and population variance. Of course, in a strict sense, if the distributions are identical then all the moments are the same, but here we restrict our discussion to the first and second moments. In this context we may then express the sample mean as:

$$\bar{X} = \frac{1}{n}\sum_{i=1}^{n} X_i \tag{1.34}$$

and the sample variance as:

$$S_X^2 = \frac{1}{n-1}\sum_{i=1}^{n} (X_i - \bar{X})^2 \tag{1.35}$$

Therefore, $\bar{x}$ and s_X^2 defined in Equations 1.32 and 1.33. and computed from the observed data are realizations of the random variables, $\bar{X}$ and S_X^2, in Equations 1.34 and 1.35. This illustrates that the sample statistics are random variables, whereas the moments of the population are constants. Consequently we are interested in the expected value and variance of $\bar{X}$ and S_X^2 as we will use observations of $\bar{X}$ and S_X^2 as estimators of unknown μ_X and σ_X.

The Expected Value and Variance of $\bar{X}$

Taking the expectation of both sides of Equation 1.34 yields:

$$\mathsf{E}[\bar{X}] = \frac{1}{n}\sum_{i=1}^{n} \mathsf{E}[X_i] = \frac{1}{n} \cdot n\mu_X = \mu_X \tag{1.36}$$

Because $\mathsf{E}[\bar{X}] = \mu_X$, in Equation 1.36, $\bar{X}$, as defined in Equation 1.34, is said to be an unbiased estimator of the population mean.

Taking the variance of both sides of Equation 1.34 yields:

$$\mathsf{Var}[\bar{X}] = \left(\frac{1}{n}\right)^2 \sum_{1=i}^{n} \mathsf{Var}[X_i] = \frac{1}{n^2} \cdot n\sigma_X^2 = \frac{\sigma_X^2}{n} \tag{1.37}$$

The standard error of, $\bar{X}$, denoted by, $\mathsf{se}_{\bar{X}}$, is given by the standard deviation of $\bar{X}$,

$$\mathsf{se}_{\bar{X}} = \frac{\sigma_X}{\sqrt{n}} \tag{1.38}$$

The Expected Value of S_X^2

Taking the expectation of both sides of Equation 1.35 yields:

$$\begin{aligned}\mathsf{E}[S_X^2] &= \frac{1}{n-1}\sum_{i=1}^{n}\mathsf{E}[(X_i-\bar{X})^2] \\ &= \frac{1}{n-1}\left[\sum_{i=1}^{n}\mathsf{E}[X_i^2]-n\mathsf{E}[\bar{X}^2]\right]\end{aligned} \tag{1.39}$$

applying Equation 1.24 we find,

$$\mathsf{E}[X_i^2] = \mathsf{Var}[X_i] - \mathsf{E}^2[X_i] = \sigma_X^2 - \mu_X^2 \tag{1.40}$$

$$\mathsf{E}[\bar{X}^2] = \mathsf{Var}[\bar{X}] - \mathsf{E}^2[\bar{X}] = \frac{\sigma_X^2}{n} - \mu_X^2 \tag{1.41}$$

substituting Equations 1.40 and 1.41 into Equation 1.39

$$\begin{aligned}\mathsf{E}[S_X^2] &= \frac{1}{n-1}[n(\sigma_X^2-\mu_X^2) - n(\frac{\sigma_X^2}{n}-\mu_X^2)] \\ &= \sigma_X^2\left(\frac{n}{n-1}\right)\left(1-\frac{1}{n}\right) \\ &= \sigma_X^2\end{aligned} \tag{1.42}$$

From Equation 1.42, we see that, S_X^2, as defined in Equation 1.35 is an unbiased estimate of the population variance. Similar to the first statistical moment, as the sample of X becomes large, $n \to \infty$, the sample variance will converge to the population variance [24].

Unbiased Estimates of Skewness and Kurtosis

We may observe from the analysis presented above that the leading coefficient in Equation 1.34 was $\frac{1}{n}$, whereas in Equation 1.35 the coefficient was $\frac{1}{n-1}$. Furthermore, we may consider this coefficient related to the free degrees of freedom, denoted, dof. In estimating the sample mean, the first moment, all the degrees of freedom are free, $\mathsf{dof} = n$. Whereas when estimating the variance, the second central moment, we reduce the degrees of freedom by one because we have already estimated one statistical moment from the data, $\mathsf{dof} = n-1$. In general for the m^{th} moment we can determine the remaining free degrees of freedom as

$$n-(m-1) \tag{1.43}$$

An unbiased estimate of the coefficient of skewness, the third central moment ($m = 3$), denoted by α_{3_X}, may be found by the equation below with $(n - (3 - 1)) = (n - 2)$ free degrees of freedom.

$$\alpha_{3_X} = \frac{\sum_{i-1}^{n}(X_i - \bar{X})^3}{(n-2)S_X^3} \tag{1.44}$$

Similarly, an unbiased estimate of the coefficient of kurtosis, the fourth central moment ($m = 4$), denoted by α_{4_X}, may be found by the equation below with $(n - (4 - 1)) = (n - 3)$ free degrees of freedom.

$$\alpha_{4_X} = \frac{\sum_{i-1}^{n}(X_i - \bar{X})^4}{(n-3)S_X^4} \tag{1.45}$$

1.5.3 Probability Models for Extreme Loads

Let us first suppose that we have a time varying random load process, $X(t)$, which is assumed to be stationary over time, T. To estimate the probability distribution of L_T, the maximum load event in time T, one may construct probability models over a number of different time scales. We introduce three such models briefly in this section and describe each in more detail subsequently. In order of decreasing time scales (and hence increasing use of data), these models are the following:

Global Extreme Models: These seek to directly model, Z, the "global" (largest) extreme over T, The advantage here is that we work most directly with the extreme of interest; i.e., L_T. The drawback is that we discard all time history values below these global maxima.

Local Extreme/Random Peak Models: These models instead represent all local maxima of the load history $X(t)$, possibly excluding those that fall beneath some user-defined lower-bound threshold. (This is an example of what is sometimes referred to as a "peak-over-threshold" model.) In this work, local maxima are defined as the maximum event between up-crossings of the mean level. Compared with the global extreme models, local extreme models have the advantage of including more data in the fitting process. A potential disadvantage is that some of these data—in particular the lower-amplitude maxima—may come from a different statistical population, which should not be included in extrapolating to large loads. Shown in Chapter 2, the complication introduced from multiple populations may be avoided by an appropriate choice of a lower-bound threshold. In this work $\mathbf{Y}$ denotes the vector of random variable associated with the sequence of local maxima of $X(t)$.

Random Process Models: Finally, these models seek to statistically describe the entire time-varying load history, $X(t)$. These contain the largest possible information, e.g., all data points in a digitized history. They may yield little advantage, however, over random peak models if there

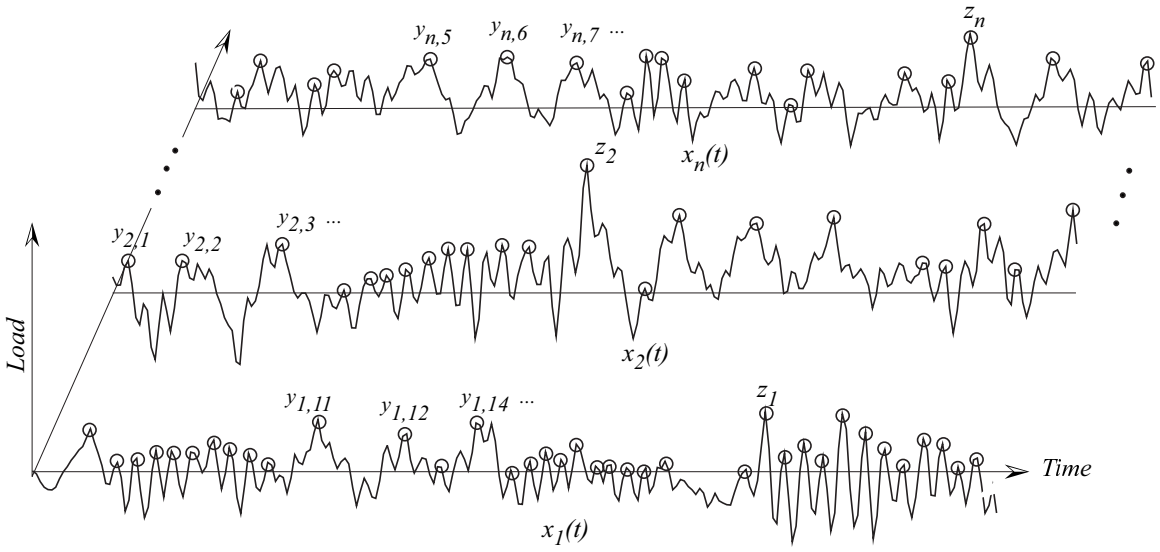

Figure 1.8: Time scales versus amount of available data: Global maximum, Z; local random peaks, Y; random process, $X(t)$.

is little additional statistically independent (i.e., relevant) information contained in the details of the time history between its peak values.

Figure 1.8, shows realizations $x_1(t), x_2(t), \ldots, x_n(t)$ of the random process $X(t)$, with realizations $\{y_{1,1}, y_{1,2}, y_{1,3}, \ldots\}, \{y_{2,1}, y_{2,2}, y_{2,3}, \ldots\}, \{y_{n,1}, y_{n,2}, y_{n,3}, \ldots\}$ of $\mathbf{Y}$, the vector of random local peaks, and realizations $z_1, z_2, , \ldots, z_n$ of the global extremes, Z. This figure graphically demonstrates the difference in time scales and the amount of available data associated with the models presented above.

1.5.4 Global Extreme Model

If we model the global extremes, we immediately have the desired probability, $P[L_T < l]$, that the maximum value L_T is less than any l as:

$$P[L_T < l] = P[Z < z] = F_Z(l) \tag{1.46}$$

It has been shown that for both the operating and parked conditions of a wind turbine, the 10-minute extreme event follows an Extreme Value Type I model fairly well [21]. Additional analysis may be required if field collected data is used [26, 27]. The expression for the Extreme Value Type I, or

Gumbel model [28, 29], is given as:

$$F_Z(z) = \exp\left(-\exp\left(-\alpha(z-u)\right)\right) \tag{1.47}$$

and the parameters α and u (α is a measure of dispersion and u is the mode of the distribution) are given in terms of the first two statistical moments of Z as:

$$\mu_Z = u + \frac{\gamma_{\text{Euler}}}{\alpha} \tag{1.48}$$

$$\sigma_Z^2 = \frac{\pi^2}{6\alpha^2} \tag{1.49}$$

where $\gamma_{\text{Euler}} \approx 0.577$.

1.5.5 Random Peak Model

If one instead models all random peaks, as previously defined and denoted Y_1, Y_2, ..., the corresponding probability $P[L_T < l]$ can be estimated as:

$$\begin{aligned} P[L_T < l] &= P[(Y_1 < l) \cap (Y_2 < l) \cap (Y_3 < l) \cap \cdots \cap (Y_{N_T} < l)] \\ &= \prod_{i=1}^{N_T} P_i[Y_i < l] = \{P[Y_i < l]\}^{N_T} = [F_Y(l)]^{N_T} \end{aligned} \tag{1.50}$$

where N_T is the number of peaks, Y_i values, in time duration T. Equation 1.50 holds assuming that the number of peaks, N_T, is deterministic and that their levels are mutually independent. The assumption of stationarity of $X(t)$ implies that all the peaks, $i = 1, 2, \ldots, N_T$, have the same probability distribution, $F_Y(y)$. None of these assumptions are strictly correct, but the approximation generally becomes more accurate as one considers extremes in the upper tail of the load probability distribution[30]. Rewriting Equation 1.50 in terms of the CDF of Z, and the complementary CDF of Y, one can apply an approximation for the exponential function as shown below:

$$F_{L_T}(l) = [1 - G_Y(l)]^{N_T} \tag{1.51}$$

$$= \left[1 - \frac{N_T\, G_Y(l)}{N_T}\right]^{N_T} \tag{1.52}$$

$$\approx \exp\left(-N_T\, G_Y(l)\right) \tag{1.53}$$

The approximation in Equation 1.53 holds for $N_T G_Y(l) \ll 1$, i.e., for large values of l.

We are looking for an estimate of the expected maximum over a duration, T. We saw above

that the distribution of 10-minute extremes was well described by the Gumbel distribution. Here we also assume that $F_{L_T}(l)$ follows a Gumbel distribution

$$F_{L_T}(l) = \exp\left(-\exp\left(-\alpha(l-u)\right)\right) \tag{1.54}$$

where the mean of L_T, denoted by μ_{L_T}, in terms of the parameters α and u is given by:

$$\mu_{L_T} = u + \frac{\gamma_{\text{Euler}}}{\alpha} \tag{1.55}$$

If we evaluate Equation 1.54 at its mean value, and set it equal to Equation 1.53, also evaluated at μ_{L_T}, and solve for $G_Y(\mu_{L_T})$, we find:

$$F_{L_T}(\mu_{L_T}) = \exp\left(-\exp\left(-\alpha(\mu_{L_T}-u)\right)\right) = \exp\left(-\exp\left(\gamma_{\text{Euler}}\right)\right) \cong \exp\left(-N_T\, G_Y(\mu_{L_T})\right) \tag{1.56}$$

$$G_Y(\mu_{L_T}) = \frac{N_T}{\exp\left(\gamma_{\text{Euler}}\right)} \tag{1.57}$$

Where Equation 1.57 gives the probability level of the distribution of Y associated with expected value of L_T. Formally,

$$\mu_{L_T} = G_Y^{-1}\left(\frac{N_T}{\exp\left(\gamma_{\text{Euler}}\right)}\right) \tag{1.58}$$

where G_Y^{-1} is the inverse of G_Y. Here we have obtained an estimate of the expected value of the maximum load in time, T, based on the probability distribution and the number of the random peaks. We shall use this result in Chapter 2.

1.5.6 Process Model

Process models seek to describe the entire time-varying load history, $X(t)$. Most research has focused on Gaussian models of $X(t)$. The Hermite transformation has been found to be useful in a range of applications in estimating the extreme statistics of non-Gaussian response processes [31, 32, 33]. As described by Winterstein [34], the Hermite polynomial given in Equation 1.59 functionally relates the fractiles of a Gaussian process to the fractiles of a non-Gaussian process. This polynomial transformation is derived in such a way that its individual terms are statistically uncorrelated. The cubic polynomial given below, which has four terms and therefore is capable of matching only the first four statistical moments, is often sufficient to capture the non-Gaussian nature of the response process.

Here, the non-Gaussian load history, $X(t)$, is presumed to be functionally related to a standard

Gaussian process $U(t)$. The Hermite polynomial for the condition when the coefficient of kurtosis, κ_X, is greater than 3, is given by:

$$x = g(u) = \mu_X + \kappa\sigma_X[u + c_3(u^2 - 1) + c_4(u^3 - 3u)] \tag{1.59}$$

where

$$\kappa = [1 + 2c_3^2 + 6c_4^2]^{-1/2} \tag{1.60}$$

A similar polynomial results from the derivation if $\kappa_X < 3$. The simplest estimates of c_3 and c_4 are given as:

$$c_3 \approx \frac{\gamma_X}{6} \qquad\qquad c_4 \approx \frac{\kappa_X - 3}{24} \tag{1.61}$$

These estimates assume there exists in the response process only small deviations from a Gaussian process and are found from the third and fourth central moments of the marginal distribution of $X(t)$. Winterstein, et al. [35] found more accurate approximations for c_3 and c_4, which are useful when $X(t)$ exhibits stronger deviations from a Gaussian process. The following equations for c_3 and c_4 are valid for $3 < \kappa_X < 15$ and $0 \leq \gamma_X^2 < \frac{2(\kappa_X - 3)}{3}$:

$$c_3 = \frac{\gamma_X}{6}\left[\frac{1 - 0.15|\gamma_X| + 0.3\gamma_X^2}{1 + 0.2(\kappa_X - 3)}\right] \tag{1.62}$$

$$c_4 = c_{40}\left[1 - \frac{1.43\gamma_X^2}{\kappa_X - 3}\right]^{1 - 0.1\kappa_X^{0.8}} \tag{1.63}$$

where

$$c_{40} = \frac{[1 + 1.25(\kappa_X - 3)]^{\frac{1}{3}} - 1}{10} \tag{1.64}$$

The Hermite polynomial transforms any fractile of a standard Gaussian distribution to the equivalent fractile of a non-Gaussian response distribution. Therefore, for this transformation to be useful in estimating fractiles of L_T we need to predict the extreme fractiles of a Gaussian process, i.e., extremes consistent with prescribed probability level. For example, we may consider the task of obtaining an estimate of the expected values of L_T, $\mathsf{E}[L_T] = \mu_{L_T}$. Again we will assume that the distribution of L_T is well described by the Gumbel distribution. The probability level, p, associated with the mean of the Gumbel distribution and hence, the expected value of L_T is

$$F_{L_T}(\mu_{L_T}) = p = \exp\left(-\exp\left(-\gamma_{\text{Euler}}\right)\right) = 0.57 \tag{1.65}$$

See Equation 1.56 as modified. Having found a probability level of interest, it then becomes of task of finding the fractile of U_{max}, the extreme of a Gaussian process associated with our prescribed

probability level, p. From Rice [36, 37], assuming the up-crossings of high levels are assumed to follow a Poisson process, it can be shown that

$$P[U_{\text{max}} \leq u] = \exp\left(-\nu_0 T \exp\left(-u^2/2\right)\right) \tag{1.66}$$

where ν_0, is the average up-crossing rate, and T is the duration. The expected number of cycles in time, T is denoted by, N_T and given as:

$$N_T = \nu_0 \times T \tag{1.67}$$

Setting $P[\cdot]$ in equation 1.66 equal to $p = 0.57$, the resulting fractile of U_{max} is given by:

$$u_{\text{max},p} = \sqrt{2 \ln\left(\frac{N_T}{\ln\left(\frac{1}{p}\right)}\right)} \tag{1.68}$$

$u_{\text{max},p}$, is an estimate of the expected maximum of a Gaussian process with up-crossing rate ν_0 in time, T. The result of Equation 1.68 is used directly in the Hermite polynomial given in Equation 1.59 to find an estimate of X_{max}=L_T. Of course the other fractiles, other than the mean, of L_T may be found by substituting other values for p in to Equation 1.68

An alternate approach to approximate the expected maximum of a standard Gaussian process in N_T cycles, which has recently been used in the analysis of extreme loads on wind turbines [21], is estimated as:

$$\mathsf{E}[U_{\text{max}}] = u_{\text{max},p} = \frac{\mathsf{E}[\max(X)] - \mu_X}{\sigma_X} \approx \sqrt{2 \ln N} + \frac{\gamma_{\text{Euler}}}{\sqrt{2 \ln N}} \tag{1.69}$$

Again applying Type I Extreme Value Theory for the distribution of L_T and recalling Equation 1.65, the probability level associated with the expected value of L_T is given as:

$$F_{L_T}(\mu_{L_T}) = \exp(-\exp(-\alpha(\mu_{L_T} - u))) = \exp(-\exp(\gamma_{\text{Euler}})) \qquad (= 0.57) \tag{1.70}$$

Setting Equation 1.70 equal to Equation 1.66, and solving for, u, yields:

$$u_{\text{max},p=0.57} = \sqrt{2 \ln N_T + 2\gamma_{\text{Euler}}} \tag{1.71}$$

Comparing the squares of Equations 1.71 and 1.69

$$(u_{\max,p=0.57})^2 = 2\ln N_T + 2\gamma_{\text{Euler}} \tag{1.72}$$

versus

$$(u_{\max,p=0.57})^2 = 2\ln N_T + 2\gamma_{\text{Euler}} + \frac{\gamma^2_{\text{Euler}}}{2\ln N} \tag{1.73}$$

For $N_T = 1,000$ these equations become:

$$(u_{\max,p=0.57})^2 = 13 + 1.1 \tag{1.74}$$

versus

$$(u_{\max,p=0.57})^2 = 13 + 1.1 + 0.024 \tag{1.75}$$

Therefore, considering $N_T = 1,000$ the approximation in Equation 1.69 introduces a difference in $u_{\max,p=0.57}$ of only about 0.1% as compared to a model based strictly on the Gumbel and Poisson distributions.

1.6 Organization

This work is divided into three major sections. The first part deals with the short-term problem, specifically, choosing probabilistic models to fit to data given the environmental conditions. The second part, building on the analysis and results of the first part, addresses the long-term problem. First, integrating the short-term models over the long-run distributions of the environmental variables. Then, two approximate approaches are investigated. The final part of this work deals with the uncertainty associated with the parameters and statistics used to describe the short-term loads models, and the long-run distributions of the environmental variables. Of particular interest is how these uncertainties impact the estimates of extreme loads on wind turbines.

Part One is made up of Chapter 2 for extreme loads and a portion of Chapter 5 which addresses fatigue. Each of these chapters address the choice of probabilistic model to fit to data. In Chapter 2 the efficacy of random peak and process models to hold sufficient information about the load process to accurately estimate the expected extreme event over a brief period of time of ten minutes to over a period of several hours is investigated. Chapter 5 introduces a new approach to fitting a probabilistic model to fatigue load ranges. The process involves using established probabilistic models, but tuning the fit of the model to the data based on expected damage. This introduces a link between the material capacity and the demand on the wind turbine. It also allows the model to be fit to the data in the region in which the data is most important, where the data has the potential to contribute

most to accumulated fatigue damage.

Part Two comprises the next three chapters. Chapter 3 presents a methodology for proceeding from conditional short-term extreme load distributions to estimates of the one-year and 50-year extreme load on an AOC 15/50 turbine, assumed to operate in an environment similar to that found in Lavrio, Greece. The methodology involves relating the moments of the data, which are used to fit the probabilistic model, to values of the environmental variables through regression analysis. Then, the short-term conditional distribution models are summed, weighted by long-run probabilities of the environmental conditions occurring. A qualitative analysis is undertaken to reduce the complexity of the integration. Prescribed deterministic fractiles of some of the variables involved in the integration are carefully chosen to account for the variability introduced if the entire distribution where included. Applying this methodology reduces one level of integration for each of the variables replaced by a prescribed fractile.

In Chapter 4 we introduce another approach for estimating long-term extremes which employs the approximate methods underlying first-order reliability analysis. In this method, contours of the critical combination of wind speed and turbulence intensity are found for prescribed reliability levels. It then becomes a straightforward task of (1) identifying an appropriate percentile of the short-term load, and (2) identifying the maximum response along the prescribed contour. Under the assumptions of first-order reliability analysis, the maximum response along the "environmental contour" is associated with the prescribed reliability level. Later, in Chapter 5 a similar methodology, from Chapter 3, is laid out for fatigue and applied to the same AOC turbine also assumed to operate in an environment similar to that in Lavrio, Greece. Note that appendices C and F consider similar analysis for both extremes and fatigue, respectively but an alternate description of the environmental conditions is used, largely based on that of Class IA conditions given by the IEC, international wind turbine code [23].

Finally, Chapter 6 discusses the sources of uncertainty in the analyzes previously presented and demonstrates how including these uncertainties affects the estimates of the one-year and 50-year extreme events on wind turbines. Some of the sources of uncertainty addressed include: uncertainty in the long-term descriptions of the environmental variables, as well as uncertainty in the model parameters of short-term load models. Also, modeling uncertainty associated with simulated loads compared with recorded field data is discussed. The impact of considering all of these sources of uncertainty on estimates of the one-year and 50-year load on wind turbine in Lavrio, Greece, is assessed.

Chapter 2

Prediction of Short-Term Extreme Load Distributions[1]

This chapter considers two distinct topics that arise in reliability-based wind turbine design. First, it illustrates how general probability models can be used to estimate long-term design loads from a set of limited-duration, short-term load histories. Second, it considers in detail the precise choice of probability model to be adopted, for both flap and edge bending loads in both parked and operating turbine conditions. In particular, a 3-moment random peak model and a 3- or 4-moment random process model are applied and compared. For a parked turbine, all models are found to be virtually unbiased and to notably reduce uncertainty in estimating extreme loads (e.g., by roughly 50 percent). For an operating turbine, however, only the random peak model is found to retain these beneficial features. This suggests the advantage of the random peak model, which appears to capture the rotating blade behavior sufficiently well to accurately predict extremes.

2.1 Introduction

Probabilistic models have gained widespread acceptance and use within a range of engineering disciplines. These models have formed the basis, either explicitly or implicitly, for a number of design codes—especially those of the LRFD (load and resistance factor design) format. Recently developed wind turbine standards [23] have begun to adopt these code formats, in analogy with long-standing practice in the building and offshore structure communities.

In applying probabilistic models to design wind turbines, a number of practical challenges remain. A first question concerns *how* a particular probability model may be used to satisfy design

[1] A portion of this chapter was previously published in the American Society of Mechanical Engineering's Journal of Solar Energy Engineering [38]

requirements as specified, for example, in wind turbine standards [39]. In particular, due to the wind turbine's complex dynamic behavior, an analyst may need to rely on a set of limited-duration load histories over a range of wind conditions. These histories may result either from measurements on prototype machines or from numerical simulation. In either case, there is a fundamental question as to how one can proceed from these *short-term* load observations to specification of appropriate *long-term* loads, as required in design codes. Future chapters address this question, presenting a general methodology to relate the short-term statistics to the desired long-run design load. Chapter 3, covers estimating long-term extreme events while Chapter 5 addresses estimating long-term distributions of fatigue loads.

A second question that arises concerns the precise details of the probabilistic modeling to be applied; namely, *which* probabilistic model or models are best suited to describe the dynamic behavior of wind turbines. As will be noted below, a number of these have been proposed and applied in the literature. These differ first in which quantity they seek to model; for example, some seek to model the entire load history $x(t)$ as a random process, others seek to model only the local peaks (maxima) of $x(t)$, while still others consider only more global peaks (e.g., 10-minute maxima). Once this choice has been made, various functional forms are available to model the relevant probability distribution at hand. In this chapter various random process and random peak models are compared, for cases of both edge and flap bending loads in both operating and parked wind turbine conditions.

2.2 Probability Models for Extreme Loads and Responses

We saw in Chapter 1 that we may construct probability models over a number of different time scales, to estimate the conditional probability distribution of L_T, the maximum load even in time T. In order of decreasing time scales (and hence increasing use of data), these include the following:

Global Extreme Models: These seek to directly model, Z, the "global" (largest) extreme over T. The advantage here is that we work most directly with the extreme of interest; i.e., L_T. The drawback is that we discard all time history values below these global maxima, see Section 1.5.4.

Local Extreme/Random Peak Models: These models instead represent all local maxima of the load history $X(t)$, possibly excluding those that fall beneath some user-defined lower-bound threshold. (This is sometimes referred to as a "peak-over-threshold" model. Also recall that we have defined local maxima as the maximum event between up-crossings of the mean level.) Compared with the global extreme models, local extreme models have the advantage of including more data in the fitting process, see Section 1.5.5. A potential disadvantage

is that some of these data—in particular the lower-amplitude maxima—may come from a different statistical population, which should not be included in extrapolating to large loads. Shown later, this can be avoided by an appropriate choice of a lower-bound threshold.

Random Process Models: Finally, these seek to statistically describe the entire time-varying load history, $X(t)$. These contain the largest possible information; e.g., all data points in the digitized history. They may yield little advantage, however, over random peak models if there is little additional statistically independent (i.e., relevant) information contained in the details of the time history between its peak values, see Section 1.5.6 .

Note that if one models global extremes directly, one immediately has the desired probability, $P[L_T < l]$, that the maximum value L_T is less than any l (Section 1.5.4). If one instead models all random peaks, here denoted Y_1, Y_2, ..., the corresponding probability $P[L_T < l]$ can be estimated as

$$P[L_T < l] = P[(Y_1 < l) \cap (Y_2 < l) \cap (Y_3 < l) \cap \cdots \cap (Y_{N_T} < l)] = \{P[Y_i < y_i]\}^{N_T} \qquad (2.1)$$

in which N_T is the number of peaks, Y_i values, in time duration T. We saw in Chapter 1 that Equation 2.1 holds assuming that the number of peaks, N_T, is deterministic and that their levels are mutually independent and identically distributed. Although none of these assumptions are strictly correct, the approximation generally becomes more accurate as one considers extremes in the upper tails of the load's probability distribution [30] (Section 1.5.5). Finally, if we instead model the entire process, $x(t)$, consistent statistics of L_T require somewhat additional effort (Section 1.5.6). An algorithm named MAXFITS has been created to automate this process, permitting the user to select between these three types of models to estimate extreme statistics [40, 41].

2.3 Data set

We used the database for the DOE/NREL/NWTC Unsteady Aerodynamics Experiment Phase III turbine as described in Section 1.4.1 in this analysis. The database contains multiple 10-minute simulations of Gaussian wind fields, and corresponding in- and out-of-plane bending moment responses. The turbine has a rotor diameter of 10m and a nominal rotor speed of 1.2 Hz. It is a three-bladed turbine with a hub height of 17m [21].

A total of 100 10-minute simulations have been performed for various choices of the mean wind speed V. These use a general-purpose, commercially available structural analysis code (ADAMS), linked with special-purpose routines to estimate aerodynamic effects [20]. The focus here is on three cases:

1. V=14m/s, typical of nominal or "rated" wind conditions;
2. V=20m/s, the maximum or "cut-out" wind speed at which the turbine operates; and
3. V=45m/s, an extreme wind speed (e.g., 50-year level) during which the turbine is parked.

The last case is somewhat analogous to extreme winds on buildings and other stationary structures, and we may expect similar statistical behavior in this wind turbine analysis. The lower-speed cases, however, correspond to operating conditions, in which the turbine blades rotationally sample the stationary wind field. Also notable here are the systematic effects of gravity on blade root in-plane (edge) bending: a strong sinusoidal trend is induced at the turbine operating speed. The work in this chapter investigates whether various probabilistic response models can remain accurate in the face of these special features that wind turbines exhibit.

2.4 Predicting Short-term Extreme Events

This section considers how the previously discussed models can be applied to estimate extreme bending loads on wind turbines. In particular, the behavior of two different types of probabilistic models are considered: (1) *Hermite* models of the load as a random process, and (2) *quadratic Weibull* models of random load peaks (over a specified threshold). The Hermite model generally utilizes four statistical moments of $x(t)$ [42], although a simplified three-moment version can be used in some special cases of limited nonlinearity [21, 43, 44]. The quadratic Weibull model is based on the first three statistical moments of the peak values, Y_i [45, 46, 47]. As noted in these references, there are no closed-form results for this model's parameters in terms of its moments; the parameters must be found numerically. Note that the MAXFITS routine implements both the quadratic Weibull and Hermite models, as well as a number of others [40, 41].

2.4.1 Sample Time Histories

Figure 2.1 shows simulated wind and load time histories from one 10-minute simulation for a target 10-minute mean wind speed of 45m/s and the turbine parked. In particular, the histories shown are brief, 10-second portions of the wind and load histories during which the wind input is maximized. It should be noted that this maximum wind episode does not generally produce the maximum bending loads.

To identify peaks from the response histories, we define a peak here as the largest value of the history between successive up-crossings of its mean level. Many alternative strategies can be used to identify peaks; e.g., the largest value per blade revolution. Later, however, we will show that

for the edge load cases presented, a threshold that excludes somewhat more load cycles—retaining roughly one peak for every two blade revolutions—is more beneficial. Figure 2.1 shows the mean levels of each history by horizontal lines, and the circled response points indicate the set of peaks that are obtained. The blade root out-of-plane (flap) bending loads are found here to roughly follow the wind speed process, although additional high-frequency content is observed. Note also that our definition of peaks—the largest response per up-crossing of the mean—serves to filter out many of these high-frequency response oscillations. The edge bending loads are of less interest in this case, showing small oscillations about the mean load.

Figures 2.2 and 2.3 show similar simulated wind and load time histories, now for a target 10-minute mean wind speed, V, of 20m/s and 14m/s during which the turbine is operating. Now the effect of gravity is clearly seen in the edge bending histories, which show a strong sinusoidal component at the operating speed of about 1.2 Hz. The flap bending histories also show systematic variations at this frequency, although it is combined with significantly larger high-frequency content here than in the edgewise cases. Again, the peak identification method implemented here removes some of this high-frequency effect. Note in the edgewise cases, however, that a somewhat anomalous effect can arise. While only one "large amplitude" peak is usually found per blade revolution, other "secondary", near-zero peaks are sometimes also identified. This arises from the high-frequency small-amplitude oscillations shown by the edgewise loads about their mean level. The resulting distribution of all peaks is found in such cases to be multi-modal; i.e., to possess a probability density function with several distinct regions of relatively high probability ("modes"). Figure 2.4 shows histograms of edge bending peaks for the two operating wind speeds investigated. Each of the histograms clearly show two distinct modes. Because our models are unimodal—i.e., designed to be fit to the single most important probability "mode"—we shall find it useful in these edgewise cases to pass a higher threshold (above the mean) to exclude these secondary peaks. We shall return to this issue below.

Finally, recall that to estimate the distribution of the *largest* peak, it is common to assume that successive peaks are mutually independent. This is the assumption inherent in the current implementation of MAXFITS[40, 41] (see, for example, Equation 2.1). To test this assumption, the correlation coefficient, ρ, between adjacent peaks y_i and y_{i+1} has been calculated for the various cases. Typical ρ values, shown in Table 2.1, are effectively negligible; for example, ρ=0.21 (flap bending, V=45m/s), ρ=0.28 (edge bending, V=45m/s), and ρ=0.15 (flap bending, V=20m/s). These values, and corresponding scatterplots of y_i vs y_{i+1} in Figures 2.5, 2.6, and 2.7, for wind speeds 45m/s, 20m/s and 14m/s respectively, confirm that the assumption of independence should not induce large modeling errors in this application. Indeed, even far higher correlations will tend to have minimal effect when extreme loads and responses are considered. For example, successive 3-hour wave

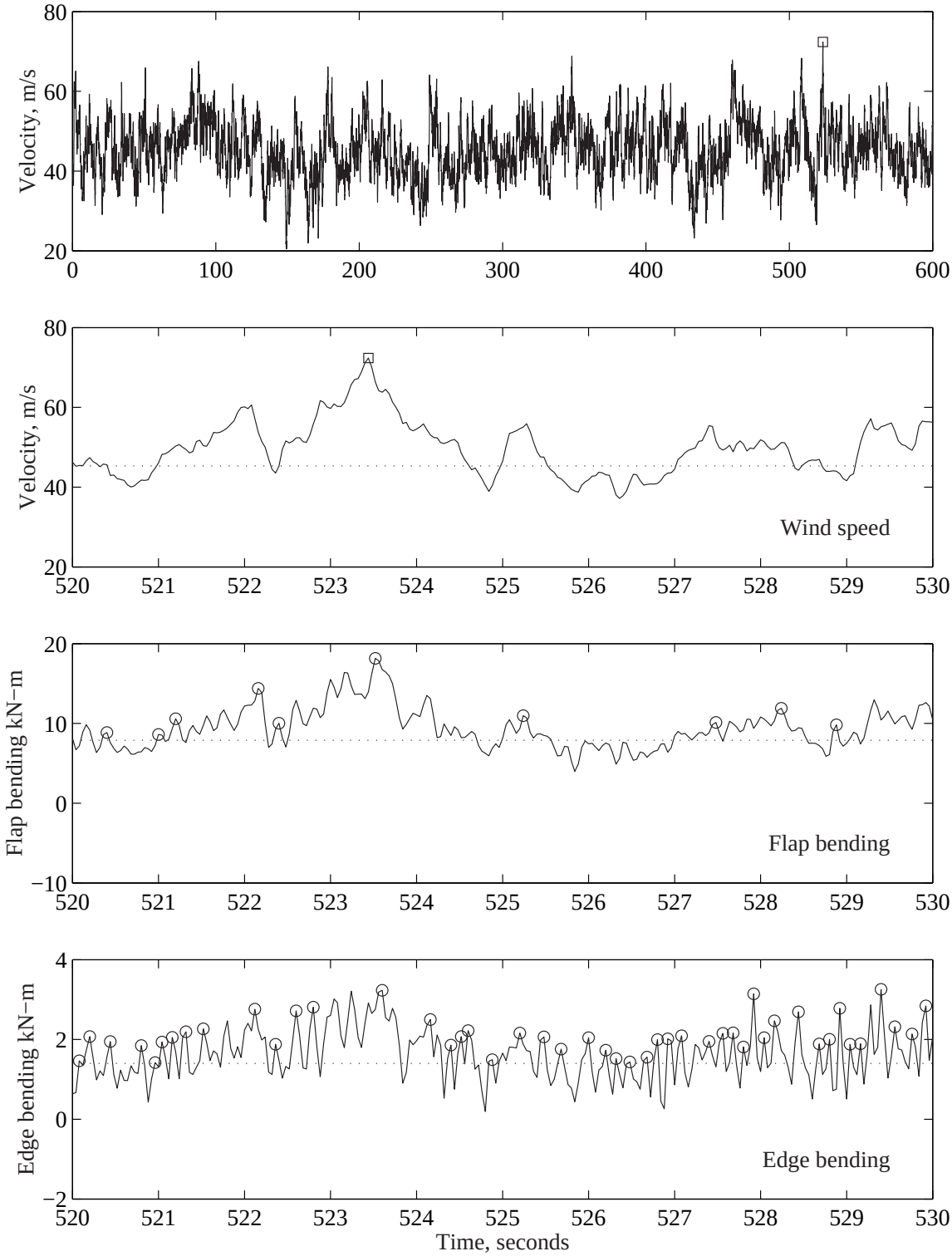

Figure 2.1: Simulated wind and blade responses; V=45m/s.

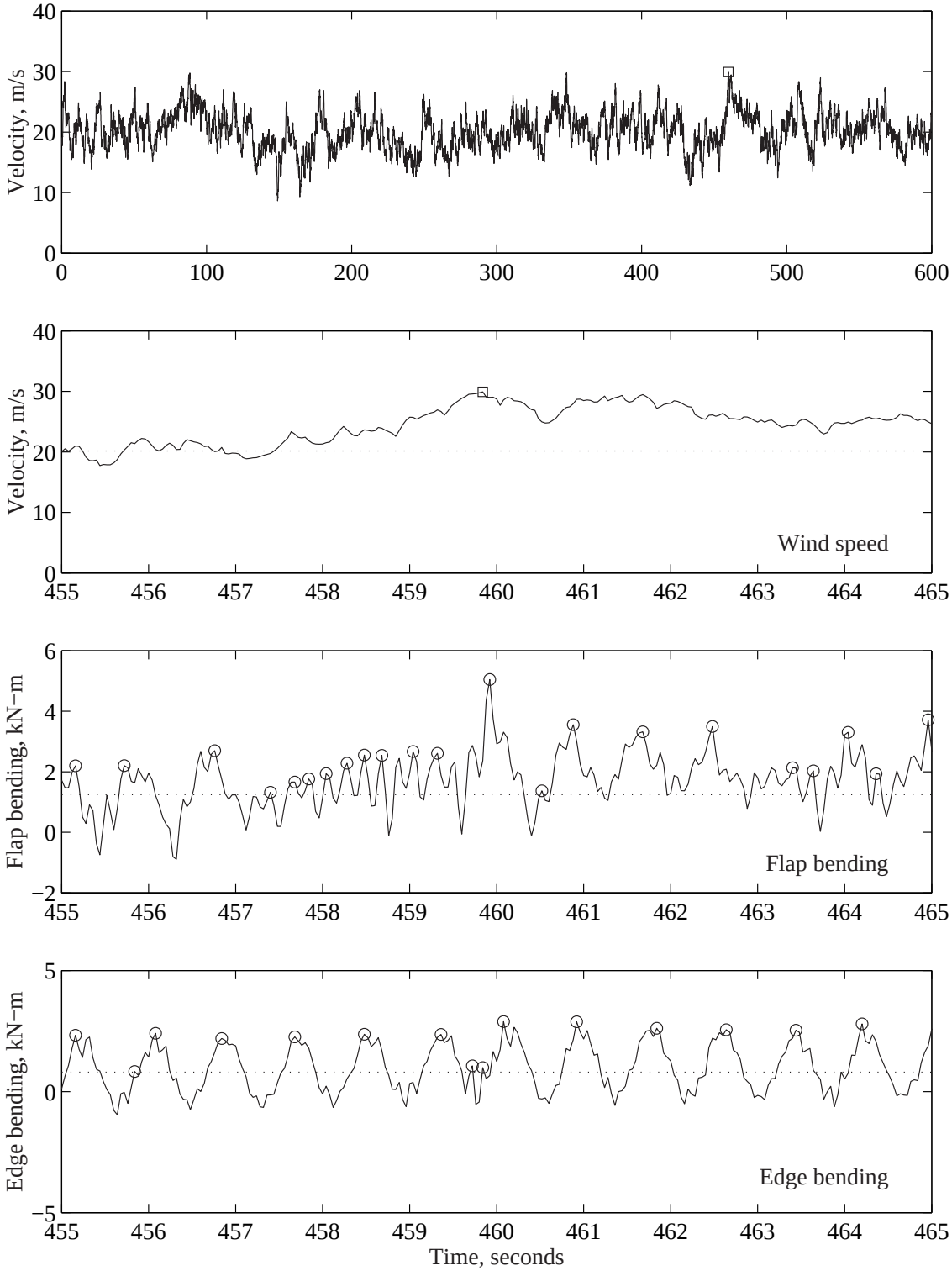

Figure 2.2: Simulated wind and blade responses; V=20m/s.

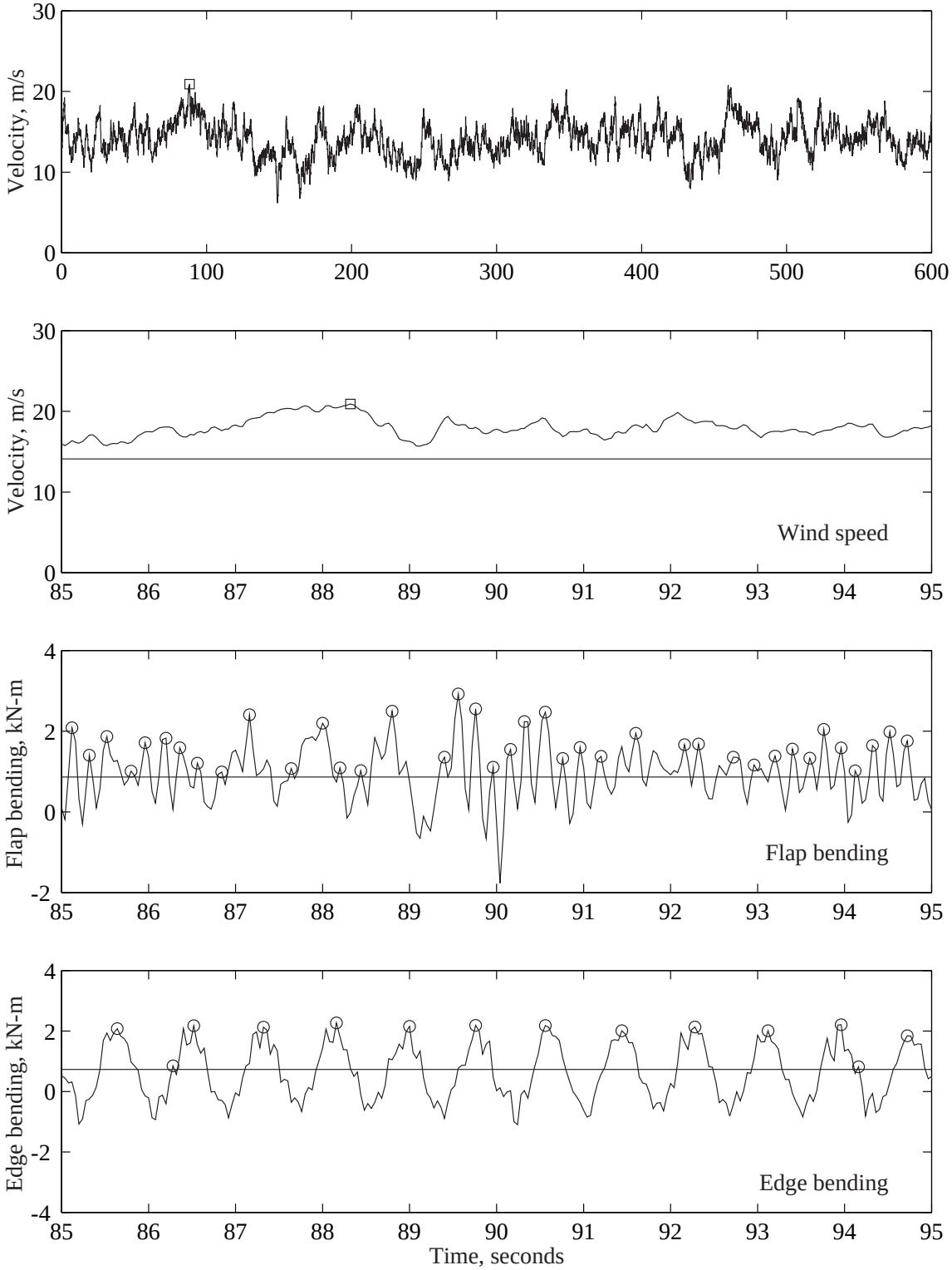

Figure 2.3: Simulated wind and blade responses; V=14m/s.

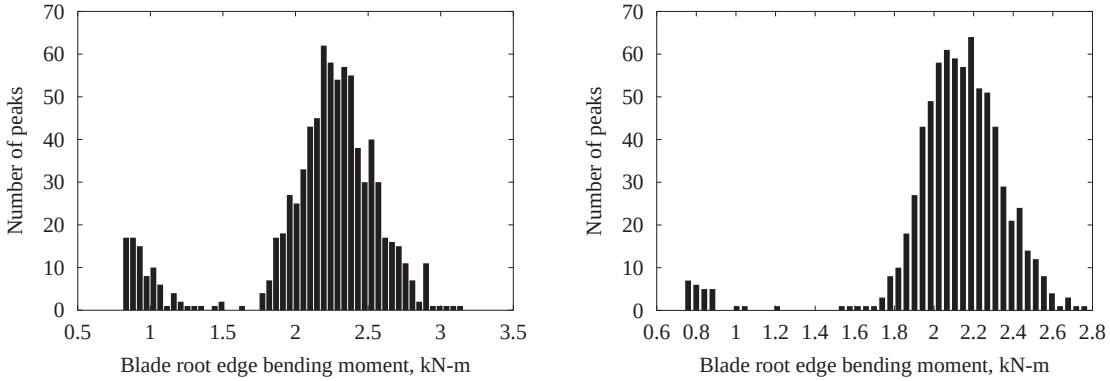

(a) 20m/s 10-minute mean wind speed

(b) 14m/s 10-minute mean wind speed

Figure 2.4: Histograms of the number of blade root edge bending peaks for V=20m/s and 14m/s.

Correlation Coefficient, ρ

Wind Speed	Flap bending peaks	Edge bending peaks	Shifted edge bending peaks
$V = 45$m/s	0.2092	0.2843	NA
$V = 20$m/s	0.1526	-0.0070	0.1249
$V = 14$m/s	0.1512	0.0770	0.1163

Table 2.1: Correlation coefficient, ρ , between adjacent peaks y_i and y_{i+1} for various 10-minute mean wind speeds

heights in the North Sea have been found to have correlation coefficient ρ=0.96[30]. Nonetheless, including the effects of this correlation is found to decrease the 100-year wave height by only about 2-3%. Note also, from the reference, that various methods are available to model this correlation, in cases when its inclusion is important. Included here are the cases where a threshold is imposed on the root edge bending peaks when the turbine is operating. In these cases only the peaks above the threshold are considered. One would expect that the correlation between peaks above a prescribed threshold would increase compared with the correlation of all the peaks, and this is the finding here. The value of the correlation coefficient for these cases, however, is still small, similar to the values found for the blade root flap bending peaks.

2.4.2 Observed vs Predicted Distributions of Peaks

First, the ability of a three-moment, quadratic Weibull distribution to accurately model the simulated response peaks across various wind conditions is tested. For illustration purposes, the results for the first (of the 100) 10-minute simulations of each of the three wind conditions are shown.

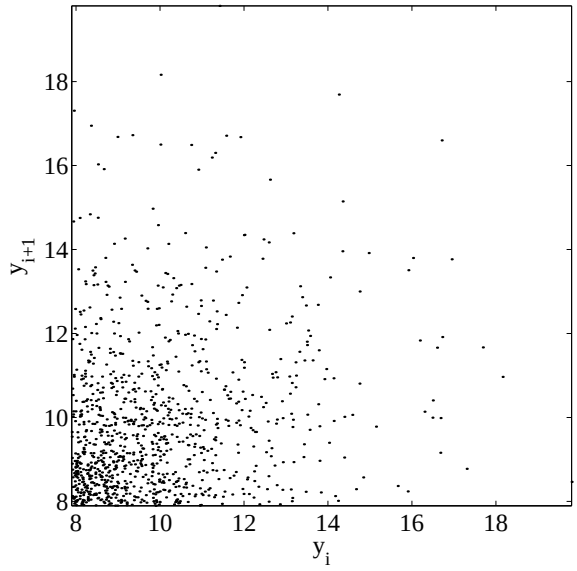

(a) Blade root flap bending peaks, ρ=0.2092

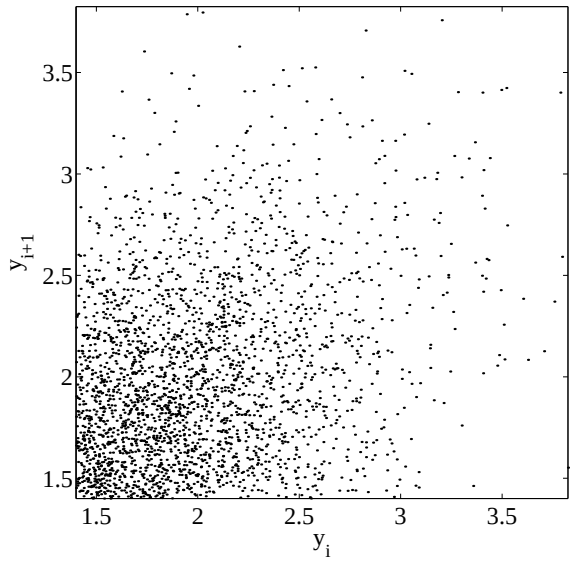

(b) Blade root edge bending peaks, ρ=0.2843

Figure 2.5: Correlation between successive blade root bending peaks; V=45m/s.

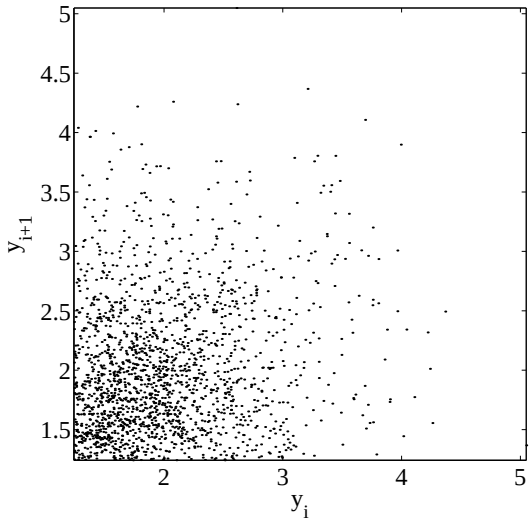

(a) Blade root flap bending peaks, ρ=0.1526

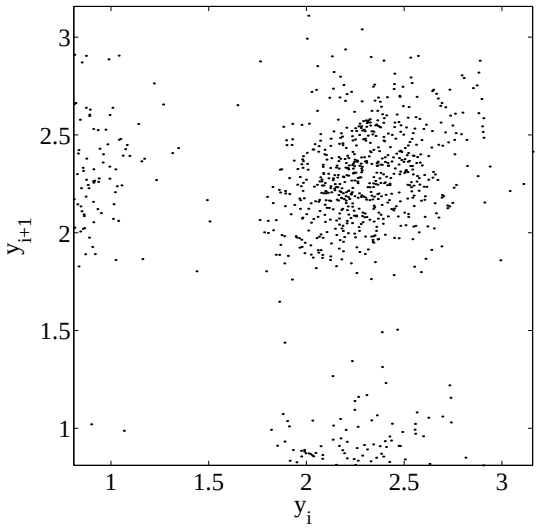

(b) Blade root edge bending peaks, ρ=-0.0070

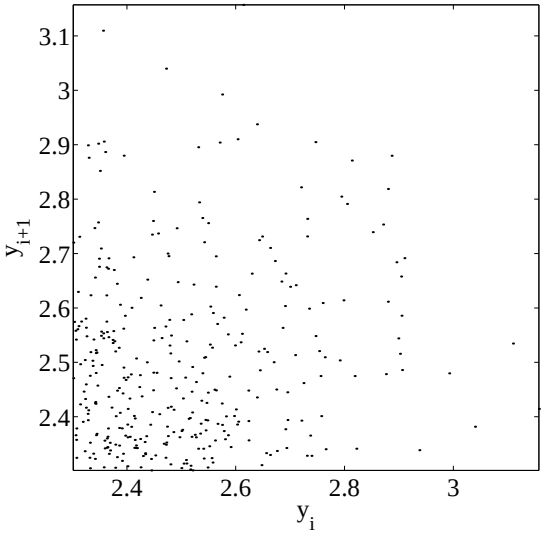

(c) Blade root edge bending peaks above threshold level, ρ=0.1249; Threshold = process mean + 1.5 kN-m

Figure 2.6: Correlation between successive blade root bending peaks; V=20m/s.

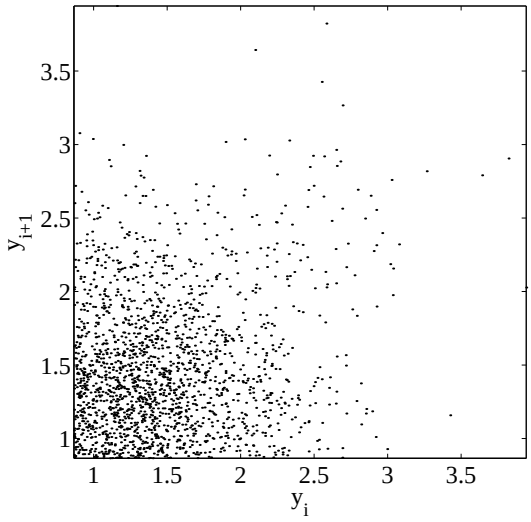

(a) Blade root flap bending peaks, ρ=0.1512

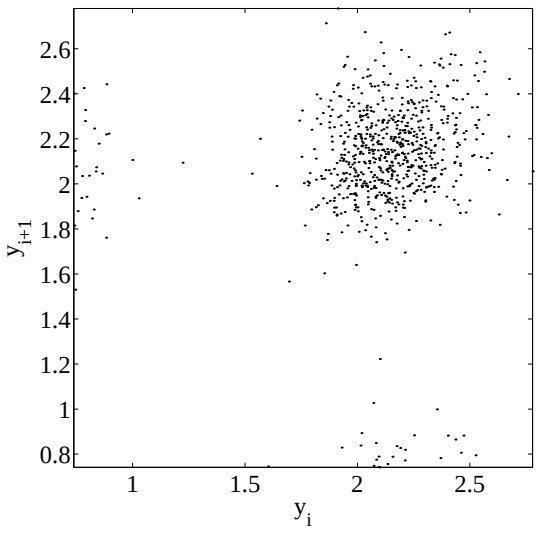

(b) Blade root edge bending peaks, ρ=0.0770

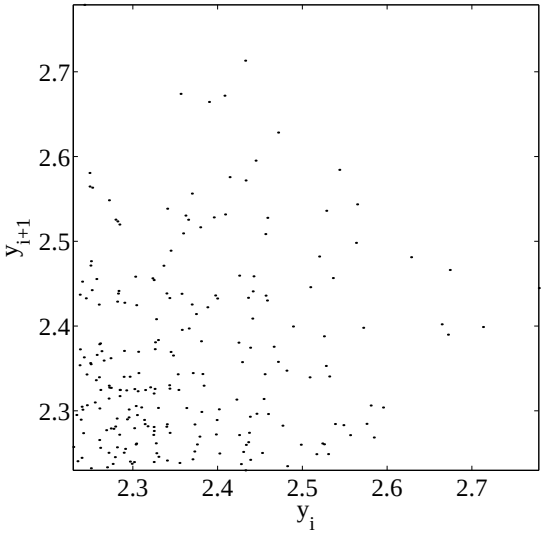

(c) Blade root edge bending peaks above threshold level, ρ=0.1163; Threshold = process mean + 1.5 kN-m

Figure 2.7: Correlation between successive blade root peaks; V=14m/s.

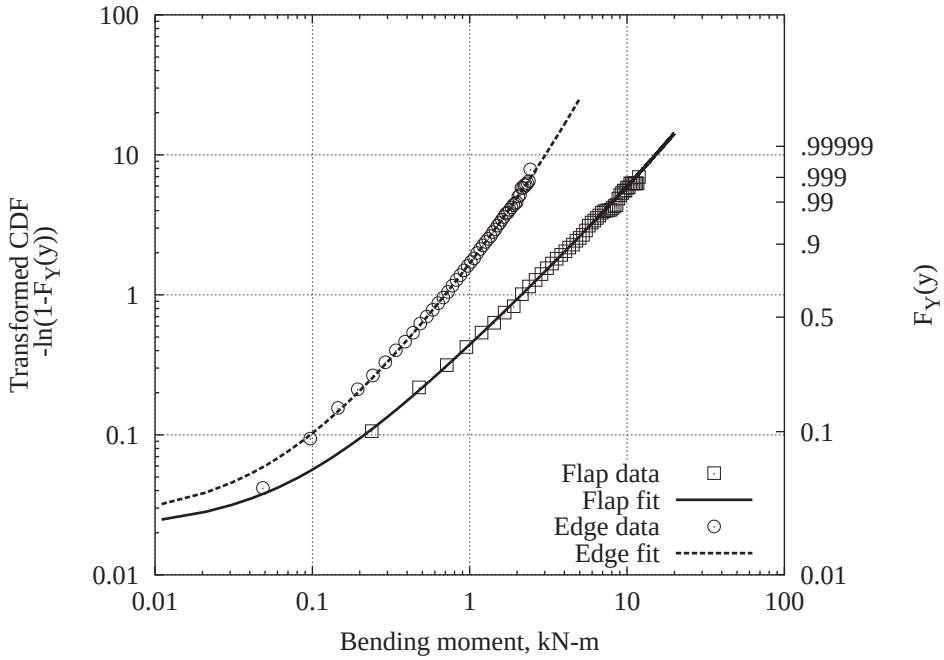

Figure 2.8: Empirical and fitted quadratic Weibull probability distributions of response peaks; V=45m/s.

We will consider the parked turbine, V=45m/s, first, whose statistical behavior may be expected to be most well-behaved. Figure 2.8 shows the cumulative probability distribution function $F_Y(y)$=$P[Y \leq y]$ of all peaks, as estimated directly from the data. Specifically, for both flap and edge cases, the peaks y_i are first ordered so that $y_1 \leq y_2 \leq ... \leq y_n$, and associated with the cumulative probabilities, p_i=$F_Y(y_i)$=$i/(n+1)$. Results are plotted on a distorted "Weibull" scale, which rather than plotting $F_Y(y)$ versus y, plots $-\ln[1-F_Y(y)]$ versus y. The results, when viewed on log-log scale, should appear as a straight line if the data follow a Weibull probability distribution model.[2]

The data here show slightly positive curvature on this Weibull scale. This suggests the value of the quadratic Weibull model, which yields a quadratically varying distribution when plotted on the Weibull scale of Figure 2.8. The right-hand y-axis contains the corresponding values of $F_Y(y)$, for clarity. This quadratic model is shown here to accurately follow both the flap and edge load data in this case.

Figures 2.9 and 2.11 shows similar Weibull scale plots of flap and edge loads in the V=20m/s and 14m/s cases respectively, during which the turbine is rotating. While the distribution of flap load peaks remains smooth, the distribution of edge load peaks shows a sharp change in behavior,

[2]This scale, however, does not emphasize the large y, small $P[Y > y]$ values of interest.

with a "corner" located at roughly y=1. This is a consequence of the bimodal character of the edge load peaks, as discussed earlier (see Figure 2.4). No smooth, single-moded distribution model can capture both the large, one-per-revolution primary peaks and the small-amplitude, secondary peaks. For both ultimate and fatigue load modeling purposes, however, these secondary peaks are of little consequence. We therefore seek to model the *truncated and shifted* peaks, $Y - 1.5$; i.e., we remove all peaks below 1.5, and report the shifted values y_i'=$y_i - 1.5$ of the remaining peaks. The shifting is used to conform with quadratic Weibull models, which generally assigns probability to all outcomes $y' \geq 0$. Figures 2.10 and 2.12 show the quadratic Weibull model to accurately follow the shifted edge loads, $Y - 1.5$, for both wind conditions. Note that the optimal choice of shift parameter may require some trial and error; e.g., comparing goodness-of-fit measures. This is a topic of ongoing study. Also, in using these models to predict extremes, the shift value must eventually be reinstated.

2.4.3 Estimating 10-Minute Mean Maxima

Finally, predicted statistics of $L_{10\,\text{min}}$, the maximum 10-minute load, are shown. In particular, we seek here to find $\hat{\mu}_{L_{10\,\text{min}}}$, an estimate of $\mu_{L_{10\,\text{min}}}$, the mean value of $L_{10\,\text{min}}$ to be expected in an arbitrary 10-minute period.

A simple, "raw" estimate of $\mu_{L_{10\,\text{min}}}$ can be found by averaging the 100 observed maxima, z_i, from each of the 10-minute simulations:

$$\hat{\mu}_{L_{10\,\text{min}}} = \bar{z} = \frac{1}{100}\sum_{i=1}^{100} z_i \tag{2.2}$$

Alternatively, an estimate of $\mu_{L_{10\,\text{min}}}$ can be found by fitting one of the foregoing models (e.g, a quadratic Weibull model) to all response peaks (perhaps above a shifted level as shown in the previous section). Here, models are fit separately to each of the 100 simulations. Denoting μ_i as the estimated value of $\mu_{L_{10\,\text{min}}}$ found from the model fit to the data of simulation i (i=1,...,100), an analogous average of these estimates is obtained:

$$\hat{\mu}_{L_{10\,\text{min}}} = \bar{\mu} = \frac{1}{100}\sum_{i=1}^{100} \mu_i \tag{2.3}$$

The subtle issue between the two estimates is that with the "raw" average we have one observation of $\bar{z}$, based on 100 z_i's from which to estimate $\mu_{L_{10\,\text{min}}}$. With the second method described above we have 100 observations of μ, (i.e., we obtain an estimate of $\mu_{L_{10\,\text{min}}}$, denoted by μ from the model fit to the data for each of the 100 simulations), from which to estimate $\mu_{L_{10\,\text{min}}}$. One advantage of the simple, "raw" estimate $\bar{z}$ is that it is always "unbiased", $\mathsf{E}[\bar{z}] = \mu_{L_{10\,\text{min}}}$; i.e., correct

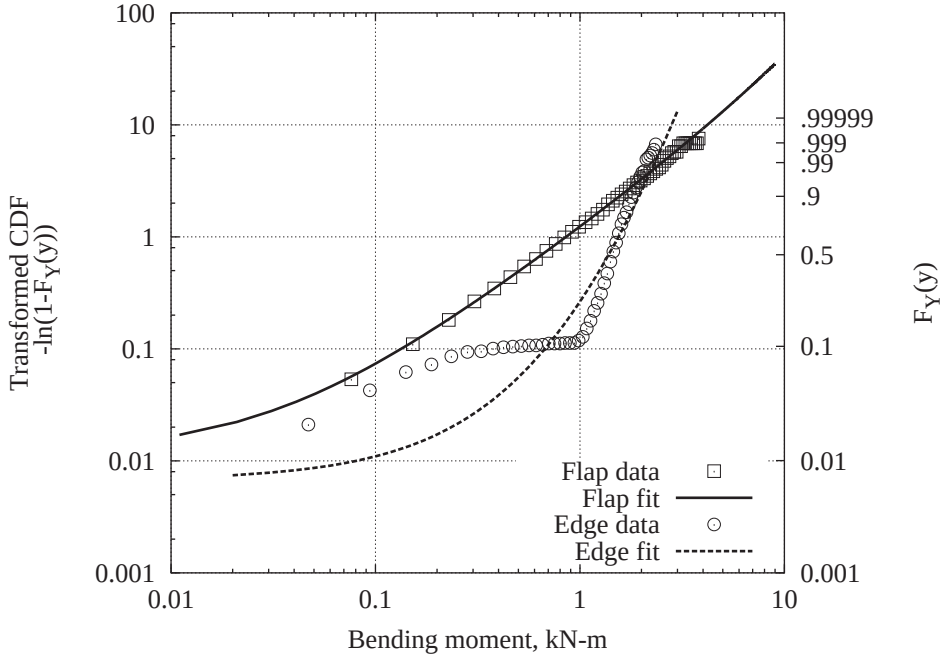

Figure 2.9: Empirical and fitted quadratic Weibull probability distributions of response peaks; V=20m/s.

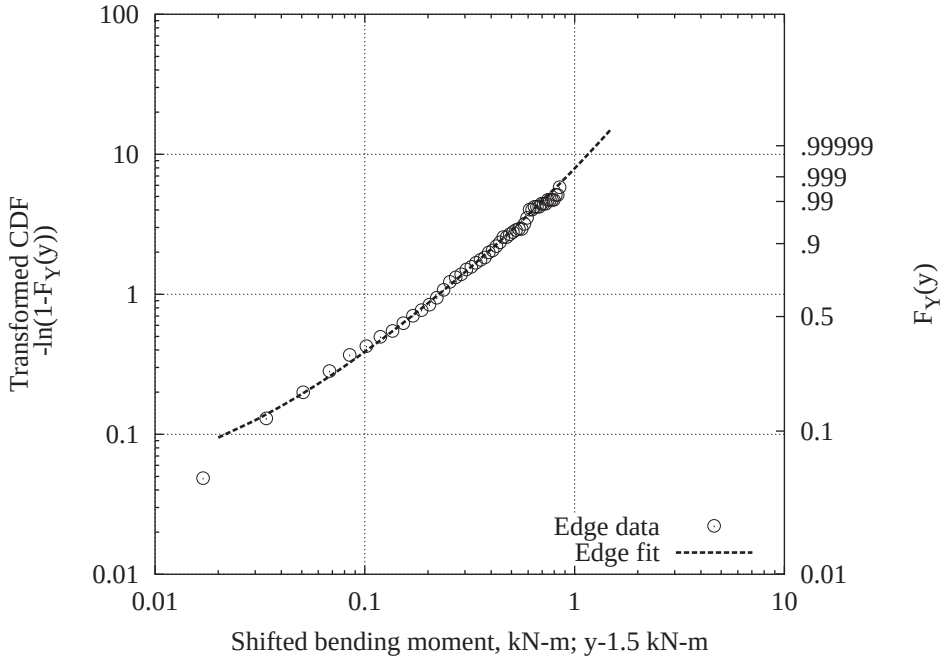

Figure 2.10: Empirical and fitted quadratic Weibull probability distributions of *shifted* edge bending response peaks above 1.5; V=20m/s.

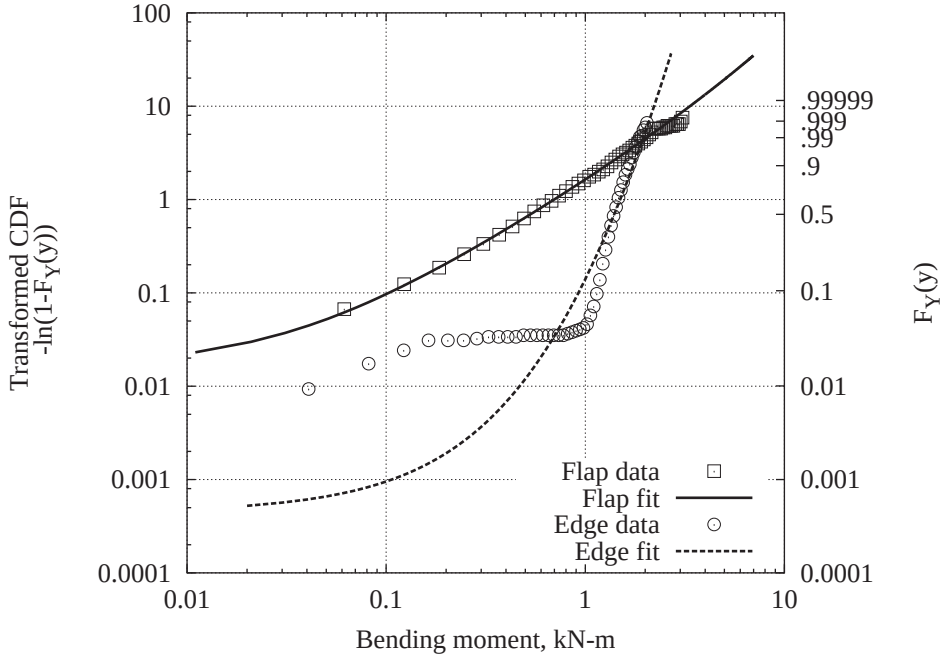

Figure 2.11: Empirical and fitted quadratic Weibull probability distributions of response peaks; V=14m/s.

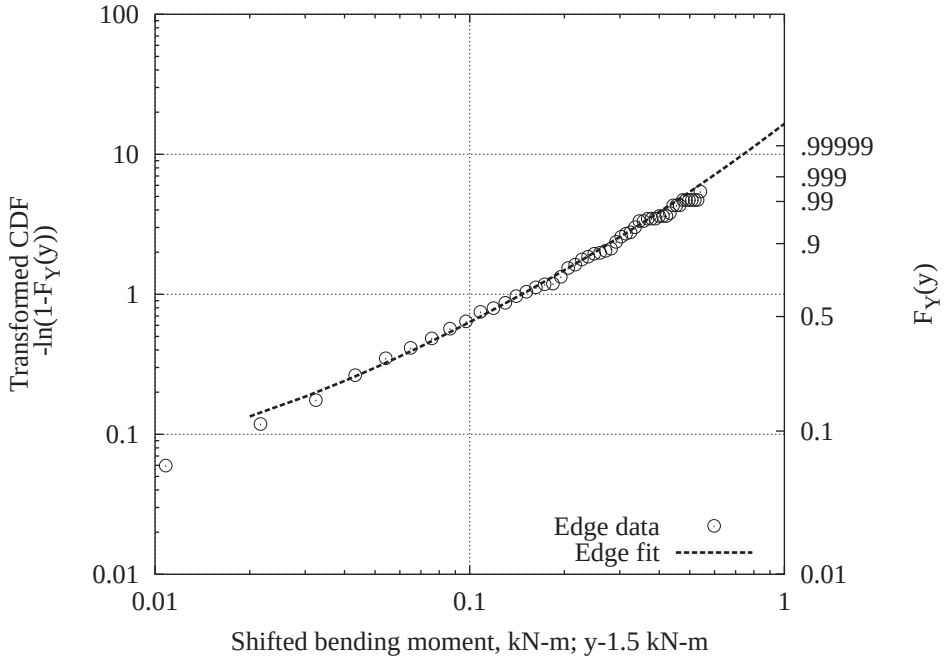

Figure 2.12: Empirical and fitted quadratic Weibull probability distributions of *shifted* edge bending response peaks above 1.5; V=14m/s.

on average. A potential disadvantage is that because it is based on only the single observed maximum in each 10-minute history, it may show considerable variability. By instead fitting probability models to form estimates μ, one hopes to achieve results that (1) remain nearly unbiased and (2) show reduced scatter, specifically, reduced standard deviation, compared with the raw estimate $\bar{z}$. To quantify these effects two factors are defined: a bias factor, defined as

$$\text{Bias (B)} = \frac{\bar{\mu}}{\bar{z}} \tag{2.4}$$

and a sigma reduction factor, defined as

$$\text{Sigma Reduction (SR)} = \frac{\sigma_\mu}{\sigma_Z} \tag{2.5}$$

One hopes to achieve bias factors of nearly unity, and sigma reduction factors far less than unity. Again, the hope for sigma reduction lies with the fact that each estimated μ_i uses more of the simulation history—specifically, each peak-over-threshold value—than the raw estimate $\bar{z}$, which uses only the single maximum z_i from each 10-minute simulation.

Figure 2.13 shows bias and SR factors, respectively, for the parked turbine (V=45m/s). Three probability models are fit: a 3-moment quadratic Weibull model ("Peak Un-shifted"), and both 3- and 4-moment Hermite models of the complete random response process $x(t)$. The three-moment simplification has been used in some mildly nonlinear wave applications, and has been derived independently for wind turbine applications [21]. Note that all models yield roughly unbiased results bias factor, B, near 1.0. The 3-moment models generally achieve a sigma reduction of 0.5 or less. Inclusion of the 4th moment, with its attendant uncertainty, leads to higher values of σ_μ and hence sigma reduction factor, SR, closer to one. Figure 2.14 shows the trend in bias and sigma reduction factors, as indicated by the 95% confidence intervals, over longer durations for the Weibull model. Longer duration time histories were obtained by placing the existing 10-minute time histories end to end. By placing all 100 10-minute time histories together in this way resulted in a 1000 minute time history, the maximum duration length available from this data set. The Bootstrap method was used to calculate the 95% confidence intervals [48]. For a prescribed length of time, the required number of 10-minute time histories were selected at random and with replacement from the data set and the observed maximum was recorded. This was done 1,000 times for a specific duration of interest. The 1,000 observations of the duration maximum were sorted and the 25^{th} and 975^{th} ordered values were used to construct the lower and upper bound of the 95% confidence interval, respectively. Both factors, Bias and Sigma Reduction, stay fairly constant over the longer durations.

Figures 2.15 and 2.16 show analogous bias and SR factors for V=20m/s and 14m/s respectively,

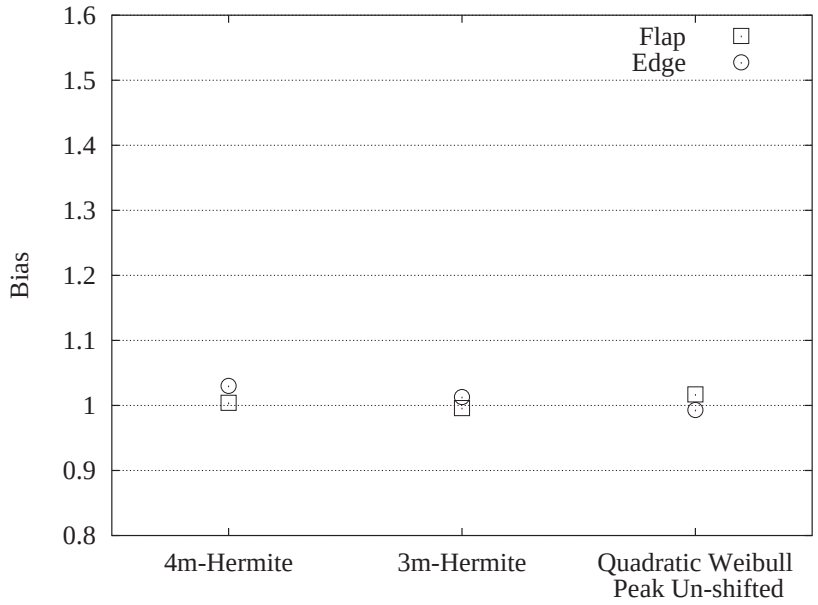

(a) Bias=$\bar{\mu}/\bar{z}$, where $\bar{\mu}$ is the average estimate of the mean 10-minute maximum over the 100 simulations and $\bar{z}$ is the average of the observed 10-minute global maxima.

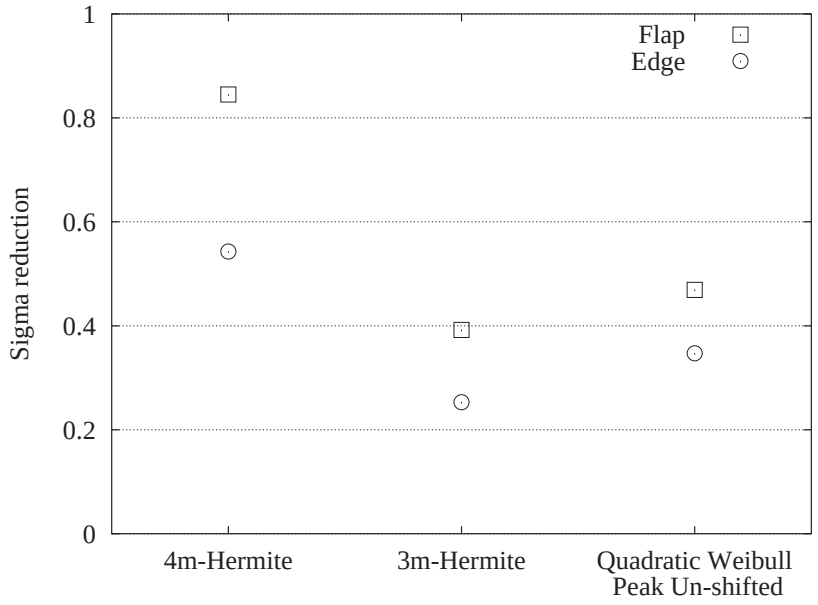

(b) Sigma reduction σ_μ/σ_Z between estimated and observed 10-minute maxima.

Figure 2.13: Bias and sigma reduction factors for three and four moment Hermite models and peak un-shifted quadratic Weibull model, V=45m/s.

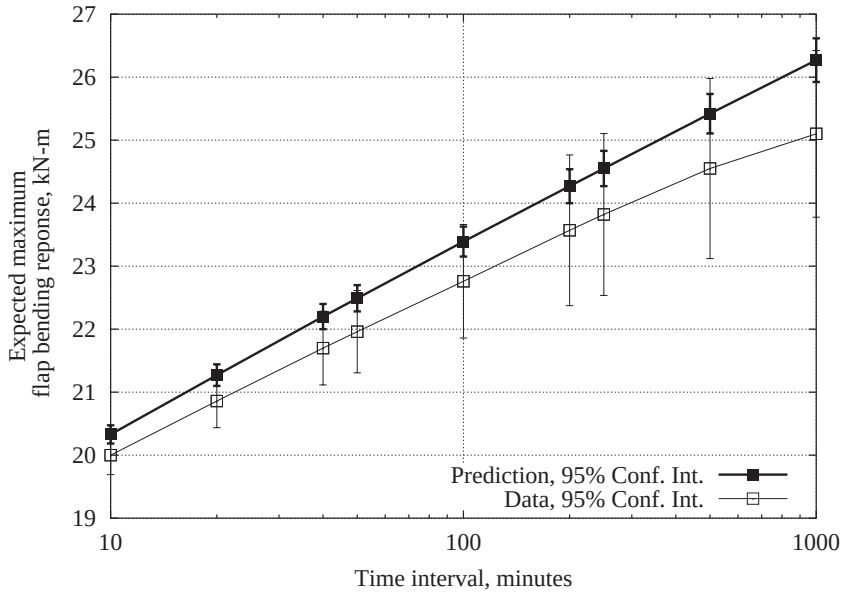

(a) Blade root flap bending

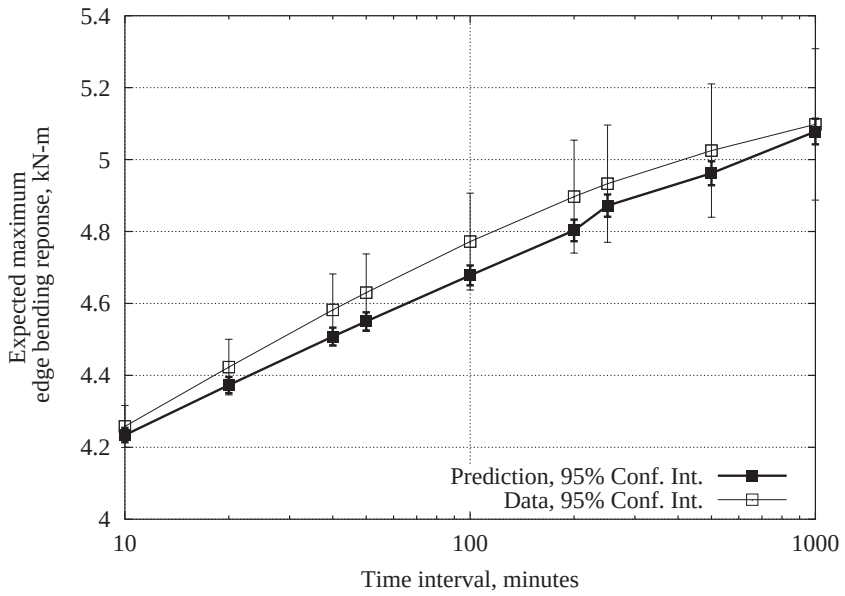

(b) Blade root edge bending

Figure 2.14: Estimated expected maxima over various time intervals, V=45m/s

the operating wind speed conditions. Here the random process (Hermite) models, which are intended to model rather general stochastic behavior, fail to accurately capture the rotating nature of the blade response. Biases of about 10% are found from conventional (4-moment) Hermite models, with considerably larger biases, 30%-50%, produced by the simpler 3-moment Hermite models.

In contrast, the quadratic Weibull models ("Peak" models in Figure 2.15(a) and 2.16(a)) remain essentially unbiased in all cases. For cases of edge loads, models have been fit both to the original data y_i "Un-shifted" and the shifted data $y_i - 1.5$ "Shifted". For this particular choice of duration (T=10-minute maxima), even the un-shifted models appear reasonably accurate. Over longer durations, however, estimates become increasingly tail-sensitive, and the use of the shift has been found more beneficial in avoiding bias. This is reflected in Figures 2.17(b) and 2.18(b), which shows the benefit of including a shift when predicting maxima over a range of T=10–1000 minutes. The shifted predictions are generally unbiased and also retain the roughly 50% sigma reduction, as shown by the 95% confidence intervals in Figures 2.17(c) and 2.18(c). Note that while these predictions with the shift lie below the data, this bias is quite small, e.g., 1.1%-3.2% for the 20m/s wind condition and 0.2%-0.8% for the 14m/s wind condition. Over the durations shown in Figure 2.17(c) the largest bias, B$\approx$1.03, occurs at the largest return period (T=1000 min.). Of course, this is based on only a single "true" observation of the 1000 minute max. In all operating and parked conditions, sigma reductions for these peak models have been found to remain at roughly 0.5 or less.

Note also that when averaging results over N simulations, the standard deviation of an estimated parameter decreases like $\sigma/\sqrt{N}$. Hence, the 50% sigma reduction shown by the quadratic Weibull fit permits a four-fold decrease in the number of simulations. For example, fitting a quadratic Weibull model to N=1 10-minute simulation is roughly equivalent to using the "raw" 10-minute maxima from N=4 simulations.

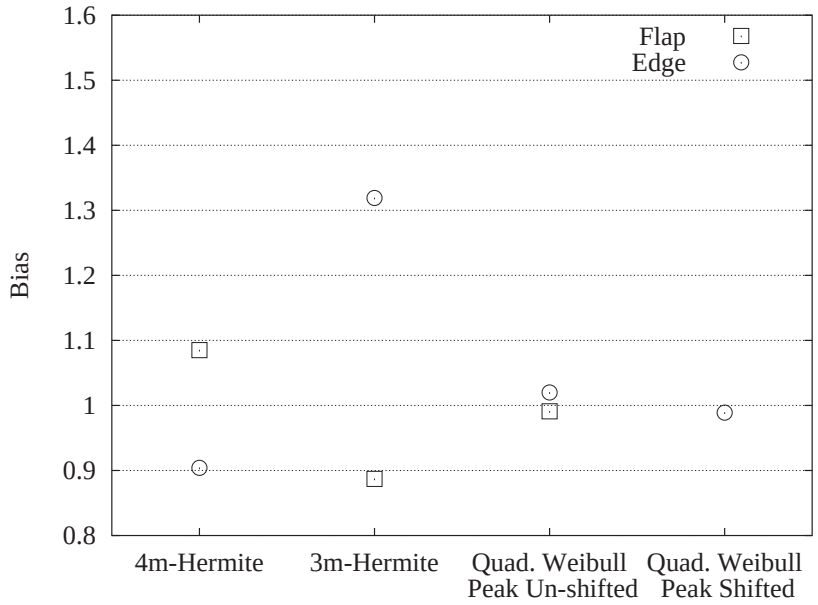

(a) Bias=$\bar{\mu}/\bar{z}$, where $\bar{\mu}$ is the average estimate of the mean 10-minute maximum over the 100 simulations and $\bar{z}$ is the average of the observed 10-minute global maxima.

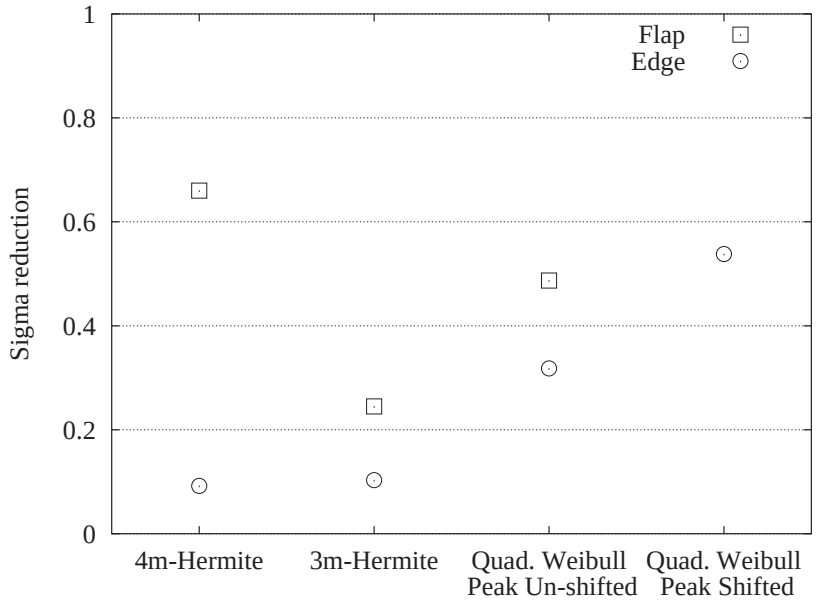

(b) Sigma reduction σ_μ/σ_Z between estimated and observed 10-minute maxima.

Figure 2.15: Bias and sigma reduction factors for three and four moment Hermite models, peak shifted, and un-shifted quadratic Weibull models, V=20m/s.

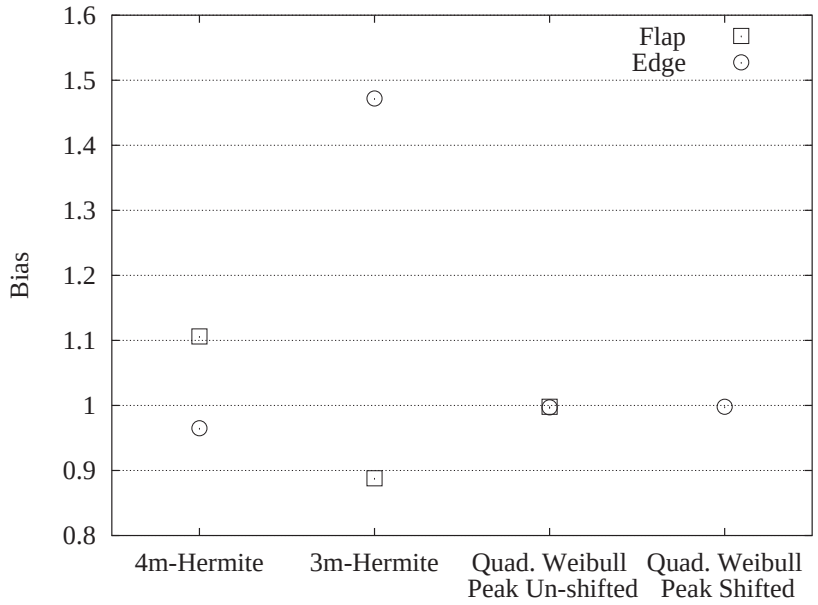

(a) Bias=$\bar{\mu}/\bar{z}$, where $\bar{\mu}$ is the average estimate of the mean 10-minute maximum over the 100 simulations and $\bar{z}$ is the average of the observed 10-minute global maxima.

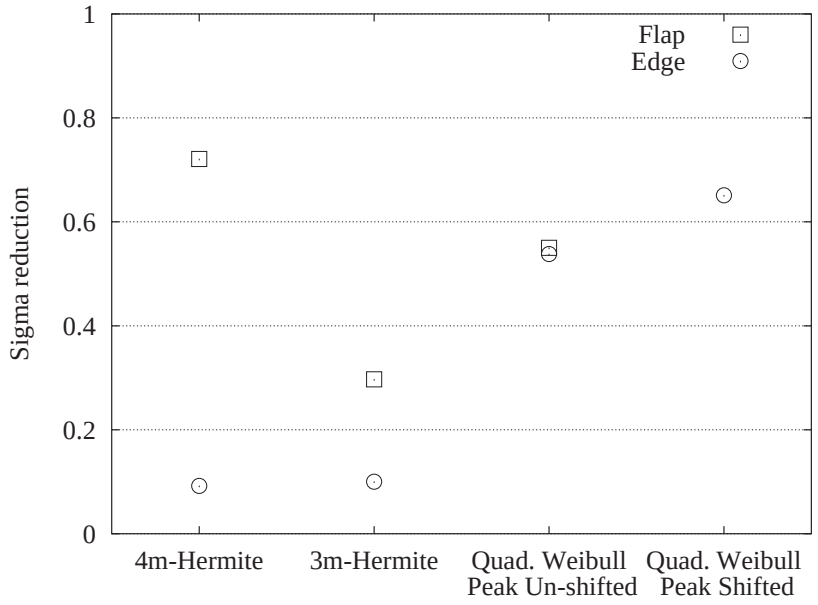

(b) Sigma reduction σ_μ/σ_Z between estimated and observed 10-minute maxima.

Figure 2.16: Bias and sigma reduction factors for three and four moment Hermite models, peak shifted, and un-shifted quadratic Weibull models, V=14m/s.

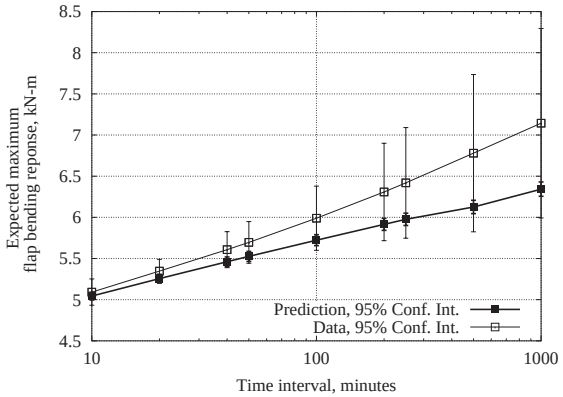

(a) Blade root flap bending: bias and sigma reduction.

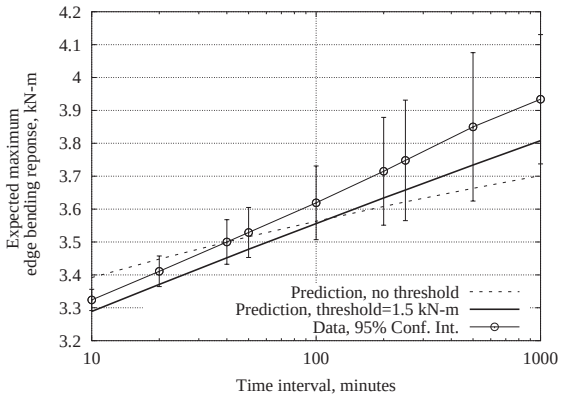

(b) Blade root edge bending: comparison of bias between prediction with and without imposed threshold.

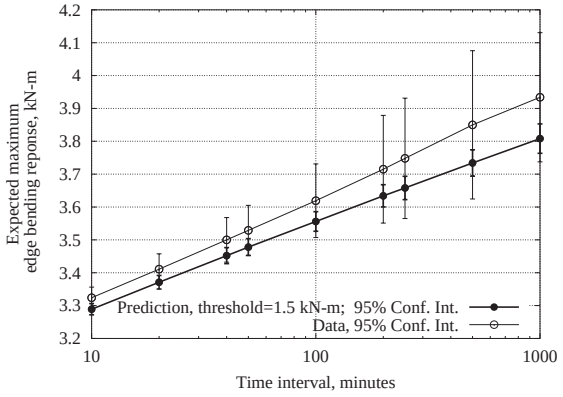

(c) Blade root edge bending: bias and associated sigma reduction of prediction based on model with imposed 1.5kN-m threshold.

Figure 2.17: Estimated expected maxima over various time intervals, V=20m/s

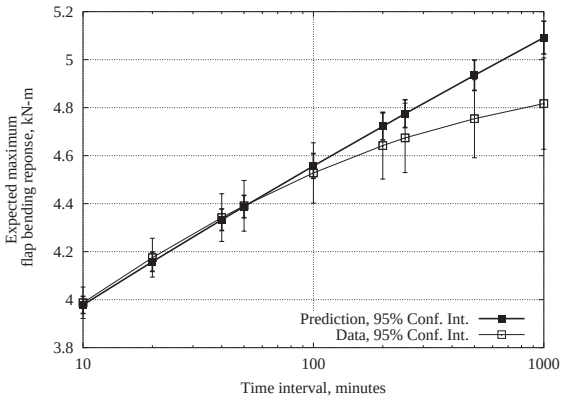

(a) Blade root flap bending: bias and sigma reduction.

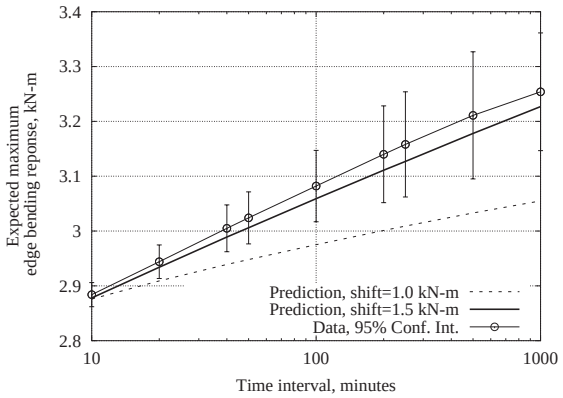

(b) Blade root edge bending: comparison of bias between prediction with and without imposed threshold.

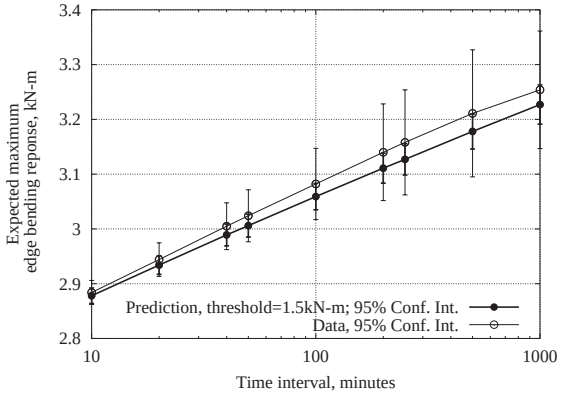

(c) Blade root edge bending: bias and associated sigma reduction of prediction based on model with imposed 1.5kN-m threshold

Figure 2.18: Estimated expected maxima over various time intervals, V=14m/s

2.5 Conclusions

This chapter has demonstrated the use of both random process and random peak models to predict wind turbine loads. In particular, it has applied 3-moment random peak models (quadratic Weibull), and 3- and 4-moment random process models (Hermite). Both the quadratic Weibull and (4-moment) Hermite models are available within MAXFITS[40, 41]. For a parked wind turbine experiencing 50-year winds, all models have been shown to be nearly unbiased, Figure 2.13(a), and to achieve a significant reduction in our uncertainty, Figure 2.13(b) in estimating the mean 10-minute maximum. For rotating blades during operation at lower wind speeds, the random process models can show notable bias: roughly 10% for the 4-moment models, and appreciably more if only 3 moments are used Figures 2.15 and 2.16. In contrast, the random peak models remain consistently accurate, and consistently beneficial (i.e., in reducing uncertainty) in all cases. This suggests that by modeling not the entire time history but rather its set of peaks, enough information about the rotating nature of the load process is retained to permit accurate estimates of extreme behavior.

In chapter 3, the short-term distributions conditional on environmental variables developed here are used to obtain long-term distributions of extreme events. This is achieved by weighting each of the conditional short-term models by the probability of the environmental conditions occurring and integrating over the range of the environmental variables. In particular, the Weibull model of local peaks discussed in this chapter and a Gumbel model of global maxima are used to model the short-term conditional loads. Given a probabilistic description of the long-run statistics of the environment, predictions of the expected annual and 50-year load are obtained. Chapter 3 details a methodology for obtaining these predictions and compares the predictions based on the two different short-term models.

Chapter 3

Prediction of the Long-term Distribution of Extreme Loads[1]

In this chapter we present a methodology for proceeding from the short-term observations of extreme loads to the long-run load distribution of these extreme events, for both flap and edge loading in both operating and parked wind turbine conditions. First, a general approach utilizing full integration, where numerical routines are used to directly integrate the conditional short-term load distribution over the annual occurrence of wind speeds and turbulence intensities, is presented. Then, starting from this general approach, a qualitative analysis is undertaken to explore the extent of the contribution of each of the three variables, in the governing equation, to the variability in the long-term extreme load distribution. From this analysis, lower order models are considered, where instead of using the entire distribution of the variables, a constant fractile of the short term extreme load distribution, turbulence intensity distribution, or both are used. Finally, recommendations are given to guide the analyst to decide when simpler, yet robust, methods which account for sufficient variability in the extreme load event may be employed with confidence.

3.1 Introduction

This chapter presents methods for calculating the long-term distribution of extreme loads. In Chapter 2, several moment-based models were presented which estimate short-term load distributions of the extremes from limited data. Continuing from this previous work, this current chapter explores methods for calculating the long-term load distribution, from the short-term statistics.

[1] A portion of this chapter was previously published in the American Society of Mechanical Engineering's Journal of Solar Energy Engineering [49]

In applying probabilistic models to design wind turbines, a number of practical challenges remain. One question concerns *how* a particular probability model may be used to satisfy design requirements as specified, for example, in wind turbine standards [39]. In particular, due to the wind turbine's complex dynamic behavior, an analyst may need to rely on a set of limited-duration load histories over a range of wind conditions. These histories may result either from measurements on prototype machines or from numerical simulation. In either case, there is a fundamental question as to how one can proceed from these *short-term* load observations to specification of appropriate *long-term* loads, as required in design codes.

In this chapter a methodology is presented for proceeding from the short-term observations of extremes to the long-run load distribution of these extreme events, for both flap and edge loading in both operating and parked wind turbine conditions. First, a general approach utilizing full integration, where numerical routines are used to directly integrate the conditional short-term load distribution over the annual occurrence of wind speeds and turbulence intensities is presented. Then, starting from the general problem where the entire distribution of the three random variables (extreme load, wind speed, and turbulence intensity) is considered, a qualitative analysis is undertaken to explore less complex models. The lower-order models consider using, instead of the entire distribution, a constant fractile of the short-term extreme load distribution, turbulence intensity distribution, or both. This results in reducing the problem from a three-fold integration over extreme event, turbulence, and wind speed to a single-fold integration, in the most reduced form, over only the annual distribution of mean wind speed. Here, the efficacy of these lower-order models to account for a sufficient portion of the variability, while reducing the necessary computations is examined. Finally, recommendations are given to guide the analyst to decide when simpler, yet robust, methods which account for sufficient variability in extreme load event may be employed with confidence.

The approach described above is conducted considering two alternatives for modeling the short-term load. In Section 3.4, an estimate of the long-term distribution of the extreme load is obtained where the short-term load is based on modeling the 10-minute extreme load, or global peak, by a Gumbel distribution. Alternatively, in Section 3.5, an estimate of the long-term distribution of the extreme load is obtained where the short-term load is based on modeling the random peaks with a quadratic Weibull model. The latter is similar to the short-term load analysis conducted in Chapter 2. We will show that the estimate of the long-term distribution of extreme loads based on modeling the random peaks is unbiased when compared to the estimate of the long-term distribution of extreme loads based on modeling the global peaks.

3.2 Estimating Long-Term Design Loads from Short-Term Histories

In Chapter 1 a discussion was presented which introduced how the load modeling problem has been divided into two parts. The first part being turbine specific and the second portion being site specific, i.e., related to the environment where the turbine will be located. We return to this discussion to provide more specific details how, once we have a description of the response of the turbine, we may proceed to generate estimates, as required by the design specifications, of the long-term extreme events on the turbine.

In general, Load Resistance Factor Design (LRFD)[9] code requirements typically compare a nominal load and resistance, $\mathcal{L}_{\text{nom}}$ and $\mathcal{R}_{\text{nom}}$, weighted respectively by factors $\gamma_{\mathcal{L}}$ and $\phi_{\mathcal{R}}$ chosen to achieve a desired reliability level:

$$\phi_{\mathcal{R}}\mathcal{R}_{\text{nom}} \geq \gamma_{\mathcal{L}}\mathcal{L}_{\text{nom}} \tag{3.1}$$

The nominal values $\mathcal{L}_{\text{nom}}$ and $\mathcal{R}_{\text{nom}}$ are commonly defined somewhat conservatively, relative to the mean load and resistance, e.g., $\mathcal{L}_{\text{nom}}$=l_N=the N-year load. Here l_N is a specific fractile of L_T, which is a random variable describing the maximum load over an interval of length T, such that the *annual* probability of exceeding l_N is $1/N$. This relationship is formally defined below.

In particular, one proposed wind turbine design check applies the 50-year wind to a parked turbine [23]. This suggests that other checks be made to ensure that this condition is satisfied with $\mathcal{L}_{\text{nom}}$=l_{50}, the 50-year *load*, which may not always coincide with the 50-year wind speed. For example, l_{50} may more likely be caused in some cases by turbines operating at lower (but more frequently occurring) wind speeds. Shown in this section is how one may consistently estimate l_{50}, properly accounting for randomness in the environmental conditions.

As noted above, it is common that the wind turbine analyst may have only limited-duration load histories—formally, observations of L_T, the maximum of the load process, $x(t)$, over a duration T much less than 50 years:

$$L_T = \max_{0\leq t\leq T} x(t); \quad T \ll 50 \text{ years} \tag{3.2}$$

Of course, as was seen in Chapter 2, there may be an advantage to modeling something other than the global maximum over duration T, e.g., the local peaks in duration T. The following development is based on modeling the global extreme. Section 3.5 will show how an estimate of the 50-year load is found using local peaks instead.

The 50-year load, l_{50}, is then commonly defined, as mentioned earlier, as a specific *fractile* of L_T, i.e., a maximum value with a prescribed probability of exceedance:

$$P[L_T > l_{50}] = \frac{T}{50} \quad T \leq 1\text{year} \tag{3.3}$$

Here, $P[\cdot]$ denotes the probability that the bracketed statement occurs. For example, with T=1 year Equation 3.3 states that the annual maximum load, $L_{1\text{ year}}$, exceeds l_{50} with probability 1/50=0.02.

Significantly, because of the small probabilities involved, the analysis is relatively insensitive to the precise choice of T. Specifically, Equation 3.3 will return virtually the same l_{50} value for all $T < 1$ year; e.g., by seeking the monthly maximum with exceedance probability .02/12, the daily maximum with exceedance probability .02/365, and so forth. Therefore, in practice, one typically reduces T to a duration during which the load process can be considered *stationary*. For wind applications, seasonal, synoptic, and diurnal variations in the wind statistics make monthly, weekly, daily, or hourly values different from annual values. These conditions result in a selection of a reference time period during which the underlying environmental processes (here, the wind speed and turbulence intensity) can be considered to remain in a statistically steady-state condition. This reference time period is less than one hour and may commonly be taken as T=10 minutes.

More formally we can obtain an estimate of the 50-year load from the long-term distribution of the extreme loads in an arbitrary 10-minutes, $F_{L_{10\text{ min}}}$, assuming independence between 10-minute observations and considering the annual long-term distribution of the extreme load, $F_{L_{1\text{ year}}}(l)$, by

$$F_{L_{1\text{ year}}}(l) = \{F_{L_{10\text{ min}}}(l)\}^N \tag{3.4}$$

$$= \{1 - G_{L_{10\text{ min}}}(l)\}^N \tag{3.5}$$

where N is the number of 10-minute segments in 1-year and $G_X(x)$ is the complimentary cumulative distribution function, $G_X(x) = 1 - F_X(x)$. Taking the Taylor series expansion of the right-hand side of Equation 3.5 yields,

$$F_{L_{1\text{ year}}}(l) \approx 1 - NG_{L_{10\text{ min}}}(l) + \frac{N(N-1)}{2!}(G_{L_{10\text{ min}}}(l))^2 - \cdots \tag{3.6}$$

$$G_{L_{1\text{ year}}}(l) \approx NG_{L_{10\text{ min}}}(l) - \frac{N(N-1)}{2!}(G_{L_{10\text{ min}}}(l))^2 + \cdots \tag{3.7}$$

For small values of $G_{L_{1\text{ year}}} \lessapprox 0.1$, a first-order approximation may be obtained by ignoring the higher order terms,

$$F_{L_{1\text{ year}}}(l) \approx 1 - NG_{L_{10\text{ min}}}(l) \tag{3.8}$$

$$1 - F_{L_{1\text{ year}}}(l) \approx NG_{L_{10\text{ min}}}(l) \tag{3.9}$$

$$G_{L_{1\text{ year}}}(l)) \approx NG_{L_{10\text{ min}}}(l) \tag{3.10}$$

Considering these assumptions above, an estimate of the 50-year load can be obtained from the

long-term distribution of extreme loads for an arbitrary 10-minutes by,

$$G_{L_{1\text{ year}}}(l_{50})) = \frac{1}{50} = 0.02 = NG_{L_{10\text{ min}}}(l) \tag{3.11}$$

$$G_{L_{10\text{ min}}}(l_{50}) = \frac{1}{50N} \tag{3.12}$$

for which Equations 3.12 or 3.3 yield the probability level associated with l_{50} as

$$P[L_{10\text{ min}} > l_{50}] = \frac{10}{50 \times 365 \times 24 \times 60} = 3.8 \times 10^{-7} \tag{3.13}$$

Similarly, for the probability level associated with the 1-year maximum, $l_{1\text{ year}}$, Equations 3.12 and 3.3 yield:

$$P[L_{10\text{ min}} > l_{1\text{ year}}] = \frac{10}{1 \times 365 \times 24 \times 60} = 1.9 \times 10^{-5} \tag{3.14}$$

By reducing T from 50 years (or 1 year) to 10 minutes, we gain the important advantage that the wind speed process remains in a steady state, characterized by V, the mean speed during that 10 minute duration. We may then perform a set of steady-state simulations at various mean wind speeds, V, calculate the conditional exceedance probability, and weight their results by $f_V(v)$, the long-term probability density of V at the site of interest, yielding:

$$P[L_{10\text{ min}} > l] = \int_{all\ v} P[L_{10\text{ min}} > l \mid v\ ] f_V(v) dv \tag{3.15}$$

Note that Equation 3.15 separates the calculation of l_{50} into the need to provide two separate terms, which respectively describe the turbine (independent of the site) and the wind conditions at the site:

Turbine-specific term: $P[L_{10\text{ min}} > l \mid v\ ]$ denotes the probability that a 10-minute maximum load exceeds a given level l, given a prescribed mean wind speed $V = v$. This is commonly known as the *short-term* problem.

Site-specific term: The remaining term on the right side of Equation 3.15, $f_V(v)dv$, defines the fraction of time the wind speed at the site lies between v and $v + dv$. In the wind turbine community it is common to choose a Rayleigh probability density form for $f_V(v)$, with mean dependent on site conditions. In general, this wind speed distribution may be found from site-specific data, or specified for design purposes by wind turbine standards (e.g., wind turbine classes I–IV [23]).

In summary, the 50-year load is calculated by first solving the short-term problem—that is, estimating $P[L_{10\text{ min}} > l \mid v\ ]$ across a range of l for various mean speeds v. These results are

combined with $f_V(v)$ through Equation 3.15, and l_{50} found as the l value returning the required probability level in Equation 3.13.

Note also that Equation 3.15 is readily modified if the wind process is instead characterized by another parameter such as turbulence intensity I—replacing V by I—or by a two-dimensional integration if both V and I are deemed to significantly help explain the observed variations in loading. In this case Equation 3.15 would become

$$P[L_{10\,\text{min}} > l] = \iint P[L_{10\,\text{min}} > l \mid v, i\,] f_{I|V}(i|v) f_V(v) di dv \tag{3.16}$$

Where now the turbine specific problem is conditioned on both V and I and the long-term probability density of turbulence intensity is conditional on V, denoted by, $f_{I|V}(i|v)$. It should be noted that both V and I usually refer to a specific height above the ground; e.g., the hub height. Also note, that additional parameters—e.g., those which characterize the vertical wind speed profile—may also be included to better describe the wind climate, and hence better separate the turbine-specific and site-specific terms.

Two challenges remain. First, to estimate the probability distribution of the maximum load, e.g., the 10-minute maximum, $L_{10\,\text{min}}$, given the environmental parameters. This was discussed in Chapter 2 and by others in the literature [38, 47, 50]. Second, solving Equation 3.16, the long-term integration problem. The latter is the focus of this chapter. Also, a discussion is presented on the significance of the environmental variables to describe the long-run variations in the loading. The work of Ronold et al. [51] has addressed a similar question assessing the probability of failure of a wind turbine rotor blade subjected to flap-wise bending during operating wind conditions, over the turbine's lifetime of 20-years. In this work, a random process model was used to model the short-term flap-wise loads, and the long-term integration was solved using an iterative first-order reliability analysis approach. The results were later used to develop appropriate partial safety factors to be applied to the characteristic load and material strength values for design of the turbine. In this chapter we address both edge and flap bending loads in both operating and parked turbine conditions; here the short-term loads are modeled using random peak models and the long-term integration is performed using numerical methods. Also, note that the paper by Fitzwater and Winterstein [38] explores the efficacy of random process models and random peak models to retain sufficient information about the load process to permit accurate estimates of extreme behavior.

In what follows in this chapter we step through the process from initial simulation runs to a final estimate of, $P[L_{10\,\text{min}} > l]$, the marginal distribution of $L_{10\,\text{min}}$. Later in Sections 3.4 and 3.5, options are discussed for simplifying Equation 3.16 considering the variability in the conditional loads and the environmental variables.

3.3 Data Set

The data set used in this analysis was for the Atlantic Orient Corporation AOC 15/50 turbine as described in Section 1.4.2 The data set consisted of multiple 10-minute simulations of Gaussian wind fields and corresponding in- and out-of-plane blade root bending moments on the AOC 15/50 horizontal axis wind turbine. The wind input processes are described by the hub height wind speed. The turbine has a rotor diameter of 15m, a fixed rotor speed of about 60 RPM, and a rated wind speed of 12m/s. It is a three-bladed, fixed pitch turbine with a hub height of 25 meters [22]. In this chapter, flap and edge bending terms refer to out-of-plane and in-plane bending, respectively.

One hundred 10-minute simulations have been performed for various choices of wind speed and turbulence class with different random seed values. The simulations were carried out using YAWDYN, an aerodynamics and dynamics analysis code for wind turbines [20]. Target 10-minute mean wind speeds, in the operating regime of the turbine were chosen from 10m/s to 24m/s in 2m/s increments. Simulations were run at each wind speed considering both class A and class B IEC turbulence classes [23]. Also, pseudo-parked conditions (turbine slowly idling) were run for both turbulence classes, with target 10-min mean wind speeds of 24, 30, 40, and 50m/s. The original data set only contained time histories corresponding to the 50m/s environmental condition. The remaining pseudo-parked conditions were later added to the data set. A plot of observed turbulence intensity versus observed mean 10-minute wind speed, calculated from the simulation data, for all 2,400 10-minute time histories is shown in Figure 3.1. It may appear from Figure 3.1 that there is significantly more scatter in the observed turbulence intensity than in the observed 10-minute mean wind speed. The coefficient of variation of the observed 10-minute mean wind speed is approximately 0.1-0.2%, while the coefficient of variation of the observed turbulence intensity is also small at approximately 2-3%. Also, as seen in Figure 3.1, a bias is present between the observed turbulence intensity calculated from the time histories, (at the hub height of the turbine) and target values of turbulence intensity for a given wind speed, as calculated from the IEC code equations [23]. Based on this result, the observed values for turbulence intensity were used for all subsequent analysis.

An additional comment is required concerning the pseudo-parked conditions. As stated earlier the original data set only contained time histories corresponding to 50m/s wind conditions. This corresponds to approximately the 50-year wind speed. Running a pseudo-parked condition came out of a constraint of the YAWDYN program, which can not simulate blade load responses for a parked turbine, so simulations were run with the turbine very slowly idling, one rotation in ten minutes. This seemed to produce acceptable results for the 50m/s high wind speed case. Later, it became apparent that just the one parked condition was not sufficient to describe the behavior of the parked turbine, so additional environmental conditions were also considered, specifically the 24m/s, 30m/s,

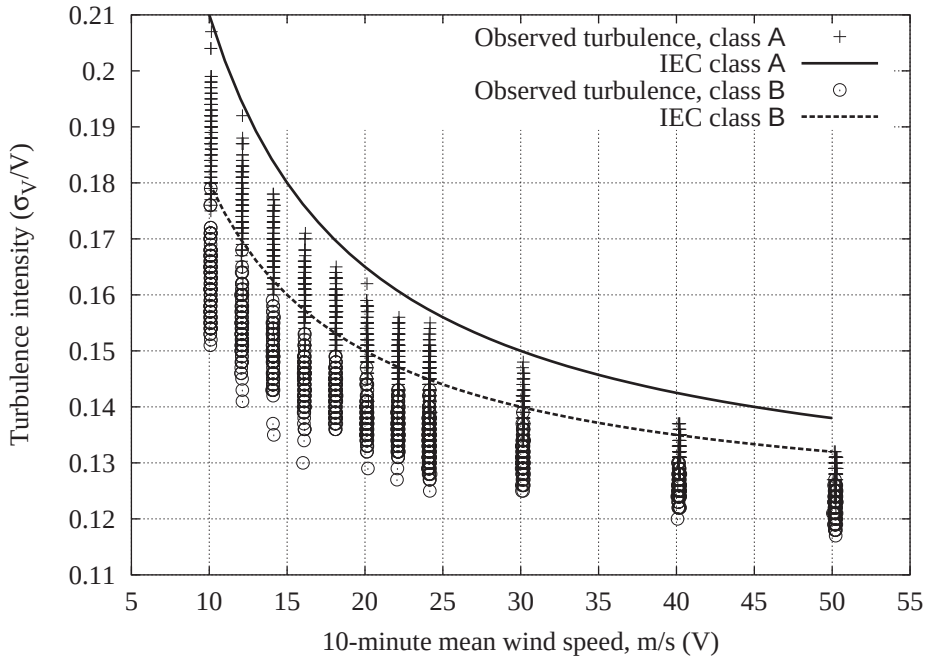

Figure 3.1: 10-minute mean wind speed and turbulence intensity for 2400 10-minute Gaussian wind input processes.

and 40m/s conditions (for both turbulence classes). For these lower wind speeds and specifically the in-plane (i.e., edge) bending (the out-of-plane, flap, bending response was not effected) the variation in the response due to the input simulated wind field was much smaller compared to the gravity cycle introduced by the slowly idling turbine. Presumably, the variation of the response due to the wind field for a parked turbine would be very closely approximated by the simulation where the turbine was slowly idling. The gravity cycle would not occur if the turbine was parked, however. A filtering technique was used to remove the gravity cycle in the edge bending response time histories for the pseudo-parked conditions. The details of how this filtering was performed on the edge bending time histories is presented in Appendix A. Figure 3.2 shows a typical edge bending time history for the 24m/s Class A wind condition before and after filtering. In Figure 3.2(a) one can clearly see the gravity cycle induced by the slowly idling turbine. These gravity cycles, if included, would have artifically inflated the magnitude of the observed global maximum for the edge bending response of the parked turbine.

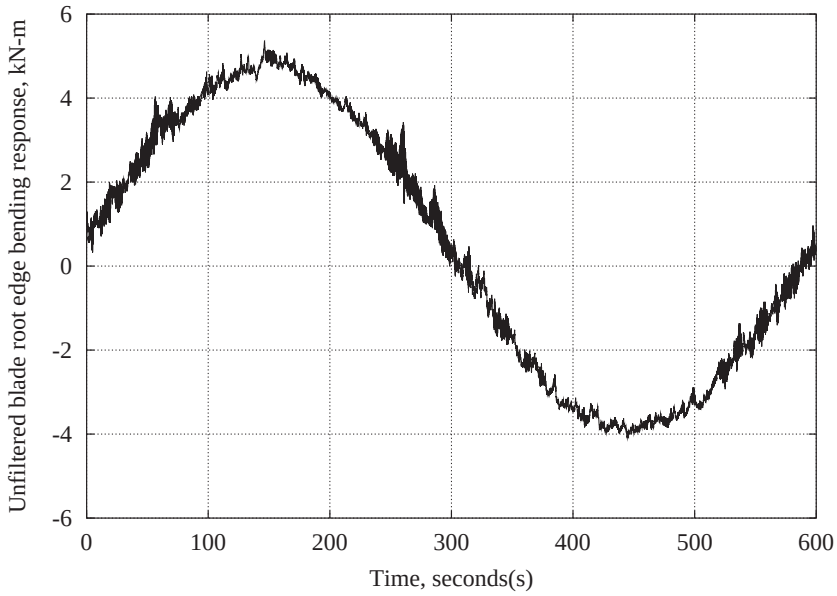

(a) Unfiltered 24m/s parked turbine, blade root edge bending response time history

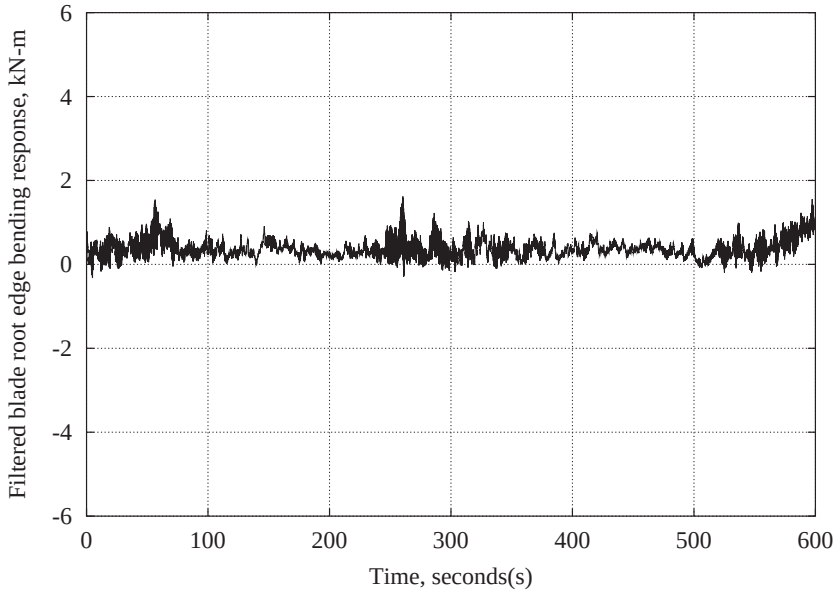

(b) Filtered 24m/s parked turbine, blade root edge bending response time history

Figure 3.2: Unfiltered and filtered time histories of blade root edge bending response for the parked turbine condition in a 24m/s turbulence class A wind environment.

3.4 Long-Term Analysis Based on Modeling Global Extremes

In this section we will step through the process of obtaining an estimate of the marginal probability distribution of the long-term load. We first relate the statistical moments of the global peak data to the environmental variables. A Gumbel distribution of the global peaks can then be obtained for each specific set of values of the environmental variables by the method of moments. Finally, an estimate of the marginal distribution of the long-term load may be obtained by summing the conditional short-term load distributions over all environmental conditions. Each conditional short-term load distribution is weighted by the probability of the associated environmental condition occurring.

3.4.1 Short-Term Analysis

In this section we are interested in estimating the conditional probability distribution of L_T, in time T, given the environmental parameters. Many models, over a number of different time scales, have been discussed in previous work [38]. The simplest of these models is the Global Extreme model or Gumbel model, which seeks to model, Z, the "global" (largest) extreme over duration T. The advantage here is that we work directly with the extreme of interest $L_{10\,\text{min}}$. Also, since we are choosing to model the global extreme directly, we immediately have the desired probability, $P[L_{10\,\text{min}} > l]$ (=$P[Z > z]$), that the maximum value $L_{10\,\text{min}}$ is greater than any l. The drawback is that we discard all time history data below these global maxima. Alternatively, as was discussed in Chapter 2, one could model all the random local peaks. We saw in Chapter 2 that compared with statistics of the global extreme, modeling the local peaks to estimate the expected extreme event provided unbiased results with lower variability.

Here we demonstrate how one can use a Gumbel distribution to model the global (10-minute) extreme events, Z, given values of the environmental variables. Then, based on this short-term model, proceed through a methodology to obtain estimates of the long-term marginal probability distribution of $L_{10\,\text{min}}$. Later in section 3.5, we demonstrate how a quadratic Weibull distribution can be used to model instead the local peaks, Y, given values of the environmental variables. Then, based on this alternate short-term model, we apply the methodology presented here to obtain estimates of the long-term marginal probability distribution of $L_{10\,\text{min}}$. It will be shown, similar to the results found in Chapter 2, that compared with the estimate of the long-term distribution of $L_{10\,\text{min}}$ based on short-term Gumbel model, the estimate of the long-term marginal distribution of $L_{10\,\text{min}}$ based on a short-term quadratic Weibull model is unbiased.

Fitting Distributions to Data

The FITS routine [52, 53] for fitting probabilistic models to data was used to fit a Gumbel model to the observed 10-minute maxima for each pair of environmental conditions: 10-minute mean wind speed, V, and turbulence intensity, I. FITS calculates the central moments from the observed data and then estimates the best model fit of the user-specified distribution type by the method of moments [24, 29]. The FITS routine contains distribution types that preserve up to the first three moments of the observed data. For purposes of the present discussion the first two moments of the observed 10-minute maxima are defined as:

$$\mu_Z = \mathsf{E}[Z] \tag{3.17}$$

$$\sigma_Z^2 = \mathsf{E}[(Z - \mu_Z)^2] \tag{3.18}$$

where $\mathsf{E}[\cdot]$ is the expectation operator. The first central moment is the mean, μ_Z, a measure of central tendency of the data. The second moment is the variance, σ_Z^2, a measure of the spread in the data.[2] Shown in Figures 3.3 and 3.4 are the mean and standard deviation of the 10-minute extreme flap (out-of-plane) and edge (in-plane) response bending moments, based on 100 simulations for each pair of nominal wind speed and turbulence intensity values. The wind turbine is operating for $V < 24$m/s, otherwise the turbine is parked. Parking the turbine will reduce the magnitude of the flap and edge loads.

Comparisons of the fitted Gumbel distributions to the observed response maxima for all simulated wind speeds in turbulence class A are shown in Figures 3.5 and 3.6 for blade root flap and edge bending respectively. In these figures the data and fitted models are plotted on a distorted "Gumbel" scale, which plots the transformed cumulative distribution function(CDF) -ln(-ln($F_Z(z)$)) rather than the standard CDF, $F_Z(z)$. The results should appear as a straight line if the data follow a Gumbel probability distribution model. For clarity the right-hand axis has the corresponding standard CDF probability values. All 100 data values for a given wind speed shown in the figure share the same turbulence class and, therefore, the same nominal turbulence intensity. However, each individual realization will have a different turbulence intensity due to its finite length. Similar results were found for the simulated wind speeds in turbulence class B. Flap bending response data and Gumbel model fit are shown in Figures 3.5(a) and 3.5(b) whereas Figures 3.6(a) and 3.6(b) contain edge bending response data.

[2] A more detailed discussion of expectation and moments of random variables may be found in Section 1.5.1.

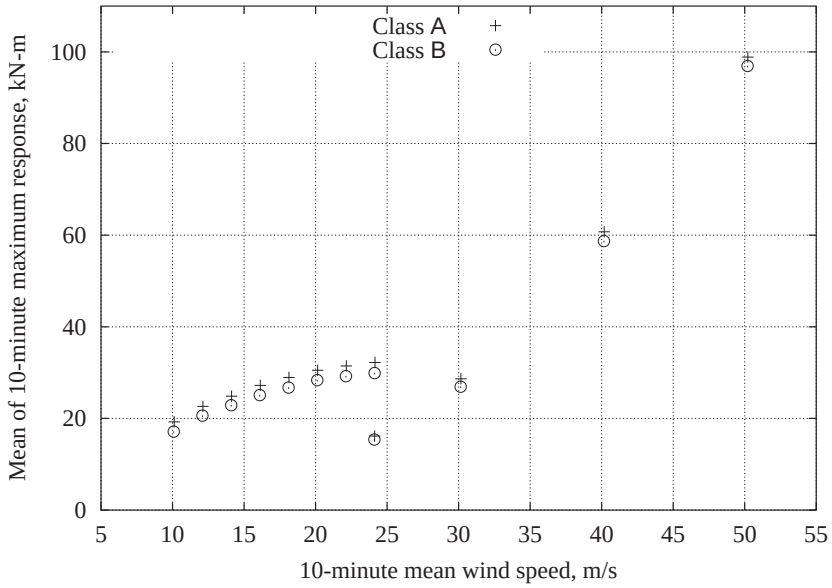

(a) Mean of 10-minute maximum blade root flap bending response.

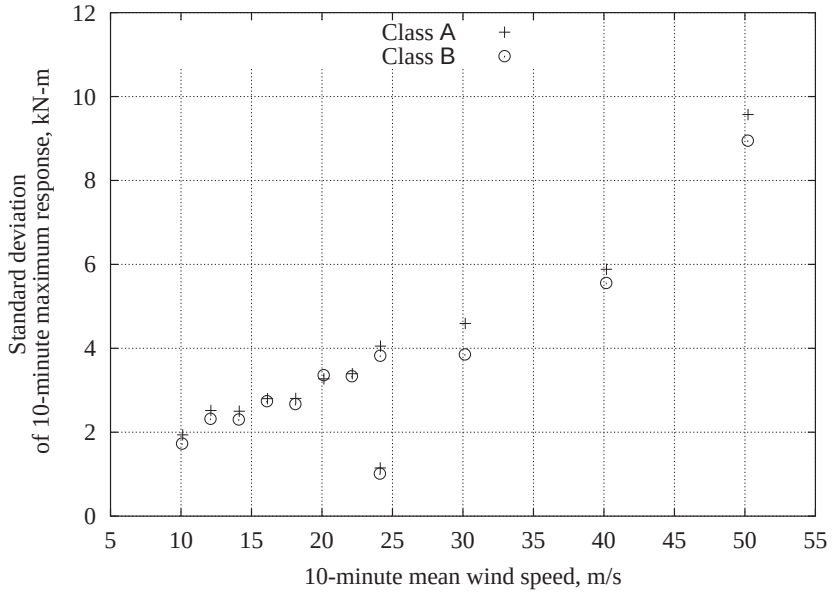

(b) Standard deviation of 10-minute maximum blade root flap bending response.

Figure 3.3: Mean and standard deviation of 10-minute maximum blade root flap bending responses for given 10-minute mean wind speeds. The wind turbine is operating for $V \leqq 24$m/s, otherwise the turbine is parked.

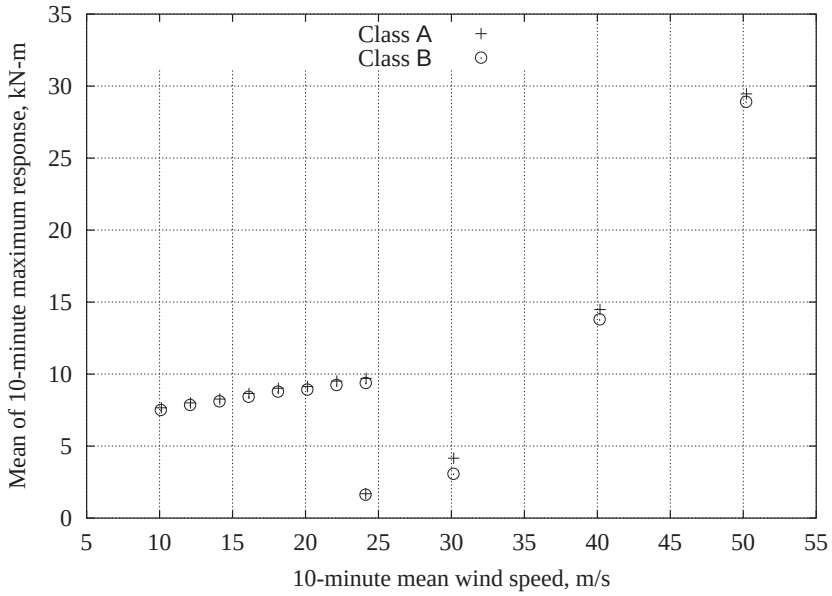

(a) Mean of 10-minute maximum blade root edge bending response.

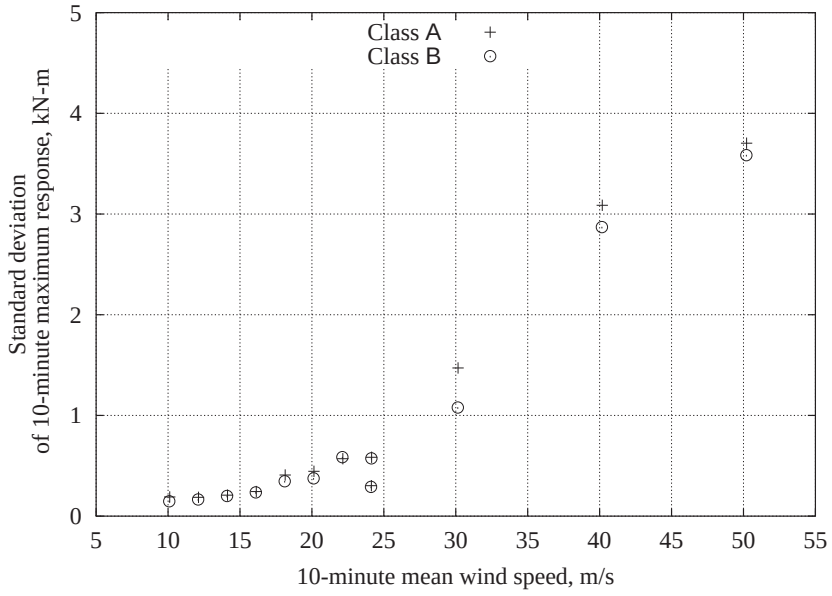

(b) Standard deviation of 10-minute maximum blade root edge bending response.

Figure 3.4: Mean and standard deviation of 10-minute maximum blade root edge bending responses for given 10-minute mean wind speeds. The wind turbine is operating for $V \leqq 24$m/s, otherwise the turbine is parked.

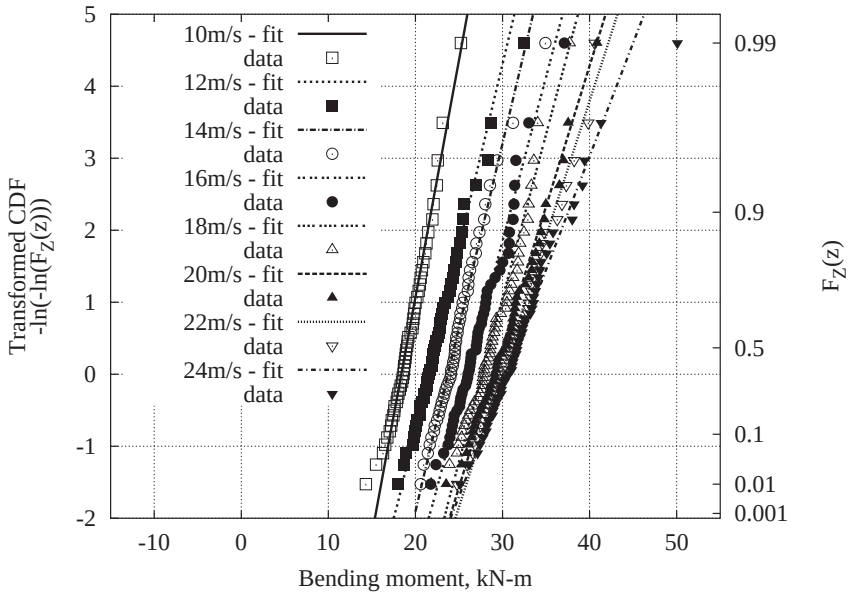

(a) Blade root flap bending moments; operating wind speeds (V <24m/s), turbulence class A.

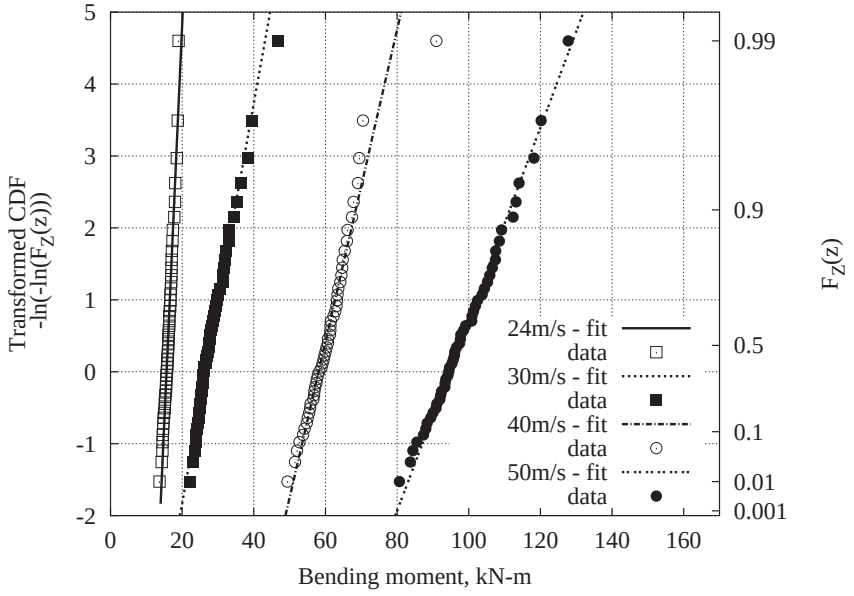

(b) Blade root flap bending moments; parked wind speeds (V >24m/s), turbulence class A.

Figure 3.5: Gumbel fit to observed blade root flap bending data for operating and parked wind speeds, turbulence class A.

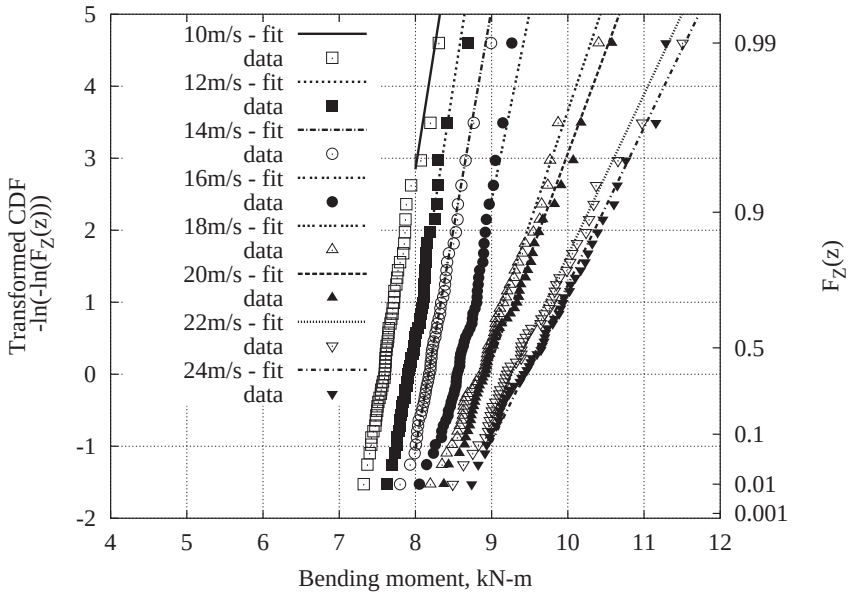

(a) Blade root edge bending moments; operating wind speeds (V <24m/s), turbulence class A.

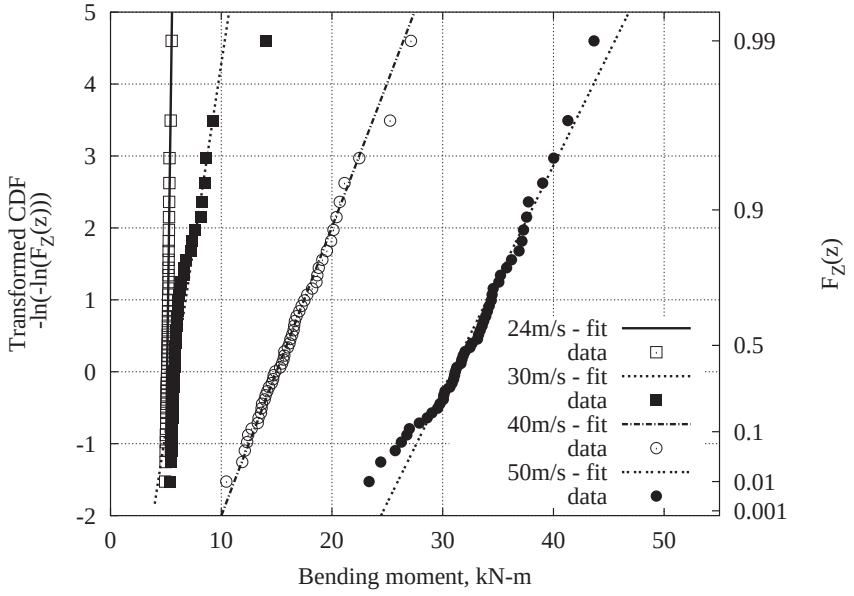

(b) Blade root edge bending moments; parked wind speeds (V >24m/s), turbulence class A.

Figure 3.6: Gumbel fit to observed blade root edge bending data for operating and parked wind speeds, turbulence class A.

Regression

We have established that we can obtain a short-term Gumbel extreme load distribution for the turbine from the first two central moments. Therefore it is sufficient to know the moments over all environmental conditions to completely define the long-term distribution of extreme loading events. Furthermore, regressing the moments over the two environmental variables, 10-minute mean wind speed and turbulence intensity, would give us this relationship between these moments, and therefore the short-term load distribution, and the environmental variables. Also, the regression analysis can assist in understanding the dependence between the environmental variables and the loading as well as the sensitivity of the loading to the environmental variables. Here we relate the statistics which describe the observed wind input process to the statistics of the observed responses of both blade root edge and flap bending. Turbulence class A and class B are considered together. The concept is to develop a functional relationship between the turbine response statistics and the entire environmental space, not a specific class environment. We should note that there is some uncertainty associated with our regression results as we generally do not have observations for all of the points in the environmental space (wind speed and turbulence intensity). This uncertainty is not addressed in this discussion of the long-term analysis but is included in discussion presented in Chapter 6 [38].

There are two distinct general loading conditions for the turbine, one when the turbine is operating and the other while the turbine is parked. Separate regression analyzes were performed under each of these conditions. During 10-minute mean wind speeds below 24m/s the turbine is assumed to be operating. This is not strictly true as there is some minimum speed (cut-in) below which the turbine is parked. For 10-minute mean wind speeds above 24m/s the turbine is assumed to be parked. So, one regression analysis considers the operating loads on the turbine for the regime of operating wind speeds and the other analysis considers parked loads on the turbine during parked wind speed conditions ($V > 24$mps). Based on the observed behavior of the turbine the statistical moments of the response (both blade root flap and edge bending) were assumed to be related to the environmental parameters following the power law function proposed by Veers and Winterstein [54], for both regimes.

$$\mu_j = a_j \left(\frac{V}{V_{\text{ref}}}\right)^{b_j} \left(\frac{I}{I_{\text{ref}}}\right)^{c_j} \quad j = 1, 2 \tag{3.19}$$

For instances where a turbine response of interest exhibited a multi-model behavior, i.e. with more than one peak as a function of wind speed, other model forms would be more appropriate. In Equation 3.19, μ_1 represents the mean and μ_2 represents the standard deviation. V_{ref} and I_{ref} are the reference 10-minute mean wind speed and turbulence intensities respectively. These reference values are calculated from the data as the geometric means of 10-minute mean wind speed and the turbulence. Although the precise choice of V_{ref} and I_{ref} is of little importance, the choice should

Blade Root Flap Bending
Regression of Statistics of 10-Minute Maximum on V and I

Mean of 10-Minute Maximum

	a (kN-m)	b	c	R^2
$V \leqq 24$m/s	25.6643	0.7928	0.7129	0.9682
$V > 24$m/s	37.3040	2.6079	0.6042	0.9985

Standard Deviation of 10-Minute Maximum

	a (kN-m)	b	c	R^2
$V \leqq 24$m/s	2.7760	0.8838	0.4424	0.9322
$V > 24$m/s	3.9338	2.9099	1.4484	0.8745

Table 3.1: Regression coefficients used in Equation 3.19 to fit statical moments of blade root flap bending loads as functions of the mean wind speed, V, and turbulence intensity, I.

Blade Root Edge Loading
Regression of Statistics of 10-Minute Maximum on V and I

Mean of 10-Minute Maximum

	a (kN-m)	b	c	R^2
$V \leqq 24$m/s	8.610	0.3231	0.2084	0.9924
$V > 24$m/s	7.2275	4.1052	0.7718	0.9965

Standard Deviation of 10-Minute Maximum

	a (kN-m)	b	c	R^2
$V \leqq 24$m/s	0.3048	1.9198	1.1430	0.9265
$V > 24$m/s	1.4120	3.5661	1.2761	0.8948

Table 3.2: Regression coefficients used in Equation 3.19 to fit statistical moments of blade root edge bending loads as functions of the mean wind speed, V, and turbulence intensity, I.

be used consistently throughout an analysis. The geometric means have been used here so that the leading regression coefficient (a) will be statistically independent from the other regression coefficients (b and c) in Equation 3.19. The V_{ref} and I_{ref} values for the operating conditions are 16.474m/s and 0.1528, respectively. The corresponding V_{ref} and I_{ref} values for the parked conditions are 34.861m/s and 0.1318, respectively. The calculated regression coefficients and R^2 statistics are shown in Tables 3.1 and 3.2 for flap and edge bending conditions, respectively. R^2 statistics near unity indicate that a large percentage of the variability in the data is explained by the regression model. Low R^2 statistics indicate that other influences not contained in the regression model may affecting the loads.

Finally, graphical regression results are shown in Figures 3.7 and 3.8 for blade root flap and

edge bending respectively. Regression results for the mean and standard deviation of the maximum 10-minute flap bending moment versus 10-minute mean wind speed are shown in Figures 3.7(a) and 3.7(b). Corresponding results for edge bending are shown in Figures 3.8(a) and 3.8(b). In all plots, the turbulence intensity has been set equal to, I_{ref}, the reference value.

3.4.2 Long-term Analysis

In the previous sections we have defined the conditional probability distribution model for the 10-minute maxima and how this model can be represented by the moments of the data. Further, we have just shown, through regression analysis, how these moments may be related to the environmental variables. In this section we demonstrate how we can combine the short-term, turbine-specific portion of Equation 3.16 with the long-run distribution of the environmental variables.

The distribution of 10-minute mean wind speed, V, and the conditional distribution of turbulence intensity are taken from the analysis by Manuel, *et al.*[50] of the MOUNTURB program data at the Lavrio, Greece test site. The 10-minute mean wind speed distribution is assumed to follow a Rayleigh probability distribution with mean[3] μ_V=10m/s:

$$f_V(v) = \frac{2v}{\alpha^2}\exp\left[-\left(\frac{v}{\alpha}\right)^2\right] \tag{3.20}$$
$$\alpha = \frac{2\mu_V}{\sqrt{\pi}}$$

The conditional probability distribution of turbulence intensity given 10-minute mean wind speed is assumed to follow a Gaussian distribution

$$f_{I|V}(i|v) = \frac{1}{\sqrt{2\pi}\sigma_{I|V}}\exp\left[-\frac{1}{2}\left(\frac{i-\mu_{I|V}}{\sigma_{I|V}}\right)^2\right] \tag{3.21}$$

with mean given by,

$$\mu_{I|V} = 2.4486v^{-0.9971} \tag{3.22}$$

and a fixed standard deviation of 0.025. In order to implement Equation 3.16 the ranges of values of the environmental variables are discretized into evenly spaced intervals. A range of 1m/s to 100m/s was considered for the 10-minute mean wind speed in intervals of 0.5m/s. Similarly, a range of approximately six standard deviations of the conditional turbulence intensity was considered, and divided into 100 evenly spaced intervals. For each pair of values of the environmental variables the corresponding short-term load distribution is generated from Equation 3.16. The load distributions

[3] μ_V is also referred to as the annual average 10-minute mean wind speed.

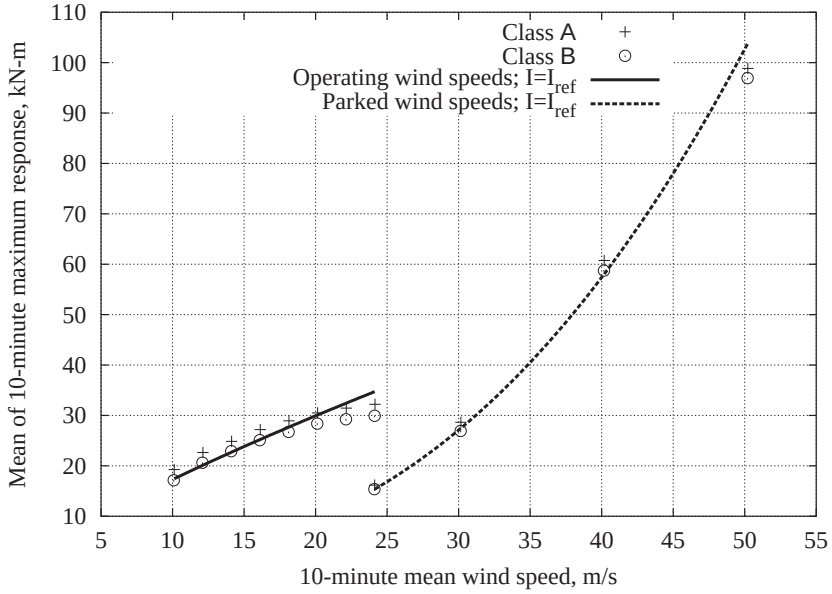

(a) Regression of the mean of 10-minute maxima on the 10-minute mean wind speed and turbulence intensity.

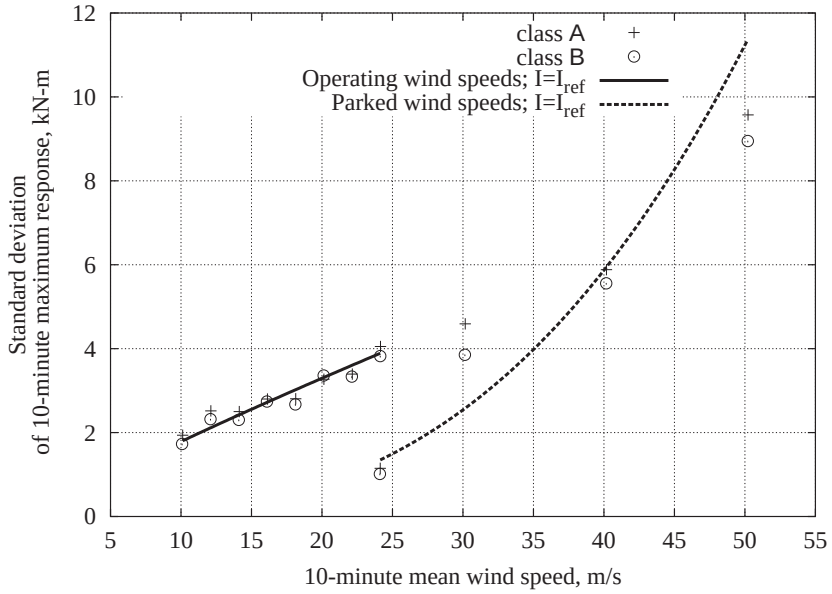

(b) Regression of the standard deviation of 10-minute maxima on the 10-minute mean wind speed and turbulence intensity.

Figure 3.7: Regression of the moments of 10-minute maximum on the 10-minute mean wind speed and turbulence intensity for blade root flap bending.

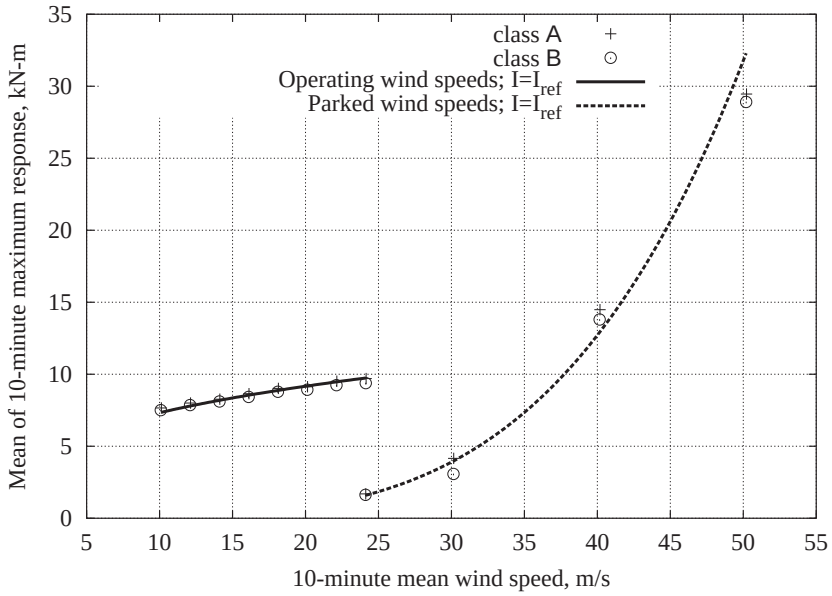

(a) Regression of the mean of 10-minute maxima on the 10-minute mean wind speed and turbulence intensity.

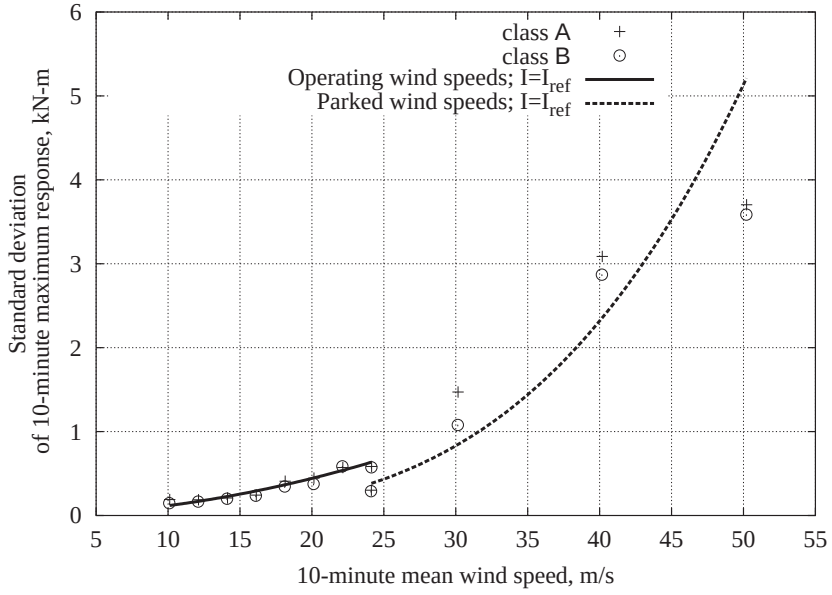

(b) Regression of the standard deviation of 10-minute maxima on the 10-minute mean wind speed and turbulence intensity.

Figure 3.8: Regression of the moments of 10-minute maximum on the 10-minute mean wind speed and turbulence intensity for blade root edge bending.

are summed together; each weighted by the probability of the respective environmental conditions, i.e., probability of the pair of values of the environmental variables occurring. The summation is performed over the entire range of environmental variables.

As stated earlier, there are two loading conditions for the turbine, operating and parked. During normal use the turbine is operating for wind speeds less than 24m/s and parked for wind speeds greater than 24m/s. In this case to develop the long-term distribution the appropriate regression model is used for each wind speed value. For wind speeds below 24m/s the regression relating operating loads is used and, correspondingly, for wind speeds above 24m/s the regression relating parked loads is used. This results in a combination of the operating and parked only long-term distributions as shown in Figure 3.9. Also shown in the figure are the long-term distributions of the load if the turbine is either parked or operating in all wind speeds. The probability levels associated with the one-year and 50-year mean return period (MRP prob. level) are also shown, note Equations 3.13 and 3.14. In all of the preceeding cases it was assumed there was 100% availability of the turbine during all winds speeds. It would require only minor modification to the procedures developed here to include the condition when the turbine was available for only a portion of the time for a given wind environment. Using the full distribution for each of the random variables, estimates for the one-year flap and edge bending load are 49.1kN-m and 11.8kN-m respectively. Correspondingly, estimates for the 50-year flap and edge bending load are 59.7kN-m and 13.7kN-m respectively.

3.4.3 Simplifying the Long-term Analysis

In this section, a methodology for simplifying the calculations required for solving Equation 3.16 is presented. The full distributions of some of the random variables are replaced with appropriate deterministic fractiles, thereby reducing the number of numerical integrations required to be performed. It is appropriate to consider this methodology for those random variables which have only a small contribution to the overall variability in our estimate of the long-term extreme load distribution. Here a qualitative analysis is employed to determine the degree to which each of the variables in Equation 3.16 contributes to the long-term extreme load distribution. Further, based on this analysis we present how an appropriate deterministic fractile of, for example, the short-term load distribution, the conditional distribution of turbulence intensity or both, may be used, instead of their full distributions.

For clarity we first consider the case, as expressed in Equation 3.15, where the wind input process is characterized by only one parameter, the 10-minute mean wind speed, V, and the short-term load is presumed to be deterministic compared with the variability in the long-term distribution of the environmental variable. In this case an important simplification arises if the mean load $\mu_L(V)$

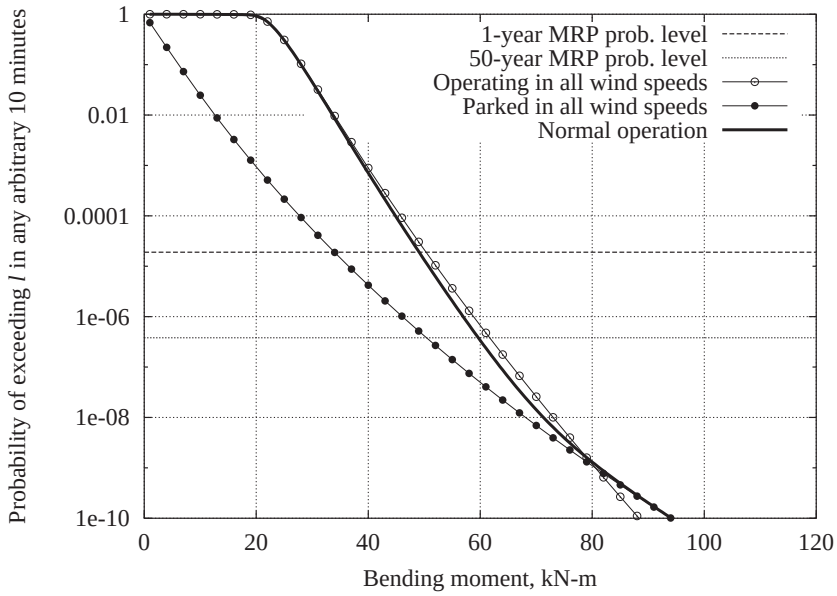

(a) Long-term distribution of extreme blade root flap bending moment for an arbitrary 10 minutes.

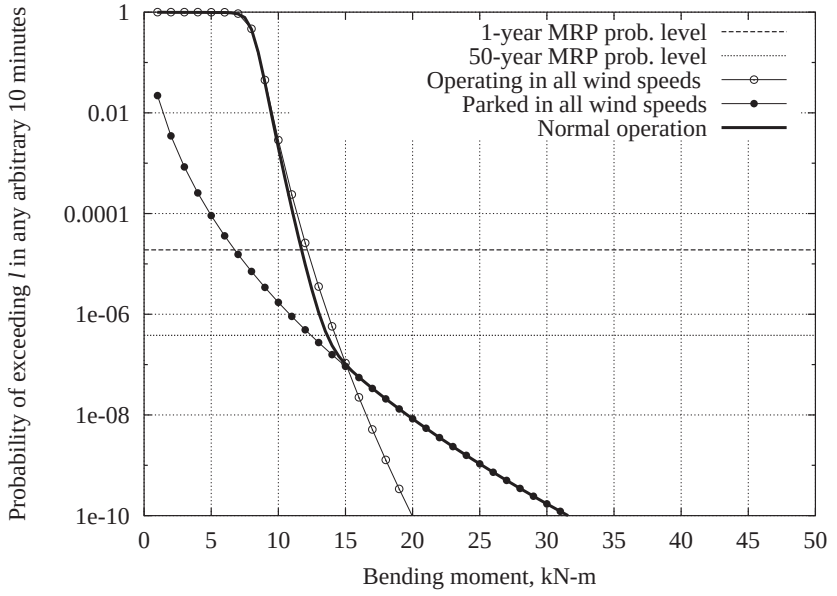

(b) Long-term distribution of extreme blade root edge bending moment for an arbitrary 10 minutes.

Figure 3.9: Long-term distributions of 10-minute extreme blade root bending moment, $L_{10\,\mathrm{min}}$, considering three turbine conditions: 1) turbine operating over all wind speeds, 2) turbine parked over all wind speeds, 3) turbine operating below cutout wind speed and parked above cutout wind speed; for both: (a) flap and (b) edge bending.

grows steadily with V, and the conditional load variability $\sigma_L(V)$ is small compared with the variability in V. Then we may estimate the 50-year load, l_{50}, as simply $\mu_L(V_{50})$, i.e., the mean load in 50-year wind conditions. This is essentially the current design load check for parked turbines (IEC load case 6.1 [23]). Formally, this will be exact in the *deterministic* load limit, i.e., as $\sigma_L(V) \to 0$. More generally it will be somewhat unconservative. In offshore structure design, for example, this unconservatism is noted and commonly adjusted by: 1) inflating the environmental variable (here, the wind speed—to a somewhat higher return period); or 2) inflating the fractile (from p=.5 to p=.80–.90) at which the load is evaluated. These inflation procedures are basically empirical, and have been calibrated with respect to long-term probability analysis (as in Equation 3.16) across many cases [55, 56].

We investigate such simplifications further in the remainder of this section. Figure 3.10 shows the long-term distribution of the 10-minute flap and edge loads for three cases that consider, in turn, the short-term load variable and each of the environmental variables deterministically. Only one variable is considered deterministic in each analysis. The other variables are assumed random and to follow the distributions defined previously. For example, in considering the 10-minute mean wind speed deterministic, i.e. $\sigma_V \to 0$, the mean value of the turbulence intensity as a function of wind speed is evaluated at the annual average wind speed (i.e., the mean value of the distribution of the 10-minute mean wind speed), $\mu_{I|V}(V) \to \mu_{I|V}(\mu_V)$, and the associated standard deviation of the conditional distribution of turbulence intensity is also evaluated at the mean value of the 10-minute mean wind speed $\sigma_{I|V}(V) \to \sigma_{I|V}(\mu_V)$. Similarly, the parameters of the short-term load distribution are evaluated considering the mean value of the 10-minute mean wind speed. From this we obtain the mean of the short-term load distribution as, $\mu_{L|I,V}(I,V) \to \mu_{L|I,V}(I,\mu_V)$ and the corresponding standard deviation as, $\sigma_{L|I,V}(I,V) \to \sigma_{L|I,V}(I,\mu_V)$. The integration over the wind speed is thus avoided. It follows from this discussion how this procedure may be used when considering the other variables, short-term load and turbulence intensity, deterministically. These three analyzes give a qualitative understanding of how the terms in Equation 3.16 contribute to the variability in the long-term load distribution. From this analysis, as shown in Figure 3.10, one would have expected the largest drop in our estimate of the 50-year load, to occur when we considered the variability in the wind speed to approach zero. Whereas, reducing the variability in the short-term load or turbulence intensity would not reduce our estimate of the 50-year load as drastically. This is what has been found in other industries such as the fields of offshore engineering and earthquake engineering. This does not appear to be the case here, however. Qualitatively, one can conclude that, less of the variability in the long-term load distribution is explained by the randomness in the wind speed and turbulence intensity, than by the variability in the short-term load, for the structure, site data, and distribution models used here.

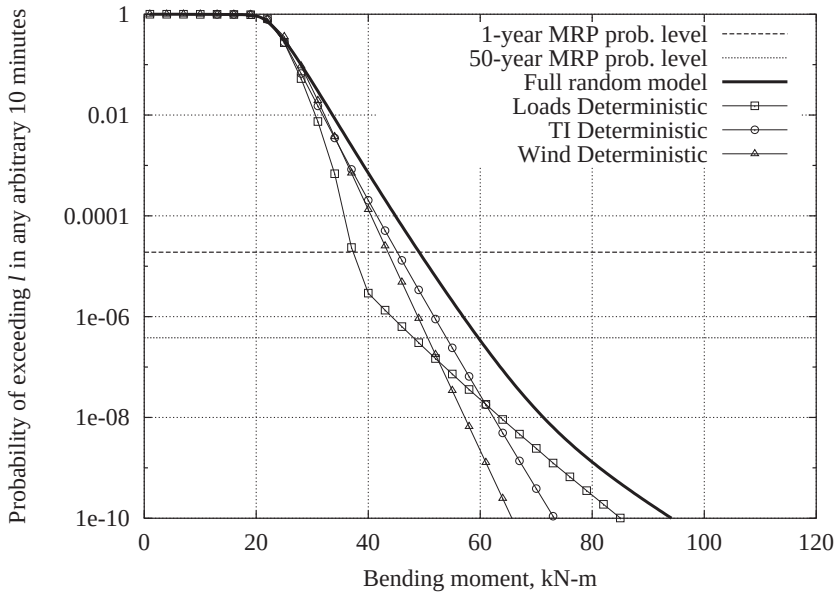

(a) Long-term distribution of extreme blade root flap bending moment for an arbitrary 10 minutes.

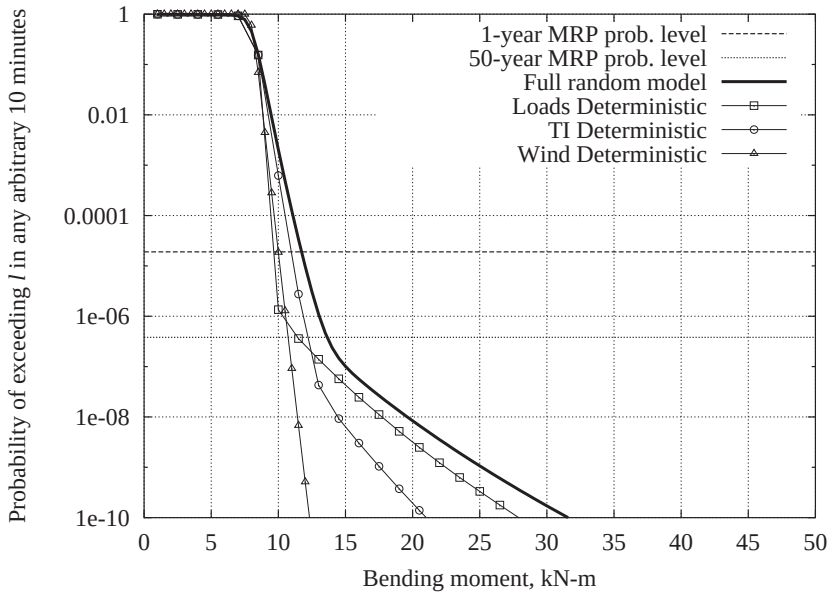

(b) Long-term distribution of extreme blade root edge bending moment for an arbitrary 10 minutes.

Figure 3.10: Long-term distributions of 10-minute extreme blade root bending moment $L_{10\,\mathrm{min}}$, considering load, turbulence intensity, and wind speed deterministically for both: (a) flap and (b) edge bending.

Following the methodology previously presented, we consider using a higher fractile of the turbulence intensity, or wind speed distributions, where we may be able to recover the associated contribution to the long-term load variability, and still achieve the reduced computational effort in calculating an estimate of the marginal distribution of $L_{10\,\text{min}}$. Note that in implementing this methodology to reduce the complexity in obtaining an estimate of the marginal distribution of $L_{10\,\text{min}}$ we resign ourselves to being unable to match the shape of the marginal distribution of $L_{10\,\text{min}}$ if we had considered all three of the variables random. Our focus here is matching the fractiles of the distributions only at the probability levels of interest, i.e., the probability levels associated with the one-year and 50-year return periods. Figure 3.11 shows the result of considering the turbulence intensity deterministic, but using the 84% fractile of the distribution rather than the mean value. Using the 84% fractile of the turbulence intensity distribution results in an estimate of the one-year flap load of 50.1kN-m, an error of 2.4% and an estimate for the one-year edge load of 11.9kN-m, an error of 1.0% with respect to the estimate using the entire distribution for the turbulence intensity. Similarly, considering the 50-year loads, the estimate for blade root flap bending is 60.2kN-m, an error of 0.8%, and the estimate for blade root edge bending is 13.8kN-m, an error of 0.7% with respect to the estimates using the entire distribution for turbulence intensity.

If we continue and consider the 84% fractile, as shown in Figure 3.12(a), rather than the mean value for the distribution of the 10-minute mean wind speed (i.e., the annual average mean wind speed) our estimates for the one-year and 50-year blade root flap bending load are 50.6kN-m,and 59.2kN-m respectively and associated errors of 3.05% and 0.8% for the one-year and 50-year load respectively. Considering the blade root edge bending shown in Figure 3.12(b) the deterministic fractile level needs to increase to 90% to recover an estimate of the one-year load of 11.9kN-m with an error of 1.2%. The fractile of the wind speed distribution must increase further to 95% to recover an estimate of the 50-year blade root edge bending load of 13.8kN-m with an error of 0.7%. If the 95% fractile was used to estimate the annual blade root edge bending load the estimate would be approximately 6% high compared with the estimate based on using the full distributions of turbulence intensity and wind speed.

This analysis, using prescribed fractiles of the distributions of the three variables, could be done based on the assumption that the short-term load contributed the least to the overall variability in the estimate of the long-term distribution, i.e., as we would have expected based on the experience of other industries. In this case Figure 3.13(a) shows the results of considering the short-term load deterministic, but using the 97.5% fractile of the distribution rather than the mean value. Using the 97.5% fractile of the load distribution results in estimates of the one-year and 50-year blade root flap bending load of 48.5kN-m and 60.5kN-m respectively with associated errors of 1.3% for both. Correspondingly the estimates of the one-year and 50-year blade root edge bending loads are

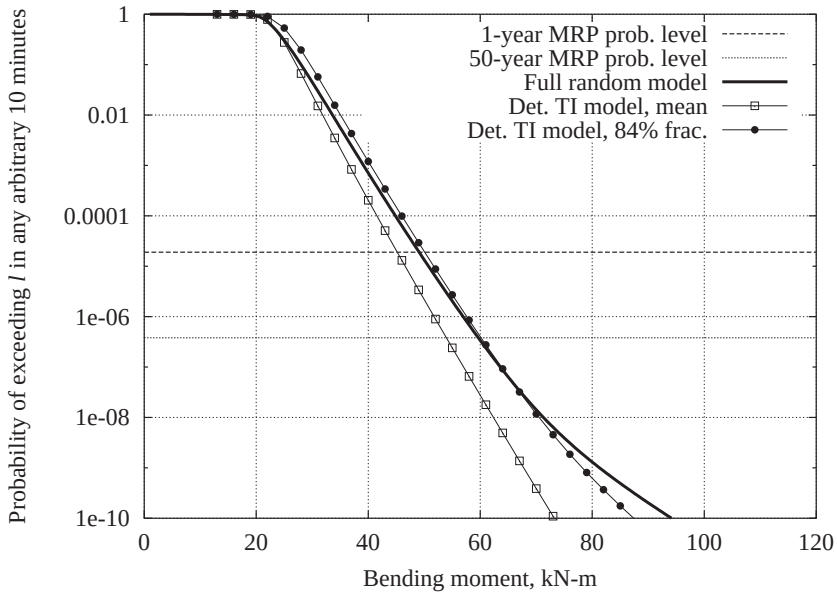

(a) Long-term distribution of extreme blade root flap bending moment for an arbitrary 10 minutes.

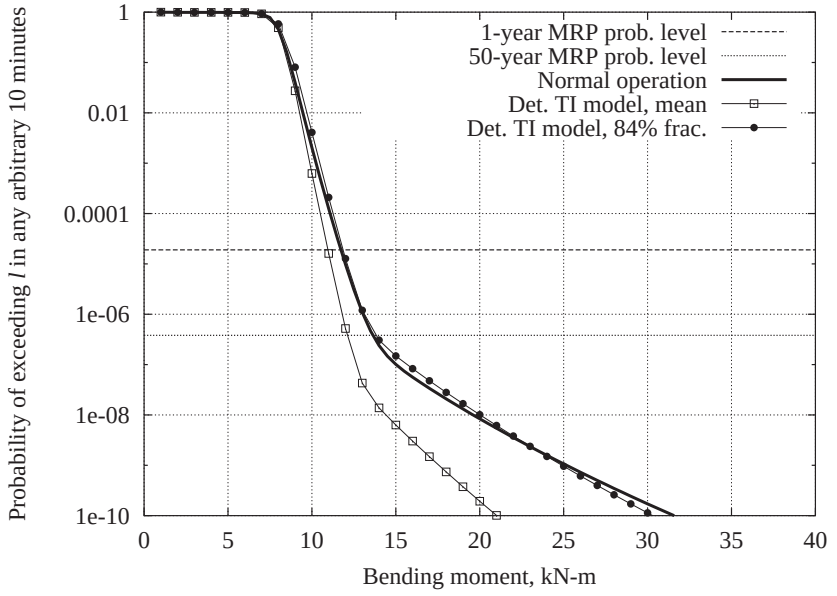

(b) Long-term distribution of extreme blade root edge bending moment for an arbitrary 10 minutes.

Figure 3.11: Long-term distributions of 10-minute extreme blade root bending moment, $L_{10\,\mathrm{min}}$, considering the turbulence intensity at prescribed deterministic levels compared with the full distribution solution; for both: (a) flap and (b) edge bending.

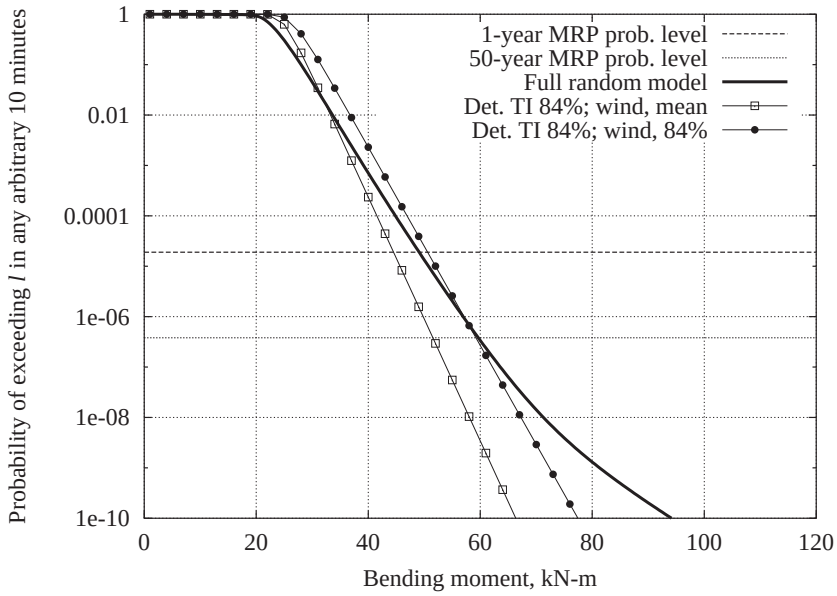

(a) Long-term distribution of extreme blade root flap bending moment for and arbitrary 10 minutes.

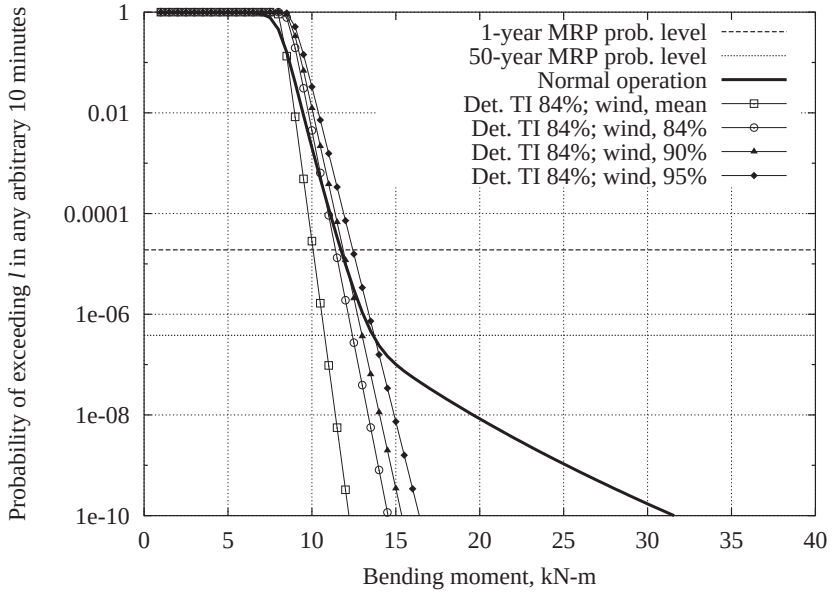

(b) Long-term distribution of extreme blade root edge bending moment for an arbitrary 10 minutes.

Figure 3.12: Long-term distributions of 10-minute extreme blade root bending moment, $L_{10\,\mathrm{min}}$, considering the turbulence intensity at the 84% fractile and 10-minute mean wind speed at prescribed deterministic levels compared with the full distribution solution.

12kN-m and 16.4kN-m respectively with associated errors of 1.5% and 19.9% for the one-year and 50-year loads respectively.

If we continue and consider the 95% fractile, rather than the mean value for the turbulence intensity distribution, as shown in Figure 3.14 the estimates for the one-year and 50-year blade root flap bending loads are 49.8kN-m and 69.3kN-m respectively with associated errors of 0.8% and 16.3% for the one-year and 50-year loads respectively. Correspondingly, the estimates for the one-year and 50-year blade root edge bending loads are 12kN-m and 20.3kN-m respectively with associated errors of 1.7% and 48% for the one-year and 50-year load respectively. It should be noted that using the same fractile level for both flap and edge loading conditions results in tending to over-estimate the 50-year blade root edge bending load, in some cases considerably.

Taking both the short-term load and turbulence intensity as deterministic fractiles of the underlying distributions would simplify Equation 3.16 to a single fold integration problem over only the distribution of annual wind speed. The results of this integration are shown in Figure 3.14. In this case, additionally, we can eliminate the remaining integration by using the complementary cumulative distribution function of the annual wind speed distribution and then evaluate the expression at the wind speed associated with the return period of interest.

3.4.4 Summary

In this section we have stepped through the process of obtaining an estimate of the marginal probability distribution of the long-term load. This was accomplished by modeling the global peaks by a Gumbel distribution for the conditional short-term load. The statistical moments of the global peak data were related to the environmental variables by a power-law functional form. The parameters of the functional form were obtained through regression analysis. Using the method of moments, a Gumbel distribution could be obtained for each specific set of values of the environmental variables. Finally, an estimate of the marginal distribution of the long-term load was obtained by summing the conditional short-term load distributions over all environmental conditions. Each conditional short-term load distribution was weighted by the probability of the associated environmental condition occurring. We found from this analysis that the estimate of the one-year and 50-year blade root flap bending loads were 49.1 kN-m and 59.7 kN-m respectively. Correspondingly the one-year and 50-year blade root edge bending loads were 11.8 kN-m and 13.7 kN-m, respectively.

We then under took a qualitative, yet systematic, analysis to determine which of the three variables—conditional short-term load, conditional turbulence, or mean wind speed—contributed the most to the variability in the distribution of the long-term load. Contrary to what we may have expected, we found that at least for the AOC 15/50 turbine, site data, and distribution models used here the conditional short-term distribution of the loads contributed the most to the variability in

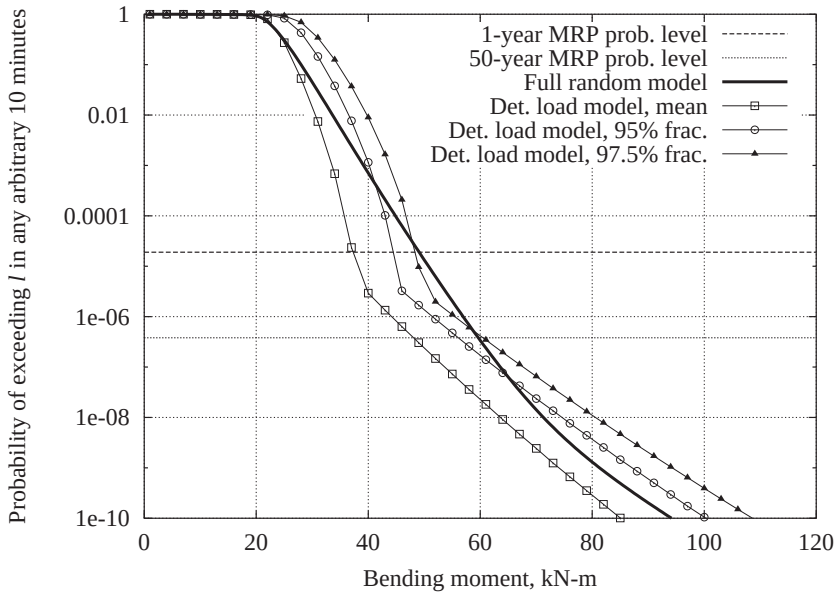

(a) Long-term distribution of extreme blade root flap bending moment for an arbitrary 10 minutes.

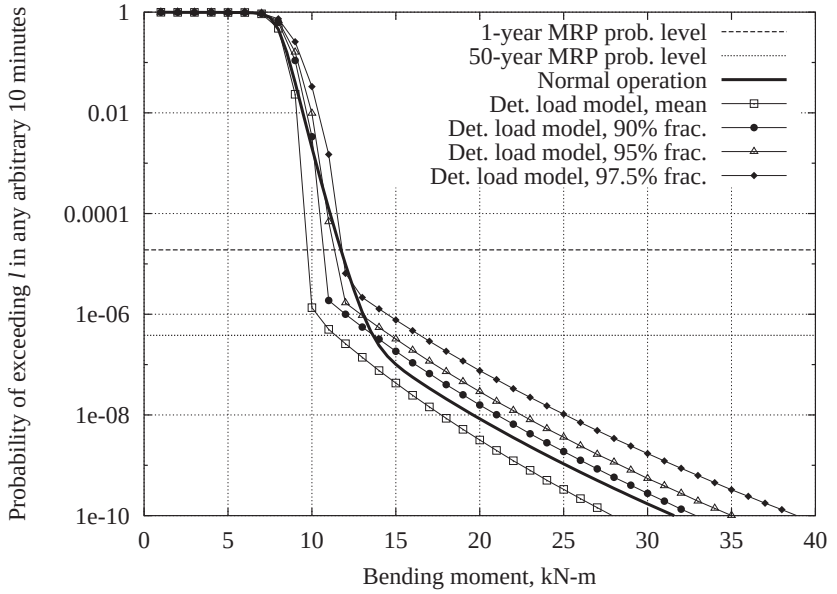

(b) Long-term distribution of extreme blade root edge bending moment for an arbitrary 10 minutes.

Figure 3.13: Long-term distributions of 10-minute extreme blade root bending moment, $L_{10\,\mathrm{min}}$, considering the short-term load at prescribed deterministic levels compared with the full distribution solution.

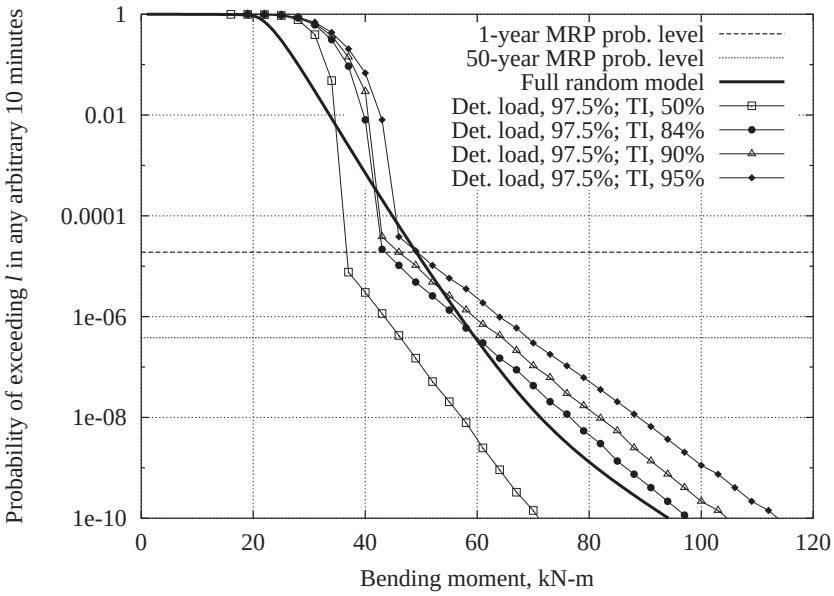

(a) Long-term distribution of extreme blade root flap bending moment for an arbitrary 10 minutes.

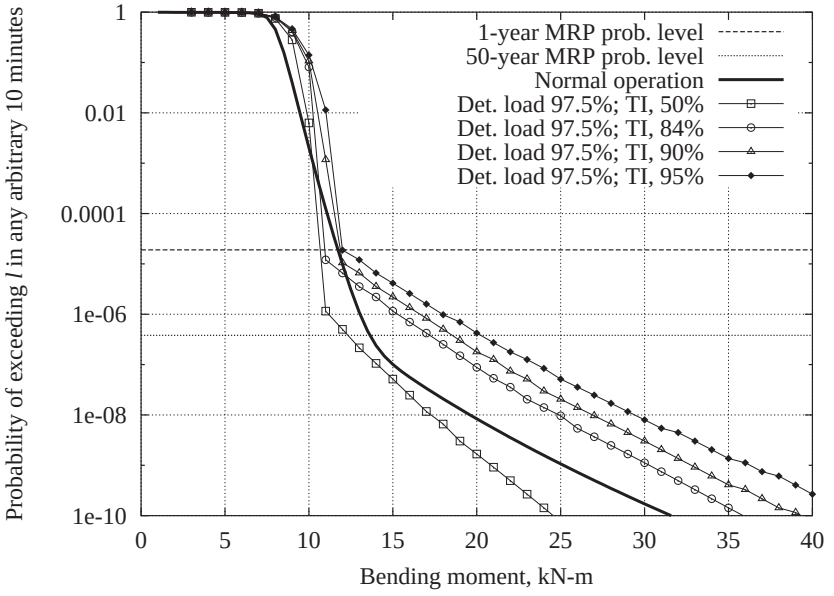

(b) Long-term distribution of extreme blade root edge bending moment for an arbitrary 10 minutes.

Figure 3.14: Long-term distributions of 10-minute extreme blade root bending moment, $L_{10\,\mathrm{min}}$, considering the short-term load at the 90% fractile and turbulence intensity at prescribed deterministic levels compared with the full distribution solution.

the distribution of the long-term load, with mean wind speed and turbulence following in ranked order. We found that by treating the environmental variables deterministic, and considering fractiles higher than the mean, much of their contribution to the variability in the distribution of the long-term load could be recovered. Specifically, considering the 84% fractile of the distribution of the mean wind speed and turbulence, our estimates of the one-year and 50-year blade root flap bending loads are 3.05% and 0.8% high respectively over our estimates employing the full distributions. For blade root edge bending, considering the 95% fractile of the mean wind speed distribution and the 84% fractile of the conditional distribution of turbulence our estimates of the one-year and 50-year root edge bending loads are 6% and 0.7% high. The next sections presents a similar analysis, only this time the short-term loads are based on modeling the random peaks with a quadratic Weibull distribution.

3.5 Long-Term Analysis Based on Modeling Local Peaks

In this section, similar to Section 3.4, we will step through the process of obtaining an estimate of the marginal probability distribution of the long-term load. In this case, however, we will use a quadratic Weibull distribution of local random peaks for our definition of the short-term load. The general procedure is very much the same as that presented in the previous section. An estimate of the marginal distribution of the long-term load, is finally obtained by summing the conditional short-term load distributions over all environmental conditions. Each conditional short-term load distribution is weighted by the probability of the associated environmental condition occurring.

3.5.1 Short-Term Analysis

The previous section demonstrated how one may obtain an estimate of the marginal long-term distribution of $L_{10\,\text{min}}$ from a short-term conditional loads model fit to Z, the global extreme over the duration of a 10-minute response time history. In this section, an estimate of the marginal long-term distribution of $L_{10\,\text{min}}$ is found following a similar procedure. In this case, however, the short-term conditional loads model is fit to, Y, the random local peaks of a 10-minute response time history, see Section 1.5.5. As discussed in the previous section, when we choose to base the short-term conditional loads model on the global extreme events we immediately have the desired probability of interest $P[L_{10\,\text{min}} < l|V, I](= P[Z < z|V, I])$. The drawback is that all time history data below these global maxima is discarded. If one instead models all the random peaks, here denoted

$Y_1, Y_2, \ldots$, the corresponding probability $P[L_{10\,\text{min}} < l|V, I]$ can be estimated as

$$P[L_{10\,\text{min}} < l|V, I] = P[Y_1 < l|V, I] \cap P[Y_2 < l|V, I] \cap P[Y_3 < l|V, I] \cap \ldots \\ \ldots \cap P[Y_{N_T} < l|V, I] = \{P[Y_i < l|V, I]\}^{N_T} \quad (3.23)$$

in which N_T is the number of peaks, Y_i values, in the 10-minute response time history. Equation 3.23 holds assuming that the number of peaks, N_T, is deterministic and that their levels are mutually independent and identically distributed. None of these assumptions are strictly correct, but the approximation generally becomes more accurate in the upper tail of the load probability distribution [30]. Based on the results of Chapter 2 a quadratic Weibull model was fit to the local peaks. The remainder of this section steps through a procedure of fitting a quadratic Weibull model to the observed local peak data, and relating the required short-term model parameters to the environmental variables. Then, based on this definition of the short-term model, we proceed to solve Equation 3.16 and obtain an estimate of the one-year and 50-year blade root flap and edge bending loads. This is similar to the procedure presented in Section 3.4.

Fitting Distributions to Data

Peaks of the response time histories were found based on the definition provided in Chapter 2, the largest value of the time history between successive up-crossings of its mean level. The process mean level and number of peaks were calculated for all blade root flap and edge bending response time histories. For each pair of environmental variables (e.g., V=10m/s and I=class A), the 100 observations of process mean or number of peaks were pooled together and the mean of these pooled observations was reported. The analysis conducted in Chapter 2 found that for operating conditions considering only the peaks in the blade root edge bending data above a prescribed threshold greater than the mean level could provide a better fit of the model to the data. A 4.75kN-m threshold was imposed on the edge bending response data only for operating conditions. Statistics, other than the process mean that describe the blade root edge bending response from operating conditions are based only on the peaks above this threshold. This threshold is discussed in more detail below. Figures 3.15 and 3.16 show the process mean and number of peaks in 10-minute response time history, respectively for both blade root flap and edge bending. These data are based on pooled observations and plotted versus 10-minute mean wind speed, for both turbulence classes.

Again, the FITS routine [52, 53] for fitting probabilistic models to data was used to fit a quadratic Weibull model to the observed local peaks for each pair of environmental conditions: 10-minute mean wind speed, V, and turbulence intensity, I. The quadratic Weibull model is a three parameter model. Thus, we can use the first three statistical moments of the data to fit the model. The first two

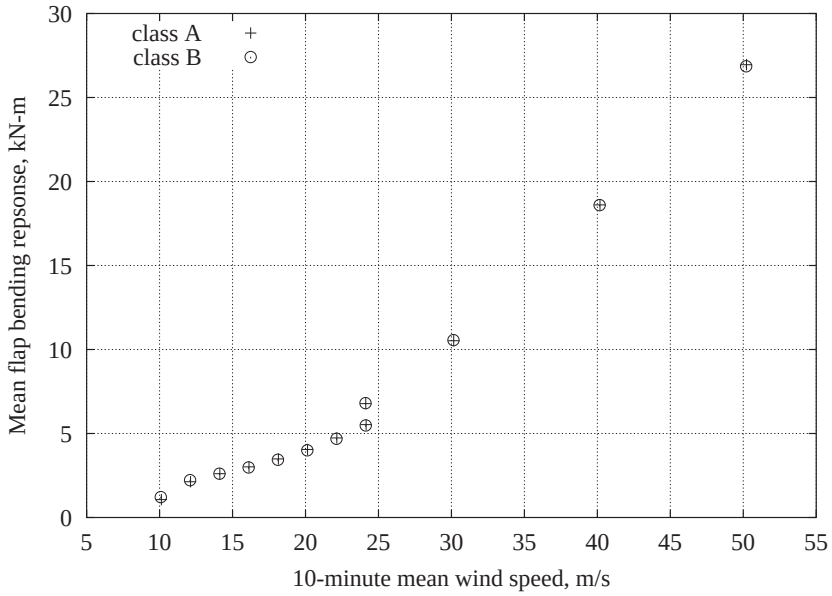

(a) Pooled process mean of 10-minute blade root flap bending response

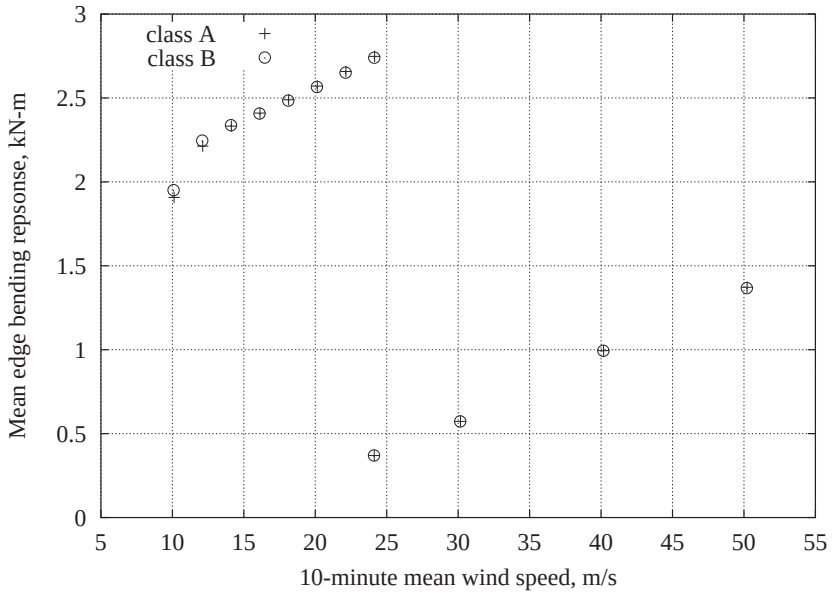

(b) Pooled process mean of 10-minute blade root edge bending response

Figure 3.15: Process mean of 10-minute blade root flap and edge bending response, based on 100 pooled observations for each 10-minute mean wind speed and turbulence class. The wind turbine is operating for $V \leqq 24$m/s, otherwise the turbine is parked.

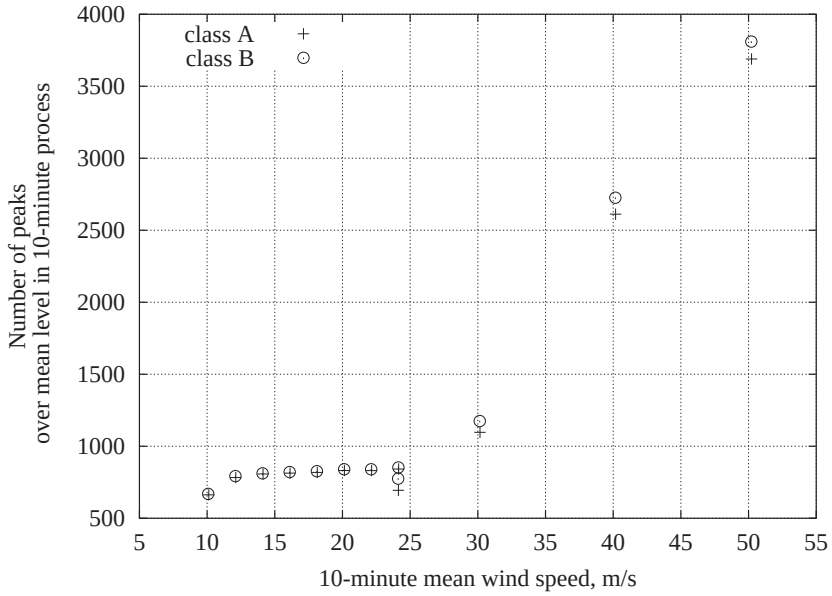

(a) Expected number of local peaks in 10-minute blade root flap bending response time history.

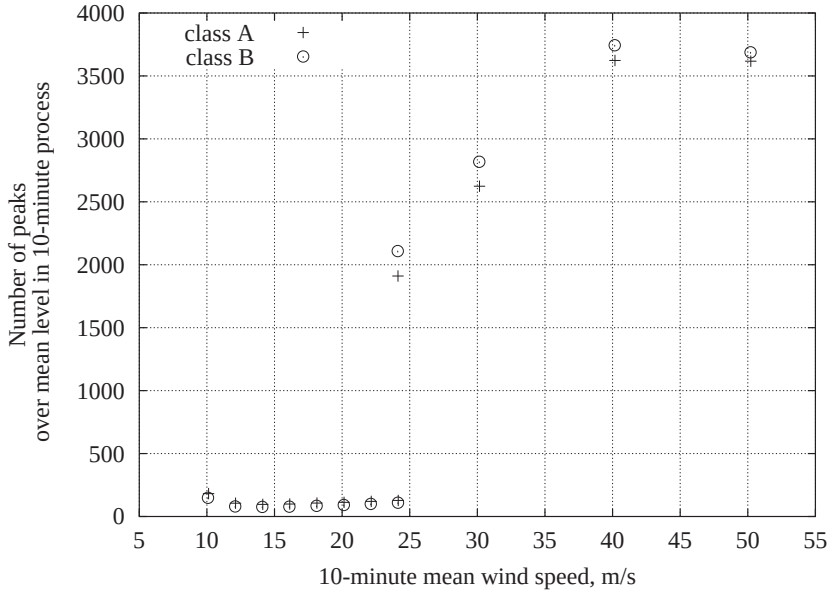

(b) Expected number of local peaks in 10-minute blade root edge bending response time history.

Figure 3.16: Expected number of local peaks in 10-minute blade root flap and edge bending responses time histories, based on 100 pooled observations for each 10-minute mean wind speed and turbulence class. The wind turbine is operating for $V \leqq 24$m/s, otherwise the turbine is parked.

statistical moments, mean (μ_Y) and variance (σ_Y^2), were defined in Section 3.4, and are repeated here. We will use the coefficient of skewness, γ_{3_Y}, a measure of asymmetry of the distribution, as a proxy for the third statistical moment. For purposes of the present discussion these statistics of the observed local peaks are defined as:[4]

$$\mu_Y = \mathsf{E}[Y] \tag{3.24}$$

$$\sigma_Y^2 = \mathsf{E}[(Y - \mu_Y)^2] \tag{3.25}$$

$$\gamma_{3_Y} = \frac{\mathsf{E}[(Y - \mu_Y)^3]}{\sigma_Y^3} \tag{3.26}$$

Shown in Figures 3.17, 3.18, and 3.19 are the observed first three central moments of the local peaks for both blade root flap and edge bending. These data are based on 100 pooled observations for each pair of 10-minute mean wind speed and turbulence class.

Comparison of the fitted quadratic Weibull distributions to observed blade root flap bending local peaks are presented in Figure 3.20. Representative blade root flap bending time histories are used, considering an operating turbine condition (V=18m/s, turbulence class A) in Figure 3.20(a) and a parked turbine condition (V=40m/s, turbulence class A) in Figure 3.20(b). In these figures, the data and fitted models are plotted on a distorted "Weibull" scale, which, rather than plotting $F_Y(y)$ versus y, plots -ln[1-$F_Y(y)$] versus y. The results, when viewed on a log-log scale, should appear as a straight line if the data follow a standard Weibull probability distribution model.[5] For clarity the right-hand axis has the corresponding $F_Y(y)$ values. Similar results were found for local blade root flap bending peaks in other wind environments (10-minute wind speed and turbulence class).

For blade root edge bending, comparison of the fitted quadratic Weibull distribution to the observed local peaks are shown in Figures 3.21 and 3.22 for turbine operating (V=18m/s, turbulence class A) and parked (V=40m/sec, turbulence class A) conditions, respectively. The data and models are plotted on the distorted Weibull scale as presented above. In Figure 3.21(a) one can see that a relatively poor fit results if we consider all the local blade root edge bending peaks from an operating turbine condition. We saw in Chapter 2, that the distribution of local edge bending peaks tends to have more than one mode induced by the gravity loading on the in-plane direction of the blade. The solution to achieve a better fit of the model to the data was to consider only the peaks above a threshold higher than the process mean level. For the analysis here, the threshold level was based on the "deterministic" gravity cycle. The amplitude of the gravity cycle for this turbine is approximately 9.5kN-m, which remains constant across the operating wind speeds analyzed here

[4] A more detailed discussion of expectation and moments of random variables may be found in Section 1.5.1.

[5] This scale, however, does not emphasize the large y, low $P[Y > y]$ of interest.

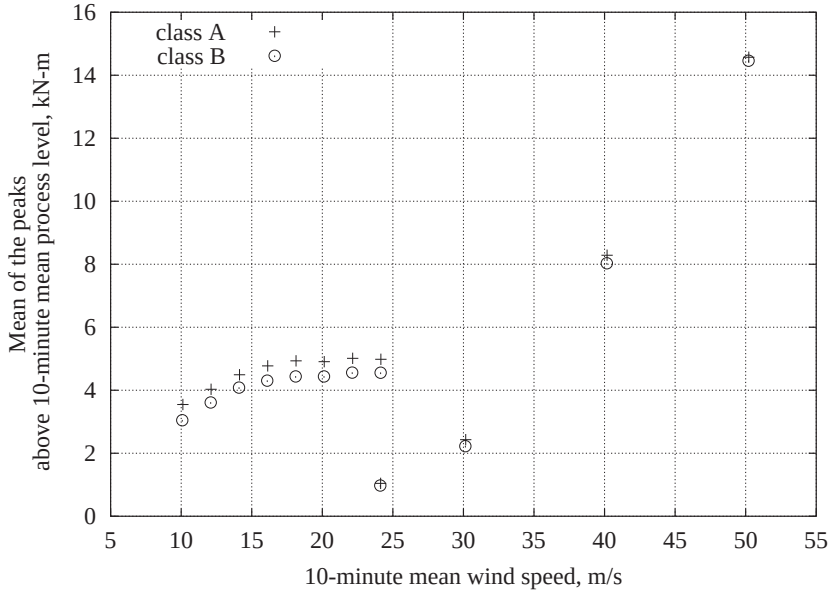

(a) Pooled statistics of the mean of the local peaks in 10-minute blade root flap bending response time history.

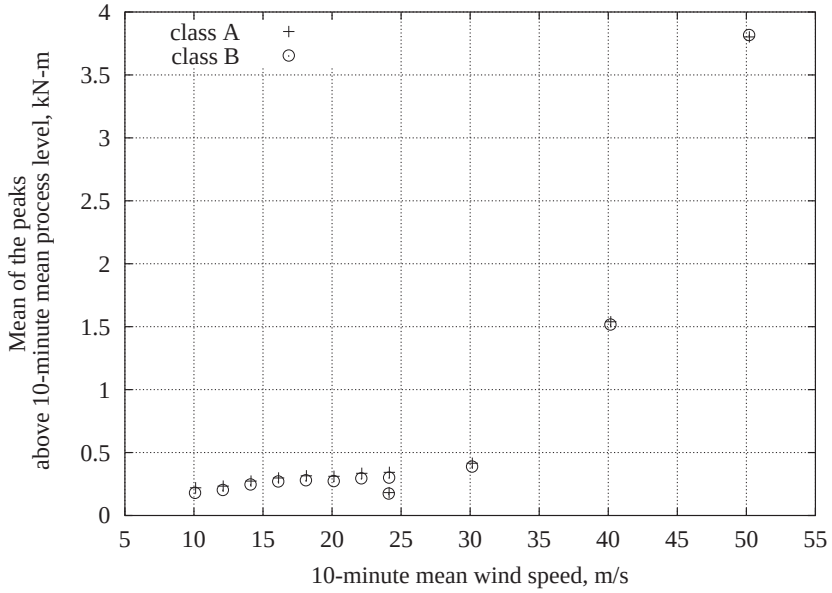

(b) Pooled statistics of the mean of the local peaks, in 10-minute blade root edge bending response time history.

Figure 3.17: Pooled statistics of the mean of the local peaks in 10-minute blade root flap and edge bending responses time histories for given 10-minute mean wind speeds. The wind turbine is operating for $V \leqq 24$m/s, otherwise the turbine is parked.

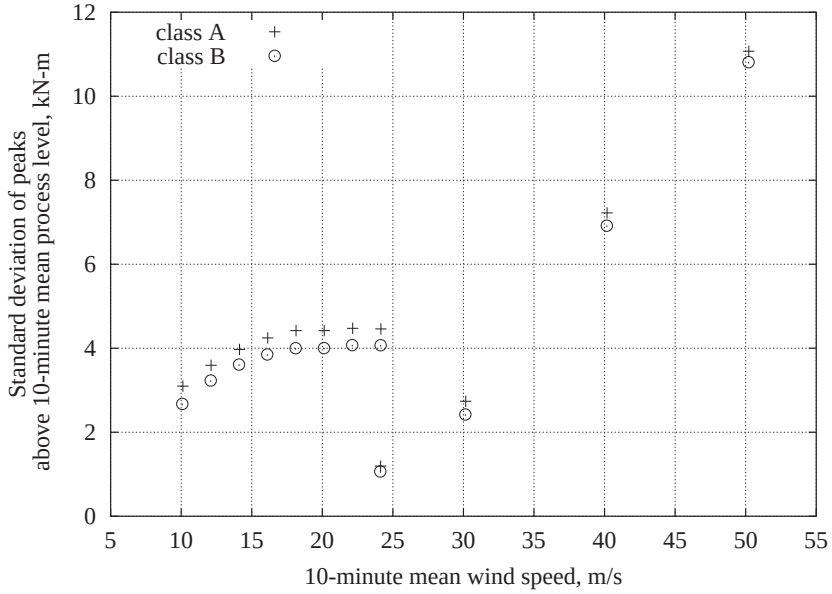

(a) Pooled statistics of the standard deviation of the local peaks in 10-minute blade root flap bending response time history.

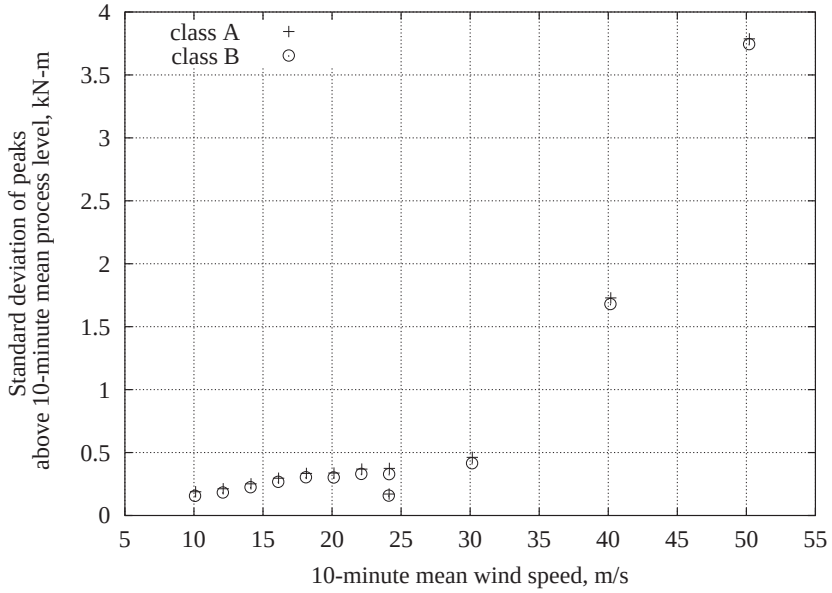

(b) Pooled statistics of the standard deviation of the local peaks in 10-minute blade root edge bending response time history.

Figure 3.18: Pooled statistics of the standard deviation of the local peaks in 10-minute blade root flap and edge bending responses time histories for given 10-minute mean wind speeds. The wind turbine is operating for $V \leqq 24$m/s, otherwise the turbine is parked.

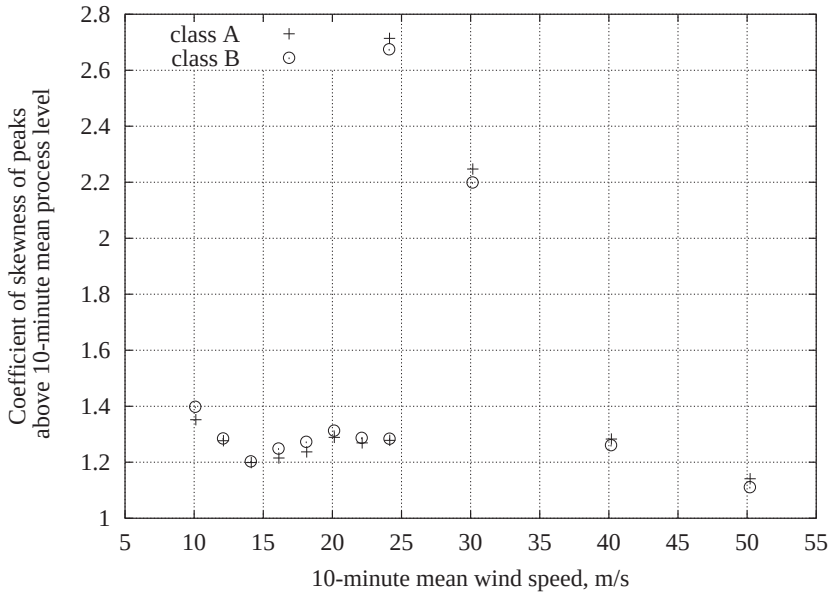

(a) Pooled statistics of the coefficient of skewness of the local peaks in 10-minute blade root flap bending response time history.

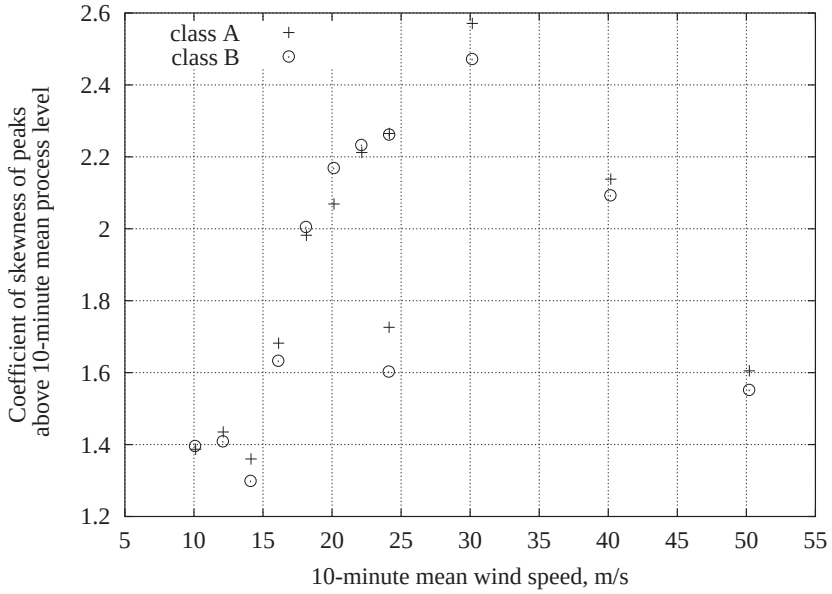

(b) Pooled statistics of the coefficient of skewness of the local peaks in 10-minute blade root edge bending response time history.

Figure 3.19: Pooled statistics of the coefficient of skewness of the local peaks in 10-minute blade root flap and edge bending responses time histories for given 10-minute mean wind speeds. The wind turbine is operating for $V \leqq 24$m/s, otherwise the turbine is parked.

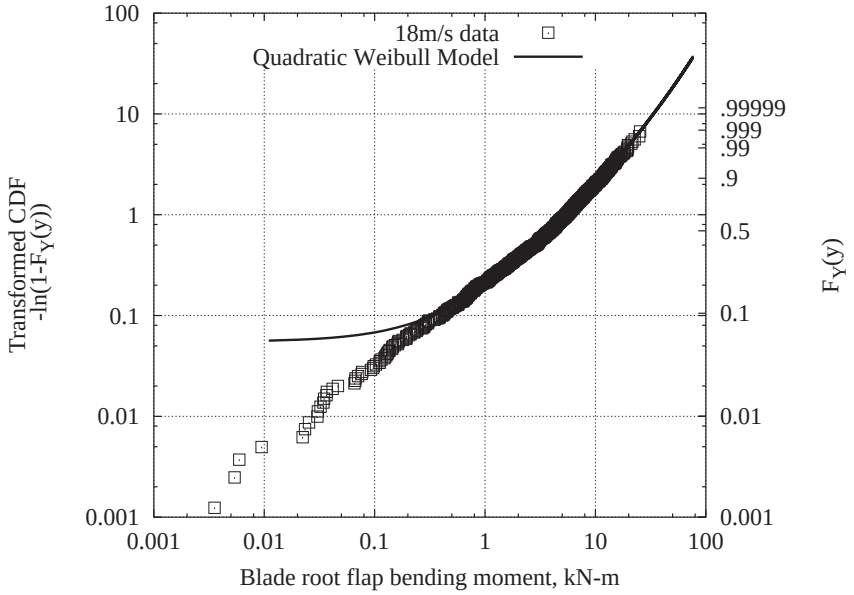

(a) Operating wind speed (18m/s)

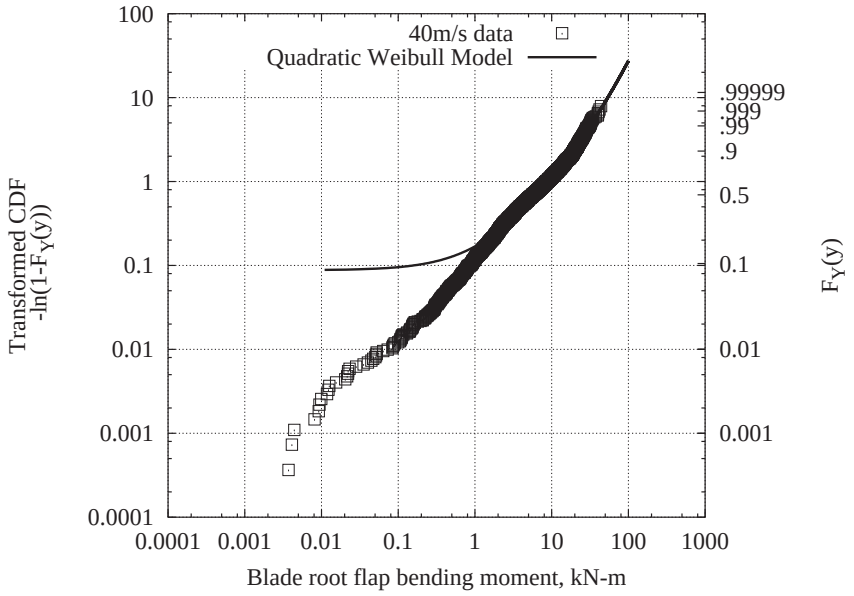

(b) Parked wind speed (40m/s)

Figure 3.20: Quadratic Weibull model fit to observed blade root flap bending data for operating (18m/s) and parked (40m/s) wind speeds, turbulence class A.

(10m/s-24m/s). In this analysis we are particularly interested in modeling the loads toward the upper tail of the distribution, therefore, we would be interested in the loads that generally occur above the positive extreme of the gravity cycle. If we assume that the gravity cycle is centered about the process mean level, the threshold that should be used is half the gravity cycle amplitude, 4.75kN-m. Figure 3.21(b) shows qualitatively an improved fit of the quadratic Weibull model to only the data above the threshold. No additional threshold or shift in the data was imposed on the local blade root edge bending peaks for the parked turbine conditions.

Regression

When obtaining a long-term estimate of the 50-year load based on a short-term distribution which models the local peaks, two parameters and three statistical moments are required. In Section 3.4 where the short-term distribution modeled the global peaks, only the relationships between two statistical moments and the environmental variables were required. We saw from the discussion that it was sufficient to know the statistical moments over all the environmental conditions to completely define the extreme loading on the turbine. Here we need the relationship between the environment and two other parameters in addition to the statistical moments required to fit the probabilistic model. These two additional parameters in this case are: the number of local peaks and the process mean. The number of peaks is required as part of Equation 3.23 to calculate $P[L_{10\,\text{min}} < l|V, I]$, and the process mean which must be added back to the estimate of the extreme load since the magnitude of the peaks was referenced to the process mean level. Therefore, instead of only having to perform two regression analyzes for a given response of interest (flap or edge bending), five analyzes are required: process mean, number of peaks, mean of the peaks, standard deviation of the peaks, and skewness of the peaks.

As discussed earlier there are two distinct general loading conditions for the turbine, one when the turbine is operating and the other while the turbine is parked. Separate regression analysis were performed under each of these conditions. During 10-minute mean wind speeds below 24m/s the turbine is assumed to be operating. For 10-minute mean wind speeds above 24m/s the turbine is assumed to be parked. Based on the observed behavior of the turbine, the moments were assumed to be related to the environmental parameters following the power law function proposed by Veers and Winterstein [54], for both regimes.

$$\mu_j = a_j \left(\frac{V}{V_{\text{ref}}}\right)^{b_j} \left(\frac{I}{I_{\text{ref}}}\right)^{c_j} \quad j = 1, 5 \tag{3.27}$$

The same values of V_{ref} and I_{ref} defined in Section 3.4 were used for this analysis. The V_{ref}

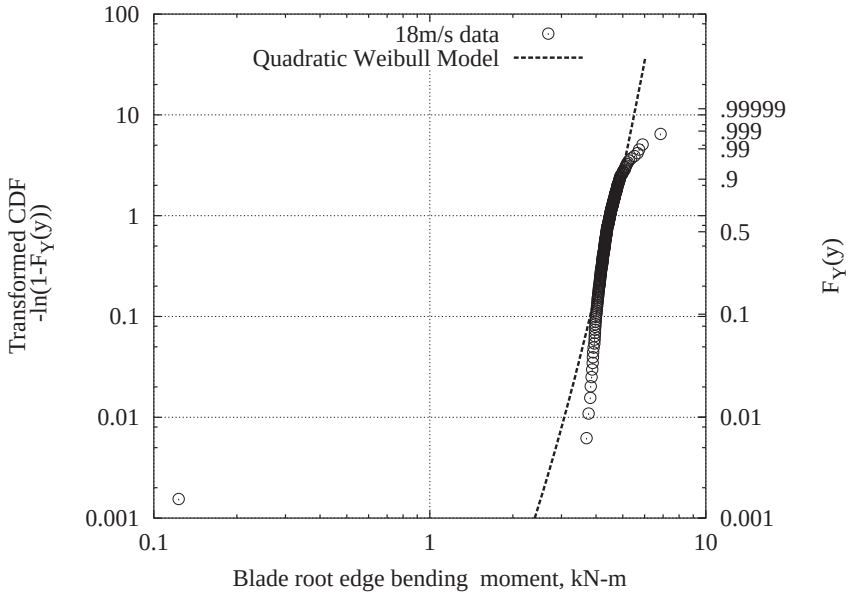

(a) Un-shifted data

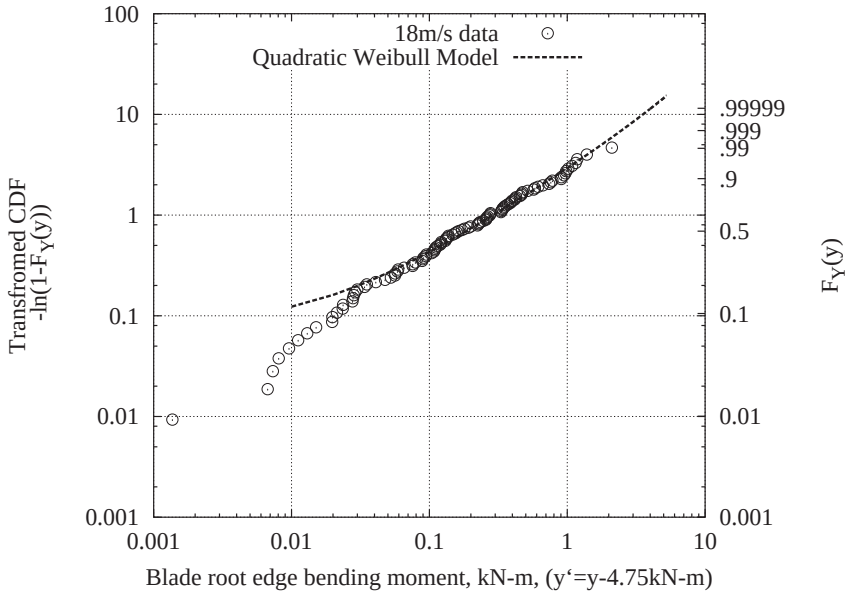

(b) Shifted data, shift=4.75kN-m

Figure 3.21: Quadratic Weibull model fit to shifted and un-shifted observed blade root edge bending data for operating wind speed equal to 18m/s, turbulence class A.

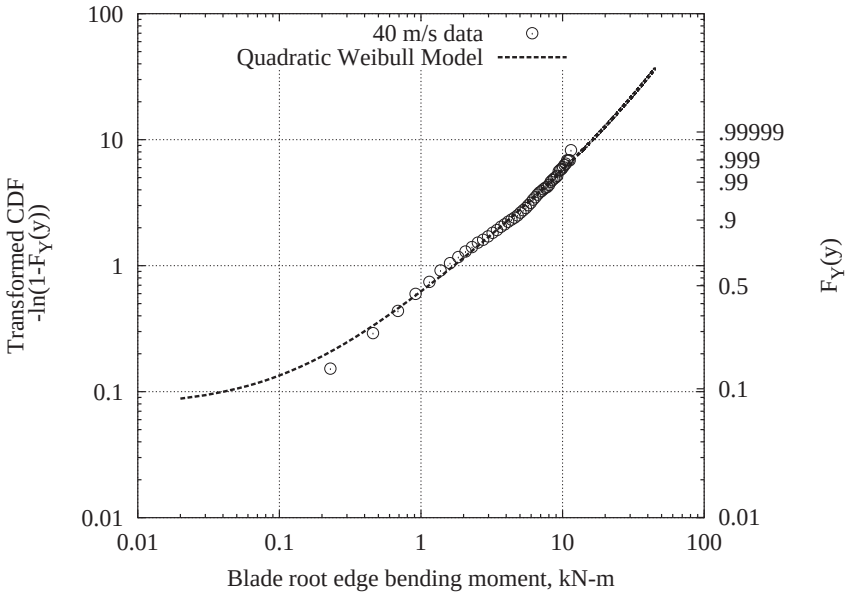

Figure 3.22: Quadratic Weibull model fit to observed blade root edge bending data for parked wind speed equal to 40m/s, turbulence class A.

and I_{ref} values for the operating conditions are 16.474m/s and 0.1528, respectively, and the corresponding values for the parked conditions are 34.861m/s and 0.1318, respectively. The calculated regression coefficients and R^2 statistics are shown in Tables 3.3 and 3.4 for both blade root flap and edge bending conditions respectively. R^2 statistics near unity indicate that a large percentage of the variability in the data is explained by the regression model. Low R^2 statistics indicate that other influences not contained in the regression model may be affecting the loads. In performing the regression analysis it was determined that the applied functional model, Equation 3.27, did not have enough flexibility to sufficiently model the observed behavior of the mean and standard deviation of the local blade root flap bending peaks. The values of the mean and standard deviation of the peaks flatten out with higher wind speeds above 17m/s as compared with the behavior below 17m/s as seen in Figures 3.17 and 3.18. Therefore a separate model was fit to each of these regions, one below 17m/s and the other above 17m/s, for both the mean and standard deviation of local blade root flap bending peaks.

Finally, graphical regression results are shown in Figures 3.23-3.27. Each figure contains regression results for both blade root flap and edge bending conditions considering: process mean, Figure 3.23; number of peaks, Figure 3.24; mean of local peaks, Figure 3.25; standard deviation of local peaks, Figure 3.26; and skewness of local peaks, Figure 3.27. In all plots, the turbulence intensity has been set equal to the reference value.

Blade Root Flap Loading
Regression of Statistics of Random Peaks on V and I

Mean of 10-Minute Response Process

	a (kN-m)	b	c	R^2
$V \leqq 24$m/s	3.0222	1.5196	-0.34972	0.95403
$V > 24$m/s	13.7604	1.8789	-0.07334	0.99857

Expected Number of Random Peaks

	a (kN-m)	b	c	R^2
$V \leqq 24$m/s	800	0.17633	-0.15389	0.71442
$V > 24$m/s	1700	2.1388	-1.1969	0.98712

Mean of Random Peaks

	a (kN-m)	b	c	R^2
$V \leqq 17$m/s	4.1829	0.96324	0.89617	0.98543
$17 < V \leqq 24$m/s	4.5654	0.32441	1.1762	0.97070
$V > 24$m/s	4.0829	3.8365	0.65347	0.99099

Standard Deviation of Random Peaks

	a (kN-m)	b	c	R^2
$V \leqq 17$m/s	3.7006	0.98592	0.86905	0.98240
$17 < V \leqq 24$m/s	4.1124	0.29532	1.1558	0.98421
$V > 24$m/s	5.2258	3.3196	1.0597	0.98509

Coefficient of Skewness of Random Peaks

	a (kN-m)	b	c	R^2
$V \leqq 24$m/s	1.2744	-0.062344	-0.099467	0.090513
$V > 24$m/s	1.7110	-1.2292	0.39315	0.96017

Table 3.3: Regression coefficients used in Equation 3.27 to fit flap load moments as functions of the mean wind speed, V, and turbulence intensity, I. The wind turbine is operating for $V \leqq 24$m/s, otherwise the turbine is parked.

Blade Root Edge Loading
Regression of Statistics of Random Peaks on V and I

Mean of 10-Minute Response Process

	a (kN-m)	b	c	R^2
$V \leqq 24$m/s	2.4063	0.33942	-0.084286	0.95275
$V > 24$m/s	0.7327	1.7925	-0.076185	0.99598

Expected Number of Random Peaks

	a (kN-m)	b	c	R^2
$V \leqq 24$m/s	105	0.44453	2.3182	0.33768
$V > 24$m/s	2928	0.67170	-1.1348	0.89983

Mean of Random Peaks

	a (kN-m)	b	c	R^2
$V \leqq 24$m/s	0.2701	0.85215	0.11290	0.92184
$V > 24$m/s	0.8037	4.3166	0.49033	0.99802

Standard Deviation of Random Peaks

	a (kN-m)	b	c	R^2
$V \leqq 24$m/s	0.2703	1.1572	1.0688	0.95583
$V > 24$m/s	0.8243	4.4614	0.81591	0.99690

Coefficient of Skewness of Random Peaks

	a (kN-m)	b	c	R^2
$V \leqq 24$m/s	1.7616	0.70937	0.092212	0.85589
$V > 24$m/s	1.9341	-0.077955	0.41886	0.048842

Table 3.4: Regression coefficients used in Equation 3.27 to fit edge load moments as functions of the mean wind speed, V, and turbulence intensity, I. The wind turbine is operating for $V \leqq 24$m/s, otherwise the turbine is parked.

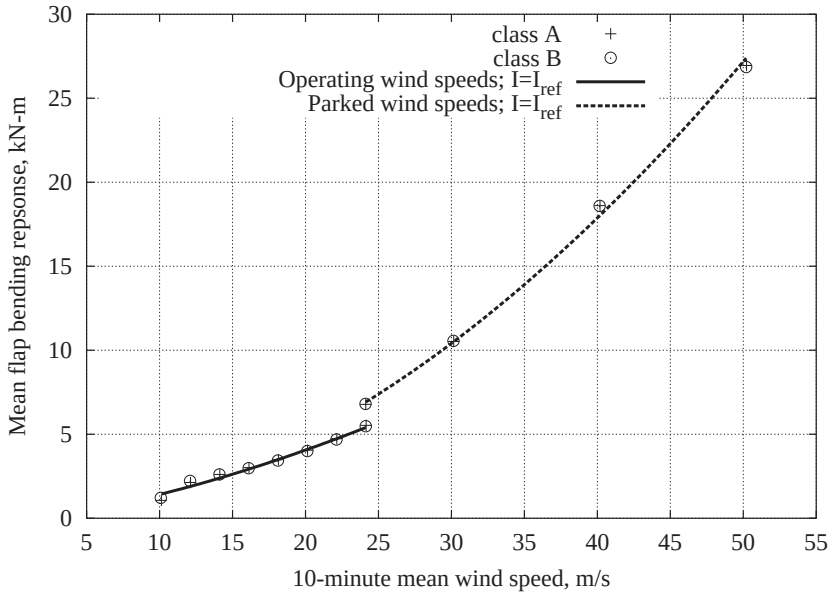

(a) Regression of the process mean of 10-minute blade root flap bending response on the 10-minute mean wind speed and turbulence intensity.

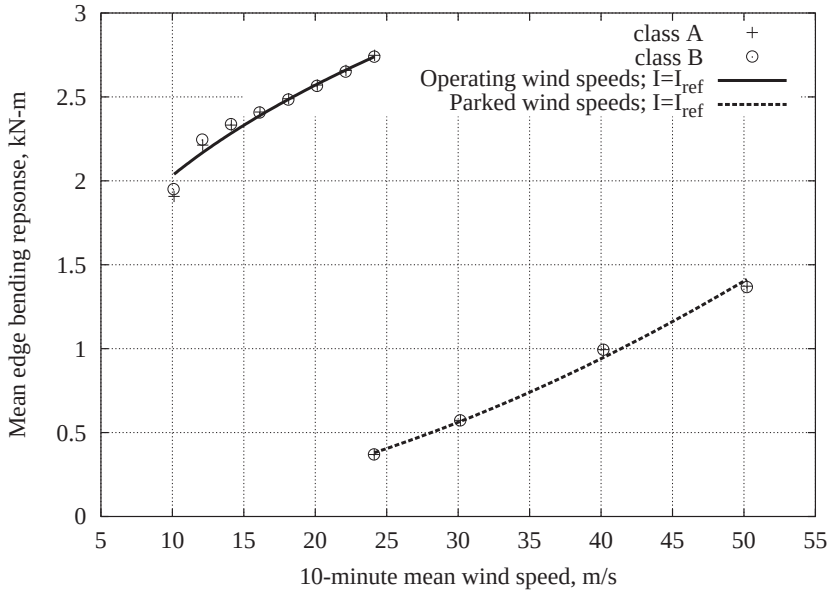

(b) Regression of the process mean of 10-minute blade root edge bending response on the 10-minute mean wind speed and turbulence intensity.

Figure 3.23: Regression of the process mean on the 10-minute mean wind speed and turbulence intensity for blade root flap and edge bending.

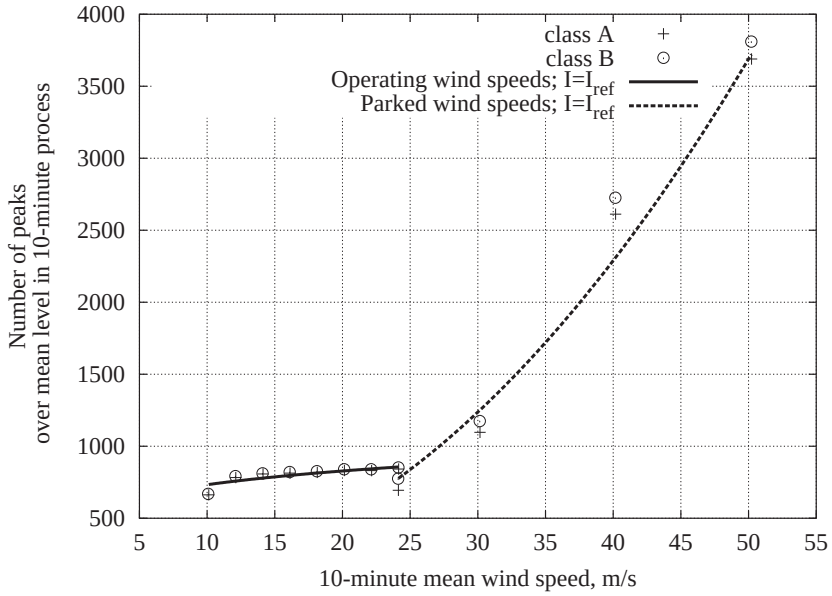

(a) Regression of the expected number of local peaks on 10-minute mean wind speed and turbulence intensity, blade root flap bending.

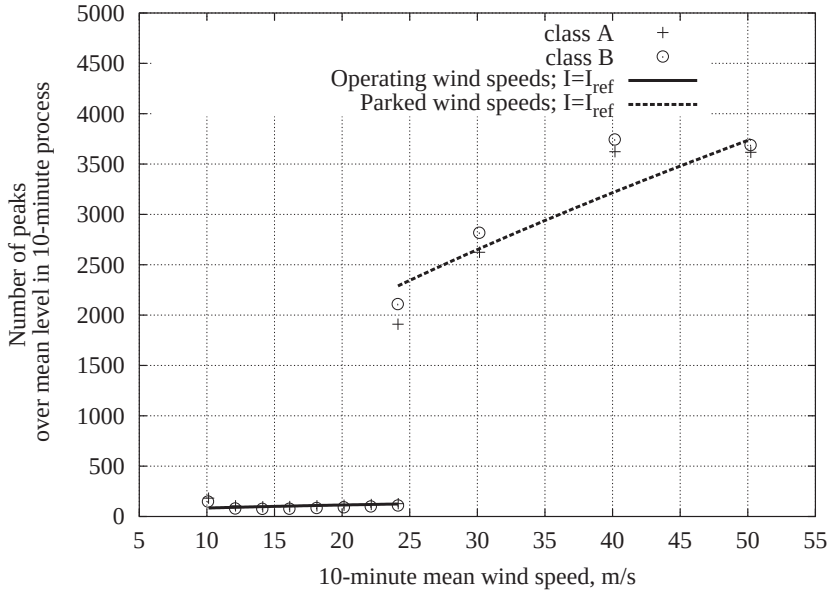

(b) Regression of the expected number of local peaks on 10-minute mean wind speed and turbulence intensity, blade root edge bending.

Figure 3.24: Regression of the expected number of local peaks on 10-minute mean wind speed and turbulence intensity for blade root flap and edge bending.

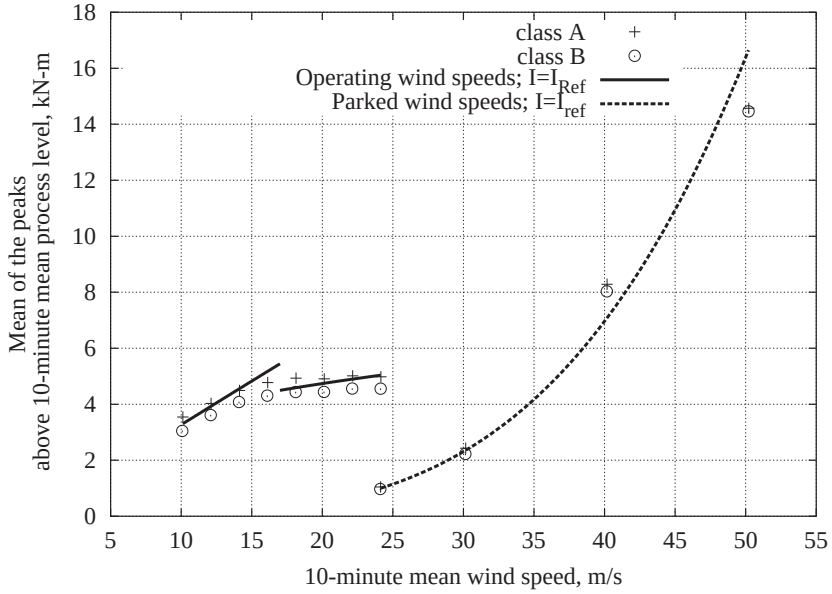

(a) Regression of the mean of the local peaks on the 10-minute mean wind speed and turbulence intensity, blade root flap bending.

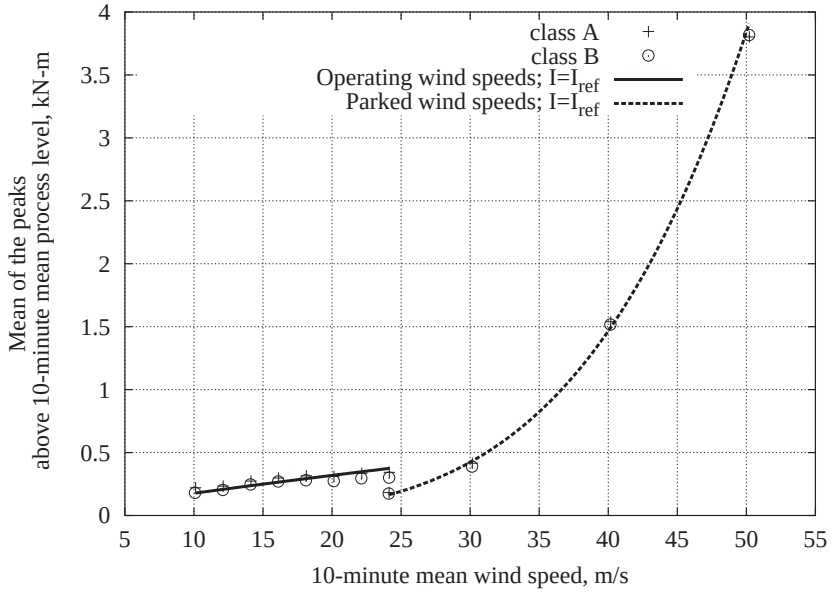

(b) Regression of the mean of the local peaks on the 10-minute mean wind speed and turbulence intensity, blade root edge bending.

Figure 3.25: Regression of the mean of the local peaks on the 10-minute mean wind speed and turbulence intensity for blade root flap and edge bending.

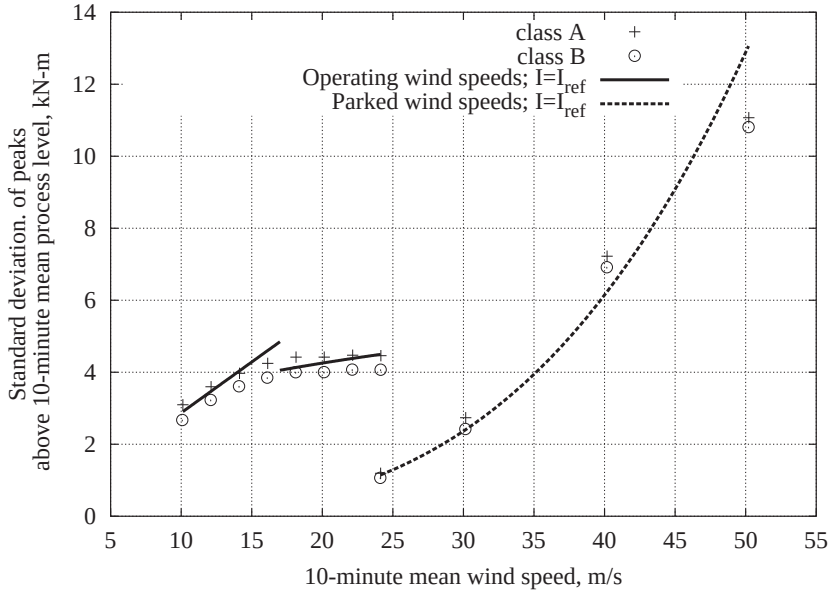

(a) Regression of the standard deviation of the local peaks on the 10-minute mean wind speed and turbulence intensity, blade root flap bending.

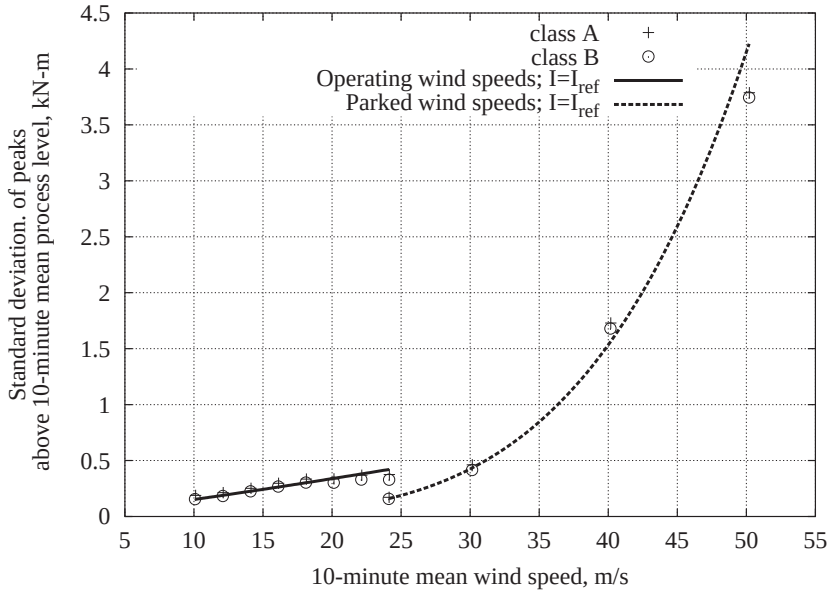

(b) Regression of the standard deviation of the local peaks on the 10-minute mean wind speed and turbulence intensity, blade root edge bending.

Figure 3.26: Regression of the standard deviation of the local peaks on the 10-minute mean wind speed and turbulence intensity for blade root flap and edge bending.

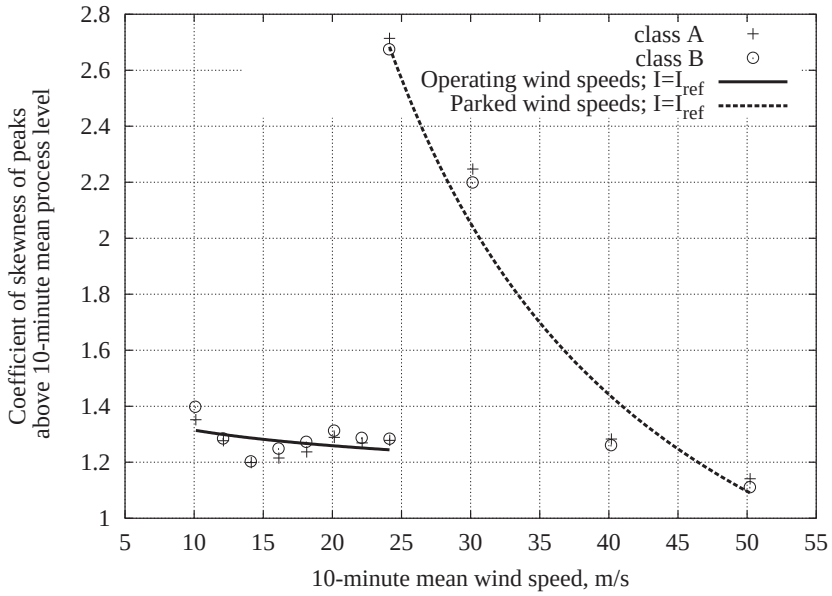

(a) Regression of the coefficient of skewness of the local peaks on the 10-minute mean wind speed and turbulence intensity, blade root flap bending.

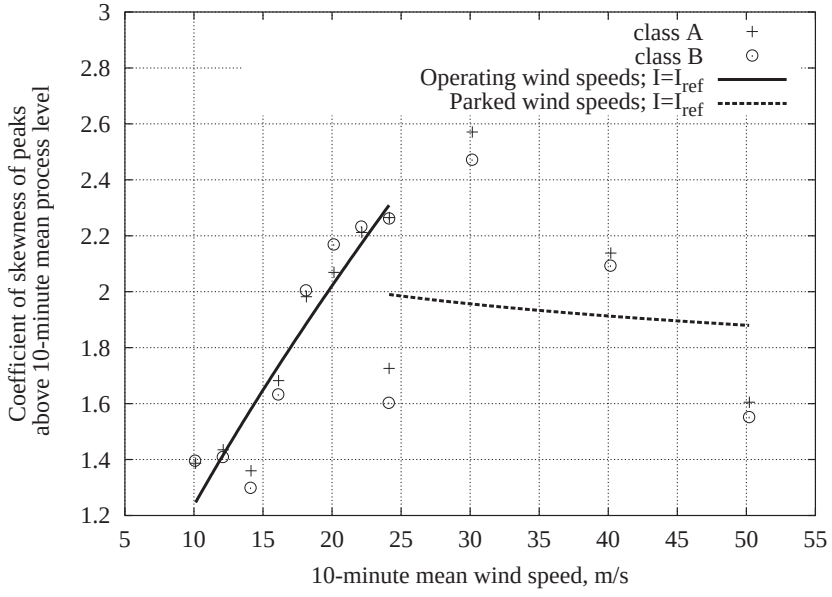

(b) Regression of the coefficient of skewness of the local peaks on the 10-minute mean wind speed and turbulence intensity, blade root edge bending.

Figure 3.27: Regression of the coefficient of skewness of the local peaks on the 10-minute mean wind speed and turbulence intensity for blade root flap and edge bending.

3.5.2 Long-term Analysis

In the previous sections we have defined the short-term probability distribution model for the local peaks and how this model can be represented by the moments of the data. Further, we have shown, through regression analysis, how these moments and associated parameters may be related to the environmental variables. In this section we demonstrate how we can combine the short-term, turbine-specific portion of Equation 3.16 with the long-run distribution of the environmental variables

The same distribution of 10-minute mean wind speed and the conditional distribution of turbulence intensity presented in Section 3.4 are used again here, for this analysis. The ranges of values of the environmental variables are discretized into evenly spaced intervals. For each pair of values of the environmental variables the corresponding short-term local peak distribution is generated. Through Equation 3.23, an estimate of the distribution of short-term extreme events, $P[L_{10\,\text{min}} < l|V, I]$, is obtained. The process mean, and any required additional threshold, are reintroduced. Then, as per Equation 3.16, the short-term extreme load distribution values are summed together; each weighted by the probability of the respective environmental conditions, i.e., the pair of values of the environmental variables occurring. The summation is performed over the entire range of environmental variables.

As stated earlier, there are two loading conditions for the turbine: operating and parked. During normal use the turbine is operating for wind speeds less than 24m/s and parked for wind speeds greater than 24m/s. In this case, to develop the long-term distribution, the appropriate regression model is used for each wind speed value. This results in a combination of the operating and parked only long-term distributions as shown in Figure 3.28. Also shown in the figure are the long-term distributions of the load if the turbine is either parked or operating in all wind speeds. The probability levels associated with the one-year and 50-year mean return period (MRP prob. level) are also shown (note Equations 3.13 and 3.14). In all the preceeding cases it was assumed there was 100% availability of the turbine during all wind speeds. Using the full distribution for each of the random variables, estimates for the one-year blade root flap and edge bending loads are 51.3kN-m and 11.7kN-m, respectively. Corresponding estimates for the 50-year blade root flap and edge bending loads are 60.8kN-m and 13.6kN-m, respectively

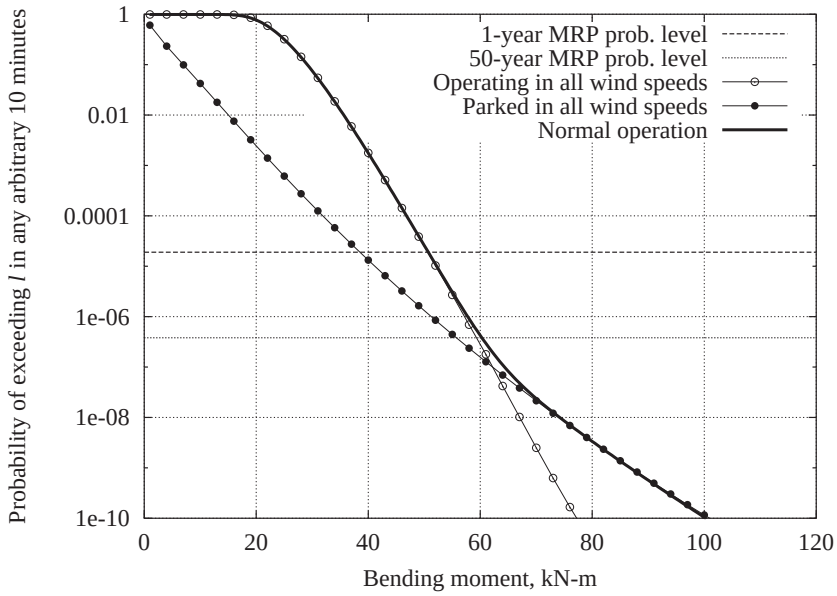

(a) Long-term distribution of extreme blade root flap bending moment for an arbitrary 10 minutes.

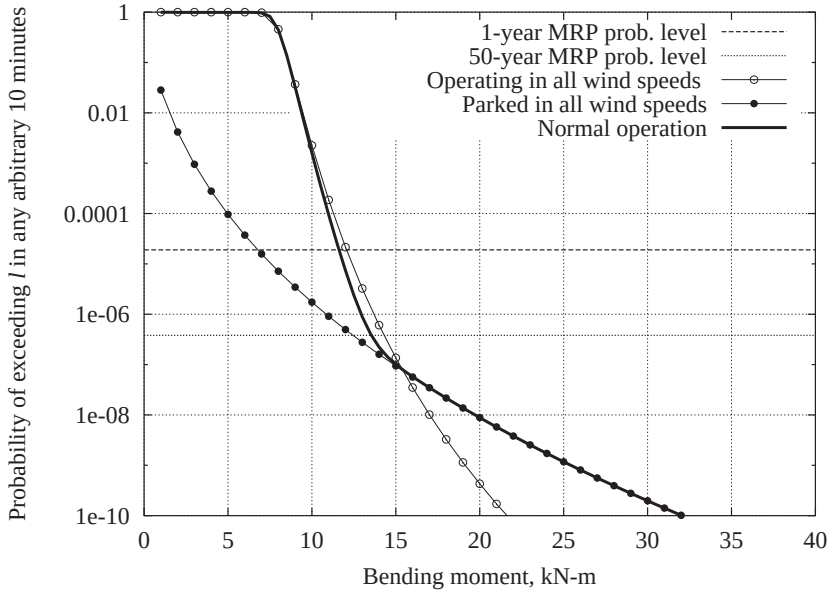

(b) Long-term distribution of extreme blade root edge bending moment for and arbitrary 10 minutes.

Figure 3.28: Long-term distributions of 10-minute extreme blade root bending moment, $L_{10\,\mathrm{min}}$, considering three turbine conditions: 1) turbine operating over all wind speeds, 2) turbine parked over all wind speeds, 3) turbine operating below cutout wind speed and parked above cutout wind speed; for both (a) flap and (b) edge bending.

3.5.3 Simplifying the Long-term Analysis

In this section we present a methodology for simplifying the calculations required for solving Equation 3.16 by replacing the full distributions of some of the random variables with appropriate deterministic fractiles. As seen previously in Section 3.4.3, it is appropriate to consider this methodology for those random variables which have only a small contribution to the overall variability in our estimate of the long-term extreme load distribution. Here, a qualitative analysis is employed to determine the degree to which each of the variables in Equation 3.16 contributes to the long-term extreme load distribution. Based on this analysis, deterministic fractiles, greater than the mean level, are used to reduce the complexity in solving equation 3.16.

Figure 3.29 shows the long-term distribution of the 10-minute flap and edge loads considering the short-term load variable and each of the environmental variables deterministically. Only one variable is considered deterministic in each analysis. The other variables are assumed random and follow the distributions defined previously. This analysis gives a qualitative understanding on how the terms in Equation 3.16 contribute to the variability in the long-term load distribution. From this analysis, one finds that the largest drop in our estimate of the 50-year load, occurs when we set the short-term load variability to zero. Whereas, reducing the variability in the turbulence intensity or wind speed does not reduce our estimate of the 50-year load as drastically. This similar result was found in the analysis presented in Section 3.4. Changing from basing the short-term model on the local peaks versus the global extreme does not seem to change the relative significance of the variability contributed by the short-term load variable. Qualitatively, one can conclude that compared to the short-term load, less of the variability in the long-term load distribution is explained by the randomness in the wind speed and turbulence intensity, at least for the structure, site data, and distribution models used here.

Following the methodology previously presented we consider using a higher fractile of the turbulence intensity, or wind speed distributions where we may be able to recover the associated contribution to the long-term load variability, and still reduce the computational effort in calculating the marginal distribution of $L_{10\,\mathrm{min}}$. Figure 3.30 shows that by considering the 90% fractile of the turbulence intensity distribution, rather than the mean value, nearly all of the variability contributed by the turbulence intensity can be recovered. Tables 3.5 and 3.6 contain estimates of the one-year and 50-year loads and their associated error, considering the estimates based on the full random models as the “true” result.

If we continue and consider an inflated fractile, rather than the mean value, for the wind speed distribution, the 90% fractile covers the one-year and 50-year load for blade root flap bending and the one-year blade root edge bending load. The fractile must be increased to 95% to cover the variability contributed by the wind speed distribution for the 50-year blade root edge bending load.

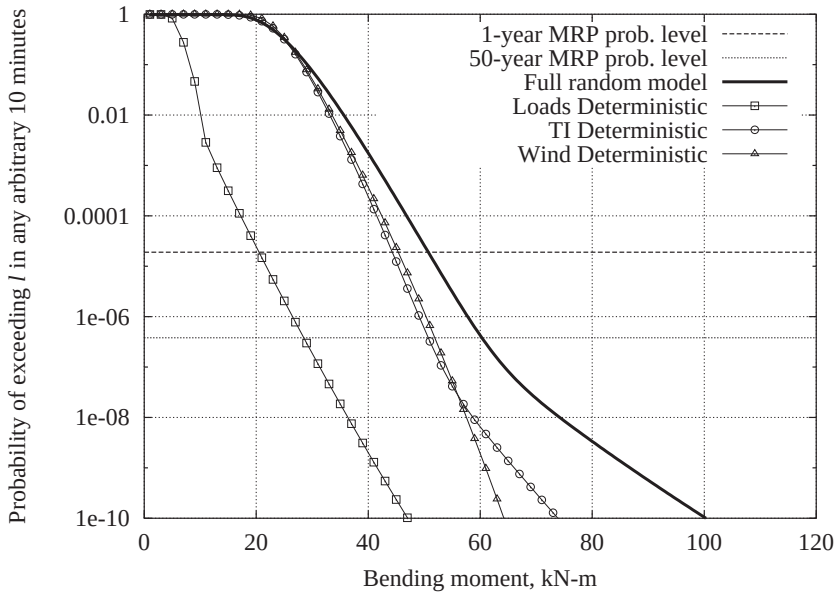

(a) Long-term distribution of blade root flap bending moment for an arbitrary 10 minutes.

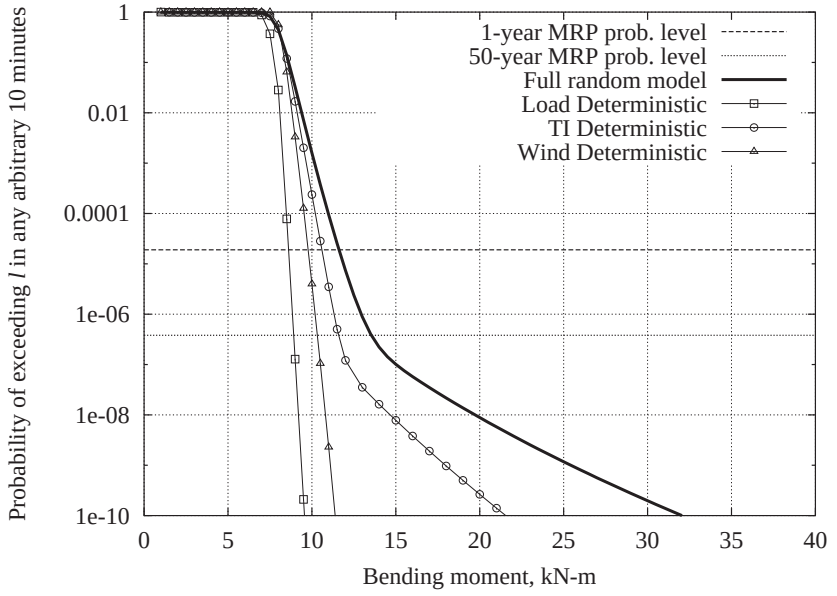

(b) Long-term distribution of blade root edge bending moment for an arbitrary 10 minutes.

Figure 3.29: Long-term distributions of 10-minute extreme blade root bending moment, $L_{10\,\mathrm{min}}$, considering load, turbulence intensity, and wind speed deterministically for both blade root (a) flap and (b) edge bending.

This is shown in Figure 3.31 and Tables 3.5 and 3.6.

This analysis, using prescribed fractiles of the distributions of the three variables, could be done based on the assumption that the short-term load contributed the least to the overall variability in the estimate of the long-term distribution. This is as we would have expected based on the experience of other industries. In this case Figure 3.32(a) shows the results for flap bending, considering the short-term load deterministic, but using the fractile associated with the mean increased by seven standard deviations of the distribution rather than just its mean value. The estimates obtained from using this fractile of the load distribution is shown in Table 3.5 along with the associated error. Correspondingly, the estimates of the one-year and 50-year blade root edge bending loads are shown in Figure 3.32(b) and the numerical results are found in Table 3.6.

Again, if we continue and consider the 84% fractile for the turbulence intensity distribution this covers the estimates for the 50-year blade root flap and edge bending loads, as seen in Figure 3.33. The fractile must be increased to approximately 99% in order to cover the variability contributed by the turbulence for the one-year blade root flap and edge bending loads. Again, numerical results for the estimates mentioned above are presented in Tables 3.5 and 3.6.

Taking both the short-term load and turbulence intensity as deterministic fractiles of the underlying distributions would simplify Equation 3.16 to a single fold integration problem over only the distribution of annual wind speed. The results of this integration are shown in Figure 3.33. In this case, additionally, we can eliminate the remaining integration by using the complementary cumulative distribution function of the annual wind speed distribution and then evaluate the expression at the wind speed associated with the return period of interest.

3.5.4 Summary

Similar to the previous section, here we have stepped through the process of obtaining an estimate of the marginal probability distribution of the long-term load. The short-term load was based on a quadratic Weibull model of local random peaks, however. The general methodology remained the same. The statistical moments were related to the environmental variables through regression analysis. Using the method of moments, the distribution of the short-term loads was obtained for each specific set of values of the environmental variables. Finally, an estimate of the marginal distribution of the long-term load was obtained by summing the conditional short-term load distributions (each weighted by the probability of the values of the environmental variables occurring) over all environmental conditions. We found from this analysis that the estimate of the one-year and 50-year blade root flap bending loads were 51.3 kN-m and 60.8 kN-m respectively. Correspondingly the one-year and 50-year blade root edge bending loads were 11.7 kN-m and 13.6 kN-m, respectively.

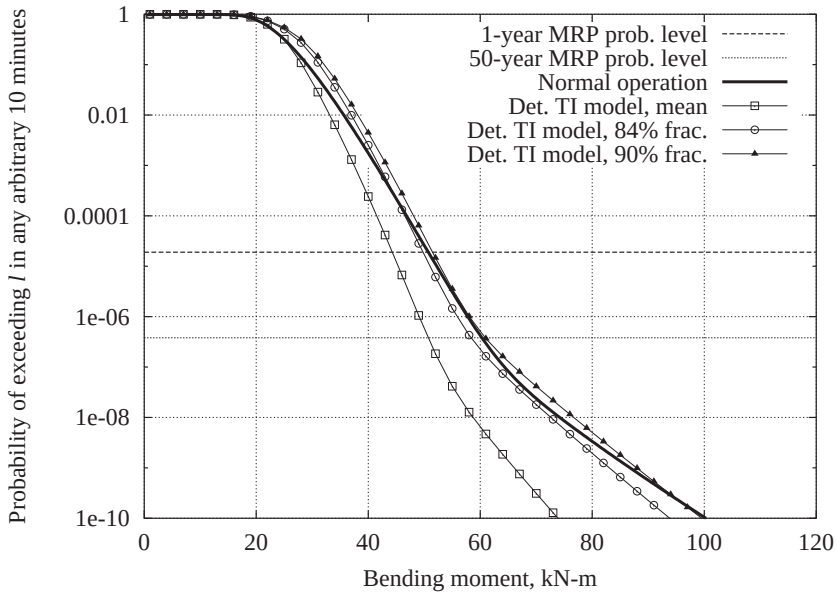

(a) Long-term distribution of extreme blade root flap bending moment for an arbitrary 10 minutes.

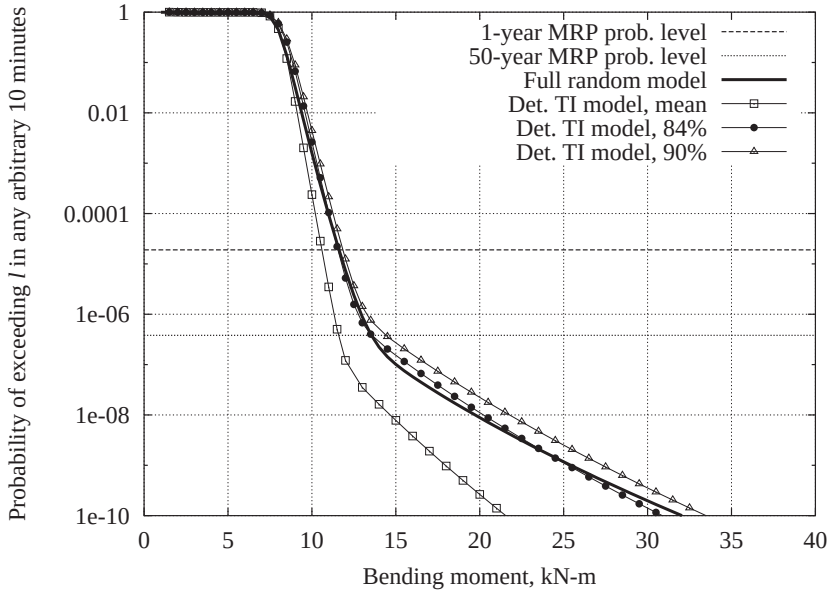

(b) Long-term distribution of extreme blade root edge bending moment for an arbitrary 10 minutes.

Figure 3.30: Long-term distributions of 10-minute extreme blade root bending moment, $L_{10\,\mathrm{min}}$, considering the turbulence intensity at prescribed deterministic fractiles compared with the full distribution solution.

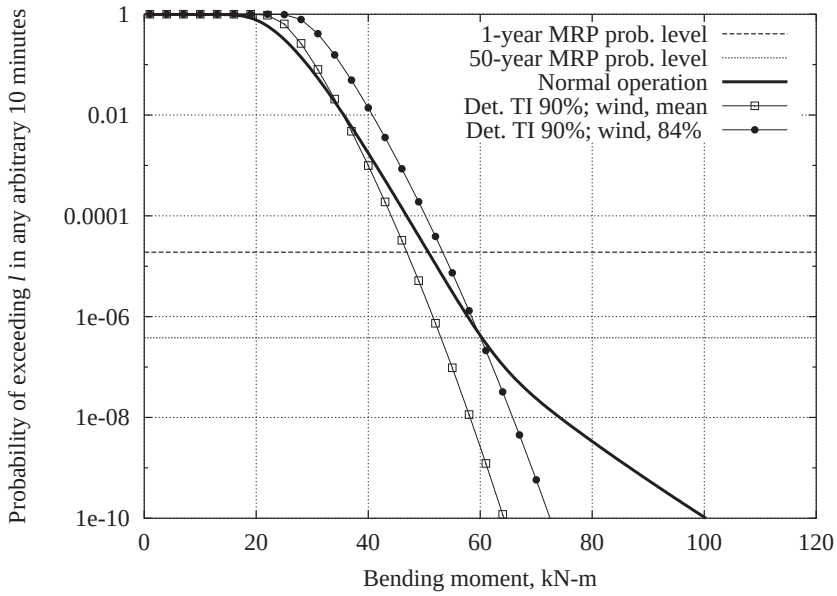

(a) Long-term distribution of extreme blade root flap bending moment for an arbitrary 10 minutes.

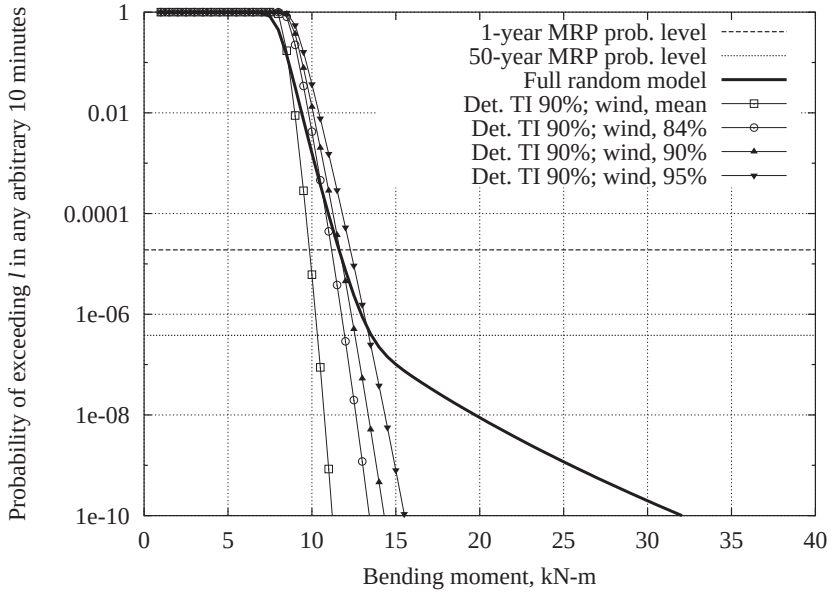

(b) Long-term distribution of extreme blade root edge bending moment for and arbitrary 10 minutes.

Figure 3.31: Long-term distributions of 10-minute extreme blade root bending moment, $L_{10\,\mathrm{min}}$, considering the turbulence intensity at the 90% fractile and 10-minute mean wind speed at prescribed deterministic levels compared with the full distribution solution.

Estimates of 1-Year and 50-Year Blade Root Flap Bending Load

Full Random Model

1-year Load	50-year Load
51.3kN-m	60.8kN-m

Deterministic Turbulence Intensity

Fractile	1-year Load	% Error	50-year Load	% Error
90%	51.1kN-m	-0.4%	60.9kN-m	0.2%

Deterministic Turbulence Intensity(90%) and Wind Velocity

Fractile	1-year Load	% Error	50-year Load	% Error
84%	53.3kN-m	4.0%	60.1kN-m	1.2%

Deterministic Short-Term Load

Fractile	1-year Load	% Error	50-year Load	% Error
$\mu_Y + 7\sigma_Y$	54.7kN-m	6.6%	60.9kN-m	0.2%

Deterministic Short-Term Load($\mu_Y + 7\sigma_Y$) and Turbulence Intensity

Fractile	1-year Load	% Error	50-year Load	% Error
84%	43.5kN-m	-15.2%	63.0kN-m	2.0%
99%	53.0kN-m	3.3%	79.0kN-m	29.9%

Table 3.5: Estimates of one-year and 50-year blade root flap bending loads, considering deterministic fractiles of conditional short-term load, turbulence intensity, and wind speed.

Estimates of 1-Year and 50-Year Blade Root Edge Bending Load

Full Random Model

1-year Load	50-year Load
11.7kN-m	13.6kN-m

Deterministic Turbulence Intensity

Fractile	1-year Load	% Error	50-year Load	% Error
90%	11.9kN-m	1.7%	14.4kN-m	6.0%

Deterministic Turbulence Intensity(90%) and Wind Velocity

Fractile	1-year Load	% Error	50-year Load	% Error
90%	11.8kN-m	0.9%	12.6kN-m	-7.4%
95%	12.4kN-m	5.9%	13.5kN-m	-0.7%

Deterministic Short-Term Load

Fractile	1-year Load	% Error	50-year Load	% Error
$\mu_Y + 7\sigma_Y$	11.5kN-m	-1.7%	12.8kN-m	-5.9%

Deterministic Short-Term Load($\mu_Y + 7\sigma_Y$) and Turbulence Intensity

Fractile	1-year Load	% Error	50-year Load	% Error
84%	11.1kN-m	-5.1%	13.9kN-m	2.2%
99%	12.0kN-m	2.6%	17.4kN-m	27.9%

Table 3.6: Estimates of one-year and 50-year blade root edge bending loads, considering deterministic fractiles of conditional short-term load, turbulence intensity, and wind speed.

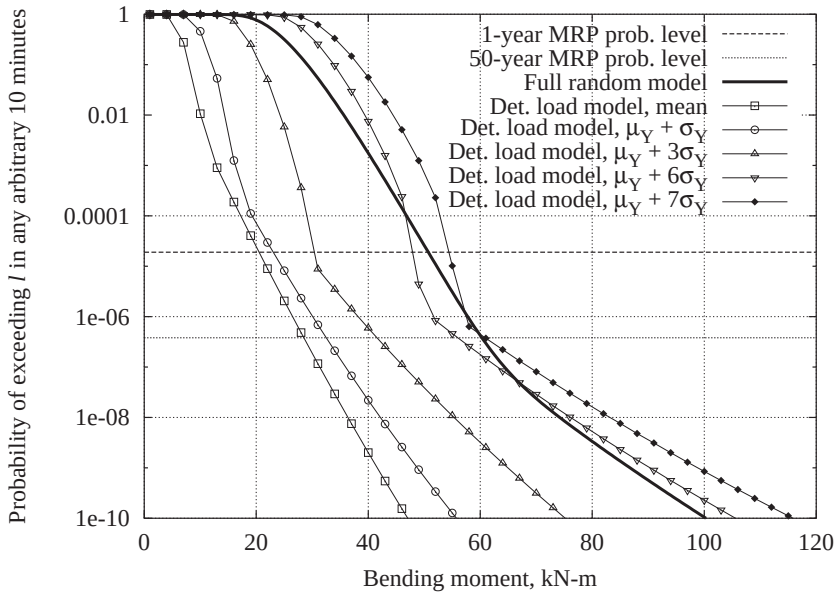

(a) Long-term distribution of extreme blade root flap bending moment for an arbitrary 10 minutes.

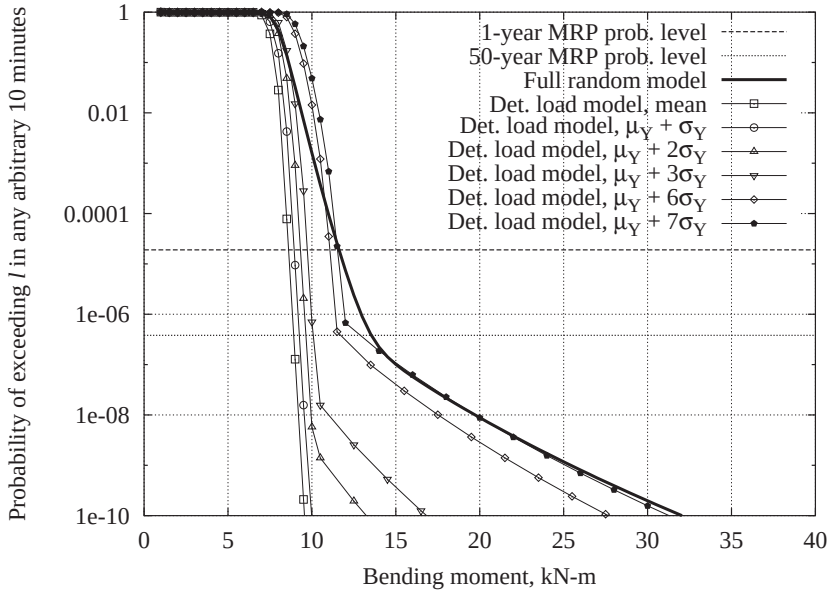

(b) Long-term distribution of extreme blade root edge bending moment for an arbitrary 10 minutes.

Figure 3.32: Long-term distributions of 10-minute extreme blade root bending moment, $L_{10\,\mathrm{min}}$, considering the load term at prescribed deterministic levels compared with the full distribution solution.

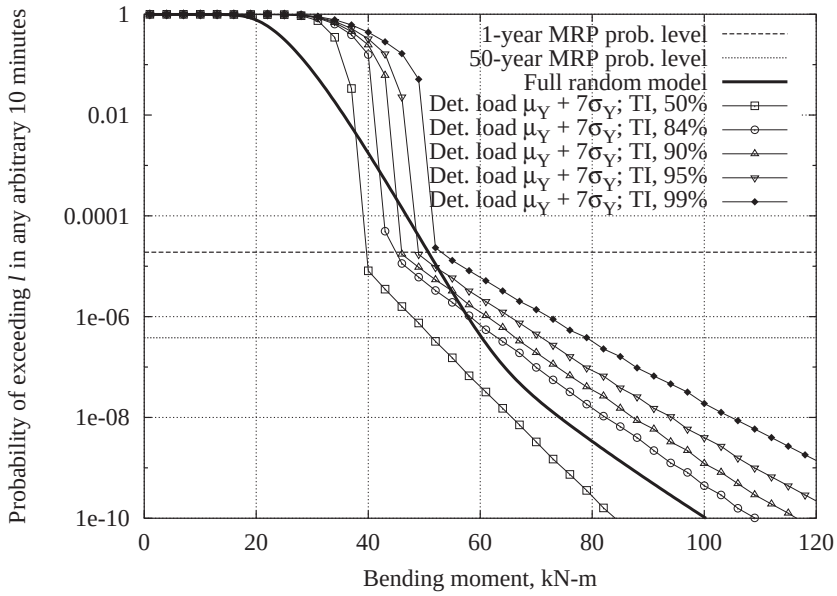

(a) Long-term distribution of extreme blade root flap bending moment for an arbitrary 10 minutes.

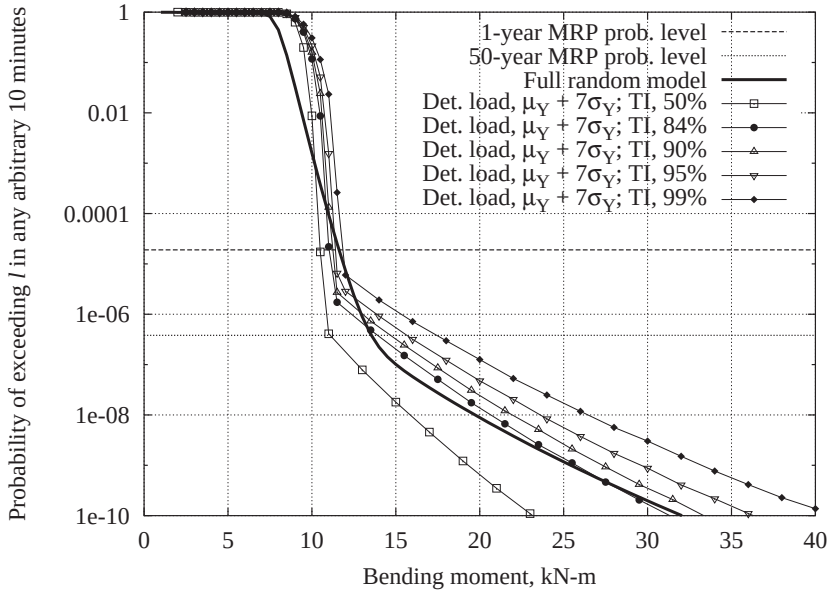

(b) Long-term distribution of extreme blade root edge bending moment for an arbitrary 10 minutes.

Figure 3.33: Long-term distributions of 10-minute extreme blade root bending moment, $L_{10\,\mathrm{min}}$, considering the short-term load at $\mu_Y + 7\sigma_Y$ level and turbulence intensity at prescribed deterministic fractiles compared with the full distribution solution.

Again, a qualitative analysis was conducted to determine which of the three variables, conditional short-term load, conditional turbulence, or mean wind speed, contributed the most to the variability in the distribution of the long-term load. We found, similar to the previous section, that at least for the AOC 15/50 turbine, site data, and distribution models used here the conditional short-term distribution of the loads contributed the most to the variability in the distribution of the long-term load, with mean wind speed and turbulence following in ranked order. We treated the environmental variables deterministic, considered fractiles higher than the mean, and were again able to recover much of the variability in the distribution of the long-term load, i.e., compared with using their full distributions. Specifically, considering the 84% fractile of the distribution of the mean wind speed and 90% fractile of the distribution of turbulence, our estimates of the one-year and 50-year blade root flap bending loads are 4.0% and 1.2% high respectively over our estimates employing the full distributions. For blade root edge bending, considering the 95% fractile of the mean wind speed distribution and the 90% fractile of the conditional distribution of turbulence our estimates of the one-year and 50-year root edge bending loads are 5.9% high and 0.7% low. The next section presents a discussion of the comparison of the results between basing the short-term loads on the distribution of global peaks and, on the other hand, basing the short-term loads on the distribution of local random peaks.

Comparison of Long-Term Estimates
Based on Short-Term Gumbel and Quadratic Weibull Models

Blade Root Flap Bending

	Gumbel Model	Quadratic Weibull Model	Percent Difference
1-year Bending Load	49.1kN-m	51.6kN-m	4.2%
50-year Bending Load	59.7kN-m	60.8kN-m	1.8%

Blade Root Edge Bending

	Gumbel Model	Quadratic Weibull Model	Percent Difference
1-year Bending Load	11.8kN-m	11.7kN-m	1.1%
50-year Bending Load	13.7kN-m	13.6kN-m	0.9%

Table 3.7: Comparison of long-term estimates of one-year and 50-year bending loads based on using Gumbel distribution fit to observed global maximum for the short-term load model versus fitting a quadratic Weibull distribution to the local peaks.

3.6 Comparison of Long-Term Estimates Based on Different Short-Term Models

In Section 3.4 we saw how one could obtain an estimate of the long-term distribution of extreme events based on modeling the 10-minute maximum event by a Gumbel distribution. Later, in Section 3.5 we saw how a similar estimate of the long-term distribution may be obtained by basing the short-term model on the quadratic Weibull distribution of local peaks. The question that arises, and follows on from the work presented in Chapter 2, is: if we consider the predictions based on the Gumbel model to be "true", are the estimates based on the alternative Weibull model unbiased? It was shown in Chapter 2 that the estimator of the mean value of the 10-minute extreme based on modeling the local peaks was unbiased and had lower standard error when compared to the estimator of the mean value of the 10-minute extreme based on the raw observations of the 10-minute extreme. Figure 3.34 shows the estimates of the long-term distribution of the 10-minute loads based on a short-term loads modeling the 10-minute extreme (Gumbel) or local peaks (Weibull). The estimates of the one-year and 50-year blade root flap and edge bending loads are presented in Table 3.7 along with the associated percent difference between the two estimates.

The data presented in Figure 3.34 and Table 3.7 show that the estimate based on modeling the local peaks is generally unbiased for both flap and edge bending compared with the estimate based on modeling the raw conditional 10-minute extremes. Therefore, we can take advantage of the more efficient estimate based on modeling random peaks, to either sample less or reduce the width of the confidence bands on the parameters. This will be discussed further in Chapter 6.

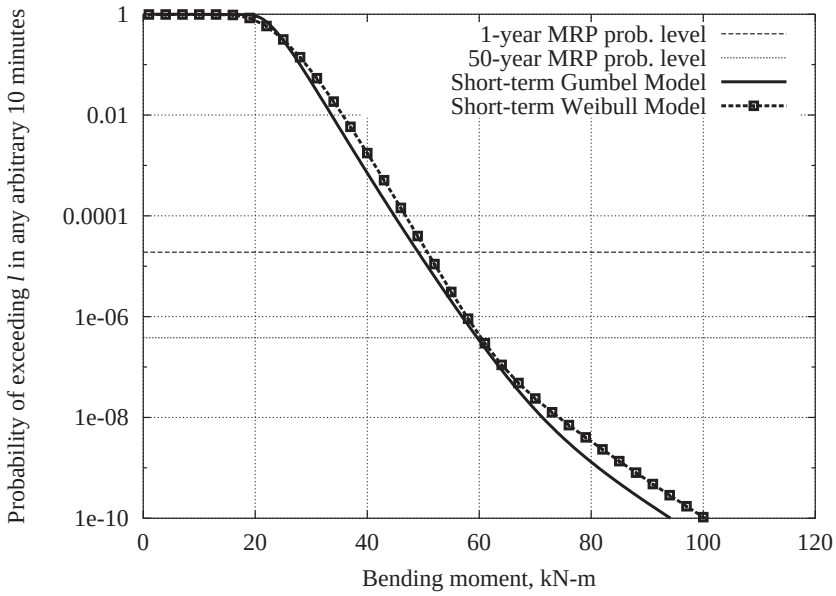

(a) Long-term distribution of extreme blade root flap bending moment for an arbitrary 10-minutes.

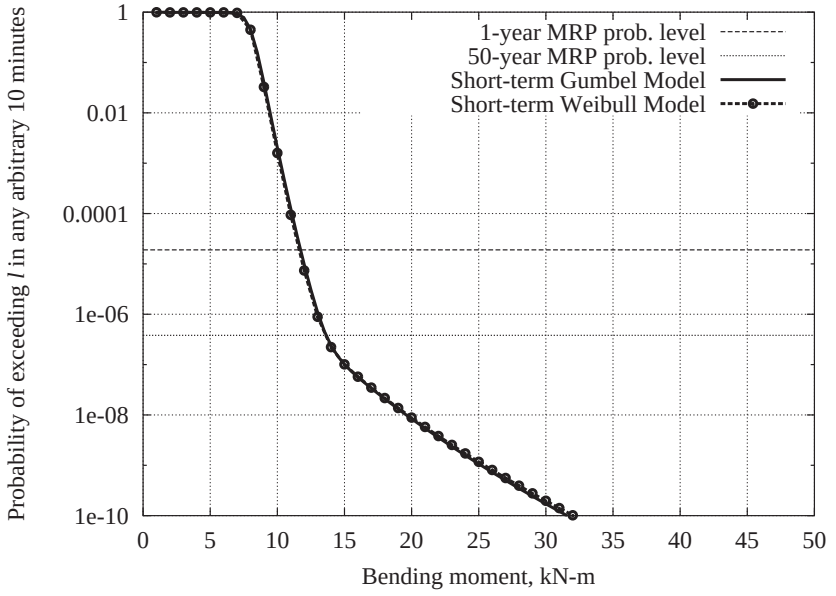

(b) Long-term distribution of blade root edge bending moment for an arbitrary 10-minutes.

Figure 3.34: Comparison of estimates of the long-term distribution of 10-minute extreme blade root bending moment, $L_{10\,\mathrm{min}}$ based short-term Gumbel model for 10-minute extreme events or a short-term Weibull model for local peaks.

3.7 Conclusions

In this chapter we have stepped through the process of calculating the probability distribution of $L_{10\,\mathrm{min}}$ by two different methods. Starting from initial simulated time histories, we fit distribution models to the observed extremes and then to the local peaks. In both cases we related the moments, which define the distribution model parameters, to the environmental variables through regression analysis. Finally, the short-term load distributions were weighted by the probability of the associated environmental conditions occurring and summed over all environmental conditions to estimate the long-term distribution. We then discussed simplifying the two-fold integration problem down to a single-fold integration by using deterministic fractiles of the short-term load, turbulence intensity, and wind speed distributions. It was shown that this methodology captures a significant portion of the contribution to the long-term load variability of these variables at the probability levels of interest. Also, the estimates based on modeling the local peaks was unbiased compared with the estimates based on modeling the observed extremes.

Note, that the fractiles, obtained from this analysis, apply to this data and moreover to the assumptions made in choosing the associated distribution models. Different fractiles may apply for other data under different assumptions. This analysis is shown here for illustration and discussion purposes. Universal fractiles, if deemed appropriate, should be chosen judiciously and with great care in choosing distribution models.

Another approach, for simplifying Equation 3.16, not explored in this chapter, employs the approximate methods underlying first-order reliability analysis. In this method, contours of the critical combination of wind speed and turbulence intensity are found for prescribed reliability levels. It then becomes a straightforward task to obtain an estimate of the 50-year load by (1) identifying an appropriate percentile of the short-term load, and (2) identifying the maximum response along the prescribed contour, e.g. 50-year contour. Under the assumptions of first-order reliability analysis, the maximum response along the contour is associated with prescribed reliability level of interest [57]. This approach is the subject of Chapter 4.

Chapter 4

Estimation of Extreme Load Events Using Environmental Contours[1]

This chapter presents and explores the application of the environmental contour method to wind turbines. Contours promise to provide both practical reliability estimation and valuable information about the combination of joint environmental variable values, e.g. wind speed and turbulence, most critical to each specific wind turbine. We present the background of the development of environmental contours as applied to wind energy systems, and apply this theory, in three examples, to develop contours based either (1) on design code description of environmental conditions, or (2) on measured field data which describes the site environment. From these contours, and a functional description of the short-term response of the turbine, implicit first-order reliability method estimates are made for the turbine response. These estimates are then compared with results obtained from numerical integration of the short-term response of the turbine over the joint distribution of wind speed and turbulence. We find that the environmental contour method provides reasonable estimates of the expected extreme load, compared with the full integration method.

4.1 Introduction

Wind turbine blades are typically designed to survive the entire operating lifetime of the system. Certification standards [23] reflect this approach when the design extreme wind speed is selected to be the 50-year maximum. If the reasonable assumption that the turbine can be parked before the worst case wind speed is encountered, the design condition is relatively easy to deal with; assume

[1] A portion of this chapter was previously published in the proceedings of the American Society of Mechanical Engineering's 22nd Wind Energy Symposium [58]

a stationary blade immersed in a uniform flow with a velocity equal to the 50-year maximum wind speed at the blade height.

Some studies have implied that the simple quasi-static maximum wind condition may not generate the maximum load. Madsen, et al. [21] suggested parked loads that include turbulence could exceed the uniform gust approach. In Chapter 3 we saw it is even possible that operating loads in much lower wind speeds can generate the highest loads in some cases. The reason that lower wind speeds can generate higher loads is twofold. First, turbulence in the inflow causes the highest load in any 10-minute sample to have higher variability. Second, when the variability in loads is combined with the greater frequency of occurrence of lower wind speeds, the extrapolation to 50 years can produce a higher design load. Add to this the fact that turbulence levels at any site are not constant, but span a range of values described by the joint probability distribution of wind speed and turbulence [23]. The designer is therefore left with the much more difficult proposition of sweeping the entire environmental space of wind speed and turbulence for the worst-case loading.

In Chapter 3 we evaluated various models of the variation in extreme loads from extensive aeroelastic simulations. We considered the entire design space of the joint distribution of wind speed and turbulence, fitting distribution models to the variation of extreme short-term loads at each combination of values of the environmental variables. Integrating the short-term distribution of extremes over the long-term joint probability distribution of wind speed and turbulence generates the long-term distribution of extreme loads. The one-year and 50-year extremes are found by picking off the once-per-year and once-per-50-year probability levels from the long-term distribution. Thus the response of the turbine and the environment of the turbine are evaluated separately and only combined in the final step. We saw in Chapter 3 that this method provides an accurate method of extrapolating to the long-term extreme from short-term simulations, although it is quite computationally expensive.

This chapter presents a method for reducing the space over which combinations of wind speed and turbulence must be evaluated from the plane to a curved line. We show that the joint distribution of mean wind speed and turbulence can be used to find a locus, or contour, of points describing in effect the once in one-year or 50-year combinations of mean and turbulence experienced in a 10-minute interval. This locus is found by using the theory of structural reliability and an approach called First-Order Reliability Method [7, 8, 12]. The contour has the property that all the points share the same associated reliability level. The contour is searched to find the point where the specific combination of values of the environmental variables engender the maximum response of the turbine. The location of this point depends on the nature of the individual turbine's sensitivity to wind speed and turbulence. Thus, again, the problem is split into the environmental part, now described by a contour instead of a joint probability density, and a turbine part that describes the

response due to specific combinations of wind-speed and turbulence.

The environmental contour concept is demonstrated here by first showing how the current IEC standard joint distribution of wind speed and turbulence can be transformed into contours of one-year and 50-year extreme combinations. This is repeated for a joint distribution derived from field measurements. Then the turbine response levels are defined using a complete mapping of the short-term (10-minute) extremes over the entire space of mean wind speed and turbulence combinations. In this chapter, we will ignore the variability of the short-term extremes. We will see later how we have considered the short-term response as random (see Figure 1.8) for the purpose of determining the short-term mean extreme response, but we ignored the variability of the short-term extreme response, i.e., we considered the short-term extreme response deterministic at its mean level. The complete mapping of the response is generated to clearly illustrate where the maximum response intersects with the contours. The intersection of the largest response with the contour defines the design load, or design point. However, in future applications the more efficient approach of only evaluating the response levels along the contour, searching for the location of the highest response, is necessary. Thus, the problem is simplified over the need to evaluate the turbine response everywhere. Results from this approach are compared with results using the long-term distribution as in Chapter 3.

4.2 Estimating the Long-term Expected Response

We are interested in finding an estimate of the capacity that should be designed into the structural system of a wind turbine. This capacity may be defined in terms of the extreme response of the turbine due to a loading environment over a period of time. More specifically, a capacity associated with a prescribed mean return period of the expected extreme response— e.g., 50-year mean return period. This can be written as

$$p_{50 \text{ years}} = P[L > l_{\text{cap}}] \tag{4.1}$$

Where, $p_{50 \text{ years}}$, is the probability associated with the 50-year mean return period, L, is the extreme response, and l_{cap} is the structural load capacity of the turbine. Our interest is in finding an estimate of l_{cap} such that the prescribed probability level, e.g., $p_{50 \text{ years}}$, is satisfied. We know that the response is a function of the loading environment. Therefore we may construct a function, h, which relates the relative characteristic random variables of the environment—e.g., mean wind speed, V, and turbulence, I, to the observed response.

$$L = h(V, I) \tag{4.2}$$

With this relationship given above, Equation 4.1 may be written as

$$p_{50\text{ years}} = P[h(V, I) > l_{\text{cap}}] \tag{4.3}$$

Furthermore, we may construct a limit state function, g, such that

$$P[g \leq 0] = P[h(V, I) > l_{\text{cap}}] \tag{4.4}$$

In this context, the expression for the limit state function which satisfies Equation 4.4 is given below as

$$g = l_{\text{cap}} - h(V, I) \tag{4.5}$$

The First-Order Reliability Method (FORM), described in Appendix D, can be used to solve for the probability that the limit state function is less than or equal to zero. FORM is an approximate method. The limit state function is approximated by a straight line tangent to the limit state surface at the point on the surface closest to the origin of standard normal space. Therefore, the smoothness of the limit state function can have an affect on the efficacy of the method to provide an accurate approximation. Using trial and error we can find an estimate of l_{cap} such that $P[g \leq 0]$ is equal to the probability associated with the prescribed mean return period. Iteratively solving for an estimate of l_{cap} in this way can be tedious.

The forward-FORM problem discussed above, seeks to find $p_f = P[g \leq 0]$. In our problem we are looking for an estimate of l_{cap} with a prescribed p_f. Therefore it would be more efficient if the process could be inverted. Winterstein, et al. [59] describes this process. Instead of transforming the random variables and limit state function from the basic space into the standard normal space and solving for p_f, with inverse-FORM, one starts with a prescribed reliability index, $\beta = \Phi^{-1}(1 - p_f)$, which describes a hyper-sphere in n-dimensional standard normal space. The hyper-sphere is then transformed to basic space. The resulting contour in basic space has the property that all the points on the contour share the same associated reliability as defined in standard normal space. The contour in basic space can then be searched for the maximum response. This is the maximum response associated with the prescribed reliability level. Using the method of inverse-FORM to develop environmental contours has been applied previously in other engineering fields including: offshore engineering [60, 61] and earthquake engineering [62].

For our problem, an estimate of l_{cap} can be obtained by searching the contour in basic space for the maximum value of $h(V, I)$. For example: searching the locus of points, $\mathcal{C}$, associated with $p_{50\text{ years}}$, we can obtain an estimate of the 50-year load, L_{50}, as:

$$L_{50} = \max_{V,T \in \mathcal{C}} [l_{\text{cap}}] = \max_{V,T \in \mathcal{C}} [h(V, I)] \tag{4.6}$$

This process of using inverse-FORM to develop environmental contours in the basic space will be demonstrated in examples, which follow this discussion. In each example, estimates of the one-year and 50-year extreme flap and edge bending loads on a horizontal axis wind turbine will be obtained. These estimates will be compared with estimates obtained through the full-integration method.

4.3 Overview of Examples

The remainder of this chapter will present three examples which apply inverse-FORM, as discussed in the previous sections, to obtain estimates of the one-year and 50-year blade root flap and edge bending loads considering two site environments and both stall-regulated and pitch-regulated turbines. For all the examples presented here, the description of the short-term extreme response of the turbine is based on modeling the global peaks by a Gumbel distribution. Also, in all the examples we consider the turbine in both operating and parked conditions. We have seen in previous chapters that there is a discontinuity in the response at the cut-out wind speed, when the turbine transitions from operating to parked conditions. This discontinuity in the limit state function will test the ability of FORM to provide a reasonably accurate approximation.

The first two examples demonstrate how estimates of the one-year and 50-year extreme blade root flap and edge bending loads on a stall-regulated AOC 15/50 turbine (see Section 1.4.2) may be obtained using environmental contours. The environment in the first example is based on the IEC class IA wind environment with turbulence variable defined as the standard deviation of the 10-minute wind process. The short-term response of the AOC 15/50 machine developed in Appendix C.3 is used with the constructed environmental contour to obtain an estimate of the one-year and 50-year blade root bending loads.

In the second example, the environment is based on an analysis of wind data from the Lavrio, Greece, test site. The description of the environment given for this site was defined in terms of the mean and coefficient of variation of the 10-minute wind process. Therefore, in the first example turbulence is defined in terms of standard deviation and in the second example turbulence is defined in terms of coefficient of variation. This is done to demonstrate the approach with both sets of variables commonly used to describe the wind environment. The reader should note that the same notation in the examples is used for turbulence, regardless of which definition is used, as either is valid.

The third example again uses the description of the environment from the Lavrio test site. In this case, however, the short-term response of the AOC 15/50 machine, in the regime of operating wind speeds, is modified to simulate the typical non-monotonic response of a pitch-regulated machine. This contributes a slope discontinuity in the limit state function, which tests the ability of FORM

to provide a reasonable approximation, with a second discontinuity. The response for parked wind speeds was not modified and, in this example, represents an unfeathered blade condition. Note in this example we only consider obtaining estimates of the one-year and 50-year blade root flap bending load.

In all of the examples, the estimates obtained from the environmental contour method are compared with estimates obtained from integrating the short-term extreme response over the long-term distribution of the environmental variables.

4.4 Example 1 — IEC Model with Stall-Regulated Turbine

In this example an AOC 15/50, stall-regulated, turbine is assumed to operate in an IEC class IA environment. The turbulence variable is defined in terms of the standard deviation of the 10-minute wind process.

4.4.1 Description of Environment

The description of the environmental variables, in this example, is based on the criteria given in the IEC wind energy safety code for a class IA environment [23]. Specifically, the annual distribution of the 10-minute mean wind speed, V, is given by the Rayleigh distribution shown below, with μ_V=10m/s.

$$f_V(v) = \frac{2v}{\alpha^2} \exp\left[-\left(\frac{v}{\alpha}\right)^2\right] \tag{4.7}$$

$$\alpha = \frac{2\mu_V}{\sqrt{\pi}}$$

The standard deviation of the 10-minute wind process is taken as the measure of wind turbulence, denoted by I. The conditional distribution of turbulence is assumed to follow the lognormal distribution shown below.

$$f_{I|V}(i|v) = \frac{1}{\sqrt{2\pi}\zeta i} \exp\left[-\frac{1}{2}\left(\frac{\ln(i) - \lambda}{\zeta}\right)^2\right] \tag{4.8}$$

The parameters of the lognormal distribution, λ and ζ, are defined as:

$$\zeta = \sqrt{\ln(\delta_{I|V}^2 + 1)} \tag{4.9}$$

$$\lambda = \ln(\mu_{I|V}) - \frac{1}{2}\zeta^2 \tag{4.10}$$

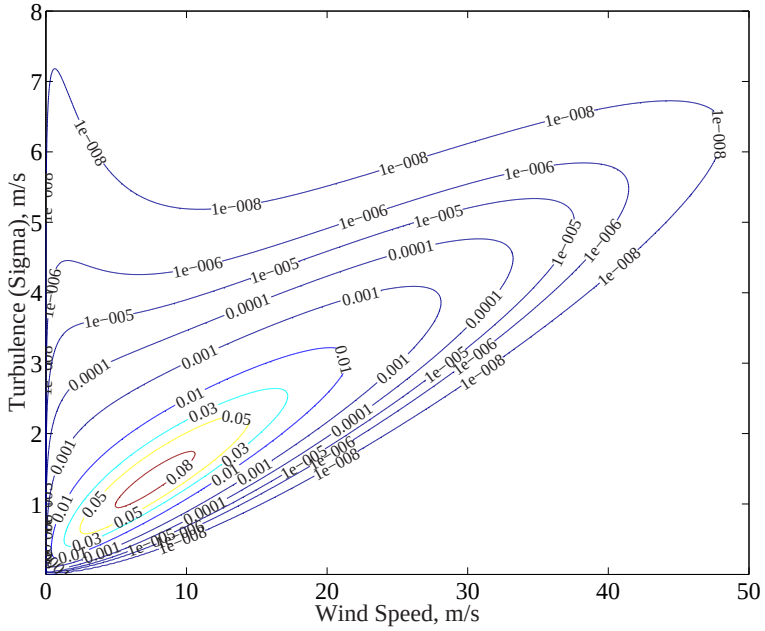

Figure 4.1: Joint probability density function based on wind class IA, μ_V=10m/s, I_{15}=0.18, a=2

with, $\delta_{I|V}$, the conditional coefficient of variation given as:

$$\delta_{I|V} = \frac{\sigma_{I|V}}{\mu_{I|V}} \tag{4.11}$$

The functions of conditional mean, $\mu_{I|V}$, and standard deviation, $\sigma_{I|V}$, of the turbulence are given by the IEC wind energy safety code. For turbulence class A, I_{15}=0.18 and a=2.

$$\mu_{I|V} = \frac{I_{15}(15\text{m/s} + av)}{(a+1)} - 2\text{m/s}\, I_{15}$$
$$\sigma_{I|V} = 2\text{m/s}\, I_{15}$$

The joint probability distribution of the environmental variables is then obtained by multiplying together Equations 4.7 and 4.8.

$$f_{V,I}(v,i) = f_{I|V}(i|v) f_V(v) \tag{4.12}$$

The resulting joint probability density function for class IA is shown in Figure 4.1.

4.4.2 Constructing the Environmental Contour

We seek to find a contour in the physical space of wind speed and turbulence such that all the points on the contour have the same level of reliability. We start in standard normal space, $U_{1,2}$, where, because of symmetry, the locus of constant reliability is a circle with radius, β (see Figure 4.2). Transforming this circle from standard normal space to the physical space will produce the contour we seek in terms of the physical variables. The equations to transform the circle, in standard normal space, into the space described by the random variables for wind speed and turbulence are given as follows.

Transformation of U_1 to wind speed, V.

The U_1 coordinates of a circle in standard normal space are transformed to the physical space where the wind speed, V, follows a Rayleigh distribution, by first equating the probability values of u_1 and v, in terms of the cumulative distribution functions (CDF) and then solving for v in terms of u_1.

$$\begin{aligned} \Phi(u_1) &= F_V(v) \\ \Phi(u_1) &= 1 - \exp\left[-\left(\frac{v}{\alpha}\right)^2\right] \\ -\exp\left[-\left(\frac{v}{\alpha}\right)^2\right] &= \Phi(u_1) - 1 \\ \left(\frac{v}{\alpha}\right)^2 &= -\ln\left(1 - \Phi(u_1)\right) \\ v &= \alpha\sqrt{-\ln\left(1 - \Phi(u_1)\right)} \end{aligned} \tag{4.13}$$

Transformation of U_2 given V to conditional turbulence, I.

After having transformed the first standard normal variable to basic space, the second random variable may be transformed. The derivation of the equation for transforming the second coordinate, U_2, of the circle in standard normal space to the basic space where the conditional turbulence, I, follows a lognormal distribution is shown below. Again, the CDFs are first equated, and then in this

case, i is found in terms of u_2 and the wind speed dependent terms λ and ζ.

$$\begin{aligned}
\Phi(u_2) &= F_{I|V}(i, v) \\
\Phi(u_2) &= \Phi\left(\frac{\ln(i) - \lambda}{\zeta}\right) \\
u_2 &= \frac{\ln(i) - \lambda}{\zeta} \\
\ln(i) &= u_2\zeta + \lambda \\
i &= \exp\left(u_2\zeta + \lambda\right)
\end{aligned} \tag{4.14}$$

4.4.3 Transform circle to contour

In order to calculate the probability levels associated with the one-year and 50-year mean return periods, we assume the statistics of the wind process remain in a steady state condition over a duration of 10-minutes. The probability levels associated with the return periods of interest are then based on the number of 10-minute segments occurring in the prescribed time interval. We saw in Chapter 3 (Section 3.2) that the probability levels associated with the one-year and 50-year loads are:

$$p_{1\text{ year}} = \frac{10}{1 \times 365 \times 24 \times 60} = 1.9 \times 10^{-5} \tag{4.15}$$

$$p_{50\text{ years}} = \frac{10}{50 \times 365 \times 24 \times 60} = 3.8 \times 10^{-7} \tag{4.16}$$

The radius, β, of the circle in standard normal space is equal to the standard normal fractile associated with a prescribed probability level. In our case, the two values of β corresponding to our return periods of interest are:

$$\begin{aligned}
\beta_{1\text{ year}} &= \Phi^{-1}(1 - p_{1\text{ year}}) = 4.1190 \\
\beta_{50\text{ years}} &= \Phi^{-1}(1 - p_{50\text{ year}}) = 4.9451
\end{aligned}$$

Figure 4.3 shows the environmental contours associated with one-year and 50-year return periods. The contours were developed by first finding the coordinates of a circle with a prescribed radius, β, in standard normal space (i.e., $u_1^2 + u_2^2 = \beta^2$, see Figure 4.2) and then transforming the circle from the standard normal space into basic space using Equations 4.13 and 4.14. For example, we may consider the point (u_1=0, u_2=$\beta_{50\text{ years}}$) on the circle in standard normal space, where wind speed is at its median level, and the conditional turbulence is at its 50-year level. This transforms into the

point,

$$\begin{aligned} v &= \alpha\sqrt{-\ln(1-\Phi(0))} \\ &= \alpha\sqrt{-\ln(0.5)} \\ &= 9.3944\text{m/s} \end{aligned}$$

where α=11.28m/s (see Equation 4.7). Next we find the corresponding value of i at this point. With $\beta_{50\text{ years}}$=4.9451,

$$i = \exp\left(4.9451\zeta + \lambda\right)$$

where ζ and λ are given by Equations 4.9 and 4.10 with parameters I_{15}=0.18 and a=2.

$$\begin{aligned} \mu_{I|V} &= \frac{0.18(15\text{m/s} + 2(9.3944\text{m/s}))}{(2\text{m/s} + 1)} - 2\text{m/s}(0.18) \\ &= 1.6673\text{m/s} \end{aligned}$$

and

$$\sigma_{I|V} = 2\text{m/s}\,(0.18) = 0.36\text{m/s}$$

implying

$$\delta_{I|V} = \frac{0.36\text{m/s}}{1.6673\text{m/s}} = 0.2159$$

so

$$\begin{aligned} \zeta &= \sqrt{\ln((0.2159)^2 + 1)} = 0.2135 \\ \lambda &= \ln(1.6673) - \frac{1}{2}(0.2135)^2 = 0.4884 \end{aligned}$$

hence

$$i = \exp\left(4.9451(0.2135) + 0.4884\right) = 4.6834\text{m/s}$$

So the point (0,4.9451) on the circle with radius β=4.9451 in the (u_1, u_2) plane maps to the point (9.3944m/s, 4.6834m/s) in the (v, i) plane. Clearly this transformation is easily programmed to provide the entire contour in basic space (v, i) corresponding to the circle (u_1, u_2) in standard normal space.

We have developed a set of contours of the environmental variables that are related to prescribed return periods. The contours describe a locus of points each of which represent a point on a circle in standard normal space such that the probability of lying in a region outside a tangent line drawn through this point, in standard normal space, is equal to the probability level associated with the

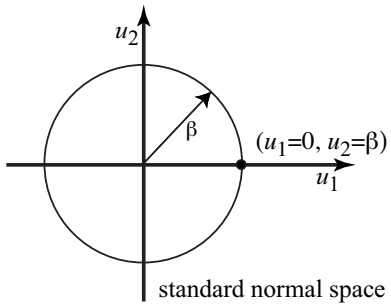

Figure 4.2: Circle in 2-D standard normal space defined by $\beta^2 = u_1^2 + u_2^2$.

prescribed return period. Note that the contours are dependent only on information that describes the environment and a prescribed reliability level.

To make use of the contour to estimate extreme events we need a description of the short-term response of the turbine—i.e., the response given a set of values of the environmental variables. In Chapter 3 we saw how we might obtain a description of the short-term response of the turbine. An estimate of the long-term extreme load can then be obtained by searching the contour for the maximum response. This estimate can be compared with an estimate obtained by integrating the short-term conditional response over the long-term distribution of the environmental parameters[49].

4.4.4 Describing the Short-Term Response

In the first two examples, we are interested in estimating the long-term extreme load on an AOC 15/50 horizontal axis wind turbine. The turbine, described in Chapter 1 (page 18), has a rotor diameter of 15m and a nominal rotor speed of 60 RPM at the rated wind speed of 12m/s. It is a three-bladed, fixed pitch turbine with a hub height of 25 meters [22]. The data set used to develop the description of the short-term response of the turbine is described in detail in Chapter 3 (page 66) and consisted of multiple 10-minute simulations of Gaussian wind fields and corresponding blade root bending moments. The wind input processes is described by the hub height wind speed.

Appendix C.3 presents a discussion on the development of the short-term extreme response of the AOC 15/50 turbine considering modeling the global peaks by a Gumbel distribution and defining the environmental variables in terms of the mean and standard deviation of the 10-minute wind process. In general, the methodology of the analysis consists of two steps. First, we compute the statistics of the response of interest, here the 10-minute extreme. Second, these statistics are related to the environmental variables. The functional form of the mean or expected short-term response

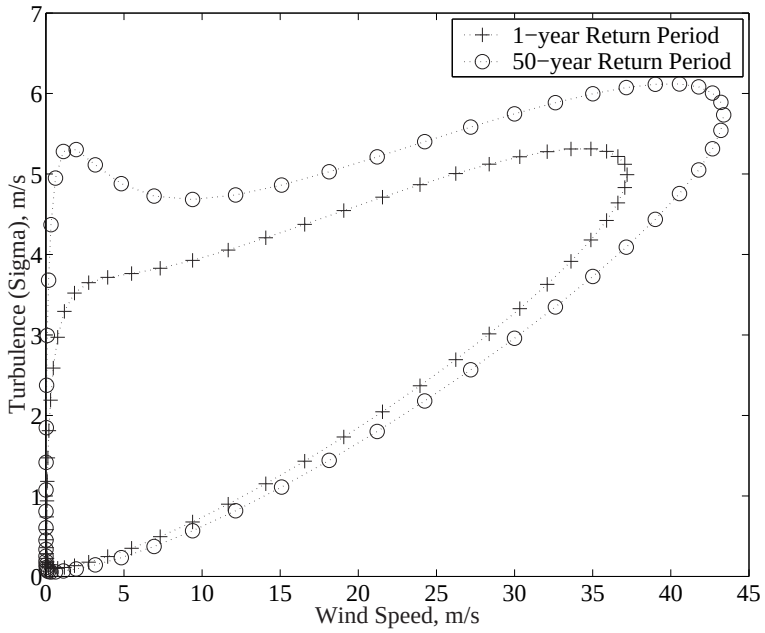

Figure 4.3: Environmental contour based on IEC IA wind class, one-year and 50-year return periods.

from Appendix C.3 is given as [54]:

$$\mu = a\left(\frac{V}{V_{\text{ref}}}\right)^{b}\left(\frac{I}{I_{\text{ref}}}\right)^{c} \tag{4.17}$$

Where V_{ref} and I_{ref} are the reference 10-minute mean wind speed and reference turbulence values respectively. In the remainder of this analysis, however, we treat the short-term extreme response as deterministic using the mean level conditioned on wind speed and turbulence. Therefore, the mean response given V and I becomes *the* response. We will come back to this point, in a later section, and discuss how the variability of the conditional short-term extreme response may be accounted for in obtaining an estimate of the long-term response. The coefficients a, b, and c were found using regression analysis.[2] The results of the regression analysis for the expected 10-minute extreme flap and edge bending loads are presented in Table 4.1. The reference wind speed and reference turbulence used in the regression analysis are given in Table 4.2. Also, with some wind turbines, e.g., pitch regulated machines, the response in the operating regime may not be monotonic with wind speed. This issue is addressed in the final example presented in this chapter.

[2]There are two load regimes for the turbine: one as a fixed structure when the turbine is parked, the other while the turbine is operating. Separate regression analyzes were conducted for each of these load regimes. The two functional forms that describe the turbine response are discontinuous at the maximum operating wind speed, see Figures C.2 and C.3.

Regression of the Mean of 10-Minute Maximum on V and I

Blade root flap bending

	a (kN-m)	b	c	R^2
$V \leqq 24$m/s	25.669	0.6090	0.0460	0.9233
$V > 24$m/s	40.181	2.5137	0.0184	0.9979

Blade root edge bending

	a (kN-m)	b	c	R^2
$V \leqq 24$m/s	8.6107	0.2693	0.0135	0.9718
$V > 24$m/s	7.2485	3.9850	0.0138	0.9960

Table 4.1: Regression coefficients used in Equation 4.17 to fit mean of the extreme 10-minute flap and edge bending loads as functions of the mean wind speed, V, and turbulence intensity, I.

Reference Wind Speed and Turbulence

	V_{ref} (m/s)	T_{ref} (m/s)
$V \leqq 24$m/s	16.474	2.5176
$V > 24$m/s	34.861	4.6074

Table 4.2: Reference wind speed and turbulence values used in Equation 4.17

4.4.5 Environmental Contours vs. Full Integration Method

Applying Environmental Contours

Figure 4.4 shows the 10-minute maximum blade root flap and edge bending iso-response lines plotted with the environmental contour from Figure 4.3. The response lines are calculated based on the regression models for the 10-minute extremes. This is done by fixing the value of the mean extreme response and plotting the V versus I contour associated with this value, and then repeating for various values of the mean extreme response. These contours are shown for the purpose of pedagogy and illustrating the respective response surfaces. In practice, it is only necessary to search the contour to find the maximum response. The maximum response corresponds to the response with the prescribed return period, as shown by the ★'s in Figure 4.4. Searching for the maximum response along the one-year mean return period contour results in an estimate of 47.4kN-m, for the blade root flap-bending load and 9.7kN-m, for the edge-bending load. Correspondingly, estimates of 69.9kN-m and 17.4kN-m were found for the flap and edge bending loads associated with the 50-year mean return period. Note that in three of the four cases the extreme is caused by the parked condition.

Figure 4.5 shows a plot of the value of the turbine response as a function of θ around the one-year and 50-year contour. The largest response is our estimate of the one-year or 50-year load respectively. Note that there may be local maxima, or instances where the global maximum is not that much larger than other peak response values along the contour. In these cases we may have a condition where multiple design points exist, where two or more sets of environmental variables yield similar load response on the turbine. Appendix D discusses how these multiple design points may affect our FORM estimates. It is clear from Figure 4.5(a), considering blade root flap bending moment, only one maximum exists for both the one-year and 50-year contours. In Figure 4.5(b) considering the one-year contour, however, it is not clear that we should necessarily discount the environmental condition at $\theta \approx 0$rad in favor of the actual global maximum shown at $\theta \approx 1$rad. In this example, a study of the shape of the limit state function in standard normal space, see Appendix D, shows that a reasonable approximation is achieved if we only consider the global maximum, little probability mass is excluded if we do not consider the set of environmental conditions at $\theta = 0$.

Full Integration Method

An alternative to the contour method shown above is to obtain an estimate of the one-year and 50-year loads from integrating the short-term response over the entire range of values of the environmental variables. Specifically, Equation 4.18 shows how an estimate of the long-term distribution of the 10-minute extreme load, L, can be obtained from integrating the distribution of the conditional

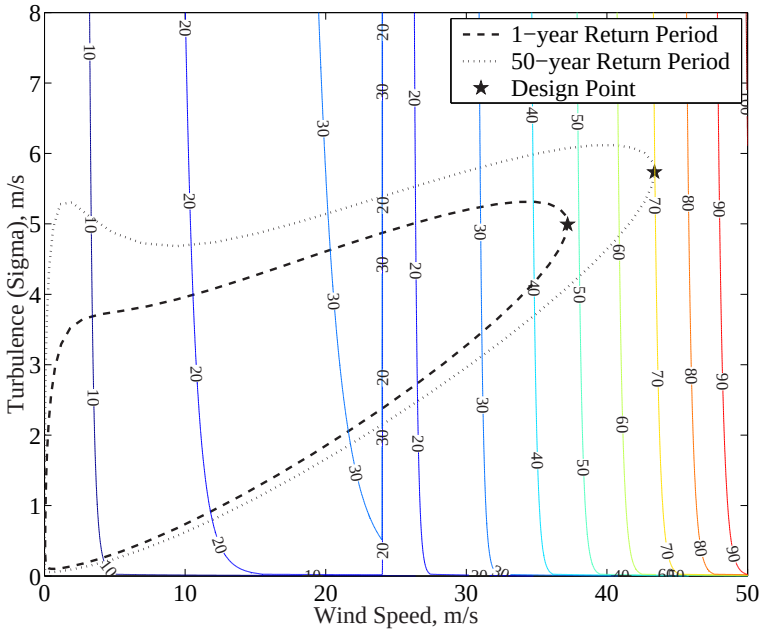

(a) Blade root flap bending

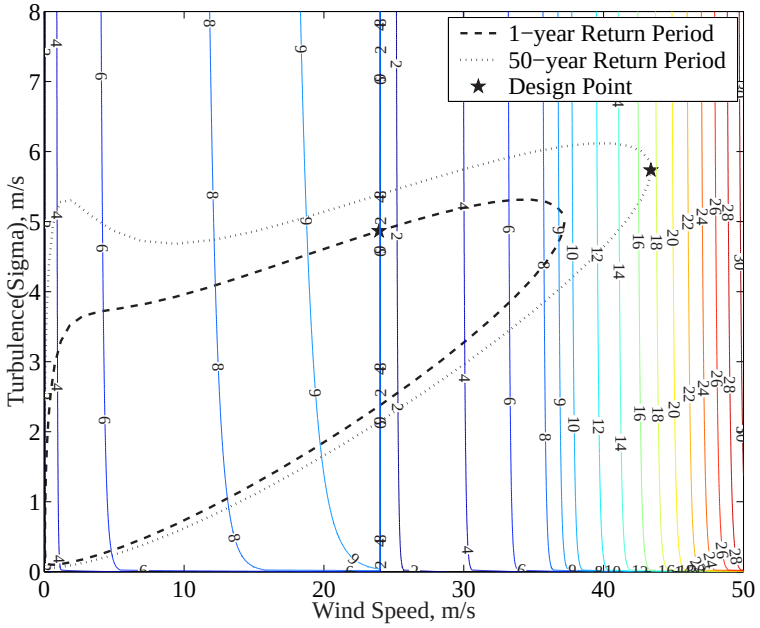

(b) Blade root edge bending

Figure 4.4: Environmental contour with blade root flap and edge bending iso-response curves. The ★'s represent the maximum response with the prescribed return period.

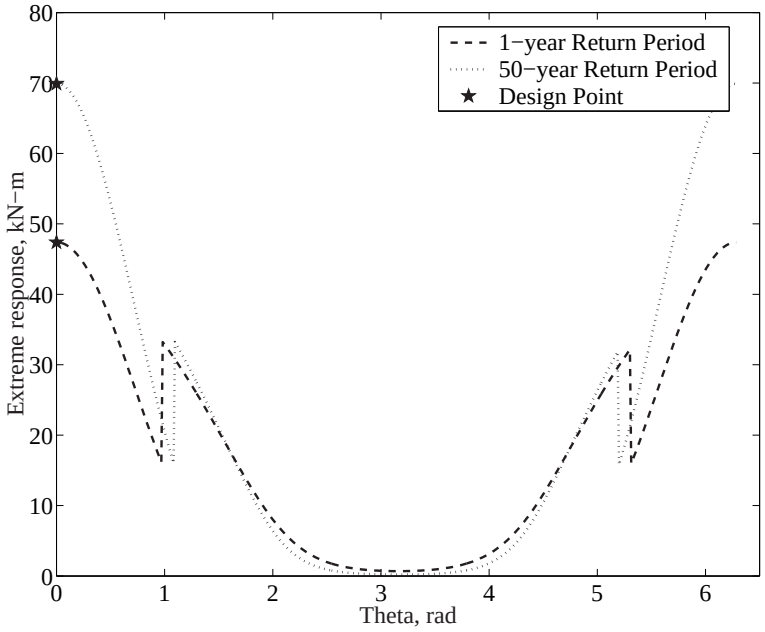

(a) Blade root flap bending

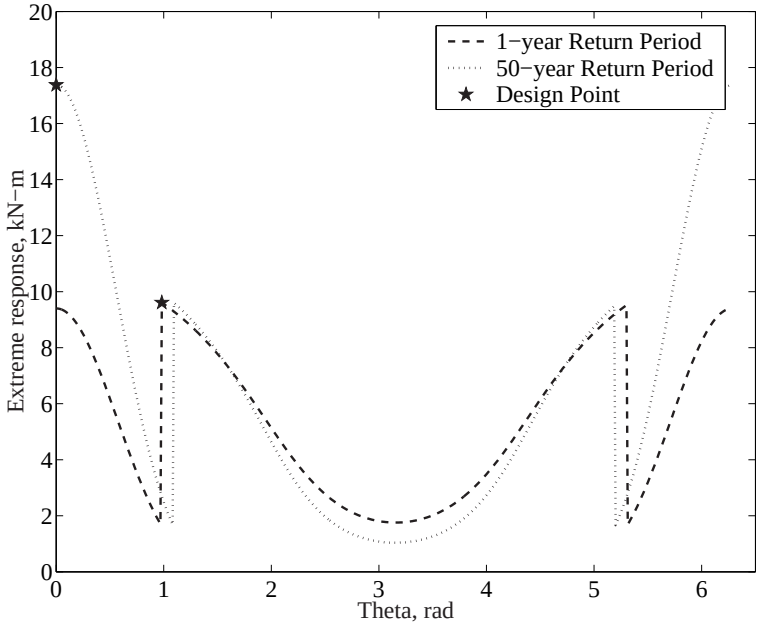

(b) Blade root edge bending

Figure 4.5: Extreme response as a function of angle, θ, in radians around circle in standard normal space for one-year and 50-year reliability levels. The ★'s represent the maximum extreme response.

short-term response over the joint probability density function of the environmental variables: wind speed V, and turbulence I.

$$P[L > l] = \iint_{\text{all v, i}} P[L > l|V, I] f_{V,I}(v, i)\, dvdi \tag{4.18}$$

In implementing Equation 4.18 the range of values of the environmental variables is discretized into evenly spaced intervals. For each pair of values of the environmental variables the corresponding distribution of the conditional short-term response is obtained. The conditional short-term response distributions are summed together; each weighted by the probability of the respective environmental variables, i.e., pair of values of the environmental variables occurring. The summation is performed over the entire range of environmental variables.

In this approach the three variables in Equation 4.18, conditional short-term response, conditional turbulence, and mean wind speed are considered random. In the examples presented in this chapter, however, the conditional short-term response is considered to be deterministic. We have shown in Chapter 3 that treating the short-term response deterministic but using a higher fractile, larger than the mean, may be used to recover the variability introduced when considering the short-term response random. We use the mean level here for simplicity and illustrative purposes; of course, other fractile levels could be used. (Note, to compare the results of the two methods, environmental contour and full integration,[3] the same fractile for the short-term response must be used for each analysis.) Figure 4.6 shows the long-term distributions of blade root flap and edge bending loads, considering the short-term response deterministic at its mean level, employing Equation 4.18 and the joint probability density function defined in Equation 4.12 and shown in Figure 4.1. Estimates of the one-year and 50-year load are the fractiles associated with the prescribed probability levels $p_{1\text{ year}}$ and $p_{50\text{ years}}$ and for blade root flap-bending are found to be equal to 47.4kN-m and 69.9kN-m, respectively. The estimates of the one-year and 50-year edge bending loads are 9.7kN-m and 17.4kN-m, respectively.

Comparison of Results

In this first example both methods return virtually the same estimates for the one-year and 50-year blade root flap and edge bending loads on the AOC 15/50 turbine installed at a hypothetical site with conditions similar to those described by the IEC class IA environment.

[3] What we refer to here as the full integration method only integrates over mean wind speed and turbulence, while fixing the short-term extreme at the mean value.

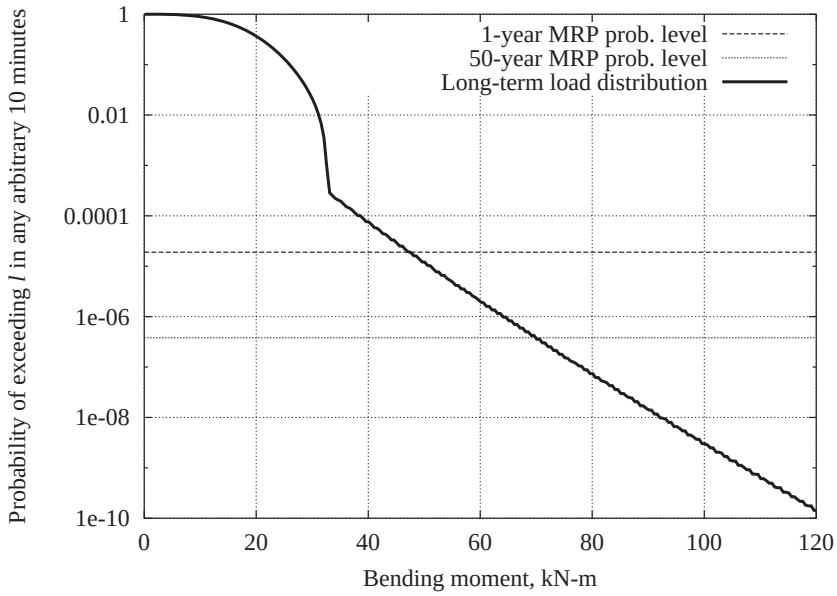

(a) Long-term distribution of extreme blade root flap bending moment for an arbitrary 10 minutes.

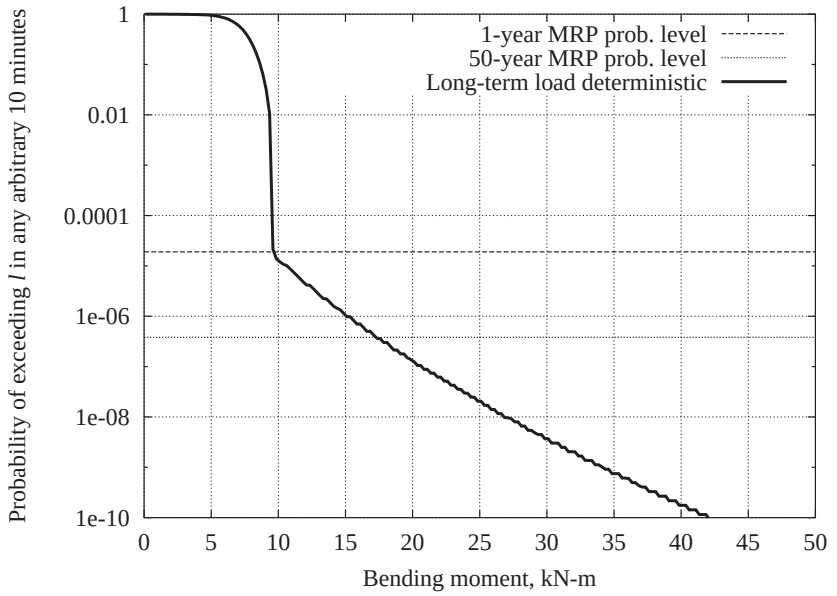

(b) Long-term distribution of extreme blade root edge bending moment for an arbitrary 10 minutes.

Figure 4.6: Long-term distributions of 10-minute extreme blade root bending moment, $L_{10\,\mathrm{min}}$, considering the short-term extreme load deterministic at mean level, for both: (a) flap and (b) edge bending. considered deterministic.

4.5 Example 2 — Field Data Model with Stall-Regulated Turbine

In this example an AOC 15/50, stall-regulated, turbine is assumed to operate at a test site in Lavrio, Greece. The turbulence variable is defined in terms of the coefficient of variation of the 10-minute wind process.

4.5.1 Description of Environment

In this second example, recorded field data is used to build a probabilistic description of the relationship between mean wind speed and turbulence. The distribution of mean wind speeds was assumed to be the same as in the first example, a Rayleigh distribution with mean, μ_V=10m/s. The data collected at a test site in Lavrio, Greece, was used to fit a rough estimate of the conditional distribution of turbulence. The analysis of the data was conducted by Manuel, et al. [50]. In this analysis the mean wind speed and turbulence are the environmental variables considered. Note that in this case the turbulence was alternatively defined as the coefficient of variation of the 10-minute wind process. (In the previous example the turbulence was defined as the standard deviation of the 10-minute wind process.) The resulting probabilistic description of these environmental variables, presented in [50], is used here. (Note that there was no attempt to match the model at the low wind speed end of the spectrum.) The conditional distribution of turbulence is given by the normal distribution shown below.

$$f_{I|V}(i|v) = \frac{1}{\sqrt{2\pi}\sigma_{I|V}} \exp\left[-\frac{1}{2}\left(\frac{i-\mu_{I|V}}{\sigma_{I|V}}\right)^2\right] \tag{4.19}$$

The functions of conditional mean and standard deviation of turbulence intensity given wind speed are shown in Equations 4.20 and 4.21, respectively.

$$\mu_{I|V} = 2.4486 v^{-0.9971} \tag{4.20}$$

$$\sigma_{I|V} = 0.025 \tag{4.21}$$

The joint probability density function of the environmental variables for the Lavrio test site is obtained by applying Equation 4.12. A plot of the resulting joint probability density function is shown in Figure 4.7. In comparing Figure 4.7, in this example, with Figure 4.1 in Example 1, the reader is reminded that in Figure 4.7, and the analysis in this second example, turbulence is defined as the coefficient of variation of the 10-minute wind process. Also note that the IEC class IA environment is intended to encompass a large variety of site conditions and is therefore generally more severe and conservative when compared to most specific sites.

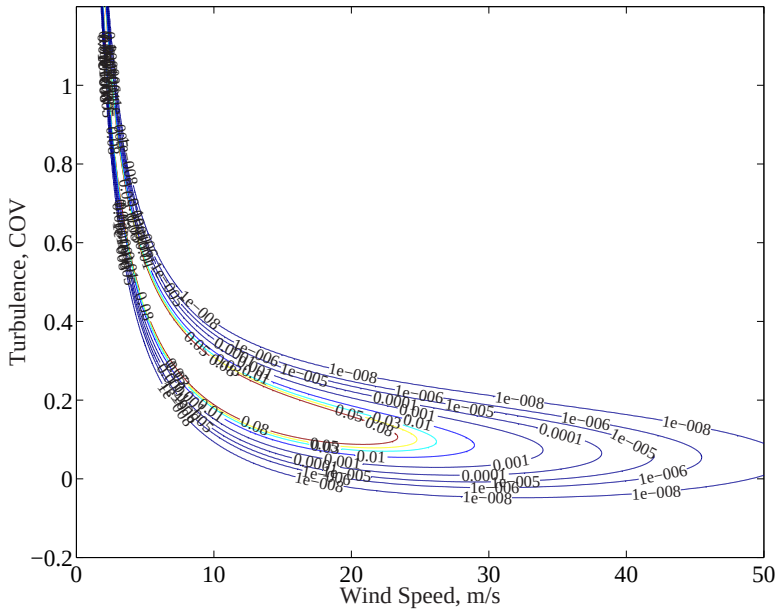

Figure 4.7: Joint probability density function for Lavrio, Greece site.

4.5.2 Constructing the Environmental Contour

In this case, the 10-minute mean wind speed follows the same probability distribution as presented in the first example. Therefore, the same transformation equation, to transform the U_1 coordinate of a circle in standard normal space to mean wind speed, V, in physical space applies and the derivation is not repeated here.

The equation for transforming the second coordinate, U_2, of a circle in standard normal space to physical space where the conditional turbulence, I, follows a normal distribution is shown below.

$$i = u_2 \sigma_{I|V} + \mu_{I|V} \tag{4.22}$$

Note the transformation is found by equating the probability levels and then solving for, i, in terms of u_2, and $\mu_{I|V}$, $\sigma_{I|V}$, the conditional mean and standard deviation of turbulence.

4.5.3 Description of Short-Term Response

The description for the short-term response of the AOC 15/50 turbine in this example is taken from Chapter 3. Note that except for the different definition of turbulence, the previous description of the short-term response of the turbine could have been used. The short-term description of the turbine can be used with any set of environmental contours, provided that environmental variables

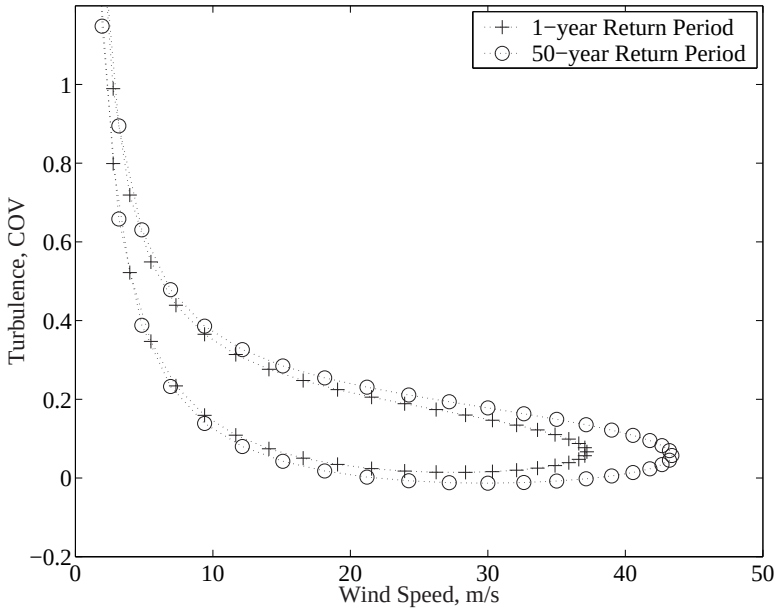

Figure 4.8: Environmental contour: Lavrio, Greece site.

are defined in a consistent manner.

The power law model in Equation 4.17 was used to relate the extreme response to the environmental variables. The results of the regression analysis in each load regime are shown in Table 4.3. The reference wind speed and reference turbulence used in the regression analysis are given in Table 4.4.

4.5.4 Environmental Contour vs. Full Integration Method

Figure 4.9 shows the 10-minute maximum iso-response lines plotted with the environmental contour from Figure 4.8. The response lines are calculated based on the regression model given in Equation 4.17 and the coefficients in Table 4.3 for the 10-minute extreme. A grid of pairs of environmental variables are evaluated and plotted as iso-response lines. Searching for the maximum response along the one-year return period contour results in an estimate of 40.2kN-m, for the one-year flap-bending load. Similarly, an estimate of 49.3kN-m was found for the 50-year flap-bending load. Correspondingly, estimates of the one-year and 50-year blade root edge bending loads are 10.2kN-m and 11.8kN-m, respectively.

Figure 4.10 shows a plot of the value of the turbine response as a function of θ around the one-year and 50-year contour. The largest response is our estimate of the one-year and 50-year load, respectively. In the cases presented in this figure, it is clear that there are no local maximums close

Regression of the Mean of 10-Minute Maximum on V and I

Blade root flap bending

	a (kN-m)	b	c	R^2
$V \leqq 24$m/s	25.664	0.7928	0.7129	0.9682
$V > 24$m/s	37.304	2.6079	0.0604	0.9985

Blade root edge bending

	a (kN-m)	b	c	R^2
$V \leqq 24$m/s	8.6100	0.3231	0.2084	0.9924
$V > 24$m/s	7.2275	4.1052	0.7718	0.9965

Table 4.3: Regression coefficients used in Equation 4.17 to fit mean flap and edge bending loads as a functions of the mean wind speed, V, and turbulence intensity, I.

Reference Wind Speed and Turbulence

	V_{ref} (m/s)	T_{ref} (%)
$V \leqq 24$m/s	16.474	15.28
$V > 24$m/s	34.861	13.18

Table 4.4: Reference wind speed and turbulence values used in Equation 4.17

in value to the global maximum as we saw in the first example. Regardless, the limit state functions, plotted in standard normal space, are shown in Appendix D.

Figure 4.11 shows the long-term distribution of flap-bending loads employing Equation 4.18 and the joint probability density function defined by Equation 4.12 and shown in Figure 4.7. In this example, the conditional short-term loads are considered to be deterministic at their mean level. Estimates of the one-year and 50-year flap-bending load are 37.8kN-m and 48.1kN-m, respectively. Corresponding estimates of the one-year and 50-year edge-bending loads are 10.0kN-m and 11.4kN-m respectively

In this example, the percent difference between the flap-bending load estimates obtained from the full integration method as compared with the environmental contour method is 6.0% and 2.4% for the one-year and 50-year extreme load, respectively. Similar results were found for edge-bending loads, i.e., 1.6% and 3.3% for the one-year and 50-year extreme loads, respectively. These estimates of the extreme loads apply to the AOC 15/50 machine, if it where installed at the Lavrio, Greece, test site. These results are lower than those predicited for the turbine if operating at a IEC class IA site. As mentioned earlier, the IEC class IA environment is intended to represent a wide range of site charateristics and is therefore more conservative when compared to most specific sites. If we contend that the IEC class IA environment is more conservative than the environment at the Lavrio, Greece, site, then we would expect to see lower estimates of extreme events at the Lavrio site than would be predicted from the IEC class IA environment. Indeed this is the result we find here.

4.6 Example 3 — Field Data Model with Pitch-Regulated Turbine

In this final example, we investigate a source of concern—if the contour method would give reasonable results, if in the operating regime the response of the turbine were not monotonic with wind speed. This behavior would be generally characteristic of a pitch-regulated turbine. To pursue this question we again consider the environmental description given in the previous example (Lavrio, Greece—turbulence defined as the coefficient of variation of the 10-minute wind process), and a hypothetical horizontal axis wind turbine with the flap-bending response behavior shown in Figure 4.12. This response behavior is based on the analysis of the AOC 15/50 turbine conducted in the previous example. However, the operating response has been modified by the author solely for the purposes of this illustration, by dividing it into two sections. The first section, below a 10-minute mean wind speed of 16.5m/s, the response increases with wind speed. The second section, above a wind speed of 16.5m/s, the response decreases with increasing wind speed. Both sections of the operating regime follow the power law model given in Equation 4.17 and the requisite coefficients

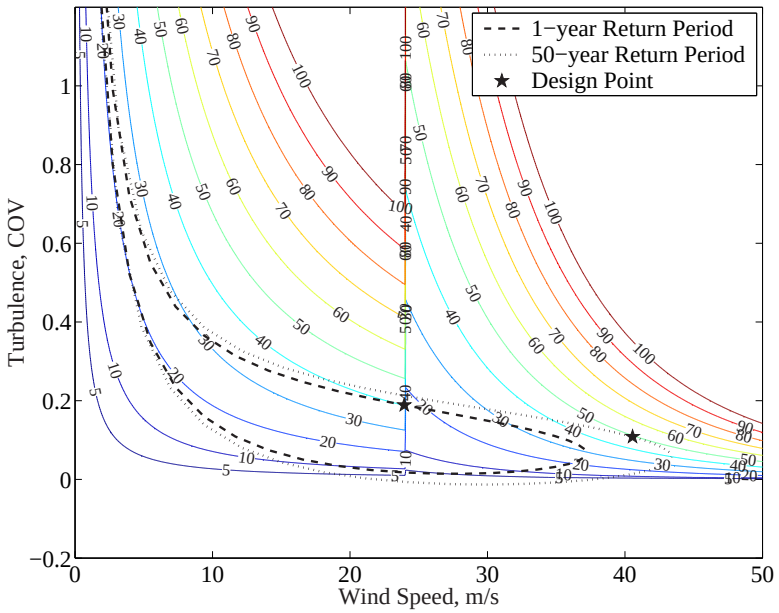

(a) Blade root flap bending

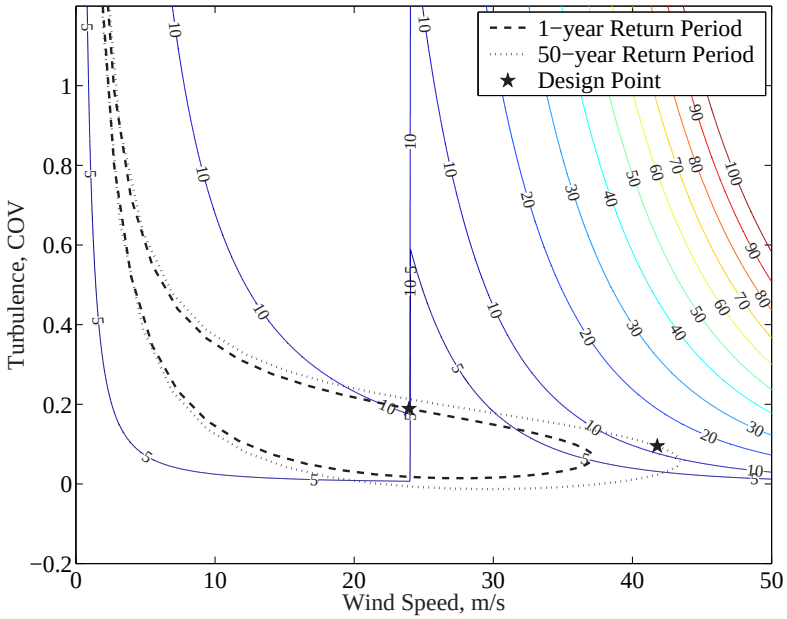

(b) Blade root edge bending

Figure 4.9: Environmental contour with flap and edge bending iso-response curves. The ★'s represent the maximum response with the prescribed return period.

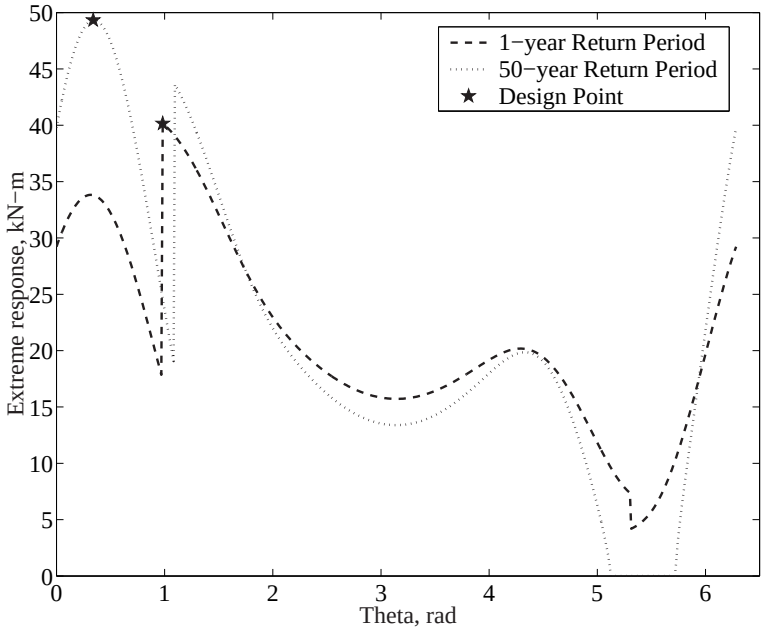

(a) Blade root flap bending

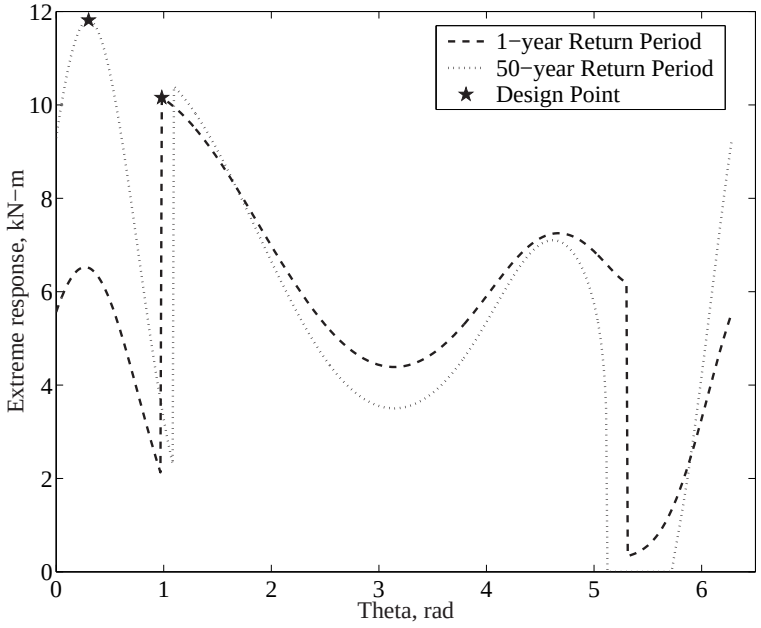

(b) Blade root edge bending

Figure 4.10: Extreme response as a function of angle, θ, in radians around circle in standard normal space for one-year and 50-year reliability levels. The ★'s represent the maximum extreme response.

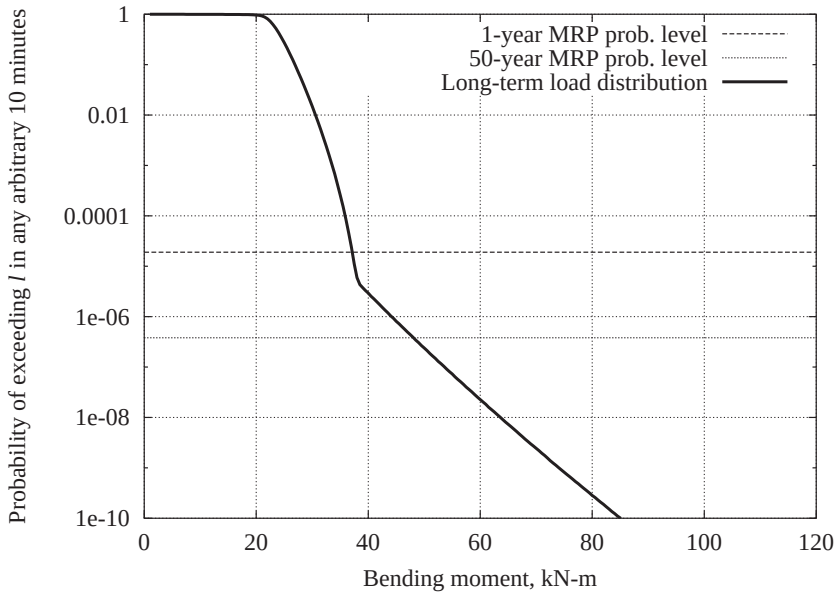

(a) Long-term distribution of extreme blade root flap bending moment for an arbitrary 10 minutes.

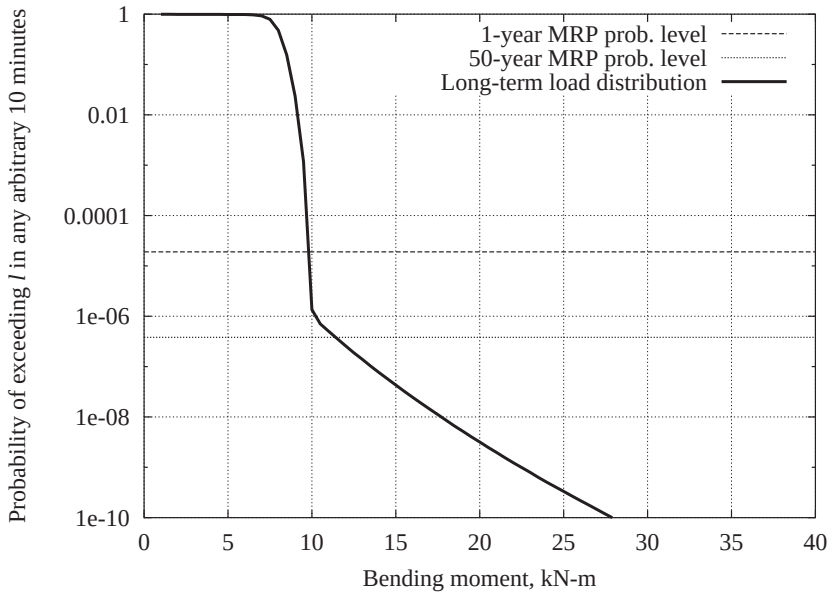

(b) Long-term distribution of extreme blade root edge bending moment for an arbitrary 10 minutes.

Figure 4.11: Long-term distributions of 10-minute extreme blade root bending moment, $L_{10\,\mathrm{min}}$, considering the short-term extreme load deterministic at mean level, for both: (a) flap and (b) edge bending. considered deterministic.

Flap Loading

Regression on Mean of 10-minute maximum

	a (kN-m)	b	c
$V \leqq 16.5$m/s	25.664	0.7928	0.7129
$16.5 < V \leqq 24$	25.664	-0.7928	0.7129
$V > 24$m/s	37.304	2.6079	0.0604

Table 4.5: Regression coefficients used in Equation 4.17 for flap load as a function of the mean wind speed, V, and turbulence intensity, T.

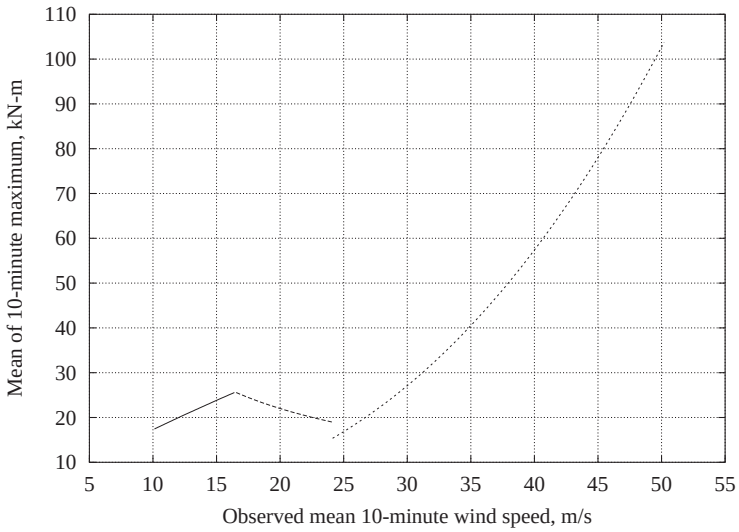

Figure 4.12: Constructed flap load response versus mean wind speed.

are shown in Table 4.5. The reference wind speed and reference turbulence used are given in Table 4.4. Note, that for the first section of the operating response (below 16.5m/s) the behavior of the turbine is the same as presented in Example 2. We have simply forced the behavior of the turbine above 16.5m/s to exhibit a non-monotonic behavior by prescribing the values of the power law model coefficients. The response in the parked wind speed regime has not been modified and represents an unfeathered blade condition. In this example, two discontinuities exist. The first discontinuity is in the operating regime of the turbine; a slope discontinuity occurs at 16.5m/s for the 10-minute mean wind speed. The second discontinuity occurs at the maximum operating 10-minute mean wind speed (24m/s), where the response of the turbine switches from the operating regime to parked regime.

4.6.1 Comparing Environmental Contour and Full Integration

Figure 4.13 shows the 10-minute maximum iso-response lines plotted with the Lavrio test site environmental contour from Figure 4.8. The response lines are calculated based on the model given in Equation 4.17 and the coefficients in Table 4.5 for the 10-minute extreme. Searching for the maximum response along the one-year return period contour, results in an estimate of 38.2kN-m, for the one-year flap-bending load. Similarly, an estimate of 49.2kN-m was found for the 50-year flap-bending load. We can see a significant change in the iso-response lines, compared with Figure 4.9, as a result of the non-monotonic description of the response of the turbine. We would expect higher extreme loads near a 10-minute mean wind speed of 16.5m/s and the iso-response lines reflect this. In the previous example we observed that the maximum response of the one-year extreme load occurred at the highest operating wind speed. For the description of the response used here, we would expect to see the maximum response along the one-year return period contour to occur closer to the 16.5m/s wind speed rather than at 24m/s, the highest operating wind speed, since in this section the extreme load is decreasing with wind speed. We find that from the contour analysis the maximum response does occur at a much lower wind speed; just below 16.5m/s, see Figure 4.13. The 50-year extreme load is still driven by higher wind speeds. We would expect this outcome as we have only slightly modified the operating regime model and the description of the environment has stayed the same.

Figure 4.14 shows a plot of the value of the turbine response as a function of θ around the one-year and 50-year contour. The largest response is our estimates of the one-year and 50-year load, respectively. In this figure we can see how the response changes as we traverse the contour. From Figure 4.13 we may anticipate, for the one-year contour, that we may have multiple design points. Figure 4.14 confirms this suggestion. The sets of environmental variables corresponding to $\theta = 0.5\pi$ and $\theta = 1.5\pi$ produce a similar load response on the turbine. A study of the shape of the limit state function plotted in standard normal space (see Appendix D) shows that under the assumptions of form analysis, similar results would be obtained if either point were used. However, a more accurate approximation may be obtained if a more complicated method of implementing second-order methods and system analysis were employed. A further discussion is presented in Appendix D. Figure 4.15 shows the long-term distribution of flap bending loads employing Equation 4.18 and the joint probability density function defined by Equation 4.12 and shown in Figure 4.7. In this example the conditional short-term loads are considered to be deterministic at their mean level. Estimates of the one-year and 50-year flap-bending load are 33.8kN-m and 48.1kN-m, respectively.

In this example, the percent difference between the flap bending load estimate obtained from the full integration method as compared with the environmental contour method is 13.0% and 2.2% for

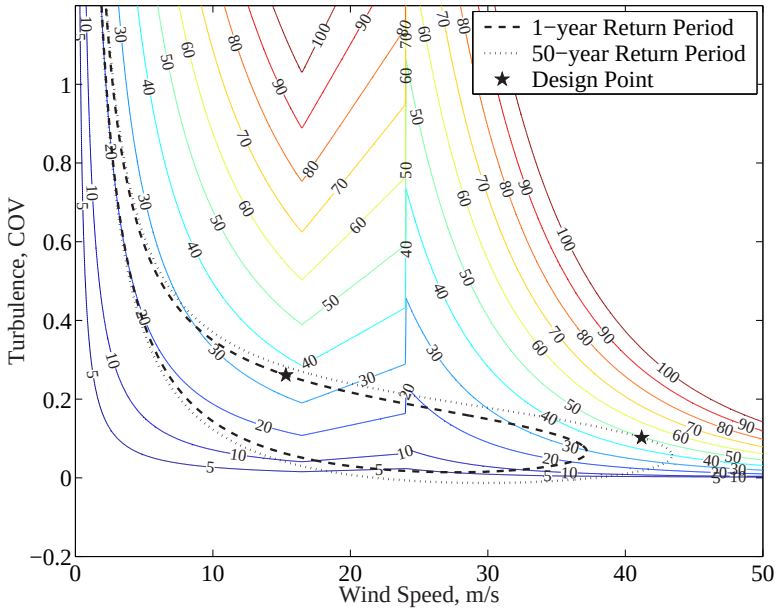

Figure 4.13: Environmental contour with flap bending iso-response curves. The ★'s represent the maximum response with the prescribed return period.

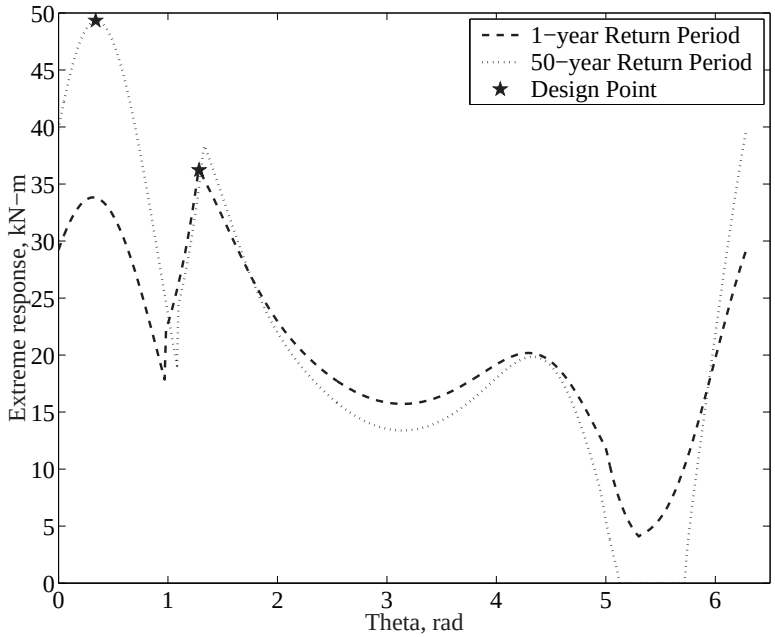

Figure 4.14: Extreme response as a function of angle, θ, in radians around circle in standard normal space for one-year and 50-year reliability levels. The ★'s represent the maximum extreme response.

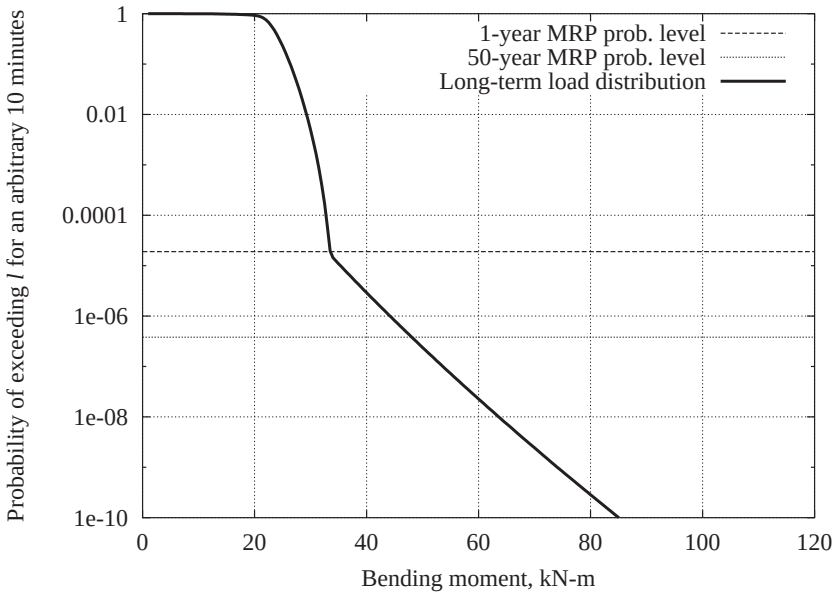

Figure 4.15: Long-term distribution of 10-minute extreme blade root flap bending moment, $L_{10\,\mathrm{min}}$, considering the short-term extreme load deterministic at mean level.

the one-year and 50-year extreme load, respectively. These results confirm the estimates obtained from the contour method for our hypothetical pitch-regulated turbine subjected to the description of the environmental conditions at the Lavrio, Greece, test site. We might attribute the larger difference in the estimates of the one-year load between the two methods as a result of the added slope discontinuity. These discontinuities present a major test to the FORM methodology. One of the underlying assumptions in FORM analysis is that the limit state function is generally smooth.

4.7 Including the Third Random Variable

In the previous examples the environmental contours were based on the two environmental random variables. The short-term extreme loads were considered deterministic. We know, however, that the short-term loads have an associated variability.

If we considered the short-term extreme response of the first example random, modeled by a Gumbel distribution, for example, as shown in Appendix C.3 and use the full-integration method, then the estimates of the one-year and 50-year flap-bending loads are 52.4kN-m and 74.3kN-m, respectively. This is a difference of 9.5% and 5.9% for the one-year and 50-year loads compared with the estimates considering the short-term extreme loads deterministic and integrating. Similarly, considering the edge bending loads, the estimates of the one-year and 50-year loads, considering

the short-term loads modeled by a Gumbel distribution, are 12.26kN-m and 19.3kN-m, respectively. This is a difference of 20.9% and 9.8% for the one-year and 50-year loads, respectively.

For the second example, if we consider the short-term extreme response random, also modeled by a Gumbel distribution (this is the analysis presented in Chapter 3), then the estimates of the one-year and 50-year flap-bending loads are 49.1kN-m and 59.7kN-m, respectively. This is a difference of 23.0% and 19.4%. Similarly, considering the edge bending loads, the estimates of the one-year and 50-year loads considering the short-term loads modeled by a Gumbel distribution are 11.8kN-m and 13.7kN-m, respectively. This is a difference of 15.3% and 16.8% for the one-year and 50-year loads, respectively. Again, these comparisons are based on implementing the integration method to demonstrate the difference between considering the short-term extremes deterministic or random. These results are summarized in Table 4.6. This topic was discussed in detail in Chapter 3. Therefore, from these comparisons we can see that the appropriate choice of the fractile of the short-term response used in the contour analysis is not a trivial matter. There are several ways to include or recover the variability of the short-term response in the contour method presented earlier. We will discuss briefly a few of them here.

We might consider using inflated fractiles, similar to the work discussed in Chapter 3(Fitzwater and Cornell [49]) or omission factors (see Winterstein, et al. [59]). In these approaches, the 2-D environmental contours are “inflated” to account for variability in the short-term load. How much the contours, based on expected extreme loads, would have to be inflated, may be based on the variability of the short-term response, which of course may differ between turbine designs. Universal fractiles would need to be chosen judiciously.

Another approach would be to consider constructing a 3-D contour including the randomness of the load variable directly. After having constructed transformation equations, a contour in 3-D space, wind speed, conditional turbulence, and conditional short-term response, could be constructed. It would then be a more involved matter to search the 3-D contour for the maximum response.

It should be noted, however, that implementing any of the methods above re-couples the problem between the wind turbine machine and the site. The contour developed would be specific to a particular site and wind turbine. The 2-D environmental contours presented in this paper are dependent only on the site conditions, and therefore any consistently defined description of short-term wind turbine response could be used. The 3-D contours developed would be applicable only to the specific turbine used in the analysis. A new analysis would have to be conducted to obtain a 3-D contour for a different wind turbine at the same site. The question of how to deal with the variability associated with a third variable (or more) continues to be a topic of ongoing research.

Comparison of One-Year and 50-Year Blade Root Flap and Edge Bending Loads Considering Conditional Short-Term Load Alternatively Random and Deterministic

Example 1—IEC Model with Stall-Regulated Turbine

	1-Year Load(kN-m)			50-year Load(kN-m)		
	Random	Deterministic	% Diff.	Random	Deterministic	% Diff.
Flap	52.4	47.4	-9.5%	74.3	69.9	-5.9%
Edge	12.3	9.7	-20.9%	19.3	17.4	-9.8%

Example 2—Field Data Model with Stall-Regulated Turbine

	1-Year Load(kN-m)			50-year Load(kN-m)		
	Random	Deterministic	% Diff.	Random	Deterministic	% Diff.
Flap	49.1	37.8	-23.0%	59.7	48.1	-19.4%
Edge	11.8	10.0	-15.3%	13.7	11.4	-16.8%

Table 4.6: Comparison of one-year and 50-year blade root flap and edge bending loads, considering conditional short-term load alternatively either random, modeled by a Gumbel distribution, or deterministic.

4.8 Conclusion

In this chapter we have presented a brief discussion of the theory of first-order reliability analysis and how through inverse-FORM, contours of design environmental conditions can be constructed.

These theories were applied in three different examples. The first two examples demonstrated how estimates of the one-year and 50-year extreme blade bending loads on an AOC 15/50 turbine might be obtained using environmental contours. The description of the environment was different in each of these examples. The environment in the first example was based on an IEC class IA wind environment. In the second example the environment was based on an analysis of field collected data at the Lavrio, Greece, test site. In both examples, the estimates obtained from the environmental contour method were compared with estimates obtained from integrating the short-term extreme loads over the long-term distribution of the environmental variables. In general, the estimates differed by only about 5%. We mentioned earlier that FORM is an approximate method, and the non-linear nature of the limit state function can have an effect on the efficacy of the method to provide an accurate approximation. We have seen in the examples considered here, even with the presence of a discontinuity in the limit state function at the cut-out wind speed, FORM provides a reasonable approximation. This is, of course, not true in general, and our result is based on the turbine, site data, and distribution models seen here. In general terms, we may expect this result, however, if it can be shown that the discontinuity in the limit state function is sufficiently far away from the design point so as not to affect the gradient calculations. The reader is referred to

Appendix D for a further discussion.

The third example again used the description of the environment from the Lavrio test site. In this case, however, the short-term response was developed to simulate the typical non-monotonic response of a pitch-regulated machine. This contributed a slope discontinuity in the limit state function. Again estimates of the one-year and 50-year extreme flap-bending loads were obtained from both methods. The estimates of the one-year load differed by about 13% while the estimates of the 50-year load differed by about 2% between the two methods. Including the additional slope discontinuity did not greatly affect the efficacy of FORM to provide an acceptable approximation, at least for the turbine, site data, and distribution models used in this analysis.

We have demonstrated that the environmental contour method provides estimates of extreme response similar to those obtained by the integration method. One advantage of using environmental contours is that the contours themselves are developed only based on data relating to the environment and a reliability criterion for the turbine. Therefore, the contours immediately give some insight into the critical combinations of environmental variables and may lead to a reduction in the required number of environmental conditions explored in the design process. In particular, instead of interrogating the entire space of combinations of environmental conditions for the critical response of the turbine, the contour identifies the critical environmental conditions. We only need to search the points along the contour to find the critical response of the turbine, for a prescribed reliability level. This can be a great benefit when running expensive computer simulations–we only need to run simulations at environmental conditions on the contour. A carefully constructed search algorithm, to interrogate the environmental contour, may lead to additional reduction in the number of environmental conditions considered in the quest to find the critical response of the turbine.

Chapter 5

Estimation of Fatigue Distributions

International standards for wind turbine certification depend on finding long-term fatigue load probability distributions that are consistent with respect to the state of knowledge for a given system. Statistical moment-based models of loads for fatigue applications are described and demonstrated here using flap and edge blade-bending data from a commercial turbine. Distributions of rain-flow-counted range data are characterized by a limited number of their statistical moments. Beyond the convenient two-moment (Weibull) model, a few higher-moment models are considered. These include: (1) a "quadratic Weibull" model, which uses a quadratic distortion of the original Weibull model to preserve the first three moments of the data; and (2) a "damage-based" Weibull model, which seeks to fit a two-moment model not to the stress ranges themselves, but to a power-law transformation of these that directly reflects "damage" (e.g., based on typical material fatigue properties). The damage-based model is shown to follow the upper tail of the observed data, while the three-moment model also gives a good tail-fit if the non-damaging low-amplitude ranges are first excluded.

5.1 Introduction

The capital cost of new product development has driven the industry toward a sophisticated reliance on numerical simulation and analysis. Fatigue loads are required to be estimated using extreme turbulence levels—intended to envelop the worst measured turbulence levels from around the world. Standards (e.g., IEC [23]) therefore specify analysis at conditions that are easily simulated, but may never be measured on a prototype in the field. Loads must be extrapolated from site conditions to design standard conditions.

Parametric, moment-based models have the ability to describe the reliance of the turbine on the

specified turbulence levels by determining the relationship between the governing parameters (moments) of the turbine response and the wind environment (average wind speed, V, and turbulence intensity, I). The fatigue response is characterized by the rain-flow counted load ranges R in the response time history. A minimal number of central moments of the rain-flow ranges can be used to characterize the distribution of ranges at a given set of inflow conditions. Remaining questions include (1) how many moments are sufficient to predict fatigue damage, which is nonlinearly related to load range amplitude, and (2) how can "higher-moment" models (i.e., including moments of higher than second order) be conveniently constructed?

Here, we present two such higher-moment models: a quadratic Weibull model based on three moments, and a "damage-based" Weibull model based on even higher moments, which are proportional to fatigue damage. The quadratic Weibull model has been previously introduced and applied to other cases of fatigue loads (e.g., Lange [63]; Veers and Winterstein [54]; Ronold et al. [46]) and we saw how this model could be applied to extreme loads in Chapters 2 and 3 (also see Fitzwater and Winterstein [38]). In contrast, the damage-based Weibull model is new, suggested here as an alternative that confers certain advantages in some fatigue applications. We demonstrate the use of these models by studying two orthogonal blade-root bending moments: "flap" (out of the plane of blade rotation) and "edge" (in the plane of rotation). The challenges in these cases for the random vibration analyst include the harmonic content of the loads from the rotational motion of the blades, as well as other less easily described nonlinear effects.

The fatigue-load spectra are calculated by splitting the problem into "short-term" and "long-term" aspects. The short-term distribution of load ranges is characterized by operation of the turbine in short (10-minute) quasi-stationary wind conditions (constant average wind speed, V, and turbulence intensity, I). The short-term distribution of load ranges is tied to the relevant statistical moments of the ranges - which, in turn, are related by regression to the input average wind speed and turbulence intensity. Thus, the short-term distribution of ranges may be predicted for any combination of wind conditions. The long-term distribution of ranges is then easily obtained by integrating over the joint annual distribution of input conditions.

The approach described above is conducted considering two alternatives for modeling the short-term load. In Section 5.4, an estimate of the long-term distribution of fatigue loads is obtained where the short-term fatigue ranges are modeled by a quadratic Weibull distribution. Alternatively, in Section 5.5, an estimate of the long-term distribution of fatigue loads is obtained where the short-term fatigue ranges are modeled by a damage-based Weibull model. In addition to obtaining estimates of the long-term distribution of fatigue stress ranges, we estimate a measure of the expected damage for different material fatigue exponent values.

5.2 Data Set

The data set used in this analysis is for the Atlantic Orient Corporation AOC 15/50 turbine, described in Chapter 1 (page 18). The turbine has a rotor diameter of 15m, a fixed rotor speed of about 60 RPM, and a rated wind speed of 12m/s. It is a three-bladed, fixed pitch turbine with a hub height of 25 meters [22]. The data set is described in detail in Chapter 3 (page 66) and consisted of multiple 10-minute simulations of Gaussian wind fields and corresponding blade root bending moments. The wind input processes is described by the hub height wind speed. The blade root flap and edge bending moment response time histories were assumed to be repeating and were rain-flow counted using the simplified rain-flow counting for repeating histories method given in ASTM standard E-1049.

5.3 Probability Models for Fatigue Loads

Similar to the analysis performed in the previous chapters, we assume here that the stress response of the wind turbine remains stationary within each 10-minute duration event. To predict fatigue damage in such an event, it is common to assume that a single stress range, R, produces damage $D \propto R^{b_f}$. More formally, the basic relation between fatigue stress ranges and the number of cycles to failure, N, is given by Basquin's Relation [64]:

$$R = \sigma'_f (N)^B \tag{5.1}$$

Where, σ'_f, is the fatigue strength coefficient, and B is the fatigue strength exponent. The damage per cycle is defined as one over, N.

$$D = \frac{1}{N} \tag{5.2}$$

Solving Equation 5.1 for N and relating to Equation 5.2, we have a relation for the damage based on the stress range.

$$D = \left(\frac{R}{\sigma'_f} \right)^{b_f} \quad \rightarrow \quad D \propto R^{b_f} \tag{5.3}$$

$$\text{where, } b_f = -\frac{1}{B}$$

If R, the stress range, is taken as a random variable, and σ'_f and b_f are deterministic coefficients, then the damage, D, will also be a random variable. The expected damage from an arbitrary cycle,

k, may be found by taking the expectation of Equation 5.3.

$$\begin{aligned}
\mathsf{E}[D_k] &= \sum_{i=1}^{\infty} d_i \; P[D = d_i] \\
&= \sum_{i=1}^{\infty} \left(\frac{r_i}{\sigma'_f} \right)^{b_f} P[R = r_i] \\
&= \left(\frac{1}{\sigma'_f} \right)^{b_f} \sum_{i=1}^{\infty} (r_i)^{b_f} \; P[R = r_i] \\
&= \left(\frac{1}{\sigma'_f} \right)^{b_f} \mathsf{E}[R^{b_f}] \\
\mathsf{E}[D_k] &\propto \mathsf{E}[R^{b_f}]
\end{aligned} \tag{5.4}$$

The important conclusion is that we should be interested in some higher moment of R (b_f, being greater than one for the materials of interest). We will refer back to this in the next sections, which describe three probability models used for estimating the distribution of fatigue ranges. This result will also be used in a later analysis to estimate the expected total damage in an arbitrary 10 minutes or over longer durations.

5.3.1 The Standard Weibull Model

A conventional approach is to model an arbitrary stress range, R, as a random variable, $W = R$, with Weibull probability distribution function:

$$P[W > w] = \exp\left[-(w/\alpha_W)^{\beta_W} \right] \tag{5.5}$$

The corresponding statistical moments of W are given by

$$\mathsf{E}[W^m] = \alpha_W^m (m/\beta_W)! \tag{5.6}$$

where $(\cdot)!$ denotes the factorial function. In practice, one estimates the first two statistical moments from the data, and uses Equation 5.6 with $m = 1$ and 2 to infer the parameter values of α_W and β_W. The mean damage per cycle, $\mathsf{E}[D] \propto \mathsf{E}[R^{b_f}]$ (Equation 5.4), is also found directly from Equation 5.6 for arbitrary $m = b_f$.

There are two main benefits of this Weibull model. First, it requires relatively little data; specifically, data sufficient only for accurate prediction of the first two moments of the stress ranges. Second, the closed-form moment results facilitate both the parameter fitting of α_W and β_W from

the data, and the consistent estimation of $\mathsf{E}[D]$ from α_W and β_W. To illustrate the fit of the standard Weibull model to data, Figure 5.1 shows range results for a turbine operating in wind conditions: 10-minute mean wind speed, $V = 24$m/s and turbulence class A. This data is taken from one of the 100 simulated samples for the turbine operating in these environmental conditions. The data are plotted on a Weibull scale for the flap data in Figure 5.1(a) and for the edge loads in Figure 5.1(b). These plots transform the vertical scale by plotting not the cumulative distribution $F_R(r) = P[R < r]$ but rather $-\ln[1 - F_R(r)]$, so that the Weibull distribution will appear as a straight line on a log-log plot. Figure 5.2 shows range results for a parked turbine. The data were taken from one of the 100 simulated samples with wind conditions: $V = 50$m/s turbulence class A, and the turbine parked. The flap loads are shown in Figure 5.2(a) and the edge loads are shown in Figure 5.2(b).

The simple two-moment characterization of the Weibull model is also its potential drawback. Typical b_f values for metals may range from 3 to 8, with lower values more typical for welded steels and higher values for aluminum. As b_f increases, $\mathsf{E}[D] \propto \mathsf{E}[R^{b_f}]$ becomes increasingly sensitive to the details of the stress range distribution in its upper tail. Any deviation from the Weibull model in this upper region can lead to erroneous damage predictions. Composites often show still higher b_f values—e.g., $b_f = 10$ or higher—and hence give still larger potential for the two-moment Weibull model to err. We describe here two models that seek to address these potential modeling errors through the use of higher-order statistical moments.

5.3.2 The Quadratic Weibull Model

The quadratic Weibull model again starts with a Weibull variable W, whose parameters α_W and β_W are chosen to preserve the first two range moments. A quadratic perturbation term is then added to better model the actual range, R:

$$R = R_0 + \kappa[W + \epsilon W^2] \tag{5.7}$$

The coefficient ϵ is chosen here so that the skewness (third normalized moment) of the range data is preserved. The remaining parameters, κ and R_0, are finally chosen to preserve the variance and mean of R respectively. (Note that Equation 5.7 is applied directly only when the skewness of R is found to exceed that of the Weibull variable W. In this case, the quadratic term ϵW^2 serves to enhance the skewness, from that of the Weibull variable to that of the observed ranges. If the skewness of R is instead found to be less than that of W, the roles of R and W in Equation 5.7 are interchanged.) Additional technical details can be found in Lange [63, 65] and Manuel, et al. [52, 53]. Other applications of this model to fatigue loads can be found in Ronold, et al. [46] and Manuel, et al. [50]. We saw how this model could be applied to extreme loads in Chapters 2 and 3;

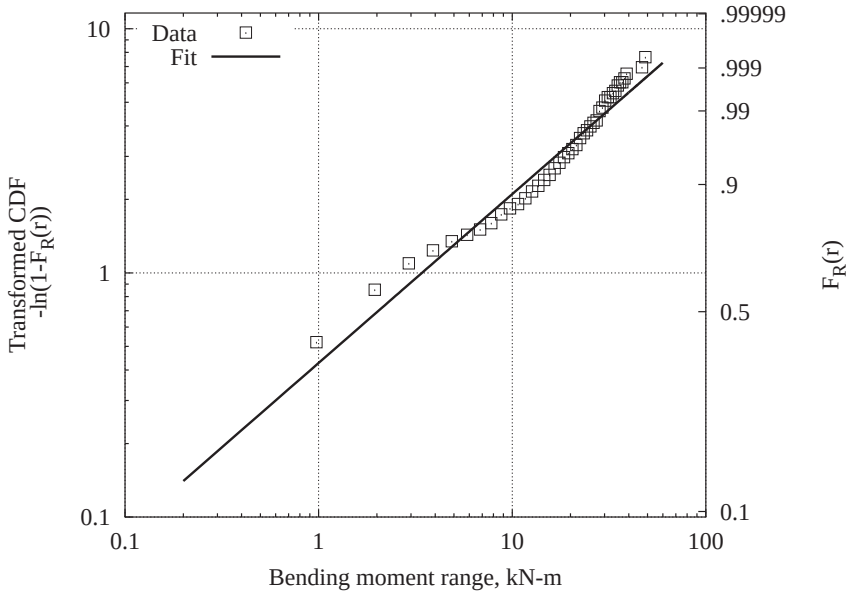

(a) Blade root flap bending.

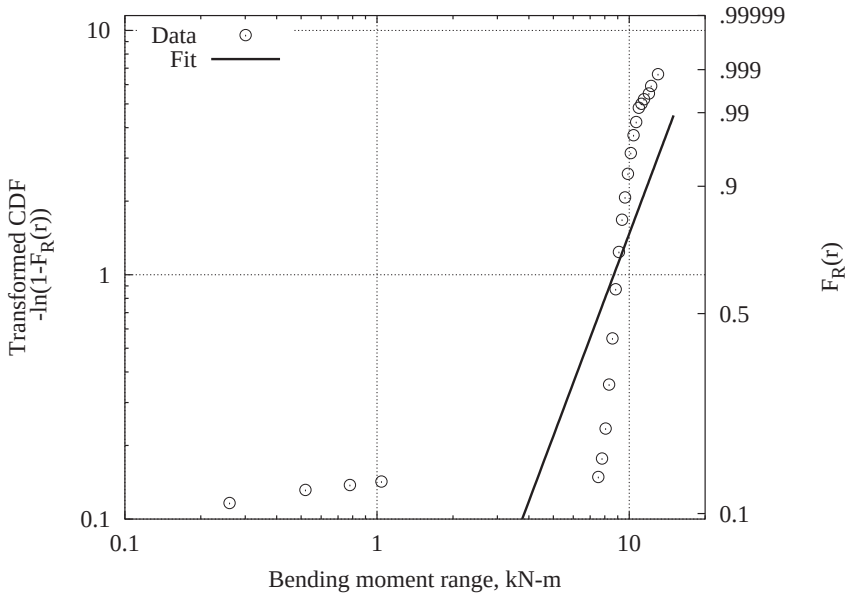

(b) Blade root edge bending.

Figure 5.1: Standard Weibull model fit to blade root flap and edge bending moment fatigue ranges for AOC 15/50 turbine operating in an environment with a 10-minute mean wind speed of 24m/s and turbulence class A.

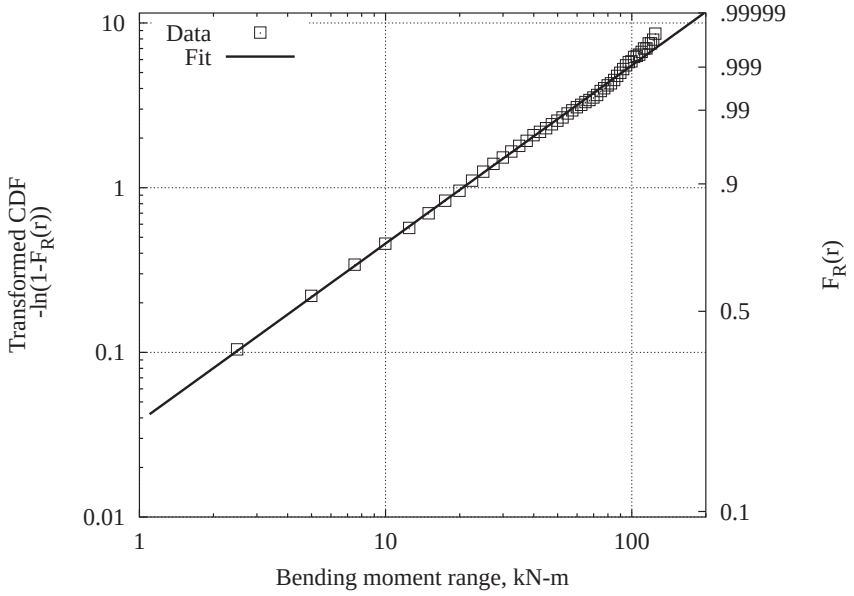

(a) Blade root flap bending.

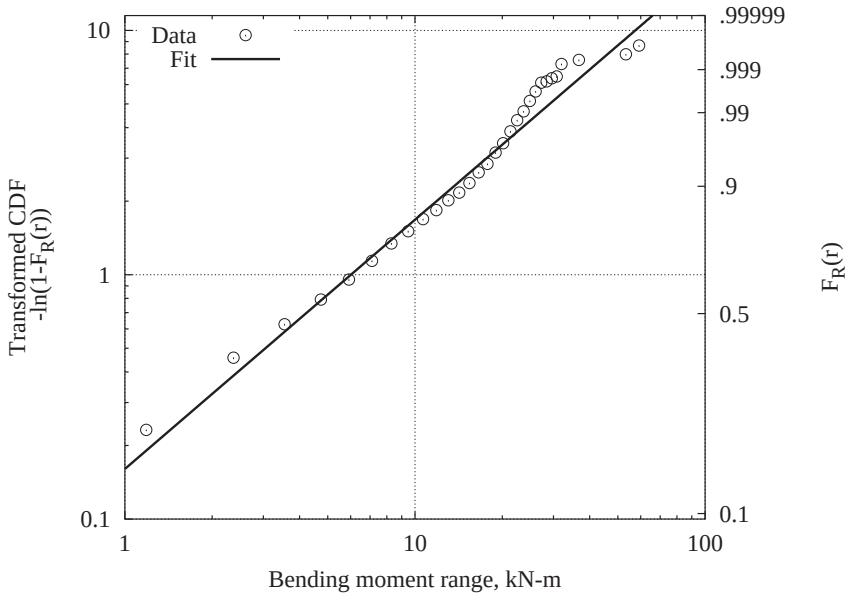

(b) Blade root edge bending.

Figure 5.2: Standard Weibull model fit to blade root flap and edge bending moment fatigue ranges for AOC 15/50 turbine parked in an environment with a 10-minute mean wind speed of 50m/s and turbulence class A.

also see Fitzwater and Winterstein [38].

Thus, the resulting quadratic Weibull distribution of R preserves the first three statistical moments of the data. Its distribution function appears as a quadratic curve when plotted on Weibull probability scale. To illustrate, quadratic Weibull models are fit to the same data, relating to the operating turbine, as presented for the standard Weibull model previously. The data are plotted on a Weibull scale for the flap data in Figure 5.3(a) and for the edge loads in Figure 5.3(b).

Figures 5.3(a) and 5.3(b) show attempts to fit the entire flap and edge data with quadratic Weibull models. As seen in Figure 5.3(a), and especially Figure 5.3(b), the data have a kinked appearance which the smooth probability distribution, in spite of its quadratic distortion, has difficulty matching. Closer examination of the data reveals that the kink is due to a large number of cycles at relatively low amplitudes. By truncating the loads at a lower-bound threshold, however, the kink in the data can be eliminated without significantly reducing the implied damage. In the edge case, there are a great number of cycles of smaller amplitude than the dominant gravity load at about 8-9kN-m (8.5kN-m was used as the filtering threshold). The flap loads have a less distinctive kink at around 10 kN-m. Figures 5.4(a) and 5.4(b) are similar to Figures 5.3(a) and 5.3(b), but include only a subset of the data by removing all ranges beneath a lower-bound threshold R_{th}, and modeling the shifted variable $R - R_{th}$ with our (positively valued) quadratic Weibull model. Clearly, the fit of the quadratic Weibull models are improved dramatically. It has also been shown (Manuel et al [50]) that the damage omitted through using a threshold can be negligible, which is consistent with findings that have long been available in the fatigue literature (e.g., Nelson and Fuchs [66]). A quadratic Weibull model fit to fatigue loads on a parked turbine for 10-minute mean wind speed of 50m/s is shown in Figure 5.5. The fit of the model to the data seems reasonable and no additional shifting and truncating of the data were performed.

In summary, the quadratic Weibull model offers the ability to match the first three moments of the data set. The resulting quadratic behavior of its distribution function, on Weibull scale, can yield a good fit to stress range data (e.g., the edge data in Figure 5.4(b)). In other cases, a simpler linear/Weibull model may suffice (e.g., the flap data in Figure 5.4(a)). The main drawbacks of the quadratic Weibull model are that (1) simple closed-form moment results are no longer available so that parameter estimation must be performed numerically; and (2) the analyst may need to first impose a lower-bound threshold to exclude uninteresting, small-amplitude ranges. Neither of these problems is insurmountable; indeed, numerical algorithms are available to facilitate the use of these higher-moment models (e.g., Manuel et al, [52, 53]). However, next we explore an alternative, the "damage-based" Weibull model that is somewhat simpler to implement.

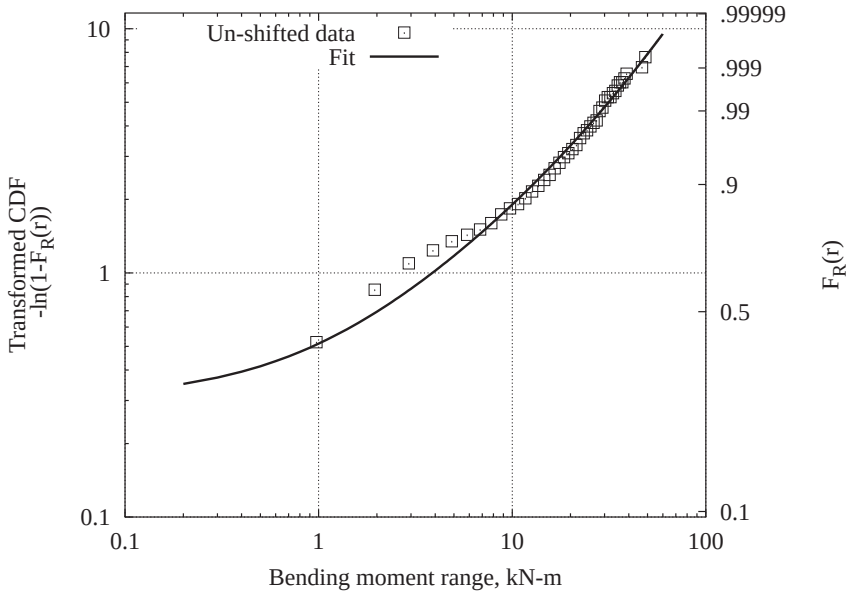

(a) Blade root flap bending.

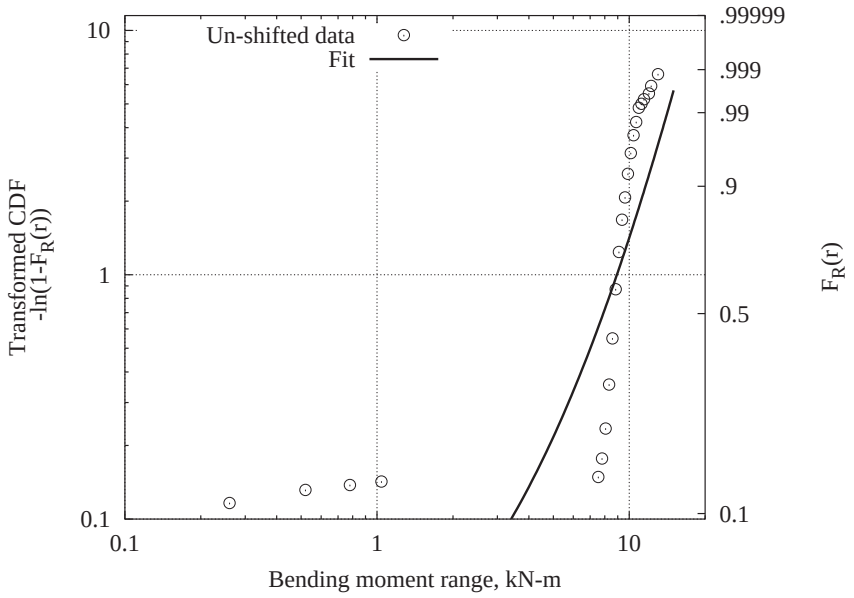

(b) Blade root edge bending.

Figure 5.3: Quadratic Weibull model fit to blade root flap and edge bending moment fatigue ranges for AOC 15/50 turbine operating in an environment with a 10-minute mean wind speed of 24m/s and turbulence class A.

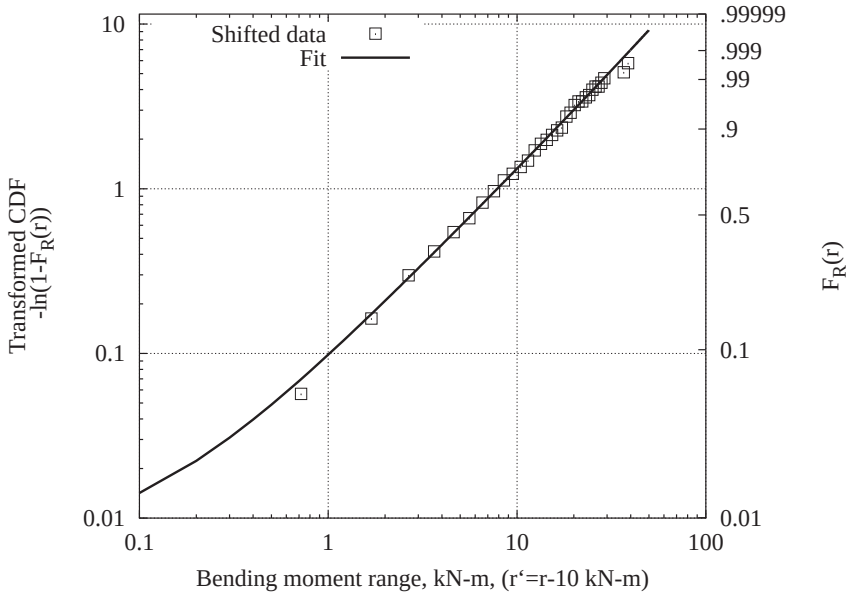

(a) Blade root flap bending, shift=10kN-m.

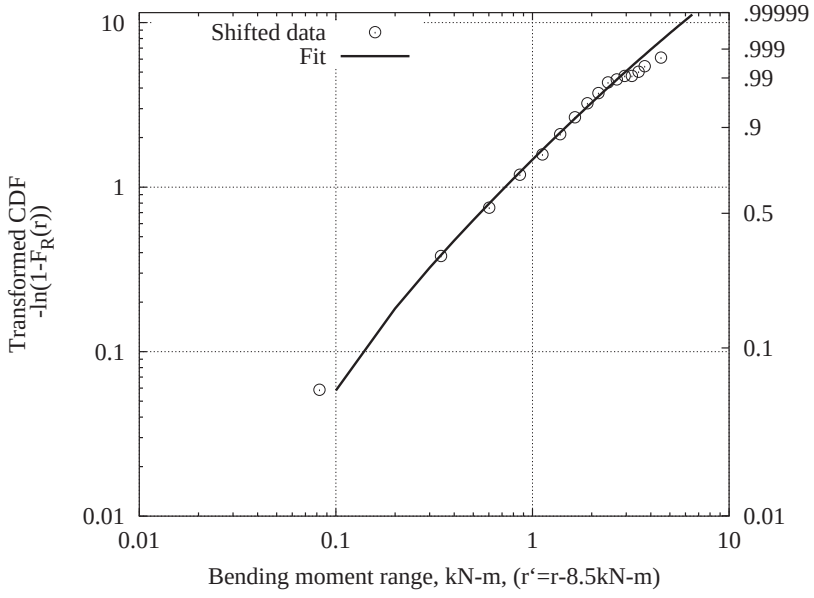

(b) Blade root edge bending, shift=8.5kN-m.

Figure 5.4: Shifted quadratic Weibull model fit to blade root flap and edge bending moment fatigue ranges for AOC 15/50 turbine operating in an environment with a 10-minute mean wind speed of 24m/s and turbulence class A.

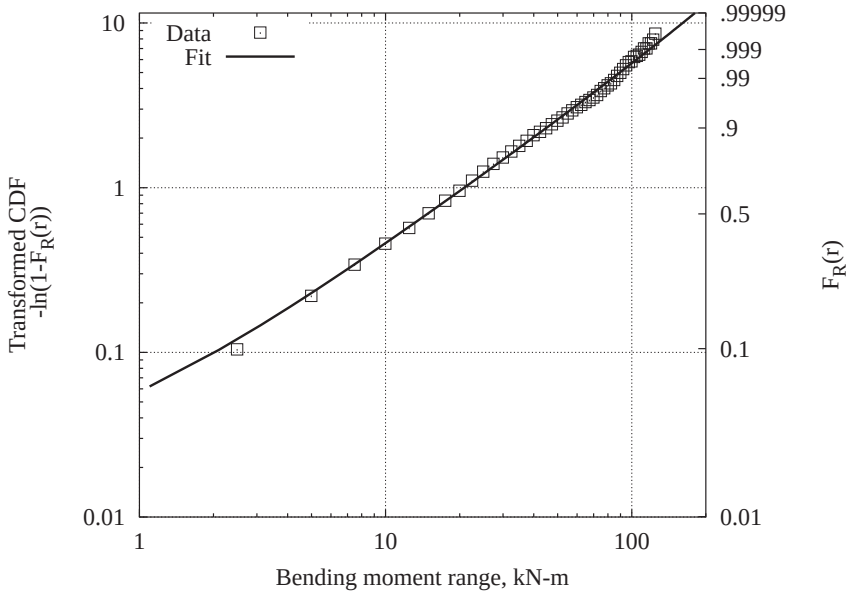

(a) Blade root flap bending.

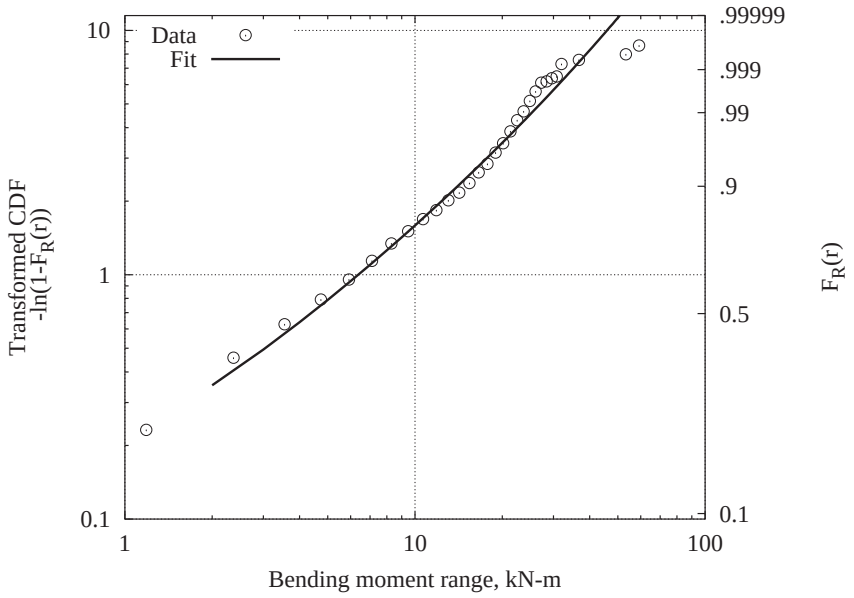

(b) Blade root edge bending.

Figure 5.5: Quadratic Weibull model fit to blade root flap and edge bending moment fatigue ranges for AOC 15/50 turbine parked in an environment with a 10-minute mean wind speed of 50m/s and turbulence class A.

5.3.3 The Damage-Based Weibull Model

As noted earlier, the damage per cycle is commonly related to R^{b_f}, the b_f^{th} power of the stress range R. Because typical b_f values far exceed unity, standard second-moment Weibull fits may not accurately predict the higher moment $\mathsf{E}[R^{b_f}]$ that drives damage accumulation. Our proposed damage-based Weibull model notes that if R follows a Weibull distribution, then the power-law transformation R^z, where z is an arbitrary power on the ranges, also follows a (modified) Weibull distribution. We therefore use a second-moment Weibull fit not of the range R, but rather an associated variable

$$W = R^z \tag{5.8}$$

By choosing $z = b_f/2$, and matching the second moment of the resulting distribution of W, the damage potential of the range distribution for a given material (where b_f is the slope of the S-N curve) is preserved. For example, with $z = 3$, this Weibull fit will preserve both $\mathsf{E}[R^3]$ and $\mathsf{E}[R^6]$, which are typical for some welded steels ($b_f = 3$) and aluminums ($b_f = 6$), respectively. For wind turbine applications, even higher moments are of interest because fiberglass composite blades possess b_f values equal to 8, 10, or even higher.

In practice, the damage-based Weibull model is fit by (1) transforming the range data R through Equation 5.8, (2) using a standard second-moment fit for the Weibull parameters α_W and β_W; and (3) plotting the resulting distribution function, $F_W(w)$, versus not w but rather $r = w^{1/z}$. The benefits of this model are that (1) it requires only a standard second-moment Weibull fitting procedure easily implemented without specialized algorithms; and (2) it explicitly ensures accurate distribution modeling in the range most relevant for damage prediction, i.e., in the upper tail of the stress range distribution. (A similar upper tail fit model could be used to predict ultimate loads as well, although in this case there is no physical motivation for a particular choice of $b_f = 2z$ value.)

Figures 5.6 and 5.7 repeat the Weibull scale distribution plots of all data for an operating turbine condition considering both flap and edge loads, respectively, for one 10-minute sample. Also shown on these figures are three damage-based Weibull predictions which utilize the parameter choices $z = 3$, 4, and 5. (A choice of $z = 5$ may be most appropriate for wind turbine blades, preserving the $b_f = 10^{\text{th}}$ moment which may govern damage of these composite components.) Similarly, Figures 5.8 and 5.9 show the damage-based Weibull model fit ($z = 3$, 4, 5) to fatigue range data for a parked turbine condition considering flap and edge loads, respectively. As may be expected, these models provide accurate load distribution estimates in the upper tail of interest. (Increasing z values leads to enhanced emphasis on the upper tail.) Note again the advantages of these models, by permitting tail-fitting in an automated, physically-based way. They also avoid the need to impose a lower-bound load threshold; all ranges may be included, and the original cycle rate preserved. Of

course, the damage-based Weibull model, because it emphasizes upper-tail behavior, will provide a poor estimate of low-fractile loads, but these loads have little or no effect on damage prediction.

5.4 Long-Term Analysis Based on Modeling Fatigue Ranges with Quadratic Weibull Model

5.4.1 Short-term Analysis

To review, the load models proposed here estimate the probability distribution of load ranges, R, by preserving a limited set of statistical moments, $\mu_i = \mathsf{E}[R^i]$. The relevant moments here are model-dependent: μ_1 and μ_2 are used for the standard Weibull model, μ_1 through μ_3 for the quadratic Weibull model, and μ_z and μ_{2z} for the damage-based Weibull model (z on the order of 3-5, $b_f = 6-10$). The moments of the fatigue ranges were calculated for all blade root flap and edge bending response time histories. For each pair of environmental variables (e.g., V=10m/s and I=class A) the 100 observations of the moments, e.g., mean, or variance, etc., were pooled together and the mean of these pooled observations was reported. We saw in Chapter 3, that the statistical moments of the global or local peaks could be related to the environmental variables through regression analysis. The same can be done here to relate the statistical moments, μ_n, of the fatigue ranges to the environmental variables: mean wind speed, V, and turbulence intensity, I, through the power-law relation we have seen before [54]:

$$\mu_i = a_i \left(\frac{V}{V_{\text{ref}}}\right)^{b_i} \left(\frac{I}{I_{\text{ref}}}\right)^{c_i} \tag{5.9}$$

Hence, for these parametric load models, the wind turbine characteristics are reflected solely through the moment relations in Equation 5.9. For example, with the quadratic Weibull model we require the 9 coefficients a_i, b_i, c_i $(i = 1, 2, 3)$ that govern the first three moments of the ranges. For clarity, we organize these coefficients here into a vector, denoted θ:

$$\theta = [a_1, b_1, c_1, a_2, b_2, c_2, a_3, b_3, c_3] \tag{5.10}$$

The other (standard or damage-based) Weibull models require only two moments, and hence 6 coefficients in the vector θ. Linear regression analysis, applied to the logarithm of Equation 5.9, yields point estimates of these coefficients. To demonstrate typical results, we pursue the quadratic Weibull model here; the alternative damage-based Weibull model will be discussed in Section 5.5. There are two distinct general loading conditions for the turbine, one when the turbine is operating

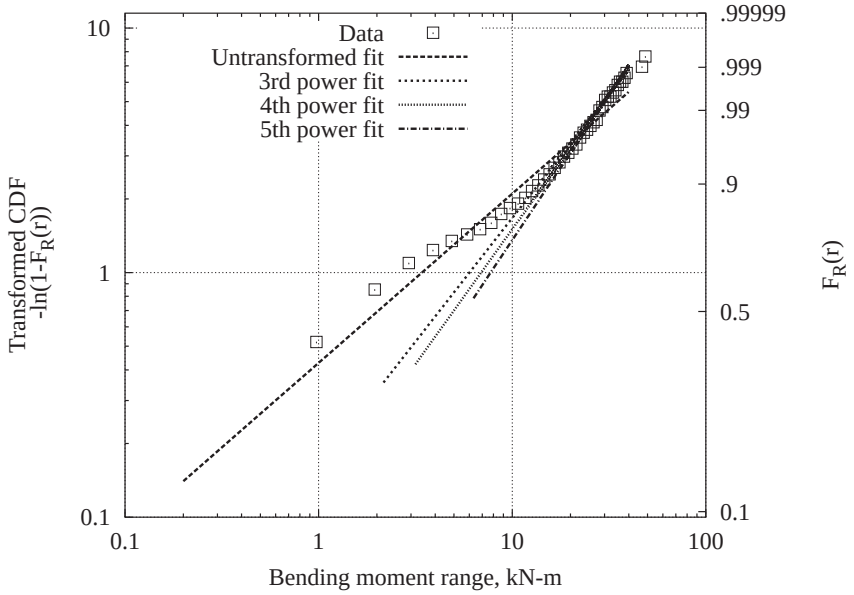

(a) All blade root flap bending fatigue ranges.

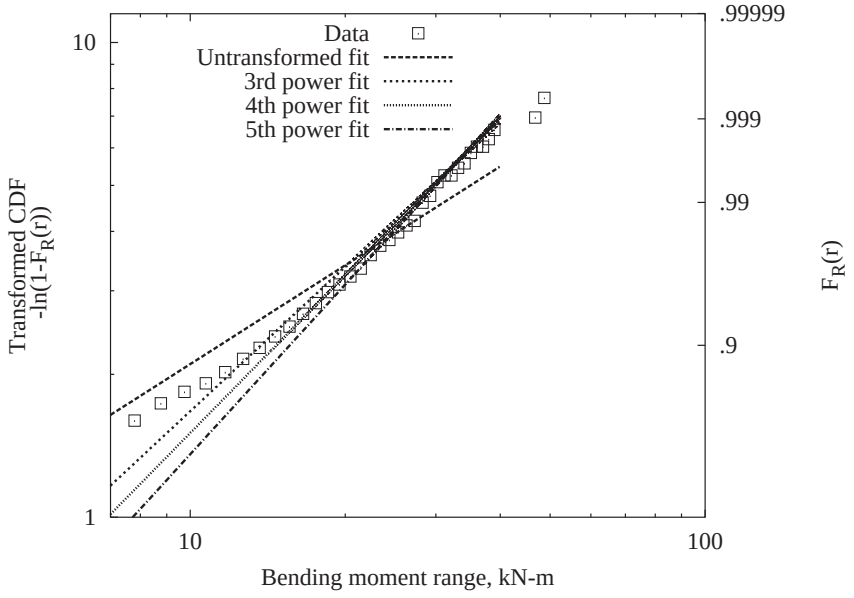

(b) Upper tail of blade root flap bending fatigue ranges.

Figure 5.6: Damage-based Weibull model fit to blade root flap bending fatigue ranges for an AOC 15/50 turbine operating in an environment with a 10-minute mean wind speed of 24m/s and turbulence class A, for $z = 3, 4, 5$.

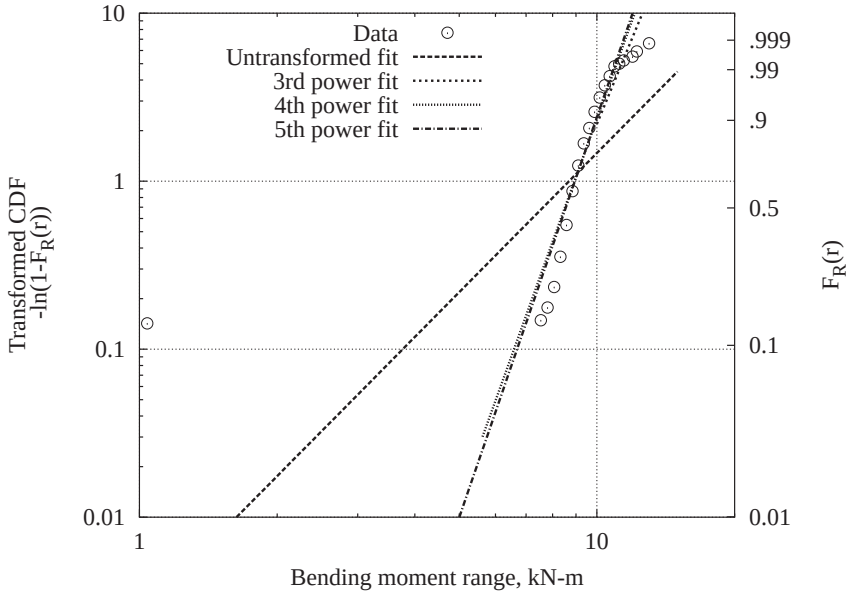

(a) All blade root edge bending fatigue ranges.

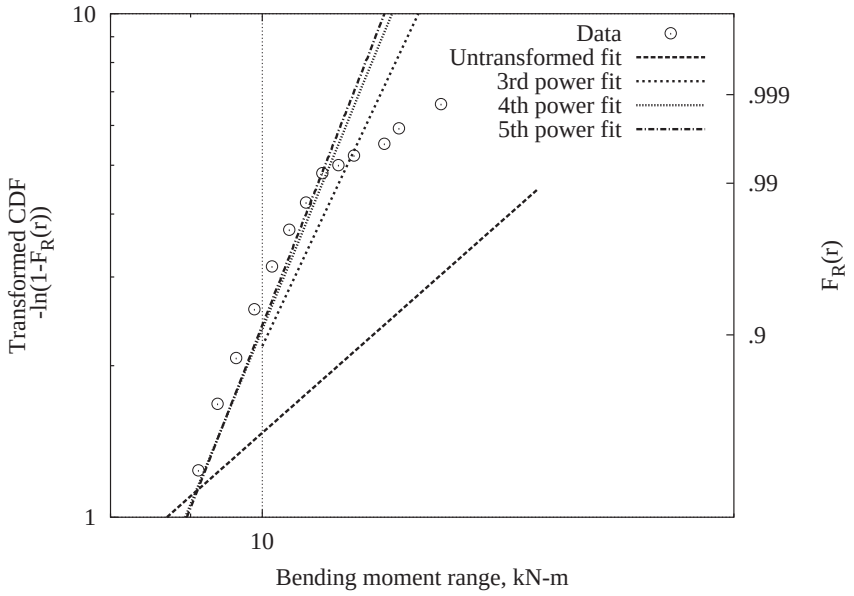

(b) Upper tail of blade root edge bending fatigue ranges.

Figure 5.7: Damage-based Weibull model fit to blade root edge bending fatigue ranges for an AOC 15/50 turbine operating in an environment with a10-minute mean wind speed of 24m/s and turbulence class A, for $z = 3, 4, 5$.

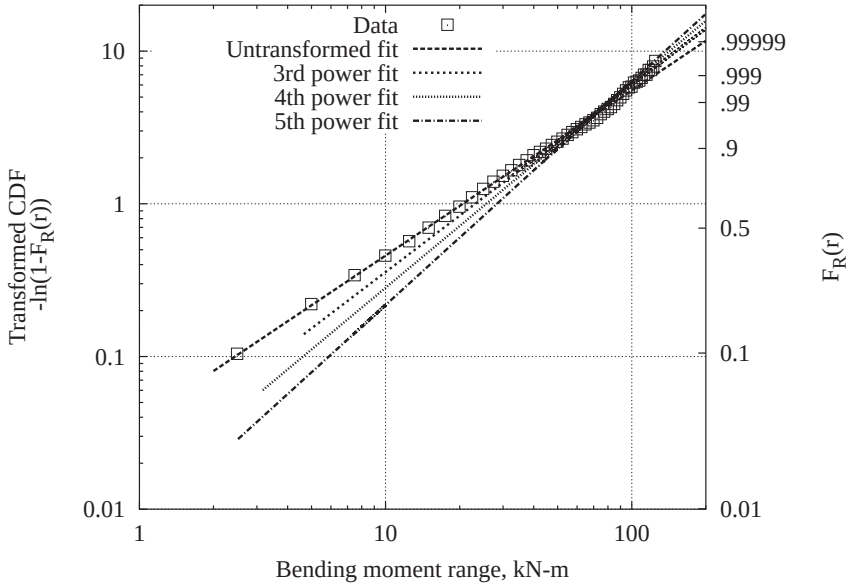

(a) All blade root flap bending fatigue ranges.

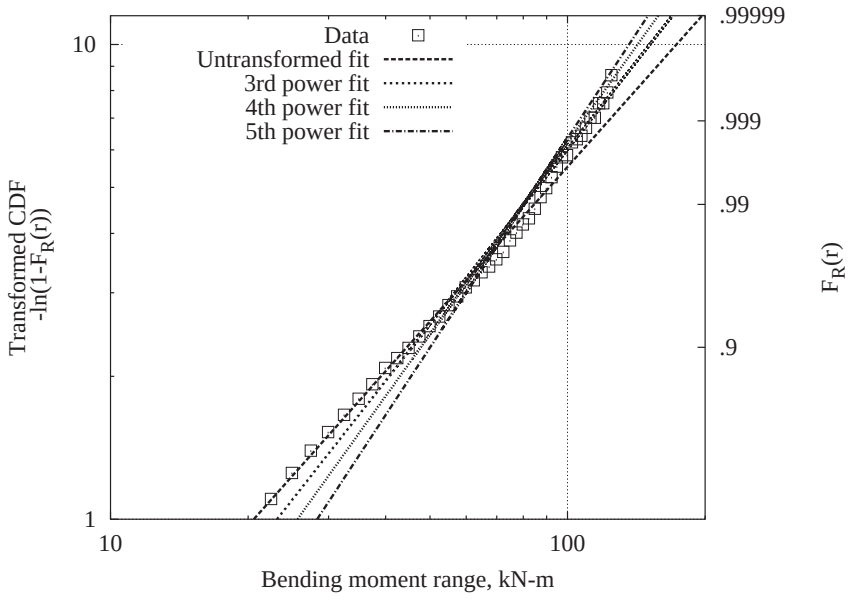

(b) Upper tail of blade root flap bending fatigue ranges.

Figure 5.8: Damage-based Weibull model fit to blade root flap bending fatigue ranges for an AOC 15/50 turbine parked in an environment with a 10-minute mean wind speed of 50m/s and turbulence class A, for $z = 3, 4, 5$.

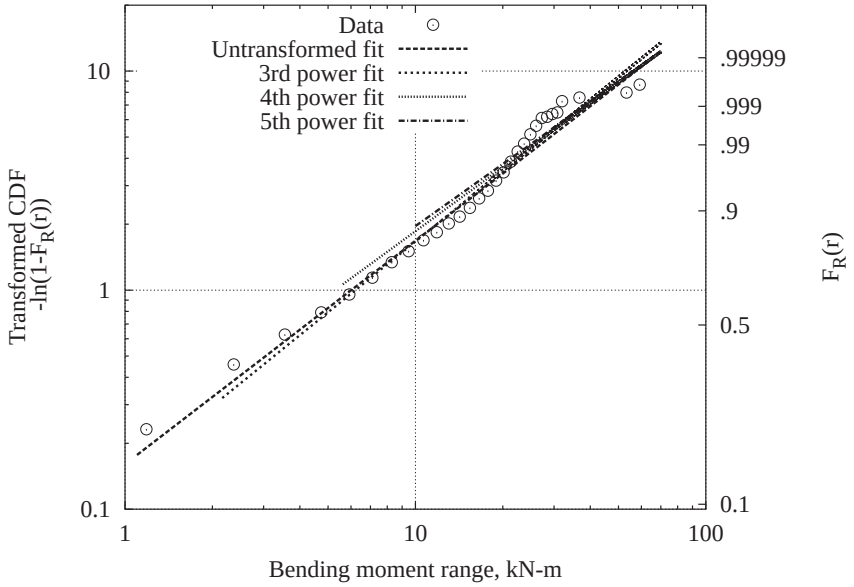

(a) All blade root edge bending fatigue ranges.

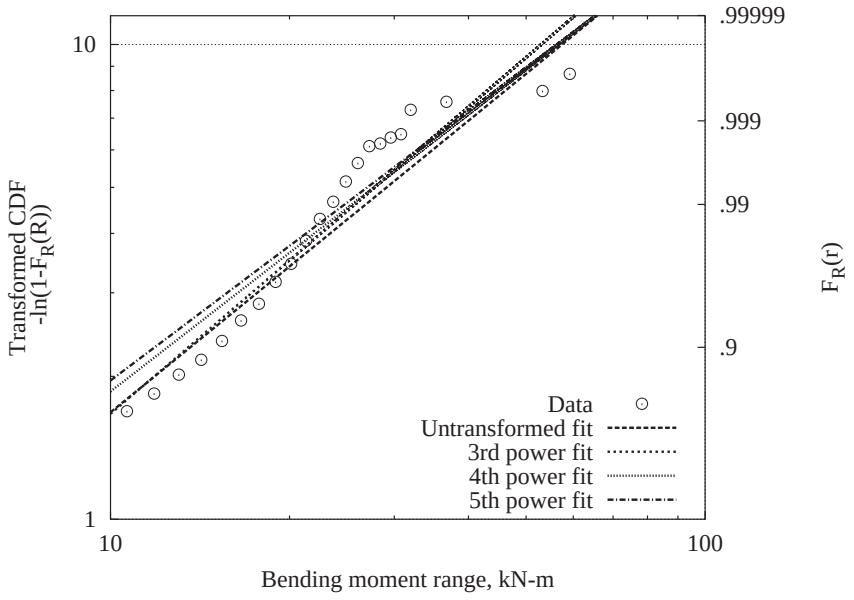

(b) Upper tail of blade root edge bending fatigue ranges.

Figure 5.9: Damage-based Weibull model fit to blade root edge bending fatigue ranges for an AOC 15/50 turbine parked in an environment with a 10-minute mean wind speed of 50m/s and turbulence class A, for $z = 3, 4, 5$.

Reference Wind Speed and Turbulence

	V_{ref} (m/s)	I_{ref} (%)
$V \leqq 24$m/s	16.474	15.28
$V > 24$m/s	34.861	13.18

Table 5.1: Reference wind speed and turbulence values used in Equation 5.9

(i.e., 10-minute mean wind speeds $\leq$ 24m/s) and the other while the turbine is parked (i.e., 10-minute mean wind speeds $>$ 24m/s). Separate regression analyzes were performed under each of these conditions. The reference wind speed and reference turbulence used in the regression analysis are given in Table 5.1. The calculated regression coefficients and R^2 statistics are shown in Tables 5.2 and 5.3 for blade root flap and edge bending fatigue ranges, respectively. R^2 statistics near unity indicate that a large percentage of the variability in the data is explained by the regression model. Low R^2 statistics indicate that other influences not contained in the regression model may be affecting the loads. We may note that the R^2 statistic for the regression analysis of the coefficient of skewness are low in a few instances (i.e., skewness–parked edge bending), implying the data exhibit variability which the model is unable to explain. In performing the regression analysis it was determined that the proposed functional model, Equation 5.9, did not have enough flexibility to sufficiently model the observed behavior of the mean and standard deviation of the blade root flap bending fatigue ranges. The values of the mean and standard deviation of the fatigue ranges flatten out with higher wind speeds above 17m/s as compared with the behavior below 17m/s. Therefore, a separate model was fit to each of these regions, one below 17m/s and the other above 17m/s, for both the mean and standard deviation of blade root flap bending fatigue ranges. A similar result was found in Chapter 3 when we considered modeling the local peaks with a quadratic Weibull model, see Figures 3.25 and 3.26.

Finally, graphical regression results are shown in Figures 5.10-5.12. Each figure contains both blade root flap and edge bending conditions considering: mean of fatigue ranges, Figure 5.10; standard deviation of fatigue ranges, Figure 5.11; and coefficient of skewness of fatigue ranges, Figure 5.12. In all plots, the turbulence intensity has been set equal to the reference value.

5.4.2 Long-Term Analysis

For the discussion here we defined the conditional probability distribution of fatigue ranges by a quadratic Weibull model. We saw how this model can be represented by the moments of the data. Further, we have just shown through regression analysis, how these statistical moments may be related to the environmental variables.

Blade Root Flap Bending
Regression of Statistics of Fatigue Ranges on V and I

Mean of Fatigue Ranges

	a (kN-m)	b	c	R^2
$V \leqq 17$m/s	6.3777	1.2545	0.9231	0.9742
$17 < V \leqq 24$m/s	7.4424	0.2782	1.3015	0.9850
$V > 24$m/s	4.4473	4.4517	0.0512	0.9948

Standard Deviation of Fatigue Ranges

	a (kN-m)	b	c	R^2
$V \leqq 17$m/s	5.6064	1.1212	0.9078	0.9889
$17 < V \leqq 24$m/s	6.5411	0.3492	1.2073	0.9843
$V > 24$m/s	4.6646	4.2613	0.6871	0.9922

Coefficient of Skewness of Fatigue Ranges

	a (kN-m)	b	c	R^2
$V \leqq 24$m/s	1.3941	0.1551	0.0398	0.4886
$V > 24$m/s	2.3150	-1.325	0.7810	0.9404

Table 5.2: Regression coefficients used in Equation 5.9 to fit flap bending moment fatigue ranges as functions of the mean wind speed, V, and turbulence intensity, I. The turbine is operating for $V \leqq 24$m/s, otherwise the turbine is parked.

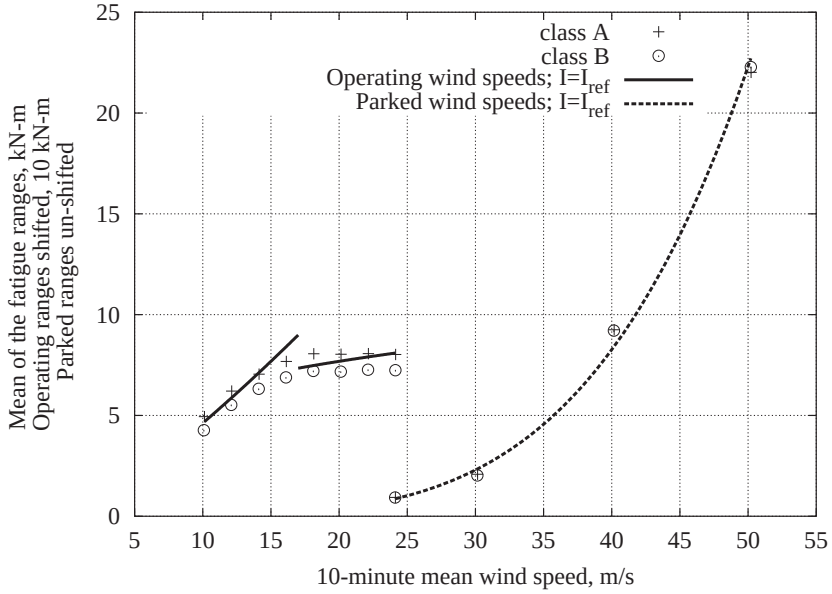

(a) Pooled statistics of the mean of the fatigue ranges in 10-minute blade root flap bending response time history.

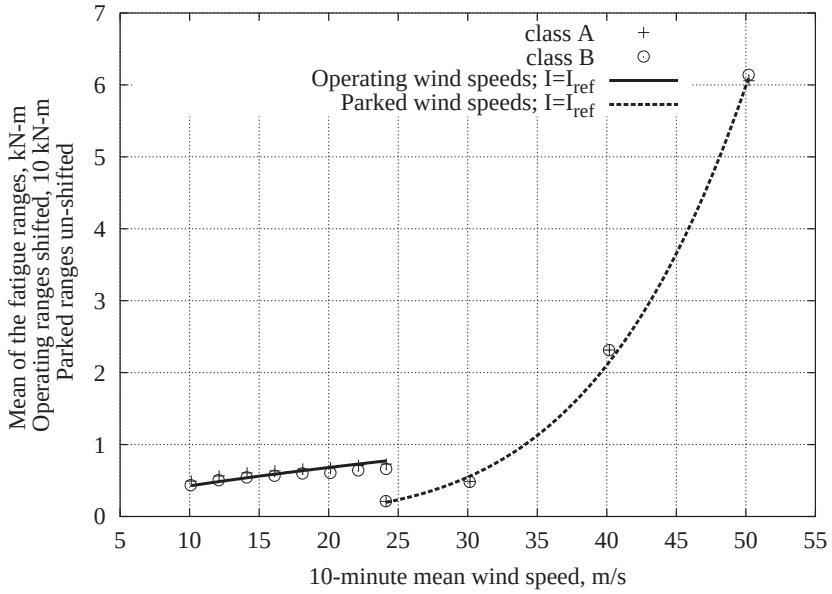

(b) Pooled statistics of the mean of the fatigue ranges in 10-minute blade root edge bending response time history

Figure 5.10: Mean fatigue range of 10-minute blade root flap and edge bending response, based on 100 pooled observations for each 10-minute mean wind speed and turbulence class. The wind turbine is operating for $V \leqq 24$m/s, otherwise the turbine is parked.

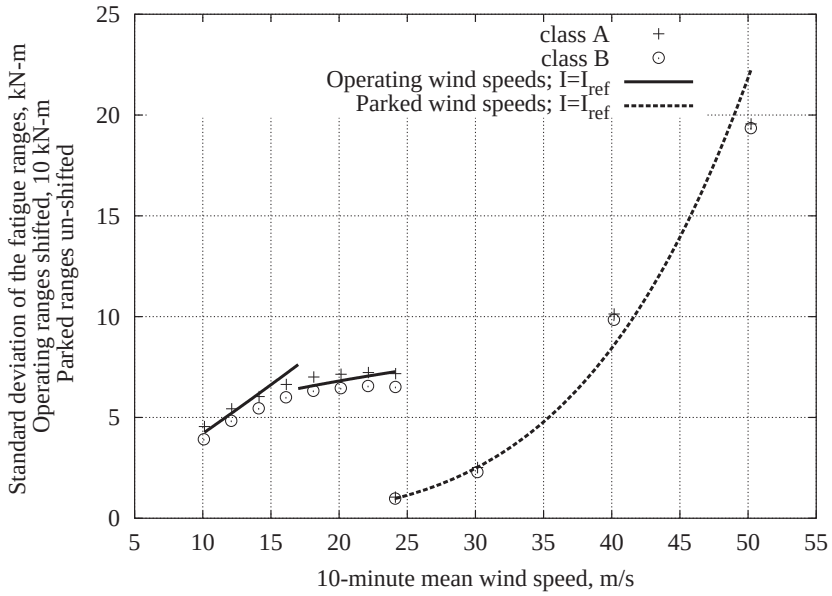

(a) Pooled statistics of the standard deviation of the fatigue ranges in 10-minute blade root flap bending response time history.

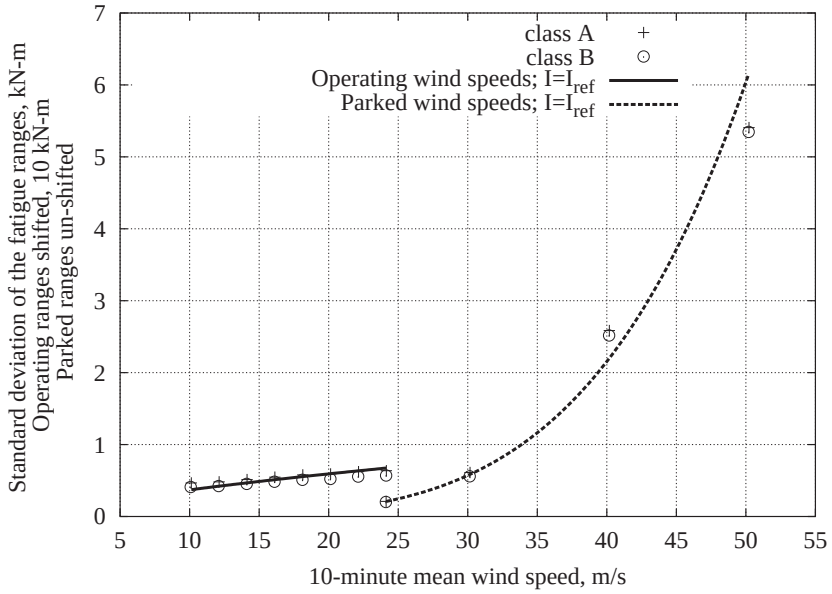

(b) Pooled statistics of the standard deviation of the fatigue ranges in 10-minute blade root edge bending response time history

Figure 5.11: Standard deviation of fatigue ranges for 10-minute blade root flap and edge bending response time histories, based on 100 pooled observations for each 10-minute mean wind speed and turbulence class. The wind turbine is operating for $V \leqq 24$m/s, otherwise the turbine is parked.

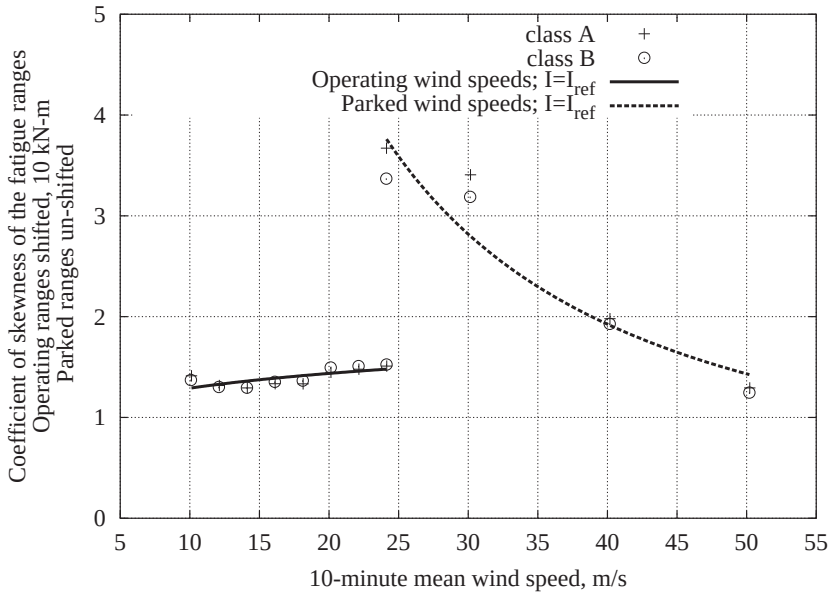

(a) Pooled statistics of the coefficient of skewness of the fatigue ranges in 10-minute blade root flap bending response time history.

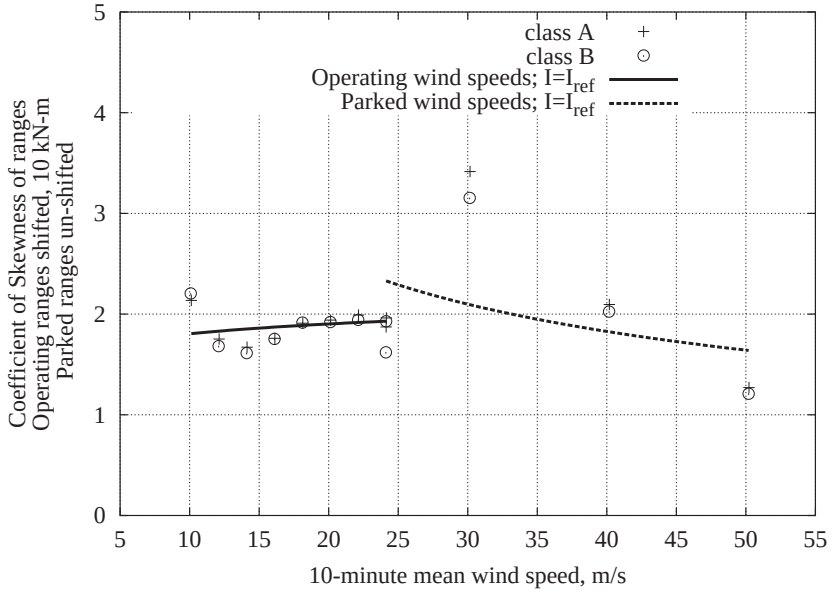

(b) Pooled statistics of the coefficient of skewness of the fatigue ranges in 10-minute blade root edge bending response time history

Figure 5.12: Coefficient of skewness of fatigue ranges for 10-minute blade root flap and edge bending response time histories, based on 100 pooled observations for each 10-minute mean wind speed and turbulence class. The wind turbine is operating for $V \leqq 24$m/s, otherwise the turbine is parked.

Blade Root Edge Bending
Regression of Statistics of Fatigue Ranges on V and I

Mean of Fatigue Ranges

	a (kN-m)	b	c	R^2
$V \leqq 24$m/s	0.5971	0.6772	0.9331	0.9572
$V > 24$m/s	1.0970	4.6834	-0.1105	0.9955

Standard Deviation of Fatigue Ranges

	a (kN-m)	b	c	R^2
$V \leqq 24$m/s	0.5194	0.6798	1.1092	0.9814
$V > 24$m/s	1.1338	4.6159	0.4885	0.9937

Coefficient of Skewness of Fatigue Ranges

	a (kN-m)	b	c	R^2
$V \leqq 24$m/s	1.8741	0.0762	0.2110	0.0232
$V > 24$m/s	1.9540	-0.4800	0.8844	0.2430

Table 5.3: Regression coefficients used in Equation 5.9 to fit edge bending moment fatigue ranges as functions of the mean wind speed, V, and turbulence intensity, I. The turbine is operating for $V \leqq 24$m/s, otherwise the turbine is parked.

The long-term distribution of fatigue load ranges, in an arbitrary 10-minute period, is found in much the same way we found the long-term distribution of extreme events in Chapter 3. To review, in Chapter 3 we saw how the turbine specific conditional probability distribution model of the 10-minute extreme load could be combined with the long-term distribution of the environmental variables, through Equation 3.16, to obtain an estimate of the long-term distribution of the extreme load. Equation 3.16 is an application of the Law of Total Probability. We can apply, with little modification, the same methodology here. In this case, Equation 3.16 can be written as:

$$F_R(r) = \int F_R(r|v,i)\, f_{V,I}(v,i)\, dvdi \tag{5.11}$$

Where, $F_{R|V,I}(r|v,i)$, is the short-term conditional distribution of fatigue ranges, and $f_{V,I}(v,i)$, the joint density function of the environmental variables. Equation 5.11 is also an application of the Law of Total Probability. Where the conditional probability distribution of the fatigue ranges, given a set of values of the environmental variables, is weighted by the probability of those values occurring and then summed over the domain of the environmental variables.

We will again assume that the AOC 15/50 turbine is installed at a site with environmental conditions similar to the Lavrio, Greece, test site, described in Chapter 3 (page 77). The long-term

distribution of the 10-minute mean wind speed is assumed to follow a Rayleigh distribution with mean, $\mu_V = 10$m/s. The conditional distribution of turbulence is given by a Gaussian distribution with conditional mean, $\mu_{I|V} = 2.4486v^{-0.9971}$ and constant standard deviation, $\sigma_{I|V} = 0.025$. A plot of the joint density function of the environmental variables is shown in Figure 4.7 (Chapter 4).[1]

The ranges of values of the environmental variables are discretized into evenly spaced intervals. For each pair of values of the environmental variables, the corresponding short-term distribution of fatigue ranges is generated, and any required threshold (*shift*) is reintroduced. Then, per Equation 5.11, the short-term conditional fatigue range distributions are summed together, each weighted by the probability of the respective environmental condition, i.e., pair of values of the environmental variables. The summation is performed over the entire domain of environmental variables.

As stated earlier, there are two loading conditions for the turbine, operating and parked. During normal use the turbine is operating for wind speeds less than 24m/s and parked for wind speeds greater than 24m/s. In this case, to develop the long-term distribution, the appropriate regression model is used for each wind speed value. For wind speeds below 24m/s the regression relating operating loads is used and, correspondingly, for wind speeds above 24m/s the regression relating parked loads is used. This results in a combination of the operating and parked long-term distributions of fatigue ranges as shown in Figure 5.13. It was assumed that there was 100% availability of the turbine during all wind speeds. Considering the blade root flap bending direction, we see in Figure 5.13(a) that the blade root flap bending moment fatigue ranges are dominated by the operating conditions. In Figure 5.13(b), we see that parking the turbine avoids increased probability of large blade root edge bending moments.

In addition to obtaining an estimate of the long-term distribution of fatigue ranges, another interesting question is how we might obtain an estimate of the fatigue damage in an arbitrary 10-minute interval. The expected fatigue damage from an arbitrary cycle, given values of the environmental variables, was given in Equation 5.4. We may then estimate the expected total damage by first calculating the expected damage in 10 minutes given values of the environmental variables as:

$$\mathsf{E}[D_{10\,\text{min}}|v,i] = \mathsf{E}[N_0(v,i)]\mathsf{E}[D|v,i] \tag{5.12}$$

Where $\mathsf{E}[N_0(v,i)]$, is the expected number of cycles as a function of wind speed and turbulence, and $\mathsf{E}[D|v,i]$, is given by Equation 5.4. It is generally assumed that $\mathsf{E}[N_0(v,i)]$ and $\mathsf{E}[D|v,i]$ are at least uncorrelated, if not independent [7]. We again turn to our regression model for a relationship between the expected number of cycles and the environmental variables. The same power law

[1] A more detailed definition of the environmental variables for the Lavrio, Greece site is given in Chapters 3 and 4.

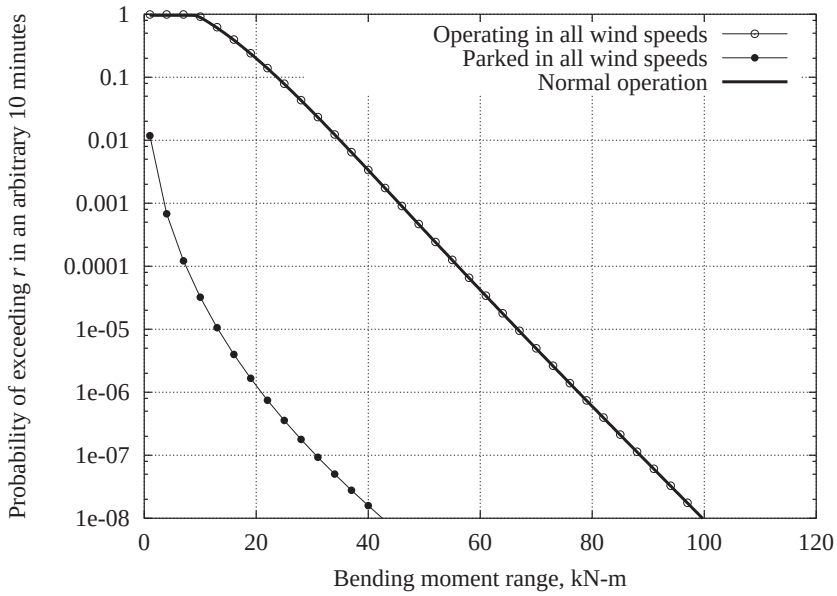

(a) Blade root flap bending.

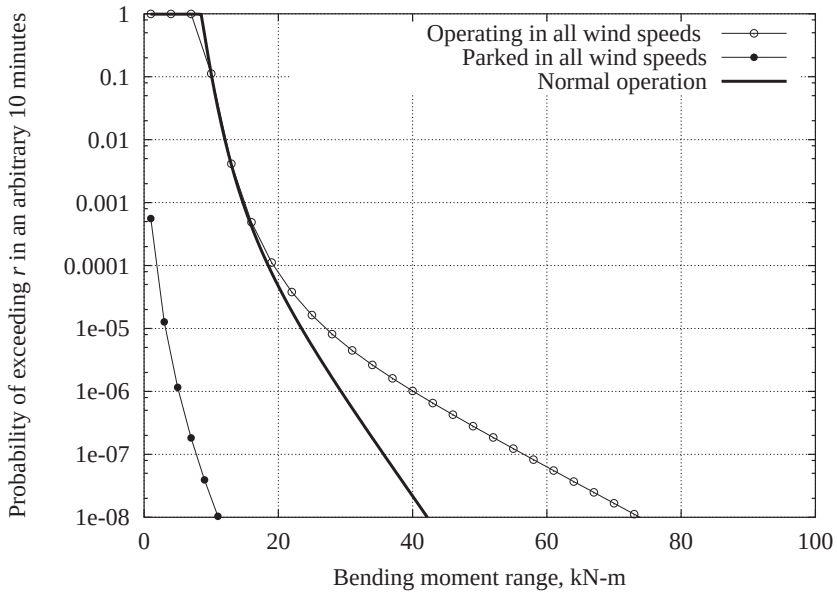

(b) Blade root edge bending.

Figure 5.13: Long-term distributions of blade root fatigue bending moment ranges, R, considering three turbine conditions: 1) turbine operating over all wind speeds, 2) turbine parked over all wind speeds, 3) turbine operating below cutout wind speed and parked above cutout wind speed; for both: blade root (a) flap and (b) edge bending.

functional form, Equation 5.9, was used.

$$\mathsf{E}[N_0(v,i)] = a\left(\frac{V}{V_{\text{ref}}}\right)^b\left(\frac{I}{I_{\text{ref}}}\right)^c \tag{5.13}$$

The calculated regression coefficients and R^2 statistics are shown in Table 5.4 for blade root flap and edge bending fatigue ranges. Graphical regression results are shown in Figure 5.14. Furthermore, the expected total damage in an arbitrary 10 minutes may be obtained by again applying the Law of Total Probability; weighting the results of Equation 5.12 by the probability of the values of the pair of environmental variables occurring and integrating over the environmental space.

$$\mathsf{E}[D_{10\text{ min}}] = \iint_{V,I}\mathsf{E}[N_0(v,i)]\mathsf{E}[D|v,i]f_{V,I}(v,i)dvdi \tag{5.14}$$

It is a simple matter to calculate the expected total damage at longer time intervals, e.g., a year, by multiplying the result of Equation 5.14 by the number of 10 minute periods in the desired time interval.

We showed earlier that $\mathsf{E}[D] \propto \mathsf{E}[R^{b_f}]$. A similar relation can be written as:

$$\mathsf{E}[D_{10\text{ min}}] \propto \iint_{V,I}\mathsf{E}[N_0(v,i)]\mathsf{E}[R^{b_f}|v,i]f_{v,i}(v,i)dvdi = \mathrm{DM}_{10} \tag{5.15}$$

In Equation 5.15 we substituted $\mathsf{E}[R^{b_f}|v,i]$ for $\mathsf{E}[D|v,i]$. DM_{10} denotes the "*damage measure in 10-minutes*" and is used as a proxy for the expected total fatigue damage in an arbitrary 10 minutes. This is not an actual estimate of the expected total fatigue damage, but it is proportional to it so that higher values of DM_{10} are associated with larger fatigue damage estimates and vise versa. The estimates of the damage measure, DM_{10}, for blade root flap and edge bending considering b_f values from 1 to 10 are presented in Table 5.5. The values in this table will be used to compare with results from modeling the short-term fatigue ranges with a damage-based Weibull model in the next section instead of the quadratic Weibull model used here.

We may also consider the portion of the expected damage contributed at different environmental conditions. Figure 5.15 presents the plot of damage density for both blade root flap and edge bending moments. Here, we only consider the 10-minute wind speed as the environmental variable of interest. The damage density is defined as the contribution to the expected total damage for a given wind speed. Since our analysis was conducted considering both the 10-minute wind speed and turbulence intensity, the values given in the figure reflect summing together all the contributions to DM_{10} from different turbulence intensities for a constant wind speed. We can see clearly from the figure that most of the damage occurs while the turbine is operating, i.e., for wind speeds below

Regression of the Number of Fatigue Ranges on V and I

Blade Root Flap Bending

	a (kN-m)	b	c	R^2
$V \leqq 24$m/s	0.5971	0.6772	0.9331	0.9572
$V > 24$m/s	1.0970	4.6834	-0.1105	0.9955

Blade Root Edge Bending

	a (kN-m)	b	c	R^2
$V \leqq 24$m/s	0.5194	0.6798	1.1092	0.9814
$V > 24$m/s	1.1338	4.6159	0.4885	0.9937

Table 5.4: Regression coefficients used in Equation 5.9 to fit the expected number of fatigue ranges, $\mathsf{E}[N_0(v,i)]$, for blade root flap and edge bending, as functions of the mean wind speed, V, and turbulence intensity, I.

Estimate of Damage Measure, DM_{10}, for Fatigue Exponent Values, $b_f = 1, \ldots, 10$.

b_f	Flap Bending	Edge Bending
1	3.490e+3	3.783e+3
2	6.381e+4	3.481e+4
3	1.349e+6	3.244e+5
4	3.281e+7	3.053e+6
5	9.134e+8	2.908e+7
6	2.884e+10	2.819e+8
7	1.024e+12	2.802e+09
8	4.054e+13	2.906e+10
9	1.776e+15	3.257e+11
10	8.569e+16	4.223e+12

Table 5.5: Estimate of damage measure, DM_{10}, for fatigue exponent values, $b_f = 1, \ldots, 10$, considering blade root flap and edge bending fatigue loads.

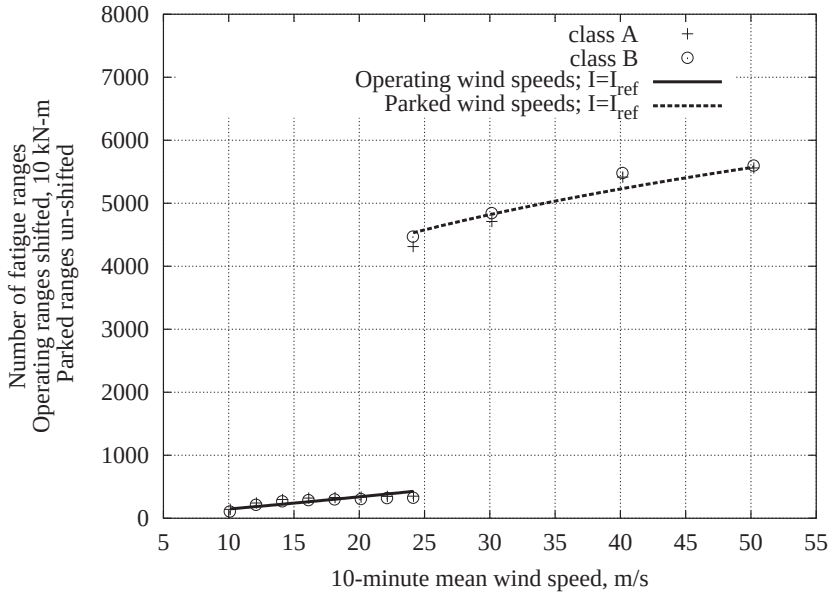

(a) Expected number of fatigue ranges in 10-minute blade root flap bending time history.

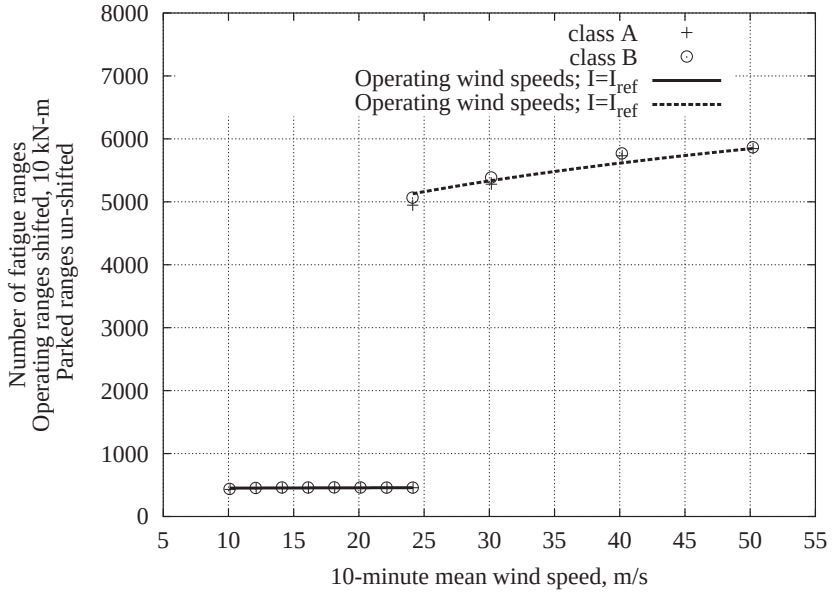

(b) Expected number of fatigue ranges in 10-minute blade root edge bending time history.

Figure 5.14: Expected number of fatigue ranges, $\mathsf{E}[N_0(v,i)]$, in 10-minute blade root flap and edge bending response time histories, based on 100 pooled observations for each 10-minute mean wind speed and turbulence class. The wind turbine is operating for $V \leqq 24$m/s, otherwise the turbine is parked.

24m/s. Also, we see from Figure 5.15 that as the value of the fatigue exponent, b_f, increases, we are relatively more sensitive to higher wind speeds while the turbine is parked.

5.4.3 Summary

In this section we have stepped through the process of obtaining an estimate of the marginal probability distribution of the long-term distribution of fatigue loads. This was accomplished by modeling the short-term distribution of fatigue ranges by a quadratic Weibull model. The statistical moments of the fatigue range data were related to the environmental variables by a power-law functional form. The parameters of the functional form were obtained through regression analysis. Using the method of moments, a quadratic Weibull distribution could be obtained for each specific set of values of the environmental variables. Finally, an estimate of the marginal distribution of the long-term fatigue loads was obtained by summing the conditional short-term load distributions over all environmental conditions. Each conditional short-term load distribution was weighted by the probability of the associated environmental condition occurring. The next section presents a similar analysis, only this time the short-term fatigue ranges are modeled with a damage-based Weibull distribution.

5.5 Long-Term Analysis Based on Modeling Fatigue Ranges with the Damage-Based Weibull Model

5.5.1 Short-Term Analysis

In the last section we considered modeling the distribution of fatigue ranges using the quadratic Weibull model. Here, in contrast, we consider modeling the distribution of the fatigue ranges using our proposed damage-based Weibull model. To review, the load models discussed here estimate the probability distribution of load ranges by preserving a limited set of statistical moments, $\mu_i = \mathsf{E}[R^i]$. The relevant moments here are model-dependent: μ_1 through μ_3 for the quadratic Weibull model, and μ_z and μ_{2z} for the damage-based Weibull model (z on the order of 3-5, b_f=6-10). In particular, in this section we will look at damage-based Weibull models in three cases, for z values equal to 3, 4, and 5. In the first case for example, where $z = 3$, this corresponds to fatigue exponent values equal to 3 and 6. The model is tuned to fit the third and sixth moment of the data. Similarly, for $z = 4$ (b_f=4 and 8), the model is tuned to fit the fourth and eighth moment of the data, and for $z = 5$ (b_f=5 and 10), the fifth and tenth moment. Separate regression analysis and long-term integration will be conducted for each of these cases. In some instances the results of only the first transformation, $z = 3$, will be presented as we find similar results for the other transformations.

In the previous section the statistical moments of the data were related to the environmental

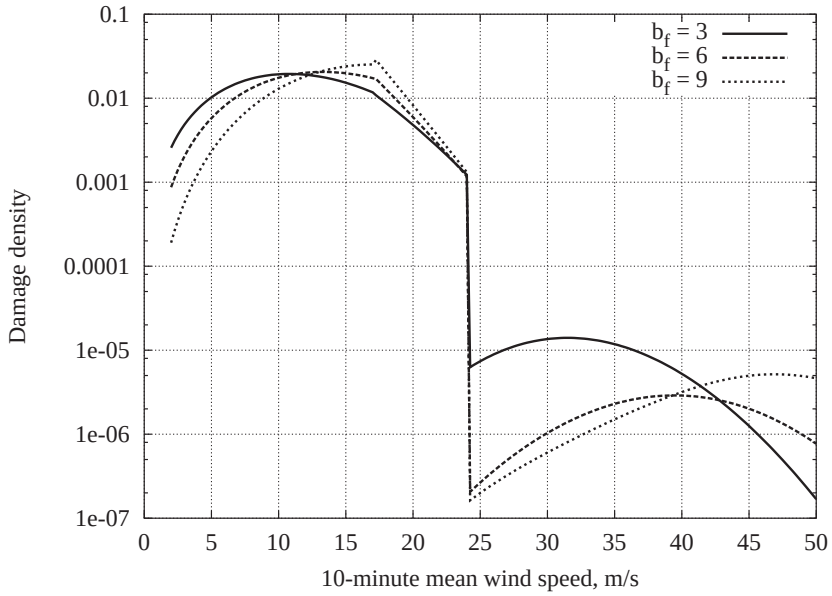

(a) Blade root flap bending moment.

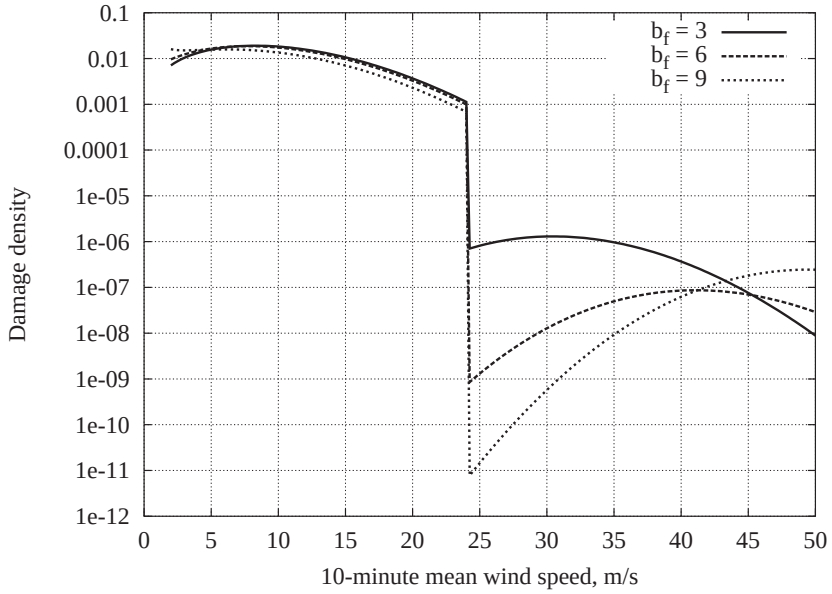

(b) Blade root edge bending moment.

Figure 5.15: Damage density for blade root flap and edge bending.

variables by the power-law model given in Equation 5.9; the same functional form and methodology are followed here, again. In this case, however, the vector θ, contains only six elements instead of nine, which we had when we considered the quadratic Weibull model which matched the first three moments. The damage-based model matches only two moments, albeit the two moments that are matched are typically of higher order. Linear regression analysis applied to the logarithm of Equation 5.9 was used to obtain estimates of the coefficients. The reference wind speed and reference turbulence used in the regression analysis are given in Table 5.1. The calculated regression coefficients and R^2 statistics are shown in Tables 5.6 and 5.7 for blade root flap and edge bending transformed, $z = 3$, fatigue ranges, respectively. Similar results are shown in Tables 5.8 and 5.9 for $z = 4$ transformed fatigue ranges and Tables 5.10 and 5.11 for $z = 5$ transformed fatigue ranges. R^2 statistics near unity indicate that a large percentage of the variability in the data is explained by the regression model. Low R^2 statistics indicate that other influences not contained in the regression model may be affecting the loads. In performing the regression analysis, it was again determined that the applied functional model, Equation 5.9, did not have enough flexibility to sufficiently model the observed behavior of the mean and standard deviation of the blade root flap bending fatigue ranges. The values of the mean and standard deviation of the fatigue ranges flatten out with higher wind speeds above 17m/s as compared with the behavior below 17m/s. Therefore, a separate model was fit to each of these regions, one below 17m/s and the other above 17m/s, for both the mean and standard deviation of blade root flap bending fatigue ranges. We saw a similar result in Section 5.4 when we fit the quadratic Weibull model to the fatigue ranges.

Finally, graphical regression results for the case where the fatigue ranges are transformed for $z = 3$, are shown in Figures 5.16 and 5.17. Each figure contains regression results for both blade root flap and edge bending conditions considering the mean of the fatigue ranges, Figure 5.16, and standard deviation of the fatigue ranges, Figure 5.17. In all plots, the turbulence intensity has been set equal to the reference value. Similar results were found for the other transformation cases and, in the interest of brevity, these additional plots are not presented.

Transformed Blade Root Flap Bending Fatigue Ranges
***z*=3**

Regression of the Mean
of Fatigue Ranges on V and I

	a (kN-m)	b	c	R^2
$V \leqq 17$m/s	910.14	3.7443	2.2384	0.93414
$17 < V \leqq 24$m/s	1354.7	0.7145	2.9149	0.9899
$V > 24$m/s	661.22	12.498	2.0233	0.9950

Regression of the Standard Deviation
of Fatigue Ranges on V and I

	a (kN-m)	b	c	R^2
$V \leqq 24$m/s	3647.1	3.3155	2.2479	0.9638
$17 < V \leqq 24$m/s	5425.1	1.0043	2.7920	0.9686
$V > 24$m/s	3358.3	10.688	2.8186	0.9944

Table 5.6: Regression coefficients used in Equation 5.9 to fit transformed ($z = 3$) flap bending moment fatigue ranges as functions of the mean wind speed and turbulence intensity. The turbine is operating for $V \leqq 24$m/s, otherwise the turbine is parked.

Transformed Blade Root Edge Bending Fatigue Ranges
***z*=3**

Regression of the Mean
of Fatigue Ranges on V and I

	a (kN-m)	b	c	R^2
$V \leqq 24$m/s	673.44	-0.0361	-0.0251	0.1926
$V > 24$m/s	9.2980	13.599	1.1361	0.9949

Regression of the Standard Deviation
of Fatigue Ranges on V and I

	a (kN-m)	b	c	R^2
$V \leqq 24$m/s	191.39	1.220	1.5619	0.9842
$V > 24$m/s	46.567	13.011	1.4599	0.9867

Table 5.7: Regression coefficients used in Equation 5.9 to fit transformed ($z = 3$) edge bending moment fatigue ranges as functions of the mean wind speed and turbulence intensity. The turbine is operating for $V \leqq 24$m/s, otherwise the turbine is parked.

Transformed Blade Root Flap Bending Fatigue Ranges
***z*=4**

Regression of the Mean of Fatigue Ranges on V and I

	a (kN-m)	b	c	R^2
$V \leqq 17$m/s	20167	4.7638	2.9951	0.9454
$17 < V \leqq 24$m/s	34234	1.0877	3.8399	0.9847
$V > 24$m/s	15041	15.723	3.2836	0.9948

Regression of the Standard Deviation of Fatigue Ranges on V and I

	a (kN-m)	b	c	R^2
$V \leqq 24$m/s	115610	4.2740	2.9899	0.9731
$17 < V \leqq 24$m/s	197600	1.5268	3.6015	0.9519
$V > 24$m/s	122030	13.3432	3.9646	0.9940

Table 5.8: Regression coefficients used in Equation 5.9 to fit transformed ($z = 4$) flap bending moment fatigue ranges as functions of the mean wind speed and turbulence intensity. The turbine is operating for $V \leqq 24$m/s, otherwise the turbine is parked.

Transformed Blade Root Edge Bending Fatigue Ranges
***z*=4**

Regression of the Mean of Fatigue Ranges on V and I

	a (kN-m)	b	c	R^2
$V \leqq 24$m/s	6041.45	0.0094	0.03198	0.0097
$V > 24$m/s	50.0689	17.307	0.86779	0.9911

Regression of the Standard Deviation of Fatigue Ranges on V and I

	a (kN-m)	b	c	R^2
$V \leqq 24$m/s	2183.3	1.1139	1.5163	0.9894
$V > 24$m/s	511.42	17.033	0.7763	0.9878

Table 5.9: Regression coefficients used in Equation 5.9 to fit transformed ($z = 4$) edge bending moment fatigue ranges as functions of the mean wind speed and turbulence intensity. The turbine is operating for $V \leqq 24$m/s, otherwise the turbine is parked.

Transformed Blade Root Flap Bending Fatigue Ranges
z=5

Regression of the Mean
of Fatigue Ranges on V and I

	a (kN-m)	b	c	R^2
$V \leqq 17$m/s	514011	5.7290	3.740	0.9548
$17 < V \leqq 24$m/s	995500	1.5177	4.7144	0.9770
$V > 24$m/s	435827	18.582	4.4772	0.9939

Regression of the Standard Deviation
of Fatigue Ranges on V and I

	a (kN-m)	b	c	R^2
$V \leqq 24$m/s	4008800	5.2460	3.7288	0.9787
$17 < V \leqq 24$m/s	7920800	2.1053	4.3682	0.9382
$V > 24$m/s	4916000	16.139	5.1216	0.9930

Table 5.10: Regression coefficients used in Equation 5.9 to fit transformed ($z = 5$) flap bending moment fatigue ranges as functions of the mean wind speed and turbulence intensity. The turbine is operating for $V \leqq 24$m/s, otherwise the turbine is parked.

Transformed Blade Root Edge Bending Fatigue Ranges
z=5

Regression of the Mean
of Fatigue Ranges on V and I

	a (kN-m)	b	c	R^2
$V \leqq 24$m/s	54502.4	0.0628	0.1017	0.2822
$V > 24$m/s	380.13	20.360	-1.1755	0.9886

Regression of the Standard Deviation
of Fatigue Ranges on V and I

	a (kN-m)	b	c	R^2
$V \leqq 24$m/s	24785	1.1121	1.5806	0.9904
$V > 24$m/s	6813.8	20.790	-0.9950	0.9883

Table 5.11: Regression coefficients used in Equation 5.9 to fit transformed ($z = 5$) edge bending moment fatigue ranges as functions of the mean wind speed and turbulence intensity. The turbine is operating for $V \leqq 24$m/s, otherwise the turbine is parked.

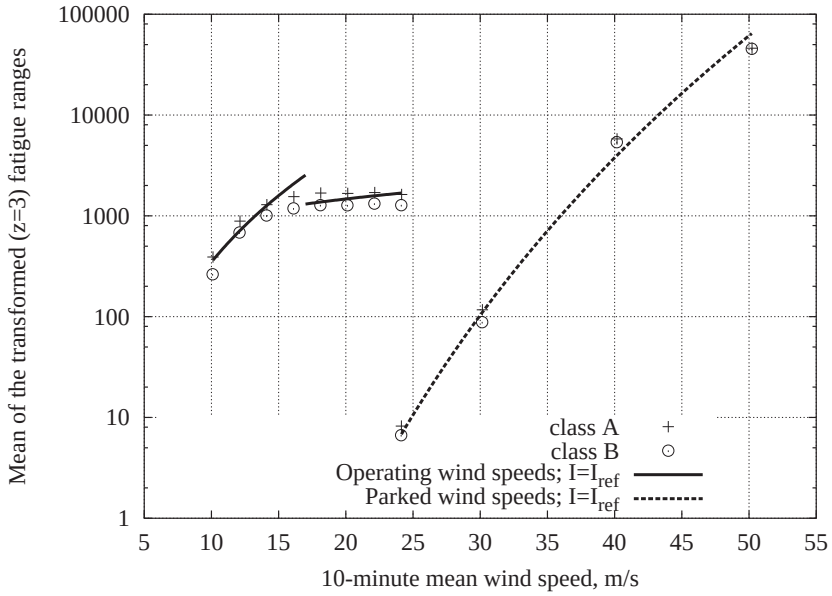

(a) Pooled statistics of the mean of transformed ($z = 3$) fatigue ranges in 10-minute blade root flap bending response time history.

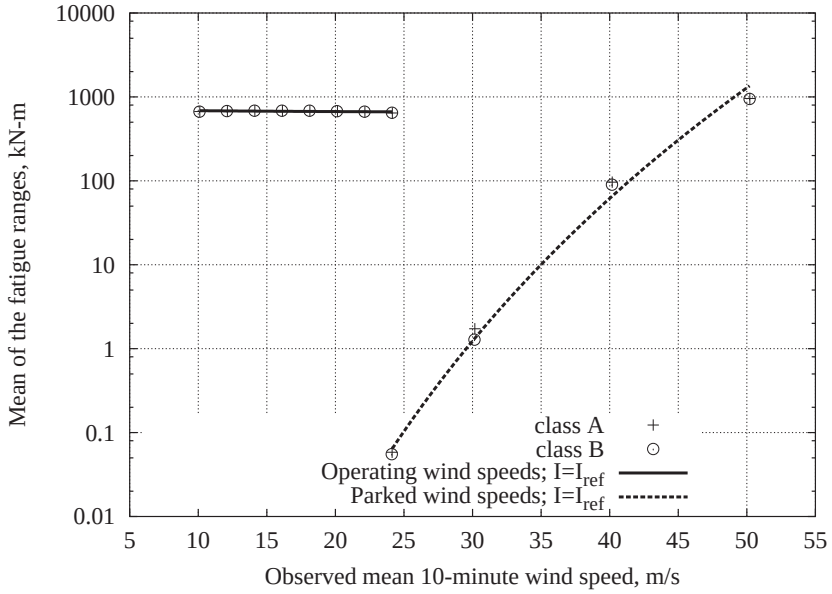

(b) Pooled statistics of the mean of transformed ($z = 3$) fatigue ranges in 10-minute blade root edge bending response time history

Figure 5.16: Mean of transformed ($z = 3$) fatigue ranges for 10-minute blade root flap and edge bending response, based on 100 pooled observations for each 10-minute wind speed and turbulence class. The wind turbine is operating for $V \leqq 24$m/s, otherwise the turbine is parked.

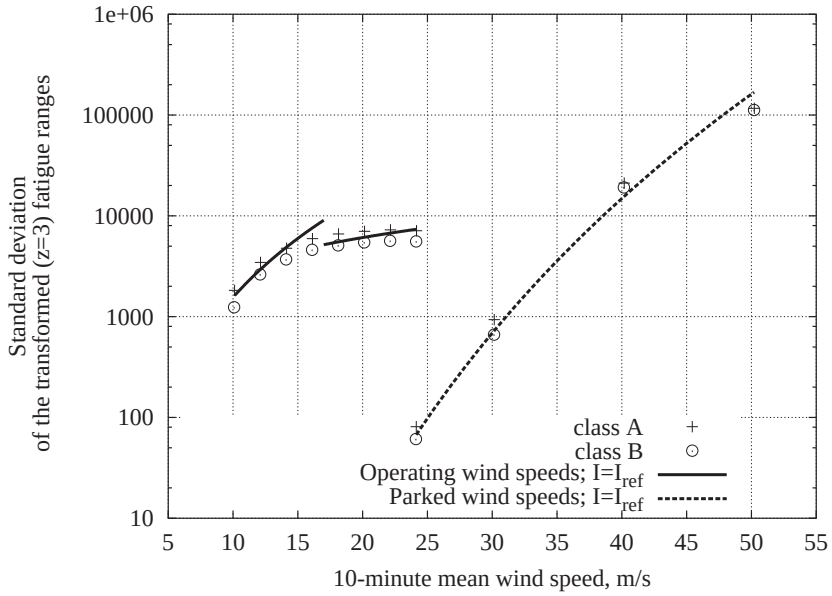

(a) Pooled statistics of the standard deviation of transformed ($z = 3$) fatigue ranges in 10-minute blade root flap bending response time history.

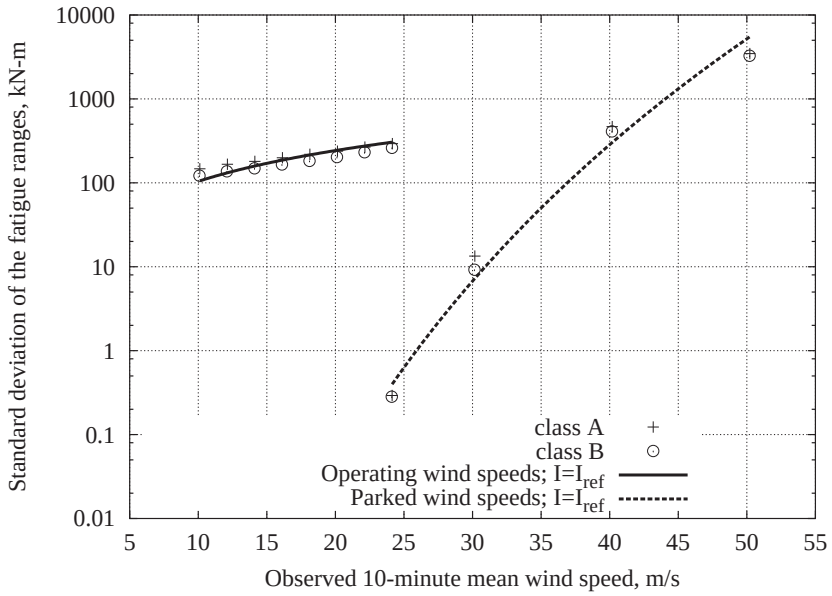

(b) Pooled statistics of the mean of transformed ($z = 3$) fatigue ranges in 10-minute blade root edge bending response time history

Figure 5.17: Standard deviation of transformed ($z = 3$) fatigue ranges for 10-minute blade root flap and edge bending response time histories, based on 100 pooled observations for each 10-minute mean wind speed and turbulence class. The wind turbine is operating for $V \leqq 24$m/s, otherwise the turbine is parked.

5.5.2 Long-Term Analysis

For the discussion here, we defined the conditional probability distribution of fatigue ranges by a damage-based Weibull model. We saw how this model can be represented by the moments of the data. Further, we have just shown through regression analysis how these statistical moments may be related to the environmental variables.

The long-term distribution of fatigue load ranges, in an arbitrary 10-minute period, is found in the same way as implemented in Section 5.4. We will again assume that the AOC 15/50 turbine is installed at a site with environmental conditions similar to the Lavrio, Greece, test site described in Chapter 3 (page 77). The long-term distribution of the 10-minute mean wind speed is assumed to follow a Rayleigh distribution with mean, $\mu_V = 10$m/s. The conditional distribution of turbulence is given by a Gaussian distribution with conditional mean, $\mu_{I|V} = 2.4486v^{-0.9971}$ and constant standard deviation, $\sigma_{I|V} = 0.025$. A plot of the joint density function of the environmental variables is shown in Figure 4.7 (Chapter 4).[2]

The ranges of the values of the environmental variables are discretized into evenly spaced intervals. For each pair of values of the environmental variables the corresponding short-term distribution of fatigue ranges is generated. Then, per Equation 5.11, the short-term conditional fatigue range distributions are summed together, each weighted by the probability of the respective environmental condition, i.e., pair of values of the environmental variables, occurring. The summation is performed over the entire range of environmental variables.

As stated earlier, there are two loading conditions for the turbine, operating and parked. During normal use the turbine is operating for wind speeds less than 24m/s and parked for wind speeds greater than 24m/s. To develop the long-term distribution of the fatigue ranges, the appropriate regression model is used for each wind speed value. Figure 5.13 shows three long-term distributions of fatigue ranges. Each distribution is based on a different transformation of the fatigue ranges ($z = 3$, 4, 5). For the most part, all of the distributions appear very similar, only at low probability levels (below 10^{-8}) do the distributions, for either blade root flap or edge bending fatigue ranges, show a significant difference.

In addition to obtaining an estimate of the long-term distribution of fatigue ranges, we saw in the previous section that we may obtain an estimate of the fatigue damage in an arbitrary 10-minute interval. We again turn to our regression model for a relationship between the expected number of cycles and the environmental variables.[3] The same power-law functional form, Equation 5.9, was

[2] A more detailed definition of the environmental variables for the Lavrio, Greece site is given in Chapters 3 and 4.

[3] When we transform the fatigue ranges, with $z = 3, 4, 5$, only the magnitude of the fatigue ranges is transformed, the number of fatigue ranges stays the same. Therefore, the expected number of fatigue ranges stays the same regardless of the transformation. The results of the regression analysis presented here is valid for any value of z used for the transformation.

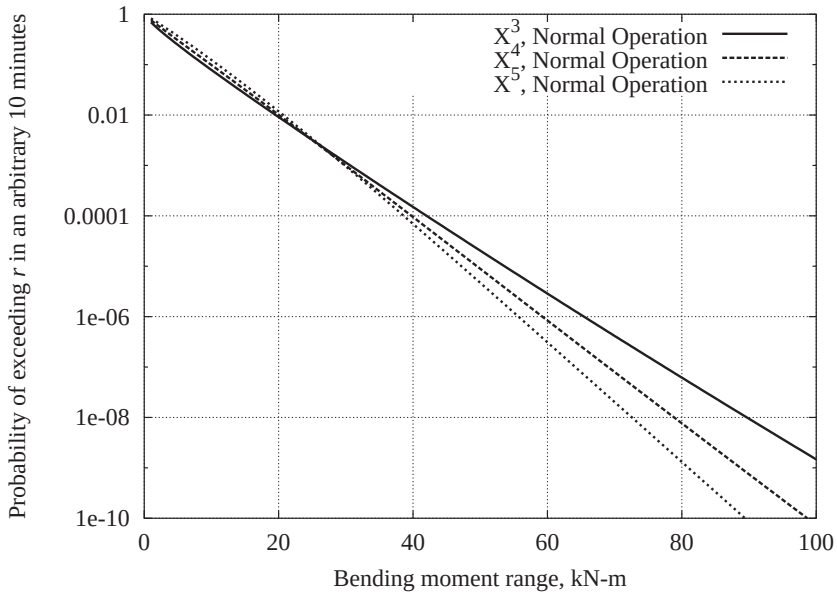

(a) Long-term distribution of blade root flap bending fatigue ranges for an arbitrary 10 minutes.

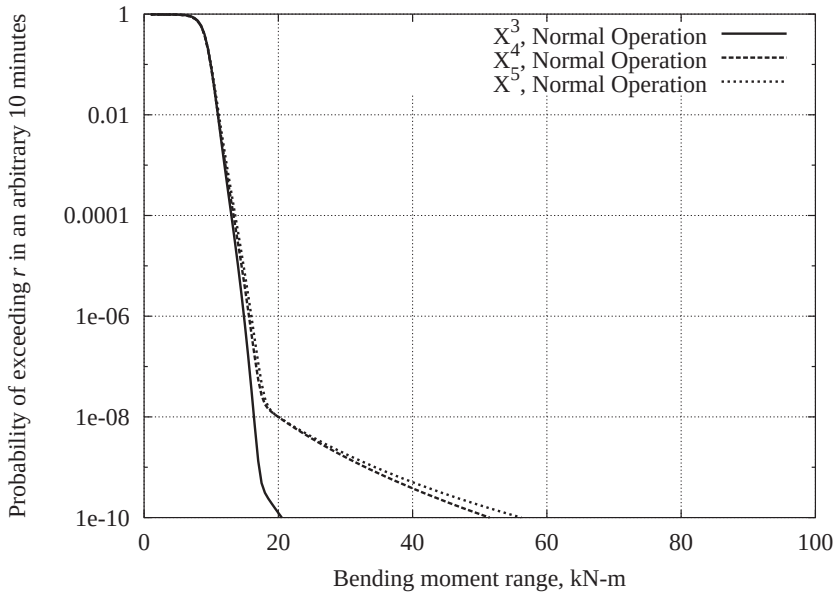

(b) Long-term distribution of blade root edge bending fatigue ranges for an arbitrary 10 minutes.

Figure 5.18: Long-term distributions of blade root fatigue bending moment ranges, R, considering three fatigue range transformations, $z = 3$, 4 and 5; for (a) flap and (b) edge bending.

Regression of the number of Fatigue Ranges on V and I

Blade Root Flap Bending

	a (kN-m)	b	c	R^2
$V \leqq 24$m/s	1764.1	-0.0977	0.03662	0.3734
$V > 24$m/s	5024.1	0.2823	-0.3971	0.9623

Blade Root Edge Bending

	a (kN-m)	b	c	R^2
$V \leqq 24$m/s	670.69	0.1326	0.1307	0.7836
$V > 24$m/s	5474.2	0.1793	-0.2630	0.9634

Table 5.12: Regression coefficients used in Equation 5.9 to fit the expected number of fatigue ranges, for blade root flap and edge bending, as functions of the mean wind speed and turbulence intensity. The turbine is operating for $V \leqq 24$m/s, otherwise the turbine is parked.

used. The calculated regression coefficients and R^2 statistics are shown in Table 5.12 for blade root flap and edge bending fatigue ranges. Graphical regression results are shown in Figure 5.19. Applying Equation 5.15, we can obtain estimates of the damage measure for blade root flap and edge bending considering b_f values corresponding to z and $2z$ for $z = 3, 4, 5$; these estimates are presented in Table 5.13. We may also consider the portion of the expected damage contributed at different environmental conditions. Figure 5.20 presents the plot of damage density for both blade root flap and edge bending moments. We can see from Figure 5.20(a), which shows damage densities for flap bending fatigue ranges and different values of b_f, that as b_f increases the damage measure is more sensitive to higher wind speeds. This trend is also seen in Figure 5.20(b), considering edge bending fatigue ranges, although for $b_f = 10$ the accumulated damage is much more sensitive to fatigue ranges resulting from high wind speeds when the turbine is parked. We might expect this behavior where the material is much more sensitive to loads above the kink in Figure 5.18(b).

5.5.3 Summary

Similar to the previous section, here we have stepped through the process of obtaining an estimate of the marginal probability distribution of the long-term distribution of fatigue ranges. The short-term fatigue loads were modeled using the damage-based Weibull model, however. The general methodology remained the same. In this case however, the statistical moments were obtained after having first transformed the fatigue ranges, e.g., $z = 3, 4, 5$. By performing this transformation when we employed the method of moments to obtain estimates of the distribution parameters, our

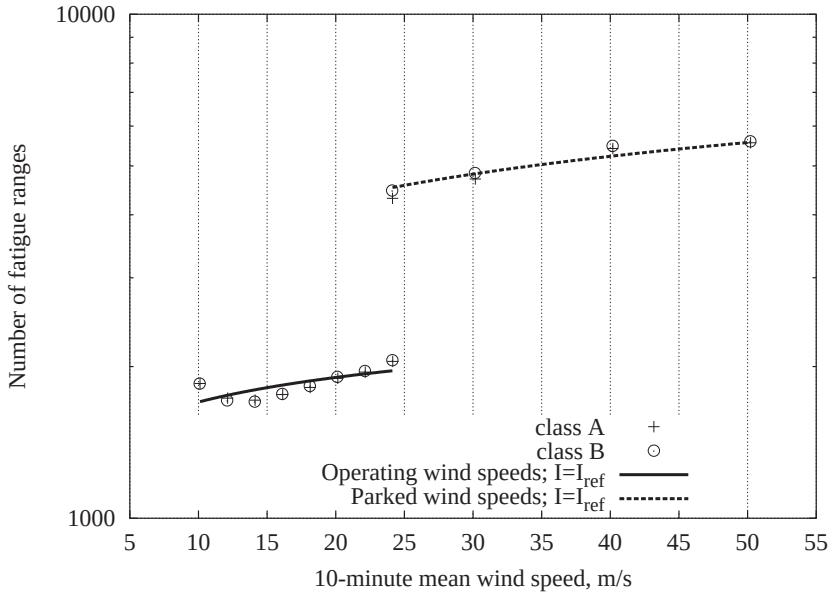

(a) Expected number of fatigue ranges in 10-minute blade root flap bending time history.

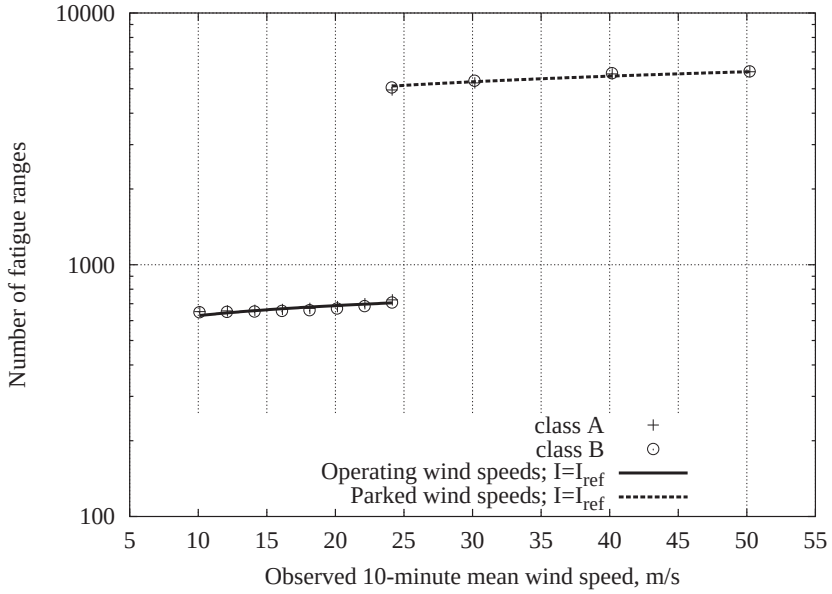

(b) Expected number of fatigue ranges in 10-minute blade root edge bending time history.

Figure 5.19: Expected number of fatigue ranges in 10-minute blade root flap and edge bending response time histories, based on 100 pooled observations for each 10-minute mean wind speed and turbulence class. The wind turbine is operating for $V \leqq 24$m/s, otherwise the turbine is parked.

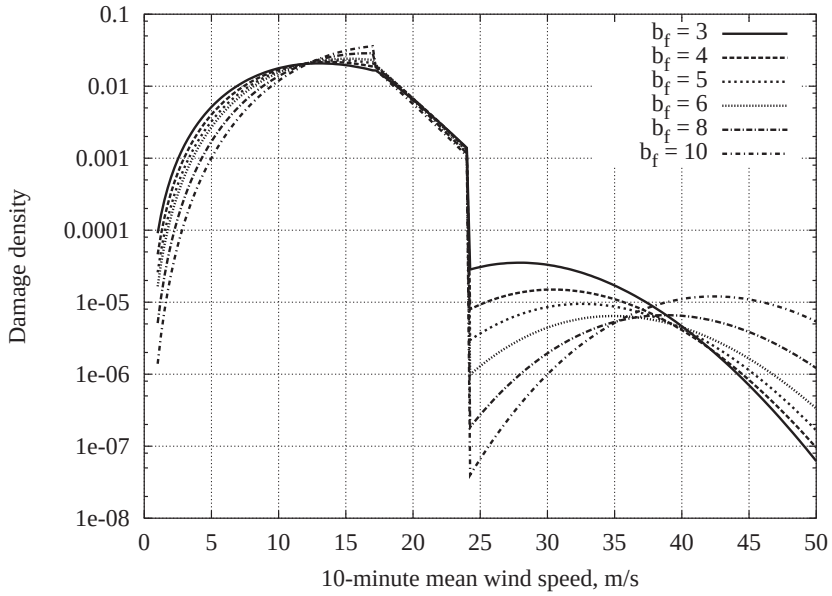

(a) Blade root flap bending moment.

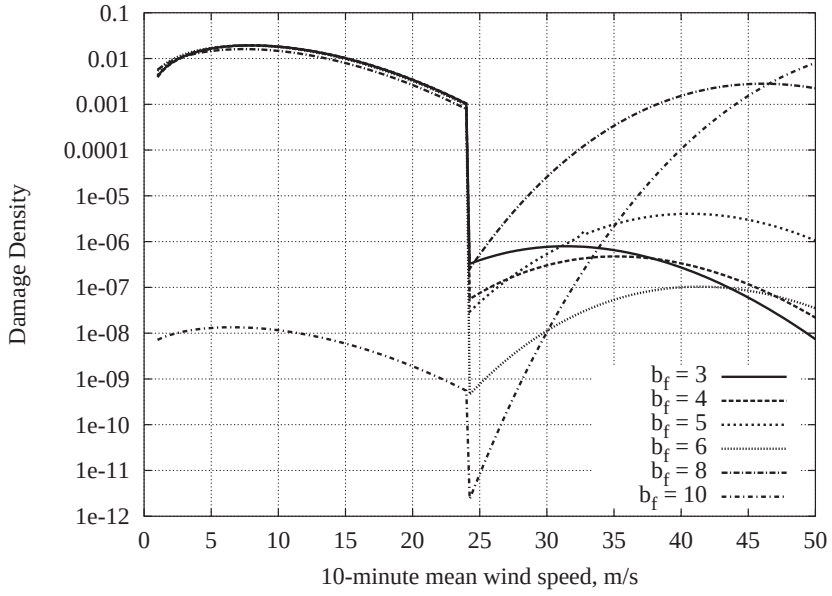

(b) Blade root edge bending moment.

Figure 5.20: Damage density for blade root flap and edge bending.

Estimate of Damage Measure, DM_{10}, for fatigue exponent values, $b_f = 1, \ldots, 10$.

	b_f	Flap	Edge
$z = 3$	3	7.909e+4	4.445e+5
	6	9.482e+9	3.416e+8
$z = 4$	4	1.487e+7	3.939e+6
	8	8.705e+12	3.512e+10
$z = 5$	5	3.574e+8	3.654e+7
	10	1.006e+16	4.142e+12

Table 5.13: Estimate of damage measure, DM_{10}, for fatigue exponent values, $b_f = 1, \ldots, 10$, considering blade root flap and edge bending loads.

model was fit to the z^{th} and $2z^{\mathrm{th}}$ moments of the untransformed data. For $z = 3$, this amounts to fitting the standard Weibull model to the third and sixth statistical moment where we suspect a material with fatigue exponent $b_f = 3$-6 would be most sensitive to these higher fatigue ranges. The statistical moments of the transformed fatigue ranges were related to the environmental variables through regression analysis. Finally, an estimate of the marginal distribution of the long-term load was obtained by summing the conditional short-term load distributions (each weighted by the probability of the values of the environmental variables occurring) over all environmental conditions. We considered three transformation cases, $z = 3$, 4, and 5. We found that the marginal long-term distributions of the fatigue ranges for an arbitrary 10-minute interval were very similar, and only exhibit significant difference at low probability levels.

5.6 Comparison of Long-Term Estimates Based on Different Short-Term Models

In Section 5.4, we saw how one could obtain an estimate of the long-term distribution of fatigue ranges based on the short-term distribution of fatigue ranges model by a quadratic Weibull model. Later, in Section 5.5, we saw how a similar estimate of the long-term distribution may be obtained by modeling the short-term distribution of fatigue ranges by a damage-based Weibull model. We have explored two alternative models for describing the short-term fatigue ranges.

Figure 5.21 shows the estimates of the long-term distribution of fatigue loads based on modeling the short-term fatigue ranges by quadratic or damage-based Weibull models. In this case, using the quadratic Weibull distribution to model the short-term fatigue ranges generates a long-term distribution with higher fatigues loads compared with the the long-term distribution of fatigue loads

Comparison of Estimates of Damage Measure, DM_{10}, Blade Root Flap Bending

		Damage-	Percent Difference		
b_f	Q. W.	Based	$z = 3$	$z = 4$	$z = 5$
3	1.349e+6	7.909e+4	-94%		
4	3.281e+7	1.487e+7		-54%	
5	9.134e+8	3.574e+8			-61%
6	2.9e+10	9.482e+9	-67%		
8	4.1e+13	8.7e+12		-78%	
10	8.6e+16	1.0e+16			-88%

Table 5.14: Comparison of damage measure, DM_{10}, estimates for blade root flap bending fatigue loads between short-term quadratic Weibull(Q.W.) model and damage-based Weibull model for $z = 3, 4, 5$ ($z = b_f/2$).

considering the damage-based model. This is the case for both blade root flap and edge bending loads. In the blade root flap bending case, the difference in the distributions is fairly uniform. In the blade root edge bending case the quadratic Weibull model does not exhibit a strong influence from the parked turbine fatigue loads, as the damage-based models do at low probability levels.

Tables 5.14 and 5.15 compare estimates of damage measures, DM_{10}, obtained from our two model definitions. We saw above that the quadratic Weibull produced higher loads for the long-term distribution for both blade root flap and edge bending loads. It would follow that we would expect to see higher damage measures. In fact, this is the case for flap loads—the damage-based Weibull models do estimate lower damage measures compared with the estimates from the quadratic Weibull model. In the edge bending case, however, even though the quadratic Weibull model does estimate higher fatigue loads, significantly higher fatigue loads at low probability levels, the damage measure estimates are just slightly lower than those estimated from the damage-based Weibull model. Even though the quadratic Weibull model predicts some higher fatigue loads, they are at extremely low probability levels and therefore occur only rarely and their contribution to the fatigue damage is limited.

We can alternatively compare our estimates of the fatigue damage measure from each of the proposed models to an empirical estimate of the fatigue damage measure. The empirical estimate of the fatigue damage measure is obtained by using the raw rainflow counted range data directly from a representative time history for a given set of values of the environmental variables. The fatigue damage measure is weighted by the probability of the values of the environmental variables. The data set examined here contained 24 different values of the environmental variables, considering the turbine during both operating and parked conditions. The weighted fatigue damage measures were

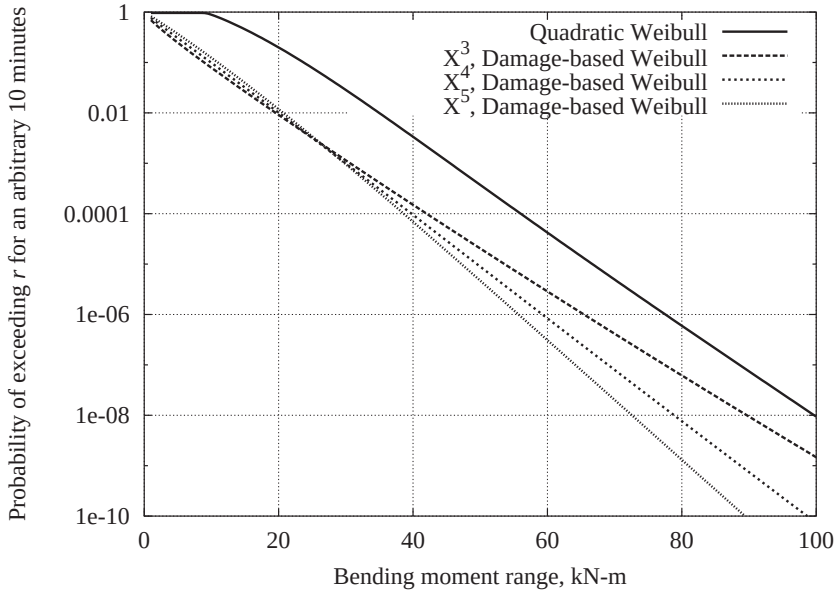

(a) Blade root flap bending.

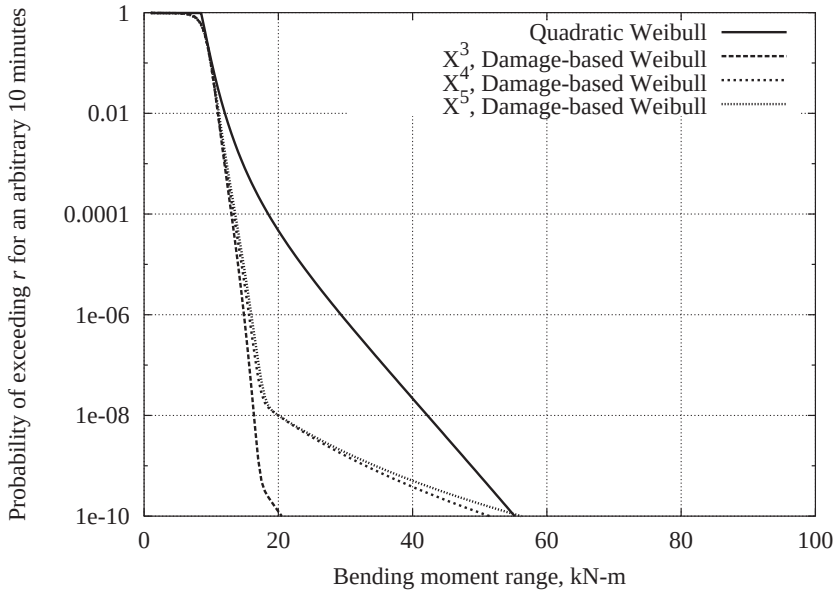

(b) Blade root edge bending.

Figure 5.21: Comparison of estimates of the long-term distribution of fatigue ranges based on quadratic or damage-based Weibull models for short-term distribution of fatigue ranges for (a) flap and (b) edge bending.

Comparison of Estimates of Damage Measure, DM_{10}, Blade Root Edge Bending

		Damage-	Percent Difference		
b_f	Q. W.	Based	$z = 3$	$z = 4$	$z = 5$
3	3.244e+5	4.445e+5	+37%		
4	3.053e+6	3.939e+6		+29%	
5	2.908e+7	3.654e+7			+26%
6	2.819e+8	3.416e+8	+21%		
8	2.9e+10	3.5e+10		+21%	
10	4.2e+12	4.1e+12			-1.2%

Table 5.15: Comparison of damage measure, DM_{10}, estimates for blade root edge bending fatigue loads between short-term quadratic Weibull(Q.W.) model and damage-based Weibull model for $z = 3, 4, 5$ ($z = b_f/2$).

summed across this range of the environmental variables.

Tables 5.16 and 5.17 show the fatigue damage measure for different values of the fatigue exponent, b_f, based on the empirical model and compared to the estimates obtained based on the quadratic Weibull and damage based models. In general, compared to the empirical model, the estimates of the fatigue damage measure for the flap bending direction, both the quadratic Weibull and damage-based models under-predict the fatigue damage measure for all fatigue exponents that we considered. We found slightly different results for the edge bending direction. In this case, the damage-based model still under-predicted the fatigue damage measure for all fatigue exponents that we considered. The quadratic based model under-predicted the fatigue damage measure for fatigue exponent values below seven, $b_f < 7$ and over-predicted for values greater than seven, $b_f > 7$. In this particular case, neither of the models does a very good job of estimating the fatigue damage measure compared with the empirical model. However, it should be noted that since the damage-based models are exact at matching the empirical damage at the moments for which they are fit it is really the regression model that is being tested. Additional research would be required to evaluate the general efficacy of these models and regression techniques to predict fatigue damage.

5.7 Conclusions

Parametric, moment-based, statistical models have been introduced to model rain-flow-counted fatigue ranges. Two "higher-moment" models (including third and/or higher moments) have been presented: (1) a quadratic Weibull model, which uses a quadratic distortion of the original Weibull model to preserve the first three moments of the data; and (2) a "damage-based" Weibull model,

Comparison of Estimates of Damage Measure, DM_{10}, for Fatigue Exponent Values, $b_f = 1, \ldots, 10$, Flap Bending

b_f	Empirical DM_{10}	Quadratic Weibull DM_{10}	Quadratic Weibull % diff.	Damage-based Weibull DM_{10}	Damage-based Weibull % diff.
1	6.612e+3	3.490e+3	-47.2%	-	-
2	8.620e+4	6.381e+4	-26.0%	-	-
3	2.105e+6	1.349e+6	-35.9%	7.909e+4	-96.2%
4	8.629e+7	3.281e+7	-62.0%	1.487e+7	-82.8%
5	5.232e+9	9.134e+8	-82.5%	3.574e+8	-93.2%
6	4.044e+11	2.884e+10	-92.8%	9.482e+9	-97.6%
7	3.493e+13	1.024e+12	-97.1%	-	-
8	3.308e+15	4.054e+13	-99.0%	8.705E+12	-99.7%
9	3.327e+17	1.776e+15	-99.5%	-	-
10	3.506e+19	8.569e+16	-99.8%	1.006e+16	-99.9%

Table 5.16: Comparison of estimates of blade root flap bending fatigue damage measure, DM_{10}, for fatigue exponent values, $b_f = 1, \ldots, 10$, considering empirical, quadratic Weibull, and damage based models.

Comparison of Estimates of Damage Measure, DM_{10}, for Fatigue Exponent Values, $b_f = 1, \ldots, 10$, Edge Bending

b_f	Empirical DM_{10}	Quadratic Weibull DM_{10}	Quadratic Weibull % diff.	Damage-based Weibull DM_{10}	Damage-based Weibull % diff.
1	5.622e+3	3.783e+3	-32.7%	-	-
2	4.938e+4	3.481e+4	-29.5%	-	-
3	4.367e+5	3.244e+5	-25.7%	4.445e+5	-96.2%
4	3.881e+6	3.053e+6	-21.3%	3.939e+6	-82.8%
5	3.467e+7	2.908e+7	-16.3%	3.654e+7	-93.2%
6	3.115e+8	2.819e+8	-9.5%	3.416e+8	-97.6%
7	2.815e+9	2.802e+9	-0.5%	-	-
8	2.564e+10	2.906e+10	13.4%	3.512E+10	-99.7%
9	2.363e+11	3.257e+11	37.8%	-	-
10	2.261e+12	4.223e+12	86.8%	4.142e+12	-99.9%

Table 5.17: Comparison of estimates of blade root edge bending fatigue damage measure, DM_{10}, for fatigue exponent values, $b_f = 1, \ldots, 10$, considering empirical, quadratic Weibull, and damage based models.

which seeks a two-moment Weibull fit, not to the fatigue ranges themselves but to power transformations that directly relate to "damage" (i.e., based on material properties defining S-N curve slope, b_f). Both models have their advantages. Compared with fatigue load data, the damage-based Weibull model is found to follow the tails of the observed data (as seen, for example, in Figure 5.6-5.9). It also requires no special numerical algorithms to estimate its parameters. In contrast, the quadratic Weibull does require such algorithms, and its accurate modeling of distribution tails can require the analyst to impose a lower-bound threshold on the load ranges to be modeled (see Figure 5.3 versus Figure 5.4). The potential benefit of the quadratic Weibull model includes its reliance only on moments through third order. The damage-based model requires moments of order $z = b_f/2$, where typical z values may range from 3 to 5 reflecting material properties $b_f = 6 - 10$. Hence, to the degree it remains accurate, the quadratic Weibull model can be fit more accurately from limited data.

Chapter 6

Uncertainty in Estimation of Extreme Loads

In the previous chapters we have presented a methodology for obtaining estimates of fatigue and extreme load distributions. In these chapters we acknowledge the natural randomness of the three constituent variables—conditional short-term load, wind speed, and turbulence—by fitting or assigning probability models to these variables. In applying these relations, however, we assumed that all the parameters of the probability models were known, i.e., the parameter values were deterministic. In this chapter we consider examining some of the sources of uncertainty in our analysis. In particular we consider how to include these sources of uncertainty and how these uncertainties influence our estimate of extreme loads.

Usually, the goal in doing an analysis of the epistemic uncertainty in an engineering design problem is to understand which variables contribute the most to the overall uncertainty. Those candidate variables are then the target of additional analysis to reduce their attendant uncertainty, and thereby increase the certainty, or confidence, in the final design. In the context of this discussion we should be interested in understanding the contribution each variable makes to the uncertainty in our prediction of the one-year load or 50-year load, for example. With this in mind, we look to address three areas of epistemic uncertainty, (1) The epistemic uncertainty in our estimates of the model parameters which define the long-term distributions of the environmental variables. (2) The epistemic uncertainty in our estimates of the regression coefficients which relate statistics of the short-term response of the turbine to the environmental variables. And finally, (3) quantifying our model uncertainty, how does our predictive model compare with observations of the response of the turbine in the field.

6.1 Introduction

In the previous discussions we have concerned ourselves with presenting a methodology for obtaining an estimate of the 1-year and 50-year extreme load in Chapters 3 and 4, or an estimate of the long-term distribution of fatigue loads in Chapter 5. In these discussions we acknowledge the natural randomness of the three constituent variables—conditional short-term load, wind speed, and turbulence—by fitting or assigning probability models to these variables. We showed how the natural randomness of these variables may be combined and contribute to the variability of the long-term distribution of fatigue or extreme loads. This was accomplished by applying the Law of Total Probability as shown in the equation below considering extreme loads,

$$P[L_{10\text{ min}} > l] = \iint P[L_{10\text{ min}} > l \mid v, i\,] f_{I|V}(i|v) f_V(v) di dv \tag{6.1}$$

where, $L_{10\text{ min}}$, is the maximum response in 10-minutes, V, and, I, are the 10-minute mean wind speed and turbulence, respectively. A similar equation, applying the Law of Total Probability was used for estimating the long-term distribution of fatigue loads. In applying these relations, however, we assumed that all the parameters of the probability models were known, i.e., the parameter values were deterministic. In this chapter we consider examining some of the sources of uncertainty in our analysis. In particular, we will consider how we might include these sources of uncertainty and to what degree these uncertainties influence our estimate of extreme loads.[1]

6.1.1 Types of Uncertainty

In this section we present a short discussion on the types of uncertainty in estimation of long-term distribution of extreme loads. These types of uncertainty are generally common to many types of predictive models, e.g., extreme wave height models for off-shore structures, ground-motion models for earthquake engineering, weather forecasting, etc.

Aleatory uncertainty The uncertainty that is associated with the nature of physical models is referred to as *aleatory* uncertainty. Other names for the aleatory uncertainty include "stochastic" or "random" uncertainty. Even under the condition of "prefect information", i.e., the model of the physical phenomenon is validated and the values of the parameters of the model are known, these aleatory uncertainties still remain. Formally, the portion of the uncertainty in our prediction of the outcome of an event which is irreducible and attributed to the natural randomness of the event is the aleatory uncertainty. Given a model, one can not reduce the

[1] A similar discussion could be presented for fatigue loads.

aleatory uncertainty by the collection of additional information. It may be possible, however, to better quantify the aleatory uncertainty by using additional data.

Epistemic uncertainty The uncertainties that arise from our lack of knowledge concerning the validity of the chosen models or the values of the parameters are referred to as *epistemic* uncertainty, as distinct from randomness (or aleatory). Sometimes, in the literature, these are referred to simply as "uncertainties". Formally, the epistemic uncertainty is the portion of uncertainty in our prediction of the outcome of an event which is related to our state, or accumulation, of knowledge of the event under observation. In other words, the epistemic uncertainty is that portion of the uncertainty in our prediction which can be reduced by continued diligent study and observation of more realizations of the process under examination.

These definitions may be more clearly explained through the following example. Let us assume that we observe the outcome of an event—the roll of a die. We do not know if the die is fair, and further we don't know the number of sides on the die. At this point we have only one outcome, and little way of quantifying the uncertainty—aleatory or epistemic—of our prediction of the outcome of the next roll of the die. After sufficient observations, we may ascertain all possible outcomes of rolling the die, and construct a probability model of the likelihood of each of these possible outcomes. With each roll, our knowledge about the possible outcomes of the event, and their relative likelihoods (i.e., long-term frequencies or next roll probabilities), has increased and our epistemic uncertainty was decreased. Which one of the possible outcomes will occur with any given roll is the irreducible aleatory uncertainty. The probability model we constructed quantifies the aleatory uncertainty. We will be able to refine the probability model, and better quantify our aleatory uncertainty by continuing to observe the outcomes of the event, but it is by definition irreducible. Which possible outcome occurs with any given future roll of the die is still unknown. Some sources, or types, of epistemic uncertainty include modeling and parametric uncertainty.

Modeling Uncertainty Represents the differences between the actual physical process that manifests the event and the simplified models used to predict the event. Here we may consider the physical processes that generate extreme blade bending loads on a wind turbine compared with the simple models used to predict these extreme events. Probabilistic models, e.g., the shape (or name) of the distribution, are also subject to such uncertainty. The modeling uncertainty can be estimated by comparing model predictions with actual, observed events.

Parameter Uncertainty Is the uncertainty associated with the estimated values of model parameters. These may include parameters in both the mechanical (deterministic) models (e.g., the blade load predictions) and the random process models (e.g., the wind speed probability

distribution model). The parametric uncertainty is quantified by observing the variation in parameters inferred from collected data.

6.1.2 Motivation

Usually the goal in doing an analysis of the epistemic uncertainty in an engineering design problem is to understand which variables contribute the most to the overall uncertainty. Those candidate variables are then the target of additional analysis to reduce their attendant uncertainty, and thereby increase the certainty, or confidence, in the final design. In the context of this discussion we should be interested in understanding the contribution each variable makes to the uncertainty in our prediction of the one-year load, or 50-year load for example. Up to now we have only considered the aleatory uncertainty, as described by the probability distributions for the variables: short-term load, 10-minute mean wind speed and turbulence. In Chapter 3 we undertook a qualitative analysis to see how the "randomness" (as we called it in Chapter 3), or "aleatory uncertainty" contributed to the variability in our estimate of the long-term distribution of extreme loads. Here, we seek to understand how including some of the sources of epistemic uncertainty contribute to the uncertainty in our estimate of the long-term distribution of extreme events.

We saw in Chapter 3 that the calculations involved in developing a prediction of the long-term distribution of extreme loads involved separating the problem into two parts: the short-term conditional distribution of the response of the turbine given prescribed environmental conditions, and the long-term distribution of the environmental variables. In the context of the IEC code, however, the parameters of these long-term distributions are legislated [23]. The resulting epistemic uncertainty is zero as the parameters are presumed known, and the aleatory uncertainty is prescribed as a result of the prescribed distributions.

The current IEC code breaks down the environmental conditions into four wind classes (wind classes I-IV), and two turbulence classes (classes A and B) [23]. For the wind classes, the long-term distribution of the 10-minute mean wind speed, V, is prescribed to follow a Rayleigh model. For each wind class a different annual average 10-minute mean wind speed, μ_V is prescribed, with class I and class IV assigned the highest and lowest values of μ_V, respectively. The long-term distribution of turbulence, conditional on wind speed, is assumed to follow either a Gaussian or lognormal model. Turbulence class A is associated with higher turbulence whereas turbulence class B is associated with lower turbulence values. Therefore, wind class IA is intended to encompass a large variety of site conditions and is therefore generally more severe and conservative than most specific sites. Class IVB is at the other end of the range of wind classes and describes a more benign wind environment than class IA.

Considering these prescribed distributions with known parameters effectively reduces the epistemic uncertainty in the environmental variables to zero. It becomes straightforward for the engineer to design and test the wind turbine to specific wind and turbulence class, as specified by the IEC code. A certifying agency reviews the design process and testing results and, hopefully, approves the turbine for use in the same wind and turbulence class for which it was intended. It is the intention of the code that wind turbines designed to higher wind classes, e.g., class IA, are more robust considering more severe environmental conditions, compared with the lower wind classes, e.g., class IVB. It is a matter then of economics to fit the right turbine to a specific set of site conditions. Generally, more robust turbines, turbines designed to a IA wind class, are more expensive since they are expected to operate in a more severe environment. Therefore, it would not necessarily be most efficient to install a class IA turbine in a benign wind environment. It is necessary then to estimate the model parameters of the environmental variables based on environmental data collected at the site. The question then becomes how good are our estimates of the model parameters for mean wind speed and turbulence. How well does the site fit the description of the four classes listed in the code? We can ask the question from another perspective. How good are our estimates of the model parameters for mean wind speed and turbulence and how does the epistemic uncertainty in our estimates of these parameters, from limited data, affect our estimate of the long-term distribution of extreme loads? This issue will be discussed in Section 6.3

The epistemic uncertainty associated with the short-term loads may be of more interest to the design engineer. We will consider two sources of epistemic uncertainty of the short-term loads, (1) parameter uncertainty, and (2) modeling uncertainty. In Chapter 3 we saw how the short-term distribution of extreme loads could be based on modeling either the global or local peaks. In either case the parameters of the model were fit to the data using the method of moments. The observed moments of the data were related to the environmental variables through regression analysis. There are several sources of epistemic uncertainty in the parameters. First, the statistical moments of the observed responses are based on limited data. Second, the moments are related to the environmental variables through regression analysis. This raises the question, “how well does the regression model fit the data?” These questions are considered in Section 6.4.1. Modeling uncertainty is considered in Section 6.4.3, where the short-term loads based on our mechanical model are compared with actual recorded data. We estimate the variability of the bias of the predictive model to the observed field data and show how we may include this uncertainty and its effect on the variability of long-term distribution of extreme events.

6.2 Data Set

The data set used in this analysis is for the Atlantic Orient Corporation AOC 15/50 turbine, described in Chapter 1 (page 18). The turbine has a rotor diameter of 15m, a fixed nominal rotor speed of about 60 RPM, and a rated wind speed of 12m/s. It is a three-bladed, fixed pitch turbine with a hub height of 25 meters [22]. The data set is described in detail in Chapter 3 (page 66) and consisted of multiple 10-minute simulations of Gaussian wind fields and corresponding blade root bending moments. The wind input processes is described by the hub height wind speed. For the analysis presented in this chapter only the blade root flap bending loads are used.

In the discussions that follow we will assume that the AOC 15/50 turbine is installed at a site with environmental conditions similar to the Lavrio, Greece, test site described in Chapter 3 (page 77). The long-term distribution of the 10-minute mean wind speed is assumed to follow a Rayleigh distribution with mean, $\mu_V = 10$m/s. The conditional distribution of turbulence is given by a Gaussian distribution with conditional mean, $\mu_{I|V} = 2.4486v^{-0.9971}$ and constant standard deviation, $\sigma_{I|V} = 0.025$. A plot of the joint density function of the environmental variables is shown in Figure 4.7 (Chapter 4).[2]

6.3 Uncertainty in Long-Term Environmental Distributions

We have seen in previous chapters how the natural randomness, or aleatory uncertainty, of the long-term distribution of the environmental variables may be described by prescribing probability models with *known* parameters, i.e., the parameters are considered known constants with no associated uncertainty. Further, we saw how an estimate of the long-term distribution of extreme loads may be obtained by combining the aleatory uncertainty of the short-term extreme response with the aleatory uncertainty of the environmental variables. This was accomplished through an application of the Law of Total Probability, as described in Chapter 3. This section presents a discussion on how we might first consider quantifying the influence of uncertainty in the parameters of the distributions of the environmental variables. The uncertainty in our estimates of the parameter values arise from having limited data, i.e., limited observations or realizations of the environmental variables. Our lack of knowledge, associated with limited observations, about the values of the parameters is a source of epistemic uncertainty.

To aid in our discussion let us consider the description of the environment at the Lavrio, Greece, test site as first presented in Chapter 3. The aspects critical to our discussion are reviewed here. The long-term distribution of the 10-minute mean wind speed, V, is assumed to follow a Rayleigh

[2] A more detailed definition of the environmental variables for the Lavrio, Greece site is given in Chapters 3 and 4.

distribution shown below,

$$f_V(v) = \frac{2v}{\alpha^2} \exp\left[-\left(\frac{v}{\alpha}\right)^2\right] \tag{6.2}$$

$$\alpha = \frac{2\mu_V}{\sqrt{\pi}}$$

This is a single parameter distribution. The standard deviation, σ_V, is given by

$$\sigma_V = \mu_V \sqrt{\frac{4}{\pi} - 1} = 0.523\mu_V \tag{6.3}$$

The coefficient of variation of the 10-minute wind process is taken as the measure of wind turbulence, denoted by I. The conditional distribution of turbulence is assumed to follow a Gaussian distribution shown below,

$$f_{I|V}(i|v) = \frac{1}{\sqrt{2\pi}\sigma_{I|V}} \exp\left[-\frac{1}{2}\left(\frac{i - \mu_{I|V}}{\sigma_{I|V}}\right)^2\right] \tag{6.4}$$

At this point we have three parameters to estimate: the annual average 10-minute mean wind speed,[3] μ_V, the conditional mean turbulence, $\mu_{I|V}$, and standard deviation, $\sigma_{I|V}$. We may consider a campaign to collect wind process data at the site of interest for installing the wind turbine. We saw in Chapter 1 how we may obtain unbiased estimates of statistical moments, e.g., our parameters of interest, from sample data. In addition, we showed how we might obtain an estimate of the uncertainty in the estimate of the mean. Formally, the standard error of estimation of the mean of a random variable, X is given by,

$$\mathsf{se}_{\hat{\mu}_X} = \frac{\hat{\sigma}_X}{\sqrt{n}} \tag{6.5}$$

Where, $\hat{\mu}_X$, and $\hat{\sigma}_X$ are our estimates of the mean and standard deviation of X from sample data and n is the number of observations of X in our sample. With respect to the standard error of estimation, or epistemic uncertainty in our estimate of the annual average 10-minute mean wind speed we can write,

$$\mathsf{se}_{\hat{\mu}_V} = \frac{\hat{\sigma}_V}{\sqrt{n}} \tag{6.6}$$

We might conclude from Equation 6.6 that in order to reduce the epistemic uncertainty in $\hat{\mu}_V$, our estimate of μ_V, we need only to increase the value of n, i.e., collect a large amount of data. Taken out of context, one might consider 1000 data points a large amount of data, even 100 data points

[3] The annual average 10-minute mean wind speed is defined as the mean of a set of measured 10-minute mean wind speed data of sufficient size and duration to serve as an estimate of the expected value of the quantity. The averaging time interval shall be a hole number of years to average out non-stationary behavior effects such as seasonality

could be considered a large amount. In the current context, or frame of reference, 1000 observations of the 10-minute mean wind speed may represent about a week of independent observations of the 10-minute mean wind speed. Note, Equation 6.6 requires that the observations be independent.

We discussed in Chapter 1 that for wind applications, seasonal, synoptic, and diurnal variations in the wind process make monthly, weekly, daily, or hourly values different from annual values. That is to say that our estimate of the annual average 10-minute mean wind speed taken over just a few months, e.g., 3-months, may be biased due to seasonal conditions. If our parameter estimates are, $\hat{\mu}_V$=10m/s and $\hat{\sigma}_V$= 5.23m/s, from about 3-months of data, we can obtain the standard error of estimation of $\hat{\mu}_V$ as,

$$\mathsf{se}_{\hat{\mu}_V} = \frac{\hat{\sigma}_V}{\sqrt{n}} = \frac{5.23\text{m/s}}{\sqrt{10,000}} = 5.23 \times 10^{-2} \tag{6.7}$$

which may mislead us to think we have about 0.52% error[4] in our estimate of the annual average 10-minute mean wind speed. In reality, our estimate may be biased due to seasonal conditions. The next 3-months of data may result in a significantly different estimate of μ_V with a presumably very similar estimate of the standard error of estimation. In this situation, data must be collected over a much longer period of time, a period which accounts for these longer time interval changes. Therefore, we see that additional analysis must be undertaken to more accurately quantify the uncertainty associated with our estimates of the distribution parameters. If we assume that we are interested in obtaining a better estimate of this uncertainty, then we would also be interested in how this uncertainty may affect our estimate of the long-term distribution of extreme loads. In the analysis presented in this section, we will assume that we can reasonably quantify our uncertainty in our estimates of the distribution parameters of the environmental variables.

In the remainder of this discussion we will consider the effect of including the epistemic uncertainty in our estimate of some of the parameters of the distributions of the environmental variables. In particular, we will consider the effect of the epistemic uncertainty in the annual average 10-minute mean wind speed, μ_V, on our estimate of the long-term distribution of extreme loads. A separate analysis will consider assessing the effect of epistemic uncertainty in the conditional mean

[4]The error discussed about is found as:

$$\mathsf{Cov}_{\mu_V} = \frac{\sigma_{\mu_V}}{\mu_V} = \frac{\mathsf{se}_{\hat{\mu}_V}}{10} = 0.52\%$$

turbulence, $\mu_{I|V}$, on our estimate of the long-term distribution of extreme loads.[5] Finally, we consider the effect of including the epistemic uncertainty in our estimates of both, μ_V and $\mu_{I|V}$. At this level we can compare qualitatively the sensitivity of our estimate of the long-term distribution of the extreme load to the epistemic uncertainty associated with μ_V and $\mu_{I|V}$. For each of these scenarios we will assume that the functions for conditional mean turbulence, and standard deviation, $\sigma_{I|V}$ given 10-minute mean wind speed previously presented for the Lavrio, Greece, site still apply. These relations are summarized below and discussed in more detail in Chapters 3 and 4.

$$\mu_{I|V} = 2.4486 v^{-0.9971} \tag{6.8}$$

$$\sigma_{I|V} = 0.025 \tag{6.9}$$

The analyzes presented below consider the AOC 15/50 turbine installed at a site with environmental conditions similar to those present at the Lavrio, Greece, test site. We will present analysis for the blade root flap bending direction only. The methodology discussed here is equally applicable to the blade root edge bending direction. The short-term blade root flap bending extreme response of the AOC 15/50 turbine based on modeling global peaks was presented and discussed in Chapter 3; these results are used in this analysis below but are not re-presented or reviewed. The reader is encouraged to refer to Chapter 3 for the details of the development of this model.

6.3.1 Estimating the Long-Term Distribution of Extreme Loads Considering Uncertain Parameters of the Distributions of Environmental Variables

Uncertain Annual Average 10-Minute Mean Wind Speed

This section considers estimating the long-term distribution of extreme blade root flap bending loads including the epistemic uncertainty associated with the parameter of the Rayleigh distribution of 10-minute mean wind speed, the annual average 10-minute mean wind speed. We will consider three cases. In each of the three cases, we will assume that we have ample information to quantify the uncertainty in our estimate of, μ_V. The level of epistemic uncertainty associated with our estimate of μ_V, we denote by δ_{μ_V}, the coefficient of variation of, μ_V. If we μ_V is known with no attendant uncertainty then δ_{μ_V}=0. We consider three cases where $\delta_{\mu_V} = 5\%$, 10%, and 20%.

[5] Note that because the Rayleigh distribution is a single parameter distribution we need not also deal with the uncertainty in σ_V. The contribution made by the epistemic uncertainty in the conditional standard deviation of turbulence to variability of the long-term distribution of the extreme loads is not considered in this analysis. The epistemic uncertainty in our estimate of the conditional standard deviation of turbulence is considered to be sufficiently small compared with that of the mean, and therefore the standard deviation is considered to be a known constant with no attendant uncertainty or bias. This may or may not be a reasonable assumption. The uncertainty in this parameter could be introduced by the same method illustrated here for the means.

The analysis used Monte Carlo simulation. For each case, the distribution of μ_V was assumed to be Gaussian with $\mathsf{E}[\mu_V] = 10$m/s (note in the long-term analysis presented in Chapter 3, $\mu_V = 10$m/s), and the coefficient of variation equal to $\delta_{\mu_V} = 5\%$, 10%, or 20%. Five hundred simulations were performed for each case. For each simulation a different realization of μ_V was obtained. This parameter defines the Rayleigh model for the long-term distribution of 10-minute mean wind speed. Each simulation then has a different long-term distribution of the 10-minute mean wind speed as defined by its particular realization of μ_V. The Gaussian model for the conditional distribution of turbulence was defined based on Equations 6.8 and 6.9. An estimate of the long-term distribution of extreme blade root flap bending loads is obtained from Equation 3.16. The values of the environmental variables are discretized into evenly spaced intervals. For each pair of values of the environmental variables, the corresponding short-term load distribution is generated. The short-term load distributions are summed together, each weighted by the probability of the respective environmental conditions, i.e., pair of values of the environmental variables (V and I) occurring. The summation is performed over the entire range of environmental variables. Following this process for each realization of μ_V results in 500 estimates of the long-term distribution of extreme blade root flap bending moments for an arbitrary 10-minute period. The median (250^{th} ranked) and mean estimates of the long-term distribution of extreme blade root flap bending moments for an arbitrary 10-minute interval considering three levels of uncertainty in μ_V (i.e., $\delta_{\mu_V} = 5\%$, 10% and 20%) are shown in Figure 6.1(a). The median estimate is found by sorting the probability of exceedance values associated with the 500 long-term distributions for a given bending moment and selecting the 250^{th} highest value. Similarly, the mean estimate is found by calculating the mean probability of exceedance value over the 500 long-term distributions for a given bending moment.

The probability distribution function that results from the above analysis is for an arbitrary 10-minute period. We defined in Chapter 3 the 50-year load as the value l such that, an estimate of the 50-year load is associated with a 0.02 probability of exceedance of the distribution of annual extreme loads.

$$1 - 1/50 = 0.98 = F_{L_{1\text{ year}}}(l) = \left(F_{L_{10\text{ min}}}(l)\right)^N \tag{6.10}$$

Where $F_{L_{1\text{ year}}}(l)$ is the distribution of the annual extreme load, $F_{L_{10\text{ min}}}(l)$ is the distribution of the 10-minute extreme load, and N is the number of 10-minute segments in one year, $N = 365 \times 24 \times 6 = 52,560$. Further, we saw in Chapter 3 that if we assume that the 10-minute segments were independent and if the value of $F_{L_{1\text{ year}}}$ is close to one, an estimate of the 50-year load could be obtained simply from the distribution of 10-minute extreme loads. The estimate was obtained by considering the appropriate probability level, i.e., the probability level associated with the 50-year

mean return period; more formally,

$$(50\text{years} \times N) G_{L_{10\,\text{min}}}(l) = 1 \tag{6.11}$$

$$G_{L_{10\,\text{min}}}(l) = \frac{1}{50N} = \frac{1}{50 \times 52,560} = 3.805 \times 10^{-7} \tag{6.12}$$

where N is the number of 10-minute segments in 1-year and $G_X(x)$ is the complimentary cumulative distribution function, $G_X(x) = 1 - F_X(x)$. In this case, where the annual average wind speed, μ_V, is itself assumed to be a random variable, our assumption of independence above is no longer valid, however. Further we are interested in all values of G from 1 to 0. The distribution of $L_{10\,\text{min}}$ is conditional on the realization of the annual average wind speed. Once we have an estimate of μ_V, it does not change from one 10-minute period to the next, but rather it is fixed with respect to time. This is an important point, as μ_V is not independent from 10-minute to 10-minute period, we can no longer perform the analysis on the basis of an *arbitrary* 10-minute segment as we did in Chapter 3. In this case we must obtain our estimate of the 50-year load as the probability level associated with the 50-year return period from the annual distribution of extreme loads. However, given a value for μ_V (i.e., instance or realization in the Monte Carlo simulation), we can assume independence and obtain an estimate of the annual long-term distribution of the extreme load, $F_{L_{1\ \text{year}}}(l)$, from the long-term distribution of the extreme load in an arbitrary 10-minutes, $F_{L_{10\ \text{min}}}$ by

$$F_{L_{1\,\text{year}}}(l) = \{F_{L_{10\,\text{min}}}(l)\}^N \tag{6.13}$$

$$= \{1 - G_{L_{10\,\text{min}}}(l)\}^N \tag{6.14}$$

Figure 6.1(b) shows the median and mean estimates of the long-term distribution of annual extreme blade root flap bending loads. The probability level associated with the 50-year mean return period is $\frac{1}{50} = 0.02 = 2\%$. The median estimate of the 50-year blade root flap bending load is 59.7kN-m for all three levels of uncertainty in μ_V, $\delta_{\mu_V} = 5\%$, 10% and 20% and $\mathsf{E}[\mu_V] = 10$m/s. We could obtain an estimate of the 50-year load by considering the load associated with a mean annual exeedance probability of 2%. In this case, our estimate of the 50-year load is 60.1kN-m for δ_{μ_V}=5% level, 62.3kN-m for δ_{μ_V}=10% level, and 78.0kN-m for δ_{μ_V}=20% level. Again, at all levels $\mathsf{E}[\mu_V] = 10$m/s. If we consider 20% uncertainty in our estimate of μ_V, then the load with a mean annual exceedance probability of 2% is 30.7% higher than if we considered μ_V deterministic. On the other hand, if the epistemic uncertainty is reduced to about 5%, the load with a mean annual exceedance probability of 2% is about 0.7% higher than considering μ_V deterministic. These results are summarized in Table 6.1.

Also shown in Figure 6.1(b) are the 95% upper confidence estimates of the long-term distribution of annual extreme blade root flap bending loads. An upper confidence level, specifically the 95% upper confidence level, is found by sorting the probability of exceedance values associated with the 500 long-term distributions for a given bending moment and selecting the 475^{th} highest value. Our 95% upper confidence limit estimates of the 50-year blade root flap bending load considering uncertain μ_V with $\delta_{\mu_V} = 5\%$, 10% and 20%, are 62.5kN-m, 70.2kN-m, and 93.5kN-m, respectively. If we consider 20% epistemic uncertainty in μ_V, our high confidence estimate of the 50-year load increases by 56.6%. On the other hand, if the epistemic uncertainty is reduced to about 5%, our 95% upper confidence limit estimate of the 50-year load increases but only by about 5%.

Uncertain Conditional Mean Turbulence

In the previous section we saw how we may obtain median and mean estimates of the long-term distribution of annual extreme blade root flap bending load including epistemic uncertainty in our estimate of the annual average 10-minute mean wind speed. Here, we consider a similar question: what is the effect on our estimate of the 50-year blade root flap bending load if we consider epistemic uncertainty in our estimate of the conditional mean turbulence?

Equation 6.8 gave the relation for the mean turbulence given 10-minute mean wind speed. Now we consider the condition where the mean turbulence is uncertain

$$\mu_{I|V} = 2.4486 v^{-0.9971} + \varepsilon_{\mu_{I|V}} \tag{6.15}$$

Were $\varepsilon_{\mu_{I|V}}$ is an error term, with $\mathsf{E}[\varepsilon_{\mu_{I|V}}] = 0$ and $\mathsf{Var}[\varepsilon_{\mu_{I|V}}]$ such that, for three separate cases, the coefficient of variation of the conditional mean turbulence, denote by $\delta_{\mu_{I|V}}$, is equal to 5%, 10%, and 20%.

A similar Monte Carlo simulation analysis was conducted to determine the long-term distribution of extreme blade root flap bending loads In this case, however, we returned to considering the annual average 10-minute mean wind speed deterministic, $\mu_V = 10$m/s. The conditional mean turbulence, $\mu_{I|V}$, was assumed to follow a Gaussian distribution with $\mathsf{E}[\mu_{I|V}] = 2.4486 v^{-0.9971}$, and the coefficient of variation $\delta_{\mu_{I|V}} = 5\%$, 10%, or 20%. Five hundred simulations were performed for each case.

In each case, the values of the 10-minute mean wind speed were discretized into evenly spaced intervals. For each value of 10-minute mean wind speed, five hundred simulations of conditional mean turbulence were obtained. The conditional standard deviation of turbulence was consider deterministic and given in Equation 6.9. In this manner, 500 observations were obtained for the conditional mean turbulence for each increment of 10-minute mean wind speed. The error terms,

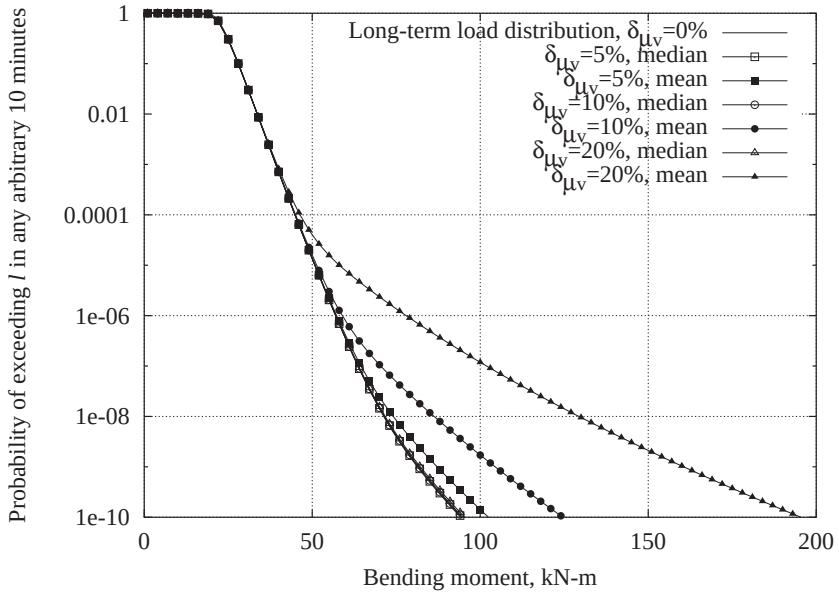

(a) Median and mean estimates of the long-term distribution of extreme blade root flap bending moment for an arbitrary 10-minutes.

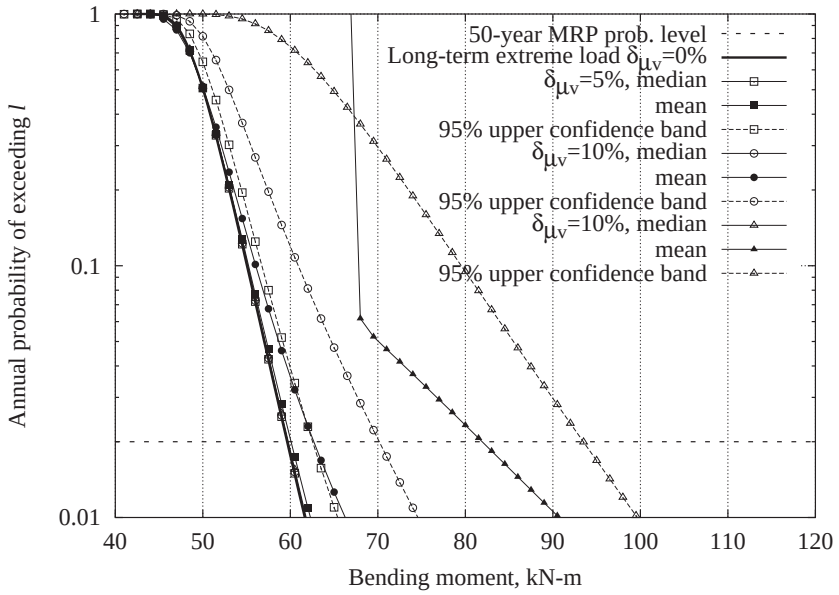

(b) Median, mean, and 95% upper confidence level estimates of the long-term distribution of annual extreme blade root flap bending moment.

Figure 6.1: Median, mean, and 95% upper confidence level estimates of the long-term distribution of extreme blade root flap bending moment, considering the parameter of the Rayleigh distribution of 10-minute mean wind speed uncertain. Three conditions are presented, $\delta_{\mu_V} = 5\%, 10\%$ and 20%. Also shown, for comparison, is the long-term distribution with all parameter values considered deterministic, $\delta_{\mu_V} = 0$.

$\varepsilon_{\mu_{I|V}}$, were assumed to be perfectly correlated from one increment of V to the next. An alternative approach would have been to use a (common) multiplicative error; this approach was not employed. The two parameters, conditional mean and standard deviation define a Gaussian model for the distribution of conditional turbulence. The values of the conditional turbulence were discretized into evenly spaced intervals.

An estimate of the long-term distribution of extreme blade root flap bending loads is obtained from Equation 3.16. For each pair of values of the environmental variables the corresponding short-term load distribution is generated. Again, here the short-term load distribution is based on modeling the global peaks as discussed in Chapter 3. The short-term load distributions are summed together each weighted by the probability of the respective environmental conditions, i.e., pair of values of the environmental variables occurring. The summation is performed over the entire range of environmental variables. This results in 500 estimates of the long-term distribution of extreme blade root flap bending moments for an arbitrary 10-minute period. The median and mean estimate of the long-term distributions of blade root flap bending moment for an arbitrary 10-minute interval are shown in Figure 6.2(a), considering the three cases where $\delta_{\mu_V} = 5\%$, 10% and 20%.

Figure 6.2(b) shows the mean and median estimates of the long-term distributions of annual extreme blade root flap bending loads. Our median estimate of the 50-year blade root flap bending load is 59.7kN-m considering uncertain $\mu_{I|V}$ with $\delta_{\mu_{I|V}} = 5\%$, 10% and 20%. This is the same value we obtained for our estimate of the 50-year load when we considered $\mu_{I|V}$ deterministic, as given in Equation 6.8. Taking our estimate of the 50-year load as the load associated with a mean annual exceedance probability of 2% results in estimates of 59.9kN-m for $\delta_{\mu_{I|V}} = 5\%$, 60.7kN-m for $\delta_{\mu_{I|V}} = 10\%$, and 63.5kN-m for $\delta_{\mu_{I|V}} = 20\%$. If we consider 20% epistemic uncertainty in our estimate of $\mu_{I|V}$, then the load with a mean annual exceedance probability of 2% is 6.4% higher than if we considered $\mu_{I|V}$ deterministic. On the other hand, if the epistemic uncertainty is reduced to about 5%, the load with a mean annual exceedance probability of 2% is about 0.3% higher than considering μ_V deterministic. These results are summarized in Table 6.1.

Also shown in Figure 6.2(b) are the 95% upper confidence estimates of the long-term distribution of annual extreme blade root flap bending loads. Our 95% upper confidence limit estimates of the 50-year blade root flap bending load considering uncertain $\mu_{I|V}$ with $\delta_{\mu_{I|V}} = 5\%$, 10% and 20%, are 61.7kN-m, 63.7kN-m, and 67.7kN-m, respectively. If we consider 20% epistemic uncertainty in our estimate of $\mu_{I|V}$, our 95% confidence limit estimate of the 50-year load is 13.4% higher than our estimate if we considered the parameter deterministic. On the other hand, if the epistemic uncertainty is reduced to about 5%, our 95% upper confidence limit estimate of the 50-year load is about 3.3% higher.

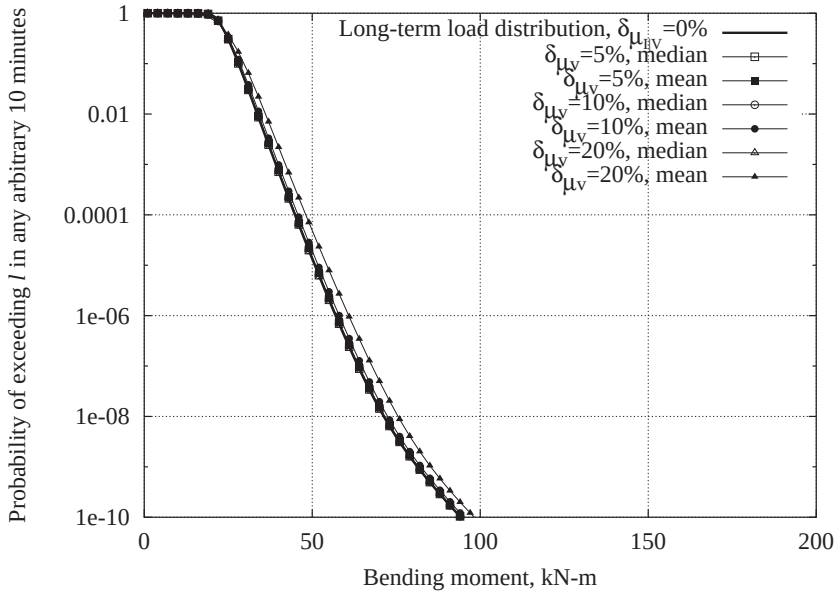

(a) Median and mean estimates of the long-term distribution of extreme blade root flap bending moment for an arbitrary 10-minutes.

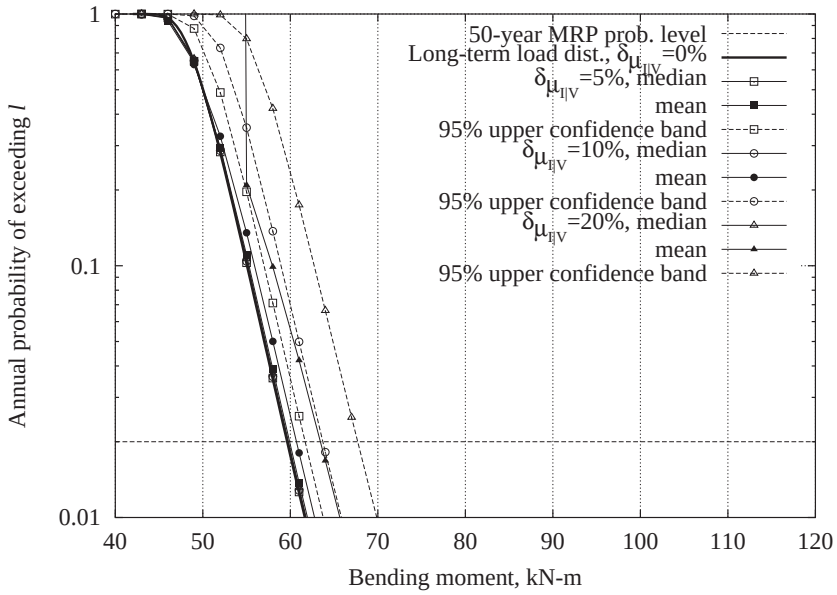

(b) Median, mean, and 95% upper confidence level estimates of the long-term distribution of annual extreme blade root flap bending moment.

Figure 6.2: Median, mean, and 95% upper confidence level estimates of the long-term distributions of extreme blade root flap bending moment, considering the mean of the Gaussian distribution of conditional turbulence uncertain. Three conditions are presented, $\delta_{\mu_I|V} = 5\%, 10\%$ and 20%. Also shown, for comparison, is the long-term distribution with all parameter values considered deterministic.

Uncertain Annual Average 10-minute Mean Wind Speed and Conditional Mean Turbulence

In the case considered here the analysis consists of nesting the uncertain conditional mean analysis within the uncertain annual average 10-minute mean wind speed analysis. Again, three cases were considered where $\delta_{\mu_V} = \delta_{\mu_{I|V}} = 5\%$, 10%, and 20%. The epistemic uncertainty in the conditional mean turbulence is considered to be independent of the epistemic uncertainty in the annual average 10-minute mean wind speed.

The Monte Carlo simulation results in multiple realizations of the long-term distribution of extreme blade root flap bending loads. The median and mean long-term distributions for an arbitrary 10-minute interval in Figure 6.3(a), considering the three cases where $\delta_{\mu_V} = \delta_{\mu_{I|V}} = 5\%$, 10% and 20%.

Figure 6.3(b) shows the median and mean estimate of the long-term distribution of annual extreme blade root flap bending loads. Our median estimate of the 50-year blade root flap bending load is 59.7 kN-m for all three conditions of uncertain μ_V and $\mu_{I|V}$ ($\delta_{\mu_V} = \delta_{\mu_{I|V}} = 5\%$, 10%, and 20%), which is the same estimate we obtained when we considered μ_V and $\mu_{V|I}$ deterministic, i.e., $\delta_{\mu_V} = \delta_{\mu_{I|V}} = 0$. Taking our estimate of the 50-year load as the load associated with a mean annual exceedance probability of 2% results in estimates of 60.2kN-m for $\delta_{\mu_{I|V}} = 5\%$, 62.7kN-m for $\delta_{\mu_{I|V}} = 10\%$, and 81.9kN-m for $\delta_{\mu_{I|V}} = 20\%$. If we consider 20% epistemic uncertainty in our estimate of μ_V and $\mu_{I|V}$, then the load with a mean annual exceedance probability of 2% is 37.2% higher than if we considered the parameters deterministic. On the other hand, if the epistemic uncertainty is reduced to about 5%, then the load with a mean annual exceedance probability of 2% is about 0.8% higher. These results are summarized in Table 6.1.

Also shown in Figure 6.3(b) are the 95% upper confidence limit estimates of the long-term distribution of annual extreme blade root flap bending loads. Our 95% upper confidence limit estimates of the 50-year blade root flap bending load considering uncertain μ_V and $\mu_{I|V}$ with $\delta_{\mu_V} = \delta_{\mu_{I|V}} = 5\%$, 10% and 20%, are 63.1kN-m, 70.2kN-m, and 93.5kN-m, respectively. If we consider 20% epistemic uncertainty in our estimate of the parameters then our upper confidence estimate of the 50-year load increases by 56.6% over our estimate if we considered the parameters deterministic. On the other hand if the epistemic uncertainty is reduced to about 5%, our 95% upper confidence limit estimate of the 50-year load increases by only about 5.5%.

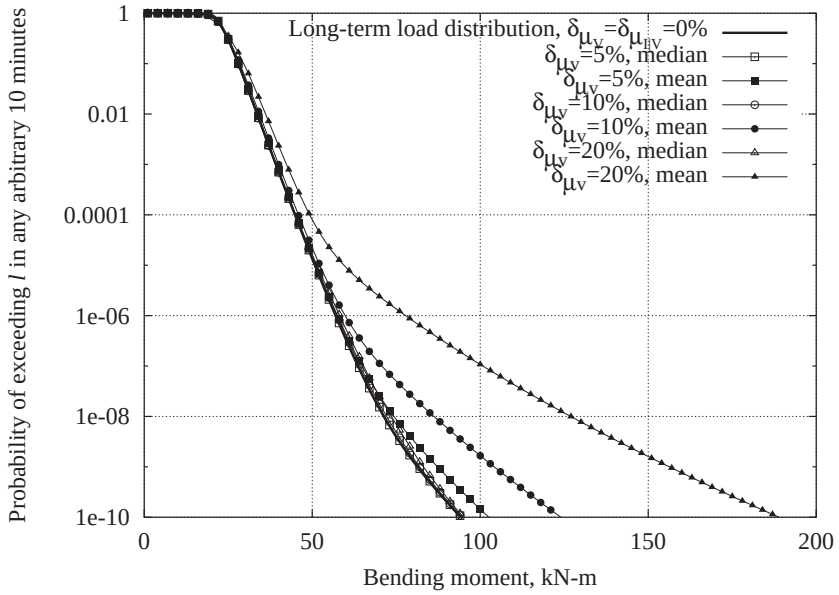

(a) Median and mean estimates of the long-term distribution of extreme blade root flap bending moment for an arbitrary 10-minutes.

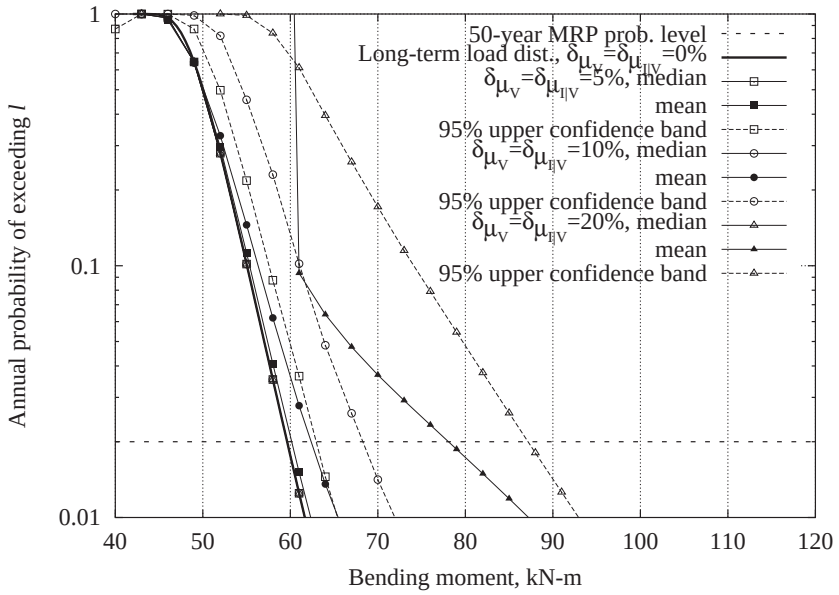

(b) Median, mean, and 95% upper confidence level estimates of the long-term distribution of annual extreme blade root flap bending moment.

Figure 6.3: Median, mean, and 95% upper confidence level estimates of the long-term distributions of extreme blade root flap bending moment, considering both the parameter of the Rayleigh distribution of 10-minute mean wind speed and the mean of the Gaussian distribution of conditional turbulence uncertain. Three conditions are presented, $\delta_{\mu_V} = \delta_{\mu_{I|V}} = 5\%, 10\%$ and 20%. Also shown, for comparison, is the long-term distribution with all parameter values considered deterministic.

Estimation of 50-year Blade Root Flap Bending Moment
Including Uncertain Long-term Environmental Variable Distribution Parameters

Parameters deterministic, 50-year load = 59.7kN-m

Wind speed	δ_{μ_V}	Median estimate (kN-m)	% diff.	Estimate with mean annual exceed Prob = 2% (kN-m)	% diff.	95% confidence estimate (kN-m)	% diff.
	5%	59.7	0%	60.1	0.7%	62.5	4.8%
	10%	59.7	0%	62.3	4.4%	68.2	14.2%
	20%	59.7	0%	78.0	30.7%	87.1	46%
Turbulence	$\delta_{\mu_{I\|V}}$						
	5%	59.7	0%	59.9	0.3%	61.7	3.3%
	10%	59.7	0%	60.7	1.7%	63.7	6.7%
	20%	59.7	0%	63.5	6.4%	67.7	13.4%
Wind speed & turbulence	$\delta_{\mu_V} = \delta_{\mu_{I\|V}}$						
	5%	59.7	0%	60.2	0.8%	63.0	5.5%
	10%	59.7	0%	62.7	5.0%	70.2	17.5%
	20%	59.7	0%	81.9	37.2%	93.5	56.6%

Table 6.1: Comparison of estimates of 50-year blade root flap bending moment, including uncertainty long-term environmental variable distribution parameters, with considering all parameters deterministic.

6.3.2 Summary

In the previous three sections we have considered three general conditions—each assessing the effect on including epistemic uncertainty in the distribution parameters on our estimate of the 50-year load. Table 6.1 summarizes the results from these previous sections. In the first section we considered including the epistemic uncertainty in our estimate of the annual average 10-minute mean wind speed. In the second section we considered including the epistemic uncertainty in our estimate of the conditional mean turbulence. We found that for the turbine, site data, and probability models considered here including the epistemic uncertainty in the conditional mean turbulence did not increase our estimate of the 50-year blade root flap bending load, defined as the load associated with a annual exceedance probability of 2%, as much as including the the epistemic uncertainty in the annual average 10-minute mean wind speed. Further analysis, which included considering the epistemic uncertainty associated with both model parameters, did not show a significant further increase in this estimate of the 50-year blade root flap bending load, about a 5% percent increase for the case with 20% coefficient of variation, over only considering epistemic uncertainty associated with the annual average 10-minute mean wind speed.

6.4 Uncertainty in short-term load distribution

6.4.1 Uncertain regression coefficients

The methodology presented in Chapter 3 for predicting the long-term extreme response, involved fitting a probability model to the observed responses for a given set of realizations of the environmental variables by the method of moments. The statistical moments of the responses were related to the realizations of the environmental variables by regression analysis. Then, finally, the conditional distributions of the responses are weighted by the probability of the respective realizations of the environmental variables occurring, and summed over the domain of the environmental variables.

In the context of understanding the sources of epistemic uncertainty in the short-term loads distribution, let us again consider the analysis of constructing the short-term loads model of extreme loads based on modeling global peaks, Z, with a Gumbel distribution as shown in Equation 6.16. We are interested in the uncertainty in our estimates of the parameters of the model, $\hat{\alpha}$ and $\hat{u}$. But we saw in Chapter 3 that we can relate the parameters of the Gumbel model to the the first two statistical moments of the observed 10-minute maximum response, i.e., global peaks, Z, defined in

Chapter 1 by the method of moments,

$$
\begin{aligned}
F_Z(z) &= \exp\left(-\exp\left(-\hat{\alpha}(z-\hat{u})\right)\right) \\
\hat{\alpha} &= \frac{\pi}{\sqrt{6\hat{\sigma}_Z^2}} \\
\hat{u} &= \hat{\mu}_Z - \frac{\gamma_{\text{Euler}}}{\hat{\alpha}} \\
\gamma_{\text{Euler}} &= 0.577
\end{aligned}
\tag{6.16}
$$

Where $\hat{\mu}_Z$ and $\hat{\sigma_Z^2}$ are the estimates of the mean and variance of the 10-minute maximum response, respectively. So we can turn our attention to the uncertainty in the estimates of the statistical moments $\hat{\mu}_Z$ and $\hat{\sigma_Z^2}$. We saw in Chapter 1 that the standard error of our estimate of the mean is,

$$
\mathsf{se}_{\hat{\mu_Z}} = \frac{\hat{\sigma_Z}}{\sqrt{n}} \tag{6.17}
$$

Where n, is the number of observations for a given pair of values of the environmental variables, (v, i). Similarly, we may assume that the standard error of the estimate of the variance is also inversely proportional to the number of observations such that,

$$
\mathsf{se}_{\hat{\sigma_Z^2}} \propto \frac{\hat{\sigma_Z^2}}{n} \tag{6.18}
$$

This is only one portion of the uncertainty in our estimates of the statistical moments, however. In the process of computing the long-term response we relate the statistical moments of the response to the environmental variables through regression analysis (see Appendix B). Specifically, we have used the power law function proposed by Veers and Winterstein [54]

$$
\hat{\mu_j} = a_j \left(\frac{V}{V_{\text{ref}}}\right)^{b_j} \left(\frac{I}{I_{\text{ref}}}\right)^{c_j} \qquad j = 1, 2 \tag{6.19}
$$

Where $\mu_1 = \mu_Z$ and $\mu_2 = \sigma_Z^2$. The uncertainty in our estimates of the regression coefficients is related to the epistemic uncertainty in the statistical moments used in the regression analysis as seen in Equation 6.19. Two methods for estimating the epistemic uncertainty in the regression coefficients are presented here. First, we consider having a large number of samples of the response for a given set of values of the environmental variables. In this case the bootstrap method [48] is used to estimate the uncertainty. Second, we could use the principals of regression analysis to estimate the uncertainty in the regression coefficients. This approach, however, assumes that the covariance matrix of the regression coefficients is known with certainty. In general, we must consider that the

covariance matrix is also unknown—we only have an estimate of it. This is the benefit of the first method. In general, the application of the bootstrap method as described below does not require *a priori* knowledge, or assumption, of the covariance matrix. It works directly with the data—as we will see. It does, however, require a large amount of data. If only a few samples have been collected for each set of values of the environmental variables (e.g. 10-20 samples) the second method would be an appropriate alternative to provide an estimate of the uncertainty. It is important to realize that this second method will discount some sources of uncertainty, i.e., because it prescribes a known covariance matrix.

6.4.2 Using Bootstrap Method to Estimate Uncertainty in Regression Coefficients

In this analysis, a bootstrap [48] methodology is employed to estimate the uncertainty associated with the regression coefficients. Let us first consider the condition where we are interested in estimating the uncertainty in the regression coefficients based on only 10 mechanical-math-model simulations for each set of values of the environmental variables from which to estimate the mean and standard deviation of the 10-minute maximum response. In this case, our estimates of the statistics of the 10-minute maximum response given a set of values of the environmental variables are based on only these 10 response time histories. The reader should recall that in Chapter 3 the estimates of these statistics were based on 100 time histories.

To estimate the epistemic uncertainty associated with these estimates based on only 10 response time histories the following methodology is employed. 10 response time histories are selected at random with replacement from the set of 100 original response time histories, for each set of values of the environmental variables as described in Chapter 3. Then we obtain the statistics of the 10-minute extreme response from this *bootstrap sample*. This process is performed for each set of the values of the environmental variables. Based on this data and following the procedure developed in Chapter 3, we obtain an estimate of the distribution of $L_{10\,\text{min}}$, the long-term distribution of the extreme 10-minute flap bending load. This process of selecting 10 time histories with replacement and then obtaining an estimate of the distribution of $L_{10\,\text{min}}$ is performed 1000 times. At the end, we have 1000 estimates of the distribution of $L_{10\,\text{min}}$. The median (500^{th} ranked) and mean estimates of the long-term distribution of blade root flap bending moments for an arbitrary 10-minute interval considering 10, 20, 50 and 100 mechanical-math-model simulations are shown in Figure 6.4. The median estimate is found by sorting the probability of exceedance values associated with 1000 long-term distributions for a given bending moment and selecting the 500^{th} highest value. Similarly, the mean estimate is found by calculating the mean probability of exceedance value over the 1000 long-term distributions for a given bending moment.

Figure 6.5 shows the median and mean estimates of the long-term distribution of annual extreme

blade root flap bending loads using 10, 20, 50, and 100 mechanical-math-model simulations upon which to base the estimates of the statistics of the 10-minute extreme response, and thereby affect the uncertainty in the estimates of the regression coefficients. The reader is reminded that our estimate of the 50-year load in Chapter 3, where we assumed the regression coefficients were known, was 59.7kN-m. From Figure 6.5(a), using the bootstrap method to obtain an estimate of the uncertainty in the regression coefficients, our median estimate of the 50-year load ranges from 107.2kN-m (if based on 10 mechanical-math-model simulations for each set of values of the environmental variables) to 60.4kN-m (if based on all 100 simulations). Considering an estimate of the 50-year load given as the load with a mean annual probability of exceedance of 2% is only 1.1% higher (60.4kN-m) than our estimate from Chapter 3. Similarly, the load with a mean annual probability of exceedance of 2% based on 50 simulations is 206kN-m, 245% higher. Estimates of the 50-year load defined as the load with a mean annual probability of exceedance of 2% are significantly higher if only 10 or 20 simulations are used, on the order of 6,000 kN-m, or more.

Also shown in Figure 6.5 are the 95% upper confidence limit estimates of the long-term distribution of annual extreme blade root flap bending loads. The 95% upper confidence level is found by sorting the probability of exceedance values associated with 1000 long-term distributions for a given bending moment and selecting the 950^{th} highest value. Our 95% upper confidence limit estimate of the 50-year load considering all 100 simulations is 11.4% higher (66.5kN-m) than our estimate from Chapter 3. Similarly, our 95% upper confidence limit estimate of the 50-year load based on 50 simulations is 270kN-m, 352% higher. Our upper confidence level estimates of the 50-year load are significantly higher if only 10 or 20 simulations are used, on the order of 9,500kN-m, or more. These results are summarized in Table 6.2. Note that the results based on only a few simulations are far beyond the range of realistic design loads, and further illustrates the effect of higher levels of epistemic uncertainty.

Uncertain Regression Coefficients with Known Covariance

In this section we consider using the principals of regression analysis to estimate the uncertainty in the regression coefficients. The variance in the regression coefficients is related to the variance of the residuals. The variance of the residuals is discussed below. We may consider the general form of the regression problem,[6]

$$\mathbf{Y} = \mathbf{X}\boldsymbol{\beta} + \boldsymbol{\varepsilon} \tag{6.20}$$

Where, $\mathbf{Y}$ is the vector of predicted values, $\mathbf{X}$ is the matrix of predictor variables (parameters), $\boldsymbol{\beta}$, is the vector of regression coefficients, and $\boldsymbol{\varepsilon}$ is the vector of residuals. Here the elements of the

[6] Additional discussion on regression analysis is presented in Appendix B. See also Weisburg [67] and Rice [24]

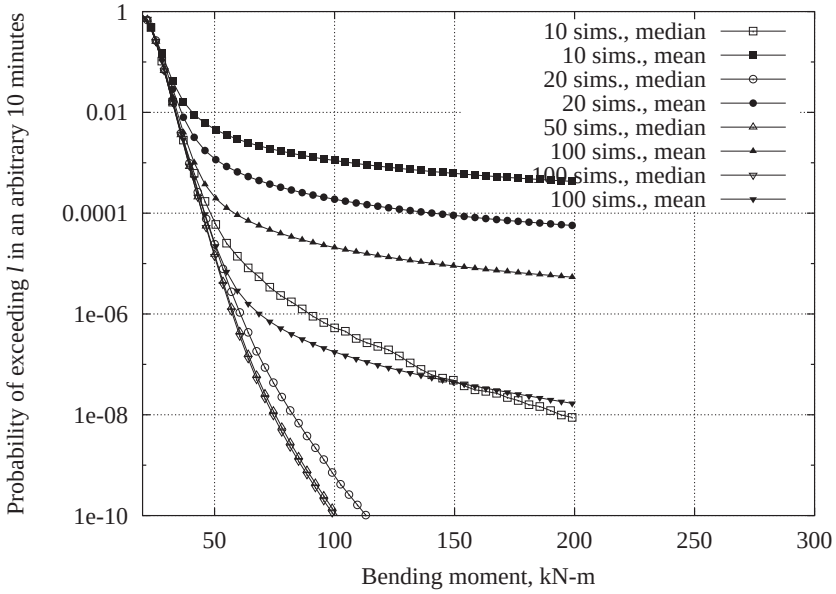

Figure 6.4: Median and mean estimates of the long-term distribution of extreme blade root flap bending moment for an arbitrary 10-minutes, considering regression coefficients uncertain. The bootstrap method was used to estimate uncertainty in regression coefficients.

Estimation of 50-year Blade Root Flap Bending Moment Including Uncertain Regression Coefficients—Bootstrap Method

Regression coefficients deterministic, 50-year load = 59.7kN-m

Number of time history simulations	Median estimate (kN-m)	% diff.	Estimate with mean annual exceed. prob. = 2% (kN-m)	% diff.	95% confidence estimate (kN-m)	% diff
10	107	79.5%	224,000	375,000%	1.35×10^6	NA
20	64.5	8.1%	6,345	10,500%	9,515	15,000%
50	61.0	2.2%	206	245%	270	352%
100	60.4	1.1%	65.9	10.4%	66.5	11.4%

Table 6.2: Comparison of estimates of 50-year blade root flap bending moment, considering uncertain regression coefficients. The bootstrap method was used to estimate uncertainty. Estimates of the 50-year blade root flap bending moment are compared with results obtained with regression coefficients considered deterministic.

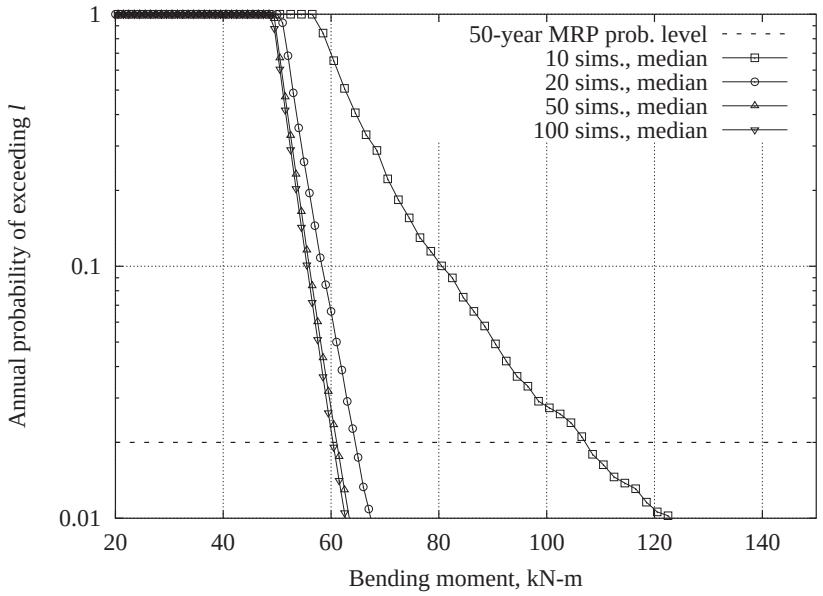

(a) Median estimates of the long-term distribution of annual extreme blade root flap bending moment.

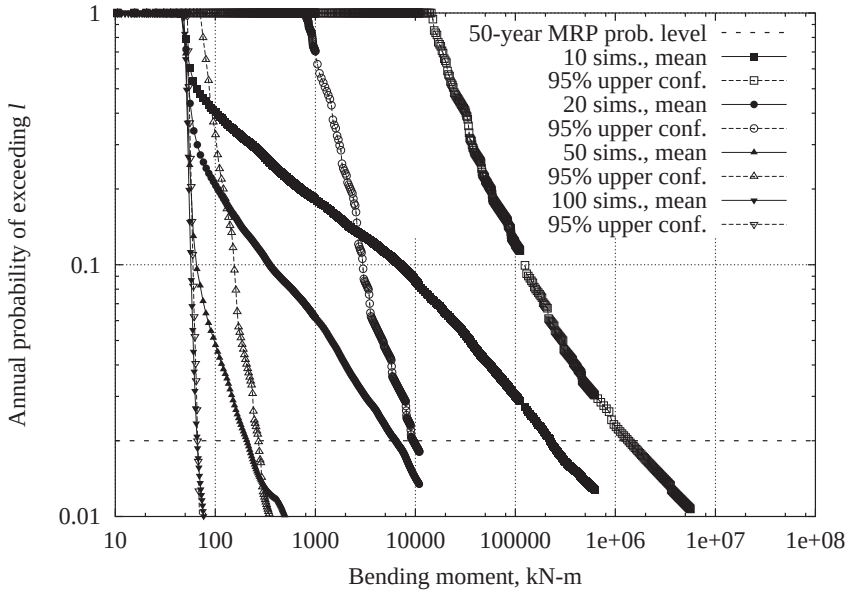

(b) Mean estimates of the long-term distribution of annual extreme blade root flap bending moment.

Figure 6.5: Median and mean estimates of the long-term distribution of extreme blade root flap bending moment, considering regression coefficients uncertain. The bootstrap method was used to estimate uncertainty in regression coefficients.

vector of regression coefficients are: $\ln(a)$, b, and c. An estimate for $\boldsymbol{\beta}$ can be found by,

$$\hat{\boldsymbol{\beta}} = (\mathbf{X}^T\mathbf{X})^{-1}\mathbf{X}\mathbf{Y} \tag{6.21}$$

From Weisburg [67], if $\mathsf{E}[\boldsymbol{\varepsilon}] = \mathbf{0}$ and $\mathsf{Var}[\boldsymbol{\varepsilon}] = \sigma^2\mathbf{I}_n$, then $\hat{\boldsymbol{\beta}}$ is unbiased, $\mathsf{E}[\hat{\boldsymbol{\beta}}] = \boldsymbol{\beta}$, and

$$\mathsf{Var}(\hat{\boldsymbol{\beta}}) = \Sigma_{\beta\beta} = \sigma^2(\mathbf{X}^T\mathbf{X})^{-1} \tag{6.22}$$

where $\Sigma_{\beta\beta}$ denotes the covariance matrix of the regression coefficients, and an estimate of σ^2 can be found from,

$$\hat{\sigma^2} = \frac{RSS}{n' - p} \tag{6.23}$$

with n' equal to the number of pairs of values of the environmental variables, $(V, I)_j$, (j=1,...,n'), p is the number of parameters in the regression analysis, i.e., p=3, and the sum of squared residuals (RSS) is

$$RSS = \hat{\boldsymbol{\varepsilon}}^T\hat{\boldsymbol{\varepsilon}} = (\mathbf{Y} - \mathbf{X}\hat{\boldsymbol{\beta}})^T(\mathbf{Y} - \mathbf{X}\hat{\boldsymbol{\beta}}) \tag{6.24}$$

so

$$\widehat{\mathsf{Var}}(\hat{\boldsymbol{\beta}}) = \hat{\sigma^2}(\mathbf{X}^T\mathbf{X})^{-1} \tag{6.25}$$

We may consider this error the model fit error, i.e., the uncertainty associated with the lack of fit of the functional form of the model to the data.

The total model error, includes model fit error but also uncertainty in our estimates of the statistics of the response, i.e., mean and standard deviation of the 10-minute maximum response. If we were to know that the functional form of the model was correct, then, given enough observations of the response at different environmental conditions, i.e., pairs of V and I, the model error would approach zero. The total model error in this case would only depend on the number of observations/simulations per environmental conditions. In this case, we could potentially drive the uncertainty to zero, purely by continuing to collect data, across both multiple observations of the response for a given specific set of environmental conditions and also across a range of different environmental conditions. If on the other hand the functional form does not contain enough flexibility to fit to the data, or the data actually follows some other functional form, then the model fit error is irreducible beyond some point, even as we continue to collect data. Data collected for the response at additional different environmental conditions will not reduce this error because the functional form is not "correct". Multiple observations of the response for a given environmental condition will reduce the standard error of the statistics and reduce the total error. However, in the limit with enough observations the total model error will only reduce to equal the model fit error.

Figure 6.6 shows mean and median estimates of the long-term distribution of extreme blade root flap bending loads for arbitrary 10 minutes, where the statistics of the maximum response are based on an increasing number of mechanical-math-model simulations. For each condition, the required number of mechanical-math-model simulations are selected at random from the pre-existing data set where 100 mechanical-math-model simulations were performed at each set of values on the environmental variables. The pooled statistics of the maximum response are calculated and a regression analysis performed. From the regression analysis, the covariance matrix of the regression coefficients is obtained. We assume the residuals of the regression analysis follow a Gaussian distribution and therefore our estimates of the regression coefficients also follow a Gaussian distribution. The covariance matrix of the regression coefficients is used to determine the uncertainty in the regression coefficients for the Monte Carlo analysis.

One thousand simulations of a Monte Carlo analysis were conducted where the regression coefficients are considered uncertain. The error terms of the regression coefficients are calculated as follows: $\mathbf{U}$ is the matrix of uncorrelated standard normal error terms, $\mathbf{L}$ is the resulting lower triangular matrix of a Cholesky decomposition of $\mathbf{\Sigma}_{\beta\beta}$. The matrix of correlated normal error terms, $\mathbf{U_c}$ is found by

$$\mathbf{U_c} = \mathbf{LUL}^T \tag{6.26}$$

for each set of error terms is added to the expected regression coefficients and the moments calculated for each. The standard process of calculating the estimate of the long-term distribution of extreme flap bending loads follows from this point. At the end of the Monte Carlo simulation 1000 estimates of the long-term distribution of extreme loads are obtained. Figure 6.7 shows the median and mean estimates of the long-term distribution of annual extreme blade root flap bending loads using 10, 20, 50, and 100 mechanical-math model simulations upon which to base the estimates of the statistics of the 10-minute extreme response. From Figure 6.7(a), all our median estimates of the 50-year load are in a narrow range from a minimum of 57.3kN-m for the case when 50 mechanical-math-model simulations for each set of values of the environmental variables are used, to 64.1kN-m if based on only 10 simulations. It is important to point out here that the estimates obtained here are specific to the set of data randomly selected for our sample of 10, 20, or 50. If a different sample of similar size were chosen, with different expected value of the regression coefficients, different median values would result. This is why we observe a lower estimate when only 20 simulations are used instead of 50—another set of 20 simulations may result in a estimate higher than the estimate obtained from the 50 simulations used here. (Note, the bootstrap method, discussed above, inherently includes this additional uncertainty). An estimate of the 50-year load given as the load with a mean annual probability of exceedance of 2%, using all 100 simulations, is 0.9% higher (60.3kN-m) than our estimate from Chapter 3. Similarly, the load with a mean annual probability of exceedance

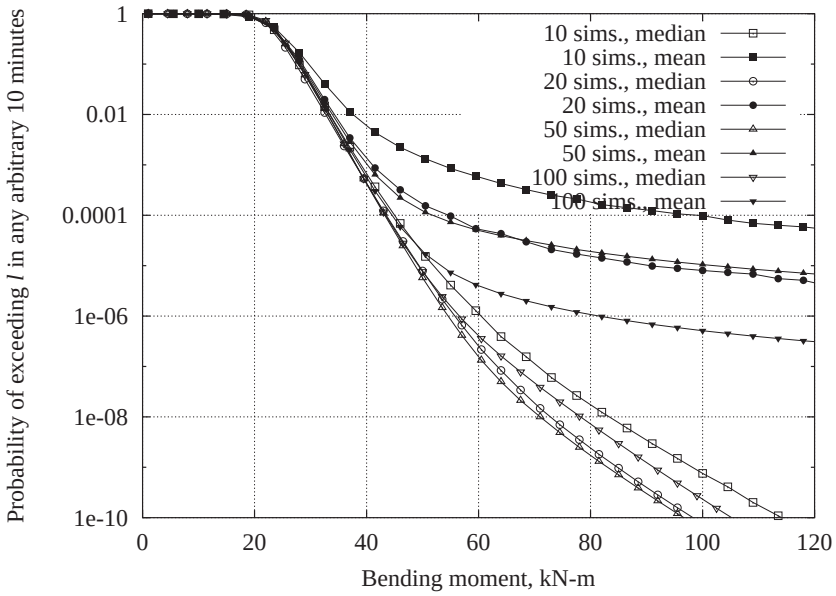

Figure 6.6: Median and mean estimates of the long-term distribution of extreme blade root flap bending moment for an arbitrary 10-minutes, considering regression coefficients uncertain with fixed covariance matrix.

of 2% based on 10 simulations is 907.5kN-m, 1420% higher. These results are summarized in Table 6.3. The width of the distance between median and mean annual probability of exceedance (at the 2% level) estimates calculated assuming a known covariance is smaller compared with the width between median and mean annual probability of exceedance (at the 2% level) estimates based on using the bootstrap method for all of the different number of mechanical-math model simulations analyzed here. Therefore, we may conclude that there is some uncertainty that is not accounted for by considering the covariance matrix of the regression coefficients fixed. Although, when the number of simulations included in the analysis becomes large (e.g., 100) we observed only a small difference in the estimates obtained from the two methods.

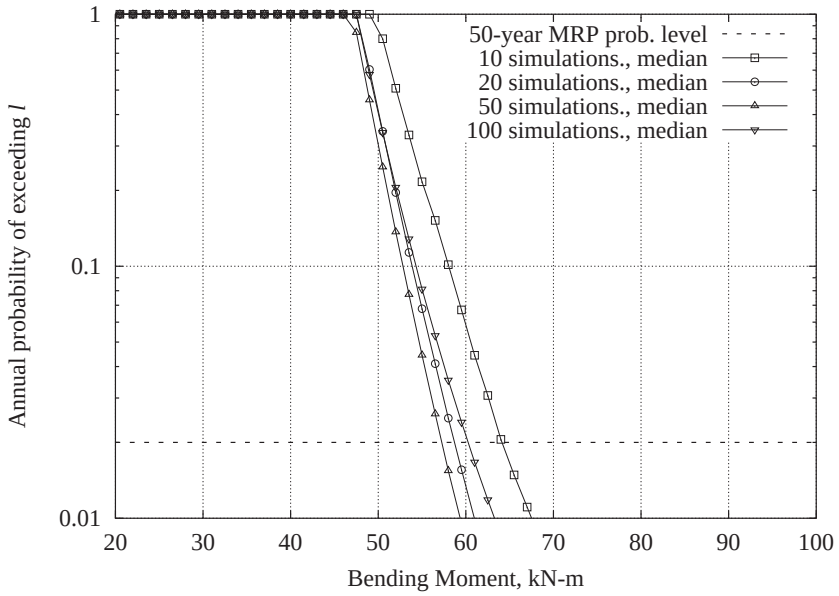

(a) Median estimates of the long-term distribution of annual extreme blade root flap bending moment.

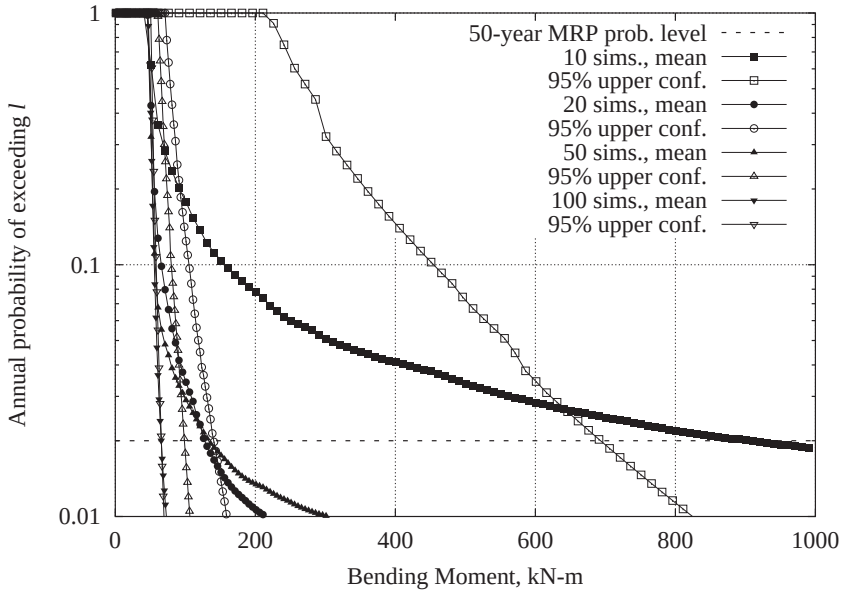

(b) Mean estimates of the long-term distribution of annual extreme blade root flap bending moment.

Figure 6.7: Median and mean estimates of the annual long-term distributions of extreme blade root flap bending moment, considering regression coefficients uncertain. Regression coefficients considered uncertain with fixed covariance matrix.

Estimation of 50-year Blade Root Flap Bending Moment
Including Uncertain Regression Coefficients with Known Covariance

Regression coefficients deterministic, 50-year load = 59.7kN-m

Number of time history simulations	Median estimate (kN-m)	% diff.	Estimate with mean annual exceed. prob. = 2% (kN-m)	% diff.	95% confidence estimate (kN-m)	% diff
10	64.1	7.4%	908	1,420%	693	1,061%
20	58.7	-1.7%	128	114%	140	135%
50	57.3	-4.1%	133	123%	98.7	65%
100	60.3	0.9%	65.5	9.7%	65.7	10%

Table 6.3: Comparison of estimates of 50-year blade root flap bending moment, considering uncertain regression coefficients with known covariance. Estimates of the 50-year blade root flap bending moment are compared with results obtained with regression coefficients considered deterministic.

6.4.3 Model Uncertainty

In the previous section we discussed epistemic uncertainty with respect to the regression coefficients. Here, we discuss the uncertainty associated with our estimate of the 10-minute maximum response from simulated mechanical-model-based data versus observed field data.

The National Renewable Energy Laboratory collected field data on an AOC 15/50 turbine installed at the National Wind Technology Center test site in Boulder, Colorado. They recorded 152 10-minute time histories at different sets of values of 10-minute mean wind speed and turbulence were recorded during November and December, 1999.[7] This included both time histories of the wind process and time histories of the response blade root flap and edge bending moments. Only the blade root flap bending moment data is used in the analysis considered here. Of the 152 time histories, two of the time histories were removed from the data set because erroneous data had been recorded.Figure 6.8 shows plots of the statistics of the environmental conditions for each time history of the wind process. The coefficient of variation of the 10-minute wind process versus 10-minute mean wind speed is shown in Figure 6.8(a). The standard deviation of the 10-minute wind process versus 10-minute mean wind speed is shown in Figure 6.8(b).

The observed 10-minute maximum blade root bending moment is plotted versus 10-minute mean wind speed in Figure 6.9(a). For each set of environmental conditions shown in Figure 6.8(a) one simulated response was generated using the YAWDYN [20] aerodynamics and dynamics model first presented in Chapter 3. This is the same mechanical model and analysis code that was used to generate the simulation data used to develop the description of the short-term load models in Chapter 3 and later used for the fatigue analysis in Chapter 5. Figure 6.9(b) shows the 10-minute maximum blade root flap bending load from simulation versus the 10-minute mean wind speed for the same set of values of the environmental variables. Each simulated or observed response, for a given set of environmental conditions, represents one draw from an unknown population of responses. We know that if we ran a second simulation at the same set of environmental variables we would get a different estimate of the 10-minute maximum blade root flap bending load. We saw this in Chapter 3 where we ran 100 simulations for the same set of values of the environmental variables. In one case in Chapter 3 we fit a Gumbel model to the distribution of the 100 realizations of the 10-minute maximum response. In this case, we acknowledge that we have some irreducible uncertainty, i.e., randomness in the 10-minute maximum response. This is aleatory uncertainty. The epistemic uncertainty results in our lack of knowledge in estimating the Gumbel model parameters which define the model. In this analysis we are interested in concentrating on the epistemic uncertainty. Taking only the one draw, i.e., on observation from the population of either simulated data or observed data for a given set of environmental conditions, allows us to consider the epistemic

[7] This data was provided by Rick Santos of the National Renewable Energy Laboratory

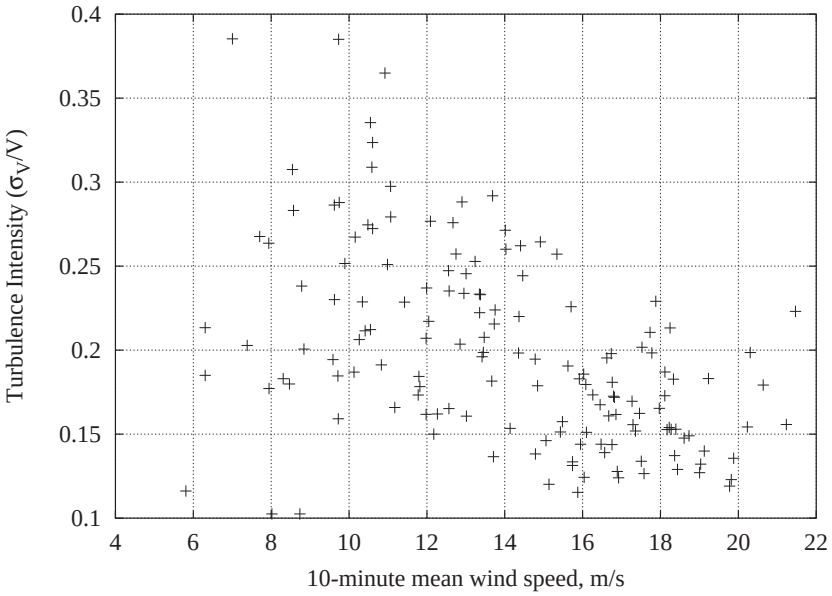

(a) Coefficient of variation of 10-minute wind process, $I = \frac{\sigma_V}{V}$, versus 10-minute mean wind speed.

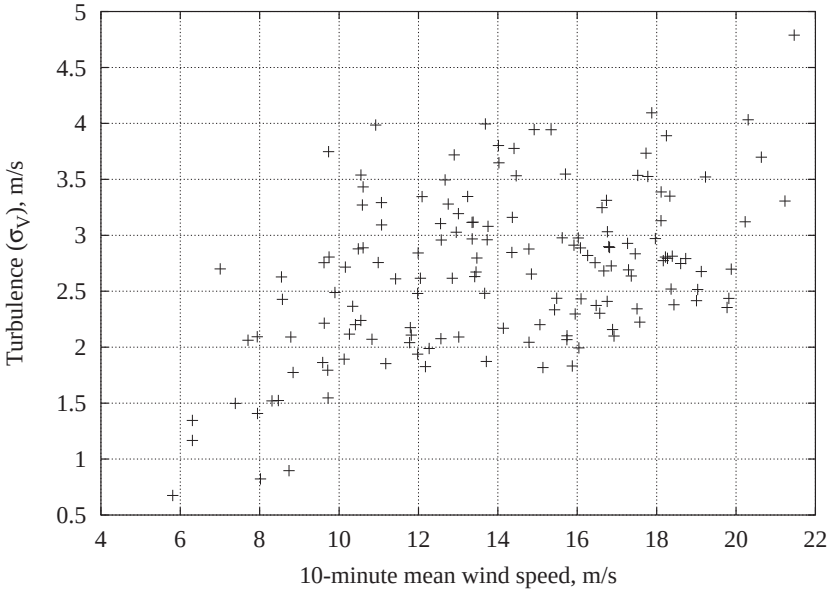

(b) Standard deviation of 10-minute wind process, $I = \sigma_V$, versus 10-minute mean wind speed.

Figure 6.8: Environmental conditions for 150 field recorded time histories.

Regression of the Observed 10-minute Maximum on Predicted 10-minute Maximum

Blade root flap bending

$\hat{\beta}$	$\hat{\sigma}_{\varepsilon_m}$	R^2
1.3569 kN-m	37.675 (kN-m)^2	.44204

Table 6.4: Numerical results of regression of the observed 10-minute maximum blade root flap bending moment on the predicted 10-minute maximum blade root flap bending moment from simulation. (Figure 6.10)

uncertainty on a individual draw basis without the additional complication of considering any irreducible uncertainty. In some respect, with only the one draw, all of the uncertainty is epistemic, or based on our lack of knowledge.

We may ask at this point if any bias exists between our prediction of the maximum 10-minute blade root flap bending load compared with the observed response based on individual draws from each population, as discussed above. Figure 6.10 shows observed versus predicted 10-minute maximum blade root flap bending moment. A simple linear regression analysis with zero intercept, i.e.,

$$L_{\text{obs}} = \beta L_{\text{pred}} + \varepsilon_m \tag{6.27}$$

was used to determine the bias factor, β, between the predicted response, L_{pred}, and the observed response, L_{obs}. Where ε_m is a random error term with $\mathsf{E}[\varepsilon_m] = 0$ and $\mathsf{Var}[\varepsilon_m] = \sigma^2_{\varepsilon_m}$. The regression results are shown in Table 6.4. From the regression analysis we find that the bias factor, i.e, slope of the regression line, is about 1.36. (Note that if there had been no bias, β would equal one.) Our observations, from field data, are about 36% higher on average than what was predicted from the mechanical-math-model. The standard deviation of the residuals, σ_{ε_m}, is 6.14kN-m.

Additionally, we may consider a measure of error that is based on the ratio of observed response to predicted response. Where the ratio is greater than one are instances where the analysis based on the mechanical model under-predicted the response. Conversely, where the ratio is less than one the mechanical model over-predicts the response. Figure 6.11 shows the ratio of observed to predicted 10-minute maximum blade root flap bending moment versus 10-minute mean wind speed. We find that most of the ratios are greater than one and would indicate that our model under-predicted the response of the turbine. This is consistent with the results found from the regression analysis.

We may obtain a mean estimate of the long-term distribution of extreme blade root flap bending loads including model uncertainty by inflating our estimates of the mean and standard deviation of the short-term extreme loads model developed from the mechanical-math-model data presented

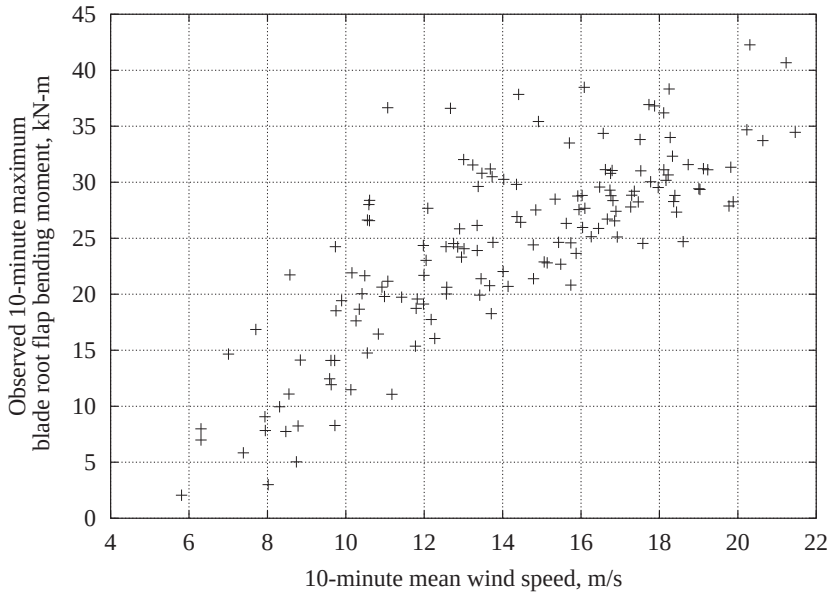

(a) Observed 10-minute maximum blade root flap bending moment versus 10-minute mean wind speed.

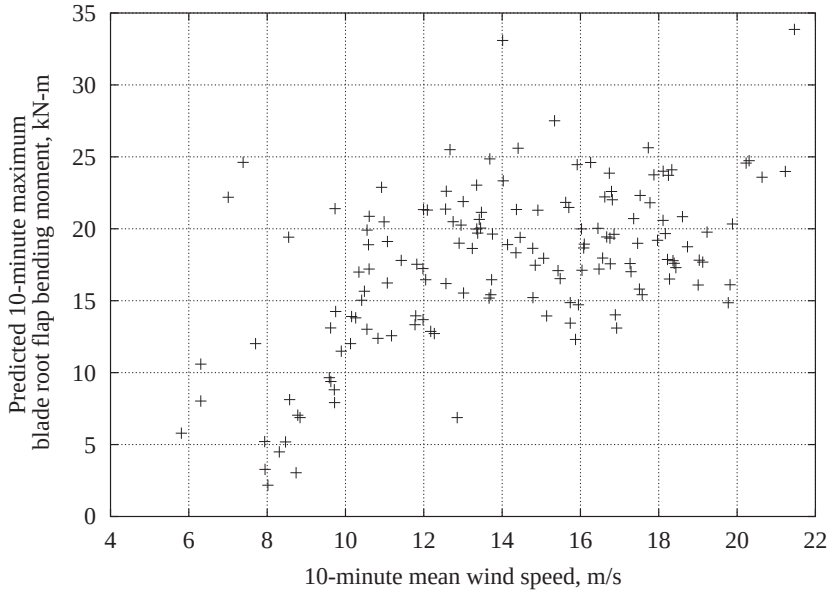

(b) Predicted 10-minute maximum blade root flap bending moment versus 10-minute mean wind speed.

Figure 6.9: Observed and predicted 10-minute maximum blade root flap bending moment versus 10-minute wind speed.

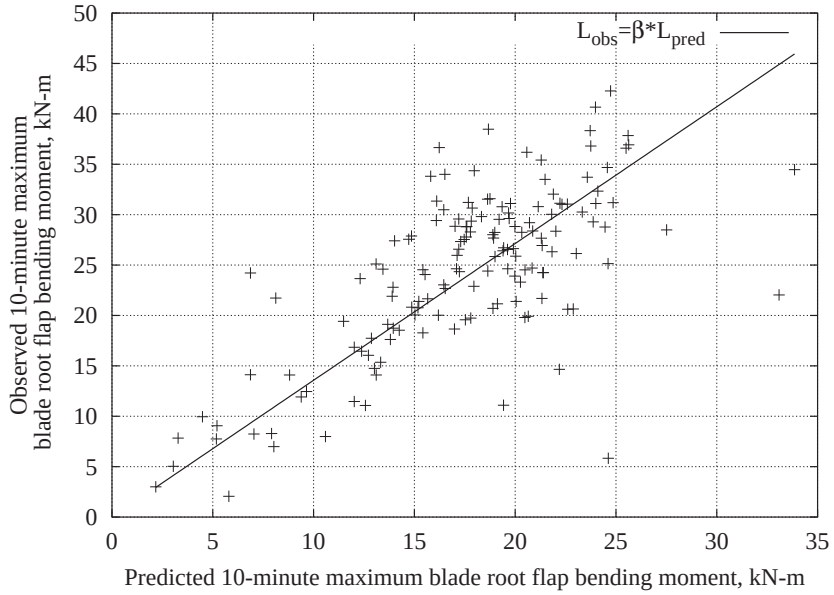

Figure 6.10: Observed versus predicted 10-minute maximum blade root flap bending moment.

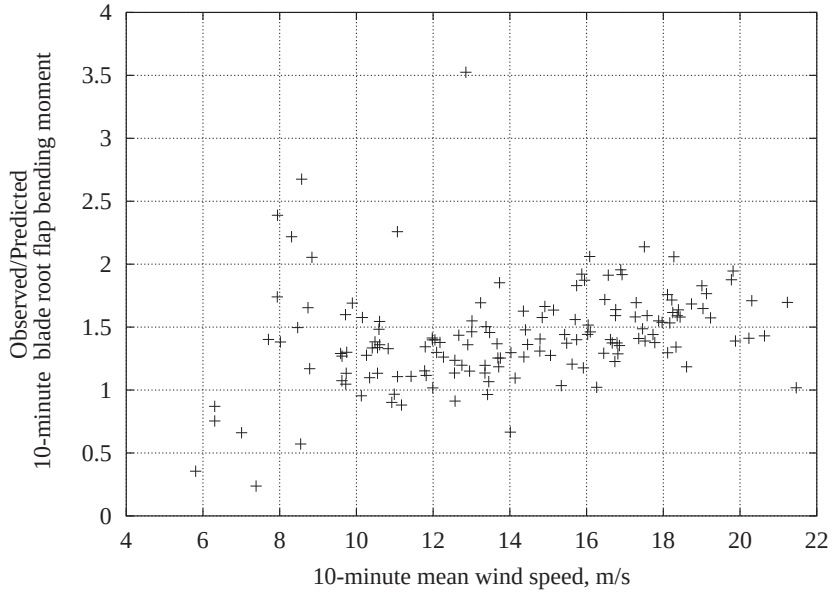

Figure 6.11: A measure of error: observed/predicted 10-minute maximum blade root flap bending moment versus 10-minute mean wind speed.

in Chapter 3 to reflect the model error as described by Equation 6.27 and Table 6.4. In Chapter 3 the short-term extreme load distribution was based on modeling the global peaks from simulated data. We showed in the analysis in this chapter that the predicted flap loads were on average biased by about 1.36 and the standard deviation of the model error residuals was 6.14kN-m. To correct for the bias we include a multiplicative term to the results we obtain from the regression analysis that relates the mean 10-minute maximum response to the environmental variables. We can write Equation 3.19 from Chapter 3 considering the mean 10-minute maximum blade root flap bending load and including the bias correction factor, $\hat{\beta}$ as

$$\mu_Z = 25.66\text{kN-m}\left(\frac{V}{V_{\text{ref}}}\right)^{0.7928}\left(\frac{I}{I_{\text{ref}}}\right)^{0.7129} \times \hat{\beta} \tag{6.28}$$

Where $\hat{\beta} = 1.36$ We can include the uncertainty associated with regression analysis, i.e., randomness associated with the prediction error by adding the variance of the residuals, $\sigma^2_{\varepsilon_m}$, to the variance predicted by our model in Chapter 3. In this case, we can write Equation 3.19 considering the standard deviation of the 10-minute maximum, blade root flap bending load and including the uncertainty, $\sigma^2_{\varepsilon_m}$, in our prediction error as

$$\sigma_Z = \sqrt{\left(8.61\text{kN-m}\left(\frac{V}{V_{\text{ref}}}\right)^{0.3231}\left(\frac{I}{I_{\text{ref}}}\right)^{0.2084}\right)^2 + \sigma^2_{\varepsilon_m}} \tag{6.29}$$

Where $\sigma^2_{\varepsilon_m} = 37.675(\text{kN-m})^2$. Figure 6.12 shows the expected estimate of the long-term distribution of maximum blade root flap bending loads for an arbitrary year. Our estimate of the 50-year blade root flap bending load, defined as the load with a mean annual exceedance probability of 2%, considering uncertainty in our prediction from the mechanical model, is 107kN-m. An estimate of the 50-year load of 59.7kN-m was obtained if we considered our mechanical-math-model to be correct. Including a correction for the model error and the uncertainty associated with the model error, our estimate of the 50-year load increases by 79.2%. 36% is due to the bias—the rest is due to "model error".

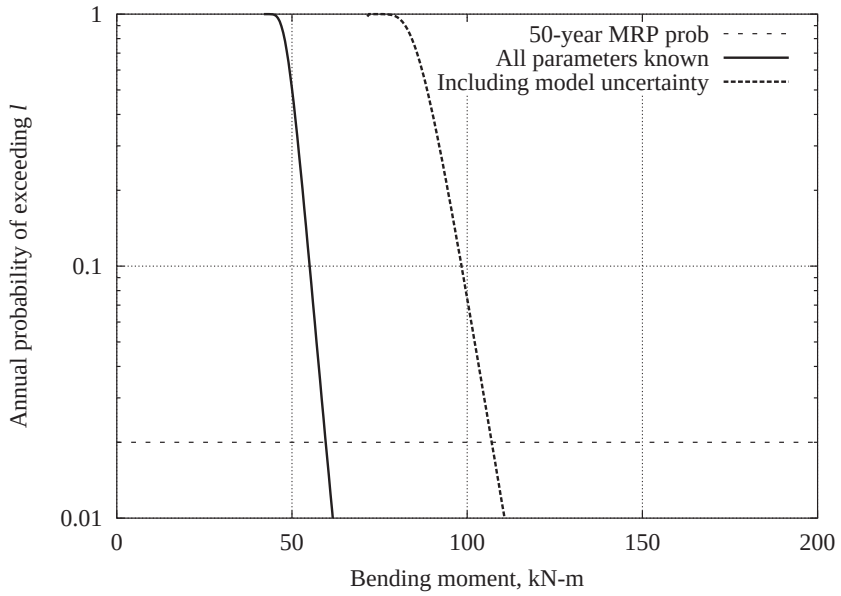

Figure 6.12: Mean long-term distribution of annual extreme blade root flap bending moment, including model uncertainty.

6.5 Conclusions

In this chapter we have discussed some of the sources on epistemic uncertainty in our analysis of estimating the long-term distribution of extreme blade root flap bending loads. We considered the effect of including the epistemic uncertainty associated with estimates of the long-term distribution parameters of the environmental variables. Including the uncertainty associated with the annual average 10-minute mean wind speed, the parameter for the Rayleigh model of long-term 10-minute mean wind speed had a greater contribution to the estimate of the long-term distribution of extreme flap bending loads, than did including the epistemic uncertainty associated with the conditional mean turbulence parameter, for the same level of parametric uncertainty of 20%. Including 20% epistemic uncertainty in our estimate of the annual average 10-minute mean wind speed, our estimate of the 50-year load, based on a mean annual exceedance probability of 2%, was 30.7% higher than if we assumed the annual average 10-minute mean wind speed to be known. On the other hand, including the 20% epistemic uncertainty in the conditional mean turbulence parameter our estimate of the 50-year load, again based on a mean annual exceedance probability of 2%, was only 6.4% higher than if we assumed this parameter was known. This shows that in this analysis the long-term distribution of the extreme response is more sensitive to epistemic uncertainty in the annual average 10-minute mean wind speed. It is critical to consider both the uncertainty and the sensitivity of the analysis to the uncertainty. Even though we have the same uncertainty in both parameters, annual average 10-minute mean wind speed and conditional mean turbulence, the analysis is more sensitive to changes in the annual average 10-minute mean wind speed. Given the choice, it would be a better use of resources to collect data to reduce the epistemic uncertainty in the estimate of the annual average 10-minute mean wind speed than the conditional mean turbulence if they have the same level of uncertainty, because the analysis is more sensitive to changes in the former.

We considered two approaches for estimating the uncertainty associated with the regression coefficients from limited data: (1) bootstrap method and (2) variance of coefficients through regression analysis. In the first approach, the bootstrap method was used to estimate the uncertainty in the regression coefficients. In the bootstrap method, a few time-histories at a time were randomly selected from the database. Then, based on this *bootstrap sample*, we obtained an estimate of the long-term distribution of the 10-minute extreme flap bending loads. This was repeated several times in order to obtain median and mean estimates of the long-term distribution of extreme blade root flap bending loads. We found that, in this case, if we considered 100 simulations at each set of values of the environmental conditions our estimate of the 50-year load, based on a mean annual exceedance probability of 2%, was 65.9kN-m about 10% higher than if we assumed the regression coefficients were known. If we considered only 50 simulations at each set of values of the environmental conditions our estimate of the 50-year load, again based on a mean annual exceedance

probability of 2%, increased to 206kN-m, about 3 times greater increase than if we used twice as many simulations.

The second approach utilized the assumptions in regression analysis to obtain a estimate of the variance of the regression coefficients. This approach may be useful if only a few (i.e. less than 20) simulations were run at each set of values of the environmental variables. In implementing this method, however, we assume that the covariance matrix of the regression coefficients remains fixed, or known. This eliminates one potential source of additional epistemic uncertainty. Monte Carlo simulation was used to randomly select sets of regression coefficients from jointly correlated Gaussian distributions. These distributions were defined by the mean vector of regression coefficients and the associated covariance matrix. One hundred mechanical-math-model simulations at each set of values of the environmental conditions resulted in an estimate of the 50-year load, based on a mean annual exceedance probability of 2%, of 65.5kN-m, about 10% higher than if the regression coefficients were known. If we considered only 50 simulations at each set of values of the environmental conditions, our estimate of the 50-year load, again based on a mean annual exceedance probability of 2%, increased to 133kN-m, about 2 times more than if we used twice as many simulations. The width of the distance between median and mean annual probability of exceedance (at the 2% level) estimates calculated assuming a known covariance is smaller compared with the width between median and mean annual probability of exceedance (at the 2% level) estimates based on using the bootstrap method for all numbers of mechanical-math-model simulations analyzed here. For example, the width of the distance between median and mean annual probability of exceedance estimates for 50 mechanical-math-model simulations using the bootstrap method is 145kN-m. Whereas, the distance between these estimates for the same number of simulations but assuming a known covariance matrix is 75.7kN-m. Therefore, we may conclude that there is some uncertainty that is not accounted for by considering the covariance matrix of the regression coefficients fixed. Although, when the number of simulations included in the analysis becomes large (e.g., 100), we observed only a small difference in the estimates obtained from the two methods.

Keeping the results of the long-term analysis in mind, the analysis considering the model uncertainty showed that there was enough bias, and variability in the bias, that if included would inflate our estimate of the 50-year load by 79.2%. Just from these simple analyzes we can determine the most effective areas to assign resources to reduce the epistemic uncertainty and then more accurately estimate the 50-year load.

Chapter 7

Summary and Conclusions

The purpose of this work has been to provide a probabilistic based approach to estimate fatigue and extreme load distributions on wind turbines. We started our discussion by looking at how we might model the short-term extreme response conditional on variables which describe the wind environment acting on the turbine. These models were then used to build estimates of the long-term distributions of extreme load events, i.e., extreme blade bending moment, from which we were able to estimate the one-year and 50-year loads. Subsequent to this work, we considered alternative methods to simplify the intensive calculations to obtain these estimates and also how we might quantify the associated uncertainty due to limited data in these estimates. Quantifying the epistemic uncertainty, and qualitatively understanding the sensitivity to the sources of uncertainty, provide a guideline to effectively target resources for further study and analysis. Additionally, we showed how the methodology developed for estimating long-term distributions of extreme loads could be applied to obtain estimates of the long-term distribution of fatigue ranges and estimates of fatigue damage. The next few sections reflect on each of these points in more detail and present suggestions for further research in several areas on the topic of fatigue and extreme load estimation for wind turbines.

7.1 Modeling Short-Term Extremes

We started with considering the appropriate choice of short-term extreme load models (i.e., process model, local peak model, or global peak model). Chapter 2 demonstrated the use of both random process and random peak models to predict short-term extreme wind turbine loads. In particular, we studied the efficacy of 3-moment random peak models, i.e., quadratic Weibull, and 3- and 4-moment random process Hermite models. We found that for a parked wind turbine experiencing 50-year winds, all models were nearly unbiased, and achieved a significant reduction, e.g., about

50%, in our epistemic uncertainty in estimating the mean 10-minute maximum load, compared with the statistics of the *raw* data. i.e., maximum event from 10-minute response time history of blade root flap or edge bending moment. On the other hand, for rotating blades during operation, at lower wind speeds, the random process models showed a notable bias. In contrast, the random peak models remained consistently accurate, and displayed consistently lower epistemic uncertainty in all cases. This suggested that rather than model the entire 10-minute time history, we could model a set of its local peaks and retain enough information about the rotating nature of the load process to permit obtaining accurate estimates of extreme behavior. Having found an accurate way of estimating the short-term extreme loads given prescribed environmental conditions, we needed a way to combine these short-term loads to estimate the marginal distribution of the extreme loads.

7.2 Estimating Long-Term Extreme Events

7.2.1 Integration Method

In Chapter 3 we presented a methodology for obtaining an estimate of the marginal distribution of the extreme loads by applying the Law of Total Probability. Starting from initial simulated response time histories of the AOC 15/50 turbine, we fit distribution models to first the observed 10-minute extremes and then later to the set of local peaks in a 10-minute response time history. In both cases the statistical moments that define the distribution model parameters were related to the environmental variables—which describe the wind processes—through regression analysis. Finally, an estimate of the long-term distribution of extreme blade root flap and edge bending moments were obtained by integrating the conditional short-term blade root bending moment distributions over the long-term distribution of the environmental variables. We found that the estimate of the long-term distributions of extreme blade root flap and edge bending moments based on modeling the local peaks were unbiased compared with the estimates of the long-term distributions of bending moments based on modeling the observed 10-minute extremes. Solving the two-fold integration is computationally intense, however. We discussed one method for mitigating this issue that simplified the two-fold integration problem down to a single-fold integration by using deterministic fractiles of the short-term load, turbulence intensity, and wind speed distributions. We showed that this methodology captured a significant portion of the contribution that these variables made to the variability of the long-term extreme bending moment distributions.

We should note that the fractiles obtained from the analysis presented in Chapter 3 apply to the data considered (turbine response and site description) in this analysis and moreover to the assumptions made in choosing the associated distribution models. Different fractiles may apply for other turbine response data under different assumptions. In particular, basing our expectations on

the results of similar analysis in other fields, i.e., off-shore structures, and earthquake engineering, we would have expected that the randomness in the short-term loads was less important than the randomness associated with the environmental variables. We found that, in general, this was not the case for the data used in our analysis. It would be beneficial to validate these results by looking at other stall-regulated turbines using different mechanical-math-model simulation techniques, and different site conditions. It would be of interest to determine if the results found here were typical of the conditions of wind turbine behavior, or for some reason pathological in this case.

7.2.2 Environmental Contour Method

Chapter 4 presented an alternate approximate approach for estimating the one-year and 50-year extreme turbine blade bending moment load. This approach essentially employed the approximate methods underlying first-order reliability analysis or FORM. In this method, contours of the critical combination of wind speed and turbulence intensity are found for a prescribed acceptable reliability level. It then becomes a straightforward task of (1) identifying an appropriate percentile of the short-term load, and (2) identifying the maximum response along the prescribed contour. Under the assumptions of FORM analysis, the maximum response along the contour is associated with prescribed reliability level of interest. These theories were applied in three different examples where the short-term extreme loads were considered deterministic at the mean level.

The first two examples demonstrated how estimates of the one-year and 50-year extreme blade bending loads on an AOC 15/50 turbine might be obtained using environmental contours, considering two different site environments. In both cases operating and parked loads on the turbine were considered. This introduced a discontinuity in the limit state function. One of the key assumptions in FORM analysis is that the limit state function is generally smooth. The reliability is approximated based on a straight line tangent to the limit state function at the point of highest probability density along the limit state function. If large discontinuities exist in the limit state function, then potentially significant areas of probability density may not be accounted for properly. The fact that this discontinuity is present is a challenge to the effectiveness of FORM to provide a reasonable approximation. In both examples the estimates obtained from the environmental contour method were reasonable (e.g., 0-6% difference) compared with estimates obtained from integrating the deterministic short-term extreme loads over the long-term distribution of the environmental variables. Even in the presence of the discontinuity in the limit state function at the cut-out wind speed, we found that FORM still provided a reasonable approximation (e.g., 2-13% difference), compared with the results from integration.

In the third example, the short-term response was developed to simulate the typical non-monotonic

response of a pitch-regulated machine. This contributed a slope discontinuity in the limit state function, in addition to the discontinuity at the cut-out wind speed. Again, estimates of the one-year and 50-year extreme flap-bending loads were obtained from both methods. We found that including the additional slope discontinuity did not greatly affect the efficacy of FORM to provide an acceptable approximation, at least for the turbine, site data, and distribution models used in this example.

We demonstrated that the environmental contour method provides reasonable estimates of extreme response similar to those obtained by the integration method. One advantage of using the two-dimensional environmental contours, presented in Chapter 4, is that the contours themselves are developed based only on data relating to the environment and a reliability criterion for the turbine. Therefore, the contours immediately give some insight into the critical combinations of environmental variables and may lead to a reduction in the required number of environmental conditions explored in the design process. In particular, instead of interrogating the entire space of combinations of environmental conditions for the critical response of the turbine, the contour identifies the critical environmental conditions. We only need to search the points along the contour to find the critical response of the turbine, for a prescribed reliability level. This can be a great benefit when running expensive computer simulations—we only need to run simulations at environmental conditions on the contour. A carefully constructed search algorithm, to interrogate the environmental contour, may lead to additional reduction in the number of environmental conditions considered in the quest to find the critical response of the turbine.

We might ask, "which fractile of the short-term extreme response should be used"? In the analysis presented in Chapter 4, we used the mean value of the short-term extreme response. We saw, however, in Chapter 3 that considering the short-term extreme response deterministic at its mean level and integrating over the long-term distribution of the environmental variables resulted in an estimate of the one-year and 50-year loads that was at times significantly lower, i.e., about 5%-25%, than had we included the randomness of the short-term extreme response. There may be some concern about how we account for the variability of the short-term extreme response in the environmental contour method. Some approaches to this problem were discussed in Chapter 4. It is important to point out that applying any of these methods discussed in Chapter 4 would re-couple the short-term turbine specific portion of the problem with the long-term environment specific portion of the problem. There is a parallel, however, with the discussion of simplifying the long-term integration problem presented in Chapter 3. Here we showed that considering the short-term loads deterministic, but at a higher fractile above the mean, we could recover the randomness that the short-term extreme load distribution contributed to the variability of the long-term distribution of extreme loads. This same fractile concept could potentially be used for the environmental contour method. In that case, if a universal fractile could be found that would cover a sufficiently large

number of stall-regulated turbines the fact that the problem has effectively been re-coupled may be mitigated. The reader should note that it is anticipated that a different fractile might be required for pitch-regulated turbines, because the nature of the loading is different.

7.3 Modeling Fatigue Ranges and Damage

These first chapters addressed estimating the long-term distribution of extreme loads. The method developed in Chapter 3 was then applied to estimating the long-term distribution of fatigue load distributions in Chapter 5. Parametric, moment-based, statistical models were introduced to model short-term rain-flow-counted fatigue ranges. Two "higher-moment" models (including third and/or higher moments) have been presented: (1) a quadratic Weibull model, which uses a quadratic distortion of the original Weibull model to preserve the first three moments of the data; and (2) a "damage-based" Weibull model, which seeks a two-moment Weibull fit, not to the fatigue ranges themselves but to power transformations that directly relate to "damage". Both models have their advantages. Compared with fatigue load data, the "damage-based" Weibull model was found to follow the tails of the observed data. It also requires no special numerical algorithms to estimate its parameters. In contrast, the quadratic Weibull does require such algorithms, and its accurate modeling of distribution tails can require the analyst to impose a lower-bound threshold on the load ranges to be modeled. The potential benefit of the quadratic Weibull model includes its reliance only on moments through third order. This may also be its draw back as the third moment may not be high enough to fit the model to upper tail of the distribution where we anticipate the loads will contribute the most to the accumulated fatigue damage. The damage-based model requires moments of higher order—typically three to five—which reflect material fatigue exponent values of six to ten.

From the analysis, we found that the two models gave two different estimates of the expected damage for the same value of the fatigue exponent. We stated that the quadratic Weibull model was fit to the first three moments of the data. Although the third moment affects the fit of the model in the tail of the data, the fit is still primarily influenced by the body of the data. To the degree that we believe that a majority of the fatigue damage will be caused by loads in the upper tail, this model, being fit to the body of data with some influence to the tail of the data, may not fit very well to the extreme tail of the data. Conversely, the damage-based model is fit to the higher moments than the third moment, is less influenced by the body of the data, and is tuned to the behavior of the extreme tail. Although, as we have mentioned, this is where we anticipate the loads to contribute the most to the fatigue damage, some damage should be expected from the body of the data. The damage-based model may not fit to this data very well. It may be overly influenced by the extreme tail of the data, and either over- or under-predict the loads in the body of the data.

Another point is that when implementing the quadratic Weibull model, either for modeling short-term fatigue ranges or short-term local peaks, a threshold was applied and the data was truncated and shifted to improve the fit of the model to the data. In these cases, the purpose of imposing the threshold was to remove a second population of either fatigue ranges or local peaks. In either case, where to impose the threshold is a difficult question. In our work here, the thresholds were based on qualitative examination of the data. It would be extremely helpful to establish some guidelines to help the engineer implement a reasonable threshold value—trading off the benefits of the goodness of the fit of the model to the data with the amount of data retained. Also, in general, assessing the goodness of fit of the model to the data, has been a qualitative evaluation. If the processes laid out in the previous chapters are to be implemented in an automatic way, we need to establish some quantitative evaluation of the goodness of fit of the model to the data. Poorly fit models to the observed or simulated data will only lead to erroneous estimates of the design loads.

7.4 Quantifying Epistemic Uncertainty

Finally, having established a methodology for estimating the long-term distribution of fatigue and extreme loads, we considered some of the possible sources of uncertainty in the analysis and showed how, at least at a first pass, the epistemic uncertainty may be incorporated into the analysis and it may affect our estimate of the 50-year load. We considered the effect of including the epistemic uncertainty associated with estimates of the long-term distribution parameters of the environmental variables. The analysis showed that the long-term distribution of the extreme response is more sensitive to epistemic uncertainty in the annual average 10-minute mean wind speed. It is critical to consider both the uncertainty and the sensitivity of the system to the uncertainty. If we have the same uncertainty in both parameters, annual average 10-minute mean wind speed and conditional mean turbulence, the system considered in Chapter 6 was more sensitive to changes in the annual average 10-minute mean wind speed. Given the choice, for this system, it would be a better use of resources to collect additional data to reduce the epistemic uncertainty in the estimate of the annual average 10-minute mean wind speed than the conditional mean turbulence if they have the same level of uncertainty.

Keeping the results of the long-term analysis in mind, we considered how we might incorporate some of the sources of uncertainty in the short-term conditional loads. Two sources of epistemic uncertainty were considered: (1) uncertainty associated with the regression coefficients and (2) model uncertainty. In the latter, we were concerned with how we might quantify the uncertainty associated with differences between the results from our mechanical model of the turbine compared with actual data from the turbine collected in the field.

We considered two approaches for estimating the uncertainty associated with the regression coefficients from limited data: (1) bootstrap method and (2) variance of coefficients through regression analysis. In the first approach—the bootstrap method—a few time-histories at a time were randomly selected from the database and then based on this *bootstrap sample* we obtained an estimate of the long-term distribution of the 10-minute extreme flap bending loads. This was repeated several times in order to obtain mean and median estimates of the the long-term distribution. The second approach utilized the assumptions in regression analysis to obtain an estimate of the variance of the regression coefficients. This approach may be useful if only an few (e.g. less than 20) simulations were run at each set of values of the environmental variables. In implementing this method, however, we assume that the covariance matrix of the regression coefficients remains fixed or known. Monte Carlo simulation was used to select sets of regression coefficients from jointly correlated Gaussian distributions. Their distributions were defined by the mean vector of regression coefficients and the associated covariance matrix. We observed that the width of the distance between the median estimate and the estimate obtained by considering the load with a mean annual exceedance probability of 2%, calculated assuming a known covariance, is smaller compared with the width between these estimates if obtained based on using the bootstrap method. Therefore, we may conclude that there is some uncertainty that is not accounted for by considering the covariance matrix of the regression coefficients fixed. Although, when the number of simulations included in the analysis becomes large (e.g., 100) we observed only a small difference in the estimates obtained from the two methods.

The analysis considering the model uncertainty showed that there was enough bias and variability in our estimate that if included, would inflate our estimate of the 50-year load by 80%. About half of this increase (36%) was due to the bias and the rest was due to case to case variability in model error. Just from these simple analyzes we can determine the most effective areas to assign resources to reduce the epistemic uncertainty and then more accurately estimate the 50-year load on wind turbines.

Bibliography

[1] Veers, P. S., 1996. "Forward." Journal of Solar Energy Engineering, Transactions of the ASME, **118**, p. 197.

[2] American Wind Energy Association. "Wind Energy: An Untapped Resource." Wind Energy Fact Sheet, www.awea.org.

[3] Wind Power Monthly. "Windicator." World Wide Web, www.windpower-monthly.com.

[4] Rohy, D. and Laurie, R., 1997. "1996 Energy Technology Status Report." Tech. Rep. 500-96-006, California Energy Commission, Sacramento, California.

[5] National Wind Turbine Technology Center. "Wind in a Minute." World Wide Web, www.nrel.gov/wind.

[6] American Wind Energy Association. "Comparative Cost of Wind and Other Energy Sources." Wind Energy Fact Sheet, www.awea.org.

[7] Madsen, H. O., Krenk, S., and Lind, N. C., 1986. *Methods of Structural Safety*. Prentice-Hall International Series in Civil Engineering and Engineering Mechanics, Prentice-Hall, Inc., Englewood Cliffs, New Jersey.

[8] Melchers, R. E., 1999. *Structural Reliability Analysis and Prediction*. Second edn. John Wiley and Sons Ltd., Chichester, England.

[9] AISC, 1986. *Manual of Steel Design, Load and Resistance Factor Design*, first edn.

[10] ACI, 1992. *Building Code Requirements for Reinforced Concrete*, ACI 318-89 edn.

[11] Cornell, C. A., 1969. "A Probability-Based Structural Code." Journal of the American Concrete Institute, **66**(12), pp. 974–985.

[12] Hasofer, A. M. and Lind, N., 1974. "An Exact and Invariant First-Order Reliability Format." Journal of Engineering Mechanics Division ASCE, **100(EM1)**, pp. 111–121.

[13] Ditlevsen, ., 1979. "Generalized Second-Moment Reliability Index." Journal of Engineering Mechanics, **7**(4), pp. 435–451.

[14] Bunditz(Chairman), R. J., Apostolakis, G., Cluff, L. S., Coppersmith, K. J., Cornell, C. A., and Morris, P. A., 1997. "Recommendations for Probabilistic Seismic Hazard Analysis: Guidance on Uncertainty and Use of Experts." Tech. Rep. NUREG/CR-6372, UCRL-ID-122160, Vol. 1, Senior Seismic Hazard Analysis Committee (SSHAC), Lawerance Livermore National Laboratory.

[15] Ross, S., 1996. *Stochastic Processes*. Second edn. John Wiley and Sons Inc., New York, New York.

[16] Grimmett, G. R. and Stirzaker, D. R., 1992. *Probability and Random Processes*. Second edn. Oxford University Press, Inc., New York New York.

[17] Luco, N. and Cornell, C. A., 2001. "Structure-Specific Scalar Intensity Measures for Near-Source and Ordinary Earthquake Ground Motions." Earthquake Spectra.

[18] Haghighi, T. K., 2002. "Stochastic Load Models From Limited Data: A General Approach with Applications to Wind and Waves." Ph.D. thesis, Stanford University.

[19] Simms, D. A., Hand, M. M., Figersh, L. J., and Jager, D. W., 1999. "Unsteady Aerodynamics Experiment Phases II-IV Test Configurations and Available Data Campaigns." Tech. Rep. NREL/TP-500-25950, National Renewable Energy Laboratory, Golden, Colorado.

[20] Hansen, A. C., 1996. *Users Guide to the Wind Turbine Dynamics Computer Programs YawDyn and AeroDyn for ADAMS*. Mechanical Engineering Department, University of Utah, Salt Lake City, Utah.

[21] Madsen, P. H., Pierce, K., and Buhl, M., Jan 1999. "Predicting Ultimate Loads for Wind Turbine Design." *A Collection of the 1999 ASME Wind Energy Symposium, at the 37th AIAA Aerospace Sciences Meeting*. AIAA-99-0069, Reno, Nevada.

[22] Atlantic Orient Corporation. *AOC 15/50 Specification*. www.aocwind.net.

[23] IEC/TC8, 1998. *61400-1 Wind Turbine Generator Systems - Part 1: Safety Requirements*. International Electrotechnical Commission, Geneva, Switzerland.

[24] Rice, J. A., 1995. *Mathematical Statistics and Data Analysis*. Second edn. Duxbury Press, Belmont, California.

[25] Pitnam, J., 1993. *Probability*. Springer-Verlag, New York.

[26] Sutherland, H. J., 2002. "Analysis of the Structural and Inflow Data from the LIST Turbine." Journal of Solar Energy Engineering, Transactions of the ASME, **124**.

[27] Sutherland, H. J. and Kelley, N. D., Jan 2003. "Inflow and Fatigue Response of the NWTC advanced research turbine." *A Collection of the 2003 ASME Wind Energy Symposium, at the 41th AIAA Aerospace Sciences Meeting*. AIAA-2003-0862, Reno, Nevada.

[28] Gumbel, E. J., 1958. *Statistics of Extremes*. Columbia University Press, New York, New York.

[29] Benjamin, J. R. and Cornell, C. A., 1970. *Probability, Statistics, and Decision for Civil Engineers*. McGraw-Hill, Inc., New York, New York.

[30] Winterstein, S. R., Kleiven, G., and Øistein, H., 2001. "Comparing Extreme Wave Estimates from Hourly and Annual Data." *to appear: Proceedings of* ISOPE-*2001*. ISOPE.

[31] Sweetman, B., 2001. "Airgap Analysis of Floating Structures Subject to Random Seas: Prediction of Extremes Using Diffraction Analysis Versus Model Test Results." Ph.D. thesis, Stanford University.

[32] Liu, Y. and Bergdahl, L., 1998. "Extreme Mooring Cable Tensions Due to Wave-Frequency Excitations." Applied Ocean Research, **20**(4), pp. 237–249.

[33] Jensen, J. J. and Dogliani, M., 1996. "Wave-Induced Ship Hull Vibrations in Stochastic Seaways." Marine Structures, **9**(3-4), pp. 353–387.

[34] Winterstein, S. R., 1988. "Nonlinear Vibration Models for Extremes and Fatigue." Journal of Engineering Mechanics, **114**(10), pp. 1772–1790.

[35] Winterstein, S. R. and Ness, O. B., 1989. "Hermite Moment Analysis of Nonlinear Random Vibration." *Computational Mechanics of Probabilistic and Reliability Analysis*, edited by W. K. Liu and T. Belytschko. Elme Press, Lausanne, Switzerland.

[36] Rice, S. O., 1944. "Mathematical Analysis of Random Noise." Bell System Technical Journal, **23**, pp. 282–332.

[37] Rice, S. O., 1944. "Mathematical Analysis of Random Noise." Bell System Technical Journal, **24**, pp. 46–156.

[38] Fitzwater, L. M. and Winterstein, S. R., 2001. "Predicting Design Wind Turbine Loads from Limited Data: Comparing Random Process and Random Peak Models." Journal of Solar Energy Engineering, Transactions of the ASME, **123**, pp. 364–371.

[39] McCoy, T. J., Malcom, D. J., and Griffin, D. A., Jan 1999. "An Approach to the Development of Turbine Loads in Accordance with IEC 1400-1 and ISO 2394." *A Collection of the 1999 ASME Wind Energy Symposium, at the 37th AIAA Aerospace Sciences Meeting*. AIAA-99-0020, Reno, Nevada.

[40] Fitzwater, L. M. and Winterstein, S. R., 2000. "Estimation of Extremes from Limited Time Histories: The Routine MaxFits with Wind Turbine Examples." Tech. Rep. RMS–39, Reliability of Marine Structures Program, Civil and Environmental Engineering Department, Stanford University, Stanford, California. Under review for publication as a technical report by Sandia National Laboratory.

[41] Fitzwater, L. M. and Winterstein, S. R., 2001. "Estimation of Extremes from Limited Time Histories: The Routine MAXFITS with Wind Turbine Examples." Tech. Rep. SAND2001-3750, Sandia National Laboratories, Albuquerque, New Mexico.

[42] Winterstein, S. R., 1988. "Nonlinear Vibration Models for Extremes and Fatigue." Journal Engineering Mechanics, **114**(10), pp. 1772–1790.

[43] Jha, A. K. and Winterstein, S. R., 1997. "Nonlinear Random Ocean Waves: Prediction and Comparison with Data." Tech. Rep. RMS–24, Reliability of Marine Structures Program, Civil and Environmental Engineering Department, Stanford University, Stanford, California.

[44] Jha, A. K. and Winterstein, S. R., 2000. "Nonlinear Random Ocean Waves: Prediction and Comparison with Data." *Proceedings 19th International Offshore Mechanical Arctic Engineering Symposium*. Paper No. OMEA 00-6125, ASME.

[45] Lange, C. H. and Winterstein, S. R., 1996. "Fatigue Design of Wind Turbine Blades: Load and Resistance Factors from Limited Data." *Wind Energy 1996*. ASME.

[46] Ronold, K. O., Wedel-Heinen, J., and Christensen, C. J., 1999. "Reliability-Based Fatigue Design of Wind Turbine Rotor Blades." Engineering Structures, **21**, pp. 1101–1114.

[47] Winterstein, S. R. and Kashef, T., 2000. "Moment-Based Load and Response Models with Wind Engineering Applications." Journal of Solar Energy Engineering, Transactions of the ASME, **122**(3), pp. 122–128.

[48] Efron, B. and Tibshirani, R. J., 1998. *An Introduction to the Bootstrap*, vol. 57 of *Monographs on Statistics and Applied Probability*. Chapman and Hall/CRC, New York, New York.

[49] Fitzwater, L. M. and Cornell, C. A., 2002. "Predicting the Long-Term Distribution of Extreme Loads from Limited Duration Data: Comparing Full Integration and Approximate Methods." Journal of Solar Energy Engineering, Transactions of the ASME, **124**(4), pp. 378–386.

[50] Manuel, L., Veers, P. S., and Winterstein, S. R., Jan 2001. "Parametric Models for Estimating Wind Turbine Fatigue Loads for Design." *A Collection of the 2001 ASME Wind Energy Symposium, at the 39th AIAA Aerospace Sciences Meeting*. AIAA-2001-0047, Reno, Nevada.

[51] Ronold, K. O. and Larsen, G. C., 1999. "Reliability-Based Design of Wind-Turbine Rotor Blades Against Failure in Ultimate Loading." Engineering Structures, **22**, pp. 565–574.

[52] Manuel, L., Kashef, T., and Winterstein, S. R., 1999. "Moment-Based Probability Modeling and Extreme Response Estimation: The FITS Routine, Version 1.2." Tech. Rep. RMS–38, Reliability of Marine Structures Program, Civil and Environmental Engineering Department, Stanford University, Stanford, California.

[53] Manuel, L., Kashef, T., and Winterstein, S. R., 1999. "Moment-Based Probability Modeling and Extreme Response Estimation: The FITS Routine, Version 1.2." Tech. Rep. SAND99–2985, Sandia National Laboratories, Albuquerque, New Mexico.

[54] Veers, P. S. and Winterstein, S. R., 1998. "Application of Measured Loads to Wind Turbine Fatigue and Reliability Analysis." Journal of Solar Energy Engineering, Transactions of the ASME, **120**(4).

[55] Haver, S., Sagli, G., and Gran, T., 1998. "Long Term Response Analysis of Fixed and Floating Structures." *Proceedings Wave'98–Ocean Wave Kinematics, Dynamics and Loads on Structures*. International OTRC Symposium.

[56] Winterstein, S. R. and Engebretsen, K., 1998. "Reliability-Based Prediction of Design Loads and Responses for Floating Ocean Structures." *Proceedings, 17th International Offshore Mechanical Artic Engineering Symposium*. ASME.

[57] Engebretsen, K. and Winterstein, S. R., 1998. "Probabilistic Specification of Metocean Criteria: Generating and Searching N-Year Contours for Extreme Response Estimation." Tech. Rep. RMS–32, Reliability of Marine Structures Program, Civil and Environmental Engineering Department, Stanford University, Stanford, California.

[58] Fitzwater, L. M., Cornell, C. A., and Veers, P. S., Jan 2003. "Using Environmental Contours to Predict Extreme Events on Wind Turbines." *A Collection of the 2003 ASME Wind Energy Symposium, at the 41st AIAA Aerospace Sciences Meeting*. AIAA-2003-0865, Reno, Nevada.

[59] Winterstein, S. R., Ude, T. C., Cornell, C. A., Bjerager, P., and Haver, S., 1993. "Environmental Parameters from Extreme Response: Inverse Form with Omission Factors." *Proceedings* ICOSSAR*93*. Innsbruck, Austria.

[60] Winterstein, S. R., Kumar, S., and Kleiven, G., 1995. "Environmental Contours and Extreme Response of Deep-Water Floating Structures." *Engineering Mechanics Proceedings of the 10th Conference*, edited by S. Sture. ASCE, Boulder, Colorado.

[61] Bhattacharya, B., Wang, S., Basu, R., Ma, K., and Menon, B., 1999. "Reliability-Based Combination of Environmental Parameters for the Design of Novel Floating Structures." *Proceedings of the 18th International Conference on Offshore Mechanics and Artic Engineering*. New Foundland, Canada.

[62] Bazzurro, P., Winterstein, S. R., Ude, T. C., and Cornell, C. A., 1996. "Magnitude-Distance Contours for Probabilistic Seismic Hazard Analysis." *Proceedings of the 7th Specialty Conference on Probabilistic Mechanics and Structural Reliability*, edited by D. M. Frangopol and M. D. Grigoriu. ASCE, Worcester, Ma.

[63] Lange, C. H., 1996. "Probabilistic Fatigue Methodology and Wind Turbine Reliability." Ph.D. thesis, Stanford University.

[64] Basquin, O. H., 1910. "The Exponential Law of Endurance Tests." Proceedings ASTM, **10**(Part II), p. 625.

[65] Lange, C. H., 1996. "Probabilistic Fatigue Methodology and Wind Turbine Reliability." Tech. Rep. SAND96–1246, Sandia National Laboratories, Albuquerque, New Mexico.

[66] Nelson, D. V. and Fuchs, H. O., 1977. "Predictions of Cumulative Fatigue Damage Using Condensed Load Histories." *Fatigue under Complex Loading: Analysis and Experiments, Advances in Engineering*, edited by R. Wetzel, vol. 6. SAE, Warrendale, Pennsylvania.

[67] Weisberg, S., 1985. *Applied Linear Regression*. Second edn. John Wiley & Sons, New York, New York.

[68] Rackwitz, R. and Fiessler, B., 1978. "Structural Reliability Under Combined Random Load Sequences." Comp Struct, **9**, pp. 484–494.

[69] Rackwitz, R., 2001. "Reliability Analysis—A Review and Some Perspectives." Structural Safety, **23**, pp. 365–395.

Appendix A

Filtered Time Histories

In Chapter 3 we noted that the time histories for blade root edge bending response of the parked turbine were filtered. This appendix briefly presents the methodology used in filtering these time histories.

The simulations of the load response of a pseudo-parked AOC 15/50 turbine at different wind speeds were run using YAWDYN. Running a pseudo-parked condition came out of a constraint of the YAWDYN program, which can not simulate blade load responses for a parked turbine. Therefore, the simulations were run with the turbine very slowly idling, one rotation in ten minutes. Presumably, the variation of the response due to the wind field for a parked turbine would be very closely approximated by the simulation where the turbine was slowly idling. This seemed to produce acceptable results for the 50m/s high wind speed case. For the lower wind speeds, specifically the in-plane, edge, bending response (the out-of-plane, flap, bending response was not effected), the variation in the response due to the input simulated wind field was much smaller compared to the gravity cycle introduced by the slowly idling turbine, see Figures A.1(a), A.2(a), and A.2(a). This gravity cycle would not occur if the turbine was parked, however.

In order to remove the erroneous gravity cycle from these parked turbine response time histories, a Discrete Fast Fourier Transform (DFFT) was applied to the edge-bending response time histories. By applying the DFFT to the time history we are able to determine the frequency content of the time history as well as the power associated with the various frequencies. In the frequency domain then it was simple to establish the once per 10 minute cycle (i.e. 1.67e-3 Hz) and set the power associated with this frequency to zero, effectively removing this frequency from the spectrum. An inverse-DFFT was applied to the modified frequency spectrum to recover a revised time history without the offending gravity cycle. This process was applied to all the edge bending response time histories for the three parked turbine conditions with 10-minute mean wind speeds of 24, 30, and 40m/s. Figures A.1, A.2, and A.3 show example unfiltered and filtered time histories.

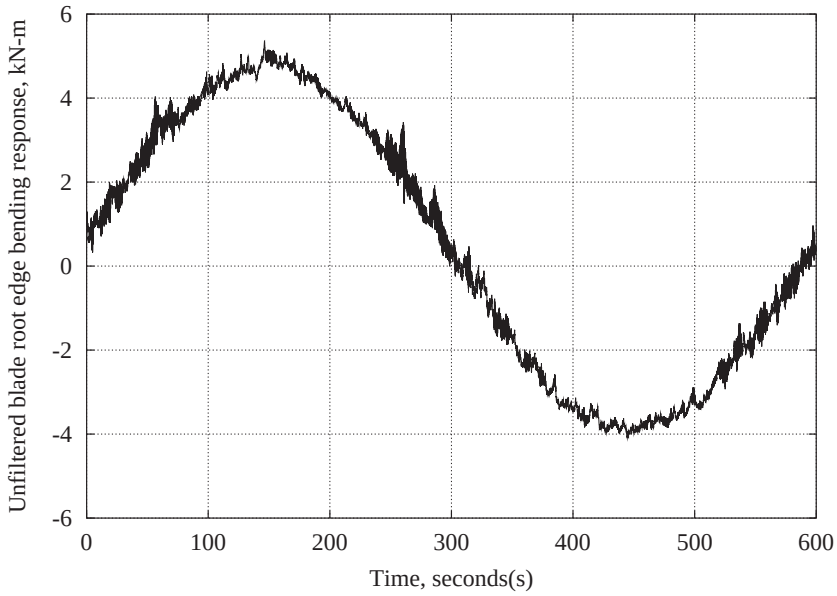

(a) Unfiltered 24m/s parked turbine, blade root edge bending response time history

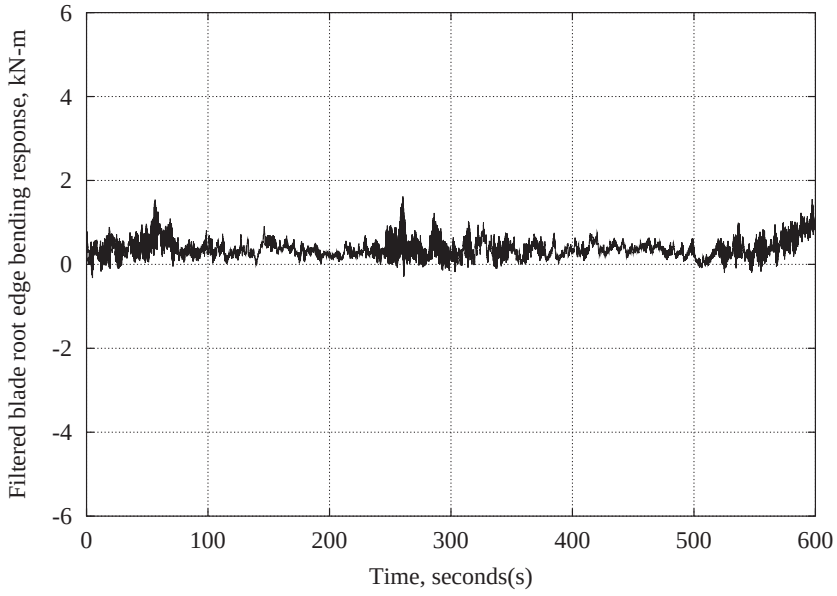

(b) Filtered 24m/s parked turbine, blade root edge bending response time history

Figure A.1: Unfiltered and filtered time histories of blade root edge bending response for the parked turbine condition in a 24m/s turbulence class A wind environment.

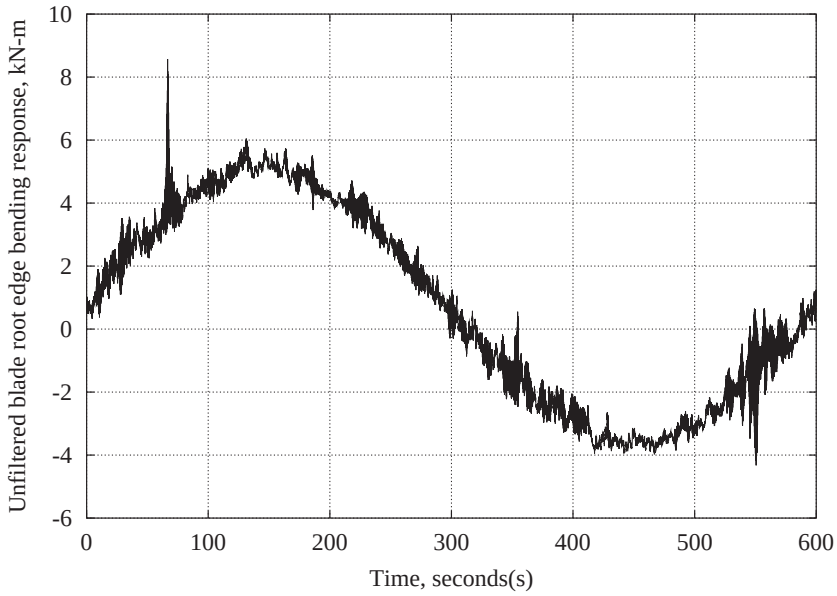

(a) Unfiltered 30m/s parked turbine, blade root edge bending response time history

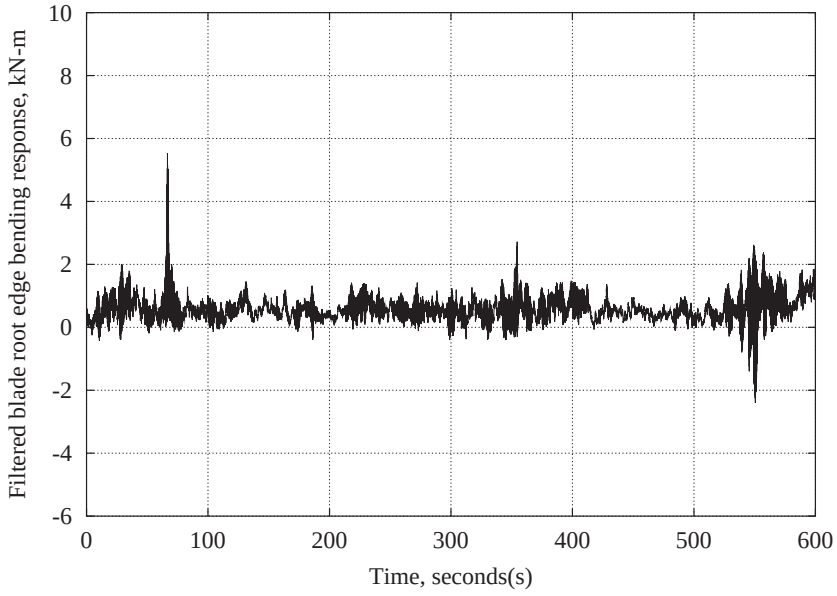

(b) Filtered 30m/s parked turbine, blade root edge bending response time history

Figure A.2: Unfiltered and filtered time histories of blade root edge bending response for the parked turbine condition in a 30m/s turbulence class A wind environment.

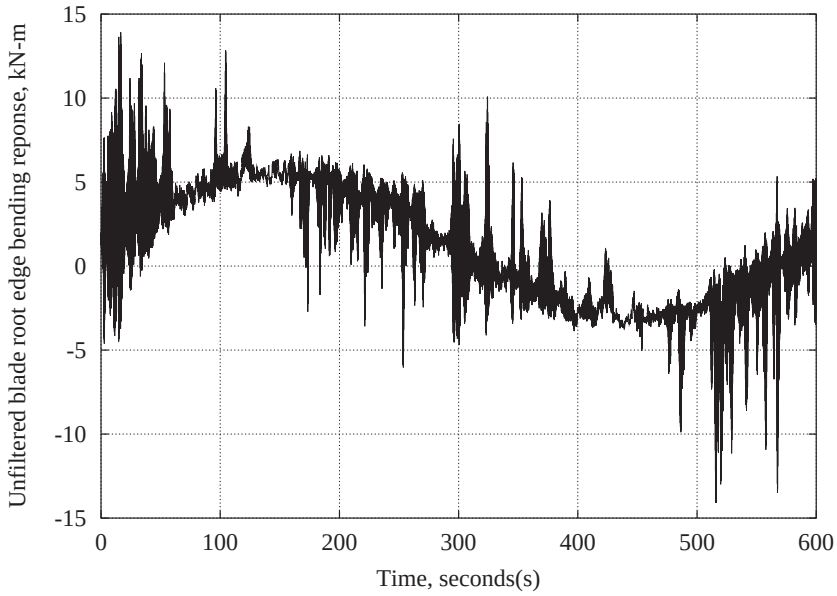

(a) Unfiltered 40m/s parked turbine, blade root edge bending response time history

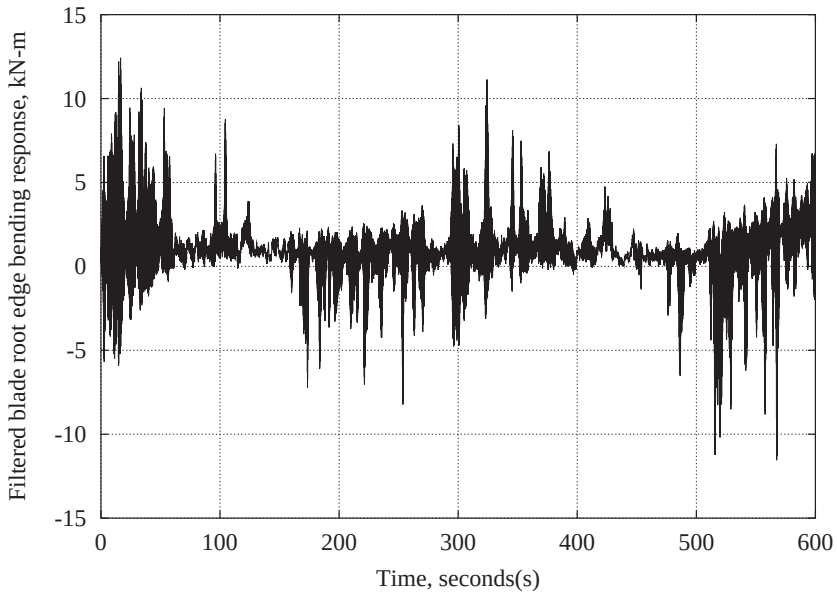

(b) Filtered 40m/s parked turbine, blade root edge bending response time history

Figure A.3: Unfiltered and filtered time histories of blade root edge bending response for the parked turbine condition in a 40m/s turbulence class A wind environment.

Appendix B

Regression Analysis

B.1 Introduction

This appendix presents a summary of the concepts of linear regression analysis. Additional information on the topics presented here can be found in Rice [24] and Weisberg [67].

Regression analysis is concerned with the prediction of a variable Y based on information provided by a set of other variables $X_1, X_2, \ldots, X_m$. The case where the relationship between Y and X is linear is called *linear regression*. This relationship can be written as,

$$Y = \beta_0 + \beta_1 X_1 + \beta_2 X_2 + \cdots + \beta_p X_p + \varepsilon \tag{B.1}$$

Where the X's are called *independent* or *predictor* variables and are not random. The β's are called regression parameters or regression coefficients, and ε is random error term. Y is called the *dependent* variable or *response* and is random as a result of ε.

The case where there is only one predictor variable, i.e., $Y = \beta_0 + \beta_1 X_1 + \varepsilon$, is called *simple linear regression*. On the other hand, the case where there are multiple predictor variables is called *multiple regression*. Our interest here, in this discussion, lies with multiple regression. Before we continue further, one point should be made about the X's, the "independent" variables. This name can be somewhat misleading, as the X's may be related to each other. Therefore, it is possible to model relationships that have non-linear terms in X. For example we may consider the relationship $Y = \beta_0 + \beta_1 X + \beta_2 X^2 + \varepsilon$, which may be modeled in a linear regression context by setting $X_1 = X$ and $X_2 = X^2$. In other words, the important point is that the linear regression model is linear with respect to the β's, the parameters, but not necessarily in the X's.

B.2 Multiple Linear Regression—Matrix Formulation

We will use matrix notation to ease the discussion of multiple regression. In general, vectors and matrices will be denoted by boldface letters such as: $\mathbf{X}$, $\mathbf{e}$, $\boldsymbol{\beta}$, etc. Elements of vectors and matrices are denoted as: $x_{i,j}$, e_j, and β_j.

The values of the β's and the statistics of ε are not known, but can be estimated from a sample of observations of Y and the corresponding X's. For the i^{th}, ($i = 1, \ldots, n$) observation, Equation B.1 can be written written as,

$$y_i = \beta_0 + \beta_1 X_{i1} + \beta_2 X_{i2} + \cdots + \beta_p X_{ip} + \epsilon_i \tag{B.2}$$

where y_i is the i^{th} observation of Y, X_{ij} is the i^{th} observation of the j^{th}, ($j = 1, \ldots, p$) independent variable, and ϵ_i is the i^{th} observation of ε.

Equation B.2 can be written in terms of matrices as,

$$\begin{bmatrix} y_1 \\ y_2 \\ \vdots \\ y_n \end{bmatrix} = \begin{bmatrix} 1 & x_{1\,1} & x_{1\,2} & \ldots & x_{1\,p} \\ 1 & x_{2\,1} & x_{2\,2} & \ldots & x_{1\,p} \\ \vdots & \vdots & & \vdots & \\ 1 & x_{n\,1} & x_{n\,2} & \ldots & x_{n\,p} \end{bmatrix} \begin{bmatrix} \beta_0 \\ \beta_1 \\ \vdots \\ \beta_p \end{bmatrix} + \begin{bmatrix} \epsilon_1 \\ \epsilon_2 \\ \vdots \\ \epsilon_n \end{bmatrix} \tag{B.3}$$

defining

$$\mathbf{Y} = \begin{bmatrix} y_1 \\ y_2 \\ \vdots \\ y_n \end{bmatrix}; \quad \mathbf{X} = \begin{bmatrix} 1 & x_{1\,1} & x_{1\,2} & \ldots & x_{1\,p} \\ 1 & x_{2\,1} & x_{2\,2} & \ldots & x_{1\,p} \\ \vdots & \vdots & & \vdots & \\ 1 & x_{n\,1} & x_{n\,2} & \ldots & x_{n\,p} \end{bmatrix}; \quad \boldsymbol{\beta} = \begin{bmatrix} \beta_0 \\ \beta_1 \\ \vdots \\ \beta_p \end{bmatrix}; \quad \boldsymbol{\epsilon} = \begin{bmatrix} \epsilon_1 \\ \epsilon_2 \\ \vdots \\ \epsilon_n \end{bmatrix} \tag{B.4}$$

Equation B.3 can be written as,

$$\mathbf{Y} = \mathbf{X}\boldsymbol{\beta} + \boldsymbol{\epsilon} \tag{B.5}$$

If we consider the condition where we assume $\mathsf{E}[\epsilon_i] = 0$, and $\mathsf{Var}[\epsilon_i] = \sigma^2$ with $\mathsf{Cov}[\epsilon_i, \epsilon_j] = 0$ which implies,

$$\mathsf{E}[\boldsymbol{\epsilon}] = 0 \tag{B.6}$$

and

$$\mathsf{Var}[\boldsymbol{\epsilon}] = \mathsf{E}[\boldsymbol{\epsilon}\boldsymbol{\epsilon}^T] = \sigma^2\mathbf{I} \tag{B.7}$$

where $\boldsymbol{\epsilon}^T$ denotes the transpose of $\boldsymbol{\epsilon}$, and $\mathbf{I}$ is the identity matrix. From Equations B.6 and B.7 the

expected value of $\mathbf{Y}$ can be found by,

$$\begin{aligned} \mathsf{E}[\mathbf{Y}] &= \mathsf{E}[\mathbf{X}\boldsymbol{\beta} + \boldsymbol{\epsilon}] \\ &= \mathbf{X}\boldsymbol{\beta} + \mathsf{E}[\boldsymbol{\epsilon}] \\ &= \mathbf{X}\boldsymbol{\beta} \end{aligned} \tag{B.8}$$

B.3 Least Squares Estimation of $\boldsymbol{\beta}$

One common method for obtaining an estimate for the regression coefficients $\beta_0, \beta_1, \beta_2, \ldots, \beta_p$ is the least squares method, which minimizes the the sum of the squares of the residuals. We will denote the vector of residuals by $\mathbf{e}$ and is defined as,

$$\mathbf{e} = \mathbf{Y} - \mathbf{X}\hat{\boldsymbol{\beta}} \tag{B.9}$$

Where $\hat{\boldsymbol{\beta}}$ is our estimate of the vector of regression coefficients. Therefore, and estimate of $\boldsymbol{\beta}$ may be found by minimizing RSS the residual sum of squares, or the sum of the squares of the elements of $\mathbf{e}$, more formally:

$$\begin{aligned} RSS &= \mathbf{e}^T\mathbf{e} \\ &= (\mathbf{Y} - \mathbf{X}\hat{\boldsymbol{\beta}})^T(\mathbf{Y} - \mathbf{X}\hat{\boldsymbol{\beta}}) \\ &= \mathbf{Y}^T\mathbf{Y} - \mathbf{Y}^T\mathbf{X}\hat{\boldsymbol{\beta}} - \mathbf{Y}\mathbf{X}^T\hat{\boldsymbol{\beta}}^T + \hat{\boldsymbol{\beta}}^T\mathbf{X}^T\mathbf{X}\hat{\boldsymbol{\beta}} \end{aligned} \tag{B.10}$$

However, the term $\mathbf{Y}^T\mathbf{X}\hat{\boldsymbol{\beta}}$ is a scalar and can be replaced by its transpose. Substituting into Equation B.10 yields,

$$RSS = \mathbf{Y}^T\mathbf{Y} - 2\hat{\boldsymbol{\beta}}^T\mathbf{X}\mathbf{Y} + \hat{\boldsymbol{\beta}}^T\mathbf{X}^T\mathbf{X}\hat{\boldsymbol{\beta}} \tag{B.11}$$

We want to minimize the residual sum of squares, RSS, so we differentiate RRS, Equation B.11 above with respect to $\hat{\boldsymbol{\beta}}$ which yields,

$$\frac{\partial RSS}{\partial \hat{\boldsymbol{\beta}}} = -2\mathbf{X}^T + 2\mathbf{X}^T\mathbf{X}\hat{\boldsymbol{\beta}} \tag{B.12}$$

Setting Equation B.12 equal to zero gives,

$$\mathbf{X}^T\mathbf{X}\hat{\boldsymbol{\beta}} = \mathbf{X}^T\mathbf{Y} \tag{B.13}$$

which yields the least square estimate of $\boldsymbol{\beta}$ as

$$\hat{\boldsymbol{\beta}} = (\mathbf{X}^T\mathbf{X})^{-1}\mathbf{X}^T\mathbf{Y} \tag{B.14}$$

B.4 Expected Value and Variance of $\hat{\boldsymbol{\beta}}$

Taking the expectation of both sides of Equation B.14 yields:

$$\begin{aligned}
\mathsf{E}[\hat{\boldsymbol{\beta}}] &= \mathsf{E}[(\mathbf{X}^T\mathbf{X})^{-1}\mathbf{X}^T\mathbf{Y}] \\
&= (\mathbf{X}^T\mathbf{X})^{-1}\mathbf{X}^T\mathsf{E}[\mathbf{Y}] \\
&= (\mathbf{X}^T\mathbf{X})^{-1}\mathbf{X}^T\mathbf{X}\boldsymbol{\beta} \\
&= \boldsymbol{\beta}
\end{aligned} \tag{B.15}$$

Because $\mathsf{E}[\hat{\boldsymbol{\beta}}] = \boldsymbol{\beta}$, in Equation B.15, $\hat{\boldsymbol{\beta}}$, as defined in Equation B.14 is said to be an unbiased estimator.

Taking the variance of both sides of Equation B.14 yields:

$$\begin{aligned}
\mathsf{Var}[\hat{\boldsymbol{\beta}}] = \boldsymbol{\Sigma}_{\hat{\boldsymbol{\beta}}} &= \mathsf{Var}[(\mathbf{X}^T\mathbf{X})^{-1}\mathbf{X}^T\mathbf{Y}] \\
&= (\mathbf{X}^T\mathbf{X})^{-1}\mathbf{X}^T\boldsymbol{\Sigma}_{\mathbf{Y}}\mathbf{X}(\mathbf{X}^T\mathbf{X})^{-1}
\end{aligned} \tag{B.16}$$

where under the assumptions given in Equations B.6 and B.7 $\boldsymbol{\Sigma}_{\mathbf{Y}}$ can be obtained as,

$$\begin{aligned}
\boldsymbol{\Sigma}_{\mathbf{Y}} &= \mathsf{E}[(\mathbf{Y} - \mathsf{E}[\mathbf{Y}])(\mathbf{Y} - \mathsf{E}[\mathbf{Y}])^T] \\
&= \mathsf{E}[(\mathbf{Y} - \mathbf{X}\boldsymbol{\beta})(\mathbf{Y} - \mathbf{X}\boldsymbol{\beta})^T] \\
&= \mathsf{E}[\boldsymbol{\epsilon}\boldsymbol{\epsilon}^T] \\
&= \sigma^2\mathbf{I}
\end{aligned} \tag{B.17}$$

Substituting Equation B.17 into Equation B.16 yields:

$$\begin{aligned}
\boldsymbol{\Sigma}_{\hat{\boldsymbol{\beta}}} &= (\mathbf{X}^T\mathbf{X})^{-1}\mathbf{X}^T\sigma^2\mathbf{I}\mathbf{X}(\mathbf{X}^T\mathbf{X})^{-1} \\
&= \sigma^2(\mathbf{X}^T\mathbf{X})^{-1}\mathbf{X}^T\mathbf{X}(\mathbf{X}^T\mathbf{X})^{-1} \\
&= \sigma^2(\mathbf{X}^T\mathbf{X})^{-1}
\end{aligned} \tag{B.18}$$

Weisburg [67] states that an estimate of σ^2 can be obtained as,

$$\hat{\sigma^2} = \frac{RSS}{n - p'} \tag{B.19}$$

were n is the number of observations in $\mathbf{Y}$ and therefore also the number of observations in $\mathbf{e}$, and $p' = p+1$, the number of predictor variables, p, plus the intercept. We may obtain an estimate of the covariance matrix of the regression coefficients by substituting our estimate of σ^2 into Equation B.18 which yields,

$$\widehat{\mathsf{Var}}(\hat{\boldsymbol{\beta}}) = \widehat{\boldsymbol{\Sigma}_{\hat{\boldsymbol{\beta}}}} = \hat{\sigma^2}(\mathbf{X}^T\mathbf{X})^{-1} \tag{B.20}$$

B.5 Coefficient of Determination, R^2

The coefficient of determination is a statistic which gives a measure of the proportion of the variability of Y explained by the regression on $\mathbf{X}$. The coefficient of determination is defined as,

$$\mathrm{R}^2 = 1 - \frac{\mathsf{Var}[\mathbf{e}]}{\mathsf{Var}[\mathbf{Y}]} = 1 - \frac{s^2_{\mathbf{e}}}{s^2_{\mathbf{Y}}} \tag{B.21}$$

where $s^2_{\mathbf{e}}$ is the sample variance of the residuals and $s^2_{\mathbf{Y}}$ is the sample variance of the response.

Appendix C

Estimation of Long-Term Extremes with IEC Environment

C.1 Introduction

In this appendix we consider a similar analysis of the estimation of the long-term distribution of extreme loads to that presented in Chapter 5 with two major differences. First, in the analysis that will be presented here the turbulence intensity is defined as the standard deviation of the 10-minute wind process rather than the coefficient of variation of the wind process. Second, the long-term description of the environment is derived from the IEC design code [23]. In particular we consider a site that conforms to the class IA standard.

C.2 Data Set

The data set used in this analysis is for the Atlantic Orient Corporation AOC 15/50 turbine, described in Chapter 1 (page 18). The turbine has a rotor diameter of 15m and a nominal rotor speed of 60 RPM at the rated wind speed of 12m/s. It is a three-bladed, fixed pitch turbine with a hub height of 25 meters [22]. The data set is described in detail in Chapter 3 (page 66) and consisted of multiple 10-minute simulations of Gaussian wind fields and corresponding blade root bending moments. The wind input processes is described by the hub-height wind speed. A plot of observed turbulence intensity, standard deviation of the hub-height wind process, versus observed 10-minute mean wind speed, calculated from the simulation data, for all 10-minute time histories is shown in Figure C.1.

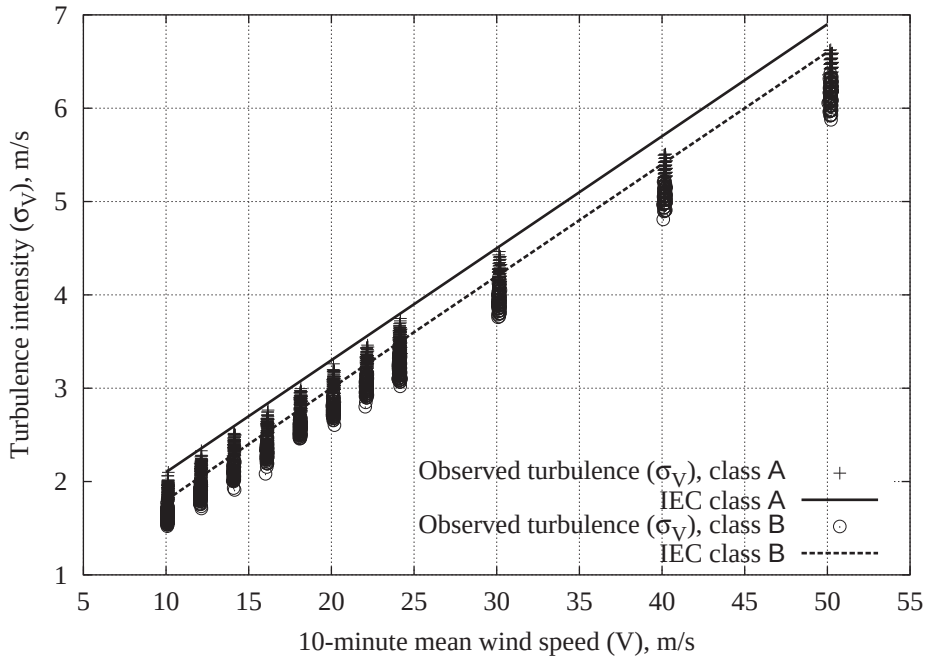

Figure C.1: 10-minute mean wind speed and turbulence intensity for 2400 10-minute Gaussian wind input processes.

C.3 Long-Term Analysis Based on Modeling Global Extremes

C.3.1 Short-Term Analysis

In this section we consider estimating the long-term distribution of extremes based on modeling the global peaks. The short-term conditional distribution of global peaks is modeled using the Gumbel model. To review, the load models discussed in Chapter 3 and considered again here, estimate the probability distribution of short-term extreme load ranges by preserving a limited set of statistical moments: $\mu_i = \mathsf{E}[Z^i]$ $(i = 1, 2)$ for the Gumbel model of global peaks, or $\mu_i = \mathsf{E}[Y^i]$ $(i = 1, 3)$ for the quadratic Weibull model of local peaks. In particular, in this section we will look at estimating the long-term distribution of extreme loads based on modeling the global peaks by a Gumbel model. This model is fit to the first two moments of the data. Separate regression analysis and long-term integration will be conducted. Later in Section C.4 we will consider estimating the long-term distribution of extreme loads by modeling the local peaks with a quartic Weibull model.

Chapter 3 showed how the statistical moments of the data could be related to the environmental variables: mean wind speed, V, and turbulence intensity, I, through the power-law relation we have

seen before [54]:

$$\mu_i = a_i \left(\frac{V}{V_{\text{ref}}} \right)^{b_i} \left(\frac{I}{I_{\text{ref}}} \right)^{c_i} \tag{C.1}$$

Where, V_{ref} is the reference 10-minute mean wind speed, and I_{ref} is the reference turbulence intensity.[1] This functional form and methodology are followed here again with some modification. In this case, with the definitions chosen for the environmental variables, mean and standard deviation of the 10-minute wind process, for 10-minute mean wind speed and turbulence intensity respectively, the variables are highly correlated, $\rho = 0.9911$. In order to avoid problems with the regression analysis due to highly correlated predictor variables a constrained regression analysis was performed. For constrained regression analysis, a simple linear regression of the statistics of the extreme load is performed on the first predictor variable, the 10-minute mean wind speed. The residuals are then in turn regressed on the second predictor variable, turbulence intensity. The issue with highly correlated predictor variables is that they tend to explain the same variability in the data. Following the procedure above, we prescribe the 10-minute mean wind speed to be the more important predictor variable and through the simple linear regression remove the variability explained by the 10-minute mean wind speed first. The second predictor variable is left to explain the variability which is left over, that portion of the variability it can explain that did not overlap (i.e. correlate) with the first predictor variable, which with highly correlated variables is generally very little. As a result the second predictor variable will play a less significant role than the first predictor variable.

The constrained linear regression analysis described above, applied to the logarithm of Equation C.1, yields point estimates of the coefficients. To demonstrate typical results, we pursue modeling the global extremes by a Gumbel model here; the alternate approach based on modeling the local peaks by a quadratic Weibull model in Section C.4. The V_{ref} and I_{ref} values for the operating conditions are 16.474m/s and 2.518m/s respectively. The corresponding V_{ref} and I_{ref} values for the parked conditions are 34.861m/s and 4.607m/s respectively. The calculated regression coefficients and R^2 statistics are shown in Tables C.1 and C.2 for flap and edge bending conditions respectively. R^2 statistics near unity indicate that a large percentage of the variability in the data is explained by the regression model. Low R^2 statistics indicate that other influences not contained in the regression model may be affecting the loads.

Finally, graphical regression results are shown in Figures C.2 and C.3 for blade root flap and edge bending respectively. Regression results for the mean and standard deviation of the maximum 10-minute flap bending moment versus 10-minute mean wind speed are shown in Figures C.2(a) and C.2(b). Corresponding results for edge bending are shown in Figures C.3(a) and C.3(b). In all plots the turbulence intensity has been set equal to, I_{ref}, the reference value.

[1] Recall that the turbulence intensity in this analysis is defined as the standard deviation of the 10-minute wind process, rather than the coefficient of variation as considered at times in previous chapters.

Blade Root Flap Bending
Regression of Statistics of 10-Minute Maximum on V and I

Mean of 10-Minute Maximum

	a (kN-m)	b	c	R^2
$V \leqq 24$m/s	25.6694	0.6090	0.0460	0.9233
$V > 24$m/s	40.1812	2.5137	0.01839	0.9979

Standard Deviation of 10-Minute Maximum

	a (kN-m)	b	c	R^2
$V \leqq 24$m/s	2.7765	0.7698	0.0287	0.9214
$V > 24$m/s	3.955	2.6841	0.0259	0.8713

Table C.1: Regression coefficients used in Equation C.1 to fit statical moments of blade root flap bending loads as functions of the mean wind speed, V, and turbulence intensity, I.

Blade Root Edge Loading
Regression of Statistics of 10-Minute Maximum on V and I

Mean of 10-Minute Maximum

	a (kN-m)	b	c	R^2
$V \leqq 24$m/s	8.6107	0.2693	0.0135	0.9718
$V > 24$m/s	7.2485	3.9850	0.0138	0.99602

Standard Deviation of 10-Minute Maximum

	a (kN-m)	b	c	R^2
$V \leqq 24$m/s	0.3049	1.6252	0.0739	0.9105
$V > 24$m/s	1.4264	3.3673	0.0232	0.8932

Table C.2: Regression coefficients used in Equation C.1 to fit statistical moments of blade root edge bending loads as functions of the mean wind speed, V, and turbulence intensity, I.

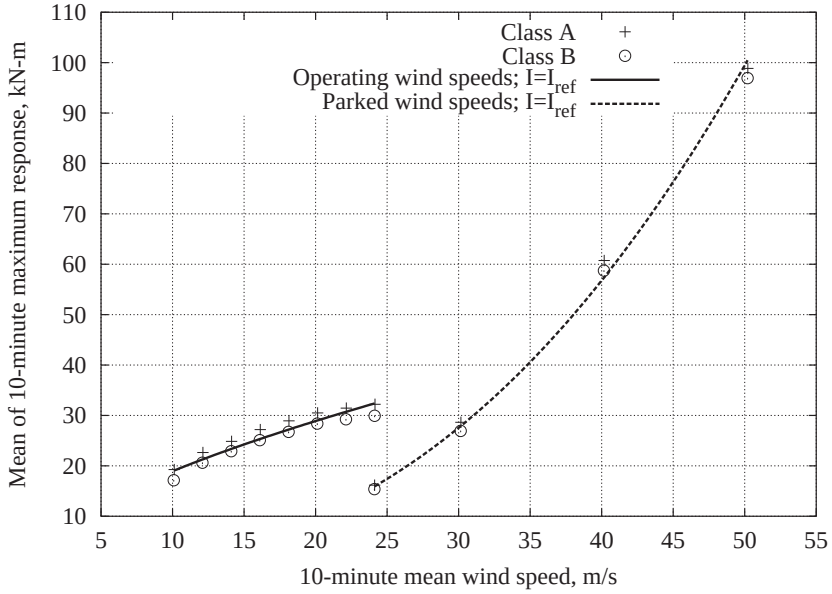

(a) Regression of the mean of 10-minute maxima on the 10-minute mean wind speed and turbulence intensity.

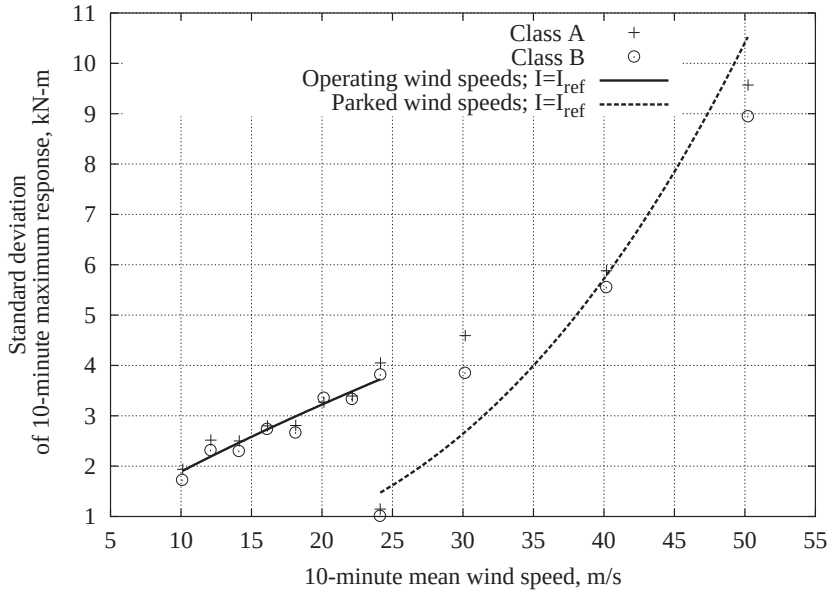

(b) Regression of the standard deviation of 10-minute maxima on the 10-minute mean wind speed and turbulence intensity.

Figure C.2: Regression of the moments of 10-minute maximum on the 10-minute mean wind speed and turbulence intensity for blade root flap bending.

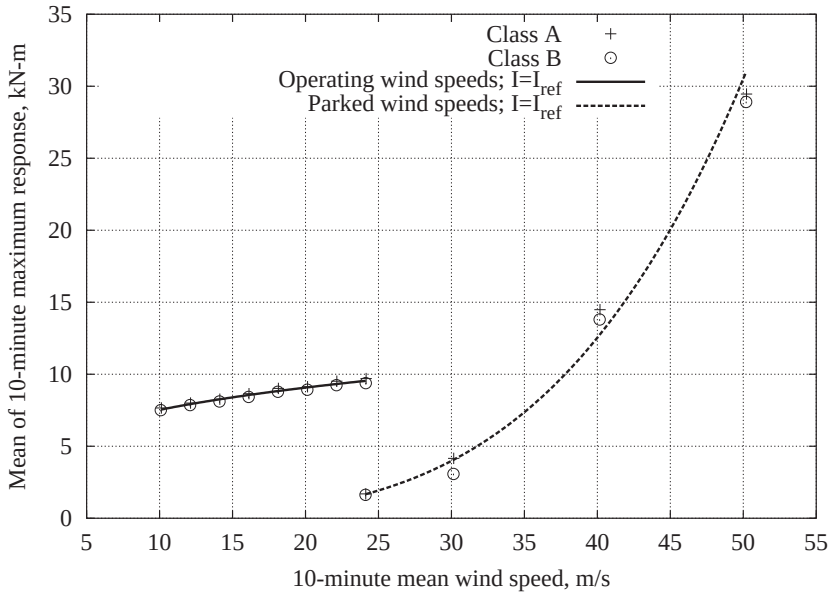

(a) Regression of the mean of 10-minute maxima on the 10-minute mean wind speed and turbulence intensity.

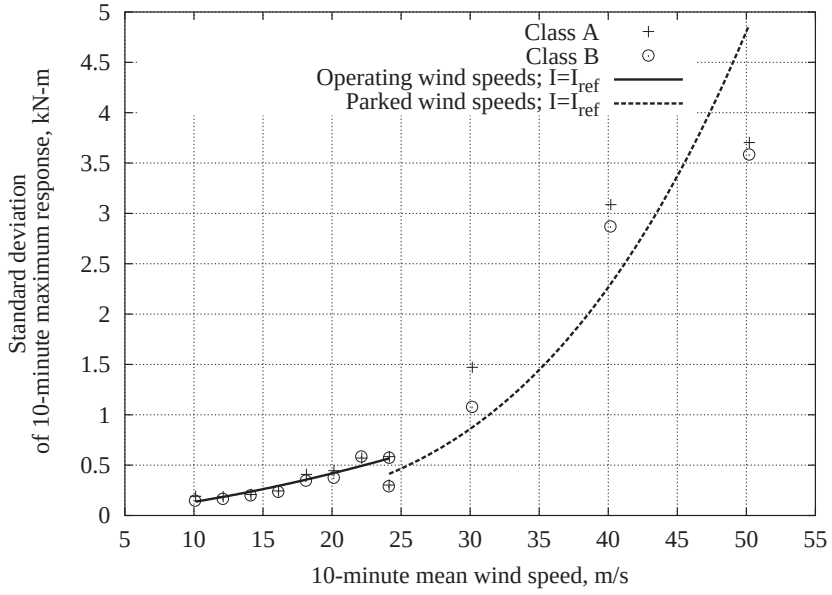

(b) Regression of the standard deviation of 10-minute maxima on the 10-minute mean wind speed and turbulence intensity.

Figure C.3: Regression of the moments of 10-minute maximum on the 10-minute mean wind speed and turbulence intensity for blade root edge bending.

C.3.2 Long-term Analysis

For the discussion here, we defined the conditional short-term probability distribution of global peaks by a Gumbel model. Further, the moments of the global peaks have been related to the environmental variables through regression analysis.

The long-term distribution of extreme loads, in an arbitrary 10-minute period, is found in the same way as described in Section 3.4.2; by performing the integration below,

$$F_L(l) = \iint F_{L|V,I}(l|v,i) f_{V,I}(v,i) dv di \tag{C.2}$$

Where, $F_{L|V,I}(l|v,i)$, is the short-term conditional distribution of extreme loads, and $f_{V,I}(v,i)$, the joint density function of the environmental variables.

We will assume that the AOC 15/50 turbine is installed at a site with environmental conditions conforming to a IEC class IA site. The description of the environmental variables is based on the criteria given in the IEC wind energy safety code for a class IA environment [23]. Specifically, the annual distribution of the 10-minute mean wind speed, V, is given by the Rayleigh distribution shown below, with μ_V=10m/s.

$$f_V(v) = \frac{2v}{\alpha^2} \exp\left[-\left(\frac{v}{\alpha}\right)^2\right] \tag{C.3}$$

$$\alpha = \frac{2\mu_V}{\sqrt{\pi}}$$

The standard deviation of the 10-minute wind process is taken as the measure of wind turbulence intensity. The conditional distribution of turbulence intensity is assumed to follow the lognormal distribution shown below.

$$f_{I|V}(i|v) = \frac{1}{\sqrt{2\pi}\zeta i} \exp\left[-\frac{1}{2}\left(\frac{\ln(i)-\lambda}{\zeta}\right)^2\right] \tag{C.4}$$

The parameters of the lognormal distribution, λ and ζ, are defined as:

$$\zeta = \sqrt{\ln(\delta_{I|V}^2 + 1)} \tag{C.5}$$

$$\lambda = \ln(\mu_{I|V}) - \frac{1}{2}\zeta^2 \tag{C.6}$$

with, $\delta_{I|V}$, the conditional coefficient of variation given as:

$$\delta_{I|V} = \frac{\sigma_{I|V}}{\mu_{I|V}} \tag{C.7}$$

The functions of conditional mean, $\mu_{I|V}$, and standard deviation, $\sigma_{I|V}$, of the turbulence are given by the IEC wind energy safety code [23]. For turbulence class A, I_{15}=0.18 and a=2.

$$\mu_{I|V} = \frac{I_{15}(15\text{m/s} + av)}{(a+1)} - 2\text{m/s}\, I_{15} \tag{C.8}$$

$$\sigma_{I|V} = 2\text{m/s}\, I_{15} \tag{C.9}$$

A plot of the joint density function of the environmental variables is shown in Figure 4.1 (Chapter 4).

The ranges of values of the environmental variables are discretized into evenly spaced intervals. For each pair of values of the environmental variables the corresponding short-term distribution of the extreme load is generated. Then, per Equation C.2, the short-term conditional fatigue range distributions are summed together each weighted by the probability of the respective environmental condition, i.e., pair of values of the environmental variables occurring. The summation is performed over the entire domain of environmental variables.

As stated earlier, there are two loading conditions for the turbine, operating and parked. During normal use the turbine is operating for wind speeds less than 24m/s and parked for wind speeds greater than 24m/s. In this case to develop the long-term distribution the appropriate regression model is used for each wind speed value. This results in a combination of the operating and parked only long-term distributions as shown in Figure C.4. Also shown in the figure are the long-term distributions of the load if the turbine is either parked or operating in all wind speeds. The probability levels associated with the one-year and 50-year mean return period (MRP prob. level) are also shown (note Equations 3.13 and 3.14). In all of the preceeding cases it was assumed there was 100% availability of the turbine during all winds speeds. It would require only minor modification to the procedures developed here to include the condition when the turbine was available for only a portion of the time for a given wind environment. Using the full distribution for each of the random variables, estimates for the one-year flap and edge bending load are 52.4kN-m and 12.3kN-m respectively. Correspondingly estimates for the 50-year flap and edge bending load are 74.3kN-m and 19.3kN-m respectively.

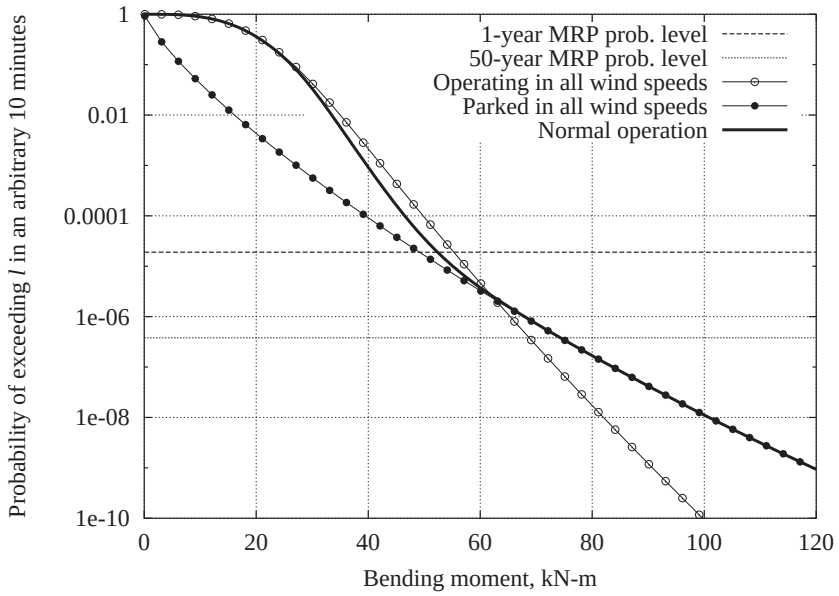

(a) Long-term distribution of extreme blade root flap bending moment for an arbitrary 10 minutes.

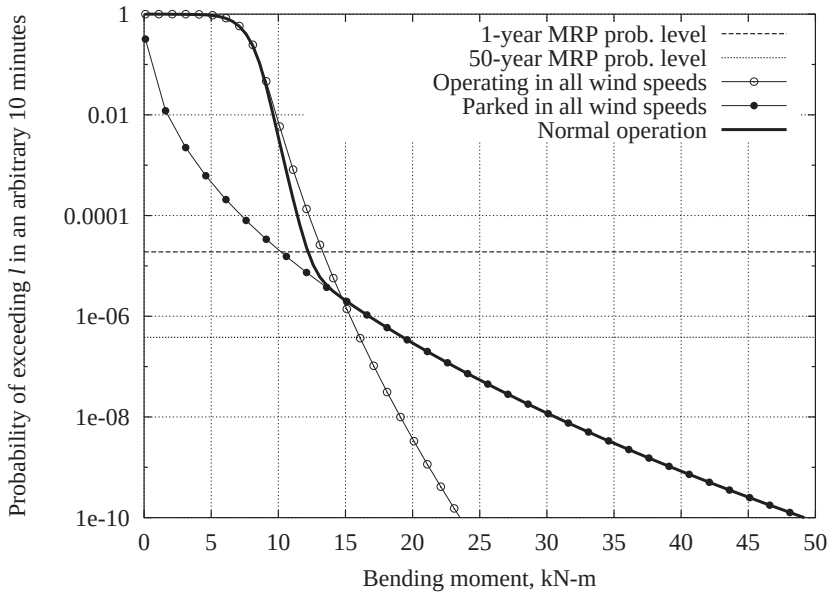

(b) Long-term distribution of extreme blade root edge bending moment for an arbitrary 10 minutes.

Figure C.4: Long-term distributions of 10-minute extreme blade root bending moment, $L_{10\,\mathrm{min}}$, considering three turbine conditions: 1) turbine operating over all wind speeds, 2) turbine parked over all wind speeds, 3) turbine operating below cutout wind speed and parked above cutout wind speed; for both: (a) flap and (b) edge bending.

C.3.3 Simplifying the Long-term Analysis

In this section a methodology for simplifying the calculations required for solving Equation C.2 is presented. The full distributions of some of the random variables are replaced with appropriate deterministic fractiles, thereby reducing the number of numerical integrations required to be performed. It is appropriate to consider this methodology for those random variables which have only a small contribution to the overall variability in our estimate of the long-term extreme load distribution. Here a qualitative analysis is employed to determine the degree to which each of the variables in Equation C.2 contributes to the long-term extreme load distribution. Further based on this analysis we present how an appropriate deterministic fractile of, for example, the short-term load distribution, the conditional distribution of turbulence intensity or both, may be used, instead of their full distributions.

We investigate such simplifications further in the remainder of this section. Figure C.5 shows the long-term distribution of the 10-minute flap and edge loads for three cases that consider, in turn, the short-term load variable and each of the environmental variables deterministically. Only one variable is considered deterministic in each analysis, the other variables are assumed random and to follow the distributions defined previously. These three analyzes give a qualitative understanding of how the terms in Equation C.2 contribute to the variability in the long-term load distribution. From this analysis one finds that the considering the turbulence intensity deterministic does not affect the results at all. This is not completely unexpected and is a result of the constrained regression. We saw from the regression analysis that very little of the variability in the data, which was not already explained by the wind speed, was explained by the turbulence intensity. Therefore, we should not expect the turbulence to play much of a role in the long-term distribution of the extreme response. The largest drop in our estimate of the 50-year load did occur, however, when we set the wind speed variability to zero. Whereas reducing the variability in the short-term load did not reduce our estimate of the 50-year load as drastically. Qualitatively, one can conclude that, less of the variability in the long-term load distribution is explained by the randomness in the short-term load, than by the variability in wind speed, for the structure, site data, and distribution models used here.

From this analysis, we may consider using prescribed fractiles of the distribution of the short-term load. In this case, Figure C.6(a) shows the results of considering the short-term load deterministic, but using the 86% fractile of the distribution rather than the mean value. Using the 86% fractile of the load distribution results in estimates of the one-year and 50-year blade root flap bending load of 52.1kN-m and 76.9kN-m respectively with associated errors of 0.5% and 3.5%, respectively. In Figure C.6(b) we see that using the 74% fractile of the short-term load distribution results in an estimate of the 50-year blade root edge bending load of 18.8kN-m with an associated error of 2.5%. The fractile must be increased to the 90% fractile of the short-term load distribution to obtain an

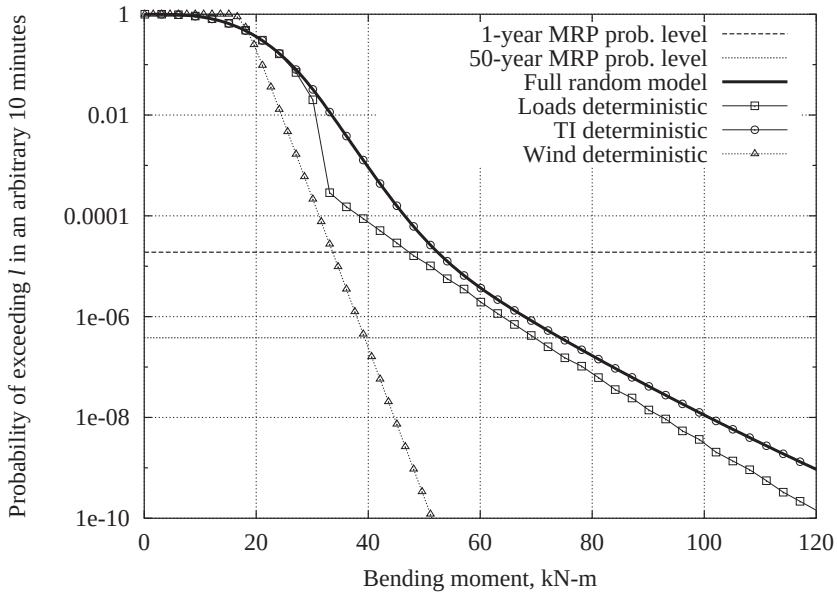

(a) Long-term distribution of extreme blade root flap bending moment for an arbitrary 10 minutes.

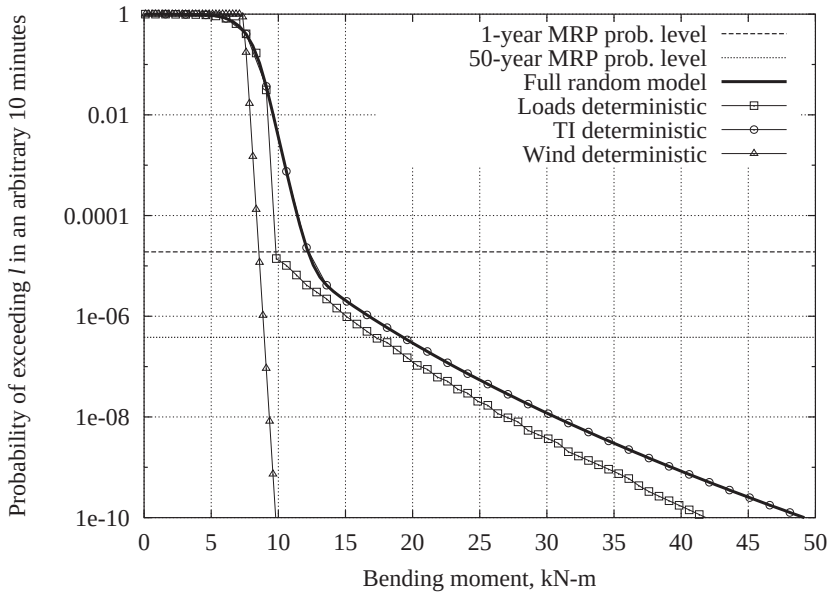

(b) Long-term distribution of extreme blade root edge bending moment for an arbitrary 10 minutes.

Figure C.5: Long-term distributions of 10-minute extreme blade root bending moment $L_{10\,\mathrm{min}}$, considering load, turbulence intensity, and wind speed deterministically for both: (a) flap and (b) edge bending.

estimate of the one-year blade root edge bending load of 11.8kN-m with an associated error of 4.1%.

Considering the short-term load deterministic simplifies Equation C.2 to a single fold integration problem over only the distribution of annual wind speed. The results of this integration are shown in Figure C.6. In this case, additionally, we can eliminate the remaining integration by using the complementary cumulative distribution function of the annual wind speed distribution and then evaluate the expression at the wind speed associated with the return period of interest.

C.3.4 Summary

In this section, we obtained an estimate of the marginal probability distribution of the long-term load. This was accomplished by modeling the global peaks by a Gumbel distribution for the conditional short-term load. The statistical moments of the global peak data were related to the environmental variables by a power-law functional form. The parameters of the functional form were obtained through regression analysis. Using the method of moments, a Gumbel distribution could be obtained for each specific set of values of the environmental variables. Finally, an estimate of the marginal distribution of the long-term load was obtained by summing the conditional short-term load distributions over all environmental conditions. Each conditional short-term load distribution was weighted by the probability of the associated environmental condition occurring. We found from this analysis that the estimate of the one-year and 50-year blade root flap bending loads were 52.1kN-m and 74.3kN-m respectively. Correspondingly, the one-year and 50-year blade root edge bending loads were 12.3kN-m and 19.3kN-m, respectively.

We then under took a qualitative, yet systematic, analysis to determine which of the three variables—conditional short-term load, conditional turbulence, or mean wind speed—contributed the most to the variability in the distribution of the long-term load. We found that at least for the AOC 15/50 turbine, site data, and distribution models used here the wind speed distribution of the loads contributed the most to the variability in the distribution of the long-term load, with the conditional short-term load contributing less. The turbulence intensity variable was essentially tuned out by the constrained regression analysis. We found that by treating the conditional short-term load deterministic, and considering fractiles higher than the mean, much of the contribution to the variability in the distribution of the long-term load could be recovered. Specifically, considering the 86% fractile of the distribution of the conditional short-term load, our estimates of the one-year and 50-year blade root flap bending loads are 0.5% and 3.5% high respectively, over our estimates employing the full distributions. For blade root edge bending, considering the 74% fractile of the conditional short-term load distribution, our estimate of the 50-year root edge bending load is 2.5% low. We needed to consider the 90% fractile of the conditional short-term load distribution for an estimate of the one-year root edge bending load that was 4.1% low. The next sections presents a

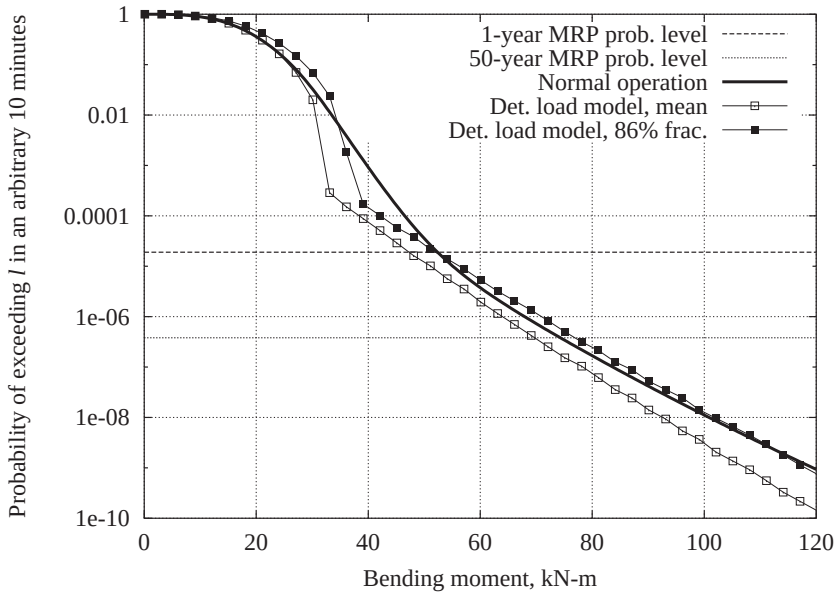

(a) Long-term distribution of extreme blade root flap bending moment for an arbitrary 10 minutes.

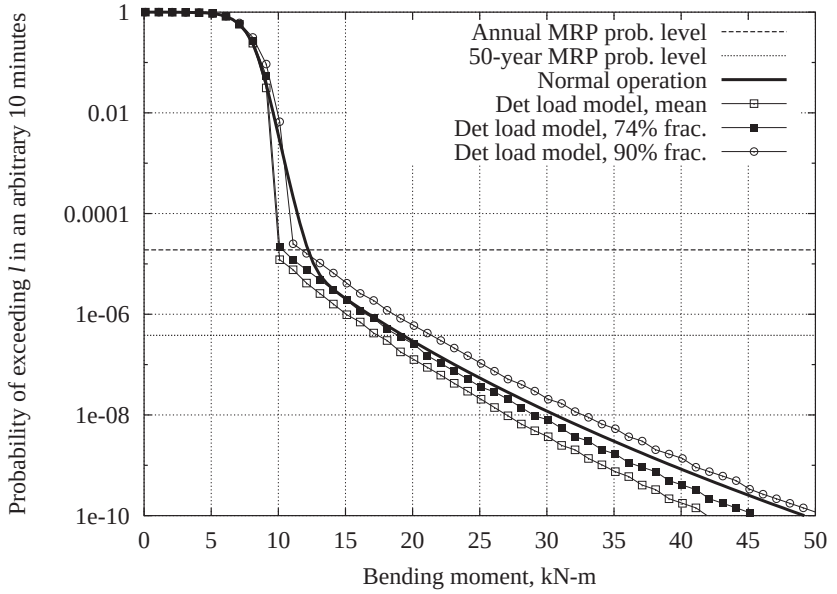

(b) Long-term distribution of extreme blade root edge bending moment for an arbitrary 10 minutes.

Figure C.6: Long-term distributions of 10-minute extreme blade root bending moment, $L_{10\ \mathrm{min}}$, considering the short-term load at prescribed deterministic levels compared with the full distribution solution.

similar analysis, only this time the short-term loads are based on modeling the random peaks with a quadratic Weibull distribution.

C.4 Long-Term Analysis Based on Modeling Local Peaks

C.4.1 Short-Term Analysis

In the previous section, we obtained an estimate of the marginal long-term distribution of $L_{10\,\text{min}}$ from a short-term conditional loads model fit to Z, the global extreme over the duration of a 10-minute response time history. In this section an estimate of the marginal long-term distribution of $L_{10\,\text{min}}$ is found following a similar procedure. In this case, however, a quadratic Weibull model for the short-term conditional load is fit to, Y, the random local peaks of a 10-minute response time history, see Section 1.5.5.

Peaks of the response time histories where found based on the definition provided in Chapter 2, the largest value of the time history between successive up-crossings of its mean level. The process mean level and number of peaks were calculated for all blade root flap and edge bending response time histories. For each pair of environmental variables (e.g., V=10m/s and I=class A) the 100 observations of process mean or number of peaks were pooled together and the mean of these pooled observations was reported. A 4.75kN-m threshold was imposed on the edge bending response data for operating conditions only, to provide a better fit of the quadratic Weibull to data. Statistics other than the process mean that describe the blade root edge bending response from operating conditions are based only on the peaks above this threshold.

In the previous section the statistical moments of the data were related to the environmental variables by the power-law model given in Equation C.1, the same methodology is used again, here. When obtaining a long-term estimate of the 50-year load based on a short-term distribution which models the local peaks, two parameters and three statistical moments are required. In Section C.3, where the short-term distribution modeled the global peaks, only the relationships between two statistical moments and the environmental variables were required. In this case, we need the relationship between the environment and two other parameters in addition to the statistical moments required to fit the probabilistic model. These two additional parameters in this case are: the number of local peaks and the process mean.

The same values of V_{ref} and I_{ref} defined in Section C.3 were used for this analysis. The V_{ref} and I_{ref} values for the operating conditions are 16.474m/s and 2.518m/s, respectively and the corresponding values for the parked conditions are 34.861m/s and 4.607m/s, respectively. The calculated regression coefficients and R^2 statistics, calculated from constrained regression analysis, are shown

in Tables C.3 and C.4 for both blade root flap and edge bending conditions, respectively. R^2 statistics near unity indicate that a large percentage of the variability in the data is explained by the regression model. Low R^2 statistics indicate that other influences not contained in the regression model may be affecting the loads. In performing the regression analysis it was determined that the applied functional model, Equation C.1, did not have enough flexibility to sufficiently model the observed behavior of the mean and standard deviation of the local blade root flap bending peaks. The values of the mean and standard deviation of the peaks flatten out with higher wind speeds above 17m/s as compared with the behavior below 17m/s as seen in Figures C.9 and C.10. Therefore a separate model was fit to each of these regions, one below 17m/s and the other above 17m/s, for both the mean and standard deviation of local blade root flap bending peaks.

Finally, graphical regression results are shown in Figures C.7-C.11. Each figure contains regression results for both blade root flap and edge bending conditions considering: process mean, Figure C.7; number of peaks, Figure C.8; mean of local peaks, Figure C.9; standard deviation of local peaks, Figure C.10; and skewness of local peaks, Figure C.11. In all plots, the turbulence intensity has been set equal to the reference value.

C.4.2 Long-term Analysis

For the discussion here, we defined the conditional short-term probability distribution of local peaks by a quadratic Weibull model. Further, the moments of the local peaks and parameters have been related to the environmental variables through regression analysis.

The long-term distribution of extreme loads, in an arbitrary 10-minute period is found in the same way as described in Section C.3.2. We will again assume that the AOC 15/50 turbine is installed at a site with environmental conditions conforming to a IEC class IA site, described in Section C.3.2. The long-term distribution of the 10-minute mean wind speed is assumed to follow a Rayleigh distribution with mean, $\mu_V = 10$m/s. The conditional distribution of turbulence is given by a lognormal distribution with conditional mean and standard deviation given by Equations C.8 and C.9, respectively. A plot of the joint density function of the environmental variables is shown in Figure 4.1 (Chapter 4).

The ranges of values of the environmental variables are discretized into evenly spaced intervals. For each pair of values of the environmental variables the corresponding short-term local peak distribution is generated. Through Equation 3.23, an estimate of the distribution of short-term extreme events, $P[L_{10\,\text{min}} < l|V, I]$, is obtained. The process mean and any required additional threshold are re-introduced. Then as per Equation C.2 the short-term extreme load distribution values are summed together each weighted by the probability of the respective environmental conditions, i.e., the pair of values of the environmental variables occurring. The summation is performed over the

Blade Root Flap Loading
Regression of Statistics of Random Peaks on V and I

Mean of 10-Minute Response Process

	a (kN-m)	b	c	R^2
$V \leqq 24$m/s	3.0234	1.6105	-0.0022	0.95250
$V > 24$m/s	13.7605	1.8909	-0.0013	0.99855

Expected Number of Random Peaks

	a (kN-m)	b	c	R^2
$V \leqq 24$m/s	800	0.2163	-0.0095	0.70233
$V > 24$m/s	1700	2.3252	-0.0212	0.98381

Mean of Random Peaks

	a (kN-m)	b	c	R^2
$V \leqq 17$m/s	3.950	0.7021	0.1877	0.84633
$17 < V \leqq 24$m/s	4.6571	0.0850	0.2609	0.26266
$V > 24$m/s	4.0833	3.7348	0.0118	0.99099

Standard Deviation of Random Peaks

	a (kN-m)	b	c	R^2
$V \leqq 17$m/s	3.500	0.7327	0.18203	0.85968
$17 < V \leqq 24$m/s	4.1934	0.0600	0.2548	0.25144
$V > 24$m/s	3.8721	3.1545	0.0191	0.98368

Coefficient of Skewness of Random Peaks

	a (kN-m)	b	c	R^2
$V \leqq 24$m/s	1.2745	-0.0365	-0.0071	0.07286
$V > 24$m/s	215.3	-1.2905	0.0039	0.95904

Table C.3: Regression coefficients used in Equation C.1 to fit flap load moments as functions of the mean wind speed, V, and turbulence intensity, I.

Blade Root Edge Loading
Regression of Statistics of Random Peaks on V and I

Mean of 10-Minute Response Process

	a (kN-m)	b	c	R^2
$V \leqq 24$m/s	2.4066	0.3613	-0.0053	0.95099
$V > 24$m/s	0.7327	1.8043	-0.0013	0.99596

Expected Number of Random Peaks

	a (kN-m)	b	c	R^2
$V \leqq 24$m/s	104	-0.1581	0.1445	0.05724
$V > 24$m/s	2927	0.8485	-0.0201	0.87987

Mean of Random Peaks

	a (kN-m)	b	c	R^2
$V \leqq 24$m/s	0.2697	0.5587	0.0734	0.81101
$V > 24$m/s	0.8038	4.2402	0.0087	0.99785

Standard Deviation of Random Peaks

	a (kN-m)	b	c	R^2
$V \leqq 24$m/s	0.2699	0.8794	0.0708	0.91066
$V > 24$m/s	0.8244	4.3343	0.014649	0.99645

Coefficient of Skewness of Random Peaks

	a (kN-m)	b	c	R^2
$V \leqq 24$m/s	1.7613	0.68540	0.0077871	0.85539
$V > 24$m/s	1.9343	-0.0143	0.0077	0.04407

Table C.4: Regression coefficients used in Equation C.1 to fit edge load moments as functions of the mean wind speed, V, and turbulence intensity, I.

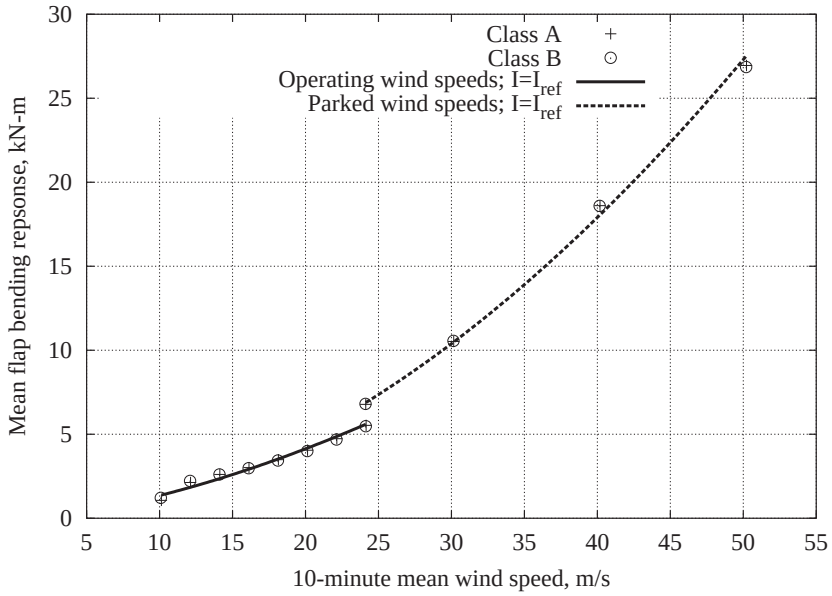

(a) Regression of the process mean of 10-minute blade root flap bending response on the 10-minute mean wind speed and turbulence intensity.

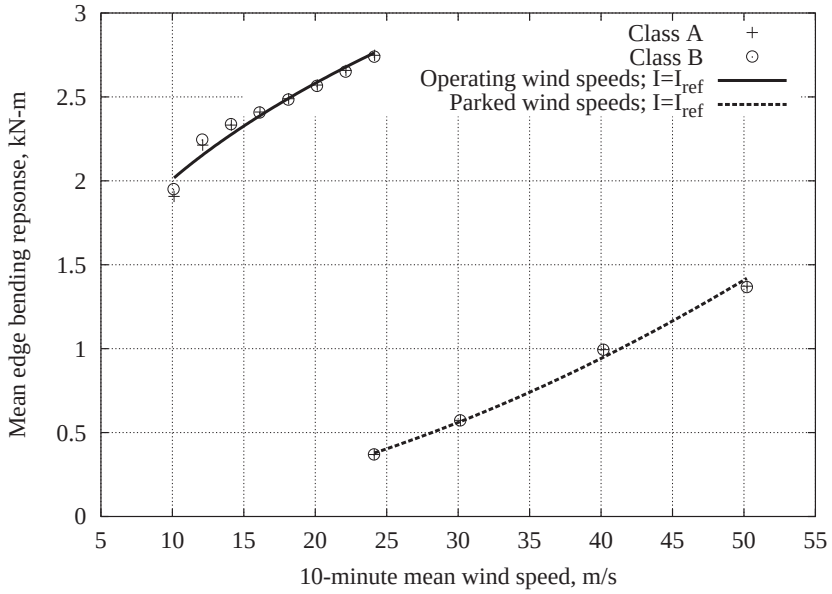

(b) Regression of the process mean of 10-minute blade root edge bending response on the 10-minute mean wind speed and turbulence intensity.

Figure C.7: Regression of the process mean on the 10-minute mean wind speed and turbulence intensity for blade root flap and edge bending.

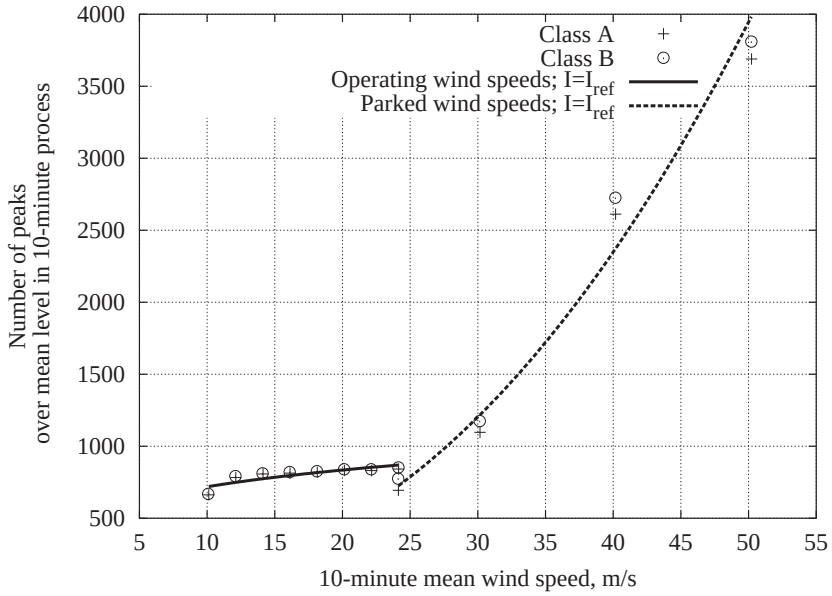

(a) Regression of the expected number of local peaks on 10-minute mean wind speed and turbulence intensity, blade root flap bending.

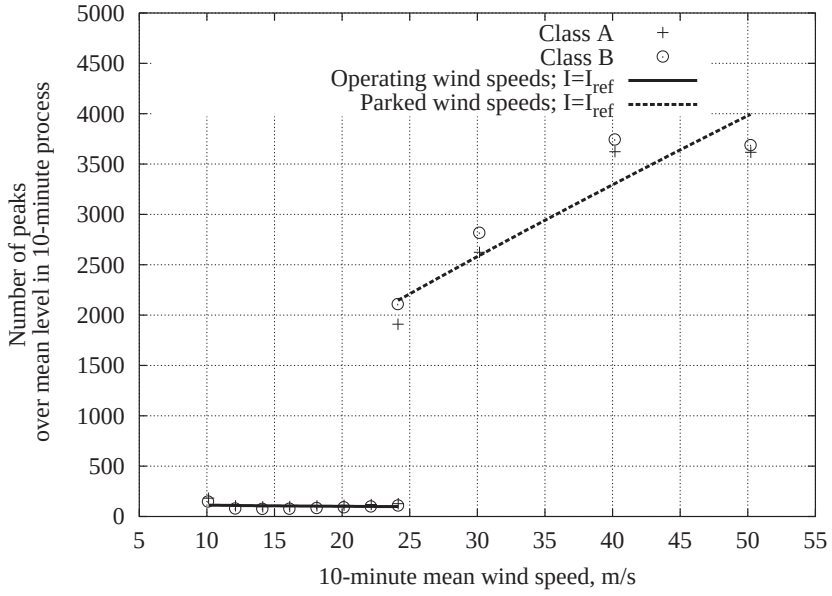

(b) Regression of the expected number of local peaks on 10-minute mean wind speed and turbulence intensity, blade root edge bending.

Figure C.8: Regression of the expected number of local peaks on 10-minute mean wind speed and turbulence intensity for blade root flap and edge bending.

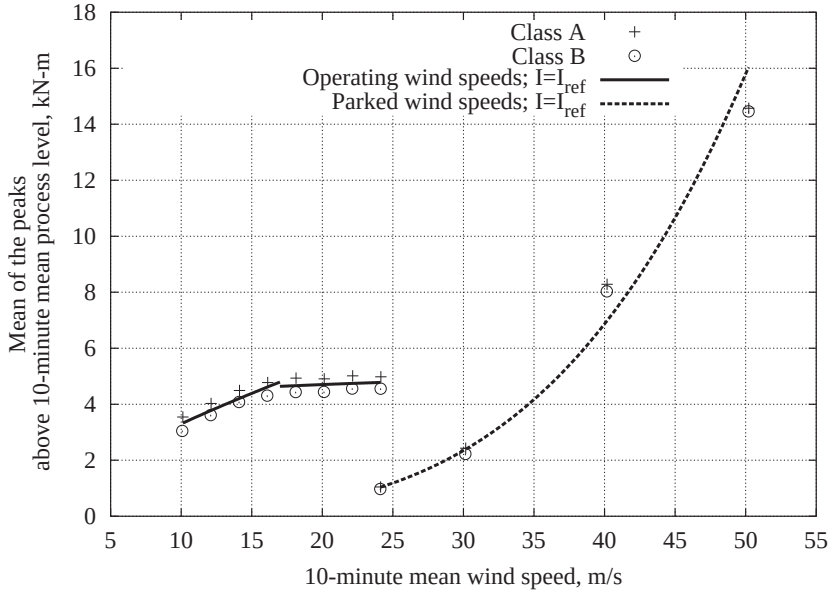

(a) Regression of the mean of the local peaks on the 10-minute mean wind speed and turbulence intensity, blade root flap bending.

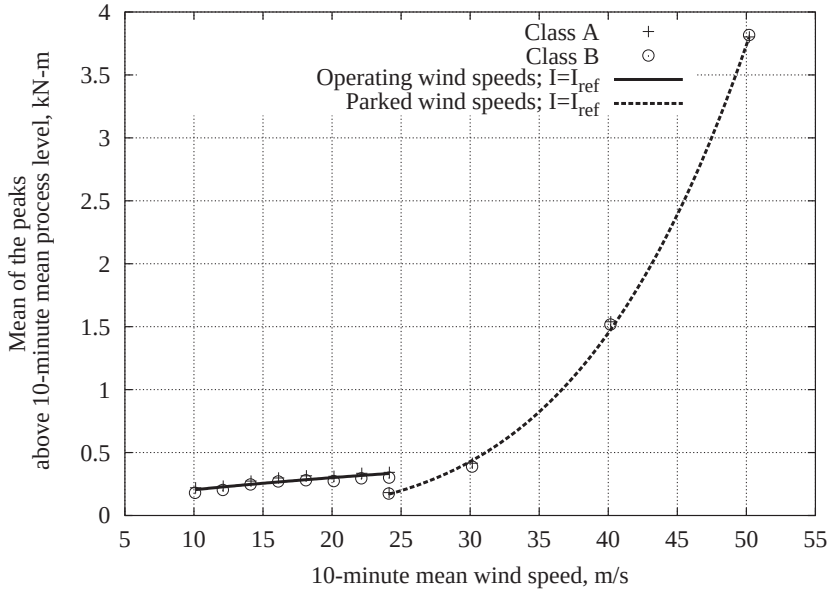

(b) Regression of the mean of the local peaks on the 10-minute mean wind speed and turbulence intensity, blade root edge bending.

Figure C.9: Regression of the mean of the local peaks on the 10-minute mean wind speed and turbulence intensity for blade root flap and edge bending.

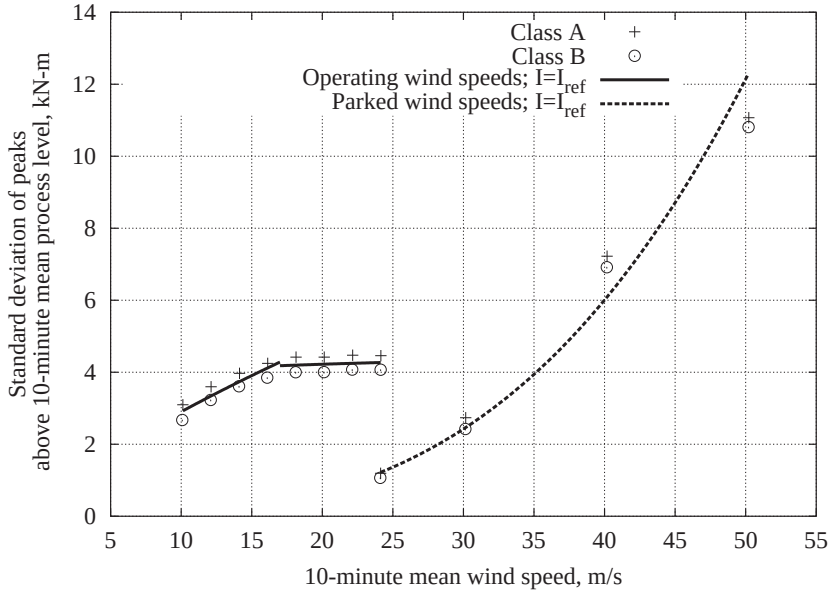

(a) Regression of the standard deviation of the local peaks on the 10-minute mean wind speed and turbulence intensity, blade root flap bending.

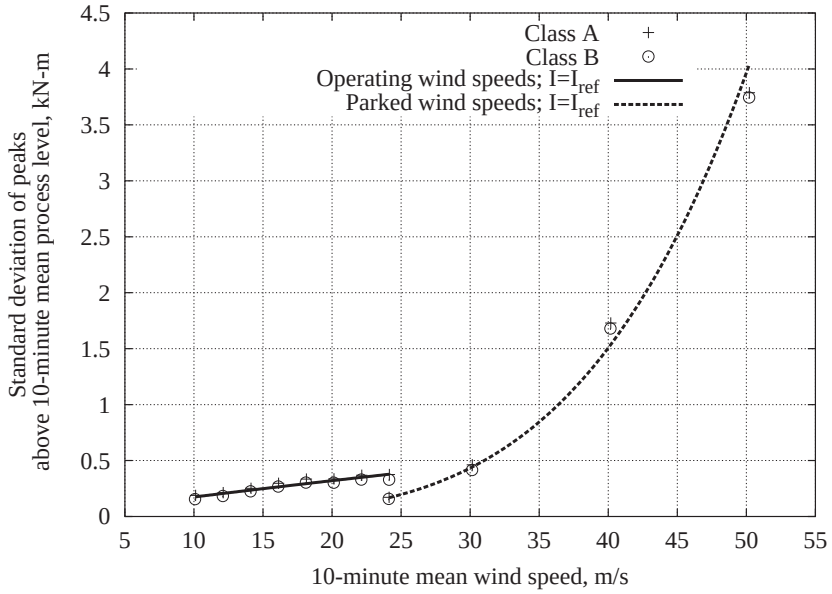

(b) Regression of the standard deviation of the local peaks on the 10-minute mean wind speed and turbulence intensity, blade root edge bending.

Figure C.10: Regression of the standard deviation of the local peaks on the 10-minute mean wind speed and turbulence intensity for blade root flap and edge bending.

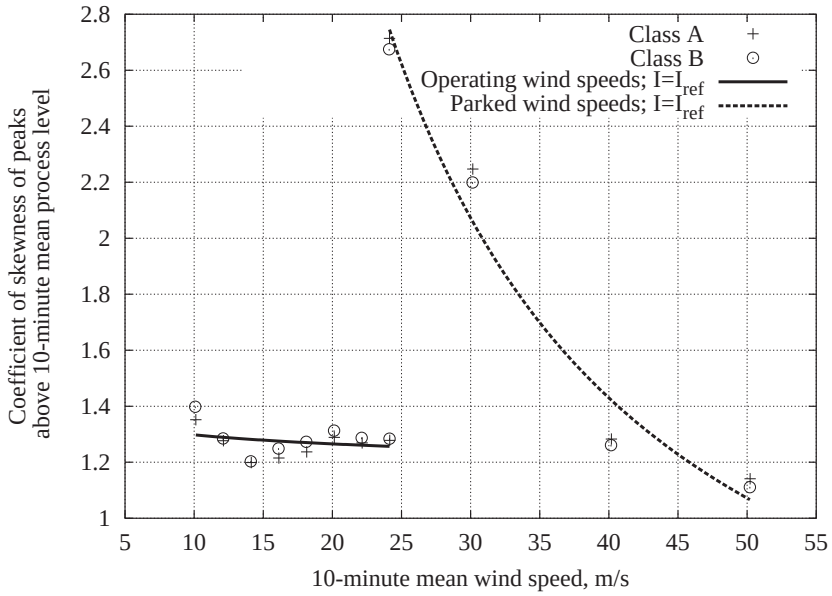

(a) Regression of the coefficient of skewness of the local peaks on the 10-minute mean wind speed and turbulence intensity, blade root flap bending.

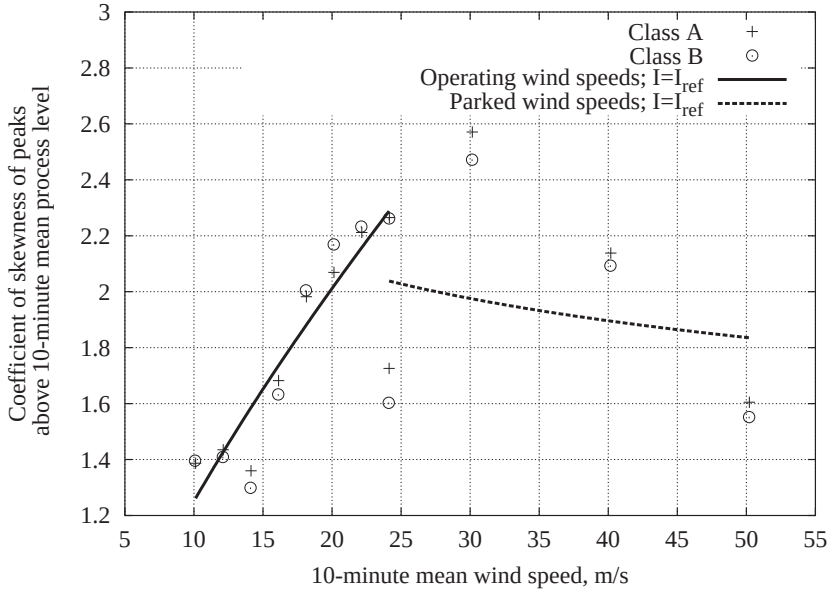

(b) Regression of the coefficient of skewness of the local peaks on the 10-minute mean wind speed and turbulence intensity, blade root edge bending.

Figure C.11: Regression of the coefficient of skewness of the local peaks on the 10-minute mean wind speed and turbulence intensity for blade root flap and edge bending.

entire range of environmental variables.

As stated earlier, there are two loading conditions for the turbine, operating and parked. During normal use the turbine is operating for wind speeds less than 24m/s and parked for wind speeds greater than 24m/s. In this case to develop the long-term distribution the appropriate regression model is used for each wind speed value. This results in a combination of the operating and parked only long-term distributions as shown in Figure C.12. Also shown in the figure are the long-term distributions of the load if the turbine is either parked or operating in all wind speeds. The probability levels associated with the one-year and 50-year mean return period (MRP prob. level), are shown (note Equations 3.13 and 3.14). In all of the preceeding cases it was assumed there was 100% availability of the turbine during all winds speeds. It would require only minor modification to the procedures developed here to include the condition when the turbine was available for only a portion of the time for a given wind environment. Using the full distribution for each of the random variables, estimates for the one-year blade root flap and edge bending loads are 51.9kN-m and 12.0kN-m, respectively. Corresponding estimates for the 50-year blade root flap and edge bending loads are 76.7kN-m and 20.0kN-m, respectively

C.4.3 Simplifying the Long-term Analysis

In this section, we consider simplifying the calculations required for solving Equation 3.16, by replacing the full distributions of some of the random variables with appropriate deterministic fractiles. As seen previously, Section C.3.3 it is appropriate to consider this methodology for those random variables which have only a small contribution to the overall variability in our estimate of the long-term extreme load distribution. Here, a qualitative analysis is employed to determine the degree to which each of the variables in Equation C.2 contributes to the long-term extreme load distribution.

Figure C.13 shows the long-term distribution of the 10-minute flap and edge loads considering the short-term load variable and each of the environmental variables deterministically. Only one variable is considered deterministic in each analysis, the other variables are assumed random and follow the distributions defined previously. This analysis gives a qualitative understanding on how the terms in Equation C.2 contribute to the variability in the long-term load distribution. From this analysis one finds that the largest drop in our estimate of the 50-year load to occur when we set the short-term load variability to zero. Whereas, reducing the variability in the wind speed does not reduce our estimate of the 50-year load as drastically. We found the opposite result in the analysis presented in Section C.3. The turbulence intensity variable was essentially tuned out by the constrained regression analysis. Qualitatively one can conclude that compared to the short-term load less of the variability in the long-term load distribution is explained by the randomness in the

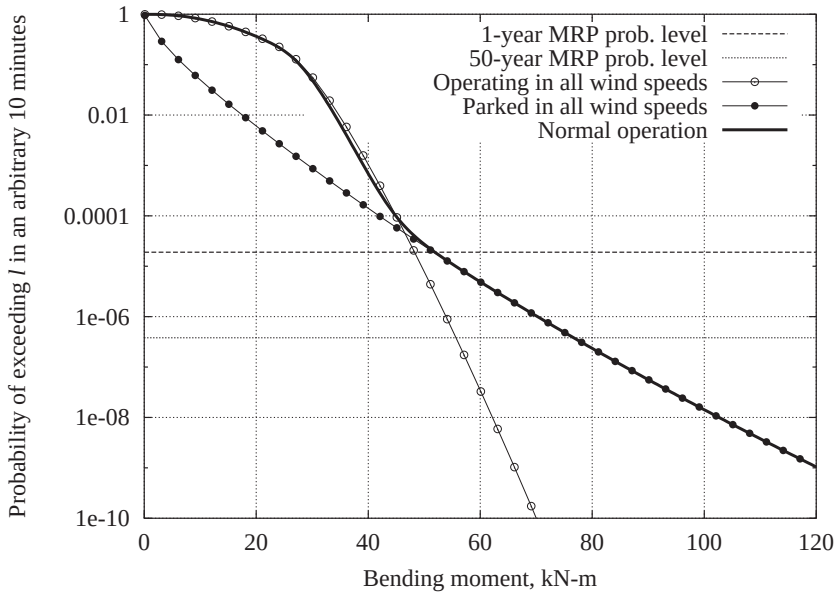

(a) Long-term distribution of extreme blade root flap bending moment for an arbitrary 10 minutes.

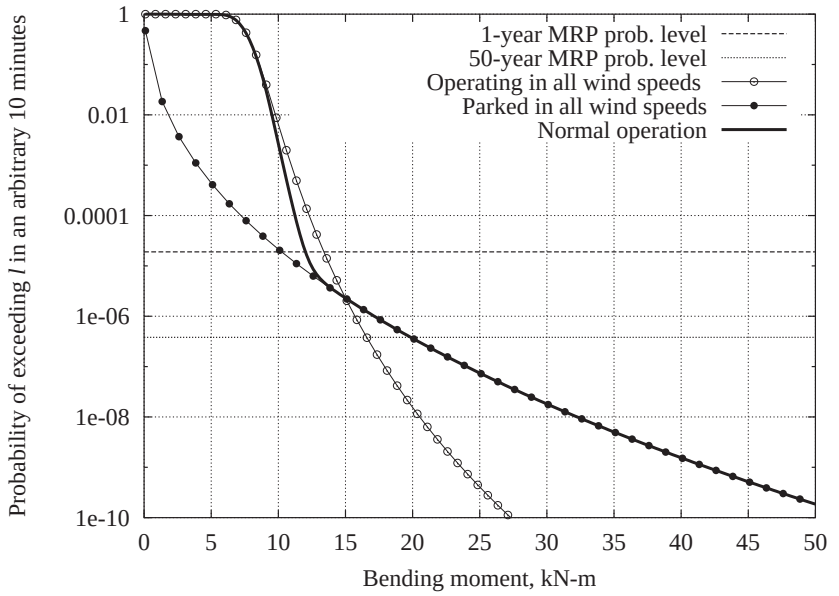

(b) Long-term distribution of extreme blade root edge bending moment for and arbitrary 10 minutes.

Figure C.12: Long-term distributions of 10-minute extreme blade root bending moment, $L_{10\,\mathrm{min}}$, considering three turbine conditions: 1) turbine operating over all wind speeds, 2) turbine parked over all wind speeds, 3) turbine operating below cutout wind speed and parked above cutout wind speed; for both blade root (a) flap and (b) edge bending.

wind speed, at least for the structure, site data, and distribution models used here.

Following the methodology previously presented, we consider using a higher fractile of the wind speed distribution where we may be able to recover the associated contribution to the long-term load variability, and still reduce the computational effort in calculating the marginal distribution of $L_{10\,\mathrm{min}}$. Figure C.14 shows that even by considering the 99% fractile of the wind speed distribution we are unable to recover the variability contributed by the the wind speed, for flap bending. If we consider edge bending using the 95% fractile of the wind speed distribution, rather than the mean value, we are able to recover a reasonable estimate, of about 11.8kN-m, for the one-year load. This is 1.6% different compared to the result from the full random model. Again, however, even with the 99% fractile of the wind speed distribution we are unable to recover a reasonable estimate of the 50-year edge bending load.

Figure C.15(a) shows the results for flap bending considering, alternatively, the short-term load deterministic, but using the fractile associated with the mean increased by six standard deviations of the distribution rather than just its mean value. The estimates of the one-year and 50-year loads are 49.8kN-m and 77.1kN-m, respectively. These estimates have associated errors of 4.1% and 0.6% compared with the results of the full random model. Correspondingly, Figure C.15(b) shows the results for blade root edge bending if we consider the fractile associated with the mean increased by 8 standard deviations. Our estimates of the one-year and 50-year blade root edge bending loads are 10.7kN-m and 20.3kN-m, respectively. These estimates have associated errors of 11.0% and 2.0% compared with the results of the full random model.

C.4.4 Summary

Similar to the previous section, here we obtained an estimate of the marginal probability distribution of the long-term load. The short-term load was based on a quadratic Weibull model of local random peaks, however. The general methodology remained the same. The statistical moments were related to the environmental variables through regression analysis. Using the method of moments, the distribution of the short-term loads was obtained for each specific set of values of the environmental variables. Finally, an estimate of the marginal distribution of the long-term load was obtained by summing the conditional short-term load distributions (each weighted by the probability of the values of the environmental variables occurring) over all environmental conditions. We found from this analysis that the estimate of the one-year and 50-year blade root flap bending loads were 51.9kN-m and 76.7kN-m, respectively. Correspondingly, the one-year and 50-year blade root edge bending loads were 12.0kN-m and 20.0kN-m, respectively.

Again, a qualitative analysis was conducted to determine which of the three variables—conditional

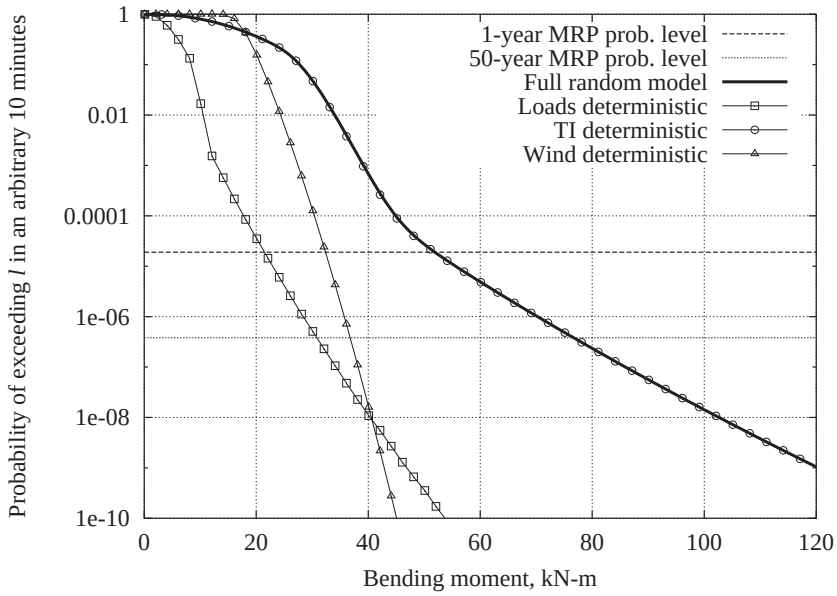

(a) Long-term distribution of blade root flap bending moment for an arbitrary 10 minutes.

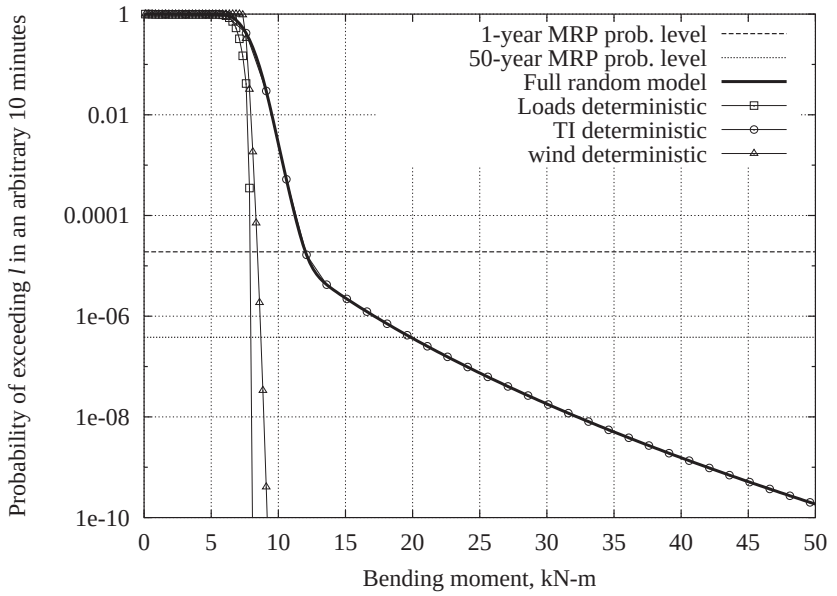

(b) Long-term distribution of blade root edge bending moment for an arbitrary 10 minutes.

Figure C.13: Long-term distributions of 10-minute extreme blade root bending moment, $L_{10\,\mathrm{min}}$, considering load, turbulence intensity, and wind speed deterministically for both blade root (a) flap and (b) edge bending.

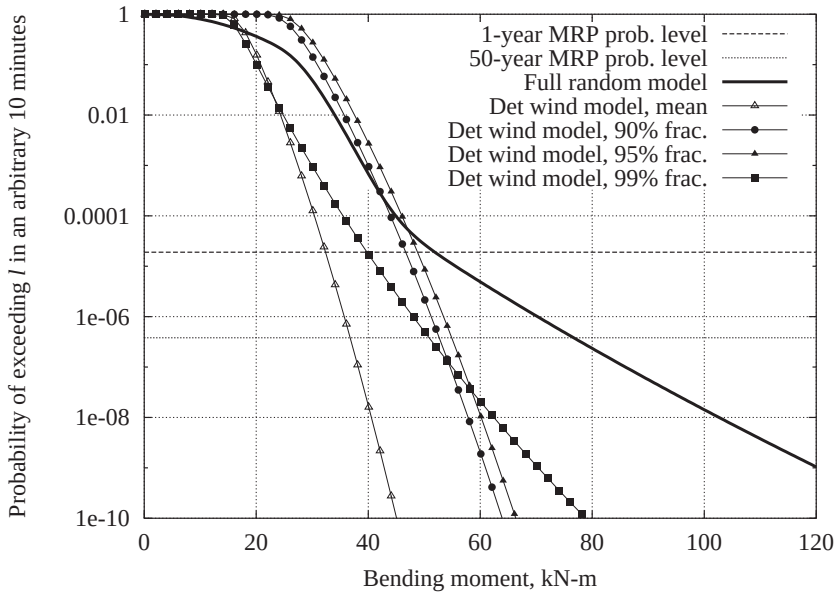

(a) Long-term distribution of extreme blade root flap bending moment for an arbitrary 10 minutes.

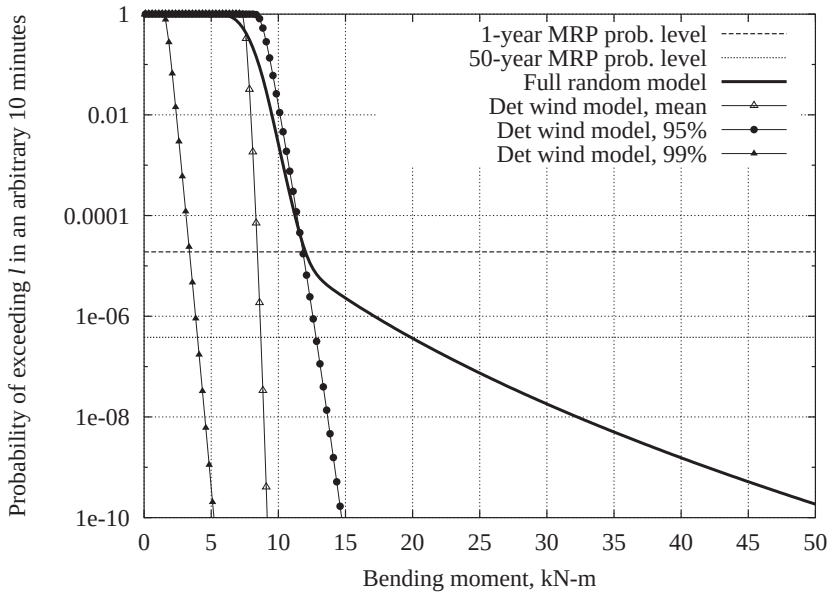

(b) Long-term distribution of extreme blade root edge bending moment for an arbitrary 10 minutes.

Figure C.14: Long-term distributions of 10-minute extreme blade root bending moment, $L_{10\,\mathrm{min}}$, considering the 10-minute mean wind speed at prescribed deterministic fractiles compared with the full distribution solution.

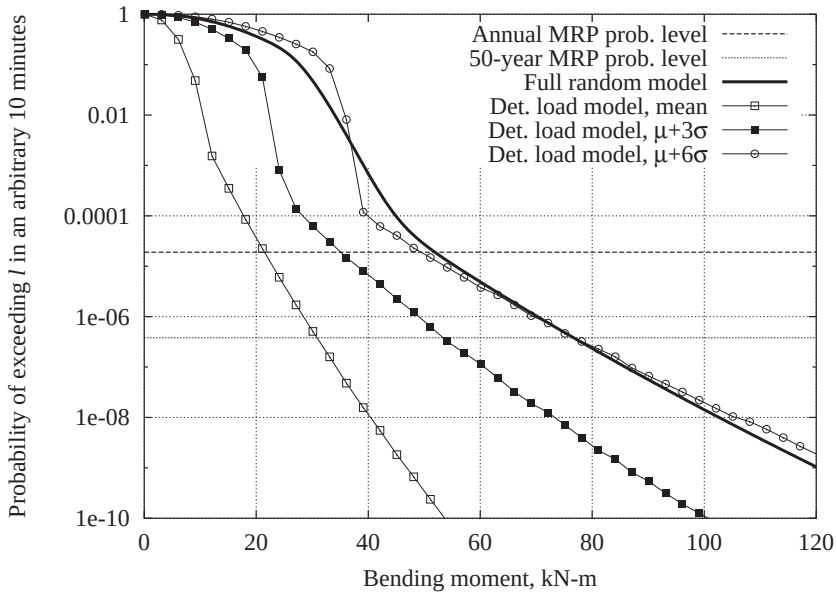

(a) Long-term distribution of extreme blade root flap bending moment for an arbitrary 10 minutes.

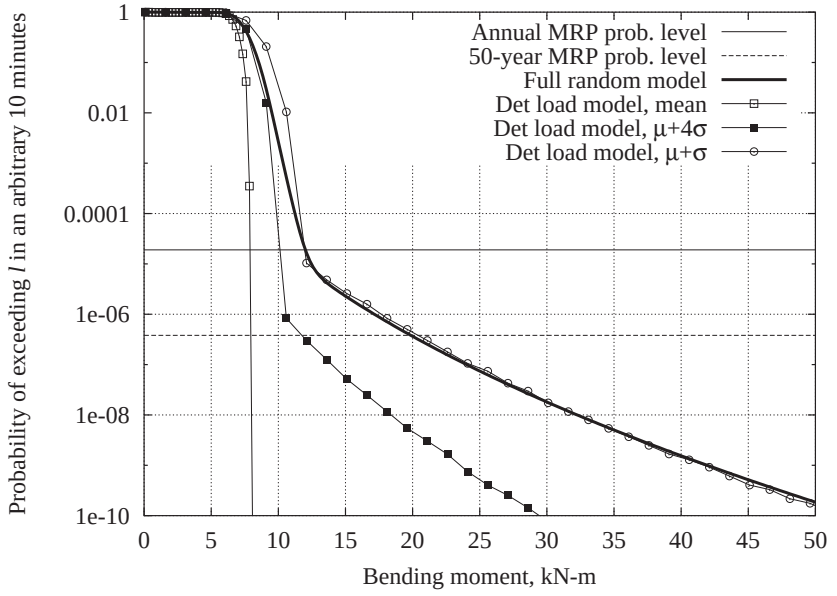

(b) Long-term distribution of extreme blade root edge bending moment for and arbitrary 10 minutes.

Figure C.15: Long-term distributions of 10-minute extreme blade root bending moment, $L_{10\,\mathrm{min}}$, considering the conditional short-term extreme load at prescribed deterministic levels compared with the full distribution solution.

short-term load, conditional turbulence, or mean wind speed—contributed the most to the variability in the distribution of the long-term load. We found that at least for the AOC 15/50 turbine, site data, and distribution models used here the conditional short-term model of the loads contributed the most to the variability in the distribution of the long-term load, with the mean wind speed contributing less. We treated the wind speed distribution deterministic, considering fractiles higher than the mean, and were unable to recover much of the variability in the distribution of the long-term load. Considering the short-term load distribution deterministic, we found using the fractile associated with mean increased by six standard deviations for the blade root flap bending load that our estimates of the one-year and 50-year loads were 4.1% and 0.6% high, respectively. Correspondingly, for the blade root edge bending loads if we considered the fractile associated with the mean increase by 8 standard deviations for the short-term blade root edge bending loads our estimate of the one-year load was low by about 11% and high by about 2.0% for the 50-year load.

C.5 Comparison of Long-Term Estimates Based on Different Short-Term Models

In Section C.3, we obtained an estimate of the long-term distribution of extreme events based on modeling the 10-minute maximum event by a Gumbel distribution. Later, in Section C.4 we obtained a similar estimate of the long-term distribution based on modeling the short-term local peaks with a quadratic Weibull distribution. Figure C.16 shows a comparison of the estimates of the long-term distribution of the 10-minute loads based on a short-term loads modeling the 10-minute extreme (Gumbel) or local peaks (Weibull). The estimates of the one-year and 50-year blade root flap and edge bending loads are presented in Table C.5 along with the associated percent difference between the two estimates.

The data presented in the figure and the corresponding table show that the estimate based on modeling the local peaks is generally unbiased for both blade root flap and edge bending compared with the estimate based on modeling the raw conditional 10-minute extremes.

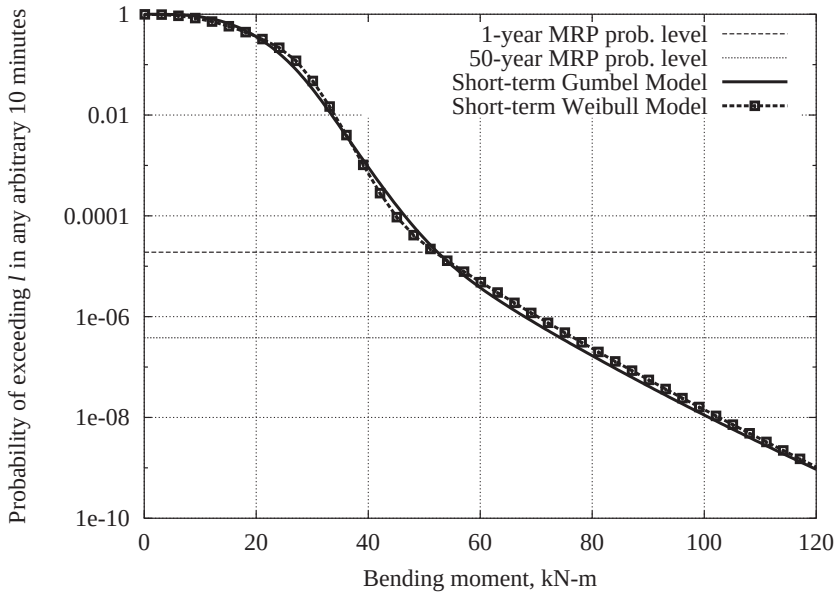

(a) Long-term distribution of extreme blade root flap bending moment for an arbitrary 10-minutes.

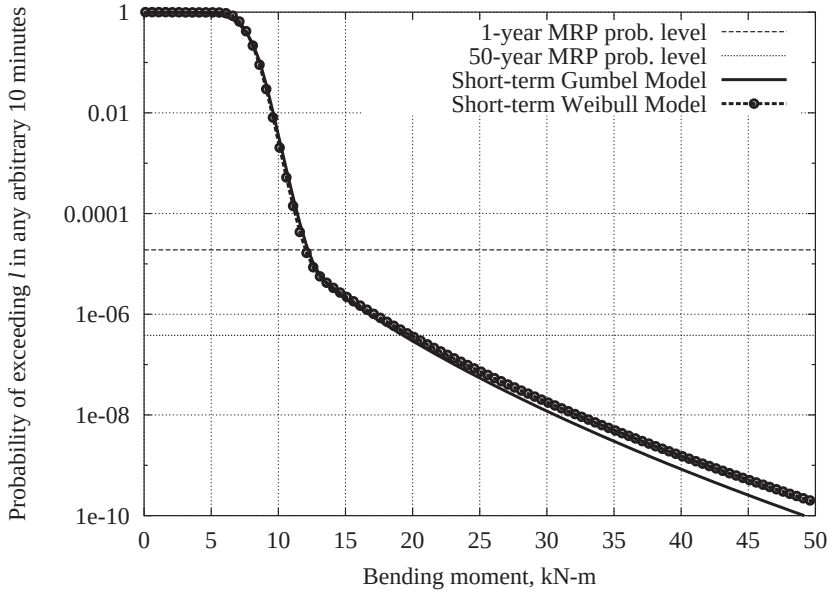

(b) Long-term distribution of blade root edge bending moment for an arbitrary 10-minutes.

Figure C.16: Comparison of estimates of the long-term distribution of 10-minute extreme blade root bending moment, $L_{10\,\mathrm{min}}$ based short-term Gumbel model for 10-minute extreme events or a short-term Weibull model for local peaks.

Comparison of Long-Term Estimates
Based on Short-Term Gumbel and Quadratic Weibull Models

Blade Root Flap Bending

	Gumbel Model	Quadratic Weibull Model	Percent Difference
1-year Bending Load	52.4kN-m	51.9kN-m	1.0%
50-year Bending Load	74.3kN-m	76.7kN-m	3.2%

Blade Root Edge Bending

	Gumbel Model	Quadratic Weibull Model	Percent Difference
1-year Bending Load	12.3kN-m	12.0kN-m	2.4%
50-year Bending Load	19.3kN-m	20.0kN-m	3.6%

Table C.5: Comparison of long-term estimates of one-year and 50-year bending loads based on using Gumbel distribution fit to observed extreme events for the short-term load model versus fitting a quadratic Weibull distribution to the local peaks for the short-term load model.

Appendix D

First Order-Reliability Method

D.1 Introduction

The purpose of this appendix is to provide the reader with a short discussion of the first-order reliability method (FORM). The reader is encouraged to consider the references in the text for further detailed discussion of the topics presented.

D.2 Background

The objective of reliability analysis is to provide an assessment of the performance of a structure or other engineering system, while taking into account the randomness of the design critical variables and uncertainties associated with limited data. The performance is evaluated based on a set of criteria or *limit states*, which define acceptable behavior. In general, if the response of the structure violates a limit state the performance is unacceptable, and often referred to as "failure".

Here we let $\mathbf{X} = \{X_1, \ldots, X_n\}$ denote the vector of random variables which influence the performance of the structure. From this vector we can formulate a limit state function, $g(\mathbf{X})$, such that $g(\mathbf{X})$=0 defines a boundary in the $\mathbf{X}$ space between the safe and failure states of the structure. We furthermore define $g(\mathbf{X}) \leq 0$ as the failure region and $g(\mathbf{X}) > 0$ as the safe region. The probability of failure can then be obtained by solving the n-fold integral below.

$$p_f = \int_{g(\mathbf{x}) \leq 0} f_{\mathbf{X}}(\mathbf{x})\, d\mathbf{x} \tag{D.1}$$

One major problem associated with evaluating Equation D.1 is that only in special cases does there exist an analytical solution. Additionally, evaluation of the multifold integral numerically can be intensive. However, approximate methods that provide good estimates of the probability of failure

do exist, e.g. first-order reliability method.

D.3 First-Order Reliability Method (FORM)

As noted above, one major obstacle in reliability assessment is the evaluation of Equation D.1. Here we are interested in presenting a brief discussion of the theory underlying the first-order reliability method. For a more detailed discussion the reader is referred to the work of Madsen, et al. [7] or Melchers [8].

The first-order reliability method takes advantage of two special properties of the standard multivariate normal distribution: total radial symmetry of the joint probability density function about the origin, and that the probability density function decays exponentially in both the radial and tangential directions. We will come back to the important role these properties play later in this discussion. In order to take advantage of these properties, the basic random variables, $\mathbf{X}$, must be transformed into a set of standard normal variates, $\mathbf{U} = \{U_1, \ldots, U_n\}$, with a joint probability density function given by

$$\phi_{\mathbf{U}}(\mathbf{u}) = \frac{1}{(2\pi)^{n/2}} \exp\left(-\frac{1}{2}\mathbf{u}^T\mathbf{u}\right) \tag{D.2}$$

The transformation can be written as $\mathbf{u} = \mathbf{u}(\mathbf{x})$, e.g., Equation 4.14 shows u_2 as a function of i. Note that if one or more of the x_i's are non-normal then the transformation is nonlinear. It is sufficient for this discussion to acknowledge that the transformation takes place. Methods for conducting the transformation are given in Madsen, et al. [7] and Melchers [8]. Note also that the limit state function in standard normal space, $G(\mathbf{u})$, must also be transformed, i.e., $G(\mathbf{u}) = g(\mathbf{x}(\mathbf{u}))$. Where $\mathbf{x}(\mathbf{u})$ is the inverse of $\mathbf{u}(\mathbf{x})$; e.g., in Equation 4.14 we see i as a function of u_2. These transformation processes are illustrated in Figure D.1.

In the original space the probability of failure was given by Equation D.1. After the transformation to standard normal space the probability of failure can be written as

$$p_f = \int_{G(\mathbf{u})\leq 0} \phi_{\mathbf{U}}(\mathbf{u})\, d\mathbf{u} \tag{D.3}$$

In general, Equation D.3 is as difficult to solve as Equation D.1. The standard normal space has two properties that enable us to obtain an accurate estimate of Equation D.3. These two properties as mentioned earlier are (1) the radial symmetry of $\phi_{\mathbf{U}}(\mathbf{u})$, and (2) the exponential decay of $\phi_{\mathbf{U}}(\mathbf{u})$ in the radial and tangential directions. As a result of these properties, the point, $\mathbf{u}^*$, on the limit state function, $G(\mathbf{U})$, closest to the origin has the highest probability density among all the points in the failure space. It is common to refer to this point as the failure point or design point. The design point is found using a constrained optimization algorithm [12, 68]. Due to the exponential

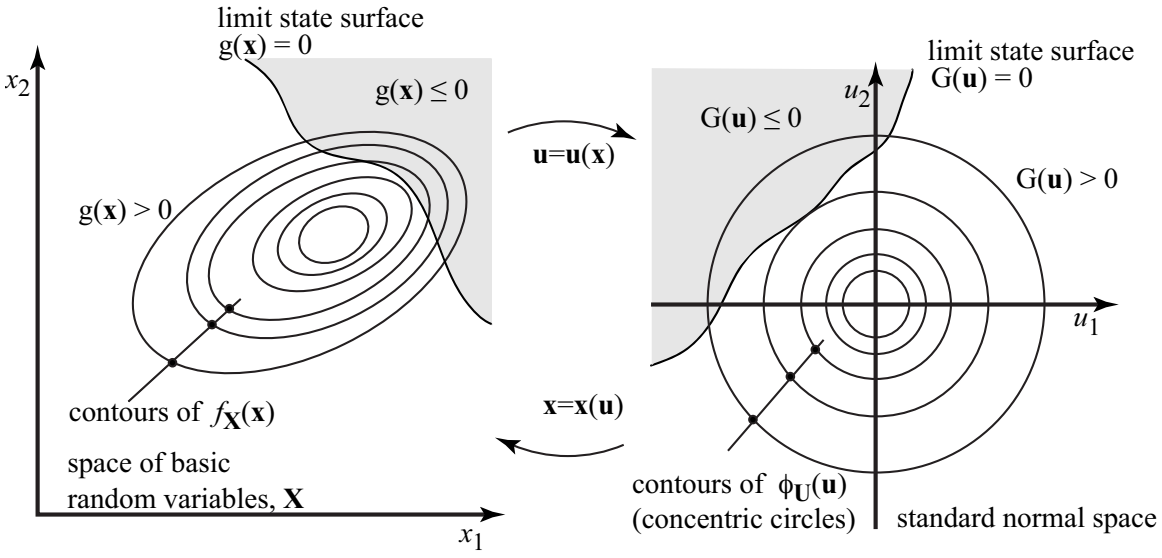

Figure D.1: Transformation of basic random variables to standard normal space.

decay of the probability density when the probability of failure is small, most of the contribution to Equation D.3 comes from the region very close to the design point. Therefore, this suggests that a good approximation to Equation D.3 can be obtained by replacing the limit state surface by a tangent line at the design point and computing the probability content of the region beyond the tangent line as shown in Figure D.2. The distance, β, from the origin to the design point is given as:

$$\beta = \alpha^T \mathbf{u}^* \tag{D.4}$$

where α is the unit normal vector to the tangent line. A first-order (FORM) estimate of Equation D.3 is given as[12]

$$p_f \approx \Phi(-\beta) \tag{D.5}$$

It is important to note that while $\mathbf{u}^*$ is the most likely failure point in the standard normal space, $\mathbf{x}^* = \mathbf{x}(\mathbf{u}^*)$, is not necessarily the most likely failure point in the original space. For most problems, however, $\mathbf{x}^*$ is close to the most likely failure point in the original space. The error associated with a FORM estimate of p_f depends on how curved the limit state function is in the standard normal space. This curvature may arise from the fact that the limit state function is non-linear in the original space to begin with, or may be due to the non-linear transformation of non-normal variables to the standard normal space. Experience has shown that for most structural engineering problems the accuracy is sufficient [69]. Note that the method (curiously) works better in the tails (i.e. when β is large). For $\beta = 0$, the exponential decay is not in effect.

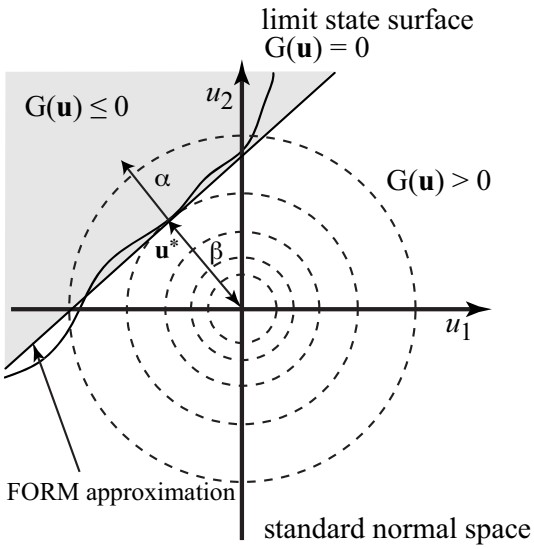

Figure D.2: Probability content behind first-order approximation of limit state function at design point, $\mathbf{u}^*$.

D.4 Affect of Multiple Design Points on FORM Estimate

In Chapter 4 we discussed the occasion of multiple design points. In this section we present a brief discussion on the effect of these multiple design points on our FORM estimates.

Figure D.3 shows a plot of the limit state function in standard normal space for the first example shown in Chapter 4, for both blade root flap and edge bending moment. For Figure D.3(a), blade root flap bending, it is clear that there is only one design point. Figure D.3(b), blade root edge bending shows that there are two points that may be design points. The question is, "how do we account for the probability mass associated with the second design point"?

The starting premise for implementing the environmental contour method discussed in Chapter 4, was that the locus of points associated with the same β value, i.e., reliability level, formed a circle in standard normal space. More formally, the probability content outside a line drawn tangent to any point on the surface of the circle is constant. The issue here is that with multiple design points, other design points may not be included in the area outside the line drawn tangent to the circle at the most probable design point (i.e., design point closest to the origin). The further these other design points are from the FORM estimate the less accurate the FORM estimate becomes in estimating the reliability. In general, a system reliability analysis is required to accurately account for the probability mass associated with multiple design posts, see Melcher [8] and Madsen, et al. [7]. We will not discuss system reliability here but the reader is encouraged to consult the listed references. Instead we will take a qualitative look at the location of the design point and the shape of the limit

state function in standard normal space, for the three examples presented in Chapter 4 to determine if the FORM estimate misses a significant portion of the probability mass associated with additional design points.

The implication is that if multiple design points exist and contribute additional probability mass not already included in the FORM estimate the estimate may be inaccurate and unconservative. In our examples in Chapter 4 we have inherently assumed that there will be only one design point. This is evident in the fact that the β value is directly related the number of 10-minute segments in a prescribed return period, and this β value defines the radius of the circle in standard normal space. If multiple design points occurred, and for example a second design point contributed probability mass not included in the FORM estimate for the most probable point, then a simple tangent at the most probable point would not be sufficient. In this case, two tangent lines would be appropriate and the probability mass that overlapped in the two regions would need to be discounted so that it was not accounted for twice, i.e., system reliability analysis. If system reliability analysis is required to account for the added probability mass associated with multiple design points, an iterative method may be required to find the appropriate scaled circle in standard normal space associated with the reliability, taking into account the contribution for all relevant design points.

Turning our attention to Figure D.3(b) the shape of the limit state function at the design point with the FORM estimate shown indicates that very little probability mass is encompassed by the limit state function. If this was the only design point then the FORM estimate would significantly over estimate the probability mass. In this case, however, a second design point exists which includes a large probability mass, to which our FORM estimate would give a good approximation. Note that both the limit state function and our FORM estimate are straight lines. So in this case one might argue that we have offsetting errors. Our FORM estimate is drawn at a point where the limit state function contains very little probability mass, but we have another potential design point not contained in the FORM estimate which does define a comparable probability mass.

Figures D.4 and D.5 show a plot of the design points and limit state functions for Examples 2 and 3 of Chapter 4 considering both blade root flap and edge bending. In Figure D.4, for Example 2, the second design point is not included with the FORM estimate at the most probable point. Although, the amount of probability mass not included with the FORM estimate appears to be small. We would expect that our estimate would be reasonable if only a small portion of probability mass was excluded, and the results shown in Chapter 4 confirm this assumption. It should be noted that if we underestimated the probability mass we would expect our estimate of the one-year load, based on the FORM estimate, to be slightly higher than indicated by the integration. This is because the circle based on only one tangent line would be larger than the circle associated with the probability content rescaled to account for probability mass associated with two tangent lines. This is also

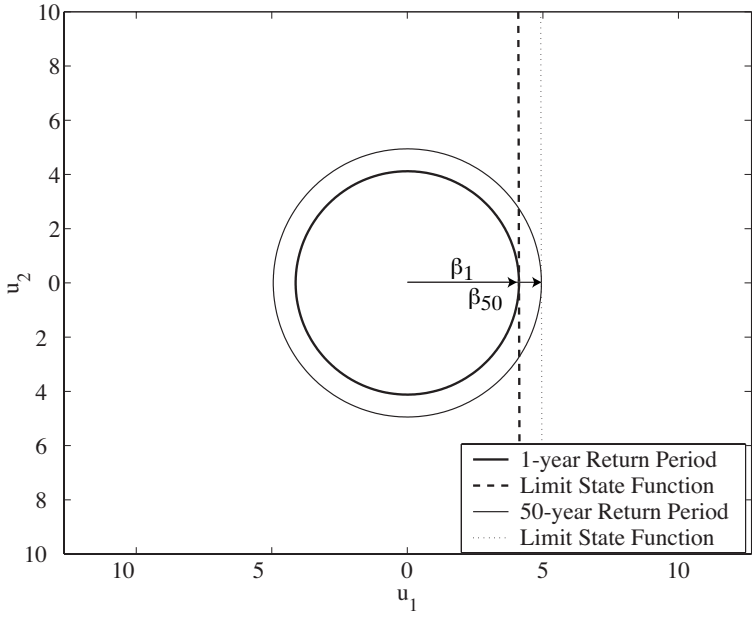

(a) Blade root flap bending.

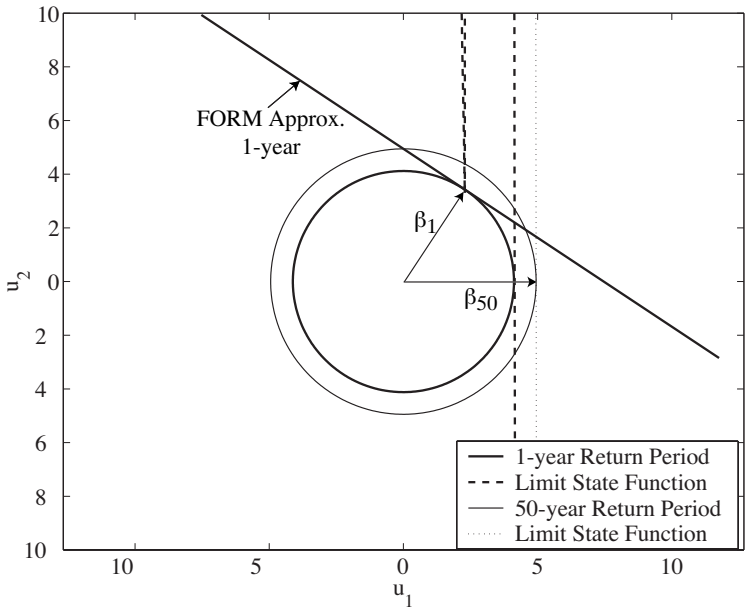

(b) Blade root edge bending.

Figure D.3: Plot of limit state functions in standard normal space for Example 1—IEC Model with Stall-Regulated Turbine, from Chapter 4, for (a) flap and (b) edge bending.

confirmed by the results shown in Chapter 4, our estimate based on FORM analysis is slightly larger than the estimate based on integration. Figure D.5, for Example 3, shows that a second design point is not included in the FORM estimate at the most probable point, and in this case a more significant portion of probability mass is neglected. Qualitatively, it seems that it may be advantageous in this case to conduct a system reliability analysis to account for the additional probability mass. This would potentially reduce the 13% difference in our estimates of the 1-year load based on FORM and integration methods.

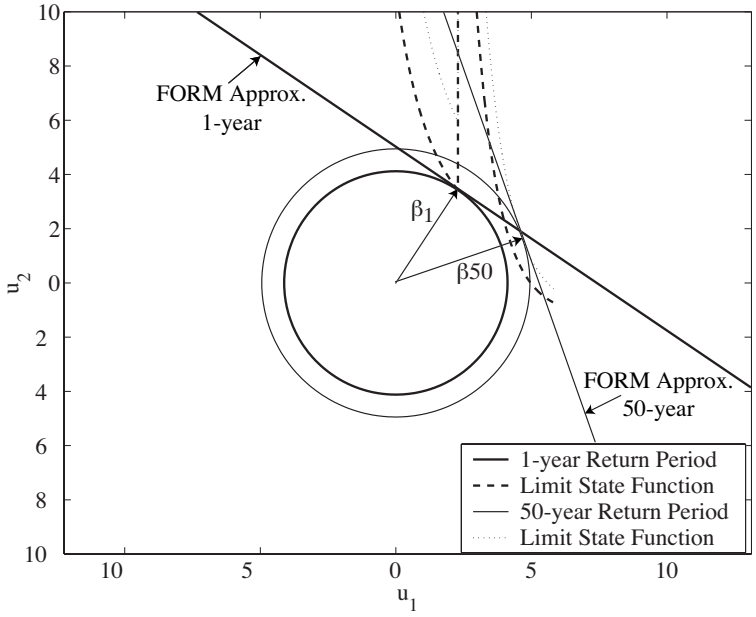

(a) Blade root flap bending.

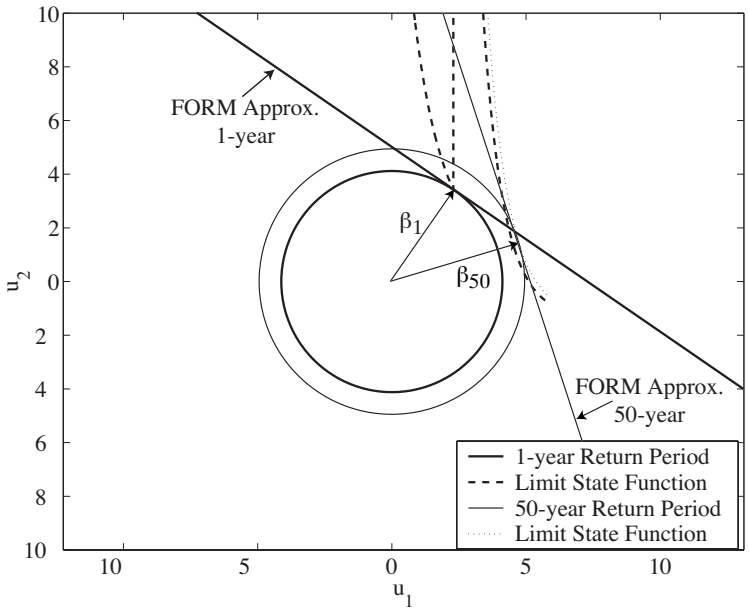

(b) Blade root edge bending.

Figure D.4: Plot of limit state functions in standard normal space for Example 2—Field Data Model with Stall-Regulated Turbine, from Chapter 4, for (a) flap and (b) edge bending.

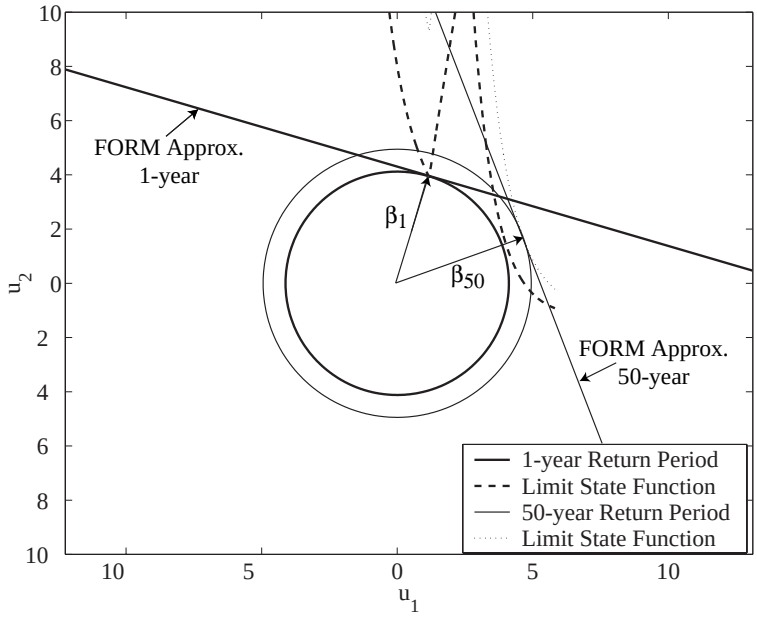

Figure D.5: Plot of limit state functions in standard normal space for Example 3—IEC Model with Pitch-Regulated Turbine, from Chapter 4, for blade root flap bending.

Appendix E

Environmental Contours Based on Propsed Changes to IEC 61400-1

E.1 Introduction

The IEC technical committee responsible for revising the international standard of safety requirements for wind turbine generator systems (IEC 61400-1) [23] has proposed several changes to the existing code. In particular, the technical committee has proposed three wind classes (I-III) instead of the current four wind classes, as well as three turbulence classes (A,B,C) instead of the current two turbulence classes. We present a brief discussion of developing environmental contours for these new wind turbine generator system classes. In particular, in the last section of this appendix we show how the environmental contours can be normalized with respect to turbulence class. The reader should note that in this analysis we have assumed that the turbulence intensity is well described by a lognormal distribution.

E.2 Definition of Environmental Random Variables

E.2.1 Wind Speed

The annual distribution of the 10 minute mean wind speed, V, is given by a Rayleigh distribution defined as:

$$f_V(v) = \frac{2v}{\alpha^2} \exp\left[-\left(\frac{v}{\alpha}\right)^2\right] \tag{E.1}$$

$$\alpha = \frac{2\mu_V}{\sqrt{\pi}}$$

Where μ_V is shown in Table E.1 for wind speed classes I-III.

Wind Speed Class	V_{ref} m/s	μ_V m/s
I	50	10
II	42.5	8.5
III	37.5	7.5

Table E.1: Mean value of annual distribution of 10-minute mean wind speed, for wind classes I-III.

E.2.2 Turbulence Intensity

The standard deviation of the 10-minute wind process is taken as the measure of turbulence, denoted by I. The conditional distribution of turbulence is assumed to follow the lognormal distribution shown below.

$$f_{I|V}(i|v) = \frac{1}{\sqrt{2\pi}\zeta i} \exp\left[-\frac{1}{2}\left(\frac{\ln(i) - \lambda}{\zeta}\right)^2\right] \tag{E.2}$$

The parameters of the lognormal distribution, λ and ζ, are defined as:

$$\zeta = \sqrt{\ln(\delta_{I|V}^2 + 1)}$$
$$\lambda = \ln(\mu_{I|V}) - \frac{1}{2}\zeta^2$$

with, $\delta_{I|V}$, the conditional coefficient of variation given as:

$$\delta_{I|V} = \frac{\sigma_{I|V}}{\mu_{I|V}}$$

The functions of conditional mean, $\mu_{I|V}$, and standard deviation, $\sigma_{I|V}$, of the turbulence are given by the equations below

$$\mu_{I|V} = I_{\text{ref}}(0.75v + c) \tag{E.3}$$
$$\sigma_{I|V} = 1.44 I_{\text{ref}} \tag{E.4}$$

The parameters I_{ref} and c are found in Table E.2 for turbulence classes A through C.

Turbulence Class	I_{ref}	c (m/s)
A	0.16	3.8
B	0.14	3.8
C	0.12	3.8

Table E.2: Parameters I_{ref} and c for annual conditional distribution of turbulence, for Turbulence classes A-C.

E.2.3 Joint Probability Density Function of Environmental Variables

The joint probability density function of the environmental variables is obtained by multiplying together Equations E.1 and E.2.

$$f_{V,I}(v,i) = f_{I|V}(i|v) f_V(v) \tag{E.5}$$

The resulting joint probability density function for class IA is shown in Figure E.1.

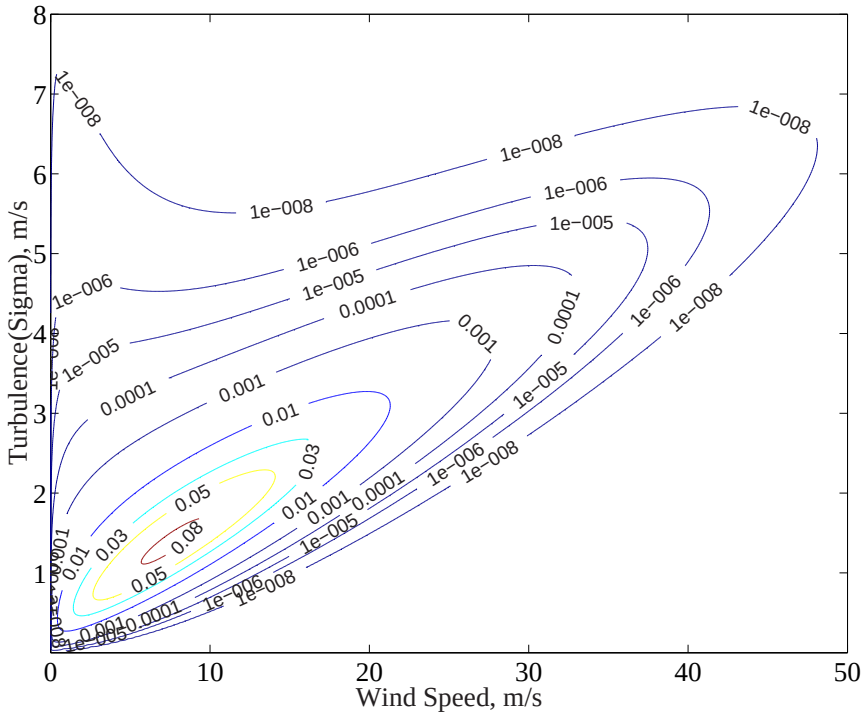

Figure E.1: Joint probability density function for wind class IA, μ_V=10m/s, I_{ref}=0.16, c=3.8

E.3 Transformation Equations

The equations to transform a circle in standard normal space, $U_{1,2}$, into the basic space described by the random variables for wind speed, V, and turbulence, I, are given below.

E.3.1 Transformation of U_1 to basic space, wind speed, V

The U_1 coordinates of a circle in standard normal space are transformed to the basic space where the wind speed, V, follows a Rayleigh distribution, by first equating the probability values of u_1 and v, in terms of the cumulative distribution functions (CDF) and then solving of v in terms of u_1.

$$\begin{aligned}
\Phi(u_1) &= F_V(v) \\
\Phi(u_1) &= 1 - \exp\left[-\left(\frac{v}{\alpha}\right)^2\right] \\
-\exp\left[-\left(\frac{v}{\alpha}\right)^2\right] &= \Phi(u_1) - 1 \\
\left(\frac{v}{\alpha}\right)^2 &= -\ln\left(1 - \Phi(u_1)\right) \\
v &= \alpha\sqrt{-\ln\left(1 - \Phi(u_1)\right)}
\end{aligned} \tag{E.6}$$

E.3.2 Transformation of U_2, given V, to basic space, turbulence, I

After having transformed the first standard normal variable to basic space, the second random variable may be transformed. The derivation of the equation for transforming the second coordinate, U_2, of the circle in standard normal space where (conditional on V) the turbulence, I, follows a lognormal distribution is shown below. Again, the CDFs are first equated, and then in this case i is found in terms of u_2 and the wind speed dependent terms λ and ζ.

$$\begin{aligned}
\Phi(u_2) &= F_{I|V}(i, v) \\
\Phi(u_2) &= \Phi\left(\frac{\ln(i) - \lambda}{\zeta}\right) \\
u_2 &= \frac{\ln(i) - \lambda}{\zeta} \\
\ln(i) &= u_2\zeta + \lambda \\
i &= \exp\left(u_2\zeta + \lambda\right)
\end{aligned} \tag{E.7}$$

E.4 Plot of Environmental Contours for Wind Classes IA-IIIC

Figures E.2 through E.10 are plots of environmental contours, as discussed in Chapter 4, for wind classes I-III and turbulence classes A through C, corresponding to 1-year and 50-year return periods.

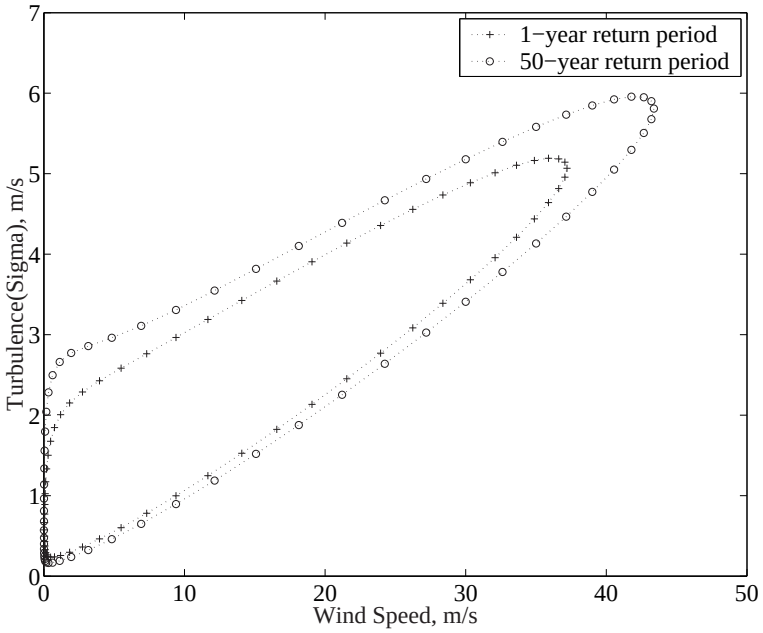

Figure E.2: Environmental contour, wind class IA, 1-year and 50-year return periods.

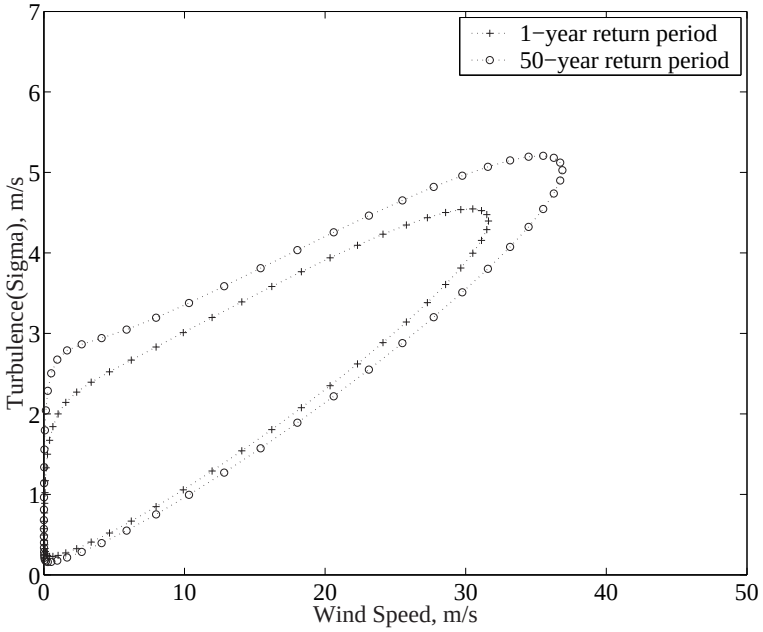

Figure E.3: Environmental contour, wind class IIA, 1-year and 50-year return periods.

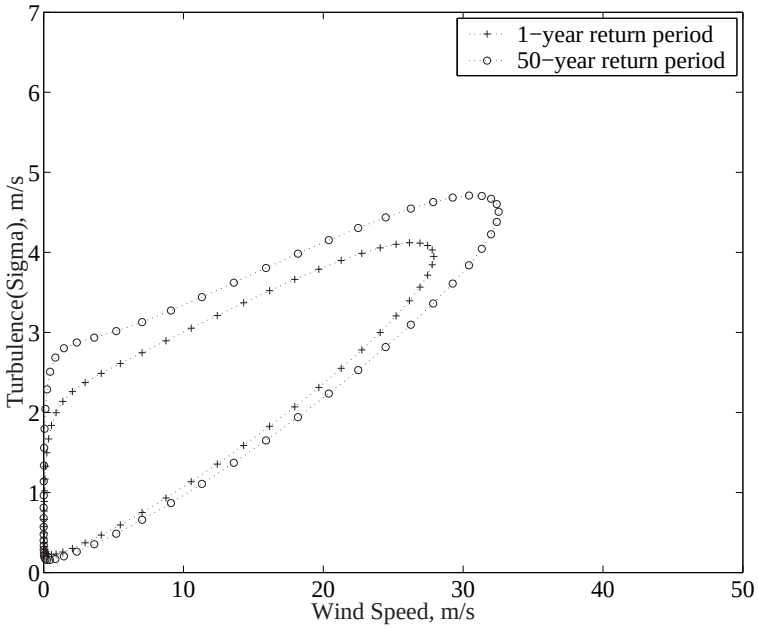

Figure E.4: Environmental contour, wind class IIIA, 1-year and 50-year return periods.

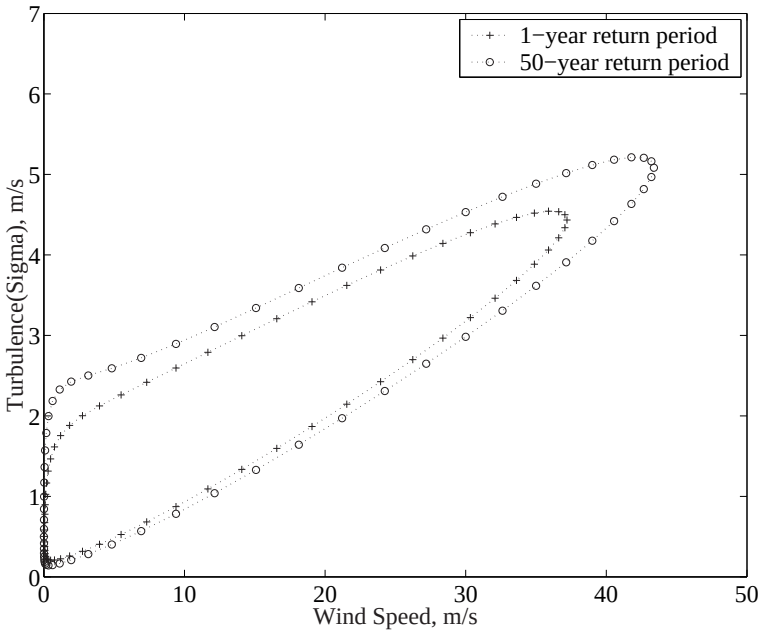

Figure E.5: Environmental contour, wind class IB, 1-year and 50-year return periods.

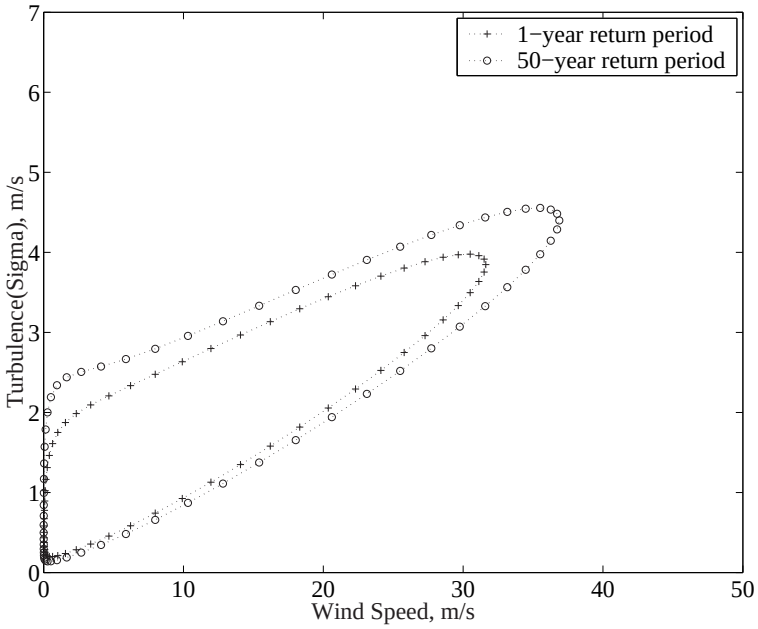

Figure E.6: Environmental contour, wind class IIB, 1-year and 50-year return periods.

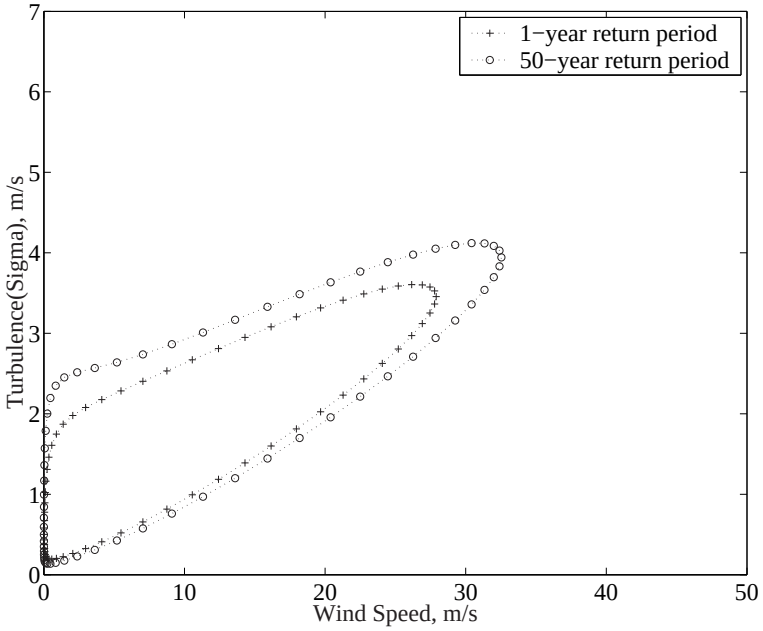

Figure E.7: Environmental contour, wind class IIIB, 1-year and 50-year return periods.

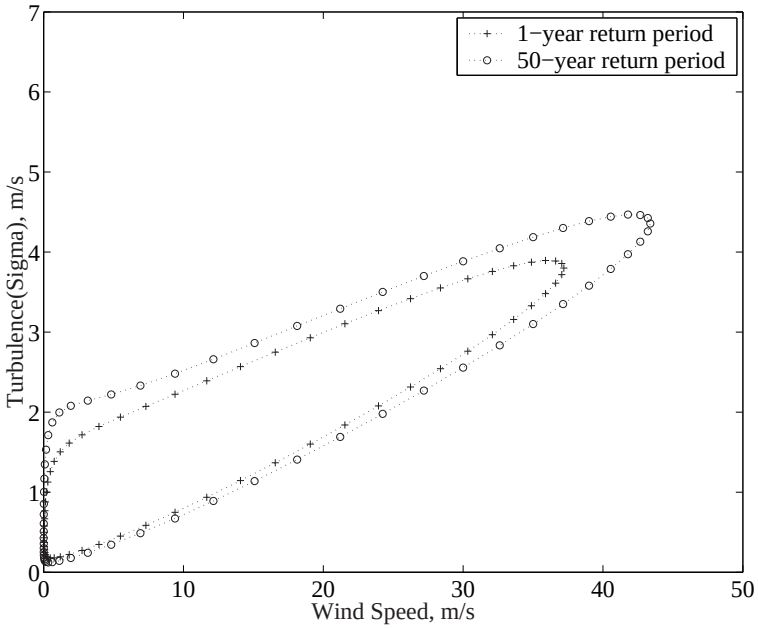

Figure E.8: Environmental contour, wind class IC, 1-year and 50-year return periods.

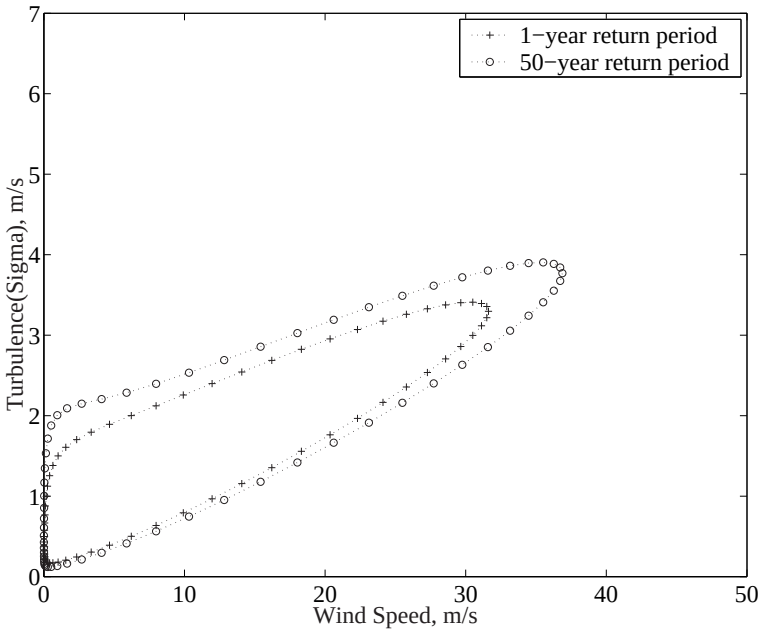

Figure E.9: Environmental contour, wind class IIC, 1-year and 50-year return periods.

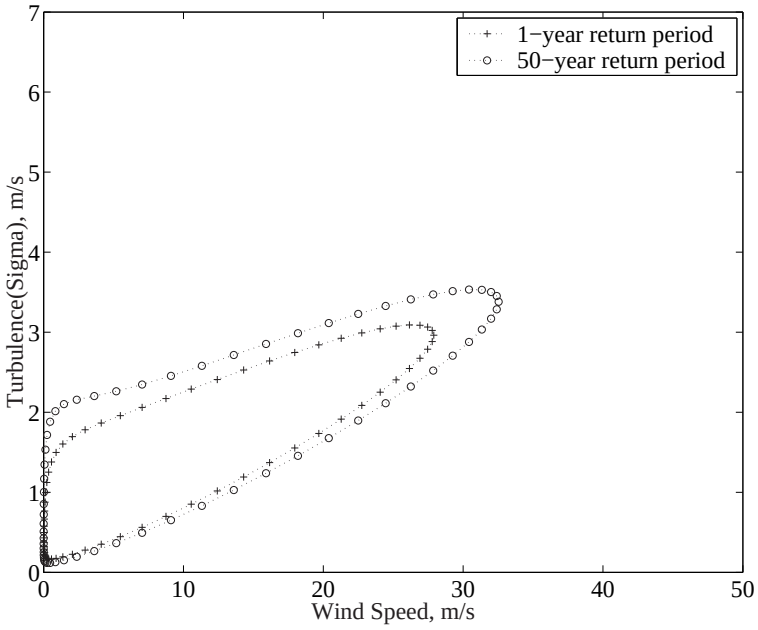

Figure E.10: Environmental contour, wind class IIIC, 1-year and 50-year return periods.

E.5 Normalized Contours

In this section, we consider normalizing the turbulence variable, such that one contour can represent the three classes of turbulence initially introduced in Table E.2. The normalized turbulence is obtained by dividing Equations E.3 and E.4 by the conditional standard deviation of turbulence (Equation E.4). As shown in the equations below.

The conditional mean normalized turbulence is given as,

$$\mu_{I|V} = \frac{I_{\text{ref}}(0.75v + c)}{1.44 I_{\text{ref}}} = \frac{0.75v + c}{1.44} \tag{E.8}$$

The conditional standard deviation of normalized turbulence is given as,

$$\sigma_{I|V} = \frac{1.44 I_{\text{ref}}}{1.44 I_{\text{ref}}} = 1 \tag{E.9}$$

These normalized equations are used in Equation E.2 The general form of the transformation equations presented earlier, however, remain unchanged. The normalized contours are shown in Figures E.11 and E.12 for 1-year and 50-year return periods, respectively.

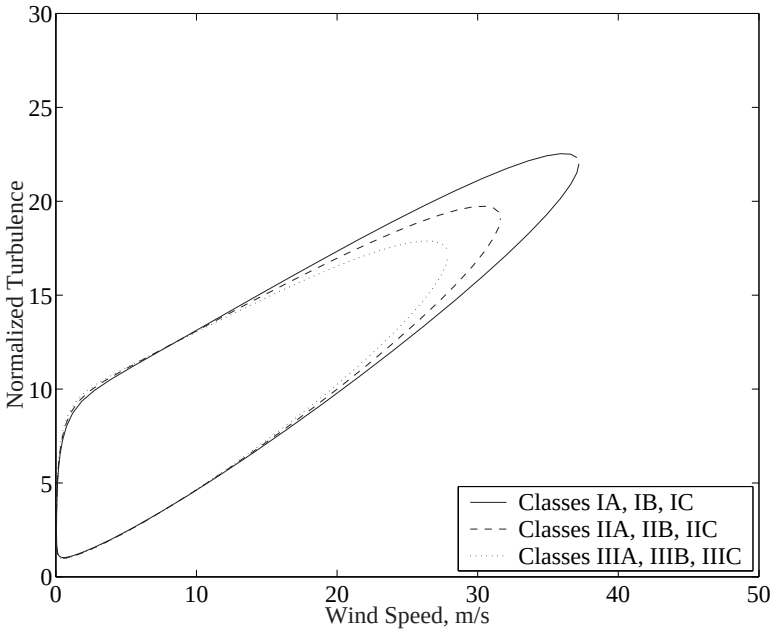

Figure E.11: Environmental contour with normalized turbulence intensity, wind classes I-III, 1-year return period.

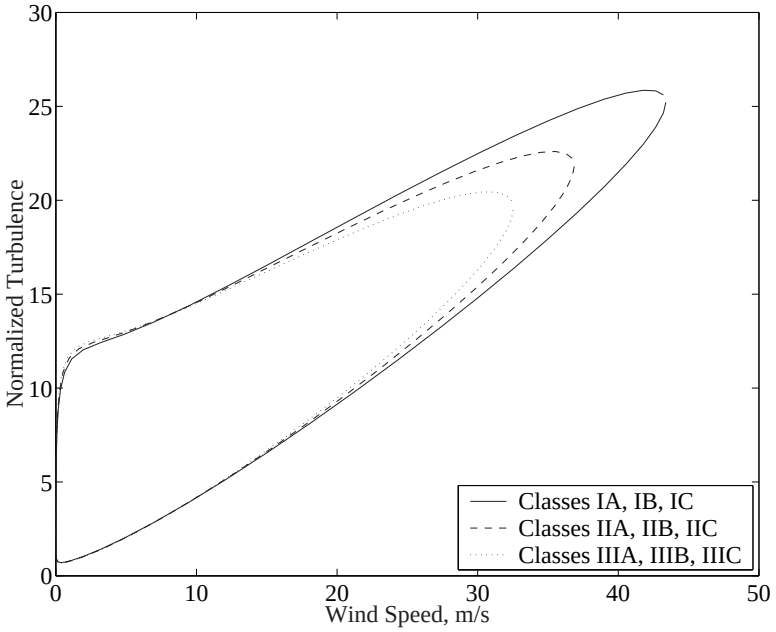

Figure E.12: Environmental contour with normalized turbulence intensity, wind classes I-III,50-year return period.

Appendix F

Estimation of Fatigue Distributions with IEC Environment

F.1 Introduction

In this appendix, we consider a similar analysis of the estimation of fatigue load distributions and fatigue damage to that presented in Chapter 5 with two major differences. First, in the analysis that will be presented here the turbulence intensity is defined as the standard deviation of the 10-minute wind process rather than the coefficient of variation of the wind process. Second, the long-term description of the environment is derived from the IEC design code [23], in particular we consider a site that conforms to the class IA standard.

F.2 Data Set

The data set used in this analysis is for the Atlantic Orient Corporation AOC 15/50 turbine, described in Chapter 1 (page 18). The turbine has a rotor diameter of 15m and a nominal rotor speed of 60 RPM at the rated wind speed of 12m/s. It is a three-bladed, fixed pitch turbine with a hub height of 25 meters [22]. The data set is described in detail in Chapter 3 (page 66) and consisted of multiple 10-minute simulations of Gaussian wind fields and corresponding blade root bending moments. The wind input processes is described by the hub height wind speed. A plot of observed turbulence intensity versus observed mean 10-minute wind speed, calculated from the simulation data, for all 10-minute time histories is shown in Figure F.1. The blade root flap and edge bending moment response time histories were assumed to be repeating and were rain-flow counted using the simplified rain-flow counting for repeating histories method given in ASTM standard E-1049.

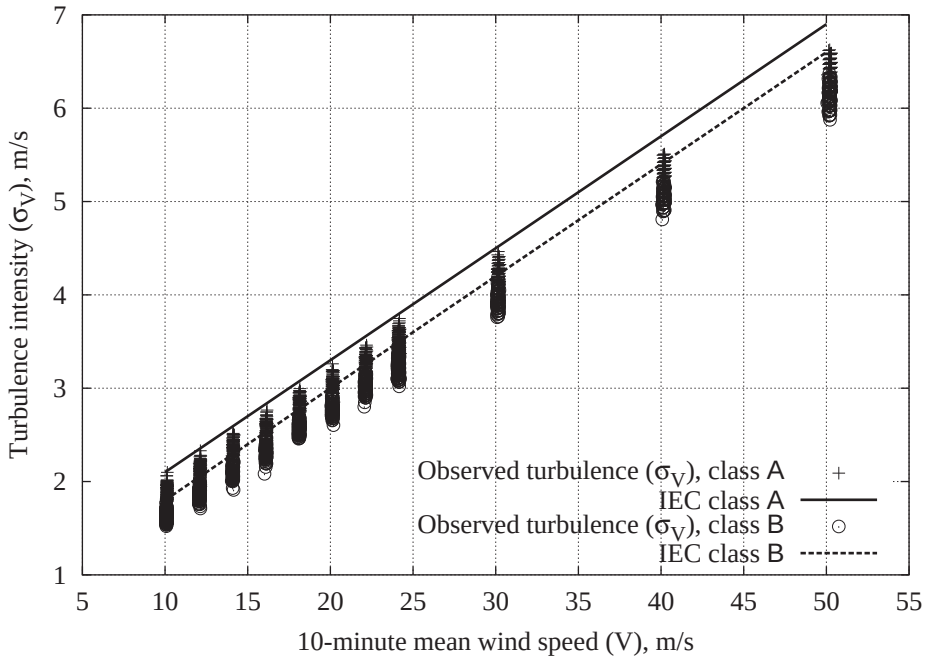

Figure F.1: 10-minute mean wind speed and turbulence intensity for 2400 10-minute Gaussian wind input processes.

F.3 Long-Term Analysis Based on Modeling Fatigue Ranges with Quadratic Weibull Model

F.3.1 Short-term Analysis

In this section, we consider modeling the distribution of fatigue ranges using the quadratic Weibull model. This model is fit to the first three moments of the data. To review, the load models, discussed in Chapter 5 and considered again here, estimate the probability distribution of load ranges by preserving a limited set of statistical moments, $\mu_i = \mathsf{E}[R^i]$. The relevant moments are model-dependent: μ_1 through μ_3 for the quadratic Weibull model, and μ_z and μ_{2z} for the damage-based Weibull model (z on the order of $3-5$, fatigue exponent, b_f equal to $2z = 6-10$). The moments of the fatigue ranges were calculated for all blade root flap and edge bending response time histories. For each pair of environmental variables (e.g., V=10m/s and I=class A) the 100 observations of the moments, e.g., mean, variance, etc., were pooled together and the mean of these pooled observations was reported.

Chapter 5 showed how the statistical moments of the data could be related to the environmental variables: mean wind speed, V, and turbulence intensity, I, through the power-law relation we have

seen before [54]:

$$\mu_i = a_i \left(\frac{V}{V_{\text{ref}}} \right)^{b_i} \left(\frac{I}{I_{\text{ref}}} \right)^{c_i} \tag{F.1}$$

Where, V_{ref} is the reference 10-minute mean wind speed, and I_{ref} is the reference turbulence intensity.[1] This functional form and methodology are followed here again with some modification. In this case, with the definitions chosen for the environmental variables, mean and standard deviation of the 10-minute wind process, for 10-minute mean wind speed and turbulence intensity respectively, the variables are highly correlated, $\rho = 0.9911$. In order to avoid problems with the regression analysis due to highly correlated predictor variables a constrained regression analysis was performed. For constrained regression analysis, a simple linear regression of the statistics of the fatigue ranges is performed on the first predictor variable, the 10-minute mean wind speed. The residuals are then in turn regressed on the second predictor variable, turbulence intensity. The issue with highly correlated predictor variables is that they tend to explain the same variability in the data. Following the procedure above, we prescribe the 10-minute mean wind speed to be the more important predictor variable and through the simple linear regression remove the variability explained by the 10-minute mean wind speed first. The second predictor variable is left to explain the variability which is left over, that portion of the variability it can explain that did not overlap (i.e. correlate) with the first predictor variable, which with highly correlated variables is generally very little. As a result the second predictor variable will play a less significant role than the first predictor variable.

The constrained linear regression analysis described above, applied to the logarithm of Equation F.1, yields point estimates of the coefficients. To demonstrate typical results, we pursue the quadratic Weibull model here; the alternative damage-based Weibull model will be discussed in Section F.4. There are two distinct general loading conditions for the turbine, one when the turbine is operating (i.e., 10-minute mean wind speed ≤ 24m/s) and the other while the turbine is parked (i.e., 10-minute mean wind speed > 24m/s). Separate regression analysis were performed under each of these conditions. The reference wind speed and reference turbulence used in the regression analysis are given in Table F.1. The calculated regression coefficients and R^2 statistics are shown in Tables F.2 and F.3 for blade root flap and edge bending fatigue ranges, respectively. R^2 statistics near unity indicate that a large percentage of the variability in the data is explained by the regression model. Low R^2 statistics indicate that other influences not contained in the regression model may be affecting the loads. We may note that the R^2 statistic for the regression analysis of the coefficient of skewness are low in a many cases, the data exhibit variability which the model is unable to explain. In performing the regression analysis it was determined that the proposed functional model, Equation F.1, did not have enough flexibility to sufficiently model the observed behavior of

[1] Recall that the turbulence intensity in this analysis is defined as the standard deviation of the 10-minute wind process, rather than the coefficient of variation as considered at times in previous chapters.

Reference Wind Speed and Turbulence

	V_{ref} (m/s)	I_{ref} (m/s)
$V \leqq 24$m/s	16.474	2.518
$V > 24$m/s	34.803	4.607

Table F.1: Reference wind speed and turbulence values used in Equation F.1

the mean and standard deviation of the blade root flap bending fatigue ranges. The values of the mean and standard deviation of the fatigue ranges flatten out with higher wind speeds above 17m/s as compared with the behavior below 17m/s. Therefore a separate model was fit to each of these regions, one below 17m/s and the other above 17m/s, for both the mean and standard deviation of blade root flap bending fatigue ranges. A similar result was found in Chapter 3 when we considered modeling the local peaks with a quadratic Weibull model, see Figures 3.25 and 3.26.

Finally, graphical regression results are shown in Figures F.2-F.4. Each figure contains both blade root flap and edge bending conditions considering: mean of fatigue ranges, Figure F.2; standard deviation of fatigue ranges, Figure F.3; and coefficient of skewness of fatigue ranges, Figure F.4. In all plots, the turbulence intensity has been set equal to the reference value.

Blade Root Flap Bending
Regression of Statistics of Fatigue Ranges on V and I

Mean of Fatigue Ranges

	a (kN-m)	b	c	R^2
$V \leqq 17$m/s	6.0105	0.9855	0.1933	0.8935
$17 < V \leqq 24$m/s	7.6080	0.0133	0.2868	0.2387
$V > 24$m/s	4.4478	4.4437	0.0010	0.9948

Standard Deviation of Fatigue Ranges

	a (kN-m)	b	c	R^2
$V \leqq 17$m/s	5.2900	0.8567	0.1902	0.8871
$17 < V \leqq 24$m/s	6.6759	0.1034	0.2630	0.2678
$V > 24$m/s	4.6655	4.1542	0.0124	0.9918

Coefficient of Skewness of Fatigue Ranges

	a (kN-m)	b	c	R^2
$V \leqq 24$m/s	1.3940	0.1447	0.0003	0.4873
$V > 24$m/s	2.3154	-1.4468	0.0140	0.9369

Table F.2: Regression coefficients used in Equation 5.9 to fit flap bending moment fatigue ranges as functions of the mean wind speed, V, and turbulence intensity, I. The turbine is operating for $V \leqq 24$m/s, otherwise the turbine is parked.

Blade Root Edge Bending
Regression of Statistics of Fatigue Ranges on V and I

Mean of Fatigue Ranges

	a (kN-m)	b	c	R^2
$V \leqq 24$m/s	0.5963	0.4346	0.0598	0.8292
$V > 24$m/s	1.0970	4.7006	-0.0019	0.9954

Standard Deviation of Fatigue Ranges

	a (kN-m)	b	c	R^2
$V \leqq 24$m/s	0.5186	0.3915	0.0711	0.7747
$V > 24$m/s	1.1339	4.5399	0.0089	0.9936

Coefficient of Skewness of Fatigue Ranges

	a (kN-m)	b	c	R^2
$V \leqq 24$m/s	1.8736	0.0213	0.0138	0.0064
$V > 24$m/s	1.9544	-0.6177	0.0161	0.2369

Table F.3: Regression coefficients used in Equation 5.9 to fit edge bending moment fatigue ranges as functions of the mean wind speed, V, and turbulence intensity, I. The turbine is operating for $V \leqq 24$m/s, otherwise the turbine is parked.

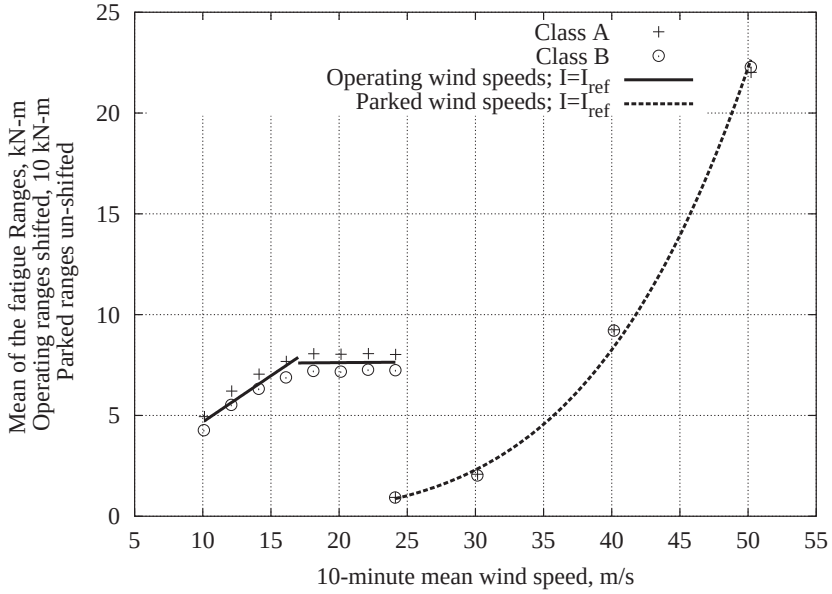

(a) Pooled statistics of the mean of the fatigue ranges in 10-minute blade root flap bending response time history.

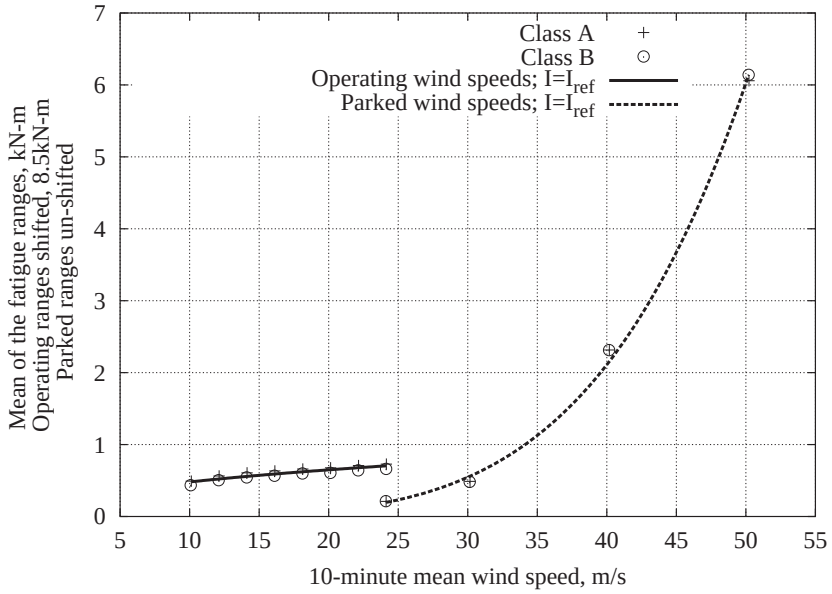

(b) Pooled statistics of the mean of the fatigue ranges in 10-minute blade root edge bending response time history

Figure F.2: Mean fatigue range of 10-minute blade root flap and edge bending response, based on 100 pooled observations for each 10-minute mean wind speed and turbulence class. The wind turbine is operating for $V \leqq 24$m/s, otherwise the turbine is parked.

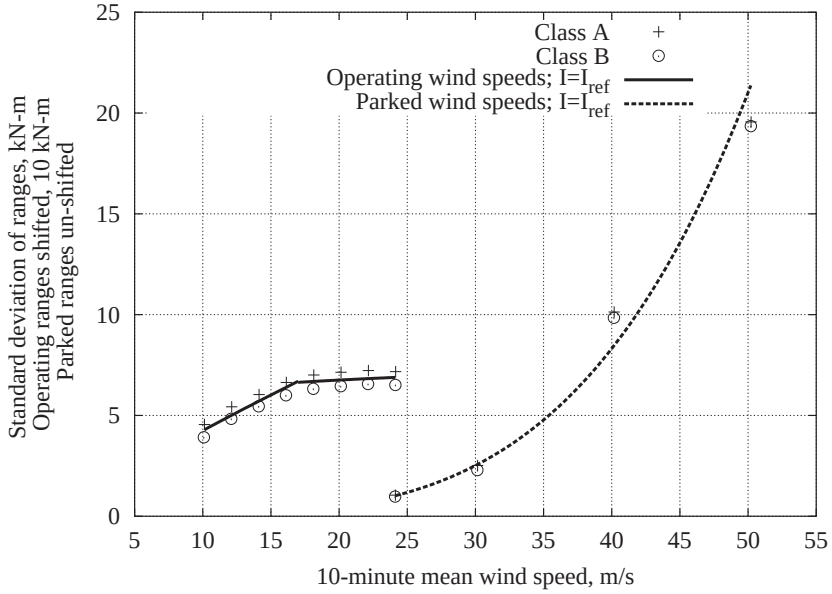

(a) Pooled statistics of the standard deviation of the fatigue ranges in 10-minute blade root flap bending response time history.

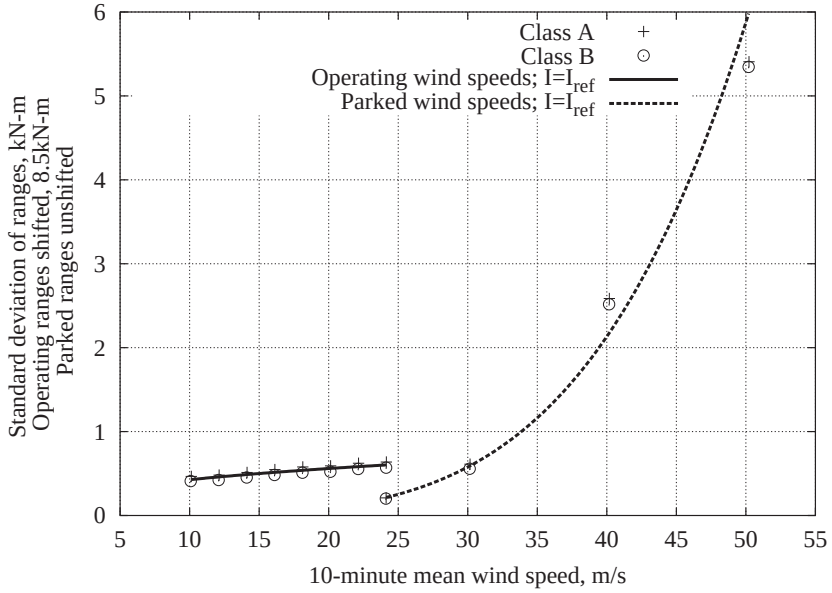

(b) Pooled statistics of the standard deviation of the fatigue ranges in 10-minute blade root edge bending response time history

Figure F.3: Standard deviation of fatigue ranges for 10-minute blade root flap and edge bending response time histories, based on 100 pooled observations for each 10-minute mean wind speed and turbulence class. The wind turbine is operating for $V \leqq 24$m/s, otherwise the turbine is parked.

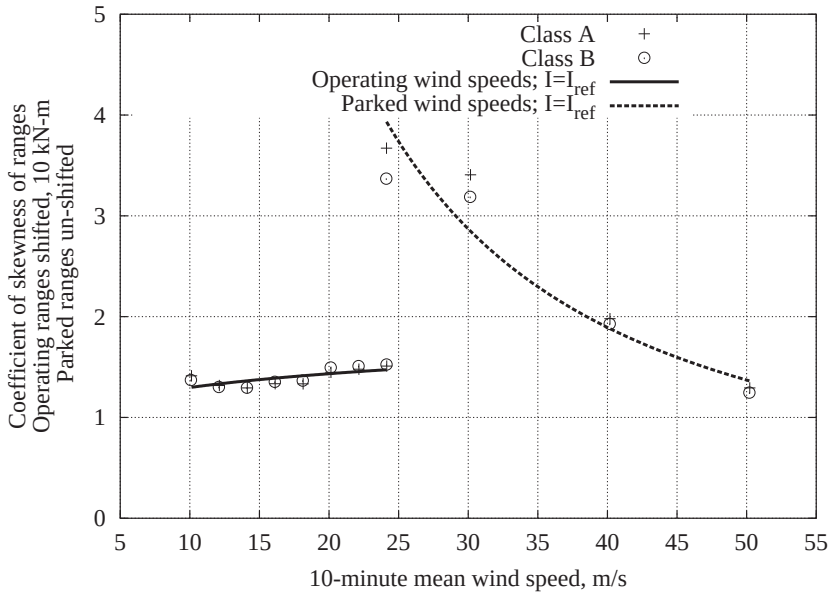

(a) Pooled statistics of the coefficient of skewness of the fatigue ranges in 10-minute blade root flap bending response time history.

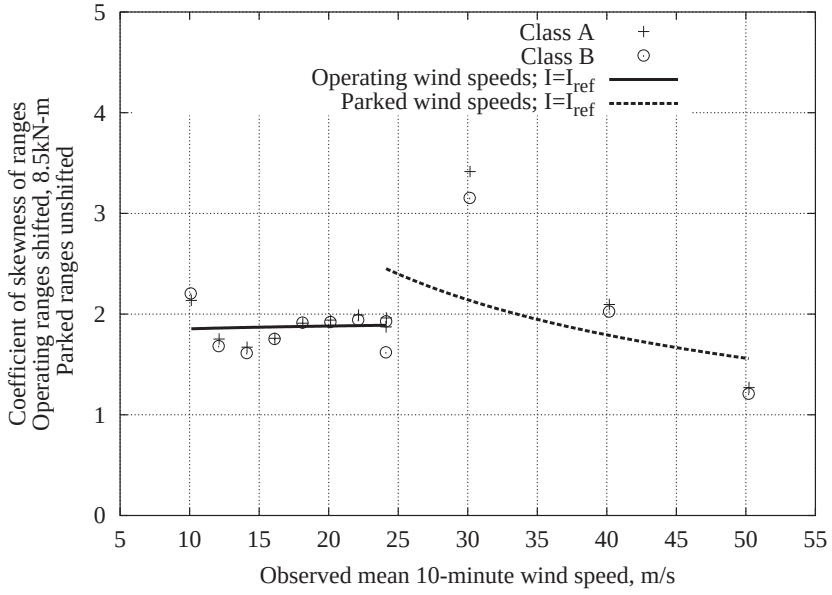

(b) Pooled statistics of the coefficient of skewness of the fatigue ranges in 10-minute blade root edge bending response time history

Figure F.4: Coefficient of skewness of fatigue ranges for 10-minute blade root and edge bending response time histories, based on 100 pooled observations for each 10-minute mean wind speed and turbulence class. The wind turbine is operating for $V \leqq 24$m/s, otherwise the turbine is parked.

F.3.2 Long-Term Analysis

For the discussion here we defined the conditional probability distribution of fatigue ranges by a quadratic Weibull model. Further, the moments of the fatigue ranges have been related to the environmental variables through regression analysis.

The long-term distribution of fatigue load ranges, in an arbitrary 10-minute period is found in the same way as described in Section 5.4; by performing the integration below,

$$F_R(r) = \int F_{R|V,I}(r|v,i)\, f_{V,I}(v,i)\, dvdi \tag{F.2}$$

Where, $F_{R|V,I}(r|v,i)$, is the short-term conditional distribution of fatigue ranges, and $f_{V,I}(v,i)$, the joint density function of the environmental variables.

We will assume that the AOC 15/50 turbine is installed at a site with environmental conditions conforming to a IEC class IA site. The description of the environmental variables is based on the criteria given in the IEC wind energy safety code for a class IA environment [23]. Specifically, the annual distribution of the 10-minute mean wind speed, V, is given by the Rayleigh distribution shown below, with μ_V=10m/s.

$$f_V(v) = \frac{2v}{\alpha^2} \exp\left[-\left(\frac{v}{\alpha}\right)^2\right] \tag{F.3}$$

$$\alpha = \frac{2\mu_V}{\sqrt{\pi}}$$

The standard deviation of the 10-minute wind process is taken as the measure of wind turbulence intensity. The conditional distribution of turbulence intensity is assumed to follow the lognormal distribution shown below.

$$f_{I|V}(i|v) = \frac{1}{\sqrt{2\pi}\zeta i} \exp\left[-\frac{1}{2}\left(\frac{\ln(i)-\lambda}{\zeta}\right)^2\right] \tag{F.4}$$

The parameters of the lognormal distribution, λ and ζ, are defined as:

$$\zeta = \sqrt{\ln(\delta^2_{I|V}+1)} \tag{F.5}$$

$$\lambda = \ln(\mu_{I|V}) - \frac{1}{2}\zeta^2 \tag{F.6}$$

with, $\delta_{I|V}$, the conditional coefficient of variation given as:

$$\delta_{I|V} = \frac{\sigma_{I|V}}{\mu_{I|V}} \tag{F.7}$$

The functions of conditional mean, $\mu_{I|V}$, and standard deviation, $\sigma_{I|V}$, of the turbulence are given by the IEC wind energy safety code. For turbulence class A, I_{15}=0.18 and a=2.

$$\mu_{I|V} = \frac{I_{15}(15\text{m/s} + av)}{(a+1)} - 2\text{m/s}\, I_{15} \tag{F.8}$$

$$\sigma_{I|V} = 2\text{m/s}\, I_{15} \tag{F.9}$$

A plot of the joint density function of the environmental variables is shown in Figure 4.1 (Chapter 4).

The ranges of values of the environmental variables are discretized into evenly spaced intervals. For each pair of values of the environmental variables the corresponding short-term distribution of fatigue ranges is generated, and any required threshold (*shift*) is reintroduced. Then, per Equation F.2, the short-term conditional fatigue range distributions are summed together, each weighted by the probability of the respective environmental condition, i.e., pair of values of the environmental variables. The summation is performed over the entire domain of environmental variables.

As stated earlier, there are two loading conditions for the turbine, operating and parked. During normal use the turbine is operating for wind speeds less than 24m/s and parked for wind speeds greater than 24m/s. In this case, to develop the long-term distribution of fatigue ranges, the appropriate regression model is used for each wind speed value. This results in a combination of the operating and parked only long-term distributions as shown in Figure F.5. Also shown in the figure are the long-term distribution of the fatigue ranges if the turbine is parked or operating in all wind speeds. We see in Figure F.5(a) that the blade root flap bending moment fatigue ranges are dominated by the operating conditions. In Figure 5.13(b) we see that the blade root edge bending moment fatigue ranges are also dominated by the operating conditions expect at very low probability levels were the parked condition dominates. This is similar to what was seen with the extreme load problem addressed in Chapter 3 and Appendix C

In addition to obtaining an estimate of the long-term distribution of fatigue ranges, we saw in Chapter 5 how we may obtain and estimate of the fatigue damage in an arbitrary 10-minute interval from,

$$\mathsf{E}[D_{10\,\text{min}}] \propto \iint_{V,I} \mathsf{E}[N_0(v,i)]\mathsf{E}[R^{b_f}|v,i] f_{V,I}(v,i)\,dv\,di = \text{DM}_{10} \tag{F.10}$$

Where $\mathsf{E}[N_0(v,i)]$, is the expected number of cycles as a function of wind speed and turbulence, and $\mathsf{E}[R^{b_f}|v,i]$, is the b_f^{th} conditional moment of the fatigue ranges. DM_{10} denotes the "*damage*

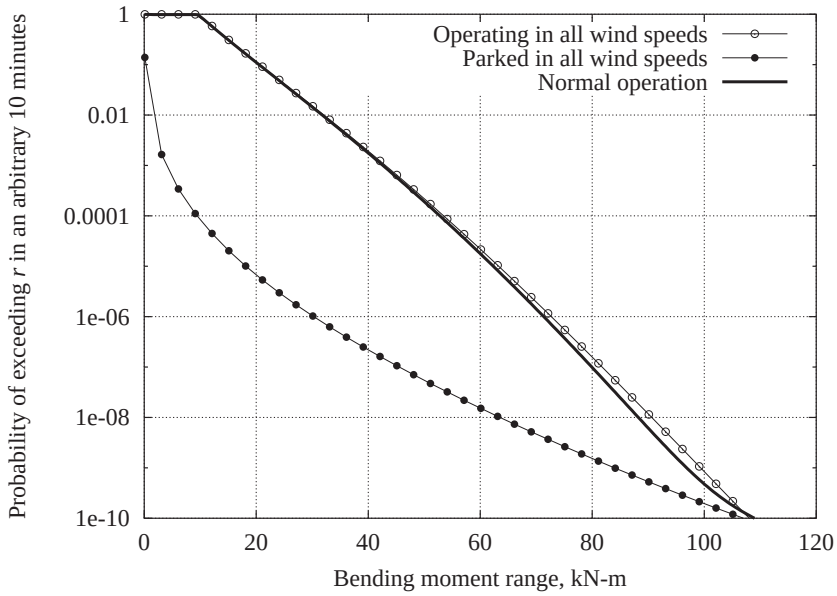

(a) Blade root flap bending.

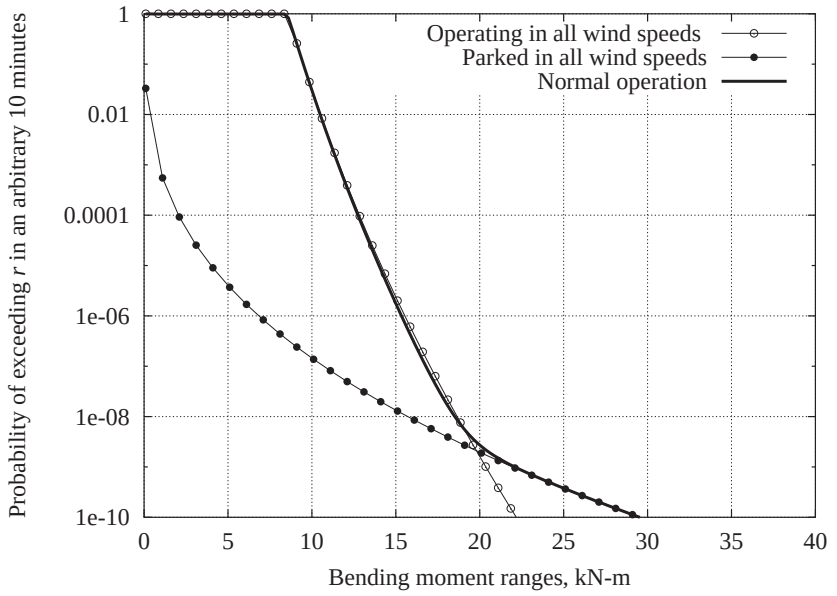

(b) Blade root edge bending.

Figure F.5: Long-term distributions of blade root fatigue bending moment ranges, R, considering three turbine conditions: 1) turbine operating over all wind speeds, 2) turbine parked over all wind speeds, 3) turbine operating below cutout wind speed and parked above cutout wind speed; for both: blade root (a) flap and (b) edge bending.

Regression of the Number of Fatigue Ranges on V and I

Blade Root Flap Bending

	a (kN-m)	b	c	R^2
$V \leqq 24$m/s	268	0.9776	0.0593	0.7219
$V > 24$m/s	5178	0.3440	-0.0070	0.9462

Blade Root Edge Bending

	a (kN-m)	b	c	R^2
$V \leqq 24$m/s	455	0.0502	-0.0080	0.5686
$V > 24$m/s	5476	0.0203	-0.0047	0.9965

Table F.4: Regression coefficients used in Equation 5.9 to fit the expected number of fatigue ranges, for blade root flap and edge bending, as functions of the mean wind speed, V, and turbulence intensity, I.

measure in 10-minutes" and is used as a proxy for the expected total fatigue damage in an arbitrary 10 minutes. This is not an actual estimate of the expected total fatigue damage, but it is proportional to it so that higher values of DM_{10} are associated with larger fatigue damage estimates and vise versa. The expected number of cycles is related to the environmental variables through regression analysis. The same power-law functional form, Equation F.1, was used. The calculated regression coefficients and R^2 statistics are shown in Table F.4 for blade root flap and edge bending fatigue ranges. Graphical regression results are shown in Figure F.6. Applying Equation F.10 then we can obtain estimates of the damage measure, DM_{10} for blade root flap and edge bending considering b_f values from 1 to 10 are presented in Table F.5. The values in this table will be used to compare with results from modeling the short-term fatigue ranges with a damage-based Weibull model in the next section instead of the quadratic Weibull model used here.

We may also consider the portion of the expected damage contributed at different environmental conditions. Figure F.7 presents a plot of damage density for both blade root flap and edge bending moments. Here, we only consider the 10-minute wind speed as the environmental variable of interest. The damage density is defined as the contribution to the expected total damage for a given wind speed. Since our analysis was conducted considering both the 10-minute wind speed and turbulence intensity, the values given in the figure reflect summing together all the contributions of different turbulence intensities for a constant wind speed. We can see clearly from the figure that most of the damage occurs while the turbine is operating, i.e., for wind speeds below 24m/s when the turbine is assumed to be operating. Also we see from Figure F.7 that as the value of the fatigue exponent, b_f, increases we are relatively more sensitive to higher wind speeds, while the turbine is parked.

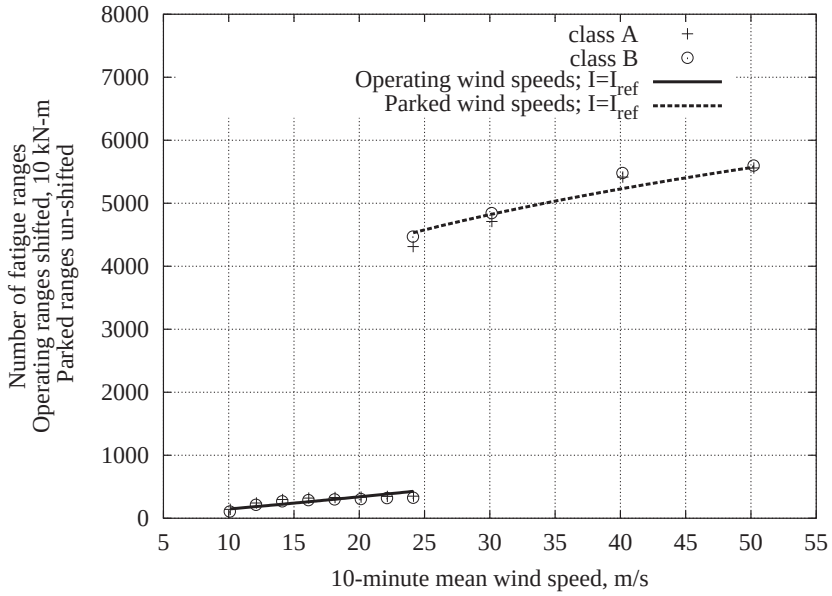

(a) Expected number of fatigue ranges in 10-minute blade root flap bending time history.

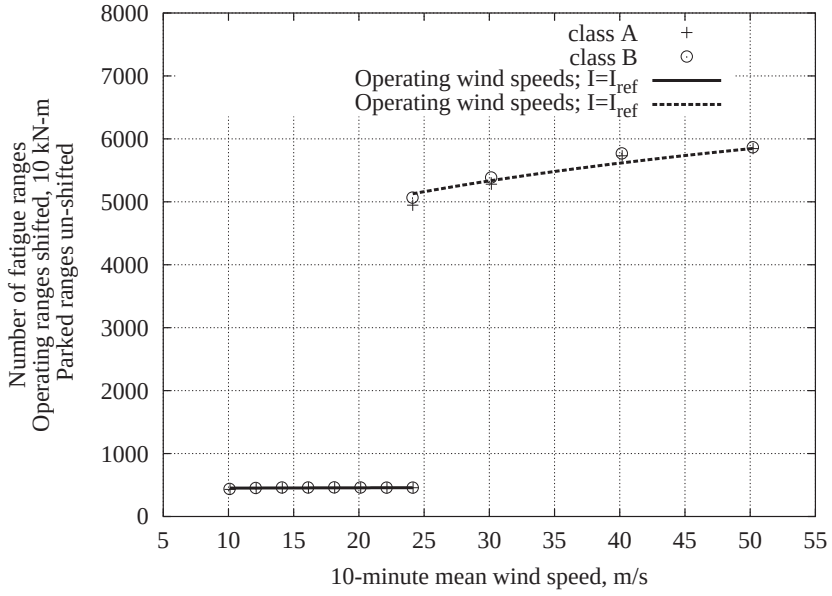

(b) Expected number of fatigue ranges in 10-minute blade root edge bending time history.

Figure F.6: Expected number of fatigue ranges in 10-minute blade root flap and edge bending response time histories, based on 100 pooled observations for each 10-minute mean wind speed and turbulence class. The wind turbine is operating for $V \leqq 24$m/s, otherwise the turbine is parked.

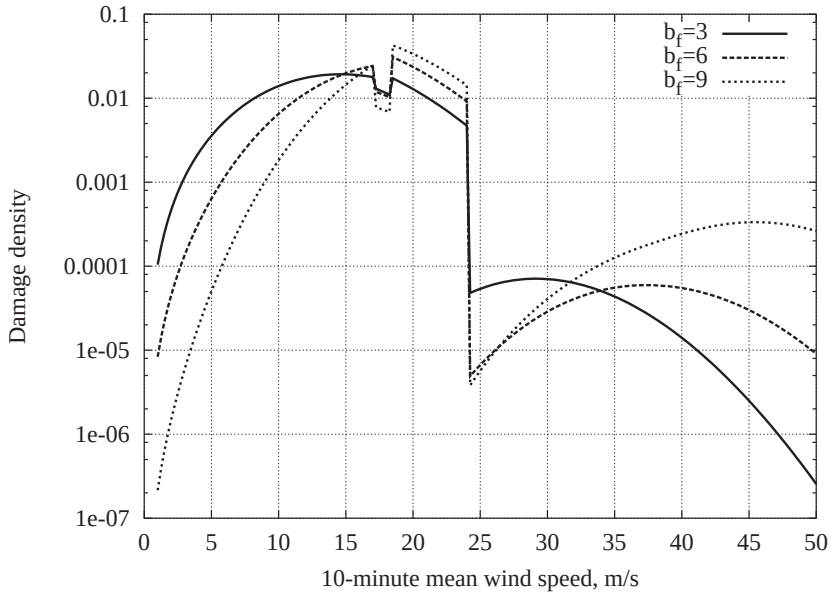

(a) Blade root flap bending moment.

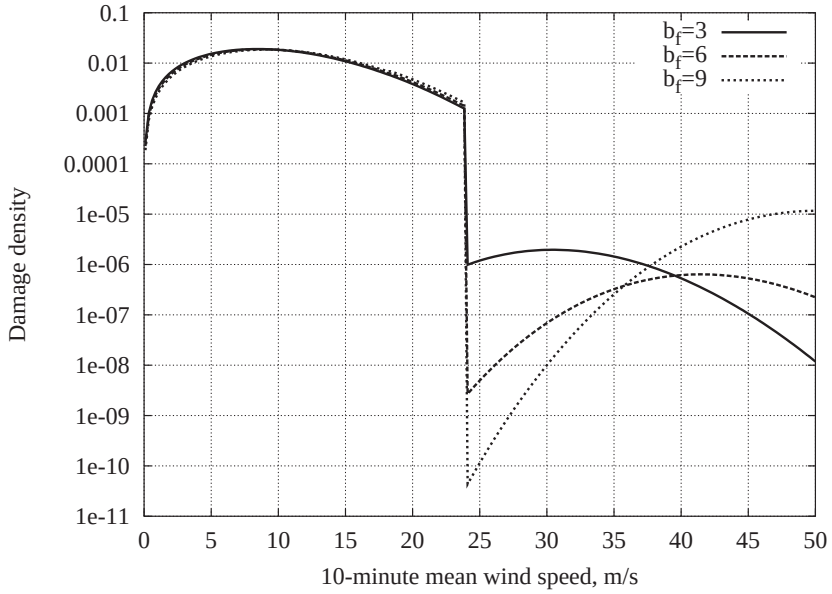

(b) Blade root edge bending moment.

Figure F.7: Damage density for blade root flap and edge bending.

Estimate of Damage Measure, DM_{10}, for Fatigue Exponent Values, $b_f = 1, \ldots, 10$.

b_f	Flap Bending	Edge Bending
1	2.321e+3	3.929e+3
2	3.713e+4	3.505e+4
3	6.835e+5	3.146e+5
4	1.447e+7	2.833e+6
5	3.540e+8	2.557e+7
6	9.961e+9	2.316e+8
7	3.193e+11	2.140e+09
8	1.152e+13	1.920e+10
9	4.634e+14	1.459e+11
10	2.080e+16	1.623e+12

Table F.5: Estimate of damage measure, DM_{10}, for fatigue exponent values, $b_f = 1, \ldots, 10$, considering blade root flap and edge bending fatigue loads.

F.3.3 Summary

In this section we have stepped through the process of obtaining an estimate of the marginal probability distribution of the long-term distribution of fatigue loads. This was accomplished by modeling the short-term distribution of fatigue ranges by a quadratic Weibull model. The statistical moments of the fatigue range data were related to the environmental variables by a power-law functional form. The parameters of the functional form were obtained through regression analysis. Using the method of moments, a quadratic Weibull distribution was obtained for each specific set of values of the environmental variables. Finally, an estimate of the marginal distribution of the long-term fatigue loads was obtained by summing the conditional short-term load distributions over all environmental conditions. Each conditional short-term load distribution was weighted by the probability of the associated environmental condition occurring. The next section presents a similar analysis, only this time the short-term fatigue ranges are modeled with a damage-based Weibull distribution.

F.4 Long-Term Analysis Based on Modeling Fatigue Ranges with the Damage-Based Weibull Model

F.4.1 Short-Term Analysis

In the last section we considered modeling the distribution of fatigue ranges using the quadratic Weibull model. Here, in contrast, we consider modeling the distribution of the fatigue ranges using our proposed damage-based Weibull model as defined in Chapter 5. To review, the load models discussed here estimate the probability distribution of load ranges by preserving a limited set of statistical moments, $\mu_i = \mathsf{E}[R^i]$. The relevant moments here are model-dependent: μ_1 through μ_3 for the quadratic Weibull model, and μ_z and μ_{2z} for the damage-based Weibull model (z on the order of 3-5, $b_f = 6 - 10$). In particular in this section we will look at damage-based Weibull models in three cases, for z values equal to 3, 4, and 5. In the first case for example where $z = 3$ this corresponds to fatigue exponent values equal to 3 and 6. The model is tuned to fit the third and sixth moment of the data. Similarly, for $z = 4$ (b_f=4 and 8) the model is tuned to fit the fourth and eighth moment of the data, and for $z = 5$ (b_f=5 and 10), the fifth and tenth moment. Separate regression analysis and long-term integration will be conducted for each of these cases. In some instances the results of only the first transformation, $z = 3$, will be presented as we find similar results for the other transformations.

In the previous section the statistical moments of the data were related to the environmental variables by the power-law model given in Equation F.1; the same functional form and methodology are followed here, again. The damage-based model matches only two moments, albeit the two moments that are matched are typically of higher order. Constrained linear regression analysis, applied to the logarithm of Equation F.1, was used to obtain estimates of the coefficients. Recall constrained regression analysis was implemented due to the high correlation between the environmental variables, i.e., the predictor variables for the regression analysis. The reference wind speed and reference turbulence used in the regression analysis are given in Table F.1. The calculated regression coefficients and R^2 statistics are shown in Tables F.6 and F.7 for blade root flap and edge bending transformed, $z = 3$, fatigue ranges, respectively. Similar results are shown in Tables F.8 and F.9 for $z = 4$ transformed fatigue ranges and Tables F.10 and F.11 for $z = 5$ transformed fatigue ranges. R^2 statistics near unity indicate that a large percentage of the variability in the data is explained by the regression model. Low R^2 statistics indicate that other influences not contained in the regression model may be affecting the loads. In performing the regression analysis it was again determined that the applied functional model, Equation F.1, did not have enough flexibility to sufficiently model the observed behavior of the mean and standard deviation of the blade root flap bending fatigue ranges. The values of the mean and standard deviation of the fatigue ranges flatten

out with higher wind speeds above 17m/s, as compared with the behavior below 17m/s. Therefore a separate model was fit to each of these regions, one below 17m/s and the other above 17m/s, for both the mean and standard deviation of blade root flap bending fatigue ranges. We saw a similar result in Section 5.4 when we fit the quadratic Weibull model to the fatigue ranges.

Finally, graphical regression results for the case where the fatigue ranges are transformed for $z = 3$, are shown in Figures F.8 and F.9. Each figure contains regression results for both blade root flap and edge bending conditions considering the mean of the fatigue ranges, Figure F.8 and standard deviation of the fatigue ranges, Figure F.9. In all plots the turbulence intensity has been set equal to the reference value. Similar results were found for the other transformation cases and, in the interest of brevity, these additional plots are not presented.

Transformed Blade Root Flap Bending Fatigue Ranges
***z*=3**

Regression of the Mean of Fatigue Ranges on V and I

	a (kN-m)	b	c	R^2
$V \leqq 17$m/s	788	3.0914	4.689	0.8859
$17 < V \leqq 24$m/s	1471	-0.0146	0.6942	0.2636
$V > 24$m/s	662	12.183	0.0364	0.9947

Regression of the Standard Deviation of Fatigue Ranges on V and I

	a (kN-m)	b	c	R^2
$V \leqq 24$m/s	3156	2.6597	4.7121	0.8975
$17 < V \leqq 24$m/s	5869	0.3059	0.6649	0.2781
$V > 24$m/s	3361	10.249	0.0526	0.9934

Table F.6: Regression coefficients used in Equation F.1 to fit transformed ($z = 3$) flap bending moment fatigue ranges as functions of the mean wind speed and turbulence intensity. The turbine is operating for $V \leqq 24$m/s, otherwise the turbine is parked.

Transformed Blade Root Edge Bending Fatigue Ranges
***z*=3**

Regression of the Mean of Fatigue Ranges on V and I

	a (kN-m)	b	c	R^2
$V \leqq 24$m/s	673	-0.0296	-0.0017	0.1878
$V > 24$m/s	9.3	13.422	0.0207	0.9948

Regression of the Standard Deviation of Fatigue Ranges on V and I

	a (kN-m)	b	c	R^2
$V \leqq 24$m/s	105	0.8172	0.1011	0.8718
$V > 24$m/s	46.6	12.784	0.0266	0.9866

Table F.7: Regression coefficients used in Equation F.1 to fit transformed ($z = 3$) edge bending moment fatigue ranges as functions of the mean wind speed and turbulence intensity. The turbine is operating for $V \leqq 24$m/s, otherwise the turbine is parked.

Transformed Blade Root Flap Bending Fatigue Ranges
***z*=4**

Regression of the Mean of Fatigue Ranges on V and I

	a (kN-m)	b	c	R^2
$V \leqq 17$m/s	16624	3.8901	0.6276	0.8907
$17 < V \leqq 24$m/s	38139	0.1271	0.9145	0.2396
$V > 24$m/s	15054	15.212	0.0590	0.9942

Regression of the Standard Deviation of Fatigue Ranges on V and I

	a (kN-m)	b	c	R^2
$V \leqq 24$m/s	95320	3.4021	0.6266	0.9013
$17 < V \leqq 24$m/s	218818	0.6259	0.8576	0.3331
$V > 24$m/s	122149	12.815	0.0710	0.9928

Table F.8: Regression coefficients used in Equation F.1 to fit transformed ($z = 4$) flap bending moment fatigue ranges as functions of the mean wind speed and turbulence intensity. The turbine is operating for $V \leqq 24$m/s, otherwise the turbine is parked.

Transformed Blade Root Edge Bending Fatigue Ranges
***z*=4**

Regression of the Mean of Fatigue Ranges on V and I

	a (kN-m)	b	c	R^2
$V \leqq 24$m/s	6041	0.0012	0.0204	0.0009
$V > 24$m/s	50	17.172	0.0163	0.9911

Regression of the Standard Deviation of Fatigue Ranges on V and I

	a (kN-m)	b	c	R^2
$V \leqq 24$m/s	2184	0.7229	0.0981	0.8567
$V > 24$m/s	511	16.912	0.0147	0.9878

Table F.9: Regression coefficients used in Equation F.1 to fit transformed ($z = 4$) edge bending moment fatigue ranges as functions of the mean wind speed and turbulence intensity. The turbine is operating for $V \leqq 24$m/s, otherwise the turbine is parked.

Transformed Blade Root Flap Bending Fatigue Ranges
***z*=5**

Regression of the Mean of Fatigue Ranges on V and I

	a (kN-m)	b	c	R^2
$V \leqq 17$m/s	403931	4.6380	0.7838	0.8946
$17 < V \leqq 24$m/s	1137109	0.3384	1.123	0.2542
$V > 24$m/s	436263	17.885	0.0804	0.9931

Regression of the Standard Deviation of Fatigue Ranges on V and I

	a (kN-m)	b	c	R^2
$V \leqq 24$m/s	3153425	4.1583	0.7819	0.9038
$17 < V \leqq 24$m/s	8957484	1.0125	1.0402	0.3907
$V > 24$m/s	4925813	15.336	0.0925	0.9915

Table F.10: Regression coefficients used in Equation F.1 to fit transformed ($z = 5$) flap bending moment fatigue ranges as functions of the mean wind speed and turbulence intensity. The turbine is operating for $V \leqq 24$m/s, otherwise the turbine is parked.

Transformed Blade Root Edge Bending Fatigue Ranges
***z*=5**

Regression of the Mean of Fatigue Ranges on V and I

	a (kN-m)	b	c	R^2
$V \leqq 24$m/s	54502	0.0366	0.0066	0.2222
$V > 24$m/s	380	20.543	-0.0199	0.9886

Regression of the Standard Deviation of Fatigue Ranges on V and I

	a (kN-m)	b	c	R^2
$V \leqq 24$m/s	24810	0.7046	0.1023	0.8415
$V > 24$m/s	6811	20.945	-0.0167	0.9883

Table F.11: Regression coefficients used in Equation F.1 to fit transformed ($z = 5$) edge bending moment fatigue ranges as functions of the mean wind speed and turbulence intensity. The turbine is operating for $V \leqq 24$m/s, otherwise the turbine is parked.

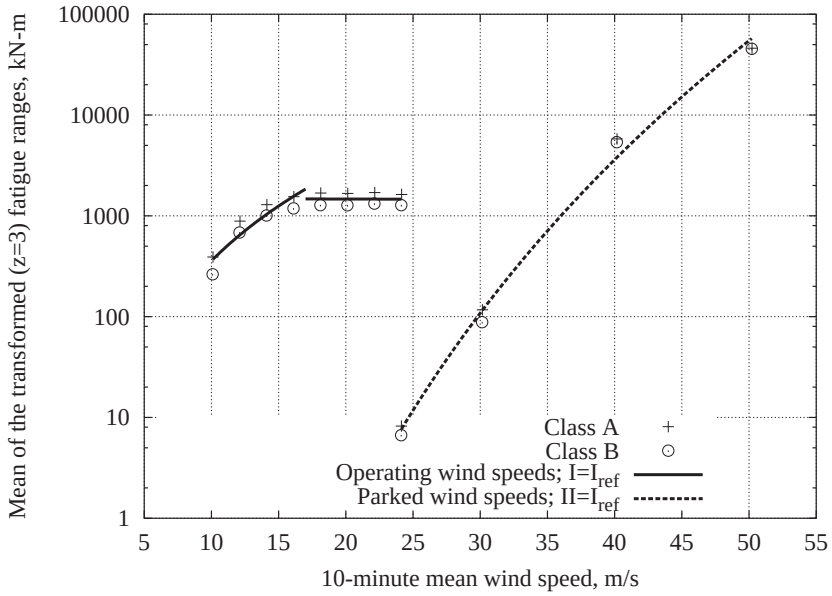

(a) Pooled statistics of the mean of transformed ($z = 3$) fatigue ranges in 10-minute blade root flap bending response time history.

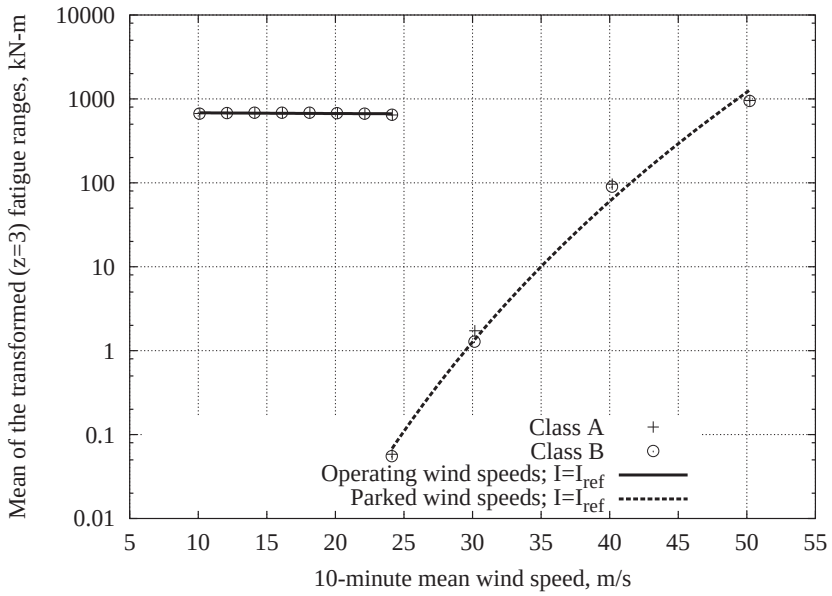

(b) Pooled statistics of the mean of transformed ($z = 3$) fatigue ranges in 10-minute blade root edge bending response time history

Figure F.8: Pooled statistics of the mean of transformed ($z = 3$) fatigue ranges in 10-minute blade root flap and edge bending response time histories for given 10-minute mean wind speeds. The wind turbine is operating for $V \leqq 24$m/s, otherwise the turbine is parked.

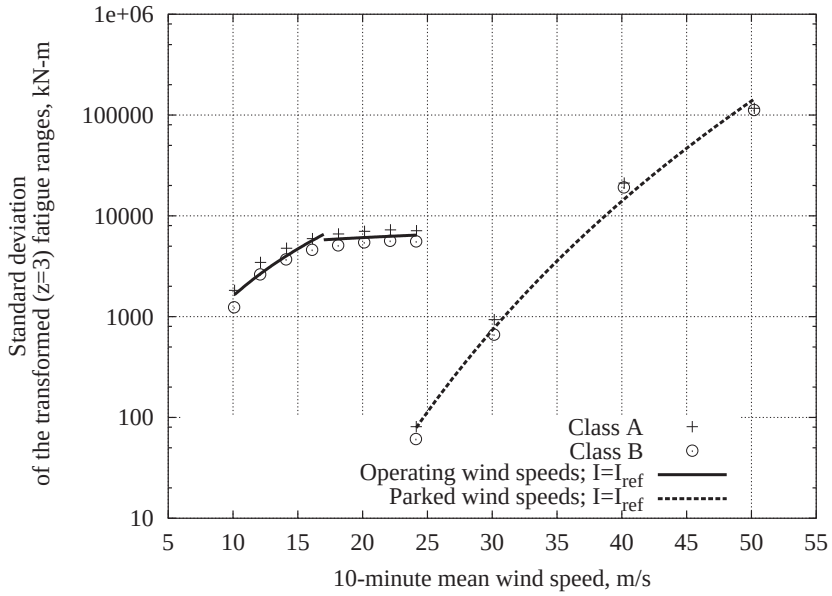

(a) Pooled statistics of the standard deviation of transformed ($z = 3$) fatigue ranges in 10-minute blade root flap bending response time history.

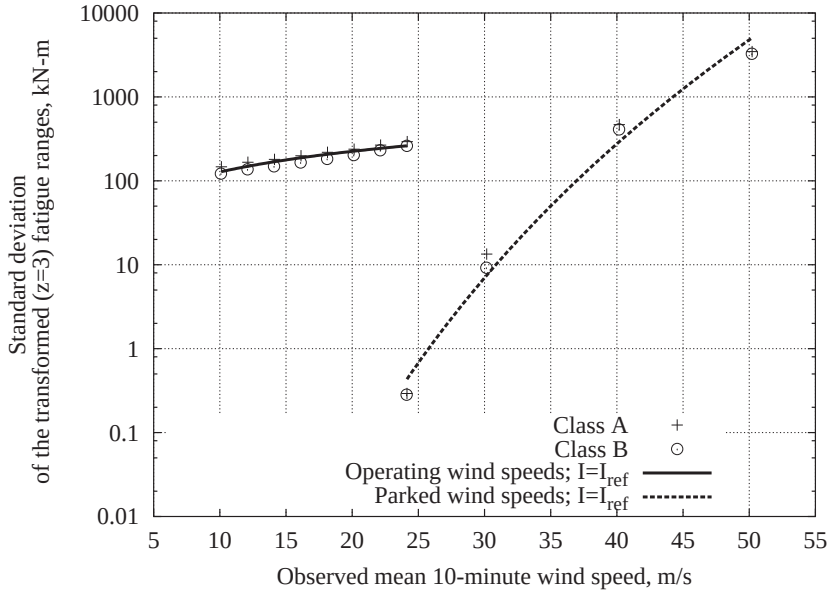

(b) Pooled statistics of the mean of transformed ($z = 3$) fatigue ranges in 10-minute blade root edge bending response time history

Figure F.9: Pooled statistics of the standard deviation of transformed ($z = 3$) fatigue ranges in 10-minute blade root flap and edge bending response time histories for given 10-minute mean wind speeds. The wind turbine is operating for $V \leqq 24$m/s, otherwise the turbine is parked.

F.4.2 Long-Term Analysis

For the discussion here we defined the conditional probability distribution of fatigue ranges by a damage-based Weibull model. Further, the moments of the data have been related to the environmental variables through regression analysis.

The long-term distribution of fatigue load ranges, in an arbitrary 10-minute period is found in the same way as discussed in Section F.3. We will again assume that the AOC 15/50 turbine is installed at a site with environmental conditions conforming to an IEC class IA site, described in Section F.3. The long-term distribution of the 10-minute mean wind speed is assumed to follow a Rayleigh distribution with mean, $\mu_V = 10$m/s. The conditional distribution of turbulence is given by a lognormal distribution with conditional mean and standard deviation given by Equations F.8 and F.9, respectively. A plot of the joint density function of the environmental variables is shown in Figure 4.1 (Chapter 4).

The ranges of the values of the environmental variables are discretized into evenly spaced intervals. For each pair of values of the environmental variables the corresponding short-term distribution of fatigue ranges is generated. Then, per Equation F.2, the short-term conditional fatigue range distributions are summed together, each weighted by the probability of the respective environmental condition, i.e., pair of values of the environmental variables, occurring. The summation is performed over the entire range of environmental variables.

As stated earlier, there are two loading conditions for the turbine, operating and parked. During normal use the turbine is operating for wind speeds less than 24m/s and parked for wind speeds greater than 24m/s. To develop the long-term distribution of the fatigue ranges the appropriate regression model is used for each wind speed value. Figure F.5 shows three long-term distributions of fatigue ranges. Each distribution is based on a different transformation of the fatigue ranges ($z = 3$, 4, 5); all of the distributions appear very similar.

In addition to obtaining an estimate of the long-term distribution of fatigue ranges, we saw in Chapter 5 how we may obtain an estimate of the fatigue damage in an arbitrary 10-minute interval. The expected number of cycles and the environmental variables through regression analysis.[2] The same power-law functional form, Equation F.1, was used. The calculated regression coefficients and R^2 statistics are shown in Table F.12 for blade root flap and edge bending fatigue ranges. Graphical regression results are shown in Figure F.11. Applying Equation F.10 we can obtain estimates of the damage measure for blade root flap and edge bending considering b_f values corresponding to z and $2z$ for $z = 3$, 4, 5, these estimates are presented in Table F.13. We may also consider the portion of

[2]When we transform the fatigue ranges, with $z = 3, 4, 5$, only the magnitude of the fatigue ranges is transformed, the number of fatigue ranges stays the same. Therefore, the expected number of fatigue ranges stays the same regardless of the transformation. The results of the regression analysis presented here is valid for any value of z used for the transformation.

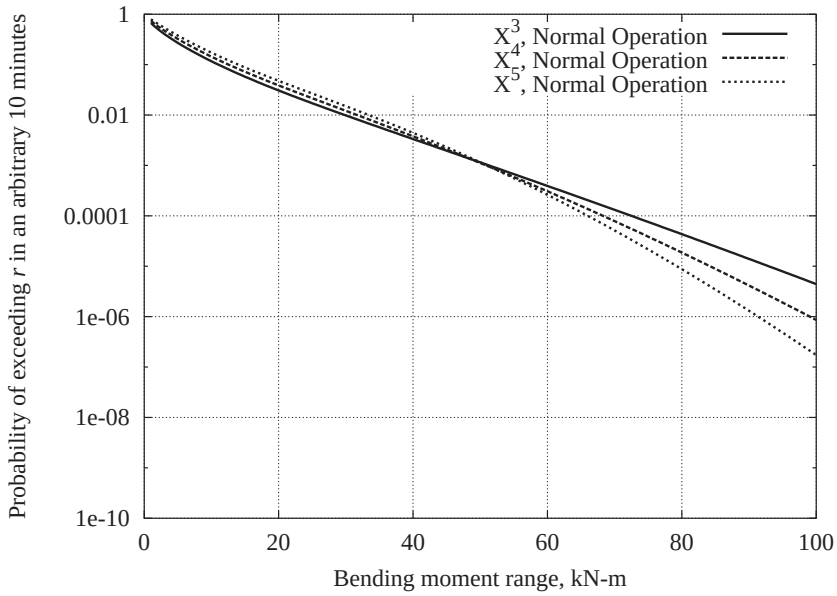

(a) Long-term distribution of blade root flap bending fatigue ranges for an arbitrary 10 minutes.

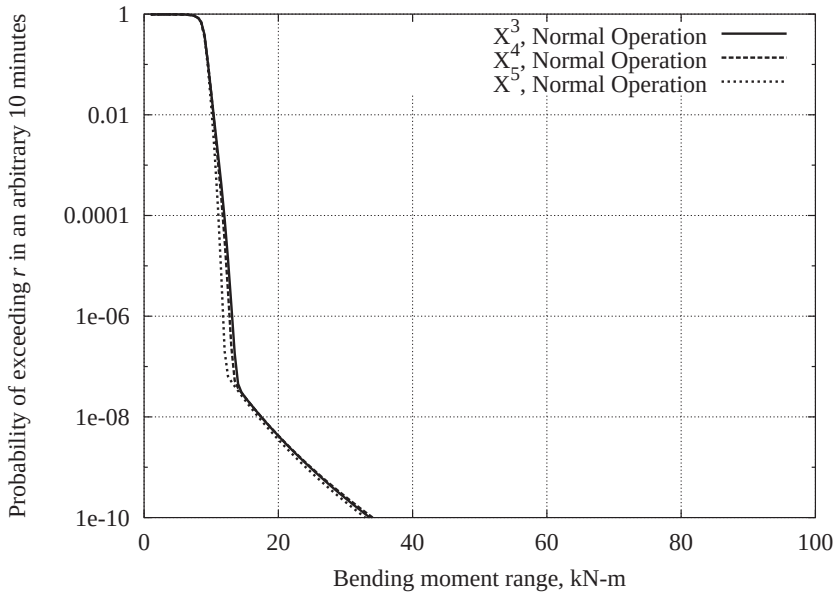

(b) Long-term distribution of blade root edge bending fatigue ranges for an arbitrary 10 minutes.

Figure F.10: Long-term distributions of blade root fatigue bending moment ranges, R, considering three fatigue range transformations, $z = 3$, 4 and 5; for (a) flap and (b) edge bending.

Regression of the number of Fatigue Ranges on V and I

Blade Root Flap Bending

	a (kN-m)	b	c	R^2
$V \leqq 24$m/s	1843	0.1488	0.0035	0.4978
$V > 24$m/s	5023	0.3442	-0.0070	0.9463

Blade Root Edge Bending

	a (kN-m)	b	c	R^2
$V \leqq 24$m/s	671	0.0989	0.0085	0.7379
$V > 24$m/s	5474	0.2203	-0.0047	0.9463

Table F.12: Regression coefficients used in Equation F.1 to fit the expected number of fatigue ranges, for blade root flap and edge bending, as functions of the mean wind speed and turbulence intensity. The turbine is operating for $V \leqq 24$m/s, otherwise the turbine is parked.

Estimate of Damage Measure, DM_{10}, for fatigue exponent values, $b_f = 1, \ldots, 10$.

	b_f	Flap	Edge
$z = 3$	3	2.315e+6	4.303e+5
	6	1.952e+11	3.123e+8
$z = 4$	4	8.788e+7	3.812e+6
	8	5.575e+14	2.552e+10
$z = 5$	5	3.897e+9	3.394e+7
	10	1.787e+18	2.085e+12

Table F.13: Estimate of damage measure, DM_{10}, for fatigue exponent values, $b_f = 1, \ldots, 10$, considering blade root flap and edge bending loads.

the expected damage contributed at different environmental conditions. Figure F.12 presents the plot of damage density for both blade root flap and edge bending moments. We can see from Figure F.12 that as b_f increases the damage measure is more sensitive to higher wind speeds.

F.4.3 Summary

Similar to the previous section, here we have stepped through the process of obtaining an estimate of the marginal probability distribution of the long-term distribution of fatigue ranges. The short-term fatigue loads were modeled using the damage-based Weibull model, however. The general methodology remained the same. In this case however, the statistical moments were obtained after having first transformed the fatigue ranges, e.g., $z = 3$, 4, 5. By performing this transformation

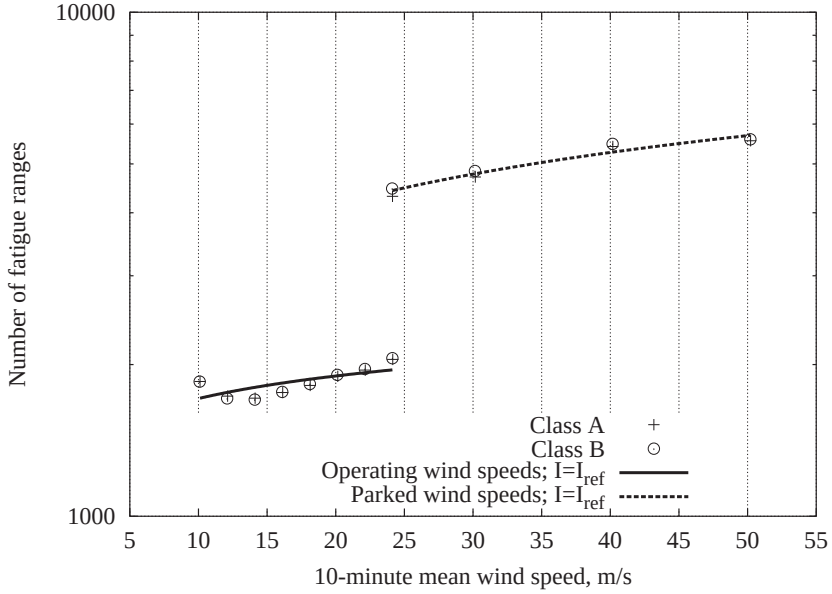

(a) Expected number of fatigue ranges in 10-minute blade root flap bending time history.

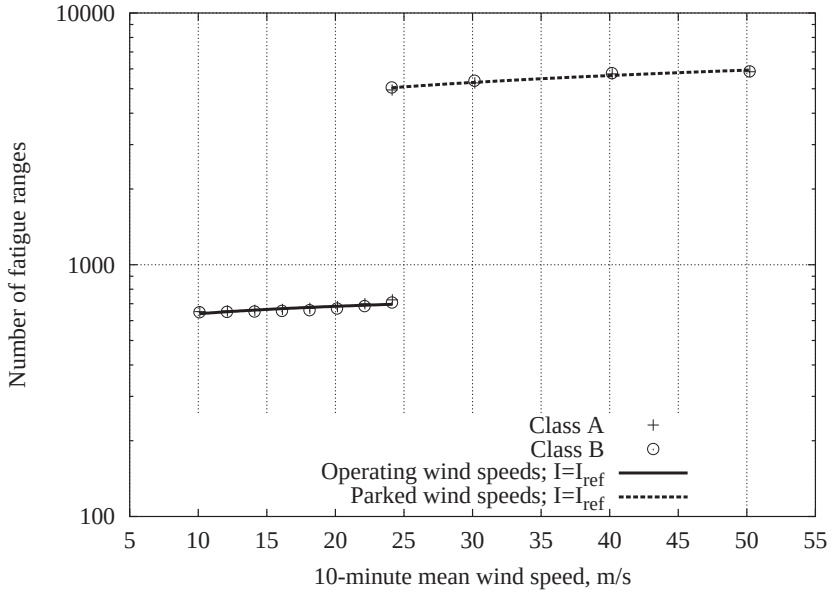

(b) Expected number of fatigue ranges in 10-minute blade root edge bending time history.

Figure F.11: Expected number of fatigue ranges in 10-minute blade root flap and edge bending response time histories, based on 100 pooled observations for each 10-minute mean wind speed and turbulence class. The wind turbine is operating for $V \leqq 24$m/s, otherwise the turbine is parked.

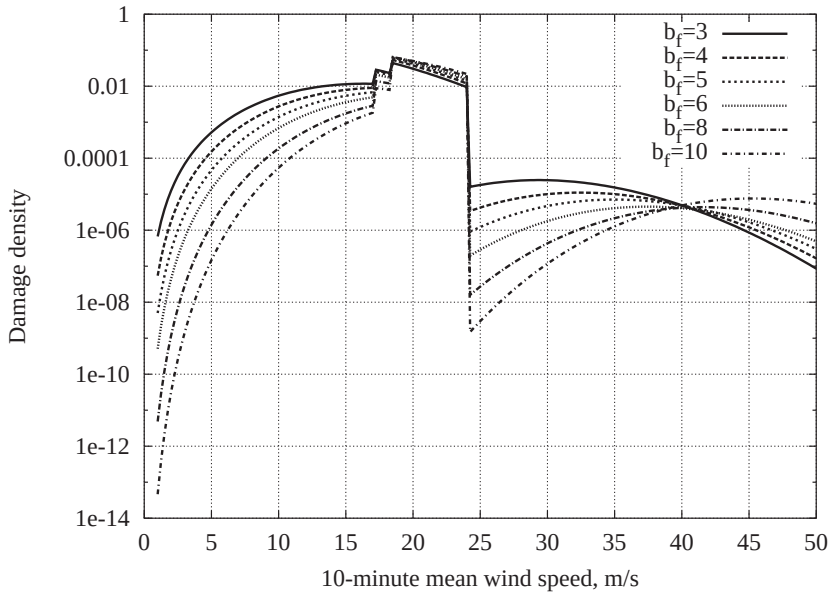

(a) Blade root flap bending moment.

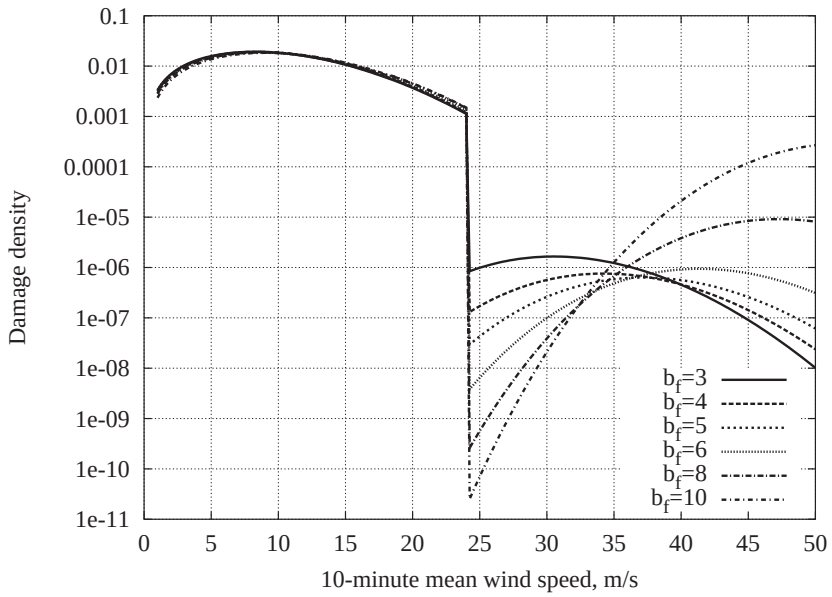

(b) Blade root edge bending moment.

Figure F.12: Damage density for blade root flap and edge bending.

when we employed the method of moments to obtain estimates of the distribution parameters, our model was fit to the z^{th} and $2z^{\text{th}}$ moments of the untransformed data. For $z = 3$, this amounts to fitting the standard Weibull model to the third and sixth statistical moment where we suspect a material with fatigue exponent $b_f =$ 3-6 would be most sensitive to these higher fatigue ranges. The statistical moments of the transformed fatigue ranges were related to the environmental variables through regression analysis. Finally, an estimate of the marginal distribution of the long-term load was obtained by summing the conditional short-term load distributions (each weighted by the probability of the values of the environmental variables occurring) over all environmental conditions. We considered three transformation cases, $z = 3$, 4, and 5. We found that the marginal long-term distributions of the fatigue ranges for an arbitrary 10-minute interval were very similar.

F.5 Comparison of Long-Term Estimates Based on Different Short-Term Models

In Section F.3, we obtained an estimate of the long-term distribution of fatigue ranges based on the short-term distribution of fatigue ranges model by a quadratic Weibull model. Later, in Section F.4 we obtained a similar estimate of the long-term distribution by modeling the short-term distribution of fatigue ranges by a damage-based Weibull model.

Figure F.13 shows the estimates of the long-term distribution of fatigue loads based on modeling the short-term fatigue ranges by quadratic or damage-based Weibull models. Considering flap bending loads, using the quadratic Weibull distribution to model the short-term fatigue ranges generates a long-term distribution with generally lower fatigues loads compared with the the long-term distribution of fatigue loads considering the damage-based model. The fatigue loads based on the quadratic Weibull model are higher for fatigue ranges less than about 20 kN-m, however. For the edge bending case, the long-term distribution of fatigue loads based on either quadratic Weibull or damage based models are very similar.

Tables F.14 and F.15 compare estimates of damage measures, DM_{10}, obtained from our two model definitions. We saw above that the quadratic Weibull produced lower loads for the long-term distribution for both blade root flap and edge bending loads. It would follow that we would expect to see lower damage measures. In fact this is the case, for flap loads, that the damage-based Weibull models do estimate much higher damage measures compared with the estimates from the quadratic Weibull model. In the edge bending case, however, even though the quadratic Weibull model does estimate similar fatigue loads the damage measure estimates are lower than those estimated from the damage-based Weibull model.

We can alternatively compare our estimates of the fatigue damage measure from each of the

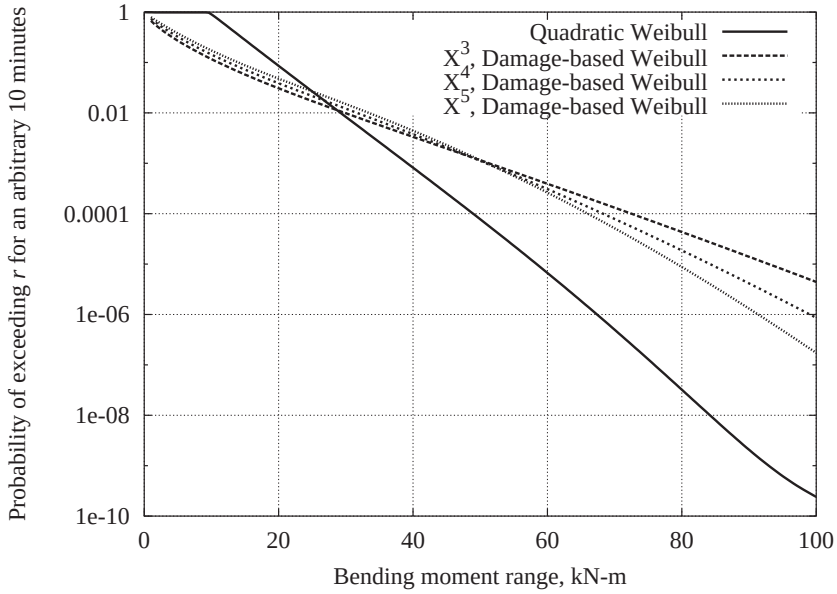

(a) Blade root flap bending.

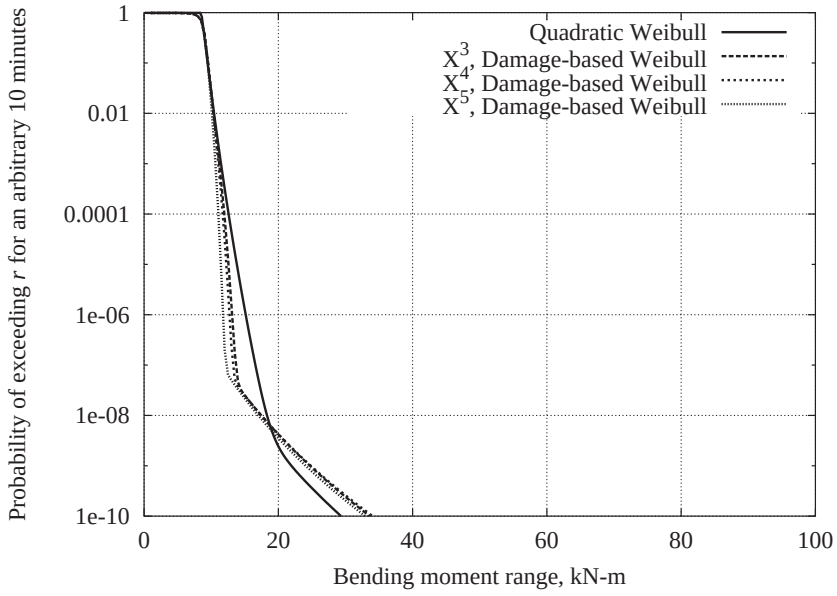

(b) Blade root edge bending.

Figure F.13: Comparison of estimates of the long-term distribution of fatigue ranges based on quadratic or damage-based Weibull models for short-term distribution of fatigue ranges for (a) flap and (b) edge bending.

Comparison of Estimates of Damage Measure, DM_{10}, Blade Root Flap Bending

		Damage-	Percent Difference		
b_f	Q. W.	Based	$z=3$	$z=4$	$z=5$
3	6.835e+5	2.315e+6	238%		
4	1.447e+7	8.788e+7		511%	
5	3.540e+8	3.897e+9			1000%
6	9.961e+9	2.0e+11	1859%		
8	1.2e+13	5.6e+14		4739%	
10	2.1e+16	1.8e+18			8491%

Table F.14: Comparison of damage measure, DM_{10}, estimates for blade root flap bending fatigue loads between short-term quadratic Weibull(Q.W.) model and damage-based Weibull model for $z = 3, 4, 5$ ($z = b_f/2$).

Comparison of Estimates of Damage Measure, DM_{10}, Blade Root Edge Bending

		Damage-	Percent Difference		
b_f	Q. W.	Based	$z=3$	$z=4$	$z=5$
3	3.146e+5	4.303e+5	+37%		
4	2.833e+6	3.812e+6		+35%	
5	2.557e+7	3.394e+7			+32%
6	2.316e+8	3.123e+8	+35%		
8	1.9e+10	2.6e+10		+33%	
10	1.6e+12	2.1e+12			28%

Table F.15: Comparison of damage measure, DM_{10}, estimates for blade root edge bending fatigue loads between short-term quadratic Weibull(Q.W.) model and damage-based Weibull model for $z = 3, 4, 5$ ($z = b_f/2$).

proposed models to an empirical estimate of the fatigue damage measure. The empirical estimate of the fatigue damage measure is obtained by using the raw rain-flow counted range data directly from a representative time history for a given set of values of the environmental variables. We saw in Chapter 5 how we could obtain an empirical estimate of the damage measure.

Tables F.16 and F.17 show the fatigue damage measure for different values of the fatigue exponent, b_f, based on the empirical model and compared to the estimates obtained based on the quadratic Weibull and damage based models. In general, compared to the empirical model the estimates of the fatigue damage measure for the flap bending direction the quadratic Weibull model under-predicts the fatigue damage measure for all fatigue exponents that we considered. The damage based model on the other hand, over-predicts damage for fatigue exponent values less that 7, $b_f < 7$ and under-predicts for values greater than 7, $b_f > 7$. We found slightly different results for the edge bending direction. In this case, the quadratic Weibull model still under-predicted the fatigue damage measure for all fatigue exponents that we considered, but not as drastically. The damage based model over predicted the fatigue damage measure for all fatigue exponent values that we considered. Similar to the results found in Chapter 5 neither of the models do a very good job of estimating the fatigue damage measure compared with the empirical model. However, it should be noted that since the damage-based models are exact at matching the empirical damage at the moments for which they are fit it is really the regression model that is being tested. Additional research would be required to evaluate the general efficacy of these models and regression techniques to predict fatigue damage.

Comparison of Estimates of Damage Measure, DM_{10}, for Fatigue Exponent Values, $b_f = 1, \ldots, 10$, Flap Bending

b_f	Empirical DM_{10}	Quadratic Weibull DM_{10}	Quadratic Weibull % diff.	Damage-Based Weibull DM_{10}	Damage-Based Weibull % diff
1	6.106e+3	2.321e+3	-62.0%	-	-
2	7.170e+4	3.713e+4	-48.2%	-	-
3	1.491e+6	6.835e+5	-54.2%	2.315e+6	55.2%
4	5.068e+7	1.447e+7	-71.5%	8.788e+7	73.4%
5	2.684e+9	3.540e+8	-86.8%	3.897e+8	45.2%
6	1.924e+11	9.961e+9	-94.8%	1.952e+9	1.46%
7	1.635e+13	3.193e+11	-98.1%	-	-
8	1.535e+15	1.152e+13	-99.2%	5.575e+12	-63.7%
9	1.538e+17	4.634e+14	-99.7%	-	-
10	1.619e+19	2.080e+16	-99.9%	1.787e+16	-89.0%

Table F.16: Comparison of estimates of blade root flap bending fatigue damage measure, DM_{10}, for fatigue exponent values, $b_f = 1, \ldots, 10$, considering empirical, quadratic Weibull, and damage based models.

Comparison of Estimates of Damage Measure, DM_{10}, for Fatigue Exponent Values, $b_f = 1, \ldots, 10$, Edge Bending

b_f	Empirical DM_{10}	Quadratic Weibull DM_{10}	Quadratic Weibull % diff.	Damage-Based Weibull DM_{10}	Damage-Based Weibull % diff
1	5.614e+3	3.929e+3	-30.0%	-	-
2	4.921e+4	3.505e+4	-28.8%	-	-
3	4.342e+5	3.146e+5	-27.5%	4.303e+5	36.8%
4	3.847e+6	2.833e+6	-26.4%	3.812e+6	34.6%
5	3.424e+7	2.557e+7	-24.7%	3.394e+7	31.7%
6	3.063e+8	2.316e+8	-24.4%	3.123e+8	34.8%
7	2.754e+9	2.140e+9	-22.3%	-	-
8	2.493e+10	1.920e+10	-23.0%	2.552E+10	32.9%
9	2.281e+11	1.759e+11	-36.0%	-	-
10	2.155e+12	1.623e+12	-24.7%	2.085e+12	28.5%

Table F.17: Comparison of estimates of blade root edge bending fatigue damage measure, DM_{10}, for fatigue exponent values, $b_f = 1, \ldots, 10$, considering empirical, quadratic Weibull, and damage based models.

C. P. Butterfield
NREL
1617 Cole Boulevard
Golden, CO 80401

J. Cadogan
Office of Wind and Hydro Technology
EE-12
U.S. Department of Energy
1000 Independence Avenue SW
Washington, DC 20585

S. Calvert
Office of Wind and Hydro Technology
EE-12
U.S. Department of Energy
1000 Independence Avenue SW
Washington, DC 20585

J. Cohen
Princeton Economic Research, Inc.
1700 Rockville Pike
Suite 550
Rockville, MD 20852

A. J. Eggers, Jr.
RANN, Inc.
744 San Antonio Road, Suite 26
Palo Alto, CA 94303

P. R. Goldman, Director
Office of Wind and Hydro Technology
EE-12
U.S. Department of Energy
1000 Independence Avenue SW
Washington, DC 20585

D. Griffin
GEC
5729 Lakeview Drive NE, Suite 100
Kirkland, WA 98033

C. Hansen
Windward Engineering
4661 Holly Lane
Salt Lake City, UT 84117

Bill Holley
3731 Oakbrook
Pleasanton, CA 94588

D. Malcolm
GEC
5729 Lakeview Drive NE, Suite 100
Kirkland, WA 98033

P. Migliore
NREL
1617 Cole Boulevard
Golden, CO 80401

A. Mikhail
Clipper Windpower Technology, Inc.
7985 Armas Canyon Road
Goleta, CA 93117

NWTC Library – (5)
NREL
1617 Cole Boulevard
Golden, CO 80401

R. Z. Poore
Global Energy Concepts, Inc.
5729 Lakeview Drive NE
Suite 100
Kirkland, WA 98033

D. Sanchez
U.S. Department of Energy
Albuquerque Operations Office
P.O. Box 5400
Albuquerque, NM 87185

Brian Smith
NREL
1617 Cole Boulevard
Golden, CO 80401

R. W. Thresher
NREL
1617 Cole Boulevard
Golden, CO 80401

W. A. Vachon
W. A. Vachon & Associates
P.O. Box 149
Manchester, MA 01944

K. Wetzel
K. Wetzel & Company, Inc.
P.O. Box 4153
Lawrence, KS 66046-1153

Paul S. Veers, Manager
Wind Energy Technology
Department 6214
Mail Stop: 0708

Herbert J. Sutherland
Department 6214
Mail Stop: 0708

David Hoover, Registrar
National Atomic Museum, Dept. 12660
1905 Mountain Road NW
Albuquerque, NM 87104

Holt Ashley
Department of Aeronautics & Astronautics
Mechanical Engineering
Stanford University
Stanford, CA 94305

Technical Library (2)
Department 9616
Mail Stop: 0899

Central Technical Files
Department 8945-1
Mail Stop: 9018

LeRoy Fitzwater (2)
The Boeing Company
P.O. Box 16858, Mail Code: P29-14
Philadelphia, PA 19142-0858

Lance Manuel
Assistant Professor – Structures
Department of Civil Engineering, C1748
University of Texas at Austin
Austin, TX 78712

Ahsan Iqbal
The Boeing Company
P.O. Box 16858, Mail Code: P29-14
Philadelphia, PA 19142-0858

Mike Warburton
The Boeing Company
P.O. Box 16858, Mail Code: P29-14
Philadelphia, PA 19142-0858